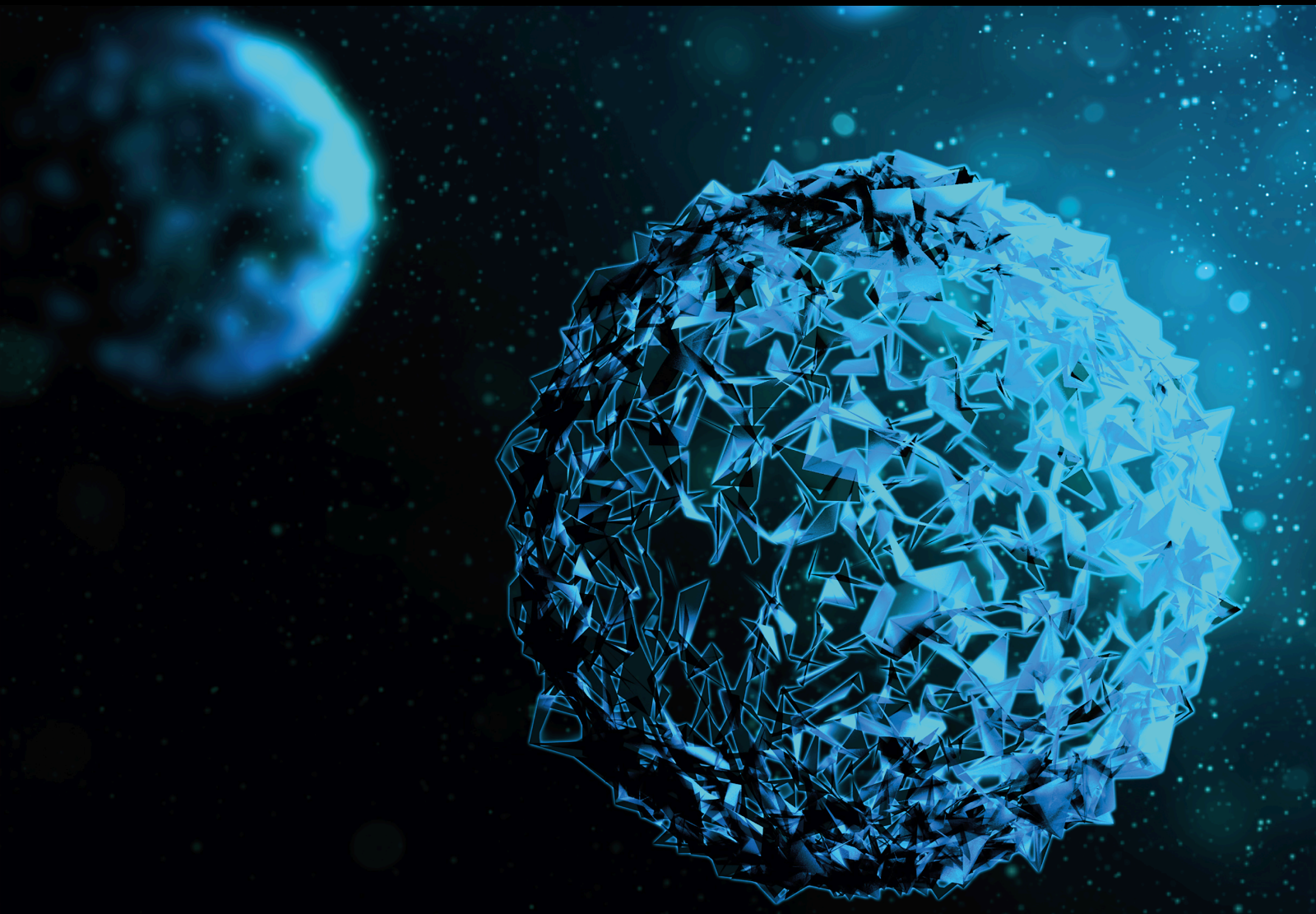# Extreme Environmental Stresses Induced Biological Effects: From Phenotype to Molecular Mechanisms

Lead Guest Editor: Xiaohua Lei
Guest Editors: Junsoo Park, Lei Zhao, Zhongquan Dai, and Akihisa Takahashi

Extreme Environmental Stresses Induced Biological Effects: From Phenotype to Molecular Mechanisms

Extreme Environmental Stresses Induced Biological Effects: From Phenotype to Molecular Mechanisms

Lead Guest Editor: Xiaohua Lei
Guest Editors: Junsoo Park, Lei Zhao, Zhongquan
Dai, and Akihisa Takahashi

Section Editors

Penny A. Asbell, USA
David Bernardo (iD), Spain
Gerald Brandacher, USA
Kim Bridle (iD), Australia
Laura Chronopoulou (iD), Italy
Gerald A. Colvin (iD), USA
Aaron S. Dumont, USA
Pierfrancesco Franco (iD), Italy
Raj P. Kandpal (iD), USA
Fabrizio Montecucco (iD), Italy
Mangesh S. Pednekar (iD), India
Letterio S. Politi (iD), USA
Jinsong Ren (iD), China
William B. Rodgers, USA
Harry W. Schroeder (iD), USA
Andrea Scribante (iD), Italy
Germán Vicente-Rodriguez (iD), Spain
Momiao Xiong (iD), USA
Hui Zhang (iD), China

Academic Editors

Cell Biology

Contents

Retraction

Retracted: Dielectrophoresis-Based Method for Measuring the Multiangle Mechanical Properties of Biological Cells

BioMed Research International

This article has been retracted by Hindawi following an investigation undertaken by the publisher [1]. This investigation has uncovered evidence of one or more of the following indicators of systematic manipulation of the publication process:

(1) Discrepancies in scope

(2) Discrepancies in the description of the research reported

(3) Discrepancies between the availability of data and the research described

(4) Inappropriate citations

(5) Incoherent, meaningless and/or irrelevant content included in the article

(6) Manipulated or compromised peer review

The presence of these indicators undermines our confidence in the integrity of the article's content and we cannot, therefore, vouch for its reliability. Please note that this notice is intended solely to alert readers that the content of this article is unreliable. We have not investigated whether authors were aware of or involved in the systematic manipulation of the publication process.

Wiley and Hindawi regrets that the usual quality checks did not identify these issues before publication and have since put additional measures in place to safeguard research integrity.

We wish to credit our own Research Integrity and Research Publishing teams and anonymous and named external researchers and research integrity experts for contributing to this investigation.

The corresponding author, as the representative of all authors, has been given the opportunity to register their agreement or disagreement to this retraction. We have kept a record of any response received.

References

[1] B. Zhu, W. Li, M. Zhu, P.-L. Hsu, L. Sun, and H. Yang, "Dielectrophoresis-Based Method for Measuring the Multiangle Mechanical Properties of Biological Cells," *BioMed Research International*, vol. 2020, Article ID 5358181, 9 pages, 2020.

Retraction

Retracted: TRPM7 Upregulate the Activity of SMAD1 through PLC Signaling Way to Promote Osteogenesis of hBMSCs

BioMed Research International

This article has been retracted by Hindawi following an investigation undertaken by the publisher [1]. This investigation has uncovered evidence of one or more of the following indicators of systematic manipulation of the publication process:

(1) Discrepancies in scope

(2) Discrepancies in the description of the research reported

(3) Discrepancies between the availability of data and the research described

(4) Inappropriate citations

(5) Incoherent, meaningless and/or irrelevant content included in the article

(6) Manipulated or compromised peer review

The presence of these indicators undermines our confidence in the integrity of the article's content and we cannot, therefore, vouch for its reliability. Please note that this notice is intended solely to alert readers that the content of this article is unreliable. We have not investigated whether authors were aware of or involved in the systematic manipulation of the publication process.

Wiley and Hindawi regrets that the usual quality checks did not identify these issues before publication and have since put additional measures in place to safeguard research integrity.

We wish to credit our own Research Integrity and Research Publishing teams and anonymous and named external researchers and research integrity experts for contributing to this investigation.

The corresponding author, as the representative of all authors, has been given the opportunity to register their agreement or disagreement to this retraction. We have kept a record of any response received.

References

[1] F. Hong, S. Wu, C. Zhang et al., "TRPM7 Upregulate the Activity of SMAD1 through PLC Signaling Way to Promote Osteogenesis of hBMSCs," *BioMed Research International*, vol. 2020, Article ID 9458983, 23 pages, 2020.

Retraction

Retracted: α_1-Adrenergic Receptor Blockade by Prazosin Synergistically Stabilizes Rat Peritoneal Mast Cells

BioMed Research International

This article has been retracted by Hindawi following an investigation undertaken by the publisher [1]. This investigation has uncovered evidence of one or more of the following indicators of systematic manipulation of the publication process:

(1) Discrepancies in scope

(2) Discrepancies in the description of the research reported

(3) Discrepancies between the availability of data and the research described

(4) Inappropriate citations

(5) Incoherent, meaningless and/or irrelevant content included in the article

(6) Manipulated or compromised peer review

The presence of these indicators undermines our confidence in the integrity of the article's content and we cannot, therefore, vouch for its reliability. Please note that this notice is intended solely to alert readers that the content of this article is unreliable. We have not investigated whether authors were aware of or involved in the systematic manipulation of the publication process.

Wiley and Hindawi regrets that the usual quality checks did not identify these issues before publication and have since put additional measures in place to safeguard research integrity.

We wish to credit our own Research Integrity and Research Publishing teams and anonymous and named external researchers and research integrity experts for contributing to this investigation.

The corresponding author, as the representative of all authors, has been given the opportunity to register their agreement or disagreement to this retraction. We have kept a record of any response received.

References

[1] N. Abe, H. Toyama, Y. Ejima et al., "α_1-Adrenergic Receptor Blockade by Prazosin Synergistically Stabilizes Rat Peritoneal Mast Cells," *BioMed Research International*, vol. 2020, Article ID 3214186, 12 pages, 2020.

Review Article

The Determinant of DNA Repair Pathway Choices in Ionising Radiation-Induced DNA Double-Strand Breaks

Lei Zhao [ID],[1] **Chengyu Bao,**[1] **Yuxuan Shang,**[1] **Xinye He,**[1] **Chiyuan Ma,**[2] **Xiaohua Lei** [ID],[2] **Dong Mi,**[3] **and Yeqing Sun** [ID][1]

[1]*Institute of Environmental Systems Biology, College of Environmental Science and Engineering, Dalian Maritime University, Dalian, 116026 Liaoning, China*
[2]*State Key Laboratory of Stem Cell and Reproductive Biology, Institute of Zoology, Chinese Academy of Sciences, Beijing, China*
[3]*College of Science, Dalian Maritime University, Dalian, Liaoning, China*

Correspondence should be addressed to Lei Zhao; zhaol@dlmu.edu.cn, Xiaohua Lei; leixh@ioz.ac.cn, and Yeqing Sun; yqsun@dlmu.edu.cn

Received 19 March 2020; Revised 13 July 2020; Accepted 30 July 2020; Published 25 August 2020

Academic Editor: Emilia Lecuona

Ionising radiation- (IR-) induced DNA double-strand breaks (DSBs) are considered to be the deleterious DNA lesions that pose a serious threat to genomic stability. The major DNA repair pathways, including classical nonhomologous end joining, homologous recombination, single-strand annealing, and alternative end joining, play critical roles in countering and eliciting IR-induced DSBs to ensure genome integrity. If the IR-induced DNA DSBs are not repaired correctly, the residual or incorrectly repaired DSBs can result in genomic instability that is associated with certain human diseases. Although many efforts have been made in investigating the major mechanisms of IR-induced DNA DSB repair, it is still unclear what determines the choices of IR-induced DNA DSB repair pathways. In this review, we discuss how the mechanisms of IR-induced DSB repair pathway choices can operate in irradiated cells. We first briefly describe the main mechanisms of the major DNA DSB repair pathways and the related key repair proteins. Based on our understanding of the characteristics of IR-induced DNA DSBs and the regulatory mechanisms of DSB repair pathways in irradiated cells and recent advances in this field, We then highlight the main factors and associated challenges to determine the IR-induced DSB repair pathway choices. We conclude that the type and distribution of IR-induced DSBs, chromatin state, DNA-end structure, and DNA-end resection are the main determinants of the choice of the IR-induced DNA DSB repair pathway.

1. Introduction

Ionising radiation (IR), such as X- or γ-rays from medical radiation treatments, high-energy charged (HZE) particles from cosmic radiation, is an unavoidable risk factor to endanger human health [1–4]. IR can attack DNA and produce a variety of DNA lesions, mainly including DNA double-strand breaks (DSBs), DNA single-strand breaks (SSBs), mismatches, modified bases, and abasic sites, which are associated with various kinds of human diseases [5]. Among these DNA lesions, DSBs are considered to be the most deleterious DNA lesions, which are the major threats to genome integrity and stability, and the main factors to determine cellular fate (to survive, to carcinogenesis, or to

die) after IR exposures [6, 7]. The evolutionarily conserved DNA repair pathways play critical roles in countering and eliciting IR-induced DSBs to ensure genome integrity and maintain genome stability [8, 9]. If these DNA lesions are not correctly repaired, residual or unrepaired DSBs can lead to the loss of genetic material and cell death, and especially incorrectly repaired DSBs can cause inappropriate end-joining and rearrangement events that may result in gene mutations, chromosome aberrations, cell transformation, carcinogenesis, etc. Therefore, the precise DSB repair is essential to reduce the IR-induced health risks. In contrast, genetic disruptions in the DNA repair pathways can cause genomic instability and enhance IR-induced health risks, especially carcinogenesis risks [10, 11].

Given the importance of DNA repair pathways in processing IR-induced DNA DSBs and reducing IR-induced health risks, many studies have been conducted to identify the critical proteins that recognise, transduce, and repair IR-induced DNA DSBs and to understand the complicated DNA DSB repair mechanisms in irradiated cells [12]. Some other studies have attempted to find the crucial gene transcriptions [13], noncoding RNAs [14], and posttranslational modifications (e.g., methylation, acetylation, and neddylation) [15] that probably implicated in the regulation of the DNA DSB repair pathways. Also, recent evidence shows that DNA repair pathways are expected to be highly evolutionarily conserved between different species [8, 9]. The conserved features of DNA repair pathways may facilitate interdisciplinary studies to expand the identification of undiscovered human DNA repair molecules for improving the new insights of the DNA repair mechanisms. Based on the conserved feature of DNA repair mechanisms, Nikitaki et al. [16] proposed an *in silico* approach to identify and rescue the candidate genes for the DNA repair pathways in plants and animals. We recently have also proposed a simplified *in silico* method of homologous comparison to investigate novel human genes implicated in DNA repair pathways. The results showed that many novel assembly proteins, transcription factors, and molecular chaperones were found to be involved in the IR-induced DNA repair pathways [17]. The innovative methods *in silico* modelling can be used to identify key DNA repair molecules and reveal IR-induced DNA DSB repair mechanisms.

There are four possible DNA repair pathways that have been employed concertedly by mammalian cells to repair DNA DSBs, such as classical nonhomologous end joining (c-NHEJ), homologous recombination (HR), single-strand annealing (SSA), and alternative end joining (alt-EJ) [18]. Accumulating evidence suggests that these repair pathways are not equal or alternative ways to handle DNA DSBs [19]. The disorder of the selections of DNA repair pathways can also cause the increases in DNA lesions, radiosensitivities, chromosomal translocations, carcinogenesis, and even other health risks [20, 21]. Indeed, a series of regulatory factors, such as the type and distribution of DNA lesions, local chromatin environment, and cell cycle phase, are employed to ensure that cells choose the suited DNA repair pathways [22–24]. Iliakis et al. [19] have proposed the hypothesis that the key factors in determining the engagements of DNA repair pathways are the degree of chromatin destabilisation generated by the DSBs. According to their opinions, indeed, different physical and biological factors have been found to determine the choices of DNA repair pathways mainly through the degree of chromatin destabilisation. However, despite all these, the understanding of the determinant of the IR-induced DNA DSB repair pathway choices is limited to date, and it is still unclear what determines the choices of major DNA repair pathways in response to IR-induced DNA DSBs.

In this review, we discuss how the mechanisms of IR-induced DSB repair pathway choices can operate in irradiated cells. We first begin with a description of the main characteristics of the major DNA repair pathways and the critical DNA repair proteins that dominate the repair of IR-induced DNA DSBs. We then mainly discuss the emerging understanding of the critical regulatory mechanisms of IR-induced DSB repair pathway choices. The overarching goal in this review is to summarize and highlight the main factors that probably determine the choices of IR-induced DSB repair pathways from different perspectives, which is of great significance for the mechanistic investigations of DNA repair pathways and consequential choices, the assessments of health risks, and even the developments of radioprotective or radiomitigative drugs after IR exposures.

2. Overview of IR-Induced DNA DSB Repair Pathways

As mentioned above, mammalian cells have probably employed four different DNA repair pathways to repair IR-induced DNA DSBs, each of which can repair DSBs using different mechanisms (Figure 1(a)). Among these pathways, c-NHEJ and HR are the two major pathways to repair IR-induced DSBs, while SSA and alt-EJ can repair the residual DSBs that are unable to be repaired by the c-NHEJ and HR [22]. Although many studies have been conducted for these pathways, the detailed molecular mechanisms of SSA and alt-EJ for repairing IR-induced DSBs are still not completely understood.

IR-induced DNA DSBs have blunt double-strand DNA ends or contain short single-strand DNA ends [18]. These kinds of IR-induced DNA DSBs can be repaired by c-NHEJ through joining two DNA ends in proximity to each other (Figure 1(a)). In contrast, IR-induced DSBs with long single-stranded DNA (ssDNA) tails and/or DNA-end resection that can be not repaired by c-NHEJ since long ssDNA tails can greatly reduce the affinity of Ku70/80, while which can be processed by the remaining pathways, HR, SSA, and alt-EJ (Figure 1(a)). The ssDNA tails in IR-induced DSBs can be stabilized by the invasions of replication protein A (RPA) [25]. The DNA-end resection can be carried out by the structure-specific nuclease (i.e., the MRE11/RAD50/NBS1 (MRN) complex) to generate "short-range resection". And, the DNA-end resection can be implemented by the helicases and exonucleases, CtBP-interacting protein (CtIP), RPA, exonuclease 1 (EXO1), DNA replication helicase/nuclease 2 (DNA2), Bloom's syndrome (BLM) helicase, *etc.*, to generate "long-range resection".

In order to clarify the determinant factors of IR-induced DNA DSB repair pathway choices next, this section will briefly introduce the main characteristics of the four possible DNA repair pathways and the critical DNA repair proteins involved in these pathways as follow.

2.1. Classical Nonhomologous End Joining. The c-NHEJ is initiated by the binding of the heterodimer Ku70/80 to the blunt or short DSB ends induced by IR. The Ku70/80 binding at DSB ends may play roles in protecting the sequence of DNA ends from unnecessary resection. And then, the Ku70/80 mediates the recruitment of the DNA-dependent protein kinase catalytic subunit (DNA-PKcs), DNA ligase IV (LIG4), and the associated scaffolding factors XRCC4,
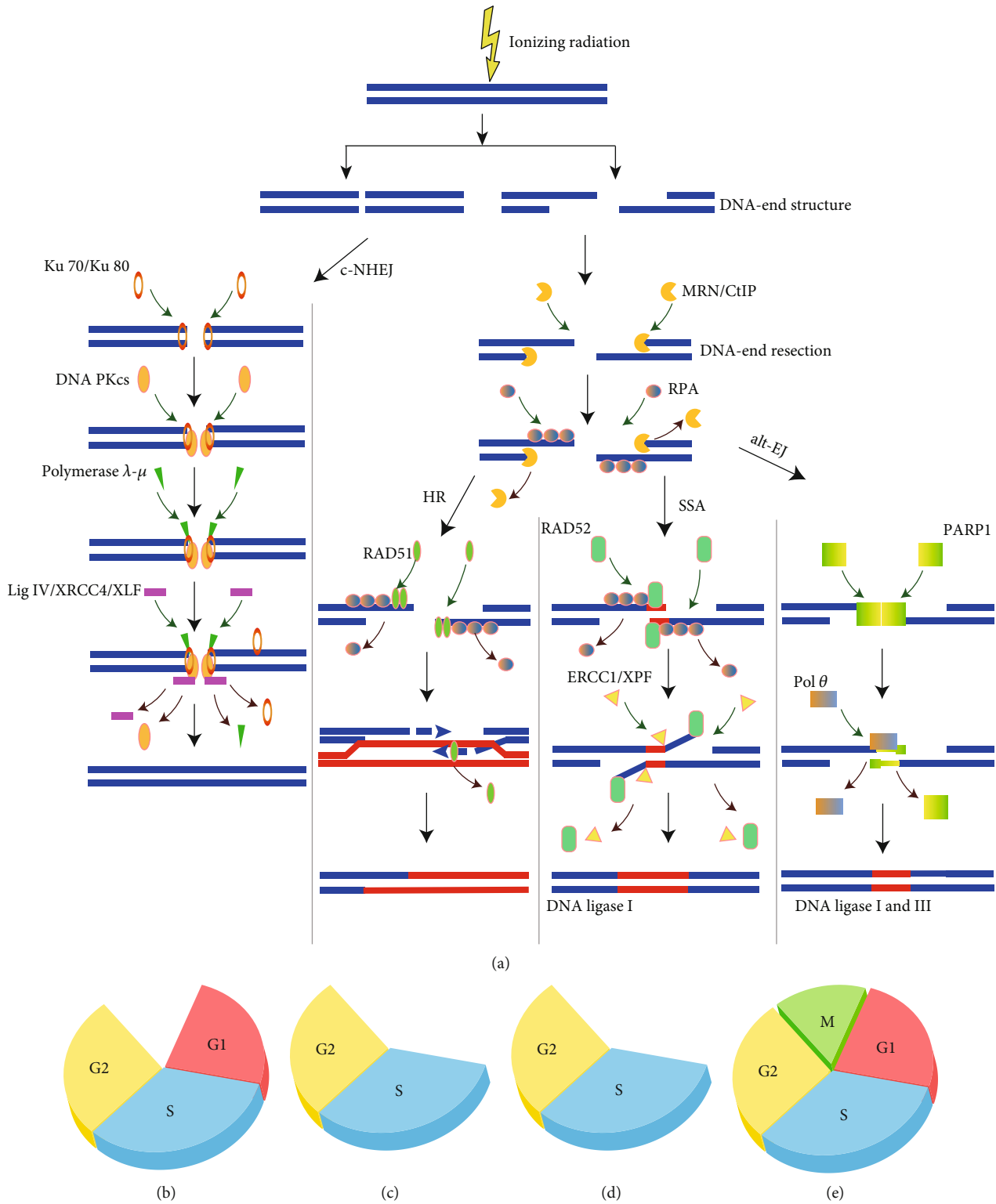
FIGURE 1: (a) Major repair pathways for DNA double-strand breaks (DSBs) generated by ionising radiation (IR). When IR-induced DNA DSBs have blunt double-strand DNA ends or contain short single-strand DNA ends, the classical nonhomologous end joining (c-NHEJ) is initiated by the binding of the Ku70/80 heterodimer followed by the recruitment of DNA-PKcs and polymerase. When DNA resection occurs, the pathways of homologous recombination (HR), alternative end joining (alt-EJ), and single-strand annealing (SSA) can be activated to repair the IR-induced DNA DSBs by the recruitments of different proteins. (b–e) The major repair pathways ((b) c-NHEJ, (c) HR, (d) SSA, and (e) alt-EJ) for processing IR-induced DNA DSBs have a distinct cell-cycle dependence.

XRCC4-like factor (XLF), and paralog of XRCC4, to ligate the broken DNA ends (Figure 1(a)) [26]. According to whether the ends can be ligated, additional end processing is needed to facilitate the c-NHEJ by several accessory factors, such as the nuclease Artemis and the specialized DNA polymerases λ and μ [27]. Also, other accessory factors, such as the Aprataxin and Aprataxin and PNK-like factor (APLF), can be involved in regulating the process of c-NHEJ. After IR exposures, histone H2AX can be phosphorylated at serine 139 through the recruitment of the above factors, resulting in forming of the discrete foci at DSB sites, which is the so-called ionising radiation-induced foci (IRIF) [28]. The γ-H2AX foci are one of the most sensitive biomarkers that can be used to reflect IR-induced DNA DSBs and plays a major role in the pathway of c-NHEJ.

In general, c-NHEJ represents the leading repair pathway to eliminate IR-induced DNA DSBs over all phases of the cell cycle except for M phase in irradiated mammalian cells (Figure 1(b)) [29]. Moreover, c-NHEJ is a simple, rapid, and highly efficient pathway to repair DSBs, which does not require a homologous sequence but depends on the blunt DNA-end structures[30]. Also, it should be noted that c-NHEJ frequently scavenges DNA ends by arbitrarily joining two ends that are very close in space. As a consequence, the c-NHEJ can result in some insertions or deletions in the genome, also known as translocations [31]. Due to the rapid speed for the repair of c-NHEJ and the fact that IR-induced DNA DSBs are usually very close to each other in space, c-NHEJ normally joins together the correct DNA ends, thus leading to low levels of translocations.

2.2. Homologous Recombination.

The second major pathway of IR-induced DNA DSB repair is HR, which requires homologous sequences between sister chromatids. Also, HR is dependent on the DNA-end resection. When the range of DNA-end resection is a few thousand base pairs, the HR can be implemented for repairing through the invasion of DNA strand transferase RAD51 to achieve the RPA displacement (Figure 1(a)), which can promote sequence alignment between the homologous regions in sister chromatids to form the structure of Holliday junction (HJ). The RAD51 foci, as one kind of IRIF, can also be used as the biomarker for IR-induced DSBs and plays a central activity in the pathway of HR. During the process of HR, some DNA-end resection regulators, such as breast cancer type 2 susceptibility protein (BRCA2) and RAD51 paralogs (such as RAD51B, RAD51C, RAD51D, XRCC2, and XRCC3), can also be involved in facilitating the RPA displacement [32].

In general, HR is in most cases the error-free repair process that can faithfully restore the original DNA structure since it carries out recombination by using the homologous sister chromatid as a template even though HR also requires error-prone polymerases and can modify the forms of sequences through gene conversion and crossover [33]. Thus, under most conditions, HR can hardly cause chromosomal translocations or sequence modifications in the genome [34]. The complex processes involved in HR suggests that this pathway is relatively slower than c-NHEJ [35]. More-

over, HR is strongly dependent on the cyclin-dependent kinase (CDK) activity and therefore is largely restricted to the S and G2 phases of the cell cycle (Figure 1(c)) [36].

2.3. Single-Strand Annealing.

SSA is also a DNA-end resection dependent pathway for DSB repair, which also requires the above-mentioned DNA-end resection proteins [37]. When the range of resection reaches a few hundred thousand base pairs, the SSA can be utilized to repair IR-induced DNA DSBs. Moreover, the repetitive sequence in the genome provides homologous regions for the engagement of SSA. However, few studies have analyzed the response of SSA in repairing IR-induced DNA DSBs.

Unlike the HR that relies on the invasion of RAD51, SSA requires the invasion of the strand accessory protein RAD52 to facilitate the displacement of RPA and to mediate the homology search between repeat regions (Figure 1(a)) [23]. Thus, RAD52 has an important role in the pathway of SSA. SSA mediates DSB end joining using the intervening sequences between the repeats in two single strands of DNA molecule. Although SSA is homology-dependent repair, SSA is still considered an error-prone repair, because the intervening sequence between the repeats can be deleted, thus resulting in the large deletions of sequences and the formation of many chromosomal translocations [38]. Similar to the HR, the SSA is also cell cycle dependent and has the potential activity during the S and G2 phases (Figure 1(d)) [19].

2.4. Alternative End Joining.

Alt-EJ, also known as microhomology-mediated end joining (MMEJ), can join two IR-induced DNA ends together, which has similar principles as c-NHEJ [39]. Unlike the c-NHEJ, alt-EJ relies on the presence of microhomologous sequences within two limited DNA-end resections, which are typically ≥2 base pairs (bp) or 2~6 bp [40, 41].

In addition to the proteins mentioned above involved in the DNA-end resection, there are also some specific proteins implicated in the alt-EJ (Figure 1(a)). For example, poly(-ADP-ribose) polymerase 1 (PARP-1) has been demonstrated to implement the displacement of Ku 70/80 or RPA, thus facilitating the pathway of alt-EJ [42]. Also, it should be emphasized that polθ has both a C-terminal polymerase domain and an N-terminal helicase like domain and can further disclose the microhomologous DNA ends and promote the joint of the DNA ends [43]. That is to say that polθ is essential for alt-EJ [41]. Furthermore, DNA ligases I and III can also be used in this pathway to promote the ligation of the DNA ends [18]. Although alt-EJ is active throughout the cell cycle, it also shows cell cycle dependence and has the maximum activity in the G2 phase (Figure 1(e)) [19].

Due to the relatively slow speed for the repair of alt-EJ and the fact that IR-induced DNA DSBs can diffuse away from the original position, alt-EJ subsequently increases the deletions and other sequence alterations and results in high levels of chromosomal translocations in the genome, which is much more extensive than those generated by c-NHEJ [23]. This mutagenic effect is generally considered to be less than those generated by the SSA.

(a)

(b)
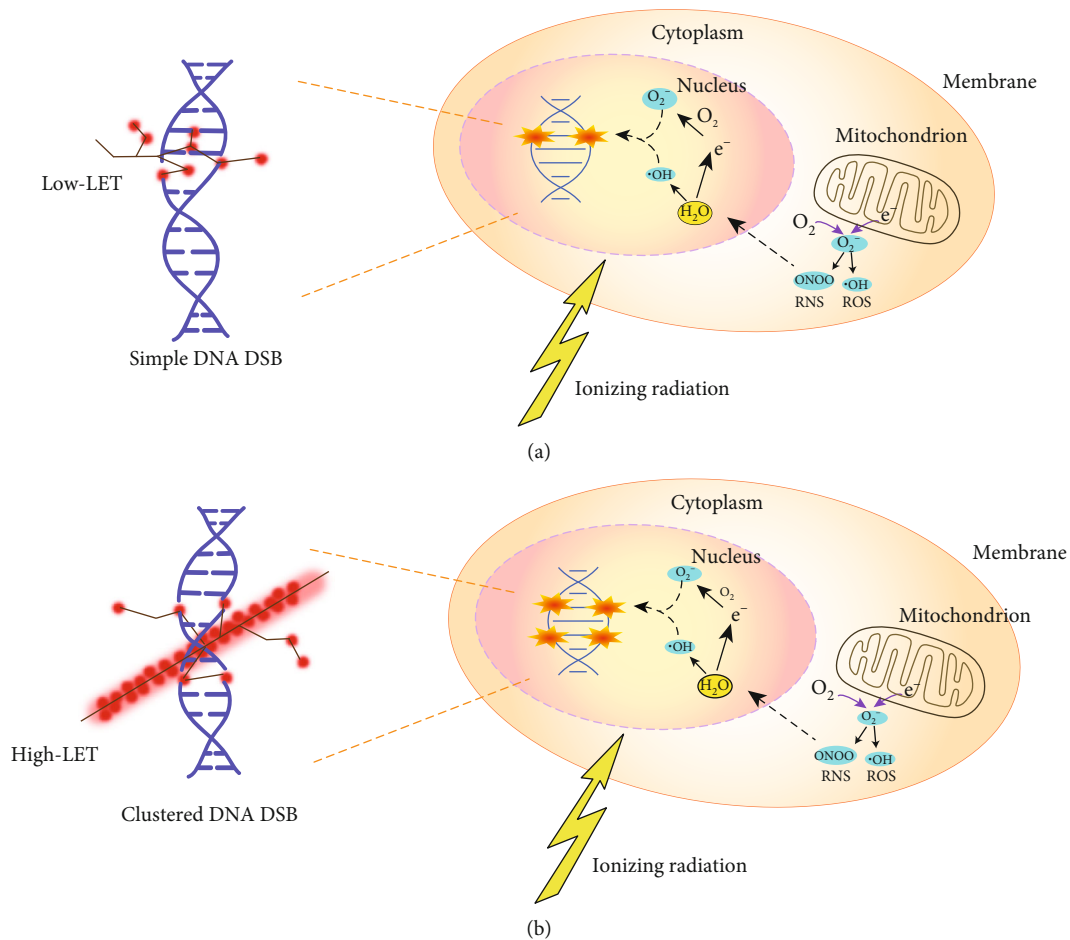
FIGURE 2: The direct and indirect effects of ionising radiation (IR) in cells. The schematic shows IR can lead to the DNA double-strand breaks (DSBs) directly by the induction of radiation energy deposition, or indirectly by the generation of reactive oxygen and nitrogen species (ROS and RNS). The direct effects are mainly determined by the radiation quality, i.e., low and high linear energy transfer (LET) can generate distinctive patterns of ionisation events on the structures of DNA molecules. When doses are the same, low-LET (a) and high-LET (b) radiation can generate different types and distributions of DNA DSBs. The IR-induced ROS and RNS are not only from the interaction of IR with water and molecules but also as a result of leakage of mitochondrial dysfunctions.

3. The Determinant of IR-Induced DNA DSB Repair Pathway Choices

As described in the above discussion, the repair pathway choices are fundamental and essential to process IR-induced DNA DSBs, which are unique and not alternative ways to decide the cell fates [22]. According to the current advances of the regulation of the repair pathway choices in mammalian cells, in this section, we will systematically summarize and discuss the main possible factors and associated challenges to determine the IR-induced DSB repair pathway choices.

3.1. The Type and Distribution of IR-Induced DSBs Contribute to Repair Pathway Choices. IR-induced DNA DSBs can occur in irradiated cells due to the direct effects through the energy deposition of IR [44–46], or the indirect effects through the generation of oxygen and nitrogen species (ROS and RNS) from the interaction of IR with water and molecules, and the leakage of mitochondrial dysfunctions

[47] (Figure 2). Recently, studies in the field indicate that IR-induced DNA DSBs are mainly determined by radiation quality [48, 49]. One important parameter for depicting the radiation quality is linear energy transfer (LET), which describes the amount of energy deposition (or ionisations) generated by IR per unit of particle-track length [50]. When doses are the same, low- and high-LET radiation can generate different types and distributions of DNA DSBs. For example, low-LET radiation (such as X-rays and γ-rays) deposits its energy uniformly within cells. It generates primary simple DNA DSB lesions (e.g., isolated DSBs (iDSBs)), which are randomly distributed in the cell nucleus (Figure 2(a)). The simple DNA DSB lesions refer to a single and individual DNA DSB induced within a chromatin loop. In contrast, high-LET radiation (such as alpha ions and heavy ions) produces high ionisation densities and deposits lots of energy in a small distance along the track of each particle and produces high levels of ROS and RNS. Through this mechanism, high-LET radiation increases the yield of DSBs and induces more complex or clustered DNA DSB lesions (e.g., clustered DSBs

(cDSBs)), which have significant track structure characteristics (Figure 2(b)) [51, 52]. The clustered DSB lesions refer to two or more close DSBs within a chromatin loop, which can also be composed of both DSB and non-DSB lesions [53]. Also, low-LET radiation with a high dose can also lead to complex or clustered DNA DSBs damage [54].

According to the review of Sridharan et al. [54], the choices of IR-induced DNA DSB repair pathways may primarily depend on radiation quality. This is mainly due to the fact that different radiation qualities can result in different complexity of DNA lesions, such as simple DNA DSB lesions and clustered DNA DSB lesions, and thereby may trigger different repair pathways. That is to say that the types and distributions of IR-induced DNA DSBs can determine the DSB repair pathway choices (Figure 3).

In general, the iDSBs induced by low-LET radiation can be mainly repaired by the pathways of c-NHEJ and HR, while the cDSBs generated by high-LET radiation are difficult to repair [55]. For example, a recent study provides the evidence that there are distinct spatial structures of key DSB repair factors, such as γ-H2AX, tumor suppressor p53-binding protein 1 (53BP1), and RAD51, in the IRIF in Hela cells after high- or low-LET radiation exposures [56], which suggest that different types and distributions of IR-induced DSBs may elicit distinct repair pathways. The study of Okayasu et al. shows that the cDSBs induced by high-LET radiation may markedly depend on c-NHEJ [57]. Also, the experimental investigation of Sridharan et al. showed that Artemis, as a key assembled-protein in the c-NHEJ, is involved the repair of the clustered DSBs induced by high-LET radiation, which supports that the c-NHEJ has important roles in the repair of cDSBs generated by high-LET radiation [58]. However, Wang et al. have also found that the complex DSBs containing short DNA fragments induced by high-LET radiation can also inhibit the c-NHEJ, which is possible due to this kind of DNA DSB lesions making it difficult for the heterodimer Ku70/80 to load onto the DNA ends and results in less efficient c-NHEJ-mediated DSB repair [59]. Also, Zafar et al. [60] investigated the contribution of DSB repair pathways in repairing DSBs induced by high-energy iron ions. They found that some key HR proteins in the process of DNA-end resection and DNA strand invasion are also involved in repairing the complex DSBs generated by high-LET radiation. In addition, they found that the assembly factors in the HR-deficient rodent cells are sensitive to high-LET radiation, resulting in enhanced induction of mutation and chromosome aberration. Therefore, the above evidence indicates that the type and distribution of IR-induced DSBs can be a leading factor to contribute to repair pathway choices. However, to our knowledge, the contributions of c-NHEJ and HR to repair cDSBs generated by high-LET radiation are still not well understood [54]. Moreover, the residual simple and clustered DSBs induced by IR with different radiation qualities can be repaired by the pathways of alt-EJ and SSA [19], while the detailed processes of the two pathways in response to high- and low-LET radiation is still unclear.

3.2. The Roles of Chromatin State in IR-Induced DSB Repair Pathway Choices.
The chromatin state can change the forms of IR-induced DSBs and therefore affect the consequences of repair processing, thus indicating that the chromatin state may also have important roles in influencing the repair pathway choices (Figure 3) [61]. In the euchromatin, the genome is active for DNA replication and transcription. Therefore, the DSBs generated by IR in this region are likely to be handled by the extensive DNA-end resection [20]. Several studies have also indicated that the IR-induced DSBs in the euchromatin are mainly repaired by c-NHEJ and HR [62, 63]. Unlike the euchromatin, the IR-induced DSBs in the region of heterochromatin disfavour the pathway of HR and prefer the pathway of alt-EJ, while remaining the activity of c-NHEJ unaltered [64]. Also, some studies found that to allow the pathway of HR for repairing IR-induced DSBs in the heterochromatin, it requires to increase the levels of the poly(ADP-ribose) polymerase (PARP) and ataxia telangiectasia mutated protein (ATM) and other assembly factors to disassemble the chromatin [65, 66]. Moreover, the repair kinetics of IR-induced DSBs in the heterochromatin is significantly slower than that of euchromatin [20], which is consistent with the above conclusions.

Taken together, we infer that the IR-induced DSBs produced in different chromatin states may lead to different consequences of DSB repair pathways. Additionally, the PARP and ATM, which may promote chromatin decondensation and remodelling, are part of early response signals to IR-induced DSBs and have important roles in determining the repair pathway choices (Figure 3). Indeed, in addition to the above mechanism, transcriptions, noncoding RNAs, and epigenetic modifications can also be implicated in determining the roles of chromatin state in pathway choices, which need be considered in the further studies.

3.3. The Roles of DNA-End Structure in IR-Induced DSB Repair Pathway Choices.
The DNA-end structure is also an important factor to determine the initial IR-induced DSB repair pathway choices (Figure 3) [20, 22]. As mentioned above, if the IR-induced DNA DSB ends are blunt, the heterodimer Ku70/80 will be prone to bind to the DNA ends to protect the DNA-end structure and facilitate the c-NHEJ. However, if the IR-induced DNA DSB ends contain long ssDNA tails or single-stranded gaps close to DNA ends, it can block the Ku70/80 binding to the DNA ends since Ku70/80 binds weakly to this kind of DNA-end structure, and directly lead to the RPA loading and PARP activation, which can result in the choices of the DNA-end resection dependent DSB repair pathways. According to the above descriptions, the DNA-end resection dependent DSB repair pathways include the HR, SSA, and alt-EJ [19]. However, if the additional end processing occurs in this kind of DNA-end structure, it may also evade end recognition by Ku70/80, which can promote the c-NHEJ.

In general, IR can generate DNA DSBs with blunt ends, or with some modified DNA ends, such as long ssDNA tails or single-stranded gaps [67, 32, 53]. Also, high-LET radiation can produce the clustered DSBs, especially the presence of the non-DSB lesions around the DSB site [54]. Thus, the IR-induced clustered DSBs with sharp DNA ends or single-stranded gaps close to DNA ends can hinder the Ku70/80
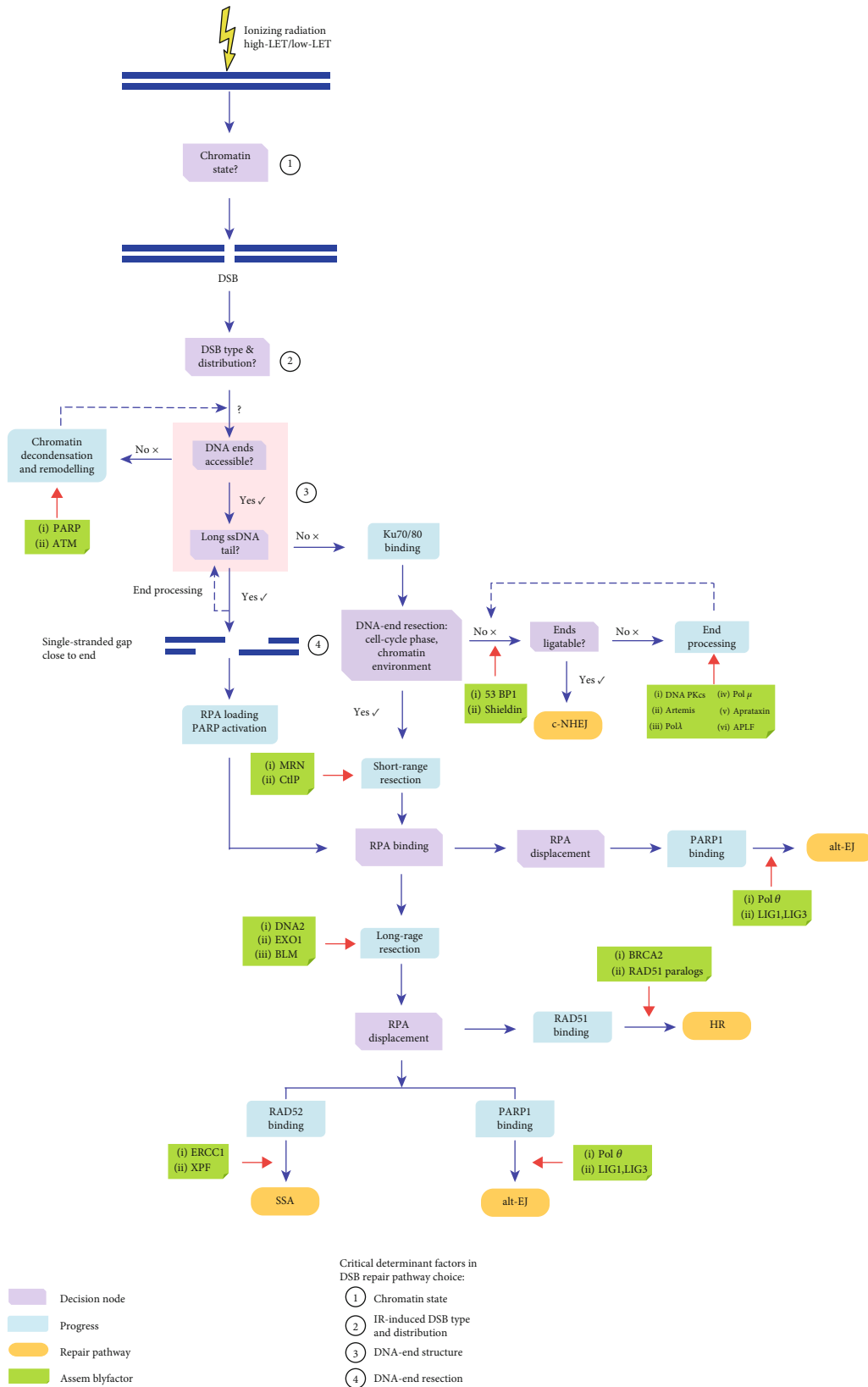
FIGURE 3: The choices of ionising radiation- (IR-) induced DNA repair pathways. The schematic shows that there are four key factors, including the chromatin state, the type and distribution of IR-induced DNA double-strand breaks (DSBs), the DNA-end structure, and the DNA-end resection, which can determine the repair pathway choices. Many critical proteins that are directly or indirectly involved in the above processes also play a critical role in determining the pathway choices. The more detailed discussions can be found in the main text.

binding to the ends of DSBs, which limits the pathway of c-NHEJ and favours the DNA-end resection-dependent DSB repair pathways. It could probably explain why, sometimes, the complex DSBs induced by high-LET radiation can inhibit the c-NHEJ and promote the HR [59]. However, the study of Povirk et al. also indicated that the Artemis nuclease can be used to process this kind of DNA-end structure induced by IR and can thereby promote the c-NHEJ [68].

Overall, the spatial structure of the IR-induced DNA DSB ends has important roles in determining the IR-induced DSB repair pathway choices (Figure 3). The IR-induced DNA-end structure primarily depends on radiation quality, while the quantitative relationship between LET and DNA-end structure is unclear.

3.4. The Roles of DNA-End Resection in IR-Induced DSB Repair Pathway Choices.

IR-induced DSBs can also be further processed through the DNA-end resection. The processes of DNA-end resection can remove the heterodimer Ku70/80 from the DNA DSB ends and activate the alternative pathways (such as HR, SSA, and alt-EJ) for DSB processing. It indicates that the DNA-end resection plays a critical and essential role in determining the IR-induced DSB repair pathway choices. And, according to recent advances, there are many factors that can affect the process of DNA-end resection [22, 23]. We will illustrate the roles of DNA-end resection in IR-induced DSB repair pathway choices from two aspects.

3.4.1. The Roles of Chromatin Environment in IR-Induced DSB Repair Pathway Choices through Regulating DNA-End Resection.

The key assembly factors in chromatin environments that block DNA-end resection can make Ku70/80 retention at DNA ends, which can promote the c-NHEJ. Conversely, the factors in chromatin environments that contribute to DNA-end resection can make the displacement of Ku70/80 and facilitate the DNA-end resection-dependent DSB repair pathways (Figure 3). For example, 53BP1 has one of the important roles in determining the DSB repair pathway choices through restricting the DSB-end resection [69]. 53BP1 can be recruited to the IR-induced DSB ends and form IRIF around DSBs, thereby promoting the chromatin compaction, blocking the DNA nucleases access to the DSB ends [70], and limiting the length of DSB end resection [71]. Therefore, 53BP1 can be considered to have an important role in promoting the pathway of c-NHEJ. The number of 53BP1 foci can also be used as another surrogate marker for DSBs and the corresponding irradiation dose, and the formation and disappearance of IR-induced 53BP1 foci are similar to those of γ-H2AX foci [72]. Recent studies reported that the Shieldin complex has similar repair functions as 53BP1, which can suppress the DNA-end resection, convert ssDNA tails into blunt ends, and facilitate the c-NHEJ [73, 74]. Conversely, BRCA2 and RAD51 paralogs, as the antagonistic of the 53BP1 and Shieldin complex, can overcome the barrier against DNA-end resection after IR exposures and promote the RAD51 loading [75] and further lead to the activation of HR.

Furthermore, the length of the DNA-end resection is most likely to be the main reason for influencing the IR-induced DSB repair pathway choices (Figure 3) [22]. If the range of resection is less than 20 bp, also known as "short-range resection," the pathway of alt-EJ will have the opportunity to be activated by an important step of the PARP1 binding. If the range of resection is relative long (about a few thousand bp), known as "long-range resection," the pathway of HR will be mainly required for repairing DSBs by the recruitment of DNA strand transferase RAD51. In addition, if the range of resection is a few hundred thousand bp, the SSA pathway can also be chosen opportunistically for repairing the residual DSBs through the invasion of RAD52 nucleofilament. Lastly, if DNA ends are the long-range resection and have the microhomologous repeat region, the alt-EJ pathway will be possibly chosen for repairing through the competitive binding of PARP1.

Indeed, many different kinds of accessory factors, such as DNA repair proteins or complex and posttranslational modifications, can contribute to the regulation of the length of DNA-end resection (Figure 3) [76, 77]. These factors can be changed by IR exposures and thereby influence the decision of IR-induced DSB repair pathway choices [19, 23, 78]. For example, MRN, CtIP, BRCA1, DNA2, EXO1, and BLM, as key DNA repair proteins or complex, are implicated in regulating the length of the DNA-end resection [19], which is very important in controlling the DSB repair pathway choices. Most of these proteins acted as the key helicase and nuclease to generate ssDNA with end resection, which is stabilized by the invasion of RPA [19]. The inhibition of any proteins mentioned above can inhibit the pathways of HR and SSA for repairing the IR-induced DSBs but allows the pathway of c-NHEJ [24].

Moreover, ATM or ATR, known as two major kinases that are differentially activated after low- and high-LET radiation [79], can recruit and phosphorylate the members of the MRN complex (MRE11, RAD50, and NBS1) and subsequently cause the phosphorylation of other key DNA repair proteins, such as CtIP, BRCA1, EXO1, and BLM. ATM or ATR can significantly enhance the efficiency of DNA-end resection and promote the related DSB repair pathways [80]. Therefore, ATM or ATR can be also considered the crucial regulators of the DNA-end resection and determine IR-induced DSB repair pathway choices. In addition, some posttranslational modifications have also been implicated in the DNA-end resection by regulating the activities of either ATM or ATR [23].

In addition to the proteins that are directly or indirectly involved in the DNA-end resection, there are other key proteins that could influence the IR-induced DSB repair pathway choices (Figure 3) [22, 23]. For example, some proteins that implicated in the displacement of RPA are capable of determining the choices of the IR-induced DSB repair pathways [22]. Specifically, the RAD51 binding to displace the RPA on the ssDNA can promote the pathway of HR, the RAD52 binding to displace the RPA can lead to the pathway of SSA, and the PARP1 and polθ binding to displace the RPA can facilitate the pathway of alt-EJ [43].

Therefore, according to the above discussions, we can conclude that DNA-end resection is considered the main factor to control the IR-induced DSB repair pathway choices. A series of critical proteins, such as 53BP1, BRCA2, RAD51

paralogs, ATM, ATR, MRN, CtIP, BRCA1, DNA2, EXO1, BLM, RPA, PARP1, and polθ, can affect IR-induced DSB repair pathway choices through regulating the length of the DNA-end resection. However, it is not very clear what the difference between low- and high-LET radiation responses of these proteins in the chromatin environment is. More radiation biological experiments and biophysical models should be used to clarify this issue.

3.4.2. The Roles of the Cell Cycle in IR-Induced DSB Repair Pathway Choices through Regulating DNA-End Resection. In addition to the above factors that can affect DNA-end resection, cell cycle is also an important factor to regulate the process of DNA-end resection (Figure 3), which can also determine the choices of IR-induced DNA DSB repair pathways. That is to say that the phase of cell cycle has an important role in DSB repair pathway choices [36]. The supporting evidence is that c-NHEJ is required for the repair of IR-induced DSBs over all phases of cell cycle except for M phase (Figure 1(b)); alt-EJ is active for repairing IR-induced DSBs throughout the cell cycle and has the maximum activity in the G2 phase (Figure 1(e)). At the same time, HR and SSA are primarily utilized during S and G2 (Figures 1(c) and 1(d)). The main reason given for these dependencies is that the CDK activity can be increased significantly when cells enter the S and G2 phases. The CDK activity can activate the DNA repair proteins through phosphorylation to perform the DNA-end resection [81]. For example, the CDK-dependent CtIP and EXO1 phosphorylations can facilitate the DNA-end resection in the S/G2 phases, which significantly promotes the pathway of HR [82, 83]. On the other hand, the impairment of the CtIP and EXO1 phosphorylations can decrease the DNA-end resection and further enhance the pathway of c-NHEJ. That is, in the G1 phase, the CDK activity can be significantly reduced to limit the DNA-end resection and therefore favours c-NHEJ over DNA-end resection dependent repair pathways [77].

Experimental evidence has shown that IR can lead to the activation of DNA lesion-dependent cell cycle checkpoint controls and result in the cell cycle arrest in G1/S or G2/M [84]. The cell cycle arrest not only provides sufficient time for DNA repair but also changes the CDK activity [85], which can regulate the process of DNA-end resection. We can, therefore, conclude that the cell cycle can also determine the IR-induced DSB repair pathway choices through CDK activity affecting the DNA-end resection. Moreover, the effects of different LETs on cell cycle checkpoint controls should be paid more attentions for further studies, which may be a key factor that cannot be ignored in regulating the IR-induced DSB repair pathway choices.

4. Conclusion

Based on the current research advances in the characteristics of IR-induced DNA DSBs and the regulation of the repair pathway choices in irradiated cells, we have systematically summarized and discussed four key factors including the type and distribution of IR-induced DSBs, chromatin state, DNA-end structure, and DNA-end resection, to determine IR-induced DSB repair pathway choices. Additionally, we have also proposed some associated challenges for future studies, including (1) the contributions of c-NHEJ and HR in repairing cDSBs induced by high-LET radiation; (2) the roles and mechanisms of alt-EJ and SSA in repairing IR-induced DSBs; (3) the roles of transcriptions, noncoding RNAs, and epigenetic modifications in regulatingthe chromatin state and thereby determining IR-induced DSB repair pathway choices, and (4) the relationships between LET and initial DNA-end structure, the critical proteins involved in DNA-end resection, and cell cycle checkpoint controls.

Conflicts of Interest

The authors declare that they have no competing interests regarding the publication of this paper.

Acknowledgments

References

[1] M. Durante, R. Orecchia, and J. S. Loeffler, "Charged-particle therapy in cancer: clinical uses and future perspectives," *Nature Reviews Clinical Oncology*, vol. 14, no. 8, pp. 483–495, 2017.

[2] M. Durante and F. A. Cucinotta, "Heavy ion carcinogenesis and human space exploration," *Nature Reviews Cancer*, vol. 8, no. 6, pp. 465–472, 2008.

[3] L. Zhao, D. Mi, and Y. Sun, "Issues and challenges of space radiation risk assessment in manned deep space exploration missions," *Chinese Science Bulletin*, vol. 63, no. 16, pp. 1523–1537, 2018.

[4] L. Zhao, Y. Shang, S. Yuan, X. He, D. Mi, and Y. Sun, "Current research progress of space radiation protection technologies in manned deep space exploration missions," *Chinese Science Bulletin*, vol. 64, no. 20, pp. 2087–2103, 2019.

[5] S. P. Jackson and J. Bartek, "The DNA-damage response in human biology and disease," *Nature*, vol. 461, no. 7267, pp. 1071–1078, 2009.

[6] K. K. Khanna and S. P. Jackson, "DNA double-strand breaks: signaling, repair and the cancer connection," *Nature Genetics*, vol. 27, no. 3, pp. 247–254, 2001.

[7] W. P. Roos, A. D. Thomas, and B. Kaina, "DNA damage and the balance between survival and death in cancer biology," *Nature Reviews. Cancer*, vol. 16, no. 1, pp. 20–33, 2016.

[8] E. M. Taylor and A. R. Lehmann, "Conservation of eukaryotic DNA repair mechanisms," *International Journal of Radiation Biology*, vol. 74, no. 3, pp. 277–286, 1998.

[9] D. Hanahan and R. A. Weinberg, "Hallmarks of cancer: the next generation," *Cell*, vol. 144, no. 5, pp. 646–674, 2011.

[10] J. H. J. Hoeijmakers, "Genome maintenance mechanisms for preventing cancer," *Nature*, vol. 411, no. 6835, pp. 366–374, 2001.

[11] P. A. Jeggo, L. H. Pearl, and A. M. Carr, "DNA repair, genome stability and cancer: a historical perspective," *Nature Reviews. Cancer*, vol. 16, no. 1, pp. 35–42, 2016.

[12] W. L. Santivasi and F. Xia, "Ionizing radiation-induced DNA damage, response, and repair," *Antioxidants & Redox Signaling*, vol. 21, no. 2, pp. 251–259, 2014.

[13] H. Lans, J. H. J. Hoeijmakers, W. Vermeulen, and J. A. Marteijn, "The DNA damage response to transcription stress," *Nature Reviews Molecular Cell Biology*, vol. 20, no. 12, pp. 766–784, 2019.

[14] N. Durut and O. M. Scheid, "The role of noncoding RNAs in double-strand break repair," *Frontiers in Plant Science*, vol. 10, article 1155, 2019.

[15] J. Her and S. F. Bunting, "How cells ensure correct repair of DNA double-strand breaks," *The Journal of Biological Chemistry*, vol. 293, no. 27, pp. 10502–10511, 2018.

[16] Z. Nikitaki, A. Pavlopoulou, M. Holá et al., "Bridging plant and human radiation response and DNA repair through an *in silico* approach," *Cancers*, vol. 9, no. 12, p. 65, 2017.

[17] L. Zhao, X. He, Y. Shang et al., "Identification of potential radiation-responsive biomarkers based on human orthologous genes with possible roles in DNA repair pathways by comparison between Arabidopsis thaliana and homo sapiens," *Science of The Total Environment*, vol. 702, article 135076, 2020.

[18] A. Schipler and G. Iliakis, "DNA double-strand-break complexity levels and their possible contributions to the probability for error-prone processing and repair pathway choice," *Nucleic Acids Research*, vol. 41, no. 16, pp. 7589–7605, 2013.

[19] G. Iliakis, E. Mladenov, and V. Mladenova, "Necessities in the processing of DNA double strand breaks and their effects on genomic instability and cancer," *Cancers*, vol. 11, no. 11, p. 1671, 2019.

[20] L. Krenning, J. van den Berg, and R. H. Medema, "Life or death after a break: what determines the choice?," *Molecular Cell*, vol. 76, no. 2, pp. 346–358, 2019.

[21] D. Setiaputra and D. Durocher, "Shieldin - the protector of DNA ends," *EMBO Reports*, vol. 20, no. 5, 2019.

[22] R. Scully, A. Panday, R. Elango, and N. A. Willis, "DNA double-strand break repair-pathway choice in somatic mammalian cells," *Nature Reviews Molecular Cell Biology*, vol. 20, no. 11, pp. 698–714, 2019.

[23] R. Ceccaldi, B. Rondinelli, and A. D. D'Andrea, "Repair pathway choices and consequences at the double-strand break," *Trends in Cell Biology*, vol. 26, no. 1, pp. 52–64, 2016.

[24] A. Shibata, "Regulation of repair pathway choice at two-ended DNA double-strand breaks," *Mutation Research/Fundamental and Molecular Mechanisms of Mutagenesis*, vol. 803, pp. 51–55, 2017.

[25] J.-H. Lee and T. T. Paull, "ATM activation by DNA double-strand breaks through the Mre11-Rad50-Nbs1 complex," *Science*, vol. 308, no. 5721, pp. 551–554, 2005.

[26] H. H. Y. Chang, N. R. Pannunzio, N. Adachi, and M. R. Lieber, "Non-homologous DNA end joining and alternative pathways to double-strand break repair," *Nature Reviews Molecular Cell Biology*, vol. 18, no. 8, pp. 495–506, 2017.

[27] B. M. Stinson, A. T. Moreno, J. C. Walter, and J. J. Loparo, "A mechanism to minimize errors during non-homologous end joining," *Molecular Cell*, vol. 77, no. 5, pp. 1080–1091.e8, 2020.

[28] L. Bee, S. Fabris, R. Cherubini, M. Mognato, and L. Celotti, "The efficiency of homologous recombination and non-homologous end joining systems in repairing double-strand breaks during cell cycle progression," *PLoS One*, vol. 8, no. 7, article e69061, 2013.

[29] B. L. Mahaney, K. Meek, and S. P. Lees-Miller, "Repair of ionizing radiation-induced DNA double-strand breaks by non-homologous end-joining," *The Biochemical Journal*, vol. 417, no. 3, pp. 639–650, 2009.

[30] S. Burma, B. P. C. Chen, and D. J. Chen, "Role of non-homologous end joining (NHEJ) in maintaining genomic integrity," *DNA Repair*, vol. 5, no. 9-10, pp. 1042–1048, 2006.

[31] H. Ghezraoui, M. Piganeau, B. Renouf et al., "Chromosomal translocations in human cells are generated by canonical non-homologous end-joining," *Molecular Cell*, vol. 55, no. 6, pp. 829–842, 2014.

[32] C. C. Chen, W. R. Feng, P. X. Lim, E. M. Kass, and M. Jasin, "Homology-directed repair and the role of BRCA1, BRCA2, and related proteins in genome integrity and cancer," *Annual Review of Cancer Biology*, vol. 2, no. 1, pp. 313–336, 2018.

[33] M. C. Marsolier-Kergoat, M. M. Khan, J. Schott, X. Zhu, and B. Llorente, "Mechanistic view and genetic control of DNA recombination during meiosis," *Molecular Cell*, vol. 70, no. 1, pp. 9–20.e6, 2018.

[34] M. Takata, M. S. Sasaki, E. Sonoda et al., "Homologous recombination and non-homologous end-joining pathways of DNA double-strand break repair have overlapping roles in the maintenance of chromosomal integrity in vertebrate cells," *The EMBO Journal*, vol. 17, no. 18, pp. 5497–5508, 1998.

[35] T. G. W. Graham, J. C. Walter, and J. J. Loparo, "Two-stage synapsis of DNA ends during non-homologous end joining," *Molecular Cell*, vol. 61, no. 6, pp. 850–858, 2016.

[36] N. Hustedt and D. Durocher, "The control of DNA repair by the cell cycle," *Nature Cell Biology*, vol. 19, no. 1, pp. 1–9, 2017.

[37] E. Rothenberg, J. M. Grimme, M. Spies, and T. Ha, "Human Rad52-mediated homology search and annealing occurs by continuous interactions between overlapping nucleoprotein complexes," *Proceedings of the National Academy of Sciences of the United States of America*, vol. 105, no. 51, pp. 20274–20279, 2008.

[38] C. Mendez-Dorantes, R. Bhargava, and J. M. Stark, "Repeat-mediated deletions can be induced by a chromosomal break far from a repeat, but multiple pathways suppress such rearrangements," *Genes & Development*, vol. 32, no. 7-8, pp. 524–536, 2018.

[39] L. N. Truong, Y. Li, L. Z. Shi et al., "Microhomology-mediated end joining and homologous recombination share the initial end resection step to repair DNA double-strand breaks in mammalian cells," *Proceedings of the National Academy of Sciences of the United States of America*, vol. 110, no. 19, pp. 7720–7725, 2013.

[40] S. Ahrabi, S. Sarkar, S. X. Pfister et al., "A role for human homologous recombination factors in suppressing microhomology-mediated end joining," *Nucleic Acids Research*, vol. 44, no. 12, pp. 5743–5757, 2016.

[41] S. Saito, R. Maeda, and N. Adachi, "Dual loss of human POLQ and LIG4 abolishes random integration," *Nature Communications*, vol. 8, no. 1, article 16112, 2017.

[42] A. Sallmyr and A. E. Tomkinson, "Repair of DNA double-strand breaks by mammalian alternative end-joining pathways,"

The Journal of Biological Chemistry, vol. 293, no. 27, pp. 10536–10546, 2018.

[43] P. A. Mateos-Gomez, F. D. Gong, N. Nair, K. M. Miller, E. Lazzerini-Denchi, and A. Sfeir, "Mammalian polymerase θ promotes alternative NHEJ and suppresses recombination," *Nature*, vol. 518, no. 7538, pp. 254–257, 2015.

[44] L. Zhao, D. Mi, B. Hu, and Y. Sun, "A generalized target theory and its applications," *Scientific Reports*, vol. 5, no. 1, article 14568, 2015.

[45] L. Zhao, D. Mi, and Y. Sun, "A novel multitarget model of radiation-induced cell killing based on the Gaussian distribution," *Journal of Theoretical Biology*, vol. 420, pp. 135–143, 2017.

[46] L. Zhao, X. Chen, J. Tian, Y. Shang, D. Mi, and Y. Sun, "Generalized multi-hit model of radiation-induced cell survival with a closed-form solution: an alternative method for determining isoeffect doses in practical radiotherapy," *Radiation Research*, vol. 193, no. 4, pp. 359–371, 2020.

[47] E. I. Azzam, J. P. Jay-Gerin, and D. Pain, "Ionizing radiation-induced metabolic oxidative stress and prolonged cell injury," *Cancer Letters*, vol. 327, no. 1-2, pp. 48–60, 2012.

[48] L. Zhao, D. Wu, D. Mi, and Y. Sun, "Radiosensitivity and relative biological effectiveness based on a generalized target model," *Journal of Radiation Research*, vol. 58, no. 1, pp. 8–16, 2017.

[49] L. Zhao, X. He, X. Chen, Y. Shang, D. Mi, and Y. Sun, "Fitting the generalized target model to cell survival data of proton radiation reveals dose-dependent RBE and inspires an alternative method to estimate RBE in high-dose regions," *Radiation Research*, vol. 192, no. 5, pp. 507–516, 2019.

[50] D. T. Goodhead, "Energy deposition stochastics and track structure: what about the target?," *Radiation Protection Dosimetry*, vol. 122, no. 1-4, pp. 3–15, 2006.

[51] D. Schardt, T. Elsasser, and D. Schulz-Ertner, "Heavy-ion tumor therapy: physical and radiobiological benefits," *Reviews of Modern Physics*, vol. 82, no. 1, pp. 383–425, 2010.

[52] A. Asaithamby, B. Hu, and D. J. Chen, "Unrepaired clustered DNA lesions induce chromosome breakage in human cells," *Proceedings of the National Academy of Sciences of the United States of America*, vol. 108, no. 20, pp. 8293–8298, 2011.

[53] T. Friedrich, M. Durante, and M. Scholz, "Modeling cell survival after photon irradiation based on double-strand break clustering in megabase pair chromatin loops," *Radiation Research*, vol. 178, no. 5, pp. 385–394, 2012.

[54] D. M. Sridharan, A. Asaithamby, S. M. Bailey et al., "Understanding cancer development processes after HZE-particle exposure: roles of ROS, DNA damage repair and inflammation," *Radiation Research*, vol. 183, no. 1, pp. 1–26, 2015.

[55] M. Shrivastav, L. P. De Haro, and J. A. Nickoloff, "Regulation of DNA double-strand break repair pathway choice," *Cell Research*, vol. 18, no. 1, pp. 134–147, 2008.

[56] J. Reindl, S. Girst, D. W. M. Walsh et al., "Chromatin organization revealed by nanostructure of irradiation induced γH2AX, 53BP1 and Rad51 foci," *Scientific Reports*, vol. 7, no. 1, article 40616, 2017.

[57] R. Okayasu, M. Okada, A. Okabe, M. Noguchi, K. Takakura, and S. Takahashi, "Repair of DNA damage induced by accelerated heavy ions in mammalian cells proficient and deficient in the non-homologous end-joining pathway," *Radiation Research*, vol. 165, no. 1, pp. 59–67, 2006.

[58] D. M. Sridharan, M. K. Whalen, D. Almendrala et al., "Increased Artemis levels confer radioresistance to both high and low LET radiation exposures," *Radiation Oncology*, vol. 7, no. 1, p. 96, 2012.

[59] H. Wang, X. Wang, P. Zhang, and Y. Wang, "The Ku-dependent non-homologous end-joining but not other repair pathway is inhibited by high linear energy transfer ionizing radiation," *DNA Repair*, vol. 7, no. 5, pp. 725–733, 2008.

[60] F. Zafar, S. B. Seidler, A. Kronenberg, D. Schild, and C. Wiese, "Homologous recombination contributes to the repair of DNA double-Strand breaks induced by high-energy Iron ions," *Radiation Research*, vol. 173, no. 1, pp. 27–39, 2010.

[61] A. Kalousi and E. Soutoglou, "Nuclear compartmentalization of DNA repair," *Current Opinion in Genetics & Development*, vol. 37, pp. 148–157, 2016.

[62] F. Aymard, M. Aguirrebengoa, E. Guillou et al., "Genome-wide mapping of long-range contacts unveils clustering of DNA double-strand breaks at damaged active genes," *Nature Structural & Molecular Biology*, vol. 24, no. 4, pp. 353–361, 2017.

[63] T. Yasuhara, R. Kato, Y. Hagiwara et al., "Human Rad52 promotes XPG-mediated R-loop processing to initiate transcription-associated homologous recombination repair," *Cell*, vol. 175, no. 2, pp. 558–570.e11, 2018.

[64] C. Lemaitre, A. Grabarz, K. Tsouroula et al., "Nuclear position dictates DNA repair pathway choice," *Genes & Development*, vol. 28, no. 22, pp. 2450–2463, 2014.

[65] A. A. Goodarzi, A. T. Noon, D. Deckbar et al., "ATM signaling facilitates repair of DNA double-strand breaks associated with heterochromatin," *Molecular Cell*, vol. 31, no. 2, pp. 167–177, 2008.

[66] A. Beucher, J. Birraux, L. Tchouandong et al., "ATM and Artemis promote homologous recombination of radiation-induced DNA double-strand breaks in G2," *The EMBO Journal*, vol. 28, no. 21, pp. 3413–3427, 2009.

[67] N. T. Strande, C. A. Waters, and D. A. Ramsden, "Resolution of complex ends by nonhomologous end joining - better to be lucky than good?," *Genome Integrity*, vol. 3, no. 1, p. 10, 2012.

[68] L. F. Povirk, T. Zhou, R. Z. Zhou, M. J. Cowan, and S. M. Yannone, "Processing of 3′-phosphoglycolate-terminated DNA double strand breaks by Artemis nuclease," *The Journal of Biological Chemistry*, vol. 282, no. 6, pp. 3547–3558, 2006.

[69] S. Panier and S. J. Boulton, "Double-strand break repair: 53BP1 comes into focus," *Nature Reviews Molecular Cell Biology*, vol. 15, no. 1, pp. 7–18, 2014.

[70] E. Bártová, S. Legartová, M. Dundr, and J. Suchánková, "A role of the 53BP1 protein in genome protection: structural and functional characteristics of 53BP1-dependent DNA repair," *Aging*, vol. 11, no. 8, pp. 2488–2511, 2019.

[71] J. R. Chapman, A. J. Sossick, S. J. Boulton, and S. P. Jackson, "BRCA1-associated exclusion of 53BP1 from DNA damage sites underlies temporal control of DNA repair," *Journal of Cell Science*, vol. 125, no. 15, pp. 3529–3534, 2012.

[72] A. Asaithamby and D. J. Chen, "Cellular responses to DNA double-strand breaks after low-dose gamma-irradiation," *Nucleic Acids Research*, vol. 37, no. 12, pp. 3912–3923, 2009.

[73] R. Gupta, K. Somyajit, T. Narita et al., "DNA repair network analysis reveals Shieldin as a key regulator of NHEJ and PARP inhibitor sensitivity," *Cell*, vol. 173, no. 4, pp. 972–988.e23, 2018.

[74] H. Dev, T. W. W. Chiang, C. Lescale et al., "Shieldin complex promotes DNA end-joining and counters homologous recombination in BRCA1-null cells," *Nature Cell Biology*, vol. 20, no. 8, pp. 954–965, 2018.

[75] B. Schwarz, A. A. Friedl, S. Girst, G. Dollinger, and J. Reindl, "Nanoscopic analysis of 53BP1, BRCA1 and Rad51 reveals new insights in temporal progression of DNA-repair and pathway choice," *Mutation Research/Fundamental and Molecular Mechanisms of Mutagenesis*, vol. 816-818, article 111675, 2019.

[76] S. Jimeno, R. Prados-Carvajal, and P. Huertas, "The role of RNA and RNA-related proteins in the regulation of DNA double strand break repair pathway choice," *DNA Repair*, vol. 81, p. 102662, 2019.

[77] L. S. Symington and J. Gautier, "Double-strand break end resection and repair pathway choice," *Annual Review of Genetics*, vol. 45, no. 1, pp. 247–271, 2011.

[78] J. Vignard, G. Mirey, and B. Salles, "Ionizing-radiation induced DNA double-strand breaks: a direct and indirect lighting up," *Radiotherapy and Oncology*, vol. 108, no. 3, pp. 362–369, 2013.

[79] J. Saha, M. L. Wang, and F. A. Cucinotta, "Investigation of switch from ATM to ATR signaling at the sites of DNA damage induced by low and high LET radiation," *DNA Repair*, vol. 12, no. 12, pp. 1143–1151, 2013.

[80] S. Matsuoka, B. A. Ballif, A. Smogorzewska et al., "ATM and ATR substrate analysis reveals extensive protein networks responsive to DNA damage," *Science*, vol. 316, no. 5828, pp. 1160–1166, 2007.

[81] Y. Aylon, B. Liefshitz, and M. Kupiec, "The CDK regulates repair of double-strand breaks by homologous recombination during the cell cycle," *The EMBO Journal*, vol. 23, no. 24, pp. 4868–4875, 2004.

[82] P. Huertas, F. Cortes-Ledesma, A. A. Sartori, A. Aguilera, and S. P. Jackson, "CDK targets Sae2 to control DNA-end resection and homologous recombination," *Nature*, vol. 455, no. 7213, pp. 689–692, 2008.

[83] N. Tomimatsu, B. Mukherjee, M. C. Hardebeck et al., "Phosphorylation of EXO1 by CDKs 1 and 2 regulates DNA end resection and repair pathway choice," *Nature Communications*, vol. 5, no. 1, article 3561, 2014.

[84] A. Maity, W. G. McKenna, and R. J. Muschel, "The molecular basis for cell cycle delays following ionizing radiation: a review," *Radiotherapy and Oncology*, vol. 31, no. 1, pp. 1–13, 1994.

[85] A. K. Weimer, S. Biedermann, and A. Schnittger, "Specialization of CDK regulation under DNA damage," *Cell Cycle*, vol. 16, pp. 143-144, 2016.

Review Article

Extreme Environmental Stress-Induced Biological Responses in the Planarian

Zhonghong Cao [ID], Hongjin Liu, Bosheng Zhao, Qiuxiang Pang, and Xiufang Zhang

School of Life Sciences, Shandong University of Technology, 266 Xincun Western Road, Zibo 255049, China

Correspondence should be addressed to Zhonghong Cao; zhcao@sdut.edu.cn

Planarians are bilaterally symmetric metazoans of the phylum Platyhelminthes. They have well-defined anteroposterior and dorsoventral axes and have a highly structured true brain which consists of all neural cell types and neuropeptides found in a vertebrate. Planarian flatworms are famous for their strong regenerative ability; they can easily regenerate any part of the body including the complete neoformation of a functional brain within a few days and can survive a series of extreme environmental stress. Nowadays, they are an emerging model system in the field of developmental, regenerative, and stem cell biology and have offered lots of helpful information for these realms. In this review, we will summarize the response of planarians to some typical environmental stress and hope to shed light on basic mechanisms of how organisms interact with extreme environmental stress and survive it, such as altered gravity, temperature, and oxygen, and this information will help researchers improve the design in future studies.

1. Introduction

Planarians are bilaterally symmetric metazoans of the phylum Platyhelminthes. They have well-defined anteroposterior and dorsoventral axes and have an anterior cephalic region which contains the brain and a pair of eyespots, a central region which includes the pharynx and the mouth, and a posterior tail region. Despite their relatively simple morphology, planarians have a highly structured central nervous system (CNS) and feature a true brain which consists of all neural cell types and neuropeptides found in vertebrates [1–3]. They have roughly 30% adult stem cells [4, 5] and possess an extensive potential of regeneration. Planarians are one of the few animal species that can easily regenerate their head including the complete neoformation of a functional brain within seven days after decapitation [6–9]. Moreover, planarians share more genes with vertebrates compared with other popular model organisms such as *Drosophila melanogaster* or *Caenorhabditis elegans* [10]. All of these make planarians a reliable and popular model in the field of developmental, regenerative, and stem cell biology.

Exploring and living somewhere beyond the Earth are always two of the dreams of humans. It means that humans had successfully walked the first step to explore the space when Soviet cosmonaut Yuri Alekseyevich Gagarin had finished his journey of 89 minutes of orbiting the planet in his space capsule, on April 12, 1961. Then, more and more astronauts successfully finished their spaceflight, and their dwell time in space also is longer and longer. But the bad news is that astronauts on a long-term mission have problems upon returning to Earth, such as bone density loss; muscle atrophy; cardiovascular and hematic changes; metabolic, endocrine, and sleep disturbances; and rapid senescence [11, 12]. These actual and potential physical effects on the body mainly come from extreme environmental stress outside the Earth, such as altered gravity, temperature, and oxygen. Then, if we want to provide a habitat that can keep organisms in it living, it is necessary to understand what the biological responses of extreme environmental stress induce. We ethically cannot directly test the impact of environmental stress on humans. We need to use appropriate animal models to learn the adaptation of mammals about environmental stress.

Planarians not only can easily regenerate the lost parts but also can survive a series of altered environment. These make the planarian an ideal model organism, help us to understand how extreme environmental stress impacted the biological responses of organisms, and help us to find out the conserved molecules and mechanisms that support organisms to survive extreme environmental stress. There are reports that environmental stress can impact the structure of cells, intercellular communication, regeneration, embryonic development, and even immunological responses [13–18]. In this review, we will summarize the impact of some typical environmental stress for the planarian and hope to shed light on basic mechanisms of how organisms interact with extreme environmental stress and survive it, such as altered gravity, temperature, and oxygen. And this information will help researchers understand the basic mechanisms and improve the design in future studies.

2. Physiological Effects of Altered Gravity and Magnetic Field

Later missions showed that space travel could be tolerated by humans, but microgravity will trigger lots of physiological responses and even some pathological reactions. If we want to keep organisms healthy and happy in altered gravity, we need to use appropriate animal models to learn the effects of altered gravity. Planarian flatworms possess remarkable regeneration ability and share more genes with vertebrates than other popular model organisms such as *Drosophila melanogaster* or *Caenorhabditis elegans* [10], so it can minimize background interference, and becomes an ideal model to learn the effects of altered gravity. This part will summarize the most relevant data from exposure of planarian to altered gravity and magnetic levels obtained through ground-based facilities or board spaceflights, sounding rockets, satellites, or space stations. We will discuss the different effects of altered gravity on planarian, including the impacts on regeneration ability, embryonic development, phototaxis response, moving behavior, and transcriptomic information.

2.1. The Regeneration and Fission Ability. In the study of Gorgiladze et al., they cut 60 freshwater planarian *Girardia tigrina* 12 to 14 h before the spacecraft starts from the Baikonur launching site. In their experiment, they cut off the planarians before and after the pharynx and collected the different fragments into 20 ml polyethylene vials which are filled with freshwater, respectively. The air temperature of the RS ISS service module ranged from 19 to 21℃, as determined by telemetry. After 10 days of journey, they found that all the amputated body parts regenerated the lost parts, and the morphometric parameters of regenerated fragments were not different from those of the control fragments. And yet, the regenerated planarians were smaller than the original "maternal" planarians until the 18th to 20th day after dissection [19].

Whole-mount and amputated fragments of *Dugesia japonica* planarian had been collected into sealed 50 ml tubes with 50%/50% air/water, then had been sent to the ISS for one month. Results showed that only the whole worms are

divided spontaneously which had been sent into space; the fission rate changed from 1.3 to 1.75. They did not find a fission phenomenon in other samples. Yet, the authors cautioned that the worms in space unavoidably experienced somewhat higher temperatures at some time periods, so we should keep admonishing for this result. After returned two months later, the number of worms that had gone to space was slightly less than the worms that were maintained on Earth [20]. For the amputated worms, the size is similar between the two groups after the space journey. And after two months of culture, the worms exposed to space grew more slowly than the Earth-only controls. The most striking phenomenon is that they found that one of the 15 pharynx fragments from space had regenerated two heads (see Figure 1), and after amputating the two heads, the headless middle fragment regenerated into a double-headed phenotype [20]. But we need to note that pharynx fragments left on Earth did not survive the duration of the mission in this work. Levin et al. thought that people should be cautious about this result; maybe it is not really induced by microgravity [21].

Teresa et al. performed their experiment in the European Space Research and Technology Centre, Noordwijk, The Netherlands. In their work, they researched the impact of simulated microgravity on the regeneration of *Schmidtea mediterranea*. They get simulated microgravity by means of the random positioning machine (RPM) set at a speed of 60°/s and 10°/s, and their results demonstrate that RPM 60°/s led to the death of trunk planarians, whereas planarians loaded into the 10°/s RPM machine appeared normally regenerated (have the normal eyes and the normal CNS and have similar mitotic activity). Moreover, they found that all planarians live and correctly regenerated the corresponding lost parts on day 5, which indicates that planarians do not die soon when sensing the effects of the 60°/s RPM but after having regenerated the main structures. They hypothesized that there are rheoreceptors in the head of planarians, and when they regenerated the whole head, they can sense the water currents which are produced in the 60°/s RPM and induce death [16]. It is necessary to analyze the effect of 60°/s RPM rotation for intact animals and definitely corroborate this hypothesis. These results demonstrate that it is not the simulated microgravity but the specific setting of rotation of the 60°/s RPM that induced the death of planarians.

They also examined the impact of hypergravity on regeneration of *Schmidtea mediterranea* and simulated hypergravity 3g, 4g, and 8g by a large diameter centrifuge (LDC). Under 3g and 4g hypergravity, planarians can regenerate missing tissues, but the proliferation rate was decreased. Under 8g hypergravity, only the larger trunk planarian fragments can regenerate the lost part, and the small planarian fragments cannot successfully regenerate the corresponding part. Although the molecular reason for this effect has not been found, the decreased proliferative rates suggest that gravity could affect the actin cytoskeleton and the assembly of microtubules, just as it happens in other organisms [22–24]. Meanwhile, they found that changed gravity had affected the fission rate of planarians, and the number of smaller
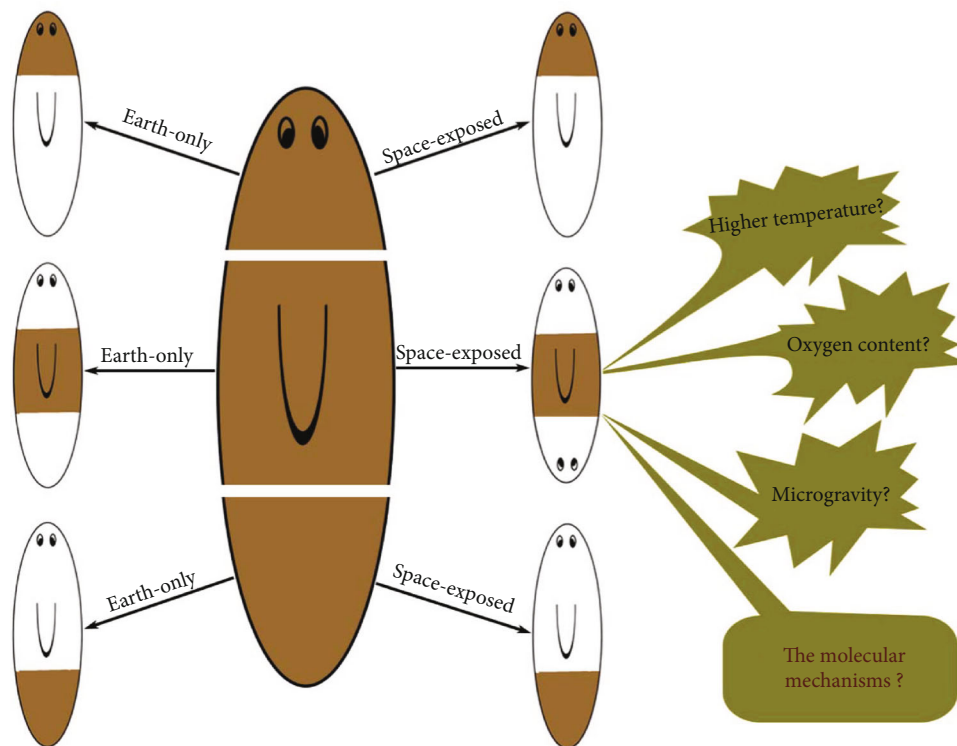
FIGURE 1: The effects of changed gravity on regenerated tissues in planarian. The left panel indicates that Earth-only planarian fragments regenerated the lost part. The right panel indicates that space-exposed head and tail fragments regenerated the lost parts, but the truncated middle planarian regenerated two heads. The immediate cause and molecular mechanisms are not well known for this phenomenon. Brown marks the original tissue, and white marks the regenerated parts.

fragments was significantly higher in LDC 4g planarians compared with the rest of the groups.

The study about 3–6 d old cocoons of *Schmidtea polychroa* showed that all cocoons in RPM 60°/s or LDC 3g conditions were taken out on the corresponding day. Immunohistochemical results of α-tubulin showed that all juveniles had a proper morphology and normal organization of the CNS and pharynx. And all animals have a similar mitotic activity. These results demonstrate that planarians can develop properly in altered gravity conditions, at least in the specific settings used in this experiment. And it called for further analysis for a more complete understanding if juveniles can survive longer times in the RPM 60°/s conditions [16].

In the research of Lu et al., they changed the gravity conditions through a large gradient high magnetic field (LG-HMF) and observed regeneration of planarians at three gravity levels (ug, 1g, and 2g). Their results demonstrate that all of the planarians normally regenerated their heads and the regeneration rate of the four groups is similar. These results indicate that planarians can correctly regenerate their heads at different gravity environments [25].

Sousa et al. in the European Space Research and Technology Centre (Noordwijk, The Netherlands) through the random positioning machine (RPM) simulated microgravity (the machine was set to a real random mode and random direction with a maximum speed of 10°/s), and the large diameter centrifuge (LDC) generated hypergravity (8g). They put intact *Schmidtea mediterranea* planarians in the RPM

and LDC at day 0; after 1 day, the planarians were amputated at pre- and postpharynx levels, and they collected trunk fragments and reloaded in the same devices. They found that all the planarian trunks exposed to s-ug or 8g correctly regenerated the lost parts [26]. There are results showing that microgravity can induce developmental retardation and cell apoptosis of mouse embryos [27], and hypergravity conditions do not affect the normal development and actin filament structures of mouse embryos [28]. But microgravity can prevent terminal differentiation of embryonic stem cells [29, 30].

There are researchers that treat decapitated planarians with weak nonuniform magnetic fields (RMFs) and found RMFs eliminated the formation of edema and blastema, which through upregulating the expression of EGR4, Netrin 2, NSE, and NPY accelerates nerve cell proliferation and function recovery [31–33]. The weak magnetic field stimulates the fission frequency of the Planarian *Dugesia* (*Girardia*) *tigrina* [32]. Alanna et al. recently found that weak magnetic fields change the accumulation of reactive oxygen species (ROS), ERK cascade, and the expression of heat shock protein 70 (Hsp70) to regulate the proliferation and differentiation of stem cells [34, 35]. The planarian will die suddenly when the geomagnetic activity is over K6 [36].

2.2. Behavior. In the experiment of Gorgiladze, the regenerated planarians have normal food behavior and locomotor activity; they can freely glide or alternate contraction and

straightening of the body on the bottom of the flask or on the water surface [19]. Morokuma et al. had sent 5 tubes with different numbers of whole worms to the ISS and found that only the sample which contains 10 whole worms that had been launched into space showed immediate unusual behavior. They curled up ventrally and are somewhat paralyzed and immobile, when they had been introduced into fresh Poland spring water. They all regained normal behavior after 2 hours. And water shock was not seen in the other samples. These results indicate that microgravity can yield different effects according to different microenvironments of culture systems. After 20 months of return to Earth, the two groups of worms showed a comparable motion rate under the stimulation of red and blue light, and the control worms spent more time in the dark compared to the space-traveled worms [20].

Lu et al. found that the planarians which regenerated heads in different gravity conditions showed similar photonegative response. During the photonegative test, most of the regenerated planarians could reach the target quadrant in 90 s, and the average times spent in the target quadrants did not significantly differ. These results showed that LG-HMF-generated microgravity and hypergravity did not affect the reestablishment of photonegative ability. But the photonegative response time of the planarians which regenerated under LG-HMF conditions was slightly suppressed, and the authors thought it was mainly due to the difference of the locomotor system instead of the reconstructed head [25]. They took the traditional planarian locomotor velocity (pLMV) assay and automated center-of-mass (COM) tracking approach and image analysis to analyze the locomotor behaviors, and the results showed that Group ug/12T has a significantly decreased locomotor function compared to the other three groups during the 8 min test. And the righting time of the simulated microgravity group also showed significantly increased compared to the other groups, but the planarians could eventually sense the reverse direction and complete the correction of the body, indicating that the function of the nervous system was normal. Histologic section staining and immunohistochemistry results showed that the circular muscle of planarians regenerated in simulated microgravity was weakened compared with the other planarian groups, and the fluorescence thickness of the epithelial cilia are significantly decreased. The authors thought that differences in locomotion velocity and righting behavior come from frail muscle [25]. There is research showing that planarian that has been exposed to 16G intensity static magnetic fields for one day significantly improved the velocity of movement [37].

2.3. Transcriptomic. In the experiment of Sousa et al., they put intact *Schmidtea mediterranea* planarians in the RPM and LDC at day 0. After 1 day, the planarians were amputated at pre- and postpharynx levels, and they collected trunk fragments and reloaded in the same devices. Five and 12 days after amputation, they collected all kinds of samples, respectively, and analyzed the transcriptome of each sample. The principal component analysis (PCA) showed that the same time samples were clustered together and the same gravity condition samples were also clustered together. They found

that after 12 dR (13 days of s-ug or 8g exposure), several genes were deferentially expressed in exposed animals compared to their corresponding controls. The number of differentially expressed genes was much higher in animals regenerating in s-ug conditions than in animals regenerating at 8 g, and there is a much higher number of deregulated genes (720 versus 77) [26].

Regarding the specific deregulated genes at s-ug, they found the downregulation of cytoskeleton and matrix genes—such as *collagen-a-1*, *piwi* genes, and the upregulation of genes which are involved in ribosome biogenesis. What makes them confused is that although supporting higher mechanical forces require strengthening the cell cytoskeleton to maintain the shape and function, they did not find significant alteration of cytoskeleton or matrix proteins in planarians regenerating at 8g conditions. Their results indicate that altered gravity conditions can severely affect genetic transcription, and these alterations potentiate molecular disorders which could promote the development of multiple diseases such as cancer [26].

2.4. The Others. In the study of Morokuma et al., the microbiome profiles of those culture-based are significantly different. In space-exposed worms, the number of colonies of *Variovorax*, *Herminiimonas*, and the unknown *Comamonadaceae* decreased and the number of *Chryseobacterium* colonies significantly increased. Their results indicate that space travel can change bacterial community composition of *D. japonica*, and this difference can exist for a few years. And they analyzed the samples of the water of the space-exposed worms and the Earth-only with liquid chromatography-mass spectrometry (LC-MS); the results revealed that both samples contained a large number of small organic molecules/metabolites. The total ion chromatograms of the two samples in the positive ion mode were quite different, and many of them correspond to long-chain fatty acids or monohydroxylated/dihydroxylated long-chain fatty acids [20].

3. Physiological Effects of Temperature and Oxygen

Temperature and oxygen are the other important factors of the environment, which can affect, regulate, and control lots of biological and pathological processes of organisms [6, 38–40]. For organisms, sensing the temperature and oxygen of the environment is very important for them to adjust behavioral strategy and escape injury. There are researchers reporting that nutrition and temperature can impact the oxygen consumption and metabolic status and impact the process of development, regeneration, injury, and escape from noxious stimulation, etc. [41–44]. And environmental stress can, through a conserved pathway, impact the biological process from planarian to human. In this session, we will discuss the impact of temperature and oxygen on planarian.

3.1. The Regeneration and Fission Ability. People found that the ROS production takes part in the regeneration in *zebrafish* and *Xenopus* [45, 46]. But the limited regeneration ability of these organisms restricted researchers that deeply explore

the function and impact of ROS in regeneration. Planarians are famous for their amazing regeneration ability; they can easily regenerate any parts of the body and include a functional head, and the new head can even have the memory of the former brain. These characters make these worms to be an ideal model.

Every live organisms need energy to maintain the function of cells; hence, every living cell needs to consume oxygen to keep the balance of metabolism. There are researches reporting that small planarians have a higher oxygen consumption rate, and injured planarians have a lower oxygen consumption rate, but injured worms have increased glycolysis during the process of regeneration [47]. Pirotte et al. researched the impact of ROS on planarian regeneration with *Schmidtea mediterranea*. They amputate the planarian into three fragments at pre- and postpharynx levels and research the impact of ROS to different part regeneration. They found that ROS burst just in a few minutes after amputation, and the production of ROS is independent of the orientation of the wound site, but it induced signals to regulate the regeneration process which appears at least after 24 h from amputation. Inhibition of the production of ROS leads to failure to regenerate the lost parts of all three fragments, and they found that reduced ROS restricted the regeneration of cephalic ganglia and the ectopic neuronal cells. And they found that disturbing the production of ROS did not affect the stem cell proliferation but restricted the neoblast differentiation into the required cell types of regeneration [48]. In addition, there are works that suggest that increased ROS do not accelerate the aging of mice and some long life-span mammals have a higher level of ROS and oxidative damage [49, 50]. Literatures showed that human protein has Met and Cyst residues, and these residues through trapping oxygen atoms prevent ROS-induced neuronal cell death [51, 52]. Tsushima et al. found that the protein of DJ-1 is conversed from human to planarian, especially the important residues for function execution; they knock down the DJ-1 gene in vivo through RNAi, and the results showed that planarian DJ-1 has antioxidant and neuroprotective functions; it indicates that planarian can be a reliable model for study oxidative stress-introduced disorders and offer the chance to explore the mechanisms [53].

There is literature reporting intact planarian preference to move to the cooler region, and even the amputated head fragment moved to the cold field [54]. It means that the head region can sense and responds to environment temperature in planarian and showed that DjTRPMa-expressing neurons sense the temperature and transduce signals to serotonergic neurons of the brain; then, serotonergic neurons exhibit thermotactic behavior. Ding et al. reported that *Dugesia japonica* planarian showed different regeneration speeds at different temperatures (15°C, 20°C, and 25°C); lower temperature decreased the regeneration speed [55]. The *Schmidtea mediterranea* trunk fragment can completely regenerate the head and tail at five days after amputation when cultured at 26°C and 28°C and shortened to two days compared with the planarian cultured at 19°C. And the eyes appeared from three days postamputation when cultured at 26°C and 28°C, but the control worms regenerated eyes at five days [56].

According to literatures showing that the fission of planarian flatworms correlates with the length and area size of worms [57], the fission frequency increased with the body size; when the body length is shorter than 4-5 mm, they cannot fission again [58]. Subsequent researchers reported that environmental stress can impact the process, such as increased temperature would decrease the fission length and increase the frequency of fission [59]. Hammoudi et al. showed that the spontaneous fission frequency multiplied significantly at 26°C and 28°C than at 19°C [56]. In addition, there have been reports that before the fission event, there was an increased proliferation of neoblast just like after amputation [60], and activating the mitotic functions through RNAi of DjP2X-A can induce higher fission frequency [61].

3.2. Behavior. Planarians can normally live and behave from 15°C to 25°C, the locomotor activity has been strongly suppressed below 10°C, the worms will lose their motility between 5 and 10°C, and high temperature almost did not affect the mobility of planarians, but they will die in 1 hour when the temperature is above 30°C [54, 56]. Hammoudi et al. reported that slowly increasing the temperature of water can elongate the live times of planarians, but they cannot survive more than 20 days when the temperature is over 30°C [56]. From 7°C to 12°C, the body of planarian has some contraction, movement is slow, and the velocity is not stable; when the temperature is between 12°C and 21°C, the velocity gradually increased to its maxim value and the body stretched along the anterior-posterior axis which probably extended 25 per cent compared with that at 10°C. Above 21°C, the locomotor rate becomes not constant again and the speed is no more than that at 21°C. When the temperature increased to 30°C, the worms become motionless [62].

Ding et al. showed that suitable living temperatures can accelerate the toxic effect of Fe^{3+}. They observed the toxic effect of Fe^{3+} for planarian at three different temperatures 15°C, 20°C, and 25°C and found that the death speed increased at 20°C and showed the lowest death speed at 15°C [55]. Normally, dorsal epidermis of planarians has excretory pores, hair cells, and rhabdites and can secrete droplets and generate mucus. The structure of epidermis has been damaged when the temperature increased over 33°C for *Girardia tigrina* and 37°C for *Girardia* sp. There were fewer rhabdites and fewer and disorganized secretory droplets [63], which form the mucus to help planarians to respond and escape stress [64, 65].

Higher temperatures did not impact the feeding behavior of planarians from 19°C to 28°C [56]; the ability to eliminate bacteria of planarians at different temperatures changed. After infection with 10^9 CFU of *S. aureus* for three hours, the worms need six days to eliminate the bacteria at 19°C and just need three days when they had been cultured at 28°C. It means that planarians have exacerbated antibacterial capabilities with the increase of temperature from 19°C to 28°C [56]. The eye action potential (OP) that evoked by a light flash in the planarian changed with the temperature. When the temperature increased from 15°C to 23°C, the amplitude increased and the latency and peak delay decreased; as the

TABLE 1: Some major advances of the effect of extreme environmental stress on planarians.

Stress conditions	The main impact on planarian	References
The effects of gravity and magnetic field		
Microgravity (space)	All the amputated body parts regenerated the lost fragments.	Gorgiladze [19]
Microgravity (space)	The whole worms had spontaneous fission. The pharynx fragment had regenerated two heads and grew more slowly. Some whole worms showed immediate unusual behavior. The microbiome profiles had changed.	Morokuma et al. [20]
Microgravity (RPM 60°/s)	The trunk planarians had died.	Adell et al. [16]
Microgravity (RPM 10°/s)	The trunk planarians appeared normally regenerated.	
Hypergravity (LDC 3g, 4g)	The amputated body parts regenerated the missing tissues; the proliferation rate was decreased.	
Hypergravity (LDC 8g)	Only the larger trunk planarian fragments can regenerate the lost part.	
Microgravity (LG-HMF ug)	The amputated body parts normally regenerated their heads. The worms have a significantly decreased locomotor function.	Lu et al. [25]
Hypergravity (LG-HMF 2g)	The amputated body parts normally regenerated their heads.	
Microgravity (RPM 10°/s)	The body parts properly regenerated head. Cytoskeleton and matrix genes had been downregulated.	Sousa et al. [26]
Hypergravity (LDC 8g)	The body parts properly regenerated head. Microtubules, cell communication, and cell cycle genes had been downregulated.	
Weak magnetic field	The nerve cell proliferation has been accelerated. The regeneration speed increased. The frequency of spontaneous increased. The velocity of movement improved.	Novikov et al. [32], Gang et al. [33]. Gang and Persinger [37]
Intense magnetic field	The planarian will suddenly die when it is over 6K.	Murugan et al. [36]
The effects of oxygen and temperature		
Inhibit ROS	Planarian fragments fail to regenerate the lost parts. The regeneration of cephalic ganglia and ectopic neuronal cells had been restricted. Neoblast differentiation has been restricted.	Pirotte et al. [48]
Increase ROS	Induce damage of DNA, lipids, and proteins.	Finkel [68]
Lower temperature (15°C)	The regeneration speed decreased. The spontaneous fission frequency increased. The movement is slow, and the velocity is not stable. The toxic effect of Fe^{3+} has been decreased.	Ding et al. [55], Hammoudi et al. [56], Herath and Lobo [59], Cole [62]
Higher temperature (25-33°C)	The regeneration speed increased. The movement is slow, and the velocity is not stable. The secretory function has been restricted. The capability to eliminate balance increased.	Ding et al. [55], Hammoudi et al. [56], Cole [62], Oliveira et al. [63]

temperature is greater than 30°C, the amplitude decreased and latency and peak delay continued to decrease until 42°C. These changes can be reversible when the temperature is lower than 30°C [66].

Ectothermic organisms respond to altered temperatures through adjusting their biochemical process but not through changing their body temperature [67]. One of the important strategies is through changing the mitochondrial oxidative phosphorylation (OXPHOS) pathways to survive, which is critical to provide energy for the eukaryotic cells. Hence, OXPHOS is important in balancing the process of metabo-

lism and the generation of reactive oxygen species (ROS). And moderate ROS is necessary for lots of important biological processes, but overproduced ROS can damage DNA, lipids, and proteins [68]. It means temperature changes OXPHOS to modify the production of ROS and then affect the signals of cells [69, 70]. Animals can respond to temperature through two steps, one is the phosphorylation system and the other is the complex I of the NADH pathway [71–75]. After 4 weeks of acclimation under low temperature, planarians can effectively increase the capacity of these related proteins [75].
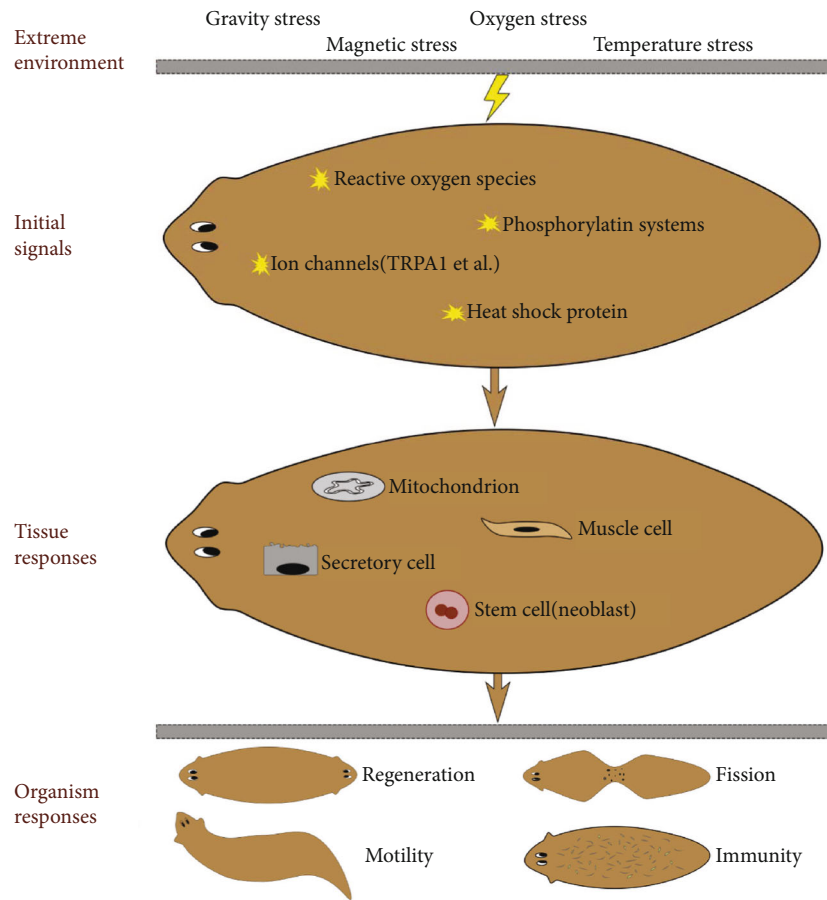
FIGURE 2: The effects of extreme environmental stress on planarians. Different kinds of extreme environmental factors irritate planarian; organisms sense it and produce the initial signal molecules (yellow star), then recruit more respond factors to join the war and change the metabolism status of different cells and organelles; at last, the organism showed changed regeneration ability, fission frequency, mobility, and immunity.

3.3. The Molecular Response. There is literature showing that the conserved ion channel TRPA1 exhibit important function to feel noxious heat and start the protective behavior [76], but Arenas et al. showed that TRAP1 cannot be directly activated by heat; they found that heat induces the production of ROS and then through RTPA1 regulates the escape process in *Schmidtea mediterranea* planarian [77]. Disturbing the regeneration of ROS or the expression of RTPA1 can lead to failure of avoiding noxious heat.

When the temperature increased to 25°C, the expression of DjHsp90 protein upregulated approximately 2-fold compared with that cultured at 18°C. When the temperature increased to 32°C, the DjHsp90 protein level decreased lower than normally (18°C) cultured planarians, but the level of *Djhsp90* mRNA is still higher at 32°C. It means that high temperature firstly restricted the process of posttranscription events [78]. Immunohistochemistry showed that the *Djhsp90*-positive cells distributed in parenchymal tissue from head to tail, just under the epidermis cells, indicating that they are suitable to sense and respond to the external environmental signals [78]. When temperature changed (increase or decrease), head-expressed *DjSpsb* mRNA will increase in *Dugesia japonica* [79]. The levels of putrescine and spermidine are also temporarily increased after heat shock or cold shock, which is essential for planarian to recover from damage [80].

4. The Controversial Issues and Future Directions

People created different experiments to explore the impact of extreme environmental stress on planarians and had obtained lots of valuable information (Table 1). But there are still some controversial issues that need to be noted and improved in future research.

4.1. Planarian Species and Planarian Density. In different researches, people used different planarian species, such as *Schmidtea mediterranea*, *Dugesia tigrina*, and *Dugesia japonica*. Jason et al. had reported that even though different species share similar anatomy and mode of reproduction, they find that each species had acquired its own distinct strategy for optimizing its reproductive success [81]. The other question is the density of planarian. In present reports, the researchers placed different numbers of planarian in a single tube and resulted in different densities of worms in each

experiment. And the density of worms can impact the fission and the expression of some molecules. This makes it complicated to directly compare the results. We need to take into account the impact of planarian species and planarian density if we want to get more reliable and to directly compare data.

4.2. The Methods and Strategies to Change Environmental Stress. Just as mentioned above, researchers use different strategies and methods to change the environment station. And these differences can lead to inconsistent results, such as the fact that the same microgravity conditions in RPM 60°/s can lead to the death of regenerated planarians but not in 10°/s; slowly increasing the temperature to 30°C makes planarian live longer times. Further analysis showed that the rheoreceptors of the intact head induced the death of planarians in RPM 60°/s but not the microgravity. When analyzing the effects of given environmental stress, we need to be cautious to the results and carefully consider the method and strategy to change the stress condition.

4.3. The Crosstalk of Different Environmental Stress. Existing research showed that microgravity did not induce failure of regeneration, but the regeneration becomes slow. And microgravity increased the spontaneous fission frequency and changed the microbiome profiles of planarian. They curled up and are immobile in spring water when they returned to Earth from space, then slowly recover to normal mobility after two hours. Researchers did not find upregulated genes of cytoskeleton or matrix related to hypergravity which has been supposed to maintain shape and strength of the cytoskeleton of cells. Temperature and oxygen are important environmental factors; oxygen is necessary for almost all animals. Research showed that temperature can impact the oxygen consumption and metabolic status, impact regeneration capacity and fission frequency, and even regulated the capacity to eliminate bacteria. Just as Figure 2 shows that different environmental factors irritate organisms, organisms sense it and produce the initial signal molecules, then recruit more response factors to join the war and change the metabolism status, protein expression levels, cell structures, and so on; at last, the organism exhibits the environmental stress effects, such as changed regeneration ability, fission frequency, mobility, and immunity. Different environmental factors can generate cross effects; there are researches showing that late loading and early retrieval can increase the success of life science experiments in space [82, 83]. Long time cold storage will increase the death frequency and induce fail of regeneration [84].

5. Conclusion

The relatively simple planarian offered a unique opportunity to study the physiological and behavioral process and to investigate the mechanisms underlying different environmental stress in whole animals. It is more helpful to understand the overall response of the organisms to facing different environmental stress than specific tissues. These could provide us with important insights about basic molecular processes

occurring in a wide range of vertebrates, including humans. But present researches analyzed the morphological and physiological changes more than molecular mechanisms, and some researches even get conflicting results for the same stress condition. These results call for further experiments to carefully consider the cross effects of different environmental stress and deeply detect the molecular mechanisms. It is still an exciting era for researchers.

Conflicts of Interest

The authors declare that they have no conflicts of interest.

Acknowledgments

References

[1] J. J. Collins, X. Hou, E. V. Romanova et al., "Genome-wide analyses reveal a role for peptide hormones in planarian germ-line development," *PLoS Biology*, vol. 8, no. 10, article e1000509, 2010.

[2] K. Mineta, M. Nakazawa, F. Cebria, K. Ikeo, K. Agata, and T. Gojobori, "Origin and evolutionary process of the CNS elucidated by comparative genomics analysis of planarian ESTs," *Proceedings of the National Academy of Sciences of the United States of America*, vol. 100, no. 13, pp. 7666–7671, 2003.

[3] S. Fraguas, S. Barberán, B. Ibarra, L. Stöger, and F. Cebri, "Regeneration of neuronal cell types in Schmidtea mediterranea: an immunohistochemical and expression study," *The International Journal of Developmental Biology*, vol. 56, no. 1-2-3, pp. 143–153, 2012.

[4] H. B. Sarnat and M. G. Netsky, "The brain of the planarian as the ancestor of the human brain," *The Canadian Journal of Neurological Sciences*, vol. 12, no. 4, pp. 296–302, 1985.

[5] K. Agata, Y. Soejima, K. Kato, C. Kobayashi, Y. Umesono, and K. Watanabe, "Structure of the planarian central nervous system (CNS) revealed by neuronal cell markers," *Zoological Science*, vol. 15, no. 3, pp. 433–440, 1998.

[6] P. W. Reddien and A. S. Alvarado, "Fundamentals of planarian regeneration," *Annual Review of Cell and Developmental Biology*, vol. 20, no. 1, pp. 725–757, 2004.

[7] D. J. Forsthoefel and P. A. Newmark, "Emerging patterns in planarian regeneration," *Current Opinion in Genetics & Development*, vol. 19, no. 4, pp. 412–420, 2009.

[8] E. Salo, J. F. Abril, T. Adell et al., "Planarian regeneration: achievements and future directions after 20 years of research," *The International Journal of Developmental Biology*, vol. 53, no. 8-9-10, pp. 1317–1327, 2009.

[9] D. D. R. Brown and B. J. Pearson, "A brain unfixed: unlimited neurogenesis and regeneration of the adult planarian nervous system," *Frontiers in Neuroscience*, vol. 11, p. 289, 2017.

[10] A. Sanchez Alvarado, "Planarian regeneration: its end is its beginning," *Cell*, vol. 124, no. 2, pp. 241–245, 2006.

[11] J. C. Buckey, *Space Physiology. Oxford*, Oxford University Press, New York, 2006.

[12] G. C. Demontis, M. M. Germani, E. G. Caiani, I. Barravecchia, C. Passino, and D. Angeloni, "Human pathophysiological adaptations to the space environment," *Frontiers in Physiology*, vol. 8, p. 547, 2017.

[13] D. Sarkar, T. Nagaya, K. Koga, and H. Seo, "Culture in vector-averaged gravity environment in a clinostat results in detachment of osteoblastic ROS 17/2.8 cells," *Environ Med*, vol. 43, no. 1, pp. 22–24, 1999.

[14] B. M. Uva, M. A. Masini, M. Sturla et al., "Clinorotation-induced weightlessness influences the cytoskeleton of glial cells in culture," *Brain Research*, vol. 934, no. 2, pp. 132–139, 2002.

[15] A. Sundaresan, D. Risin, and N. R. Pellis, "Loss of signal transduction and inhibition of lymphocyte locomotion in a ground-based model of microgravity," *In Vitro Cellular & Developmental Biology. Animal*, vol. 38, no. 2, pp. 118–122, 2002.

[16] T. Adell, E. Saló, J. J. W. A. van Loon, and G. Auletta, "Planarians sense simulated microgravity and hypergravity," *BioMed Research International*, vol. 2014, 10 pages, 2014.

[17] X. Lei, Z. Deng, H. Zhang et al., "Rotary suspension culture enhances mesendoderm differentiation of embryonic stem cells through modulation of Wnt/β-catenin pathway," *Stem Cell Reviews and Reports*, vol. 10, no. 4, pp. 526–538, 2014.

[18] X. Lei, Y. Cao, B. Ma et al., "Development of mouse preimplantation embryos in space," *National Science Review*, 2020.

[19] G. I. Gorgiladze, "Regenerative capacity of the planarian Girardia tigrina and the snail Helix lucorum exposed to microgravity during an orbital flight on board the International Space Station," *Doklady Biological Sciences*, vol. 421, no. 1, pp. 244–247, 2008.

[20] J. Morokuma, F. Durant, K. B. Williams et al., "Planarian regeneration in space: persistent anatomical, behavioral, and bacteriological changes induced by space travel," *Regeneration (Oxf)*, vol. 4, no. 2, pp. 85–102, 2017.

[21] M. Levin, J. Morokuma, and J. Finkelstein, "Space travel has effects on planarian regeneration that cannot be explained by a null hypothesis," *Regeneration (Oxf)*, vol. 4, no. 4, pp. 156–158, 2017.

[22] C. Papaseit, N. Pochon, and J. Tabony, "Microtubule self-organization is gravity-dependent," *Proceedings of the National Academy of Sciences of the United States of America*, vol. 97, no. 15, pp. 8364–8368, 2000.

[23] S. J. Crawford-Young, "Effects of microgravity on cell cytoskeleton and embryogenesis," *The International Journal of Developmental Biology*, vol. 50, no. 2-3, pp. 183–191, 2006.

[24] D. Vorselen, W. H. Roos, F. C. MacKintosh, G. J. L. Wuite, and J. J. W. A. Loon, "The role of the cytoskeleton in sensing changes in gravity by nonspecialized cells," *The FASEB Journal*, vol. 28, no. 2, pp. 536–547, 2014.

[25] H.-M. Lu, X.-L. Lu, J.-H. Zhai et al., "Effects of large gradient high magnetic field (LG-HMF) on the long-term culture of aquatic organisms: planarians example," *Bioelectromagnetics*, vol. 39, no. 6, pp. 428–440, 2018.

[26] N. de Sousa, G. Rodriguez-Esteban, I. Colagè et al., "Transcriptomic analysis of planarians under simulated microgravity or 8 g demonstrates that alteration of gravity induces genomic and cellular alterations that could facilitate tumoral transformation," *International Journal of Molecular Sciences*, vol. 20, no. 3, p. 720, 2019.

[27] Y. CAO, X. FAN, Z. SHEN, B. MA, and E. DUAN, "Nitric oxide affects preimplantation embryonic development in a rotating wall vessel bioreactor simulating microgravity," *Cell Biology International*, vol. 31, no. 1, pp. 24–29, 2007.

[28] L.-N. Ning, X.-H. Lei, Y.-J. Cao et al., "Effect of short-term hypergravity treatment on mouse 2-cell embryo development," *Microgravity Science Technology*, vol. 27, no. 6, pp. 465–471, 2015.

[29] X. Lei, Y. Cao, Y. Zhang et al., "Effect of microgravity on proliferation and differentiation of embryonic stem cells in an automated culturing system during the TZ-1 space mission," *Cell Proliferation*, vol. 51, no. 5, article e12466, 2018.

[30] X. Lei, Y. Cao, Y. Zhang, and E. Duan, "Advances of mammalian reproduction and embryonic development under microgravity," in *Life Science in Space: Experiments on Board the SJ-10 Recoverable Satellite*Research for Development, Spring, Singapore.

[31] Q. Chen, G. Lin, N. Wu et al., "Early exposure of rotating magnetic fields promotes central nervous regeneration in planarian Girardia sinensis," *Bioelectromagnetics*, vol. 37, no. 4, pp. 244–255, 2016.

[32] V. V. Novikov, I. M. Sheiman, and E. E. Fesenko, "Effect of weak static and low-frequency alternating magnetic fields on the fission and regeneration of the planarian Dugesia (Girardia) tigrina," *Bioelectromagnetics*, vol. 29, no. 5, pp. 387–393, 2008.

[33] N. Gang, G. H. Parker, R. M. Lafrenie, and M. A. Persinger, "Intermittent exposures to nanoTesla range, 7 Hz, amplitude-modulated magnetic fields increase regeneration rates in planarian," *International Journal of Radiation Biology*, vol. 89, no. 5, pp. 384–389, 2013.

[34] A. V. Van Huizen, J. M. Morton, L. J. Kinsey et al., "Weak magnetic fields alter stem cell-mediated growth," *Science Advances*, vol. 5, no. 1, p. eaau7201, 2019.

[35] R. Goodman, A. Lin-Ye, M. S. Geddis et al., "Extremely low frequency electromagnetic fields activate the ERK cascade, increase hsp70 protein levels and promote regeneration in Planaria," *International Journal of Radiation Biology*, vol. 85, no. 10, pp. 851–859, 2009.

[36] N. J. Murugan, L. M. Karbowski, W. F. Mekers, and M. A. Persinger, "Group planarian sudden mortality: is the threshold around global geomagnetic activity≥K6?," *Communicative & Integrative Biology*, vol. 8, no. 6, article e1095413, 2015.

[37] N. Gang and M. A. Persinger, "Planarian activity differences when maintained in water pre-treated with magnetic fields: a nonlinear effect," *Electromagnetic Biology and Medicine*, vol. 30, no. 4, pp. 198–204, 2011.

[38] H. B. Lillywhite, "Temperature selection by the bullfrog, Rana catesbeiana," *Comparative Biochemistry and Physiology. A, Comparative Physiology*, vol. 40, no. 1, pp. 213–227, 1971.

[39] S. Bennett, C. M. Duarte, N. Marbà, and T. Wernberg, "Integrating within-species variation in thermal physiology into climate change ecology," *Philosophical Transactions of the Royal Society of London. Series B, Biological Sciences*, vol. 374, no. 1778, p. 20180550, 2019.

[40] B. H. Brattstrom, "Thermal acclimation in anuran amphibians as a function of latitude and altitude," *Comparative Biochemistry and Physiology*, vol. 24, no. 1, pp. 93–111, 1968.

[41] M. Agathocleous and W. A. Harris, "Metabolism in physiological cell proliferation and differentiation," *Trends in Cell Biology*, vol. 23, no. 10, pp. 484–492, 2013.

[42] C. D. L. Folmes and A. Terzic, "Energy metabolism in the acquisition and maintenance of stemness," *Seminars in Cell & Developmental Biology*, vol. 52, pp. 68–75, 2016.

[43] J. K. Salabei, P. K. Lorkiewicz, C. R. Holden et al., "Glutamine regulates cardiac progenitor cell metabolism and proliferation," *Stem Cells*, vol. 33, no. 8, pp. 2613–2627, 2015.

[44] J. A. Gaspar, M. X. Doss, J. G. Hengstler, C. Cadenas, J. Hescheler, and A. Sachinidis, "Unique metabolic features of stem cells, cardiomyocytes, and their progenitors," *Circulation Research*, vol. 114, no. 8, pp. 1346–1360, 2014.

[45] C. Gauron, C. Rampon, M. Bouzaffour et al., "Sustained production of ROS triggers compensatory proliferation and is required for regeneration to proceed," *Scientific Reports*, vol. 3, no. 1, 2013.

[46] N. R. Love, Y. Chen, S. Ishibashi et al., "Amputation-induced reactive oxygen species are required for successful Xenopus tadpole tail regeneration," *Nature Cell Biology*, vol. 15, no. 2, pp. 222–228, 2013.

[47] E. A. Osuma, D. W. Riggs, A. A. Gibb, and B. G. Hill, "High throughput measurement of metabolism in planarians reveals activation of glycolysis during regeneration," *Regeneration (Oxf)*, vol. 5, no. 1, pp. 78–86, 2018.

[48] N. Pirotte, A. S. Stevens, S. Fraguas et al., "Reactive oxygen species in planarian regeneration: an upstream necessity for correct patterning and brain formation," *Oxidative Medicine and Cellular Longevity*, vol. 2015, 19 pages, 2015.

[49] R. Doonan, J. J. McElwee, F. Matthijssens et al., "Against the oxidative damage theory of aging: superoxide dismutases protect against oxidative stress but have little or no effect on life span in Caenorhabditis elegans," *Genes & Development*, vol. 22, no. 23, pp. 3236–3241, 2008.

[50] B. Andziak, T. P. O'Connor, W. Qi et al., "High oxidative damage levels in the longest-living rodent, the naked mole-rat," *Aging Cell*, vol. 5, no. 6, pp. 463–471, 2006.

[51] W. Zhou, M. Zhu, M. A. Wilson, G. A. Petsko, and A. L. Fink, "The oxidation state of DJ-1 regulates its chaperone activity toward α-Synuclein," *Journal of Molecular Biology*, vol. 356, no. 4, pp. 1036–1048, 2006.

[52] T. Taira, Y. Saito, T. Niki, S. M. M. Iguchi-Ariga, K. Takahashi, and H. Ariga, "DJ-1 has a role in antioxidative stress to prevent cell death," *EMBO Reports*, vol. 5, no. 2, pp. 213–218, 2004.

[53] J. Tsushima, K. Nishimura, N. Tashiro et al., "Protective effect of planarian DJ-1 against 6-hydroxydopamine-induced neurotoxicity," *Neuroscience Research*, vol. 74, no. 3-4, pp. 277–283, 2012.

[54] T. Inoue, T. Yamashita, and K. Agata, "Thermosensory signaling by TRPM is processed by brain serotonergic neurons to produce planarian thermotaxis," *The Journal of Neuroscience*, vol. 34, no. 47, pp. 15701–15714, 2014.

[55] X. Ding, L. Song, Y. Han et al., "Effects of Fe3+ on Acute Toxicity and Regeneration of Planarian (Dugesia japonica) at Different Temperatures," *BioMed Research International*, vol. 2019, 9 pages, 2019.

[56] N. Hammoudi, C. Torre, E. Ghigo, and M. Drancourt, "Temperature affects the biology of Schmidtea mediterranea," *Scientific Reports*, vol. 8, no. 1, p. 14934, 2018.

[57] J. B. Best, A. B. Goodman, and A. Pigon, "Fissioning in planarians: control by the brain," *Science*, vol. 164, no. 3879, pp. 565–566, 1969.

[58] C. P. Arnold, B. W. Benham-Pyle, J. J. Lange, C. J. Wood, and A. Sánchez Alvarado, "Wnt and TGFβ coordinate growth and patterning to regulate size-dependent behaviour," *Nature*, vol. 572, no. 7771, pp. 655–659, 2019.

[59] S. Herath and D. Lobo, "Cross-inhibition of Turing patterns explains the self-organized regulatory mechanism of planarian fission," *Journal of Theoretical Biology*, vol. 485, p. 110042, 2020.

[60] D. Bueno, J. Fernàndez-Rodríguez, A. Cardona, V. Hernàndez-Hernàndez, and R. Romero, "A novel invertebrate trophic factor related to invertebrate neurotrophins is involved in planarian body regional survival and asexual reproduction," *Developmental Biology*, vol. 252, no. 2, pp. 188–201, 2002.

[61] T. Sakurai, H. Lee, M. Kashima et al., "The planarian P2X homolog in the regulation of asexual reproduction," *The International Journal of Developmental Biology*, vol. 56, no. 1-2-3, pp. 173–182, 2012.

[62] W. H. Cole, "Temperature and locomotion in planaria," *The Journal of General Physiology*, vol. 9, no. 4, pp. 503–511, 1926.

[63] M. S. de Oliveira, K. A. R. Lopes, P. M. S. C. M. Leite, F. V. Morais, and N. M. R. de Campos Velho, "Physiological evaluation of the behavior and epidermis of freshwater planarians (Girardia tigrinaandGirardiasp.) exposed to stressors," *Biol Open*, vol. 7, no. 6, p. bio029595, 2018.

[64] I. D. Bowen, T. A. Ryder, and J. A. Thompson, "The fine structure of the planarianPolycelis tenuis Iijima," *Protoplasma*, vol. 79, no. 1-2, pp. 1–17, 1974.

[65] L. R. Smales and H. D. Blankespoor, "The epidermis and sensory organs of Dugesia tigrina (Turbellaria: Tricladida). A scanning electron microscope study," *Cell and Tissue Research*, vol. 193, no. 1, pp. 35–40, 1978.

[66] H. M. Brown and T. E. Ogden, "The electrical response of the planarian ocellus," *The Journal of General Physiology*, vol. 51, no. 2, pp. 237–253, 1968.

[67] H. O. Portner, "Climate variations and the physiological basis of temperature dependent biogeography: systemic to molecular hierarchy of thermal tolerance in animals," *Comparative Biochemistry and Physiology. Part A, Molecular & Integrative Physiology*, vol. 132, no. 4, pp. 739–761, 2002.

[68] T. Finkel, "Signal transduction by reactive oxygen species," *The Journal of Cell Biology*, vol. 194, no. 1, pp. 7–15, 2011.

[69] D. Abele, K. Heise, H. O. Pörtner, and S. Puntarulo, "Temperature-dependence of mitochondrial function and production of reactive oxygen species in the intertidal mud clam Mya arenaria," *The Journal of Experimental Biology*, vol. 205, Part 13, pp. 1831–1841, 2002.

[70] W. Jarmuszkiewicz, A. Woyda-Ploszczyca, A. Koziel, J. Majerczak, and J. A. Zoladz, "Temperature controls oxidative phosphorylation and reactive oxygen species production through uncoupling in rat skeletal muscle mitochondria," *Free Radical Biology & Medicine*, vol. 83, pp. 12–20, 2015.

[71] E. Gnaiger, "Capacity of oxidative phosphorylation in human skeletal muscle," *The International Journal of Biochemistry & Cell Biology*, vol. 41, no. 10, pp. 1837–1845, 2009.

[72] H. Lemieux, P. U. Blier, and E. Gnaiger, "Remodeling pathway control of mitochondrial respiratory capacity by temperature in mouse heart: electron flow through the Q-junction in permeabilized fibers," *Scientific Reports*, vol. 7, no. 1, p. 2840, 2017.

[73] H. Lemieux, S. Semsroth, H. Antretter, D. Höfer, and E. Gnaiger, "Mitochondrial respiratory control and early defects of oxidative phosphorylation in the failing human heart," *The International Journal of Biochemistry & Cell Biology*, vol. 43, no. 12, pp. 1729–1738, 2011.

[74] H. Lemieux and B. E. Warren, "An animal model to study human muscular diseases involving mitochondrial oxidative phosphorylation," *Journal of Bioenergetics and Biomembranes*, vol. 44, no. 4, pp. 503–512, 2012.

[75] K. Y. Scott, R. Matthew, J. Woolcock, M. Silva, and H. Lemieux, "Adjustments in the control of mitochondrial respiratory capacity to tolerate temperature fluctuations," *Journal Experimental Biology*, vol. 222, no. 18, p. jeb207951, 2019.

[76] M. Gallio, T. A. Ofstad, L. J. Macpherson, J. W. Wang, and C. S. Zuker, "The coding of temperature in the Drosophila brain," *Cell*, vol. 144, no. 4, pp. 614–624, 2011.

[77] O. M. Arenas, E. E. Zaharieva, A. Para, C. Vásquez-Doorman, C. P. Petersen, and M. Gallio, "Activation of planarian TRPA1 by reactive oxygen species reveals a conserved mechanism for animal nociception," *Nature Neuroscience*, vol. 20, no. 12, pp. 1686–1693, 2017.

[78] K. X. Ma, G. W. Chen, and D. Z. Liu, "cDNA cloning of heat shock protein 90 gene and protein expression pattern in response to heavy metal exposure and thermal stress in planarian Dugesia japonica," *Molecular Biology Reports*, vol. 39, no. 6, pp. 7203–7210, 2012.

[79] Z. Dong, F. Cheng, Y. Yuwen et al., "Identification and expression analysis of a Spsb gene in planarian Dugesia japonica," *Gene*, vol. 564, no. 2, pp. 168–175, 2015.

[80] K. Hamana, H. Hamana, and T. Shinozawa, "Alterations in polyamine levels of nematode, earthworm, leech and planarian during regeneration, temperature and osmotic stresses," *Comparative Biochemistry and Physiology. Part B, Biochemistry & Molecular Biology*, vol. 111, no. 1, pp. 91–97, 1995.

[81] J. A. Carter, C. H. Lind, M. P. Truong, and E.-M. S. Collins, "To each his own," *Journal of Statistical Physics*, vol. 161, no. 1, pp. 250–272, 2015.

[82] M. Hughes-Fulford, "Lessons learned about spaceflight and cell biology experiments," *Journal of Gravitational Physiology*, vol. 11, no. 1, pp. 105–109, 2004.

[83] P. Warren, A. Golden, J. Hanover, D. Love, F. Shephard, and N. J. Szewczyk, "Evaluation of the fluids mixing enclosure system for life science experiments during a commercial Caenorhabditis elegans spaceflight experiment," *Advances in Space Research*, vol. 51, no. 12, pp. 2241–2250, 2013.

[84] Vista SSEP Mission 11 Team, D. Hagstrom, C. Bartee, and E.-M. S. Collins, "Studying planarian regeneration aboard the International Space Station within the Student Space Flight Experimental Program," *Frontiers in Astronomy and Space Sciences*, vol. 5, 2018.

Research Article

Microgravity versus Microgravity and Irradiation: Investigating the Change of Neuroendocrine-Immune System and the Antagonistic Effect of Traditional Chinese Medicine Formula

Haoru Zhu,[1] Lin Zhang,[2] Meng Qian,[1] Tuo Shi,[1] Fangxin Fan,[1] Wenfei Li,[1] Sitai Zhu,[1] and Ming Xie [1]

[1]*School of Traditional Chinese Medicine, Bejing University of Chinese Medicine, Beijing 100029, China*
[2]*School of Traditional Chinese Medicine, Liaoning University of Chinese Medicine, Shenyang, Liaoning 110847, China*

Correspondence should be addressed to Ming Xie; xieming603@126.com

During spaceflight, the homeostasis of the living body is threatened with cosmic environment including microgravity and irradiation. Traditional Chinese medicine could ameliorate the internal imbalance during spaceflight, but its mechanism is still unclear. In this article, we compared the difference of neuroendocrine-immune balance between simulated microgravity (S) and simulated microgravity and irradiation (SAI) environment. We also observed the antagonistic effect of SAI using a traditional Chinese medicine formula (TCMF). Wistar rats were, respectively, exposed under S using tail suspending and SAI using tail suspending and ^{60}Co-gama irradiation exposure. The SAI rats were intervened with TCMF. The changes of hypothalamic–pituitary–adrenal (HPA) axis, splenic T-cell, celiac macrophages, and related cytokines were observed after 21 days. Compared with the normal group, the hyperfunction of HPA axis and celiac macrophages, as well as the hypofunction of splenic T-cells, was observed in both the S and SAI group. Compared with the S group, the levels of plasmatic corticotropin-releasing hormone (CRH), macrophage activity, and serous interleukin-6 (IL-6) in the SAI group were significantly reduced. The dysfunctional targets were mostly reversed in the TCMF group. Both S and SAI could lead to NEI imbalance. Irradiation could aggravate the negative feedback inhibition of HPA axis and macrophages caused by S. TCMF could ameliorate the NEI dysfunction caused by SAI.

1. Introduction

Since the last century, the exploration of space has been gradually unfolding. However, the physiological behavior of human beings is continuously threatened with extreme environmental factors in space, such as microgravity, irradiation, space noise, narrow space, and social loneliness, which has seriously affected the physical and mental health of astronauts and hindered the development of manned spaceflight partly [1].

Microgravity and irradiation are the most important factors among the complex space environment. It is reported that microgravity could affect multiple physiological systems including the cardio-cerebral-vascular system [2], nervous system [3], locomotor system [4], and immune system [5].

On the other hand, it is reported that space irradiation could lead to the dysfunction of the nervous system [6], endocrine system [7], and immune system [8]. Considering the difficulties of midcourse space experiment, such as high research cost and unsatisfied experimental space, the research on space extreme environment is generally simulated on the ground. However, most of the studies are currently focused on physiological changes caused by a single environmental factor like microgravity or irradiation, how the complexed extreme environment interferes with the human body is barely researched.

Since the immune-neuro-endocrine system was hypothesized by Besedovsky and Sorkin in 1977 [9], researchers have been proceeding a variety of studies on the internal mechanism of the neuroendocrine and immune systems. It has been

confirmed that there exists a bidirectional mechanism between the neuroendocrine system and immune system, which build the neuro-endocrine-immune (NEI) system together via a synergistic effect and antagonism. The NEI system plays an important role in homeostasis and against external environmental aggression. It is reported that the NEI system could engender a series of changes to readapt the new external environment while facing the extreme space surroundings. Nevertheless, the research on how the NEI system changes under microgravity-irradiation environment is scarcely reported.

Traditional Chinese medicine (TCM) shows its advantage on systematically reconciling the physiological function of the human body. It is reported that traditional Chinese medicine formula (TCMF), especially which is used based on TCM theory, could effectively alleviate the physical impairment caused by microgravity, irradiation, and other space environments [10]. TCMF "Taikong Xieli Decoction" (TKXLD), which was formulated by our team, has been confirmed to modulate the immunity of rats under the condition of short-term microgravity combined with irradiation [11]. However, the immunomodulatory mechanism of TKXLD is still unclear.

Overall, the research on organism adaption in space is depending rapidly, yet a lot of deficiencies still remain, especially on the comprehensive consideration of the complex space environment, systematized exploration on multiple physiological systems in the human body, and profound study on the mechanism of TCMF. Hence, we reconstructed the rat model which suffered from microgravity and irradiation to observe the changes in the NEI system and the modulated the mechanism of TKXLD. This study might give experimental support for ascertaining the influence of space environment on a mammal and the antagonistic effect of TCMF.

2. Materials and Methods

2.1. Preparation of TKXLD. TKXLD consists of Ginseng Radix et Rhizoma (*PanaxginsengC.A.Mey.*), Ophiopogonis Radix (*Ophiopogon japonicus*), Astragali Radix (*Astragalus membranaceus* (*Fisch.*) *Bge. var. mongholicus* (*Bge.*)*Hsiao*), Schisandrae Chinensis Fructus (*Schisandra chinensis* (*Turcz.*) *Baill.*), Poria (*Poria cocos* (*Schw.*) *Wolf*), Rehmanniae Radix Praeparata (*Rehmannia glutinosa Libosch.*), Drynariae Rhizoma (*Drynaria fortunei* (*Kunze*) *J.Sm.*), and Chuanxiong Rhizoma (*Ligusticum chuanxiong Hort.*). All the herbs were provided by Beijing Tong Ren Tang Chinese Medicine Company, China, and met the criterion of *Pharmacopoeia of the People's Republic of China (the 2015 edition)*. The TKXLD formula was extracted under reflux with distilled water (1 : 10 volume) twice for 1 h each. After that, the extracts were concentrated to 100%, then filtered and dried below 60°C to obtain TKXLD granules. The TKXLD granule was dissolved in 70% solution using distilled water before use.

2.2. Animals and Treatments. 40 male Wistar rats, weighing 170 g to 190 g (180 ± 10), were used in this study (Grade SPF/VAF, Certificate No: SCXK(Jing) 2002-2003, Beijing

Laboratory Animal Research Center). All animal experiments were performed strictly in accordance with the guidelines of Beijing University of Chinese Medicine Animal Care and Use Committee. The animals were maintained at an ambient temperature of 16-20°C under a 12 h : 12 h light-dark cycle. Water and food were given ad libitum. The rats were randomly divided into four groups: the control group (C), tail-suspended group (S), tail-suspended adding irradiated group (SAI), and herb (Taikong Xieli Decoction, TKXLD) group, 10 rats per group.

Rats in the S, SAI, and TKXLD groups were subjected to tail suspended of head down position of -30° to simulate microgravity and those in the SAI and TKXLD groups were irradiated with 4.5 Gy of ^{60}Co-gamma rays at the 8th day of tail suspended (the cobalt bomb was provided by Academy of military medical sciences). Rats of the TKXLD group were orally administrated with the decoction ($7 g \cdot kg^{-1} \cdot d^{-1}$) abstracted from a compound formula of traditional Chinese medicine and other groups with equivalent normal saline. All rats were anesthetized via an intraperitoneal injection of 2% sodium pentobarbital (0.25 mL/100 g) and then killed at 2 hours after intragastric administration, on the 21th day of the experiment. At that time, related tissues were extracted.

2.3. Proliferation of T Lymphocyte Measurement. Half of the spleen, which was extracted under aseptic condition, was put in a culture dish. 2 mL RPMI-1640 incomplete medium was added at the same time. After that, single-cell suspension was prepared by grinding and filtration with 80 mesh sieve. Single-cell suspension was seeded into 96-well plates at a density of 5×10^{-6} cells/mL and a volume of 100 μL/well, ConA (Sigma, USA) was added into each well at a final concentration of 5 μg/mL. The cells were incubated for 68 h at 37°C, 5%CO$_2$ after 100 μL solution was discarded in each well. Then, the culture media were eliminated and 10 μL MTT solution (5 mL, Sigma, USA) was added into each well, followed by culturing at 37°C in a 5% CO$_2$ humidified atmosphere for 4 h. 150 μL DMSO (Sigma, USA) was then added and shook up. 10 minutes later, the absorbance of the solution was measured using a microplate reader at the wavelength of 570 nm.

2.4. Phagocytosis of Macrophage Measurement. The peritoneal fluid was obtained using cold Hank's with heparin washing. After that, the peritoneal macrophages were collected by draining the solution. The cell concentration was regulated to 5×10^{-9} cells/L and added into a 96-well plate which was put in the incubator. Four hours later, neutral red solution was added and then cell lysates were added after 40 minutes. Macrophage suspension was put over the night of 4°C; then, the absorbance of the solution was measured using a microplate reader at the wavelength of 492 nm.

2.5. Radioimmunoassay (RIA). The hypothalamus was rapidly collected onto ice. After weighing, the hypothalamus was boiling in 1 mL normal saline for 3 minutes; 1 N glacial acetic acid (0.5 mL) was added and homogenized. The homogenate was neutralized with 1 N NaOH (0.5 mL) and centrifuged at 3000 r/min for 30 min. The supernatant was

drained and stored at -80°C. The level of the corticotropin-releasing hormone (CRH) was assayed using a radioimmunoassay (RIA) kit (Haikerui Biotechnology Center, Beijing, China). Pituitary suspension was drained as mentioned above, and the level of adrenocorticotropic hormone (ATCH) was measured using a RIA kit (Huaying Institute of Biotechnology, Beijing, China). Furthermore, the levels of CRH and ACTH in plasma were, respectively, measured using a RIA kit as mentioned above. The level of CORT in the serum was measured using RIA kit (Huaying Institute of Biotechnology, Beijing, China). The supernatants of splenocyte suspension and macrophage suspension were, respectively, drained by measuring interleukin 2 (IL-2), interleukin 1 beta (IL-1β) and interleukin 6 (IL-6) using a RIA kit (Science and technology development center of PLA General Hospital, Beijing, China). IL-1β, IL-2, and IL-6 levels in the serum were, respectively, measured using the RIA kit as stated above.

2.6. Reverse Transcription-Polymerase Chain Reaction (RT-PCR).
Total RNA was extracted from the splenocytes using RNA TRIzol (Gibco, USA) and reverse transcription into cDNA. The primers for glucocorticoid receptor (GR) and β-actin were shown in Table 1. RT-PCR detected fluorescence, and the levels of mRNA were normalized to β-actin expression. Primers for RT-PCR were listed as follows.

2.7. Statistical Analysis.
The experimental data was expressed as the mean ± standard deviation (X±SD). All the data were analyzed by one-way ANOVA using SPSS 23.0 software and differences were considered significant at $P < 0.05$.

3. Results

3.1. HPA Axis

3.1.1. CRH.
As shown in Figure 1, compared with the control group, the levels of the hypothalamic and plasmatic CRH in the S and SAI group were reduced significantly. Compared with the S group, the level of plasmatic CRH in the SAI group was reduced significantly. Compared with the SAI group, the levels of hypothalamic and plasmatic CRH in the TKXLD group was increased significantly.

3.1.2. ACTH.
As shown in Figure 2, compared with the control group, the levels of pituitary and plasmatic ACTH in the S and SAI groups were both increased significantly. There was no statistical difference between the S and SAI groups. Compared with the SAI group, the levels of pituitary and plasmatic ACTH in the TKXLD group were reduced significantly.

3.1.3. CORT and GR mRNA.
As shown in Figure 3(a), compared with the control group, the levels of plasmatic CORT in the S and SAI groups were both increased significantly. For CORT, there was no significant difference between the S and SAI groups. Compared with the SAI group, the level of CORT in the TKXLD group was reduced significantly. As shown in Figure 3(b), compared with the control group, the expression of splenic GR mRNA in the S and SAI group were both increased significantly. There was no significant

Table 1: Primers for RT-PCR.

Gene	Primer sequence (5′→3′)	Product size (bp)
GR	Forward:ACCCTGCTACAGTACTCATGGA Reverse:CTTGGCTCTTCAGACCTTCCT	271
β-Actin	Forward:CATCCTGCGTCTGGACCT Reverse:CACACAGAGTACTTGCGCTCA	498

difference in the GR mRNA expression between the S and SAI groups. Compared with the SAI group, the GR mRNA expression in the TKXLD group was reduced significantly.

3.2. Immune Function

3.2.1. T-Cell Function and Related Cytokines.
As shown in Figures 4(a) and 4(b), compared with the control group, the capacity of splenic T-cell proliferation and IL-2 secreting capacity in the S and SAI groups were decreased significantly. There was no significant difference of splenic T-cell proliferation and IL-2 secreting capacity between the S and SAI groups. Compared with the SAI group, the IL-2 secreting capacity in the TKXLD group was increased significantly. As shown in Figure 4(c), compared with the control group, the level of serous IL-2 in the S and SAI groups was decreased significantly. There was no statistical difference of serous IL-2 between the S and SAI groups. Compared with the SAI group, the levels of serous IL-2 in the TKXLD group had an uptrend, but there was no significant difference.

3.2.2. Celiac Macrophage Function and Related Cytokines.
As shown in Figure 5, for celiac macrophages, the phagocytosis and IL-1β level in the S and SAI groups were both significantly enhanced in comparison with the control group. The macrophagic IL-6 level in the S group was significantly increased in comparison with the control group. Compared with the S group, the phagocytosis of macrophages in the SAI group was decreased markedly, and the levels of IL-1β and IL-6 showed no statistical difference. Compared with the SAI group, the phagocytosis and IL-1β level of macrophages in the TKXLD group was decreased significantly.

As shown in Figure 6, compared with the control group, the levels of serous IL-1β and IL-6 in the S and SAI groups were significantly increased. There was no significant difference of serous IL-1β between the S and SAI groups, but the level of serous IL-6 in the SAI group was significantly decreased compared with the S group. There was no significant difference of serous IL-1β between the SAI and TKXLD groups. However, the level of serous IL-6 in the TKXLD group was significantly decreased compared with the SAI group.

4. Discussion

Microgravity and irradiation are two main factors affecting organisms during spaceflight. In this study, we simulated the microgravity state of a rat by tail suspension. Meanwhile, we also compared the neuro-endocrine-immune influence under microgravity-irradiation environment with microgravity state. Recently, there is a wide range of chosen
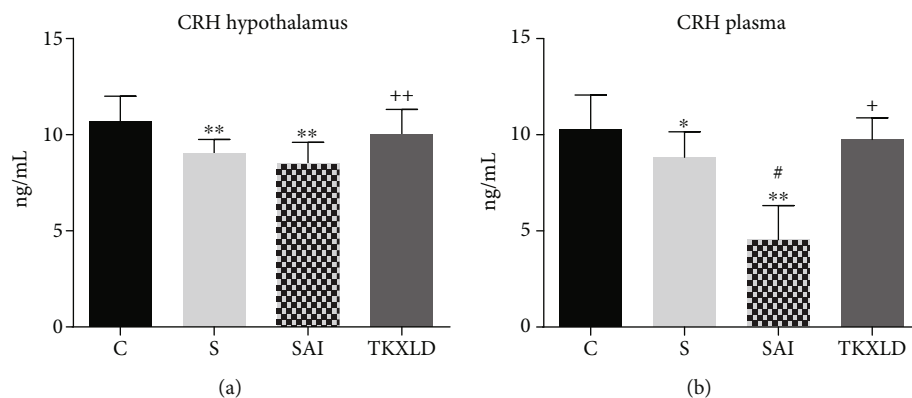
FIGURE 1: The level of CRH in the hypothalamus and plasma. (a) The level of hypothalamic CRH in each group. (b) The level of plasmatic CRH in each group. $N = 10$ for each group. $^*P < 0.05$, $^{**}P < 0.01$ compared with the control group. $^\#P < 0.05$ compared with the S group. $^+P < 0.05$, $^{++}P < 0.01$ compared with the SAI group.
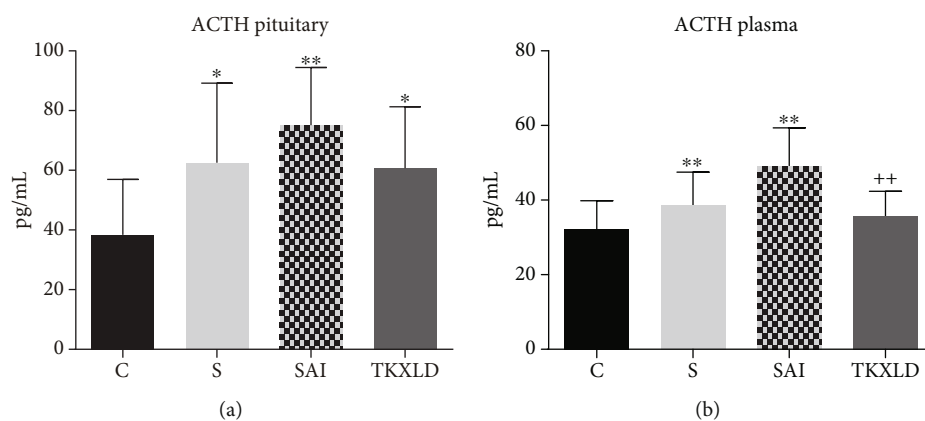
FIGURE 2: The level of ACTH in the pituitary and plasma. (a) The level of hypophyseal ACTH in each group. (b) The level of plasmatic ACTH in each group. $N = 10$ for each group. $^*P < 0.05$, $^{**}P < 0.01$ compared with the control group. $^{++}P < 0.01$ compared with the SAI group.
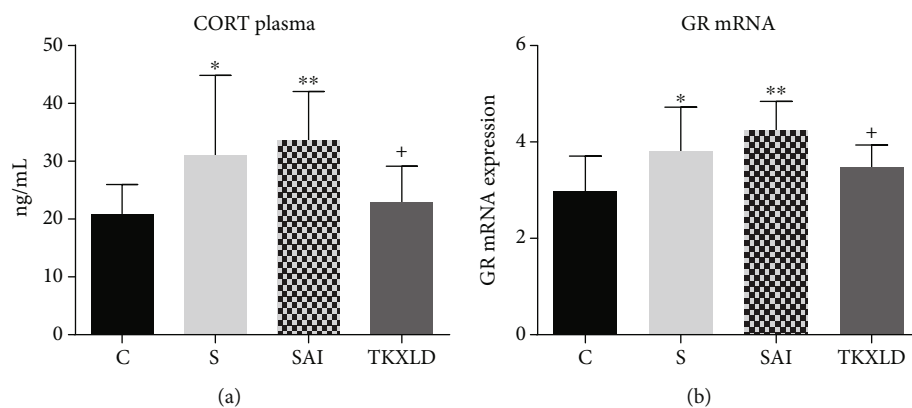
FIGURE 3: The expression of plasmatic CORT and splenic GR mRNA. (a) The level of plasmatic CORT in each group. (b) The expression of splenic GR mRNA in each group. $N = 10$ for each group. $^*P < 0.05$, $^{**}P < 0.01$ compared with the control group. $^+P < 0.05$ compared with the SAI group.

irradiation dosage which is from 0.5 Gy to 25 Gy on space irradiation research [12–14]. The designed irradiation dose is determined by species, experimental purpose, and biological endpoints [15]. Considering that the astronauts might suffer high-dose space irradiation during solar nucleon active

period or extravehicular activities, and the Wistar rat had a relative low sensitivity in comparison with other experimental animals, we used a total of 4.5 Gy irradiation dosage (0.3 Gy/min) which was a little bit higher than the commonly used irradiation dosage (2.5 Gy or thereabouts). In this
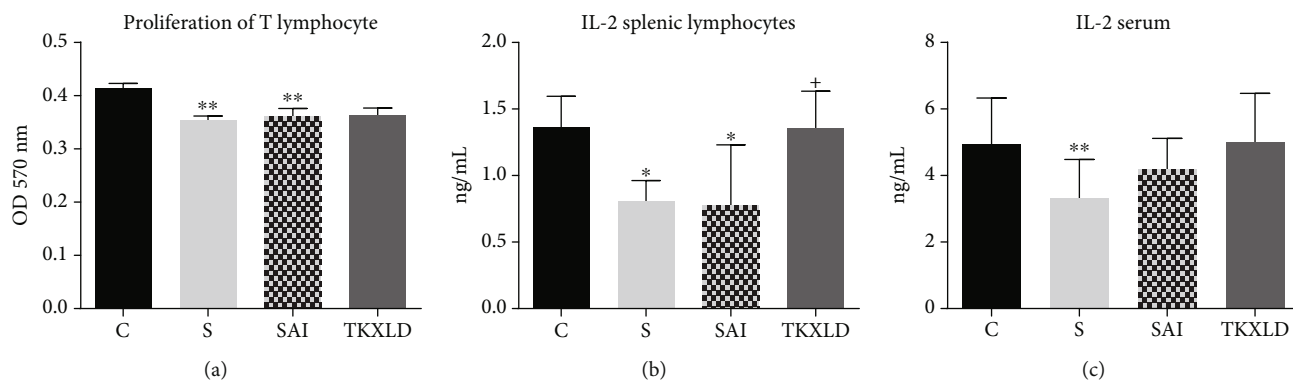
FIGURE 4: T-cell proliferation and related IL-2 level. (a) The proliferation of splenic T-cell in each group. (b) The level of splenic IL-2 in each group. (c) The level of serous IL-2 in each group. $N = 10$ for each group. $^*P < 0.05$, $^{**}P < 0.01$ compared with the control group. $^+P < 0.05$, $^{++}P < 0.01$ compared with the SAI group.
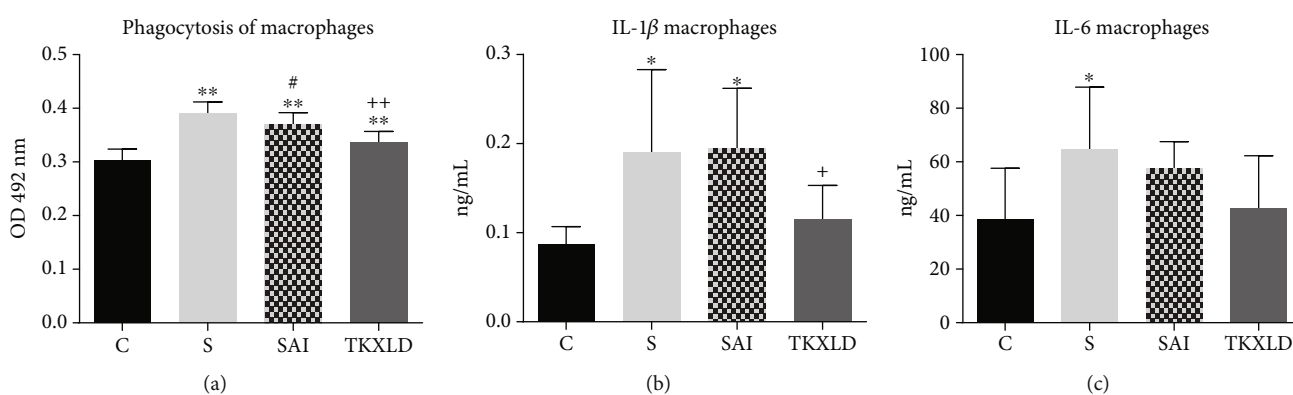
FIGURE 5: Macrophagic phagocytosis and related cytokine levels. (a) Phagocytosis of celiac macrophages in each group. (b) The level of macrophagic IL-1β in each group. (c) The level of macrophagic IL-6 in each group. $^*P < 0.05$, $^{**}P < 0.01$ compared with the control group. $^\#P < 0.05$, $^{\#\#}P < 0.01$ compared with the S group. $^+P < 0.05$, $^{++}P < 0.01$ compared with the SAI group.
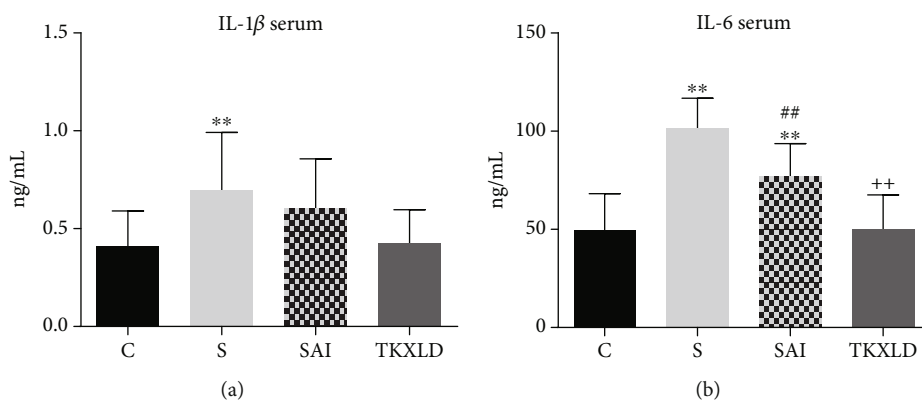
FIGURE 6: Serous IL-1β and IL-6 levels. (a) The level of serous IL-1β in each group. (b) The level of serous IL-6 in each group. $N = 10$ for each group. $^*P < 0.05$, $^{**}P < 0.01$ compared with the control group. $^\#P < 0.05$, $^{\#\#}P < 0.01$ compared with the S group. $^+P < 0.05$, $^{++}P < 0.01$ compared with the SAI group.

article, we found that, compared with the control group, the level of CRH was decreased, the ACTH and CORT level were increased, and the expression of splenic GR mRNA was upregulated in both the S and SAI groups. The proliferative and IL-2 secreting capacity of T-cell in the S and SAI group were weakened, but the phagocytosis and related cytokine secreting capacity of celiac macrophages were significantly

increased. On the other hand, the plasmatic CRH, phagocytosis of macrophages, and serous IL-6 in the SAI group were all decreased significantly compared with the S group. Furthermore, TKXLD could normalize the anomalous changing of the NEI targets to varying degrees.

There is a close correspondence between the neuroendocrine and immune systems, both of these two systems

constitute the complex NEI system. As an important part of the NEI system, there also exists a two-way communication and feedback between the HPA axis and the immune system. For one thing, plenty of cytokines like IL-1, IL-6, IL-10, and tumor necrosis factor alpha (TNF-α) could activate the HPA axis; for another, HPA could regulate the systemic inflammatory response. HPA axis is activated under hyperinflammatory state; high-level glucocorticoids are then released to inhibit the immune response by hindering the proinflammatory cytokines secreting like IL-1 and TNF-α. Meanwhile, the HPA axis could induce immune cells releasing anti-inflammatory cytokines such as IL-4, IL-10, and IL-13 to restrain the inflammation, which contributes to protecting the body from the damages caused by the excessive activation of the immune system [16].

In the microgravity state, the change of gravity leads to the imbalance of body fluids. The biofluid flows to the head, which causes the change of cerebral blood flow and hemodynamics. The cerebral metabolism, including the central nervous system (CNS) metabolism, is then adversely affected. The expression of hypothalamic proteins is disordered including oxidative imbalance [17]. The feeding frequency of the pituitary cells was disrupted, which leads to hormone secretion disorder [18]. Furthermore, the levels of humoral adrenaline, noradrenalin, dopamine, ACTH, growth hormone (GH), prolactin, and CORT were increased at the same time [19]. The redistribution of body fluids could also induce the stress response of the immune system. In this state, for immune organ atrophy, the T-cell and B-cell secreting capacity of which falls into decline simultaneously [20]. Additionally, the expression and ability of maturation markers on dendritic cells (DC) were dwindled [21]. The resistance of the body to some pathogens is enhanced by activating macrophages [22].

Irradiation could act upon the external body parts such as the skin or retina directly and influence the internal system or tissues via the bystander effect, which is different from microgravity. It is reported that radiotherapeutic irradiation could lead to endocrine dyscrasia, pituitary insufficiency, and HP axis dysfunction [23]. Space irradiation is reported to injure the hypothalamus, prefrontal lobe, and nucleus accumbens [24]. It is also reported that space irradiation could give a promotion on macrophage proliferation and enhance its phagocytic function [25].

Organisms are threatened with microgravity, irradiation, and other extreme environmental hazards in the space environment. The NEI system shows the approximate changes under space environment, including the increasing ACTH, thyroxine, CORT, and antidiuretic hormone (ADH) levels [26]; the hypofunction on T-cell [27]; and overactivation on macrophages [28].

The influence of microgravity and irradiation on the human body nearly has the similar trend, but each of which is emphasized in different directions further. It is reported that the human body could be caused to lower the CNS defense against oxidative damage [29] and reduce the quantity of lymphocytes [30] under either microgravity or irradiation condition. Remarkably, it is reported that space flight-associated anorexia and musculoskeletal degenerative changes may be driven by irradiation- and microgravity-associated mechanisms, respectively [31], which suggested that there existed a different intervention mechanism, respectively, between microgravity and irradiation. A raft of research suggested that there might be a kind of "superposition effect" on the organism while it was under the condition of both microgravity and irradiation. It is reported that the apoptosis rate of the Hmy2.CIR cell, which is the metrocyte of B-cell, under the conditions of microgravity-irradiation was way above which under the condition of single irradiation [32]. Microgravity could aggravate the genotoxicity caused by irradiation [33]. Compared with microgravity, the microgravity-irradiation environment showed the most serious oxidative stress in the cerebral cortex of mice [34].

In this study, we found that the HPA axes and macrophages in both the S group and SAI group were unanimously active, but the splenic T-cell and related cytokines were under hypofunctional state. Compared with the S group, the level of plasmatic CRH, macrophage activity, and serous IL-6 were all decreased significantly, which indicated that irradiation could antagonize the HPA and macrophage stress caused by microgravity, as well as aggravate the hypofunction of T-cell. Upon this, we hypothesized that there might be several differences on the body stress mechanism between microgravity and microgravity-irradiation, while irradiation might weaken the self-adaptive ability under the condition of microgravity.

The HPA axis consists of the hypothalamus, pituitary, and adrenal glands. CRH and arginine vasopressin (AVP) which are synthesized in the relay neurons of the paraventricular hypothalamic nucleus (PVN) are released into the anterior pituitary via the portal vein. ACTH is driven to release after that, which could activate adrenocortical cells to synthesize and secrete CORT and GC that contributes to energy mobilization and homeostasis maintaining via negative feedback regulation [35]. In this research, the ATCH and CORT levels in the S and SAI groups were both elevated, which illustrated that the HPA axis was activated. As the level of CRH was observed to be significantly decreased in the S and SAI groups, it might be caused by the hypothalamic inverse feedback signal that was given by the overexpressed GR and glucocorticoid which was caused by systemic stress.

There is a close correspondence between the HPA axis and the immune system. ACTH is known as an important immune modulator that could regulate the phagocytosis of macrophages [36]. On the one hand, a high level of CORT could lead to the inhibition of immunity and inflammation. On the other hand, the acute release of CORT could also upregulate the expression of IFN-γ receptor and promote macrophages secreting IL-6 [37]. The plasmatic CRH, mainly coming from epithelial cells and immunocyte secretion, besides hypothalamic transportation through the axons of nerve endings, could regulate cytokines via autocrine and paracrine [38]. Compared with T-cell or B-cell, macrophage shows the most sensitive immune activity to CRH [39]. CRH is indicated to promote the phagocytosis of macrophages via the PKA/PKC-ERK1/2-RhoA/Rac1 signaling pathway [40]. In this study, we indicated that the overexpression of CORT and GR mRNA led to the inhibition of T-cell

function and enhancement of macrophage activation. Microgravity combined with irradiation could downregulate the plasmatic CRH level to inhibit the hyperfunction of macrophages to some extent.

TKXLD is composed of Ginseng, Ophiopogonis, Radix Astragali, Schisandrae Chinensis Fructus, Poria, Rehmanniae, Drynariae, and Chuanxiong. In TCM theory, TKXLD is able to replenish Qi, nourish Yin, toxify the kidney, and promote blood circulation. It is reported that Ginseng and Radix Astragali show favorable antimicrogravity [41, 42] and anti-irradiation effects [43, 44] that could regulate immune response and HPA axis dysfunction caused by stress to maintain the NEI balance [45, 46]. Ophiopogonis Radix is proved to contribute to ameliorate macrophage activity [47]. There are evidences that Schisandrae Chinensis Fructus and Chuanxiong have protective effects on irradiation damage, the mechanisms of which contains reversing damage caused by irradiation and inhibiting the overactivation of the HPA axis [48–50]. Poria has been used as a good immune modulator that could resist the excessive macrophage activation induced by LPS [51]. Rehmanniae has been proved to be efficacious in retaining NEI homeostasis [52]. Drynariae is considered a kind of potential antimicrogravity medicine that has a good effect on several diseases like bone loss led by microgravity [53]. Thus, it is indicated that the compatibility of the herbs above might produce a marked effect on NEI imbalance caused by irradiation and microgravity. In this research, for the rats in the TKXLD group, the amelioration of the HPA axis, macrophage, and splenic T-cell function was observed after TKXLD treatment. Meanwhile, the expression of splenic GC mRNA was downregulated in the TKXLD group. All these evidences have demonstrated that TKXLD has a protective influence on the NEI system of rats under microgravity-irradiation conditions. The mechanism of TKXLD might be involved in different function links of CNS and peripheral parts.

Human body faces dual challenges of microgravity and irradiation during spaceflight. Current studies on physiological adaptation in space are mostly focused on the single environmental factors. There is an urgent need for physiological research that is studied under complex environments. In this article, we entirely compared the functional changes of the NEI system between microgravity and microgravity-irradiation. The efficacy of TKXLD on treating NEI dysfunction caused by microgravity-irradiation was also investigated. The results indicated that the rats were suffered from dysfunction of the NEI system in different degrees under both microgravity and microgravity-irradiation, but there still are some differences, especially those related to the pathogenesis between the two conditions. Our study might be conducive to exploring the physiological adaptation mechanism of the human body in space, developing the defense strategy against extreme space environment, and promoting the protective use of TCM on spaceflight.

However, we only observe the NEI change in medium-term spaceflight of 21 days for the rats. Only the HPA axis and representative immunocytes in the NEI system were investigated. Though we found that irradiation might superimpose its effect on microgravity by messing the NEI sys-

tem, the bioregulating mechanism against microgravity-irradiation among the subsystems of the NEI network still deserved to be explored in depth.

5. Conclusion

Both microgravity and microgravity combined with irradiation could lead to the dysfunction of the HPA axis and immunity. The hyperfunctional HPA axis might cause dysimmunity. Irradiation could not only aggravate the negative feedback inhibition of the HPA axis but also antagonize the macrophage hyperfunction caused by microgravity. TKXLD could favorably ameliorate the dysfunction of the NEI system caused by microgravity-irradiation.

Data Availability

The data used to support the findings of this study are available from the corresponding author upon request.

Conflicts of Interest

The authors declare that there is no conflict of interest regarding the publication of this paper.

Authors' Contributions

Haoru Zhu and Lin Zhang contributed equally to this work.

Acknowledgments

References

[1] B. Mishra and U. Luderer, "Reproductive hazards of space travel in women and men," *Nature Reviews Endocrinology*, vol. 15, no. 12, pp. 713–730, 2019.

[2] L. F. Zhang, "Vascular adaptation to microgravity: what have we learned?," *Journal of Applied Physiology (Bethesda, MD: 1985)*, vol. 91, no. 6, pp. 2415–2430, 2001.

[3] A. Van Ombergen, A. Demertzi, E. Tomilovskaya et al., "The effect of spaceflight and microgravity on the human brain," *Journal of Neurology*, vol. 264, no. S1, pp. 18–22, 2017.

[4] L. Vico and A. Hargens, "Skeletal changes during and after spaceflight," *Nature Reviews Rheumatology*, vol. 14, no. 4, pp. 229–245, 2018.

[5] N. Goswami, A. P. Blaber, H. Hinghofer-Szalkay, and V. A. Convertino, "Lower body negative pressure: physiological effects, applications, and implementation," *Physiological Reviews*, vol. 99, no. 1, pp. 807–851, 2019.

[6] O. D. Iancu, S. W. Boutros, R. H. J. Olsen et al., "Space radiation alters genotype-phenotype correlations in fear learning and memory tests," *Frontiers in Genetics*, vol. 9, 2018.

[7] A. R. Kennedy, J. H. Ware, J. Guan et al., "Selenomethionine protects against adverse biological effects induced by space radiation," *Free Radical Biology and Medicine*, vol. 36, no. 2, pp. 259–266, 2004.

[8] R. Fernandez-Gonzalo, S. Baatout, and M. Moreels, "Impact of particle irradiation on the immune system: from the clinic to mars," *Frontiers in Immunology*, vol. 8, 2017.

[9] H. Besedovsky and E. Sorkin, "Network of immune-neuroendocrine interactions," *Clinical and Experimental Immunology*, vol. 27, no. 1, pp. 1–12, 1977.

[10] H. Sun, S. Ling, D. Zhao et al., "Panax quinquefolium saponin attenuates cardiac remodeling induced by simulated microgravity," *Phytomedicine*, vol. 56, pp. 83–93, 2019.

[11] L. Zhang and M. Xie, "Change of splenic T cells and thymus of the rat simulated by weightlessness with irradiation and effects of Taikong Xieli decoction of traditional Chinese medicine," *Chinese Journal of Experimental Traditional Medical Formulae*, vol. 15, no. 3, pp. 35–37, 2009.

[12] J. M. Wilson, J. K. Sanzari, E. S. Diffenderfer et al., "Acute biological effects of simulating the whole-body radiation dose distribution from a solar particle event using a porcine model," *Radiation Research*, vol. 176, no. 5, pp. 649–659, 2011.

[13] J. K. Sanzari, X. S. Wan, A. J. Wroe et al., "Acute hematological effects of solar particle event proton radiation in the porcine model," *Radiation Research*, vol. 180, no. 1, pp. 7–16, 2013.

[14] J. K. Sanzari, S. X. Wan, E. S. Diffenderfer, K. A. Cengel, and A. R. Kennedy, "Relative biological effectiveness of simulated solar particle event proton radiation to induce acute hematological change in the porcine model," *Journal of Radiation Research*, vol. 55, no. 2, pp. 228–244, 2014.

[15] A. R. Kennedy, "Biological effects of space radiation and development of effective countermeasures," *Life Sciences in Space Research*, vol. 1, pp. 10–43, 2014.

[16] N. M. Jiang, M. Cowan, S. N. Moonah, and W. A. Petri, "The impact of systemic inflammation on neurodevelopment," *Trends in Molecular Medicine*, vol. 24, no. 9, pp. 794–804, 2018.

[17] P. Sarkar, S. Sarkar, V. Ramesh et al., "Proteomic analysis of mouse hypothalamus under simulated microgravity," *Neurochemical Research*, vol. 33, no. 11, pp. 2335–2341, 2008.

[18] W. C. Hymer, R. E. Grindeland, T. Salada et al., "Feeding frequency affects cultured rat pituitary cells in low gravity," *Journal of Biotechnology*, vol. 47, no. 2-3, pp. 289–312, 1996.

[19] M. Feuerecker, W. P. J. van Oosterhout, B. Feuerecker et al., "Headache under simulated microgravity is related to endocrine, fluid distribution, and tight junction changes," *Pain*, vol. 157, no. 5, pp. 1072–1078, 2016.

[20] K. X. Wang, Y. Shi, and D. T. Denhardt, "Osteopontin regulates hindlimb-unloading-induced lymphoid organ atrophy and weight loss by modulating corticosteroid production," *Proceedings of the National Academy of Sciences*, vol. 104, no. 37, pp. 14777–14782, 2007.

[21] N. Tackett, J. H. Bradley, E. K. Moore et al., "Prolonged exposure to simulated microgravity diminishes dendritic cell immunogenicity," *Scientific Reports*, vol. 9, no. 1, p. 13825, 2019.

[22] E. S. Miller, R. A. Bates, D. A. Koebel, and G. Sonnenfeld, "Antiorthostatic suspension stimulates profiles of macrophage activation in mice," *Neuroimmunomodulation*, vol. 6, no. 3, pp. 160–167, 1999.

[23] N. M. Appelman-Dijkstra, F. Malgo, K. J. Neelis, I. Coremans, N. R. Biermasz, and A. M. Pereira, "Pituitary dysfunction in adult patients after cranial irradiation for head and nasopharyngeal tumours," *Radiotherapy and Oncology*, vol. 113, no. 1, pp. 102–107, 2014.

[24] O. V. Belov, K. V. Belokopytova, A. S. Bazyan et al., "Exposure to 12C particles alters the normal dynamics of brain monoamine metabolism and behaviour in rats," *Physica Medica*, vol. 32, no. 9, pp. 1088–1094, 2016.

[25] D. L. Caudell, K. T. Michalson, R. N. Andrews et al., "Transcriptional profiling of non-human primate lymphoid organ responses to total-body irradiation," *Radiation Research*, vol. 192, no. 1, pp. 40–52, 2019.

[26] C. Tipton, J. Greenleaf, and C. Jackson, "Neuroendocrine and immune system responses with spaceflights," *Medicine & Science in Sports & Exercise*, vol. 28, no. 8, pp. 988–998, 1996.

[27] R. P. Stowe, D. L. Pierson, and A. D. T. Barrett, "Elevated stress hormone levels relate to Epstein-Barr virus reactivation in astronauts," *Psychosomatic Medicine*, vol. 63, no. 6, pp. 891–895, 2001.

[28] J. W. Armstrong, R. A. Gerren, and S. K. Chapes, "The effect of space and parabolic flight on macrophage hematopoiesis and function," *ExperimentaL Cell Research*, vol. 216, no. 1, pp. 160–168, 1995.

[29] X. W. Mao, N. C. Nishiyama, M. J. Pecaut et al., "Simulated microgravity and low-dose/low-dose-rate radiation induces oxidative damage in the mouse brain," *Radiation Research*, vol. 185no. 6, pp. 647–657, 2016.

[30] X. W. Mao, M. Boerma, D. Rodriguez et al., "Combined effects of low-dose proton radiation and simulated microgravity on the mouse retina and the hematopoietic system," *Radiation Research*, vol. 192, no. 3, pp. 241–250, 2019.

[31] P. Chowdhury, N. Akel, A. Jamshidi-Parsian et al., "Degenerative tissue responses to space-like radiation doses in a rodent model of simulated microgravity," *Annals of Clinical and Laboratory Science*, vol. 46, no. 2, pp. 190–197, 2016.

[32] B. Dang, Y. Yang, E. Zhang et al., "Simulated microgravity increases heavy ion radiation-induced apoptosis in human B lymphoblasts," *LIFE SCIENCES*, vol. 97, no. 2, pp. 123–128, 2014.

[33] M. Mognato, C. Girardi, S. Fabris, and L. Celotti, "DNA repair in modeled microgravity: Double strand break rejoining activity in human lymphocytes irradiated with γ-rays," *Mutation Research*, vol. 663, no. 1-2, pp. 32–39, 2009.

[34] X. W. Mao, N. C. Nishiyama, M. Campbell-Beachler et al., "Role of NADPH oxidase as a mediator of oxidative damage in low-dose irradiated and hindlimb-unloaded mice," *Radiation Research*, vol. 188, no. 4, pp. 392–399, 2017.

[35] N. Pecoraro, M. F. Dallman, J. P. Warne et al., "From Malthus to motive: how the HPA axis engineers the phenotype, yoking needs to wants," *Progress in Neurobiology*, vol. 79, no. 5-6, pp. 247–340, 2006.

[36] E. Ottaviani, A. Franchini, and S. Genedani, "ACTH and its role in immune-neuroendocrine functions. A comparative study," *Current Pharmaceutical Design*, vol. 5, no. 9, pp. 673–681, 1999.

[37] M. P. Yeager, C. A. Guyre, B. D. Sites, J. E. Collins, P. A. Pioli, and P. M. Guyre, "The stress hormone cortisol enhances Interferon-v–Mediated proinflammatory responses of human immune cells," *Anesthesia and Analgesia*, vol. 127, no. 2, pp. 556–563, 2018.

[38] C. Benou, Y. Wang, J. Imitola et al., "Corticotropin-releasing hormone contributes to the peripheral inflammatory response in experimental autoimmune encephalomyelitis," *Journal of Immunology*, vol. 174, no. 9, pp. 5407–5413, 2005.

[39] C. Baker, L. J. Richards, C. M. Dayan, and D. S. Jessop, "Corticotropin-releasing hormone immunoreactivity in human T

and B cells and macrophages: colocalization with arginine vasopressin," *Journal of Neuroendocrinology*, vol. 15, no. 11, pp. 1070–1074, 2003.

[40] W. C. Wang, X. Z. Zhang, D. W. Liu, J. Qiu, X. H. Wang, and J. H. Zhou, "Corticotropin-releasing hormone and urocortin promote phagocytosis of rat macrophages through convergent but distinct pathways," *Life Sciences*, vol. 122, pp. 100–107, 2015.

[41] L. Feng, X. F. Yue, Y. X. Chen et al., "LC/MS-based metabolomics strategy to assess the amelioration effects of ginseng total saponins on memory deficiency induced by simulated microgravity," *Journal of Pharmaceutical and Biomedical Analysis*, vol. 125, pp. 329–338, 2016.

[42] Y. F. Gao, X. L. Fan, Z. X. He, S. D. Wu, and X. A. Song, "Effects of Ligustrazine and Radix Astragali on activities of myosin adenosine triphosphatase of soleus muscle and muscle atrophy in tail-suspended rats," *Space Medicine & Medical Engineering (Beijing)*, vol. 18, no. 4, pp. 262–266, 2005.

[43] L. X. He, Z. F. Zhang, J. Zhao et al., "Ginseng oligopeptides protect against irradiation-induced immune dysfunction and intestinal injury," *Scientific Reports*, vol. 8, no. 1, p. 13916, 2018.

[44] J. Z. Song, S. F. Mo, Y. K. Yip, C. F. Qiao, Q. B. Han, and H. X. Xu, "Development of microwave assisted extraction for the simultaneous determination of isoflavonoids and saponins in radix astragali by high performance liquid chromatography," *Journal of Separation Science*, vol. 30, no. 6, pp. 819–824, 2007.

[45] S. Lee and D. K. Rhee, "Effects of ginseng on stress-related depression, anxiety, and the hypothalamic–pituitary–adrenal axis," *Journal of Ginseng Research*, vol. 41, no. 4, pp. 589–594, 2017.

[46] Y. Qi, F. Gao, L. Hou, and C. Wan, "Anti-inflammatory and immunostimulatory activities of astragalosides," *The American Journal of Chinese Medicine*, vol. 45, no. 6, pp. 1157–1167, 2017.

[47] X. Lu, W. Tong, S. Wang et al., "Comparison of the chemical consituents and immunomodulatory activity of ophiopogonis radix from two different producing areas," *Journal of Pharmaceutical and Biomedical Analysis*, vol. 134, pp. 60–70, 2017.

[48] N. Xia, J. Li, H. Wang, J. Wang, and Y. Wang, "Schisandra chinensis and Rhodiola rosea exert an anti-stress effect on the HPA axis and reduce hypothalamic c-Fos expression in rats subjected to repeated stress," *Experimental and Therapeutic Medicine*, vol. 11, no. 1, pp. 353–359, 2016.

[49] H. Zheng, S. Wang, P. Zhou, W. Liu, and F. Ni, "Effects of Ligustrazine on DNA damage and apoptosis induced by irradiation," *Environmental Toxicology and Pharmacology*, vol. 36, no. 3, pp. 1197–1206, 2013.

[50] L. M. Zhao, Y. L. Jia, M. Ma, Y. Q. Duan, and L. H. Liu, "Prevention effects of Schisandra polysaccharide on radiation-induced immune system dysfunction," *International Journal of Biological Macromolecules*, vol. 76, pp. 63–69, 2015.

[51] Y. Pu, Z. Liu, H. Tian, and Y. Bao, "The immunomodulatory effect of Poria cocos polysaccharides is mediated by the Ca2+/PKC/p38/NF-κB signaling pathway in macrophages," *International Immunopharmacology*, vol. 72, pp. 252–257, 2019.

[52] R. Zhang, J. Zhou, M. Li et al., "Ameliorating effect and potential mechanism of Rehmannia glutinosa oligosaccharides on the impaired glucose metabolism in chronic stress rats fed with high-fat diet," *Phytomedicine*, vol. 21, no. 5, pp. 607–614, 2014.

[53] S. Song, Z. Gao, X. Lei et al., "Total flavonoids of Drynariae Rhizoma prevent bone loss induced by hindlimb unloading in rats," *Molecules*, vol. 22, no. 7, p. 1033, 2017.

Retraction

Retracted: TRPM7 Upregulate the Activity of SMAD1 through PLC Signaling Way to Promote Osteogenesis of hBMSCs

BioMed Research International

This article has been retracted by Hindawi following an investigation undertaken by the publisher [1]. This investigation has uncovered evidence of one or more of the following indicators of systematic manipulation of the publication process:

(1) Discrepancies in scope

(2) Discrepancies in the description of the research reported

(3) Discrepancies between the availability of data and the research described

(4) Inappropriate citations

(5) Incoherent, meaningless and/or irrelevant content included in the article

(6) Manipulated or compromised peer review

The presence of these indicators undermines our confidence in the integrity of the article's content and we cannot, therefore, vouch for its reliability. Please note that this notice is intended solely to alert readers that the content of this article is unreliable. We have not investigated whether authors were aware of or involved in the systematic manipulation of the publication process.

Wiley and Hindawi regrets that the usual quality checks did not identify these issues before publication and have since put additional measures in place to safeguard research integrity.

We wish to credit our own Research Integrity and Research Publishing teams and anonymous and named external researchers and research integrity experts for contributing to this investigation.

The corresponding author, as the representative of all authors, has been given the opportunity to register their agreement or disagreement to this retraction. We have kept a record of any response received.

References

[1] F. Hong, S. Wu, C. Zhang et al., "TRPM7 Upregulate the Activity of SMAD1 through PLC Signaling Way to Promote Osteogenesis of hBMSCs," *BioMed Research International*, vol. 2020, Article ID 9458983, 23 pages, 2020.

Research Article

TRPM7 Upregulate the Activity of SMAD1 through PLC Signaling Way to Promote Osteogenesis of hBMSCs

Fanfan Hong,[1] Shali Wu,[1] Cui Zhang,[1] Liang Li,[1] Jianling Chen,[1] Yong Fu,[2] and Jinfu Wang ●[1,2]

[1]*Institute of Cell and Development Biology, College of Life Sciences, Zijingang Campus, Zhejiang University, Hangzhou, Zhejiang 310058, China*
[2]*Department of ENT, The Children's Hospital, Zhejiang University School of Medicine, National Clinical Research Center for Child Health, Hangzhou, Zhejiang, China*

Correspondence should be addressed to Jinfu Wang; wjfu@zju.edu.cn

TRPM7 is a member of the transient receptor potential cation channel (TRP channel) subfamily M and possesses both an ion channel domain and a functional serine/threonine α-kinase domain. It has been proven to play an essential role in the osteogenic differentiation of human bone marrow-derived mesenchymal stem cells (hBMSCs). However, the signaling pathway and molecular mechanism for TRPM7 in regulating osteogenic differentiation remain largely unknown. In this study, the potential role and mechanism of TRPM7 in the osteogenic differentiation of hBMSCs were investigated. The results showed that the expression of TRPM7 mRNA and protein increased, as did the osteogenic induction time. Upregulation or inhibition of TRPM7 could promote or inhibit the osteogenic differentiation of hBMSCs for 14 days. It was also found that the upregulation or inhibition of TRPM7 promoted or inhibited the activity of PLC and SMAD1, respectively, during osteogenic differentiation. PLC could promote osteogenic differentiation by upregulating the activity of SMAD1. However, inhibition of PLC alone could reduce the activity of SMAD1 but not inhibit completely the activation of SMAD1. Therefore, we inferred that it is an important signaling pathway for TRPM7 to upregulate the activity of SMAD1 through PLC and thereby promote the osteogenic differentiation of hBMSCs, but it is not a singular pathway. TRPM7 may also regulate the activation of SMAD1 through other ways, except for PLC, during osteogenic differentiation of hBMSCs.

1. Introduction

Bone marrow-derived mesenchymal stem cells (BMSCs) are a potential source of stem cells for tissue repair due to their multipotentials of differentiation into various specialized cells, including bone, fat, and muscular cells [1–4]. Among these potentials, the ability for differentiation into bone cells is widely studied. The osteogenic potential of BMSCs plays an important role in the equilibrium of bone substance. Some extreme environments, such as microgravity, play an important role in the osteogenic potential of BMSCs [5]. The differentiation of BMSCs into osteoblasts is a complex developmental process, and many signaling pathways participate in the regulation of osteogenic differentiation, such as Wnt signaling [6, 7], Hedgehog signaling, NELL-1 signaling [8],

BMP signaling [9–11], IGF signaling [12], growth hormone signaling [13], mitogen-activated protein kinase signaling (MAPKs) [14], and Notch signaling [15]. Zhang et al. [5] found that the space microgravity decreased the osteogenesis of human MSCs, which may be attributed to the decreased BMP expression and FAK activity. Here, focusing on another factor, a member of the transient receptor potential cation channel (TRP channel) subfamily M, TRPM7, which possesses both an ion channel domain and a functional serine/-threonine α-kinase domain [1, 2, 16–21], has been reported to be fundamental for murine MSC survival [2]. Previous studies also show that TRPM7 is important for bone formation [22]. However, little is known about the role of TRPM7-related signaling pathways in the osteogenic differentiation of human BMSCs (hBMSCs). Many studies have led to

the discovery of mechanosensitive ion channels and the identification of the physiological function of specific mechanosensitive ion channels [23]. TRPM7 has the constitutively active ion channel segment that is permeable to divalent cation Ca2+ and mediates the Ca2+ influx. Previous studies have demonstrated that the TRPM7 kinase domain interacts with phospholipase C (PLC, also known as heparan sulfate proteoglycan 2 (HSPG2)) [24] which can hydrolyse phosphatidylinositol 4,5-bisphosphate (PIP2) to produce inositol trisphosphate (IP3) and activate the IP3 receptor to further trigger Ca2+ release from IP3R2. Calcium functions as a second messenger to support bone remodeling and plays a vital role in the osteogenic differentiation of mesenchymal stem cells [16, 25–28]. Ca2+ signaling is mediated mainly by the Ca2+ binding protein calmodulin (CaM). CaM binds Ca2+ and activates various target proteins including calmodulin-dependent protein kinases (CaMKs). CaMK II is the major target of CaM and plays essential roles in the regulation of osteoblast differentiation [25, 29]. It has been reported that Ca2+ binds to calmodulin (CaM) and activates CaMK II in C3H10T1/2 and hBMSCs. Activated CaMK II can then phosphorylate SMAD1, inducing its translocation to the nucleus where it activates osteogenic target genes such as RUNX2, Osterix, and OCN [30]. Meanwhile, it has been reported that PLC regulates the TGF-β-induced chondrogenic differentiation of synovial mesenchymal cells via SMAD 2 and p38 MAPK signaling pathways [31]. It was also showed that BFP- (bone-forming peptide-) 3 plays a vital role in increasing the levels of osteogenic-inducing factors and regulating the ERK1/2 and SMAD1/5/8 signaling pathways in the process of regulating osteogenic differentiation of BMSCs [32]. Studies revealed that CREBH (cAMP response element-binding protein H) increased the expression of SMAD ubiquitination regulatory factor 1 (Smurf1), leading to ubiquitin-dependent degradation of SMAD1. Meanwhile, it was suggested that CREBH is a novel negative regulator of osteoblast differentiation and bone formation [33]. Here, we examine the expression of TRPM7 during the osteogenic differentiation of hBMSCs and the role of TRPM7 in the osteogenic differentiation of hBMSCs by inhibiting or promoting the activation of TRPM7 under normal gravity. We also investigate the role of PLC in the osteogenic differentiation of hBMSCs by regulating the activity of PLC. Through a series of regulation combinations of TRPM7 and PLC, we explore the relationship between TRPM7, PLC, and SMAD1 during the osteogenic differentiation of hBMSCs and found that TRPM7 might regulate the activation of SMAD1 through different pathways (not only PLC) to promote the osteogenic differentiation of hBMSCs. This study may be contributed to the researches on the effects of space microgravity on the ion channels in hBMSCs, which will be performed in the Space Station of China.

2. Materials and Methods

2.1. Preparation and Culture of hBMSCs.
The Institutional Review Board (IRB) and Ethical Committee of Zhejiang University, Hangzhou, China, approved this study. Whole-bone marrow samples were collected from healthy donors at the First Affiliated Hospital, Zhejiang University. All donors provided the written informed consent. Bone marrow cells were isolated and purified from bone marrow according to the methods of Zhang et al. [3]. The harvested cells were seeded in a 10 cm dish with α-MEM culture medium (Gibco, Shanghai, China) supplemented with 10% FBS, 100 U/mL penicillin, 100 μg/mL streptomycin (Gibco), and 5 ng/mL basic fibroblast growth factor (BFGF; Life Technologies, Shanghai, China) and cultured at 37°C, 5% CO_2, and 95% humidity. Cells at approximately 80% confluency were trypsinized and reseeded at a density of 1×10^5 cells/mL as passage 1. Cells at passage 3 were used for this study. These cells were characterized by surface markers CD19−, CD34−, CD14−, CD45−, HLA-DR−, CD105+, CD90+, CD73+, and CD29+ and showed the potentials of osteogenesis and adipogenesis.

2.2. shRNA-Mediated Knockdown of TRPM7 in hBMSCs.
shRNA with sequences targeting human TRPM7 mRNA was transfected into hBMSCs according to the manufacturer's instructions (Invitrogen, Shanghai, China). In brief, 30 nM of the shRNA fragment for TRPM7 (sense: 5′-GCA GTT CAT CTA CTA GCA TAC-3′ and antisense: 5′-CGT CAA GTA GAT GAT CGT ATG-3′) or the negative control fragment (sense: 5′-GCA CCCAGTCCGCCCTGAGCA-3′ and antisense: 5′-CGT GGG TCA GGG ACG CGT-3′) was designed and ligated to pRNAi-U6.2/Lenti-vector to construct the target plasmid. Then, the target plasmid and two lentiviral packaging plasmids (PSPAX2 and PMD2G) were cotransfected into 293T cells using Lipofectamine™ 3000 (Invitrogen). After 48 and 72 h, the virus supernatant was collected to infect hBMSCs with 60% confluency at passage 3. Cells transfected with the target plasmid exhibited RFP expression. All experiments were performed in triplicate.

2.3. Osteogenic Induction of hBMSCs.
When the cells at passage 3 reached 60-70% confluency, the osteogenic medium (Dulbecco's modified Eagle's medium (DMEM; Life Technologies)) supplemented with 10% FBS, 50 μg/mL L-ascorbic acid, 10 mM β-glycerophosphate, 0.1 μM dexamethasone, 100 U/mL penicillin, and 100 μg/mL streptomycin (Sigma, Shanghai, China) was used to replace the culture medium, and cells were incubated at 37°C and 5% CO_2 to induce the osteogenic differentiation of hBMSCs. 2-APB was used to inhibit mRNA and protein expression [34] and the function of TRPM7 [35, 36] in this study. Naltriben, a TRPM7-specific agonist, was used to activate the expression of TRPM7 [1, 37, 38]. U73122 or M-3M3FBS was reported to inhibit and induce the mRNA expression [39, 40] and protein expression [41] of PLC.

The osteogenic induction experiment of hBMSCs was divided into 7 groups: cells induced in the osteogenic medium supplemented with 50 μM 2-APB (APEXBIO, Shanghai, China) as the 2-APB group, cells induced in the osteogenic medium supplemented with 20 μM Naltriben (Meilunbio, Dalian, China) as the Naltriben group, cells induced in the osteogenic medium supplemented with 20 μM M-3M3FBS (Sigma) as the M-3M3FBS group, cells

Table 1: Primer sequences of real-time PCR.

Gene	Primer sequences	Product size (bp)
RUN2	5′-CCGCCTCAGTGATTTAGGGC-3′ (F) 5′-GGGTCTGTAATCTGACTCTGTCC-3′ (R)	132
ALP	5′-AACATCAGGGACATTGACGTG-3′ (F) 5′-GTATCTCGGTTTGAAGCTCTTCC-3′ (R)	159
COL1A1	5′-GTGCGATGACGTGATCTGTGA-3′ (F) 5′-CGGTGGTTTCTTGGTCGGT-3′ (R)	119
OPN	5′-CTCCATTGACTCGAACGACTC-3′ (F) 5′-CAGGTCTGCGAAACTTCTTAGAT-3′ (R)	230
OCN	5′-GGCGCTACCTGTATCAATGG-3′ (F) 5′-GTGGTCAGCCAACTCGTCA-3′ (R)	110
TRMP7	5′-GTTGGAAAGTATGGGGCGGAA-3′ (F) 5′-CACACACAACTACTGGAACAGG-3′ (R)	190
GADPH	5′-GGAGCGAGATCCCTCCAAAAT-3′ (F) 5′-GGCTGTTGTCATACTTCTCATGG-3′ (R)	197

induced in the osteogenic medium supplemented with $1\,\mu$M U73122 (MCE, Shanghai, China) as the U73122 group, cells induced in the osteogenic medium supplemented with $50\,\mu$M 2-APB and $20\,\mu$M M-3M3FBS as the 2-APB+M-3M3FBS group, cells induced in the osteogenic medium supplemented with $20\,\mu$M Naltriben and $1\,\mu$M U73122 as the Naltriben+U73122 group, and cells induced in the osteogenic medium without any pharmacological treatment as the control group. The osteogenic medium was changed every three days, and cells were harvested after an induction of 14 days for the following analyses.

2.4. Whole-Cell Protein Extraction and Western Blot Analysis. Cells were lysed by sonication with ice-cold lysis buffer containing RIAP protein lysate and a phosphatase inhibitor. A bovine serum albumin (BSA) protein assay kit (Beyotime, Shanghai, China) was used to detect the protein concentrations. The protein sample was separated on a 10% sodium dodecyl sulfate-polyacrylamide gel electrophoresis (SDS-PAGE) and then transferred onto a $4.5\,\mu$M PVDF membrane (Millipore, Shanghai, China). The membrane was blocked with 5% nonfat milk PBST and then incubated with anti-TRPM7 (1:1500), anti-PLC (1:1500), anti-P-PLC (1:1500), anti-SMAD1 (1:1500), anti-P-SMAD1 (1:1500), anti-COL1A1 (1:1500), anti-ALP (1:1500), anti-RUNX2 (1:1500), and anti-GADPH (1:2000) antibodies at 4°C overnight. Antibodies to PLC, Phospho-PLC, SMAD1, Phospho-SMAD1, RUNX2, COL1A1, and GADPH were purchased from Cell Signaling (Shanghai, China). The TRPM7 antibody was purchased from Abcam (Shanghai, China). After incubation, the membrane was reprobed with the appropriate secondary antibodies (conjugated with horseradish peroxidase) for 1 h. The enhanced chemiluminescence detection reagent (Thermo Scientific, Shanghai, China) and the Tanon 6600 Luminescence Imaging Workstation (Tanon, China) were used to visualize the protein bands. Western blot images were semiquantitatively analyzed with ImageJ software (NIH, USA).

2.5. Alkaline Phosphate (ALP) and Alizarin Red S (ARS) Staining Assays. Cells osteogenically induced for 14 days were washed with precooled PBS for three times before being stained with ARS to examine the matrix concentrations of calcium according to a previously described procedure [3]. The ALP Quantitative Analysis Kit (Beyotime, Shanghai, China) was used to analyze the ALP activity in cells according to the manufacturer's instructions. Definition of the ALP activity unit is as follows: hydrolysis of para-nitrophenyl (unit: μmol) per minute at 37°C in a diacetamine (DEA) buffer pH 9.8. The absorbance was measured at 405 nm. ALP staining was performed using the Gomori Staining Kit (Nanjing Jiancheng Institute, China). Finally, the samples were washed with deionized water and visualized by phase microscopy using an inverted microscope. ARS reverse quantification was by stain extraction, and the absorbance was measured at 405 nm.

2.6. Quantitative Real-Time Polymerase Chain Reaction (PCR) Assays. The TRIzol reagent (Sigma) was used to exact RNA. Reverse transcription was performed using $1\,\mu$g of total RNA and the RevertAid First Strand cDNA Synthesis Kit (Fermentas, Shanghai, China). Primers were designed as shown in Table 1. Quantitative real-time PCR reactions were performed as previously described [3]. The PCR conditions were 95°C for 5 min, followed by 40 cycles of 95°C for 15 s, 60°C for 1 min, then 72°C for 1 min, and finally 72°C for 10 min. The expression level of each gene was analyzed through the $2-\Delta\Delta$Ct method [42] and normalized to that of GAPDH.

2.7. Statistical Analyses. Data are presented as mean values ± standard deviation (SD). Statistical analysis was performed using GraphPad Prism statistical software. Statistical significance determined using Student's t-test or two-way analysis of variance followed by post hoc Bonferroni correction was set at $^{*}P < 0.05$, $^{**}P < 0.01$, and $^{***}P < 0.001$.

A

B

(a)

(b)

A

B

(c)

(d)

Figure 1: Continued.

(e)

(f)

(g)

FIGURE 1: Continued.

(h)

(i)

(j)
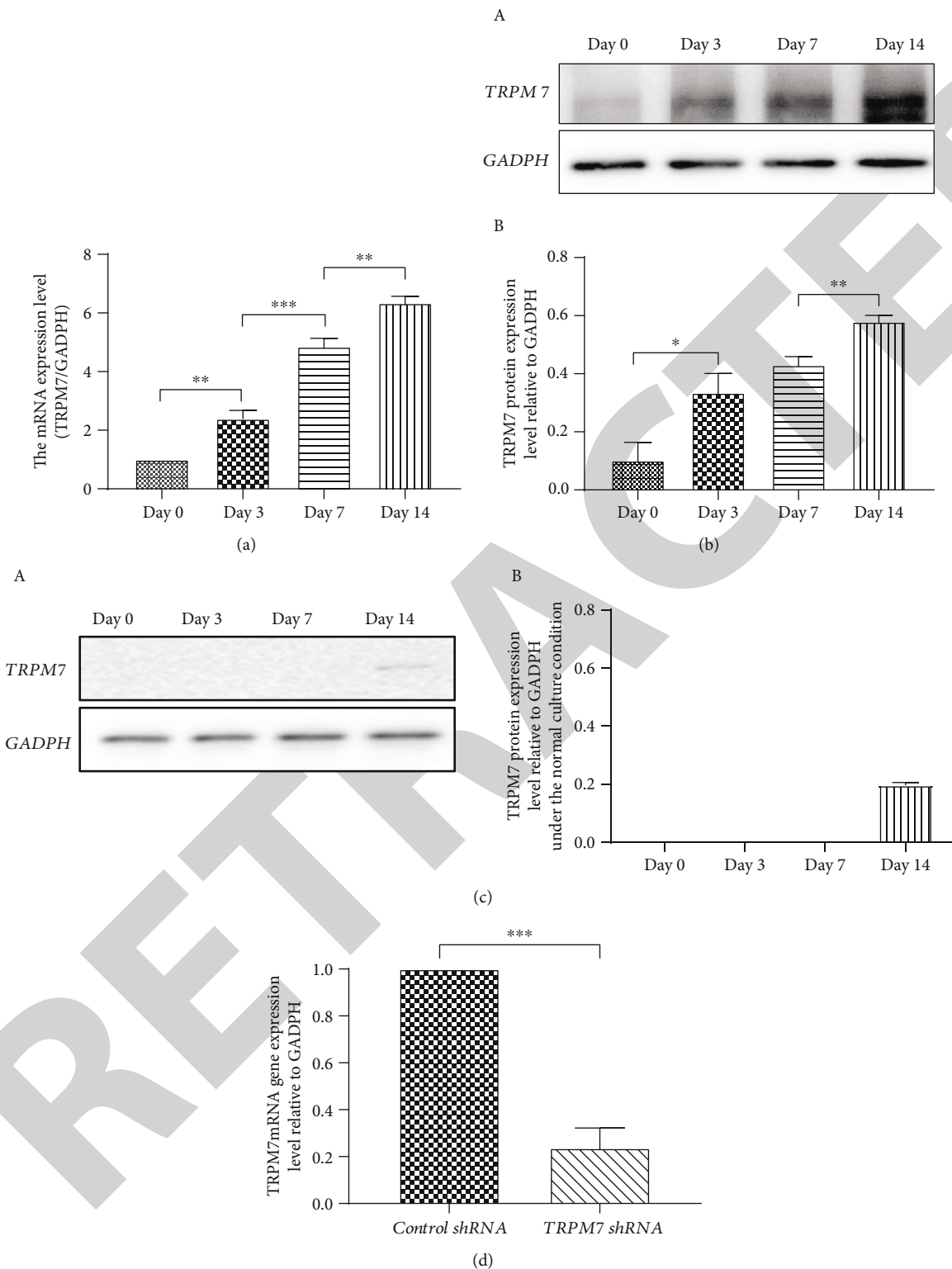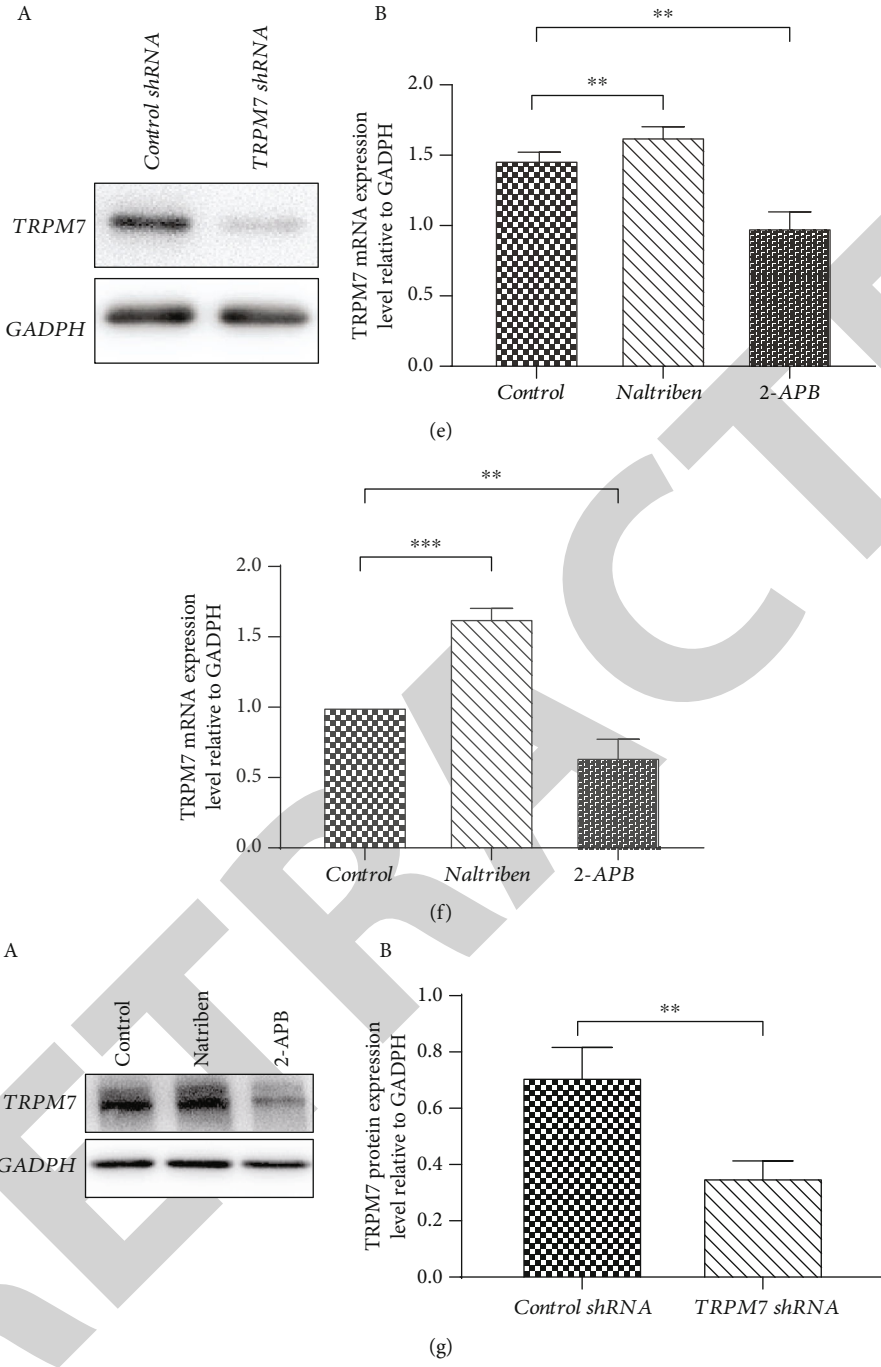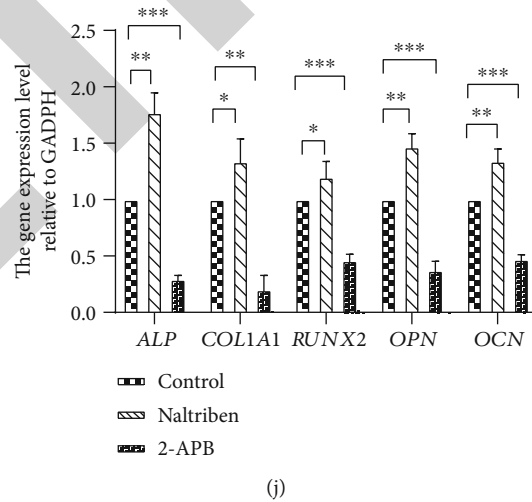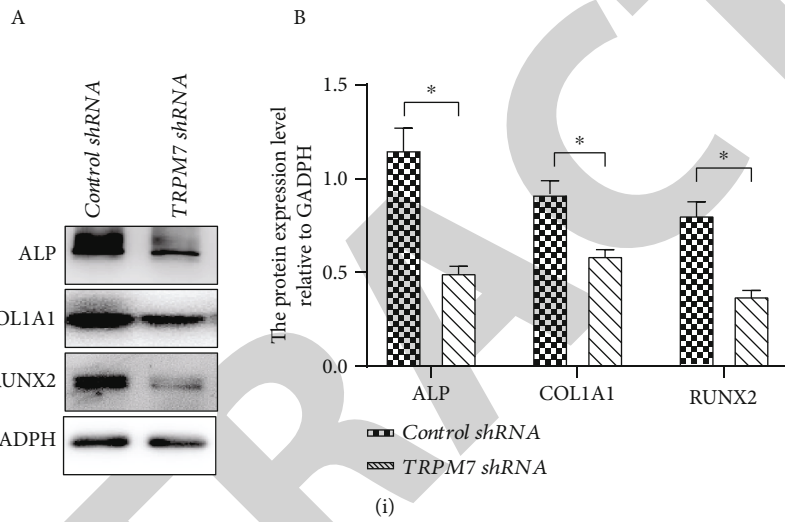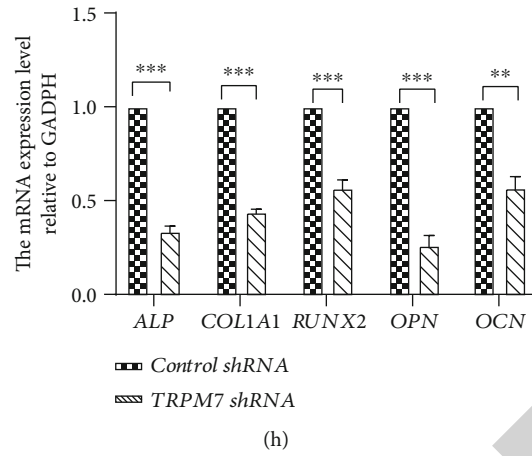
Figure 1: Continued.
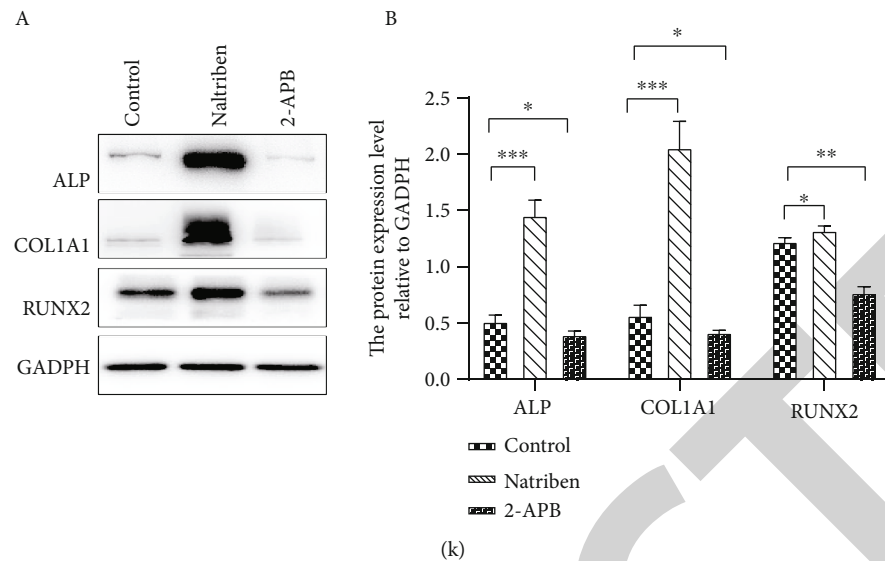
Figure 1: The effects of TRPM7 on the expression of osteogenic markers. (a) The expression of TRPM7 mRNA in cells induced for 0, 3, 7, and 14 days. (b) (A) The expression of TRPM7 protein in cells induced for 0, 3, 7, and 14 days. (B) Relative expression levels of TRPM7 protein were quantified and plotted. (c) (A) The expression of TRPM7 protein in cells noninduced for 0, 3, 7, and 14 days. (B) Relative expression levels of TRPM7 protein were quantified and plotted. (d) The expression of TRPM7 mRNA in cells treated with TRPM7 shRNA and control shRNA induced for 14 days. (e) The expression of TRPM7 protein in cells treated with TRPM7 shRNA and control shRNA induced for 14 days. The relative expression levels of TRPM7 protein were quantified and plotted. (f) The expression of TRPM7 mRNA in cells induced with the osteogenic medium or the osteogenic medium supplemented with Naltriben or 2-APB induced for 14 days. (g) (A) Western blot analysis of TRPM7 protein in cells induced with the osteogenic medium or the osteogenic medium supplemented with Naltriben or 2-APB. (B) The relative expression levels of TRPM7 protein were quantified and plotted. (h) The expression of osteogenic markers ALP, COL1A1, RUNX2, OPN, and OCN in cells treated with TRPM7 shRNA and control shRNA induced for 14 days. (i) (A)Western blot analysis of osteogenic marker proteins ALP, COL1A1, and RUNX2 in cells treated with TRPM7 shRNA and control shRNA. (B) Relative protein expression levels of osteogenic markers were quantified and plotted. (j) The expression of osteogenic markers ALP, COL1A1, RUNX2, OPN, and OCN in cells induced with osteogenic medium or osteogenic medium supplemented with Naltriben or 2-APB induced for 14 days. (k) (A) Western blot analysis of osteogenic marker proteins ALP, COL1A1, and RUNX2 in cells induced with osteogenic medium or osteogenic medium supplemented with Naltriben or 2-APB. (B) Relative protein expression levels of osteogenic markers were quantified and plotted. TRPM7 shRNA: hBMSCs transfected with TRPM7-shRNA-vector; control shRNA: hBMSCs transfected with negative control-shRNA-vector; $*P < 0.05$, $**P < 0.01$, and $***P < 0.0001$.

3. Results

3.1. TRPM7 Plays an Important Role in Osteogenic Differentiation in hBMSCs.
It has been reported that TRPM7 is fundamental for murine MSC survival [2] and plays an important role in osteogenic differentiation [16]. Hence, we examined the expression pattern of TRPM7 during osteogenic induction of hBMSCs. We measured the mRNA and protein levels of TRPM7 in different stages of osteogenic differentiation. The expression of TRPM7 mRNA and protein increased gradually from day 0 to 14 and reached their peaks at day 14 of osteogenic induction (Figures 1(a) and 1(b)). The expression of TRPM7 protein is little from day 0 to 14 without osteogenic induction (Figure 1(c)). Hence, detection was mainly done during the osteogenic differentiation. The mRNA and protein levels of ALP, RUNX2, and COL1A1, as well as the ALP staining and ARS mineralization assays in different stages of osteogenic differentiation, were undertaken to examine the osteogenic differentiation effect in induced cells for 0, 3, 7, and 14 days (Figure S1 A-F).

In our initial exploratory experiments, the time period during osteogenesis induction was 0, 3, 7, and 14 days. Multiple experiments showed that the highest expression of

TRPM7 was on the 14th day. Hence, we decided to perform the following experiment on the 14th day of the induction time. These results indicated that TRPM7 is expressed throughout osteogenic differentiation, and its expression level increases with an increase in induction time, which may imply the important role of TRPM7 in the osteogenic differentiation of hBMSCs.

To verify this role of TRPM7, hBMSCs were transfected transiently with shRNA specific to TRPM7 and control-shRNA-vector. Meanwhile, the pharmacological blocking or activating of TRPM7 to the effect of relative osteogenic markers was performed during osteogenic induction for 14 days. 2-APB was used to inhibit mRNA and protein expression [34] and the function of TRPM7 [35, 36, 43], and Naltriben, a TRPM7-specific agonist, was used to activate the expression of TRPM7 [1, 37, 38]. The expression of the TRPM7 gene and protein in cells treated with TRPM7 shRNA, 2-APB, and Naltriben was measured in Figures 1(d)–1(g). After osteogenic induction for 14 days, the expression of three osteogenic marker proteins, alkaline phosphatase (ALP), collagen type 1 alpha 1 chain (COL1A1), and runt-related transcription factor 2 (RUNX2) as well as five osteogenic marker mRNAs, ALP, COL1A1, RUNX2, osteopontin (OPN), and

(a)

(b)

(c)

(d)

(e)

(f)
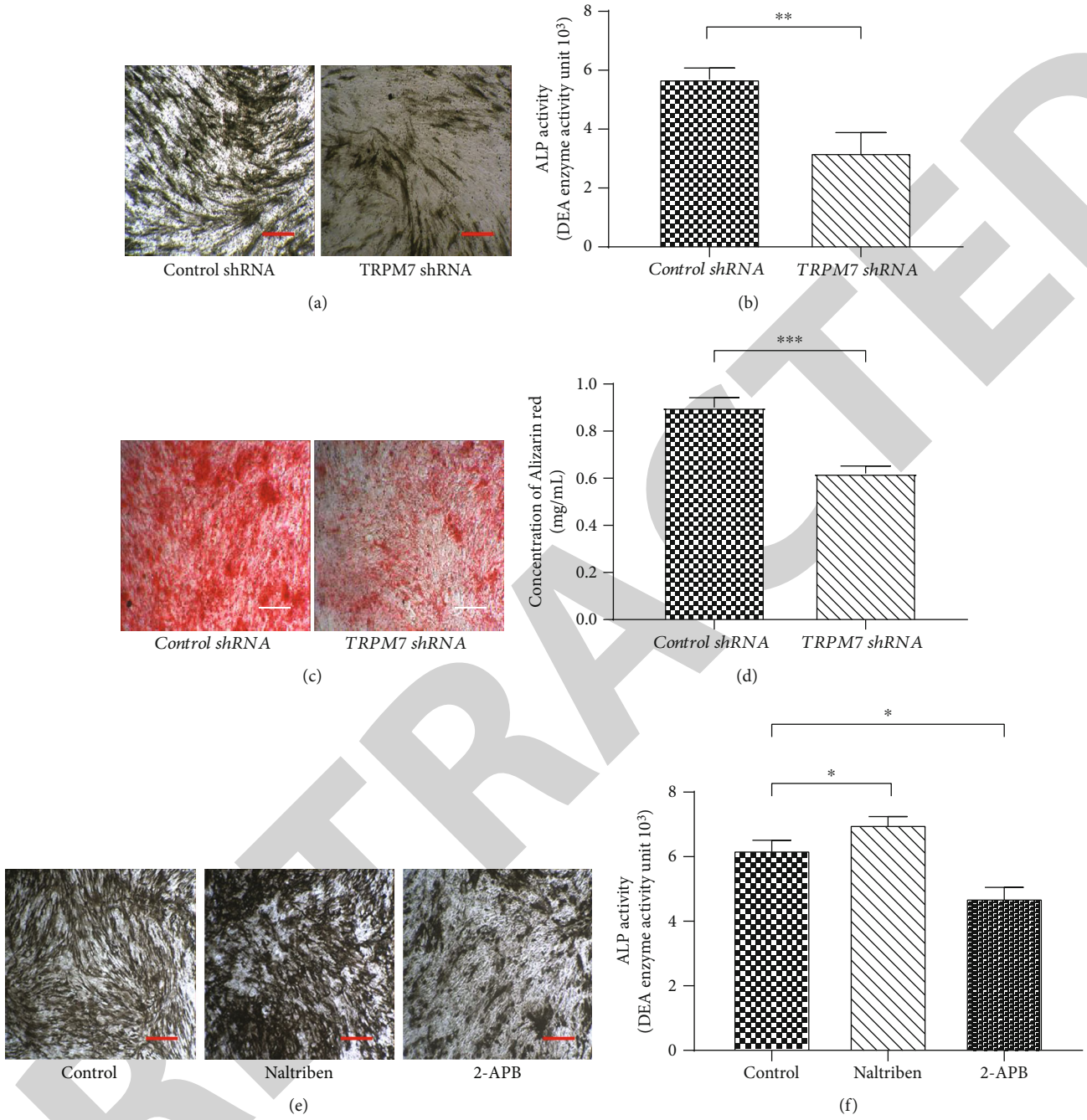
FIGURE 2: Continued.

(g)

(h)
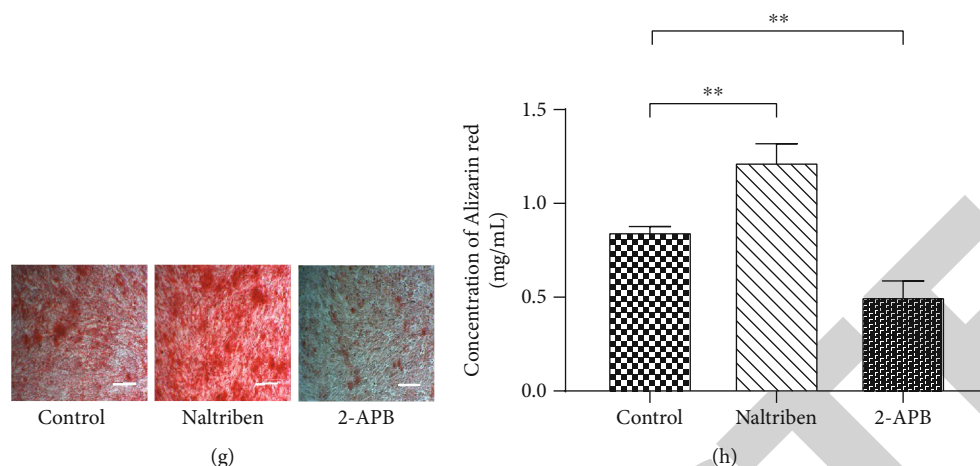
FIGURE 2: The effects of TRPM7 on the osteogenic differentiation in hBMSCs. (a) Analysis of ALP staining in cells treated with control shRNA and TRPM7 shRNA induced for 14 days. (b) Analysis of ALP activity (the unit for p-nitrophenyl: μmol) in cells treated with control shRNA and TRPM7 shRNA induced for 14 days. (c) Analysis of ARS staining in cells treated with control shRNA and TRPM7 shRNA induced for 14 days. (d) A quantification of ARS in cells treated with control shRNA and TRPM7 shRNA induced for 14 days. (e) Analysis of ALP staining in cells induced with osteogenic medium or osteogenic medium supplemented with Naltriben or 2-APB induced for 14 days. (f) Analysis of ALP activity (the unit for p-nitrophenyl: μmol) in cells induced with osteogenic medium or osteogenic medium supplemented with Naltriben or 2-APB induced for 14 days. (g) Analysis of ARS staining in cells induced with osteogenic medium or osteogenic medium supplemented with Naltriben or 2-APB induced for 14 days. (h) A quantification of ARS in cells induced with osteogenic medium or osteogenic medium supplemented with Naltriben or 2-APB induced for 14 days. Scale: 200 μm. $^*P < 0.05$, $^{**}P < 0.01$, and $^{***}P < 0.0001$.

osteocalcin (OCN), was detected. The results showed that the shRNA-mediated knockdown of TRPM7 inhibited the expression of both osteogenic marker genes and proteins (Figures 1(h) and 1(i)). Likewise, the use of 2-APB decreased the expression of both marker genes and proteins, and Naltriben promoted the osteogenic differentiation of hBMSCs (Figures 1(j) and 1(k)). Alkaline phosphatase (ALP) functional assays were used to examine ALP activity. Alkaline phosphatase staining and Alizarin red staining were used to examine matrix concentration of calcium and phosphate (Figures 2(a)–2(h)). Both shRNA-mediated knockdown of TRPM7 and use of 2-APB decreased ALP activity and mineralization in induced cells. In contrast, the use of Naltriben increased ALP activity and mineralization. These results verify that TRPM7 indeed plays an important role in the osteogenic differentiation of hBMSCs.

3.2. TRPM7 Promotes the Osteogenic Differentiation of hBMSCs by Regulating the Activity of PLC. It has been reported that TRPM7-associated PLC isozymes interact with the TRPM7 self-phosphorylating α-type Ser/Thr protein kinase domains which modulate the phosphorylation of PLC [19, 37]. Hence, we examined the activity of PLC in cells induced for 0, 3, 7, and 14 days. The activity of PLC increased with increasing induction time (Figure 3(a)), showing a similar pattern to the expression of TRPM7. As the same time, we detected the activity of PLC without the osteogenic differentiation for 0, 3, 7, and 14 days (Figure 3(b)). To investigate the function of PLC in the osteogenic differentiation of hBMSCs, we used the pharmacological method to inhibit or activate the activity of PLC. M-3M3FBS was used as a specific PLC activator and U73122 as an inhibitor of PLC. After pharmacologic treatment, we found that M-3M3FBS

increased PLC activity and promoted the osteogenic differentiation of hBMSCs by increasing the main osteogenic markers, and U73122 decreased the PLC activity and reduced the osteogenic differentiation of hBMSCs by decreasing the main osteogenic markers (Figures 3(c)–3(i)$P < 0.05$). Consequently, we analyzed the relationship between TRPM7 and PLC by inhibiting or promoting the expression of TRPM7. The shRNA-mediated knockdown of TRPM7 and the use of 2-APB inhibited the activity of PLC. Likewise, Naltriben promoted the activity of PLC (Figures 4(a) and 4(b)). To better explore the function of TRPM7 in the regulation of PLC activity during the osteogenic differentiation of hBMSCs, we adopted the method of activating TRPM7 and suppressing PLC or suppressing TRPM7 and activating PLC. The experiment was designed involving seven groups, as described in Materials and Methods. When PLC was activated with M-3M3FBS during both the inhibition and uninhibition of TRPM7 activity, the use of M-3M3FBS alone effectively promoted the expression of osteogenic markers in induced cells, and the use of 2-APB alone effectively inhibited the expression of osteogenic markers in induced cells. When inhibiting the activity of TRPM7 with 2-APB, the use of M-3M3FBS increased the expression of osteogenic markers in induced cells in comparison with the use of 2-APB alone, but this was lower than when using M-3M3FBS alone (Figures 4(c) and 4(d)$P < 0.05$). Alkaline phosphatase (ALP) functional assays and ALP staining and ARS mineralization assays were undertaken to examine the activity of ALP and the matrix concentrations of calcium and phosphate in induced cells (Figures 4(e)–4(h)). The results were consistent with the expression of osteogenic markers. Meanwhile, we inhibited the activity of PLC with U73122 under both the activation and inactivation of

(a)

(b)

(c)

Figure 3: Continued.

(d)

(e)

(f)

(g)

Figure 3: Continued.

(h)   (i)
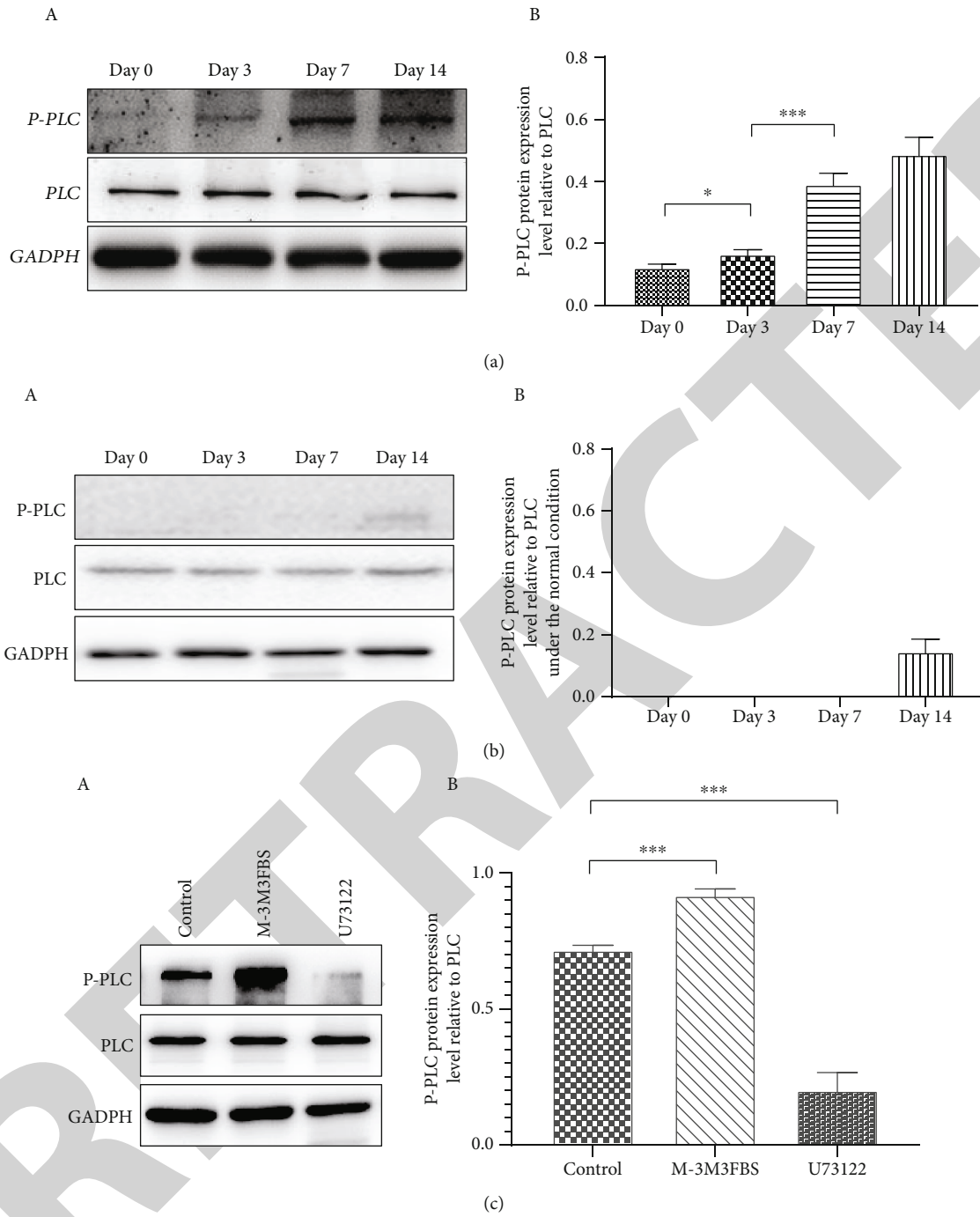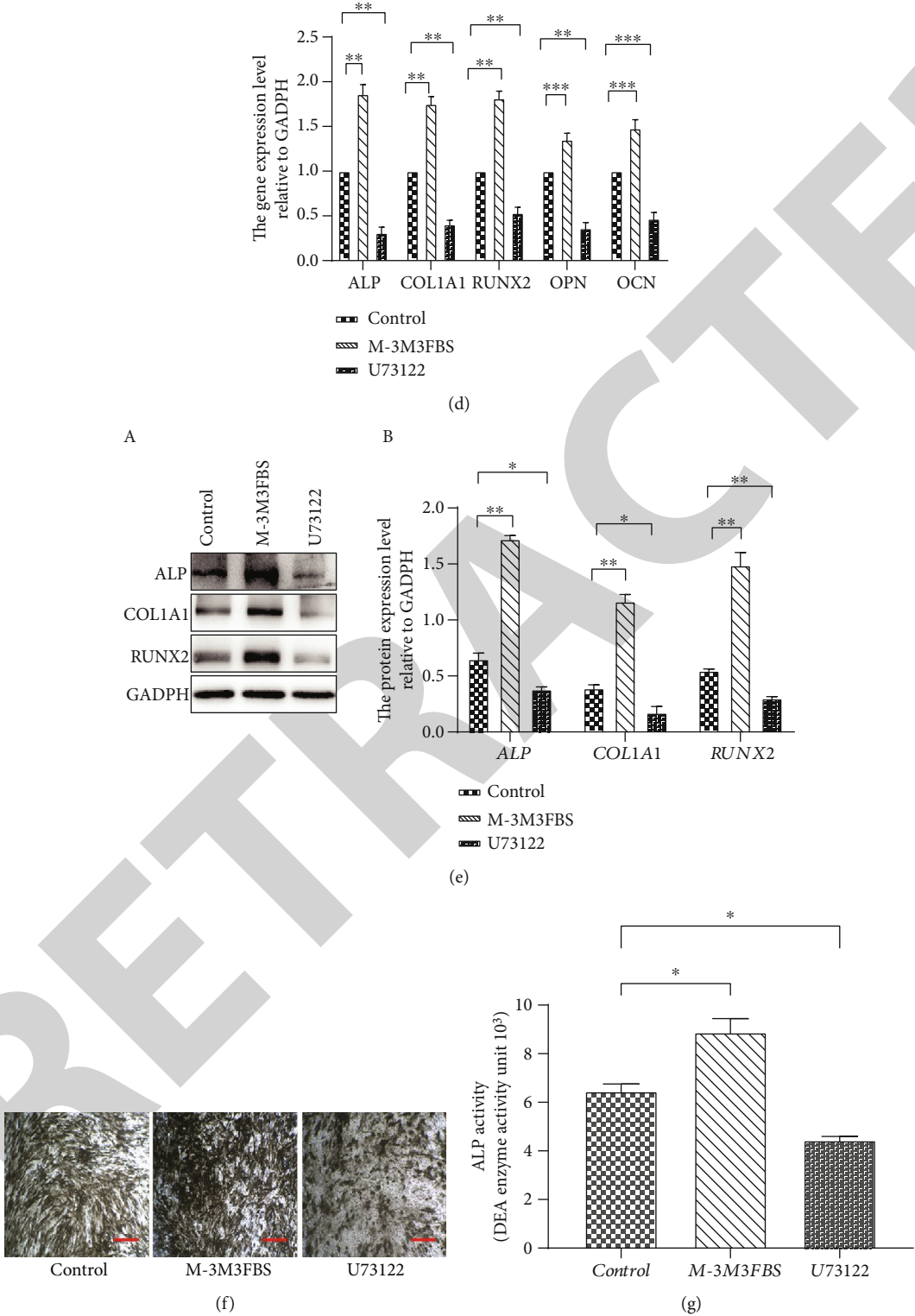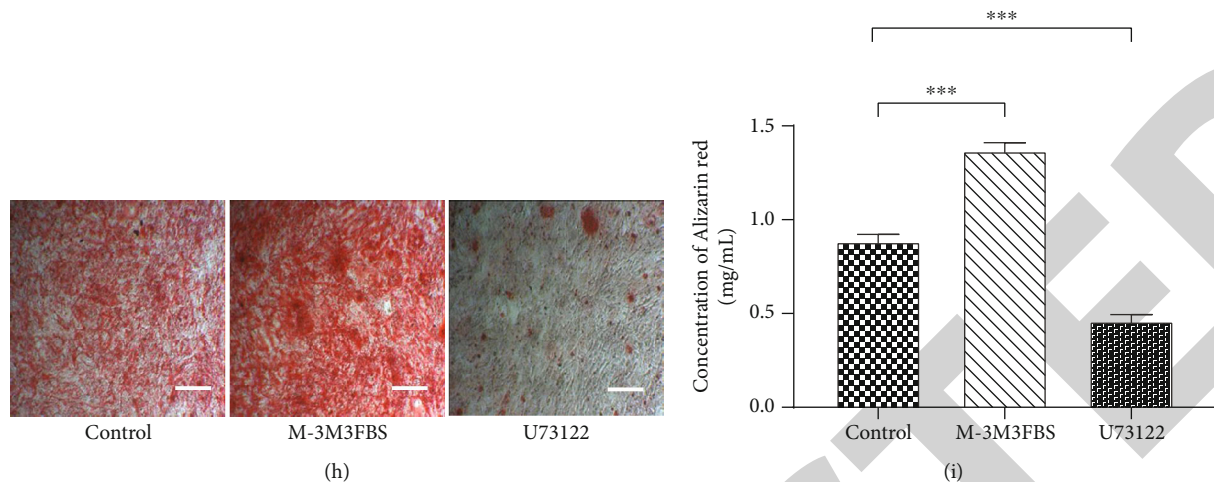
Figure 3: The effects of PLC (HSPG2) on the osteogenic differentiation of hBMSCs. (a) (A)The activity of PLC protein in cells induced with osteogenic medium for 0, 3, 7, and 14 days. (B) The relative activity of PLC protein was quantified and plotted. (b) (A) The expression of P-PLC protein in cells noninduced for 0, 3, 7, and 14 days. (B) Relative expression levels of P-PLC protein were quantified and plotted. (c) (A) Western blot analysis of PLC in cells induced with osteogenic medium or osteogenic medium supplemented with M-3M3FBS or U73122 induced for 14 days. (B) The relative activity of PLC protein was quantified and plotted. (d) RT-PCR analysis of osteogenic markers ALP, COL1A1, RUNX2, OPN, and OCN in cells induced with osteogenic medium or osteogenic medium supplemented with M-3M3FBS or U73122 induced for14 days. (e) (A) Western blot analysis of osteogenic marker proteins ALP, COL1A1, and RUNX2 in cells induced with osteogenic medium or osteogenic medium supplemented with M-3M3FBS or U73122 induced for 14 days. (B) The relative levels of osteogenic marker proteins were quantified and plotted. (f) Analysis of ALP staining in cells induced with osteogenic medium or osteogenic medium supplemented with M-3M3FBS or U73122 induced for 14 days. (g) Analysis of ALP activity (the unit for p-nitrophenyl: μmol) in cells induced with osteogenic medium or osteogenic medium supplemented with M-3M3FBS or U73122 induced for 14 days. (h) Analysis of ARS staining in cells induced with osteogenic medium or osteogenic medium supplemented with M-3M3FBS or U73122 induced for 14 days. (i) A quantification of ARS in cells induced with osteogenic medium or osteogenic medium supplemented with M-3M3FBS or U73122 induced for 14 days. Scale: 200 μm. $^{*}P < 0.05$, $^{**}P < 0.01$, and $^{***}P < 0.0001$.

TRPM7. As seen in Figures 5(a) and 5(b), the use of Naltriben alone effectively promoted the expression of osteogenic markers in induced cells. The use of U73122 alone effectively inhibited the expression of osteogenic markers in induced cells ($P < 0.05$). A combination of Naltriben and U73122 increased the expression of osteogenic markers in induced cells, in comparison to the use of U73122 alone. However, this was lower than the use of Naltriben alone. The analysis of ALP activity, ALP staining, and ARS mineralization also confirmed these results (Figures 5(c)–5(f)). Therefore, we infer that the pathway of TRPM7 promoting the expression of osteogenic markers through regulating the activity of PLC might be one of the important signaling pathways involved in the osteogenic differentiation of hBMSCs. However, these results also imply that the pathway of TRPM7 through PLC to regulate the osteogenic differentiation of hBMSCs is not a singular pathway.

3.3. The Activation of SMAD1 Is an Important Node of the TRPM7 Signaling Pathway for the Osteogenic Differentiation of hBMSCs. It has been reported that the TGF-β1-mediated activation of SMAD signaling increases the expression of TRPM7, which in turn phosphorylates SMAD proteins and ultimately contributes to collagen production and hepatic fibrosis [44]. Hence, this study examines the activity of SMAD1 in cells induced for 0, 3, 7, and 14 days. The activity of SMAD1 increased gradually with increasing induction time (Figure 6(a)), also showing a similar pattern to that of

the expression of TRPM7. At the same time, we detected the activity of SMAD1 in cells without induction for 0, 3, 7, and 14 days (Figure 6(b)). To examine whether TRPM7 promotes the osteogenic differentiation of hBMSCs through the activation of SMAD1, the activity of SMAD1 in induced cells was analyzed, as seen in Figures 6(c) and 6(d). Both the shRNA-mediated knockdown of TRPM7 and the use of 2-APB inhibited the activity of SMAD1. Naltriben upregulated the activity of SMAD1. These results indicate that TRPM7 may promote the osteogenic differentiation of hBMSCs by regulating the activity of SMAD1. The activity of SMAD1 was also analyzed under PLC-activated and PLC-inhibited conditions. M-3M3FBS upregulated the activity of SMAD1 while U73122 downregulated the activity of SMAD1 ($P < 0.05$) (Figure 6(e)). These results suggest that PLC may play an important role in the TRPM7-mediated activation of SMAD1. To examine the relationship between TRPM7, PLC, and SMAD1, the activity of SMAD1 was detected under different pharmacological treatments. As seen in Figure 6(f), the combination of Naltriben and U73122 decreased the activity of SMAD1 in induced cells, in comparison with the use of Naltriben alone but was higher than the use of U73122 alone ($P < 0.05$). Similarly, the combination of 2-APB and M-3M3FBS increased the activity of SMAD1 in induced cells in comparison with the use of 2-APB alone but was lower than the use of M-3M3FBS alone (Figure 6(g)) ($P < 0.05$). The results show that the activation of SMAD1 is an important node of the TRPM7

Figure 4: Continued.

A

B

(d)

Control   M-3M3FBS   2-APB+M-3M3FBS   2-APB

(e)

(f)

Figure 4: Continued.

(g)

(h)
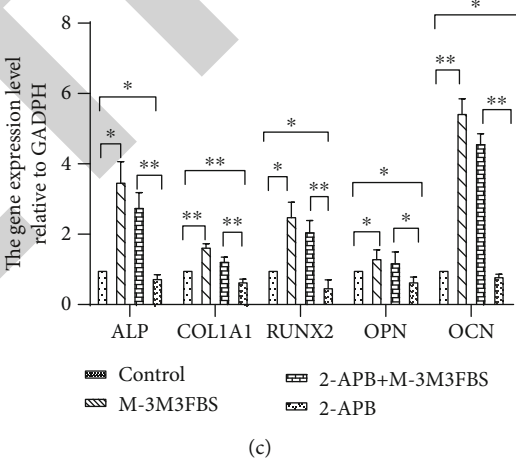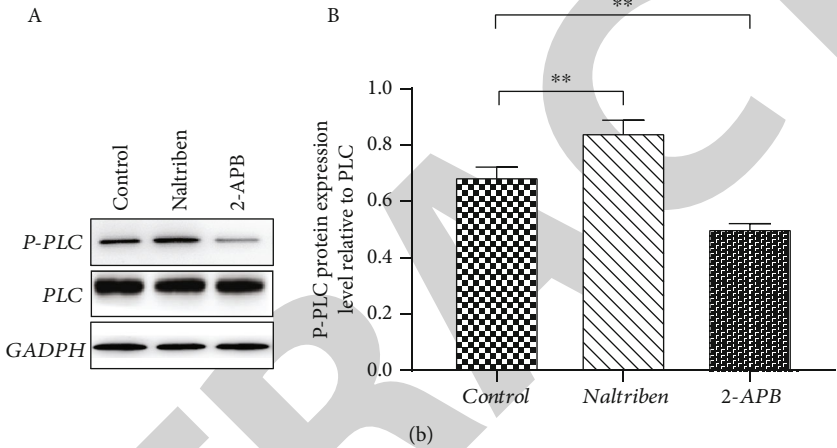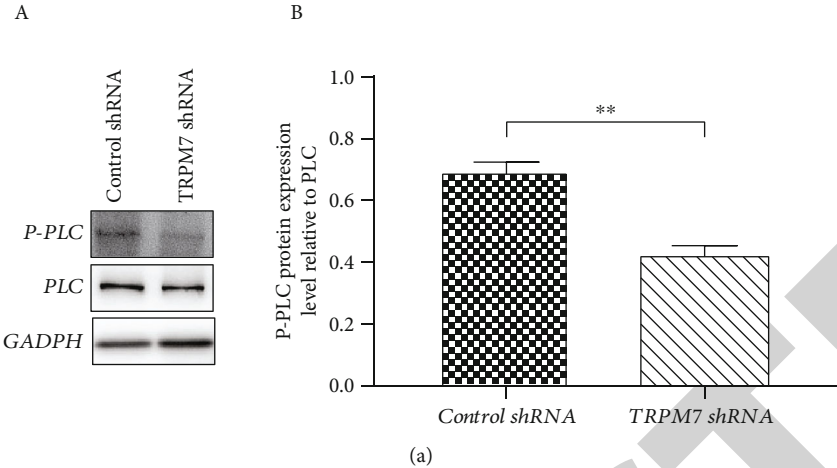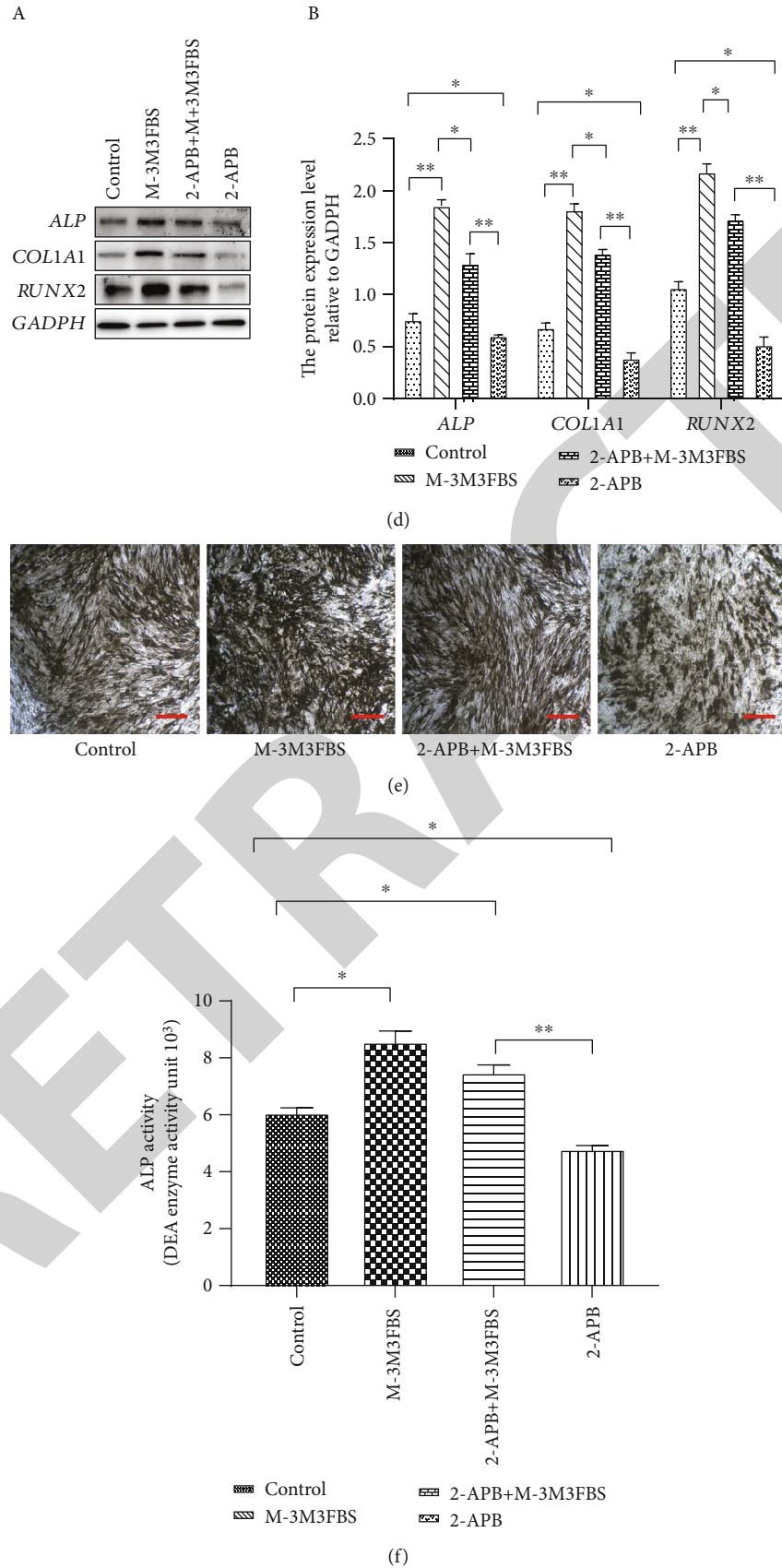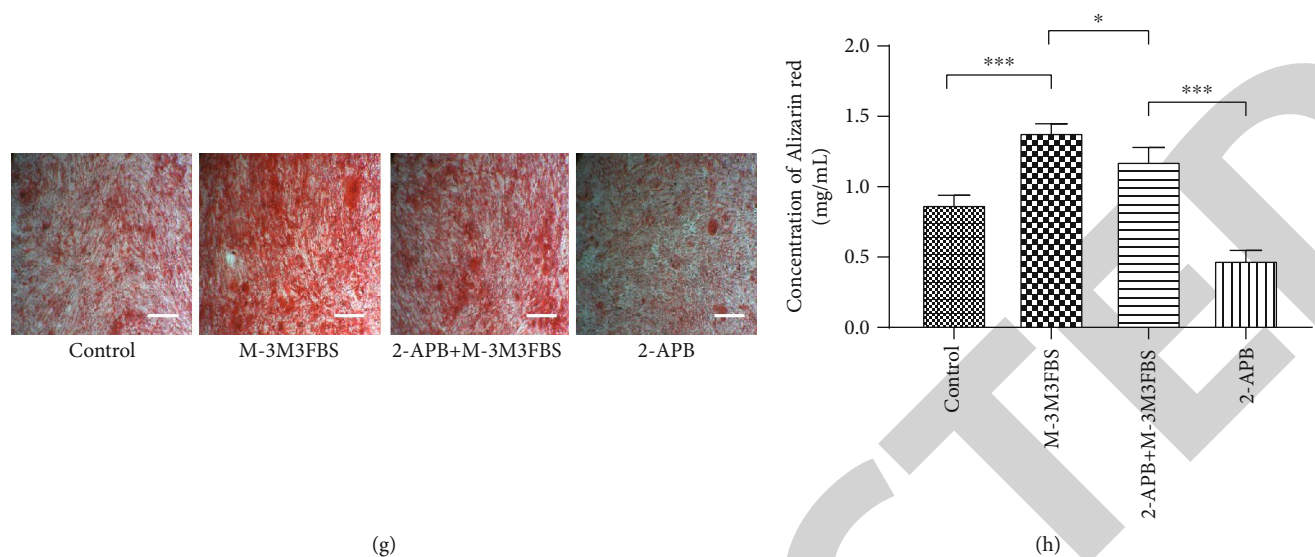
FIGURE 4: The expression of osteogenic markers and the osteogenic potential of hBMSCs under inhibiting TRPM7 and activating PLC (HSPG2). (a) (A) Western blot analysis of PLC activity in cells induced with osteogenic medium or osteogenic medium plus control shRNA or TRPM7 shRNA induced for 14 days. (B) The relative activity of PLC protein was quantified and plotted. (b) (A) Western blot analysis of the activity of PLC in cells induced with osteogenic medium or osteogenic medium plus Naltriben or 2-APB induced for 14 days. (B) The relative activity of PLC protein was quantified and plotted. Control shRNA: hBMSCs transfected with negative control-shRNA-vector; TRPM7 shRNA: hBMSCs transfected with TRPM7-shRNA-vector. (c) RT-PCR analysis of osteogenic markers ALP, COL1A1, RUNX2, OPN, and OCN in cells induced with osteogenic medium supplemented with different pharmaceuticals induced for 14 days. (d) (A) Western blot analysis of osteogenic marker proteins ALP, COL1A1, and RUNX2 in cells induced with osteogenic medium supplemented with different pharmaceuticals induced for 14 days. (B) The relative levels of osteogenic marker proteins were quantified and plotted. (e) Analysis of ALP staining in cells induced with osteogenic medium supplemented with different pharmaceuticals induced for 14 days. (f) Analysis of ALP activity (the unit for p-nitrophenyl: μmol) in cells induced with osteogenic medium supplemented with different pharmaceuticals induced for 14 days. (g) Staining of ARS in cells induced with osteogenic medium supplemented with different pharmaceuticals induced for 14 days. (h) A quantification of ARS in cells induced with osteogenic medium supplemented with different pharmaceuticals induced for 14 days. Scale: 200 μm. Control: cells induced in osteogenic medium without any pharmacological treatment; M-3M3FBS: cells induced in osteogenic medium supplemented with 20 μM M-3M3FBS; 2-APB+M-3M3FBS: cells induced in osteogenic medium supplemented with 50 μM 2-APB and 20 μM/mL M-3M3FBS; 2-APB: cells induced in osteogenic medium supplemented with 50 μM 2-APB. $^{*}P < 0.05$, $^{**}P < 0.01$, and $^{***}P < 0.0001$.

signaling pathway for the osteogenic differentiation of hBMSCs. Through the comprehensive analysis of osteogenic marker expression and SMAD1 activation in cells induced under different pharmacological treatments, we speculate that there might be another mechanism for TRPM7 to activate SMAD1 other than through phosphorylating PLC during the osteogenic differentiation of hBMSCs.

4. Discussion

A key event in bone formation is the differentiation of BMSCs into osteoblasts [19, 45], and many molecules are involved in the osteogenic differentiation of BMSCs. It has been reported that a transient receptor potential cation channel protein, TRPM7, is involved in osteoblast differentiation. In mature bone cells, the knockdown of TRPM7 inhibits osteoblast proliferation [22], and the expression of TRPM7 increases during osteoblast differentiation [2]. TRPM7 is also reported to control cell migration and is critical for tissue remodeling and regeneration [46]. Recently, it has been reported that TRPM7 is a dual-function kinase and cation channel for mediating the osteogenic differentiation of murine BMSCs in response to shear stress [17]. However,

the signaling pathway and molecular mechanism for TRPM7 to regulate the osteogenic differentiation of hBMSCs remain largely unknown. Hence, in order to further confirm the role of TRPM7 in the osteogenic differentiation of hBMSCs, we investigate the role and mechanisms of TRPM7 in the regulation of the osteogenic differentiation of hBMSCs in the present study. We found that the expression of TRPM7 and the activity of PLC and SMAD1 increase gradually with increasing osteogenic induction time, reaching a peak at day 14 of osteogenic induction. Results also showed that activating or inhibiting the activity of TRPM7 or PLC promotes or retards osteogenesis and SMAD1 activation in Figures 3(c)–3(e), 4(d), and 5(b). This implies that TRPM7 and PLC play a critical role in the osteogenic differentiation of hBMSCs and SMAD1 might be involved in this process. We then further examined the effects of TRPM7 on the activation of the PLC/SMAD1 signaling pathway during osteogenic differentiation induced for 14 days by activating or inhibiting the activity of TRPM7 or PLC. However, there is some controversy on whether TRPM7 siRNA inhibits the osteogenic differentiation in hBMSCs. Liu et al. [17] showed that the knocking down of TRPM7 decreased the osteogenic differentiation, but Castiglioni et al. [16] found that the

(a)

(b)
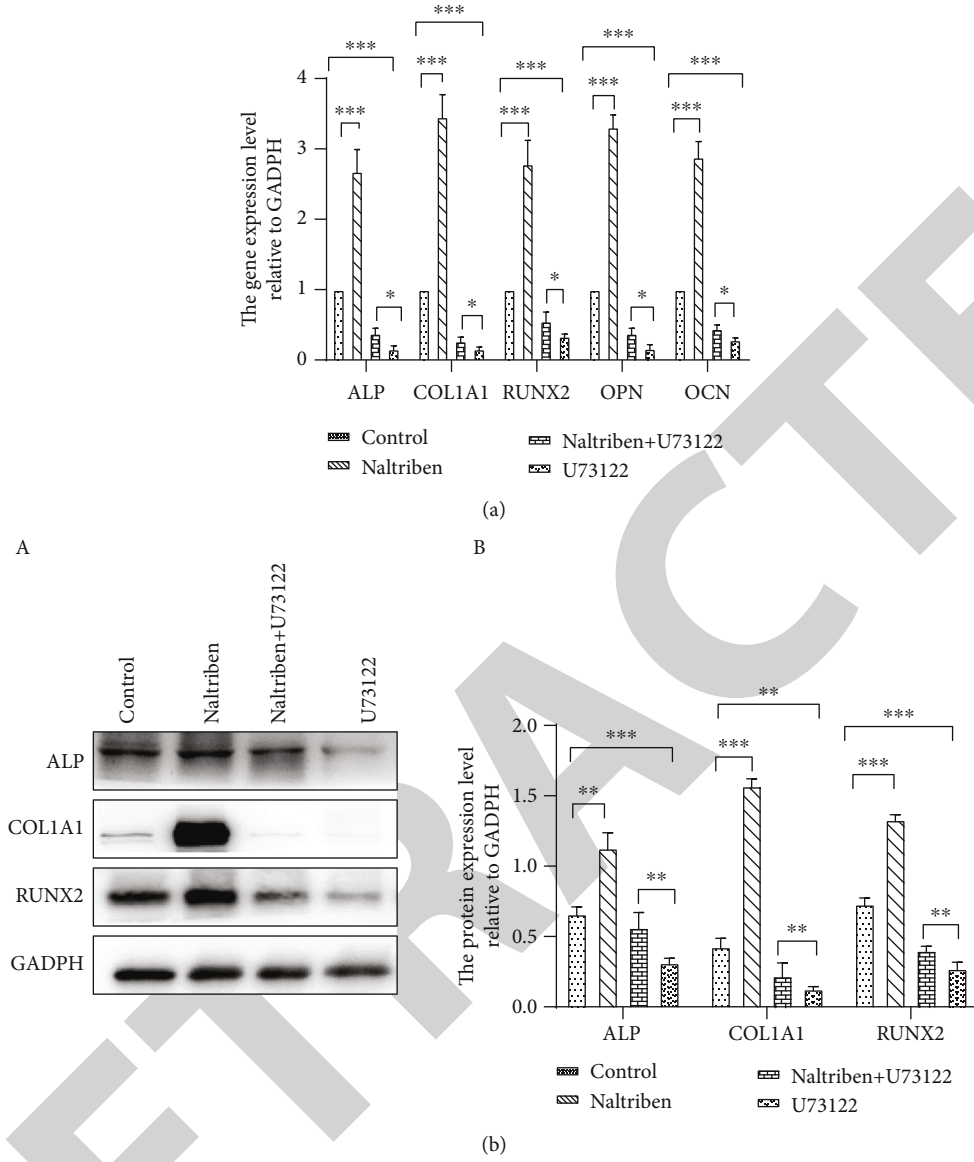
Figure 5: Continued.

(c)

(d)

(e)

(f)
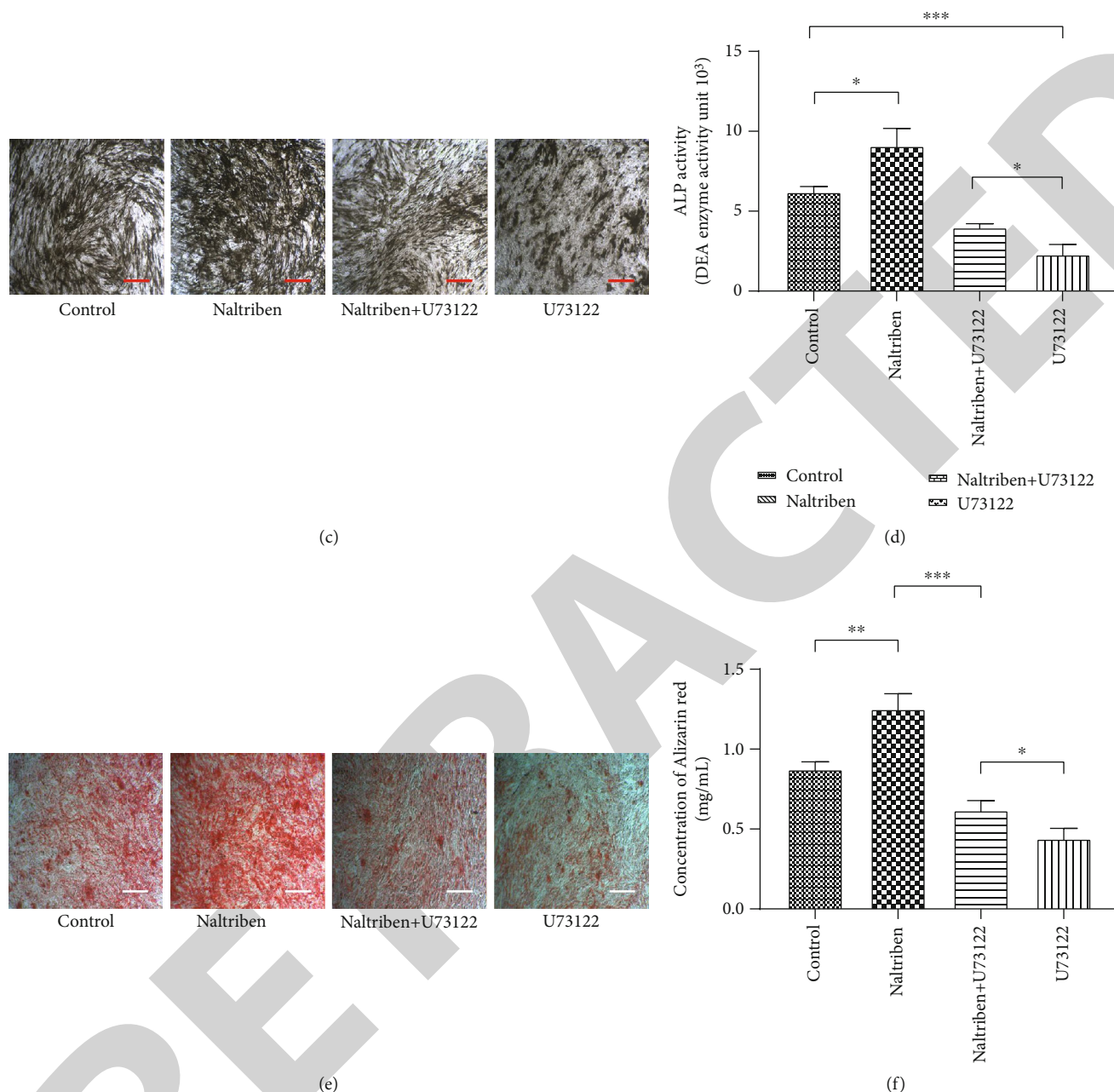
FIGURE 5: The expression of osteogenic markers and the osteogenic potential of hBMSCs under activating TRPM7 and inhibiting PLC (HSPG2). (a) RT-PCR analysis of osteogenic markers ALP, COL1A1, RUNX2, OPN, and OCN in cells induced with osteogenic medium supplemented with different pharmaceuticals induced for 14 days. (b) (A) Western blot analysis of osteogenic markers in cells induced with osteogenic medium supplemented with different pharmaceuticals induced for 14 days. (B) The relative levels of osteogenic marker proteins were quantified and plotted. (c) Analysis of ALP staining in cells induced with osteogenic medium supplemented with different pharmaceuticals induced for 14 days. (d) Analysis of ALP activity (the unit for p-nitrophenyl: μmol) in cells induced with osteogenic medium supplemented with different pharmaceuticals induced for 14 days. (e) Staining of ARS in cells induced with osteogenic medium supplemented with different pharmaceuticals induced for 14 days. (f) A quantification of ARS in cells induced with osteogenic medium supplemented with different pharmaceuticals induced for 14 days. Scale: 200 μm. Control: cells induced with osteogenic medium without any pharmacological treatment; Naltriben: cells induced with osteogenic medium supplemented with 20 μM Naltriben; Naltriben+U73122: cells induced with osteogenic medium supplemented with 20 μM Naltriben and 1 μM U73122; U73122: cells induced with osteogenic medium supplemented with 1 μM/mL U73122. $^{*}P < 0.05$, $^{**}P < 0.01$, and $^{***}P < 0.0001$.

knocking down of TRPM7 increased the osteogenic differentiation. Our final results showed that activation or inhibition of TRPM7 expression promoted or inhibited the osteogenic

differentiation of hBMSCs by increasing or decreasing the main osteogenic markers. Our observation disagreed with the result of Castiglioni et al. [16]. It may be inferred that this

(a)

(b)

(c)

Figure 6: Continued.

A

B

(d)

A

B

(e)

A

B

(f)

Figure 6: Continued.

A   B

(g)
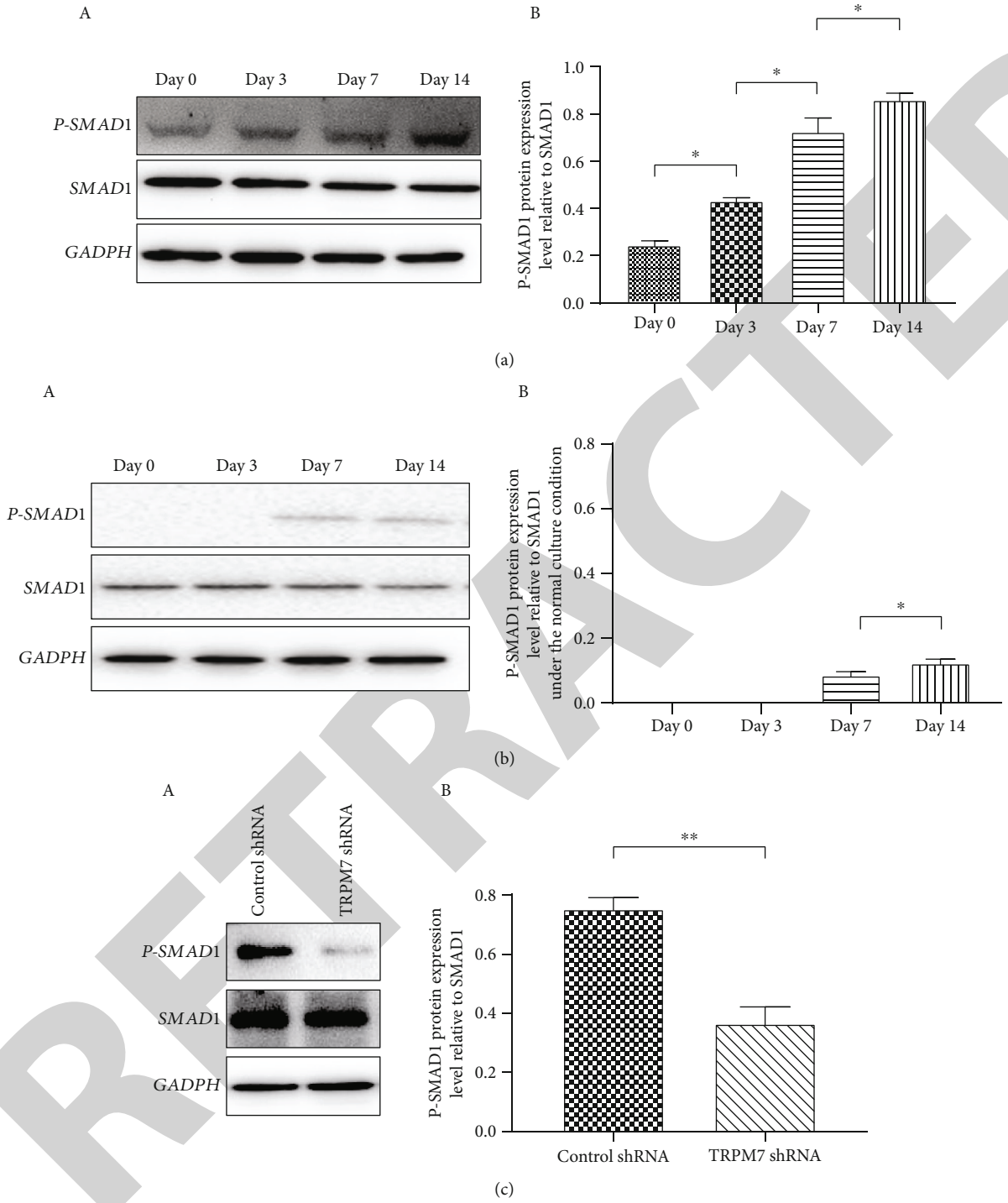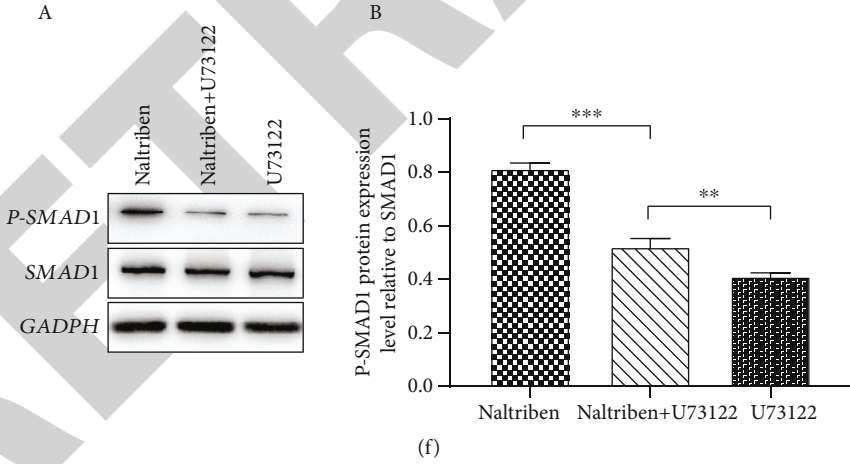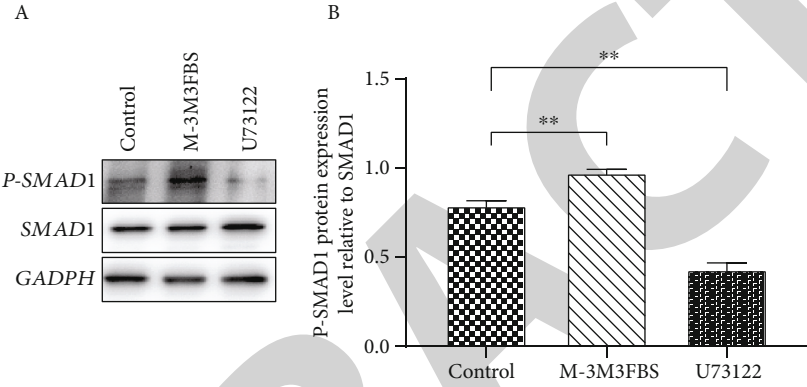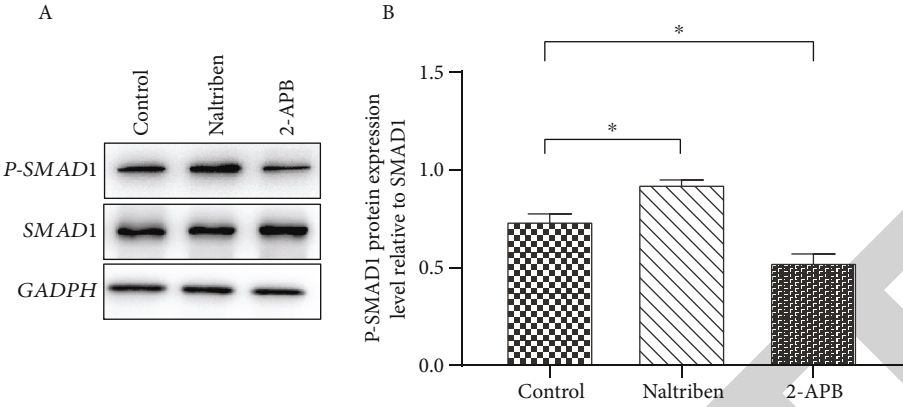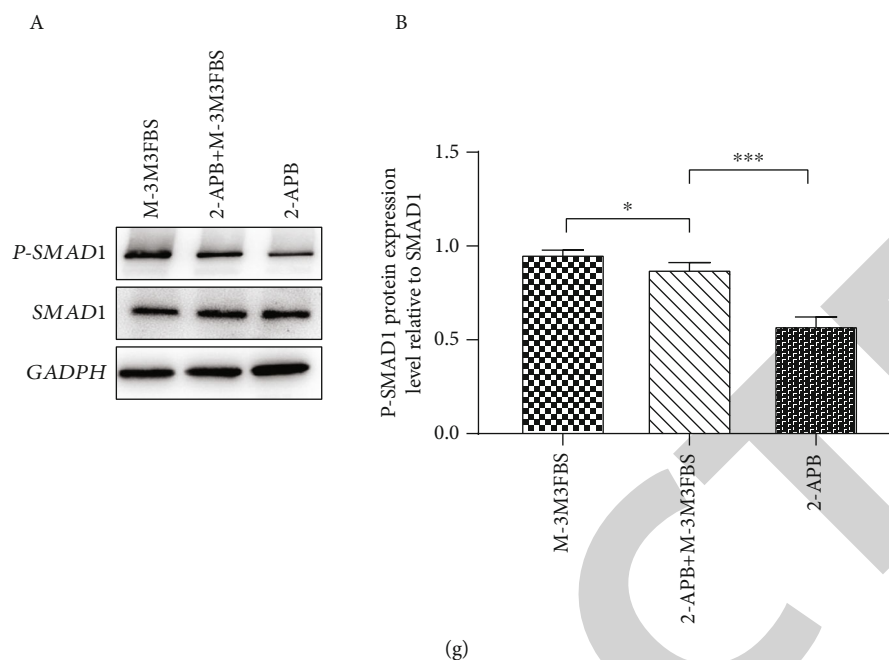
Figure 6: The analysis of SMAD1 activity under inhibiting or activating TRPM7 and inhibiting or activating PLC (HSPG2). (a) (A) The activity of SMAD1 protein in cells induced with osteogenic medium for 0, 3, 7, and 14 days. (B) The relative activity of SMAD1 protein was quantified and plotted. (b) (A) The expression of P-SMAD1 protein in cells noninduced for 0, 3, 7, and 14 days. (B) Relative expression levels of P-SMAD1 protein were quantified and plotted. (c) (A) Western blot analysis of SMAD1 protein in cells induced with osteogenic medium or osteogenic medium plus shRNA-mediated knockdown of TRPM7 induced for 14 days. (B) The relative activity of SMAD1 protein was quantified and plotted. (d) (A) Western blot analysis of SMAD1 protein in cells induced with osteogenic medium or osteogenic medium supplemented with Naltriben or 2-APB induced for 14 days. (B) The relative activity of SMAD1 protein was quantified and plotted. (e) (A) Western blot analysis of SMAD1 protein in cells induced with osteogenic medium or osteogenic medium supplemented with M-3M3FBS or U73122 induced for 14 days. (B) The relative activity of SMAD1 protein was quantified and plotted. (f) (A) Western blot analysis of SMAD1 protein in cells induced with osteogenic medium supplemented with 20 μM Naltriben or 20 μM Naltriben plus 1 μM U73122 or 1 μM/mL U73122 induced for 14 days. (B) The relative activity of SMAD1 protein was quantified and plotted. (g) (A) Western blot analysis of SMAD1 protein in cells induced with osteogenic medium supplemented with 20 μM M-3M3FBS or 50 μM 2-APB plus 20 μM M-3M3FBS or 50 μM 2-APB induced for 14 days. (B) The relative activity of SMAD1 protein was quantified and plotted. $^{*}P < 0.05$, $^{**}P < 0.01$, and $^{***}P < 0.0001$.

discordance is ascribed to the different protocols and reagents used in the experiment. For example, we used dexamethasone to induce the osteogenic differentiation of hBMSCs, which is consistent with the experiment of Liu et al. [17]. However, Castiglioni et al. [16] used vitamin D in the osteogenic induction. After the transfection with specific siRNAs for TRPM7, in addition, cells were cultured in the culture medium for 3 days before induction of osteogenic differentiation in the experiment of Castiglioni et al. [16], which is different with our experiment in that cells transfected with siRNAs for TRPM7 were induced directly for osteogenic differentiation. Of course, this inference should be verified by further experiment.

Previous studies have reported that the TRPM7 kinase phosphorylates PLC in its C2 domain at position Ser1164 and in the linker region preceding the C2 domain at position Thr1045 [24]. According to the expression or activation pattern of TRPM7, PLC, and SMAD1, we suspected that TRPM7 might play an important role in the osteogenic differentiation of hBMSCs by regulating the activation of PLC. The results of this study show that the shRNA-mediated knockdown of TRPM7 or the use of 2-APB during osteogenic

induction decreases the activity of PLC in induced cells. However, the use of Naltriben promoted the activation of PLC. This indicates that TRPM7 mediates the activation of PLC. The relationship between the TRPM7-mediated activation of PLC and the promotion of the osteogenic differentiation of hBMSCs was also analyzed by activating TRPM7 while inhibiting PLC or inhibiting TRPM7 while activating PLC. Our data suggest that TRPM7 may promote osteogenic differentiation by regulating the activity of PLC.

It has been reported that PLC can hydrolyse phosphatidylinositol 4,5-bisphosphate (PIP2) to produce inositol trisphosphate (IP3). Activating the IP3 receptor further triggers Ca2+ release from IP3R2 [2]. Ca2+ binds to calmodulin (CaM) and activates CaMK II in C3H10T1/2 and hBMSCs. In addition, it is reported that the activation of PLC in the skeletal muscle leads to the recruitment of protein kinase C (PKC) and calmodulin and the stimulation of calmodulin kinase II. Activated CaMK II can then phosphorylate SMAD1, inducing its translocation to the nucleus where it activates osteogenic target genes such as RUNX2, Osterix, and OCN [30]. In synovial mesenchymal cells, the knockdown of PLC significantly reduces the phosphorylation of

SMAD and p38 MAPK induced by TGF-β [31]. Here, we hypothesize that TRPM7 upregulates the activity of SMAD1 by activating PLC and thereby promoting the osteogenic differentiation of hBMSCs. To verify this hypothesis, the activity of SMAD1 under activating TRPM7 while inhibiting PLC or inhibiting TRPM7 while activating PLC was examined. The shRNA-mediated knockdown of TRPM7 and the use of 2-APB during the osteogenic induction of hBMSCs decreased the activity of SMAD1 in induced cells, while the use of Naltriben promoted the activation of SMAD1 in induced cells. Similarly, M-3M3FBS upregulated the activity of SMAD1 while U73122 downregulated the activity of SMAD1. These data confirm that TRPM7 regulates the activity of SMAD1 by phosphorylating PLC and the pathway of TRPM7 promoting the expression of osteogenic markers by regulating the activity of PLC/SMAD1. This may be one of the important signaling pathways involved in the osteogenic differentiation of hBMSCs.

Interestingly, the combination of Naltriben and U73122 decreased the activity of SMAD1 in induced cells in comparison with the use of Naltriben alone but was higher than the use of U73122 alone. Similarly, the combination of 2-APB and M-3M3FBS increased the activity of SMAD1 in induced cells in comparison with the use of 2-APB alone but was lower than the use of M-3M3FBS alone. The expression of osteogenic markers also shows a similar tendency under these pharmacologic treatments. These results may suggest that TRPM7 regulates the activity of SMAD1 not only through activating PLC but also through other signaling pathways during the osteogenic differentiation of hBMSCs.

Previous studies have shown that the kinase activity of TRPM7 is correlated with the phosphorylation of SMAD1/5 and p38 MAPK [17]. The activation of TRPM7/SMAD2 signaling by angiotensin II is an important mechanism leading to myocardial fibrosis in the sinoatrial node (SAN) tissues of sick sinus syndrome (SSS) rats [47]. TGF-β1 elevates TRPM7 expression in hepatic stellate cells (HSCs) via SMAD3-dependent mechanisms, which in turn contributes SMAD protein phosphorylation and subsequently increases fibrous collagen expression [43]. Meanwhile, the TRPM7 kinase can modulate SMAD2 signaling via direct phosphorylation at the C-terminal Ser465/467 motif, which is essential for its transcriptional activity [48]. Therefore, we surmise that there should be another mechanism for TRPM7 to activate SMAD1 other than by phosphorylating PLC during osteogenic differentiation. Whether it is possible for TRPM7 to activate SMAD1 directly during osteogenic differentiation of hBMSCs remains to be studied further. Elucidation of upstream and downstream regulatory components involved in the regulation of SMAD1 activity by TRPM7 will help us to better understand the regulation mechanism of TRPM7 in the osteogenic differentiation of hBMSCs. Summarily, our results may contribute to a greater understanding of the roles of TRPM7, PLC, and SMAD1 in the osteogenic differentiation of hBMSCs.

Finally, we should emphasize that this study is a preresearch for the project that will be performed in the Space Station of China. In this project, we will explore the effects of space microgravity on the activation of ion channel pro-

teins, such as TRPM7, in hBMSCs and thereby on the osteogenesis of hBMSCs. Some studies have showed that TRPM7 is a mechanosensitive protein [17, 38, 49]. Therefore, it should be important to recognize the role of TRPM7 protein in the osteogenesis of hBMSCs before we perform the space experiments.

Abbreviations

hBMSCs:	Human bone marrow-derived mesenchymal stem cells
MSCs:	Marrow-derived mesenchymal stem cells
TRPM7:	Transient receptor potential cation channel subfamily M7
PLC:	Phospholipase C
MAPKs:	Mitogen-activated protein kinases
P38 MAPKs:	Protein 38 mitogen-activated protein kinases
PIP2:	Phosphatidylinositol 4,5-bisphosphate
BMP:	Bone morphogenetic protein
IGF:	Insulin-like growth factor
TGF-β1:	Transforming growth factor-β1
BFGF:	Basic fibroblast growth factor
CaMKs:	Calmodulin-dependent protein kinases
ALP:	Alkaline phosphate
COL1A1:	Collagen type 1 alpha 1 chain
RUNX2:	Runt-related transcription factor 2
OCN:	Osteocalcin
OPN:	Osteopontin
shRNA:	Short hairpin RNA
PMSF:	Phenylmethylsulfonyl fluoride
HSPG2:	Heparan sulfate proteoglycan 2
Wnt:	Wingless/integrated
NELL-1:	Nel-like molecular 1
ERK:	Extracellular regulated protein kinases
BFP:	Bone-forming peptide
CREBH:	cAMP response element-binding protein H
IP3:	Inositol trisphosphate
Smurf1:	Smad ubiquitination regulatory factor 1.

Data Availability

The datasets generated and/or analyzed during this study are available from the corresponding author upon a reasonable request.

Conflicts of Interest

The authors indicate no potential conflicts of interest.

Authors' Contributions

F.H., S.W., C.Z., L.L., J.C., and Y.F performed the experiments and contributed to the data analysis. J.W. and F.H. drafted the conception of the study, designed the experiments, and monitored the project progression, data analysis, and interpretation. F.H prepared the initial draft of the manuscript. J.W. prepared the final version of manuscript. All authors have given approval to the submitted manuscript.

Acknowledgments

Supplementary Materials

Figure S1: The expression of osteogenic markers induced for 0, 3, 7, and 14 days. (A) The mRNA expression of ALP, COL1A1, RUNX2, OPN and OCN in cells induced for 0, 3, 7, and 14 days. (B) The protein expression of ALP, COL1A1, RUNX2 protein in cells induced for 0, 3, 7, and 14 days. Relative protein expression levels of TRPM7 protein were quantified and plotted. (C) Analysis of ALP staining in cells induced with osteogenic medium for 0, 3, 7, 14days. (D) Analysis of ALP activity (the unit for p-nitrophenyl: μmol) in cells treated with osteogenic medium for 0, 3, 7, 14days. (E) Staining of ARS in cells induced with osteogenic medium for 0, 3, 7,14 days. (F) ARS quantification by stain extraction and detected the absorbance at 405 nm. Scale: 100μm. *P< 0.05, **P< 0.01, ***P< 0.0001. (Supplementary Materials)

References

[1] E. Xiao, H. Q. Yang, Y. H. Gan et al., "Brief Reports: TRPM7 Senses Mechanical Stimulation Inducing Osteogenesis in Human Bone Marrow Mesenchymal Stem Cells," *STEM CELLS*, vol. 33, no. 2, pp. 615–621, 2015.

[2] H. Cheng, J. M. Feng, M. L. Figueiredo et al., "Transient Receptor Potential Melastatin Type 7 Channel is Critical for the Survival of Bone Marrow Derived Mesenchymal Stem Cells," *Stem Cells and Development*, vol. 19, no. 9, pp. 1393–1403, 2010.

[3] C. Zhang, F.-F. Hong, C.-C. Wang et al., "TRIB3 inhibits proliferation and promotes osteogenesis in hBMSCs by regulating the ERK1/2 signaling pathway," *Scientific Reports*, vol. 7, no. 1, p. 10342, 2017.

[4] B. Parekkadan and J. M. Milwid, "Mesenchymal Stem Cells as Therapeutics," *Annual Review of Biomedical Engineering*, vol. 12, no. 1, pp. 87–117, 2010.

[5] C. Zhang, L. Li, Y. Jiang et al., "Space microgravity drives trans-differentiation of human bone marrow-derived mesenchymal stem cells from osteogenesis to adipogenesis," *FASEB Journal*, vol. 32, no. 8, pp. 4444–4458, 2018.

[6] N. Case and J. Rubin, "β-Catenin-A supporting role in the skeleton," *Journal of Cellular Biochemistry*, vol. 110, no. 3, pp. 545–553, 2010.

[7] A. W. James, "Review of Signaling Pathways Governing MSC Osteogenic and Adipogenic Differentiation," *Scientifica*, vol. 2013, 17 pages, 2013.

[8] L. Nanni, J. E. Ming, M. Bocian et al., "The Mutational Spectrum of the Sonic Hedgehog Gene in Holoprosencephaly: SHH Mutations Cause a Significant Proportion of Autosomal Dominant Holoprosencephaly," *Human Molecular Genetics*, vol. 8, no. 13, pp. 2479–2488, 1999.

[9] Y. Mishina, M. W. Starbuck, M. A. Gentile et al., "Bone Morphogenetic Protein Type IA Receptor Signaling Regulates Postnatal Osteoblast Function and Bone Remodeling," *Journal of Biological Chemistry*, vol. 279, no. 26, pp. 27560–27566, 2004.

[10] M. Okamoto, J. Murai, H. Yoshikawa, and N. Tsumaki, "Bone Morphogenetic Proteins in Bone Stimulate Osteoclasts and Osteoblasts During Bone Development," *Journal of Bone and Mineral Research*, vol. 21, no. 7, pp. 1022–1033, 2006.

[11] E. Gazzerro, A. Smerdel-Ramoya, S. Zanotti et al., "Conditional Deletion of Gremlin Causes a Transient Increase in Bone Formation and Bone Mass," *Journal of Biological Chemistry*, vol. 282, no. 43, pp. 31549–31557, 2007.

[12] L. Xian, X. Wu, L. Pang et al., "Matrix IGF-1 maintains bone mass by activation of mTOR in mesenchymal stem cells," *Nature Medicine*, vol. 18, no. 7, pp. 1095–1101, 2012.

[13] W. Qiu, T. E. Andersen, J. Bollerslev, S. Mandrup, B. M. Abdallah, and M. Kassem, "Patients With High Bone Mass Phenotype Exhibit Enhanced Osteoblast Differentiation and Inhibition of Adipogenesis of Human Mesenchymal Stem Cells," *Journal of Bone and Mineral Research*, vol. 22, no. 11, pp. 1720–1731, 2007.

[14] C. Thouverey and J. Caverzasio, "The p38α MAPK positively regulates osteoblast function and postnatal bone acquisition," *Cellular and Molecular Life Sciences*, vol. 69, no. 18, pp. 3115–3125, 2012.

[15] F. Ugarte, M. Ryser, S. Thieme et al., "Notch signaling enhances osteogenic differentiation while inhibiting adipogenesis in primary human bone marrow stromal cells," *Experimental Hematology*, vol. 37, no. 7, pp. 867–875.e1, 2009.

[16] S. Castiglioni, V. Romeo, L. Locatelli, A. Cazzaniga, and J. A. M. Maier, "TRPM7 and MagT1 in the osteogenic differentiation of human mesenchymal stem cells in vitro," *Scientific Reports*, vol. 8, no. 1, 2018.

[17] Y.-S. Liu, Y.-A. Liu, C.-J. Huang et al., "Mechanosensitive TRPM7 mediates shear stress and modulates osteogenic differentiation of mesenchymal stromal cells through Osterix pathway," *Scientific Reports*, vol. 5, no. 1, 2015.

[18] I. Carvacho, G. Ardestani, H. C. Lee, K. McGarvey, R. A. Fissore, and K. Lykke-Hartmann, "TRPM7-like channels are functionally expressed in oocytes and modulate post-fertilization embryo development in mouse," *Scientific Reports*, vol. 6, no. 1, 2016.

[19] T. Hofmann, S. Schäfer, M. Linseisen, L. Sytik, T. Gudermann, and V. Chubanov, "Activation of TRPM7 channels by small molecules under physiological conditions," *Pflügers Archiv*, vol. 466, no. 12, pp. 2177–2189, 2014.

[20] M. Langeslag, K. Clark, W. H. Moolenaar, F. N. van Leeuwen, and K. Jalink, "Activation of TRPM7 channels by phospholipase C-coupled receptor agonists," *Journal of Biological Chemistry*, vol. 282, no. 1, pp. 232–239, 2007.

[21] K. Takahashi, C. Umebayashi, T. Numata et al., "TRPM7-mediated spontaneous Ca2+entry regulates the proliferation and differentiation of human leukemia cell line K562," *Physiological Reports*, vol. 6, no. 14, p. e13796, 2018.

[22] E. Abed and R. Moreau, "Importance of melastatin-like transient receptor potential 7 and cations (magnesium, calcium)

Retraction

Retracted: α_1-Adrenergic Receptor Blockade by Prazosin Synergistically Stabilizes Rat Peritoneal Mast Cells

BioMed Research International

This article has been retracted by Hindawi following an investigation undertaken by the publisher [1]. This investigation has uncovered evidence of one or more of the following indicators of systematic manipulation of the publication process:

(1) Discrepancies in scope

(2) Discrepancies in the description of the research reported

(3) Discrepancies between the availability of data and the research described

(4) Inappropriate citations

(5) Incoherent, meaningless and/or irrelevant content included in the article

(6) Manipulated or compromised peer review

The presence of these indicators undermines our confidence in the integrity of the article's content and we cannot, therefore, vouch for its reliability. Please note that this notice is intended solely to alert readers that the content of this article is unreliable. We have not investigated whether authors were aware of or involved in the systematic manipulation of the publication process.

Wiley and Hindawi regrets that the usual quality checks did not identify these issues before publication and have since put additional measures in place to safeguard research integrity.

We wish to credit our own Research Integrity and Research Publishing teams and anonymous and named external researchers and research integrity experts for contributing to this investigation.

The corresponding author, as the representative of all authors, has been given the opportunity to register their agreement or disagreement to this retraction. We have kept a record of any response received.

References

[1] N. Abe, H. Toyama, Y. Ejima et al., "α_1-Adrenergic Receptor Blockade by Prazosin Synergistically Stabilizes Rat Peritoneal Mast Cells," *BioMed Research International*, vol. 2020, Article ID 3214186, 12 pages, 2020.

Research Article

α_1-Adrenergic Receptor Blockade by Prazosin Synergistically Stabilizes Rat Peritoneal Mast Cells

Nozomu Abe,[1] Hiroaki Toyama,[1] Yutaka Ejima,[1] Kazutomo Saito,[1] Tsutomu Tamada,[2] Masanori Yamauchi,[1] and Itsuro Kazama [iD][3]

[1]*Department of Anesthesiology, Tohoku University Hospital, Seiryo-cho, Aoba-ku, Sendai, Miyagi, Japan*
[2]*Department of Respiratory Medicine, Tohoku University Graduate School of Medicine, Seiryo-cho, Aoba-ku, Sendai, Miyagi, Japan*
[3]*Miyagi University, School of Nursing, Gakuen, Taiwa-cho, Kurokawa-gun, Miyagi, Japan*

Correspondence should be addressed to Itsuro Kazama; kazamai@myu.ac.jp

Background. Adrenaline quickly inhibits the release of histamine from mast cells. Besides β_2-adrenergic receptors, several in vitro studies also indicate the involvement of α-adrenergic receptors in the process of exocytosis. Since exocytosis in mast cells can be detected electrophysiologically by the changes in the membrane capacitance (Cm), its continuous monitoring in the presence of drugs would determine their mast cell-stabilizing properties. *Methods.* Employing the whole-cell patch-clamp technique in rat peritoneal mast cells, we examined the effects of adrenaline on the degranulation of mast cells and the increase in the Cm during exocytosis. We also examined the degranulation of mast cells in the presence or absence of α-adrenergic receptor agonists or antagonists. *Results.* Adrenaline dose-dependently suppressed the GTP-γ-S-induced increase in the Cm and inhibited the degranulation from mast cells, which was almost completely erased in the presence of butoxamine, a β_2-adrenergic receptor antagonist. Among α-adrenergic receptor agonists or antagonists, high-dose prazosin, a selective α_1-adrenergic receptor antagonist, significantly reduced the ratio of degranulating mast cells and suppressed the increase in the Cm. Additionally, prazosin augmented the inhibitory effects of adrenaline on the degranulation of mast cells. *Conclusions.* This study provided electrophysiological evidence for the first time that adrenaline dose-dependently inhibited the process of exocytosis, confirming its usefulness as a potent mast cell stabilizer. The pharmacological blockade of α_1-adrenergic receptor by prazosin synergistically potentiated such mast cell-stabilizing property of adrenaline, which is primarily mediated by β_2-adrenergic receptors.

1. Introduction

Anaphylaxis is a severe allergic reaction and a potentially life-threatening acute multisystem syndrome caused by the sudden release of mast cell-derived mediators [1]. In the treatment, adrenaline, a nonspecific adrenergic receptor agonist, is the first-choice drug, since it immediately suppresses further release of chemical mediators from mast cells [2]. Concerning the mechanisms, β_2-adrenergic receptors are considered to be primarily responsible, because the stimulation of these receptors strongly inhibits FcεRI- (high-affinity receptors for IgE-) dependent calcium mobilization in the cells [3]. Previously, several in vitro studies also demonstrated the presence of α-adrenergic receptors in mast cells [4] and indicated their involvement in the activation of the

cells [5, 6]. Based on these findings, later in vivo studies actually showed the therapeutic efficacy of prazosin, a specific α_1-adrenergic receptor antagonist, for the histamine-induced bronchoconstriction in patients with asthma [7, 8]. To determine the effects of adrenaline or α-adrenergic receptor agonists/antagonists on the stabilization of mast cells, previous in vitro studies measured the drug-induced changes in histamine release from mast cells [6, 9–11]. However, they were not enough to monitor the whole process of exocytosis, since mast cells also release fibrogenic factors, growth factors and inflammatory cytokines in addition to chemical mediators [12]. In our series of patch-clamp studies, by detecting the changes in whole-cell membrane capacitance (Cm) in mast cells, we provided electrophysiological evidence that antiallergic drugs, antimicrobial drugs, and corticosteroids inhibit

the process of exocytosis and thus exert mast cell-stabilizing properties [13–16]. In the present study, employing the same standard patch-clamp whole-cell recording technique in rat peritoneal mast cells, we examined the effects of adrenaline on the changes in the Cm to quantitatively determine its ability to stabilize mast cells. Additionally, we examined the effects of α-adrenergic receptor agonists or antagonists on the degranulation of mast cells to determine their involvement in the stabilization of mast cells. Here, this study provides electrophysiological evidence for the first time that adrenaline dose-dependently inhibits the process of exocytosis, confirming its usefulness as a potent mast cell stabilizer. This study also shows that the pharmacological blockade of α_1-adrenergic receptor by prazosin synergistically potentiates such mast cell-stabilizing property of adrenaline, which is primarily mediated by β_2-adrenergic receptors.

2. Materials and Methods

2.1. Cell Sources and Preparation. Male Wistar rats no less than 25 weeks old were purchased from Japan SLC Inc. (Shizuoka, Japan). We profoundly anaesthetized the rats with isoflurane and sacrificed them by cervical dislocation. The protocols for the use of animals were approved by the Animal Care and Use Committee of Tohoku University Graduate School of Medicine and Miyagi University. As previously described [13–17], we washed rat peritoneum using standard external (bathing) solution which consists of (in mM) the following: NaCl, 145; KCl, 4.0; CaCl$_2$, 1.0; MgCl$_2$, 2.0; HEPES, 5.0; bovine serum albumin, 0.01% (pH 7.2 adjusted with NaOH); and isolated mast cells from the peritoneal cavity. We maintained the isolated mast cells at room temperature (22-24°C) to use within 8 hours. The suspension of mast cells was spread on a chamber placed on the headstage of an inverted microscope (Nikon, Tokyo, Japan). Mast cells were easy to distinguish from other cell types since they included characteristic secretory granules within the cells [13–17].

2.2. Quantification of Mast Cell Degranulation. Adrenaline, purchased from Daiichi Sankyo, Inc. (Tokyo, Japan); dopamine, from Kyowa Hakko Kirin Co., Ltd. (Tokyo, Japan); phenylephrine hydrochloride, from Wako Pure Chem Ind. (Osaka, Japan); and clonidine and yohimbine, from Tokyo Chemical Industry Co., Ltd. (Tokyo, Japan) were separately dissolved in the external solution at final concentrations of 1, 10, and 100 μM and 1 mM. Prazosin hydrochloride, purchased from Tokyo Chemical Industry Co., Ltd., was dissolved at final concentrations of 0.01, 0.1, and 1 μM. Butoxamine hydrochloride, purchased from Sigma-Aldrich Co. (St. Louis, MO, USA), or prazosin was also dissolved in the external solution containing 1 mM adrenaline at the final concentrations of 1 mM or 1 μM, respectively. After we incubated mast cells in these solutions or a solution without the reagents, exocytosis was externally induced by compound 48/80 (Sigma-Aldrich; final concentration 10 μg/ml) [13–17]. We obtained bright-field images from randomly chosen 0.1-mm^2 fields of view (10 views from each condition), as we described previously [13–17]. We counted degranulated mast cells (definition; cells surrounded by more than 8 granules outside the cell membrane) and calculated their ratio to all mast cells.

2.3. Electrical Setup and Membrane Capacitance Measurements. As we described in our previous studies [13–17], we employed an EPC-9 patch-clamp amplifier system (HEKA Electronics, Lambrecht, Germany) and conducted standard whole-cell patch-clamp recordings. Briefly, we maintained the patch pipette resistance between 4-6 MΩ when plugged with internal (patch pipette) solution which consists of (in mM) the following: K-glutamate, 145; MgCl$_2$, 2.0; Hepes, 5.0 (pH 7.2 adjusted with KOH). We added 100 μM guanosine 5′-o-(3-thiotriphosphate) (GTP-γ-S) (EMD Bioscience Inc., La Jolla, CA, USA) into the internal solution to endogenously induce exocytosis in mast cells [13–17]. We induced a gigaseal formation on a single mast cell spread in the external solutions containing no drug, different concentrations of adrenaline, or dopamine (1, 10, and 100 μM and 1 mM). Then, we briefly sucked the pipette to rupture the patch membrane and perfused GTP-γ-S into the cells. We maintained the series resistance below 10 MΩ during the whole-cell recordings. To monitor the membrane capacitance of mast cells, we conducted a sine plus DC protocol employing the lock-in amplifier of an EPC-9 Pulse program. We superimposed an 800 Hz sinusoidal command voltage on the holding potential of -80 mV. We continuously monitored the membrane capacitance (Cm), membrane conductance (Gm), and series conductance (Gs) during the whole-cell recording configuration. We performed all experiments at room temperature.

2.4. Statistical Analyses. Data were analyzed using PulseFit software (HEKA Electronics, Lambrecht, Germany) and Microsoft Excel (Microsoft Corporation, Redmond, Wash., USA) and reported as means ± SEM. Statistical significance was assessed by two-way ANOVA. A value of $p < 0.05$ was considered significant.

3. Results

3.1. Effects of Adrenaline and Dopamine on Degranulation of Rat Peritoneal Mast Cells. Mast cells incubated in the external solution with compound 48/80 (10 μg/ml) showed more wrinkles on their cell surface than those incubated without the compound (Figure 1(a), B vs. A). They released more secretory granules due to exocytosis (Figure 1(a), B). Mast cells that were preincubated with relatively lower doses of adrenaline, a nonselective agonist of adrenergic receptors (1 and 10 μM; Figure 1(a), C and D), showed similar findings to those that were incubated in the external solution alone (Figure 1(a), B). However, mast cells preincubated with relatively higher doses of adrenaline (100 μM, 1 mM; Figure 1(a), E and F) did not show such findings characteristic of exocytosis. On the other hand, almost all mast cells that were preincubated with dopamine, a nonselective agonist of dopamine receptors (1, 10, and 100 μM and 1 mM), showed typical findings of exocytosis regardless of their concentrations (Figure 1(a), G to J).
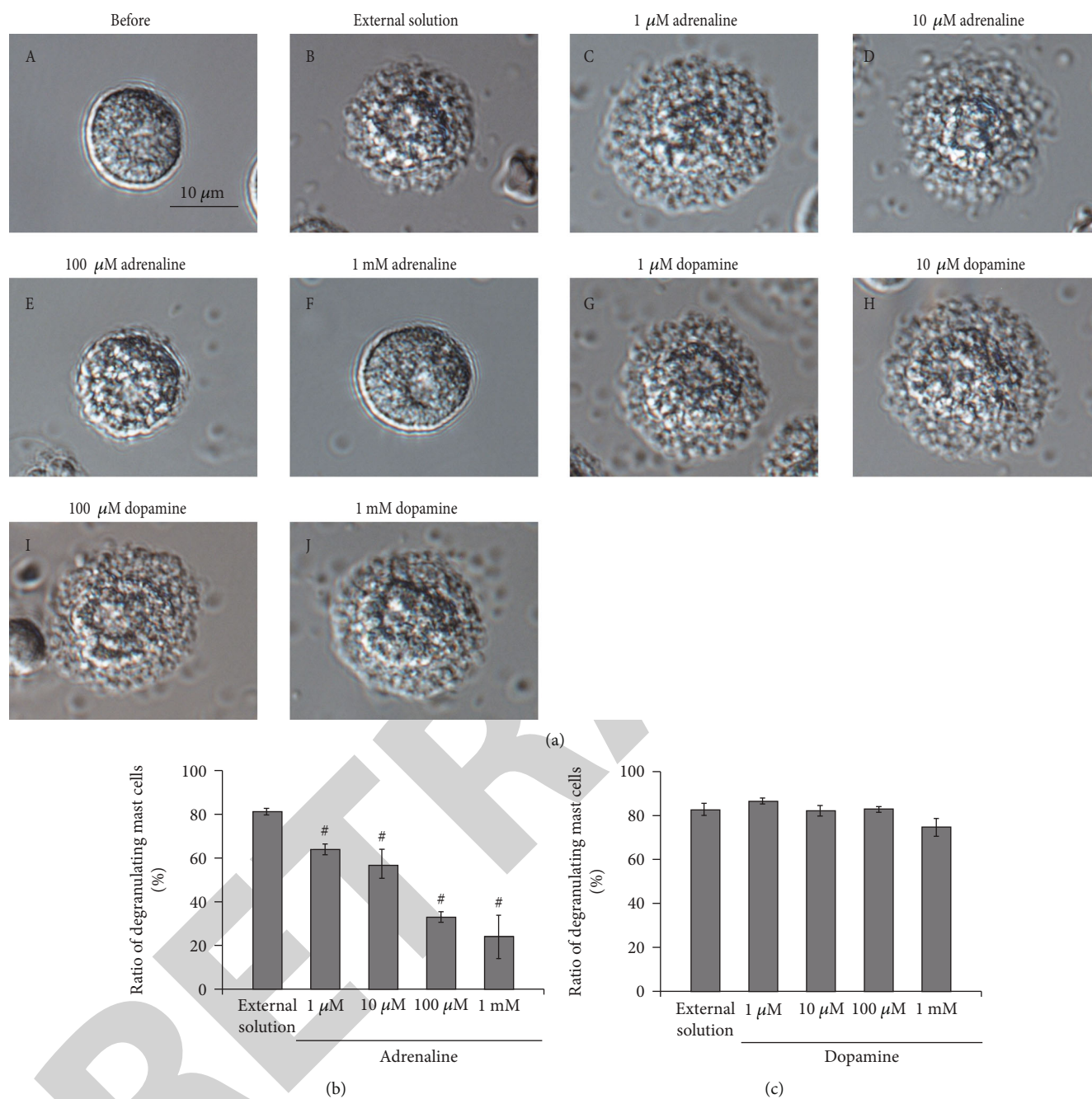
FIGURE 1: Effects of adrenaline and dopamine on mast cell degranulation. (a) Differential-interference contrast (DIC) microscopic images were taken before (A) and after exocytosis was externally induced by compound 48/80 in mast cells incubated in the external solutions containing no drug (B), 1 μM adrenaline (C), 10 μM adrenaline (D), 100 μM adrenaline (E), 1 mM adrenaline (F), 1 μM dopamine (G), 10 μM dopamine (H), 100 μM dopamine (I), and 1 mM dopamine (J). Effects of different concentrations (1, 10, and 100 μM and 1 mM) of adrenaline (b) and dopamine (c). After the mast cells were incubated in the external solutions containing no drug or either drug, exocytosis was induced by compound 48/80. The numbers of degranulating mast cells were expressed as percentages of the total mast cell numbers in selected bright fields. $^{\#}p < 0.05$ vs. incubation in the external solution alone. Values are means ± SEM. Differences were analyzed by ANOVA followed by Dunnett's test.

To quantitatively determine such effects of adrenaline and dopamine on exocytosis, we then counted the numbers of degranulating mast cells and calculated their ratio to all mast cells (Figures 1(b) and 1(c)). In the absence of adrenaline, compound 48/80 caused degranulation in 80.0 ± 1.4% of the entire mast cells ($n = 10$; Figure 1(b)). Relatively lower concentrations of adrenaline (1 and 10 μM) significantly decreased the number of degranulating mast cells dose-dependently (1 μM, 63.9 ± 2.3%, $n = 15$, $p < 0.05$; 10 μM, 56.7 ± 5.4%, $n = 14$, $p < 0.05$; Figure 1(b)). Additionally, with higher concentrations (100 μM, 1 mM), adrenaline markedly reduced the numbers of degranulating mast cells (100 μM,

(a)

(b)

(c)

(d)
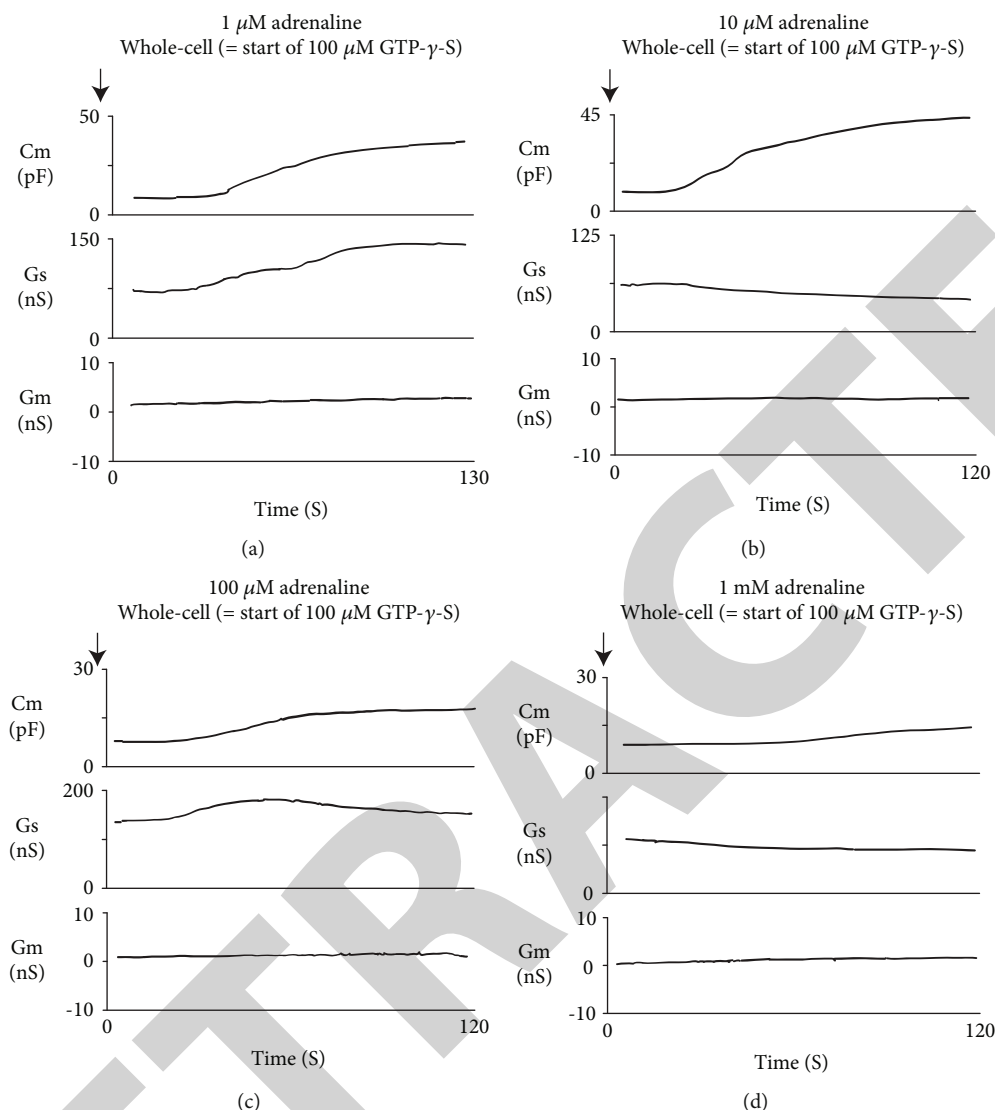
FIGURE 2: Adrenaline-induced changes in mast cell membrane capacitance and series and membrane conductance during exocytosis. After the mast cells were incubated in the external solutions containing 1 μM (a), 10 μM (b), 100 μM (c), or 1 mM adrenaline (d), the whole-cell recording configuration was established in single mast cells and dialysis with 100 μM GTP-γ-S was started. Membrane capacitance and series and membrane conductance were monitored for at least 90 sec. Cm: membrane capacitance; Gs: series conductance; Gm: membrane conductance.

$32.9 \pm 2.1\%$, $n = 14$, $p < 0.05$; 1 mM, $24.1 \pm 2.3\%$, $n = 13$, $p < 0.05$; Figure 1(b)). Differing from adrenaline, dopamine did not significantly affect the numbers of degranulating mast cells regardless of their concentrations (Figure 1(c)). From these results, consistent with the previous findings [9, 10], adrenaline, which suppresses the release of histamine, actually inhibited the degranulation of rat peritoneal mast cells dose-dependently.

3.2. Effects of Adrenaline and Dopamine on Whole-Cell Membrane Capacitance in Rat Peritoneal Mast Cells. In our previous studies, microscopic changes in megakaryocyte or lymphocyte membranes were accurately monitored by measuring the whole-cell membrane capacitance (Cm) [18–26]. Of note, in mast cells, the process of degranulation during

exocytosis was successively monitored by the increase in the Cm [13–17, 27, 28]. Hence, in our study, to quantitatively examine the effects of adrenaline or dopamine on the process of exocytosis, we preincubated mast cells in adrenaline- or dopamine-containing external solutions and measured the changes in Cm (Figures 2 and 3). In these figures, we showed the effects of 1, 10, and 100 μM and 1 mM adrenaline (Figure 2) and dopamine (Figure 3) on the Cm, Gs, and Gm. Table 1 summarizes the changes in the Cm. Representing the endogenous induction of exocytosis [13–17, 29, 30], the internal addition of GTP-γ-S into mast cells markedly increased the value of Cm (from 9.29 ± 0.37 to 34.0 ± 2.79 pF, $n = 9$, $p < 0.05$; Table 1).

When mast cells were preincubated with lower doses of adrenaline (1 and 10 μM), the addition of GTP-γ-S
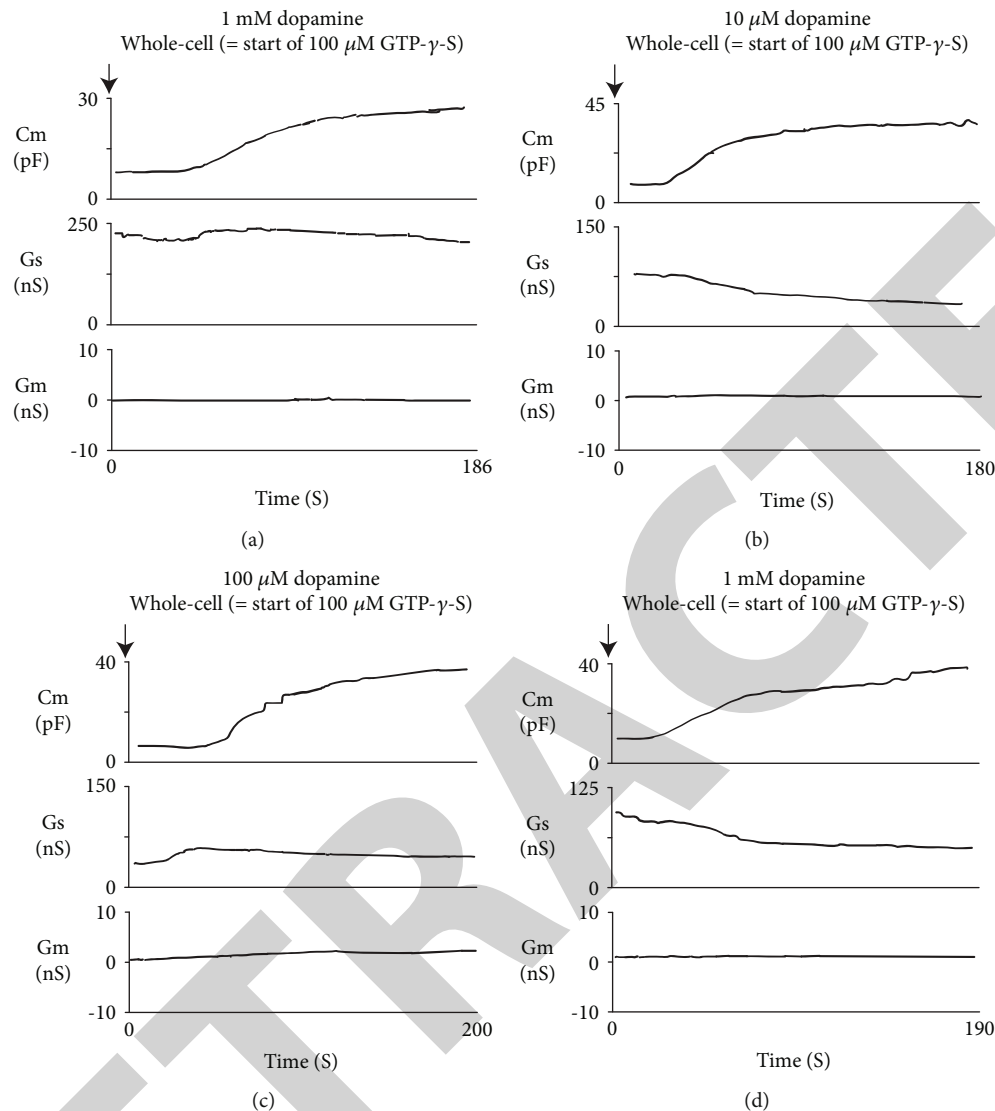
FIGURE 3: Dopamine-induced changes in mast cell membrane capacitance and series and membrane conductance during exocytosis. After the mast cells were incubated in the external solutions containing $1\,\mu$M (a), $10\,\mu$M (b), $100\,\mu$M (c), or $1\,$mM dopamine (d), the whole-cell recording configuration was established in single mast cells and dialysis with $100\,\mu$M GTP-γ-S was started. Membrane capacitance and series and membrane conductance were monitored for at least 90 sec. Cm: membrane capacitance; Gs: series conductance; Gm: membrane conductance.

tended to increase the Cm similarly to that of mast cells preincubated with the external solution alone (Figures 2(a) and 2(b)). However, compared to the external solution alone, the increase in the Cm (ΔCm) was significantly suppressed ($1\,\mu$M, 17.5 ± 6.83 pF, $n = 6$, $p < 0.05$; $10\,\mu$M, 19.0 ± 2.03 pF, $n = 7$, $p < 0.05$; Table 1). With higher doses ($100\,\mu$M, $1\,$mM), adrenaline more markedly suppressed the GTP-γ-S-induced increase in the Cm (Figures 2(c) and 2(d); $100\,\mu$M, 7.61 ± 2.49 pF, $n = 8$, $p < 0.05$; $1\,$mM, 5.41 ± 2.90 pF, $n = 6$, $p < 0.05$; Table 1). In contrast, preincubation with dopamine did not significantly affect the GTP-γ-S-induced increase in the Cm regardless of its concentrations (Figure 3, Table 1). These results provided electrophysiological evidence for the first time that adrenaline inhibits the exocytotic process of mast cells dose-dependently. This strongly supported our findings that were obtained from Figure 1.

3.3. Effects of β_2-Adrenergic Receptor Antagonist on Adrenaline-Induced Inhibition of Mast Cell Degranulation.

Mast cells express numerous receptors on their cell surface that transduce stimulatory or inhibitory signals for degranulation [31, 32]. Among them, the β_2-adrenergic receptor is the major one that transduces inhibitory signals for exocytosis [3]. Since adrenaline is one of the most potent nonspecific stimulators of adrenergic receptors, we examined the involvement of this receptor-mediated pathway in the adrenaline-induced inhibition of exocytosis. Consistent with our findings obtained from Figures 1(a) and 1(b), preincubation with $1\,$mM adrenaline halted the induction of exocytosis in mast cells (Figures 4(a), B vs. A) by markedly suppressing the numbers of degranulating cells (Figure 4(b)). However, in the presence of $1\,$mM butoxamine, a specific β_2-adrenergic receptor antagonist, such inhibitory effect of adrenaline on exocytosis

TABLE 1: Summary of changes in membrane capacitance in enternal solutions containing adrenaline or dopamine.

Agents	N	Cm before GTP-S internalization (pF)	Cm after GTP-S internalization (pF)	ΔCm (pF)
External solution (control)	9	9.29 ± 0.37	34.0 ± 2.79	24.7 ± 2.64
$1\,\mu$M adrenaline	6	9.89 ± 0.72	27.4 ± 7.21	$17.5 \pm 6.83^*$
$10\,\mu$M adrenaline	7	9.29 ± 1.07	28.3 ± 2.07	$19.0 \pm 2.03^*$
$100\,\mu$M adrenaline	8	9.73 ± 0.92	17.3 ± 2.49	$7.61 \pm 2.49^*$
$1\,\mu$M adrenaline	6	10.1 ± 0.86	15.5 ± 3.28	5.41 ± 2.90
External solution (control)	5	8.18 ± 0.94	30.8 ± 1.89	22.6 ± 7.21
$1\,\mu$M adrenaline	8	11.6 ± 1.27	$36 \pm 2 \pm 11.2$	24.5 ± 3.70
$10\,\mu$M adrenaline	5	8.22 ± 0.77	31.8 ± 3.14	23.6 ± 2.94
$100\,\mu$M adrenaline	6	8.84 ± 1.23	30.2 ± 7.69	21.3 ± 7.13
$1\,\mu$M adrenaline	8	8.05 ± 0.52	33.4 ± 4.95	25.3 ± 4.77

Values are means $\pm$ SEM. Cm: membrane capacitance. $^*p < 0.05$ vs. ΔCm in external solution.

FIGURE 4: Effects of β_2-adrenergic receptor antagonist on adrenaline-induced inhibition of mast cell degranulation. (a) Differential-interference contrast (DIC) microscopic images were taken after exocytosis was externally induced by compound 48/80 in mast cells incubated in the external solutions containing no drug (A), 1 mM adrenaline (B), or 1 mM adrenaline in the presence of 1 mM butoxamine (C). (b) After exocytosis was induced in mast cells incubated in the external solutions containing no drug and 1 mM adrenaline with or without the presence of 1 mM butoxamine, the numbers of degranulating mast cells were expressed as percentages of the total mast cell numbers in selected bright fields. $^\#p < 0.05$ vs. incubation in the external solution alone. Values are means $\pm$ SEM. Differences were analyzed by ANOVA followed by Dunnett's test.

was almost completely erased (Figures 4(a), C and 4(b)). These results confirmed the previous findings in rat peritoneal mast cells that the stimulation of β_2-adrenergic receptors, which is linked to a cyclic AMP-dependent calcium mobilization via the coupling of G-proteins [33], is the major pathway for the adrenaline-induced inhibition of exocytosis [3].

(a)

(b)
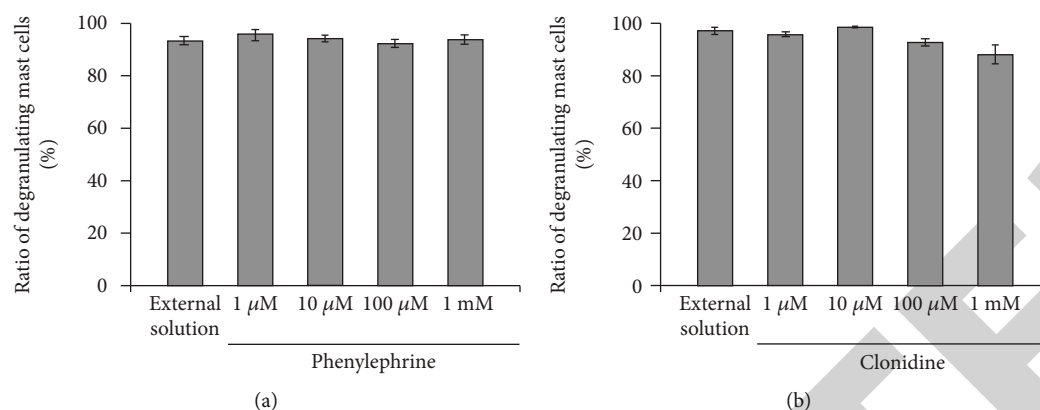
Figure 5: Effects of α_1- or α_2-adrenergic receptor agonists on mast cell degranulation. Effects of different concentrations (1, 10, and 100 μM and 1 mM) of phenylephrine (a) and clonidine (b). After the mast cells were incubated in the external solutions containing no drug or either drug, exocytosis was induced by compound 48/80. The numbers of degranulating mast cells were expressed as percentages of the total mast cell numbers in selected bright fields. Values are means ± SEM. Differences were analyzed by ANOVA followed by Dunnett's test.

3.4. Involvement of α-Adrenergic Receptors in Degranulation of Rat Peritoneal Mast Cells.

In addition to β_2-adrenergic receptors that transduce inhibitory signals for the degranulation of mast cells (Figure 4), studies revealed the localization of α_1-adrenergic receptors on mast cell membranes [4] and also provided in vivo evidence for the presence of α_2-adrenergic receptors [11, 34]. To reveal the involvement of these adrenergic receptors in the degranulation of mast cells, we examined the effects of the receptor agonists or antagonists.

3.4.1. Effects of α₁- or α₂-Adrenergic Receptor "Agonists" on Degranulation of Rat Peritoneal Mast Cells.

Consistent with our results shown in Figures 1(b) and 1(c), compound 48/80 caused degranulation in 80.0 ± 1.4% of the entire mast cells in the external solution alone ($n = 10$; Figure 5(a)). However, preincubation with 1, 10, and 100 μM and 1 mM phenylephrine, a selective α_1-adrenergic receptor agonist, did not significantly affect the numbers of degranulating mast cells regardless of their concentrations (Figure 5(a)). Similarly, preincubation with different concentrations of clonidine, a selective α_2-adrenergic receptor agonist, did not alter the ratio of degranulating mast cells, either (Figure 5(b)).

3.4.2. Effects of α₁- or α₂-Adrenergic Receptor "Antagonists" on Exocytosis of Rat Peritoneal Mast Cells.

Since α_1- and α_2-adrenergic receptor agonists did not affect the process of exocytosis in mast cells (Figure 5), we then examined the effects of α_1- and α_2-adrenergic receptor antagonists (Figure 6). The physiological concentration of prazosin, a selective α_1-adrenergic receptor antagonist, is as low as between 2.60 and 26.0 nM in humans [35], which is by far lower than that of adrenaline, dopamine, phenylephrine, and clonidine [36]. Additionally, in some in vitro studies, prazosin with concentrations as low as 0.1 μM was enough to exert inhibitory effects on the α_1-adrenergic receptor-mediated proliferation in cultured vascular smooth muscle cells [37]. Therefore, in the present study, we tried doses from

as low as 0.01 up to 1 μM (Figure 6(a)). Relatively lower doses, such as 0.01 and 0.1 μM, did not significantly affect the numbers of degranulating mast cells (Figure 6(a), A). However, 1 μM prazosin alone significantly reduced the ratio of degranulating mast cells compared to the external solution (from 84.5 ± 2.1% to 64.7 ± 3.8%, $n = 10$, $p < 0.05$). In mast cells, the process of degranulation during exocytosis was monitored by the increase in the Cm [13–17, 27, 28]. Actually, in the present study, the ratio of degranulating mast cells was well correlated with the GTP-γ-S-induced increase in the Cm (ΔCm) (Figures 1 to 3, Table 1). Therefore, we additionally examined the effects of prazosin on the ΔCm (Figure 6(a), B). Similarly to the ratio of degranulating mast cells (Figure 6(a), A), low-dose prazosin did not significantly affect the ΔCm (Figure 6(a), B). However, 1 μM prazosin alone significantly decreased the ΔCm compared to the external solution (from 19.6 ± 2.38 pF to 10.4 ± 1.68 pF, $n = 6$, $p < 0.05$; Figure 6(a), B). These results provided electrophysiological evidence that high-dose prazosin can inhibit the process of exocytosis in mast cells. In contrast, however, yohimbine, a selective α_2-adrenergic receptor antagonist, did not affect the ratio of degranulating mast cells (Figure 6(b)). These results suggested that the process of exocytosis in mast cells may be partially mediated by α_1-adrenergic receptors, but not by α_2-adrenergic receptors.

3.5. Effects of Prazosin on Adrenaline-Induced Inhibition of Mast Cell Degranulation.

From our results, since 1 μM prazosin inhibited the process of exocytosis in mast cells (Figure 6(a)), we finally examined its effect on the adrenaline-induced inhibition of exocytosis (Figure 7). Consistent with our results shown Figures 1(a) and 1(b), preincubation with 1 mM adrenaline halted the induction of exocytosis (Figure 7(a), B vs. A) and markedly reduced the numbers of degranulating mast cells (Figure 7(b)). In the presence of 1 μM prazosin, such inhibitory effect of adrenaline on exocytosis was augmented (Figure 7(b)) and the induction of exocytosis was almost totally suppressed (Figure 7(a), C). These results suggested that the blockade of α_1-adrenergic
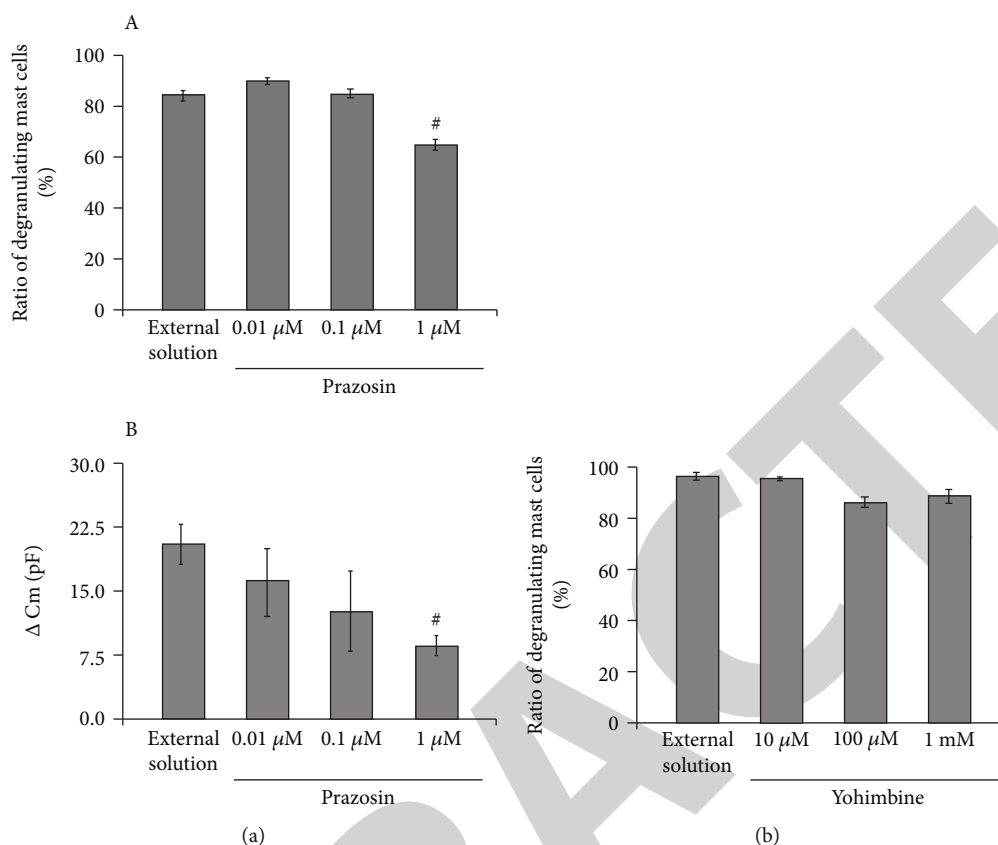
FIGURE 6: Effects of α_1- or α_2-adrenergic receptor antagonists on mast cell degranulation. (a) Effects of prazosin on mast cell degranulation and membrane capacitance. (A) After the mast cells were incubated in the external solutions containing no drug or different concentrations (0.01, 0.1, and 1 μM) of prazosin, exocytosis was induced by compound 48/80. The numbers of degranulating mast cells were expressed as percentages of the total mast cell numbers in selected bright fields. (B) After the mast cells were incubated in the external solutions containing no drug or different concentrations (0.01, 0.1, and 1 μM) of prazosin, the whole-cell recording configuration was established in single mast cells and dialysis with 100 μM GTP-γ-S was started. The GTP-γ-S-induced increase in the Cm (ΔCm) was calculated. (b) Effects of yohimbine on mast cell degranulation. After the mast cells were incubated in the external solutions containing no drug or different concentrations (10 and 100 μM and 1 mM) of yohimbine, exocytosis was induced by compound 48/80. The numbers of degranulating mast cells were expressed as percentages of the total mast cell numbers in selected bright fields. $^{\#}p < 0.05$ vs. incubation in the external solution alone. Values are means ± SEM. Differences were analyzed by ANOVA followed by Dunnett's test.

receptors by prazosin can synergistically potentiate the β_2-adrenergic receptor-mediated inhibition of exocytosis in mast cells.

4. Discussion

For people experiencing anaphylaxis or those at risks of anaphylactic reaction, intramuscular injection of adrenaline, a nonselective agonist of β-adrenergic receptors, has been the first choice of the treatment [2]. In previous studies, by measuring the amount of histamine released from mast cells, suppressive effects of adrenaline on the activation of mast cells were indirectly monitored [9, 10]. However, to precisely determine the ability of adrenaline on the stabilization of mast cells, the exocytotic process itself needs to be monitored, otherwise the release of all the chemical mediators or the inflammatory substances have to be evaluated. In our previous patch-clamp studies using rat peritoneal mast cells, the degranulating process during exocytosis was successively monitored by the gradual increase in the whole-cell Cm [15–17, 29, 38]. Employing this electrophysiological approach, our recent studies revealed the inhibitory effects of antiallergic drugs, antibiotics, and corticosteroids on the exocytotic process of mast cells [13–16]. In these studies, the mast cell-stabilizing properties of the drugs were quantitatively determined by the suppressed value of Cm which is to be increased by the GTP-γ-S internalization [13, 14]. In the present study, applying the same approach, we provided direct evidence for the first time that adrenaline actually inhibits the process of exocytosis dose-dependently and thus exerts mast cell-stabilizing property.

The physiological concentration of adrenaline in the plasma is usually below 0.1 μM at the basal level [39, 40]. However, it reaches more than 0.3 μM up to 1.5 μM after intramuscular injection in the treatment of anaphylaxis [41, 42]. In the present study, 1 μM adrenaline significantly deceased the number of degranulating mast cells by approximately 20% (Figure 1(b)), which was consistent with the
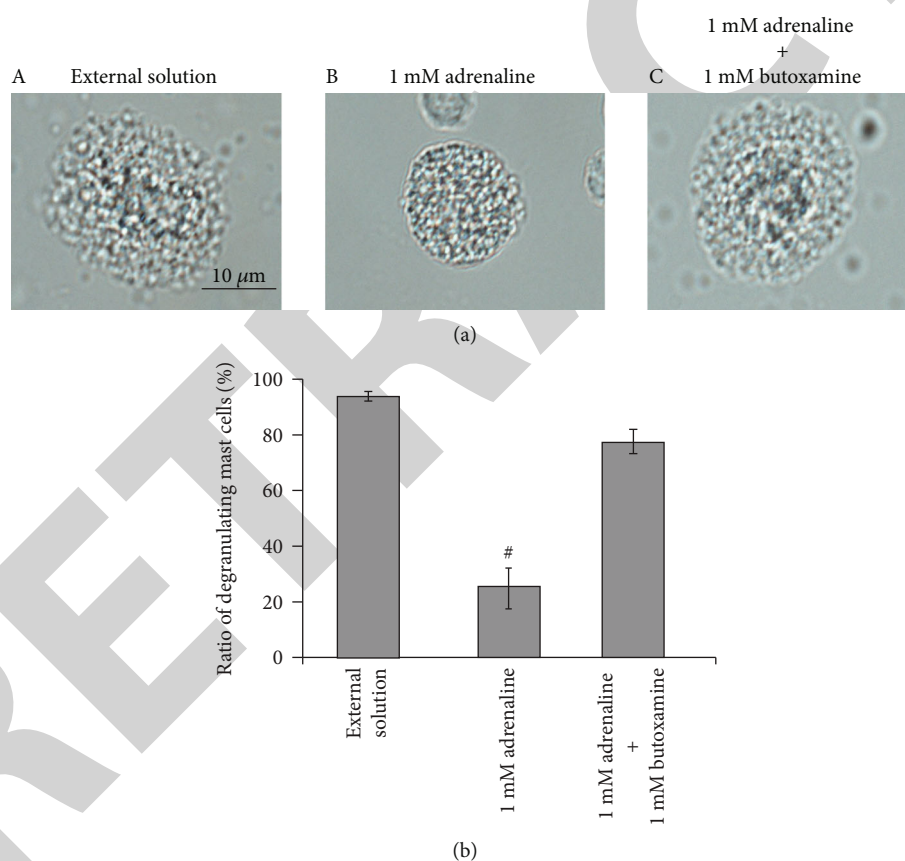
(a)

(b)
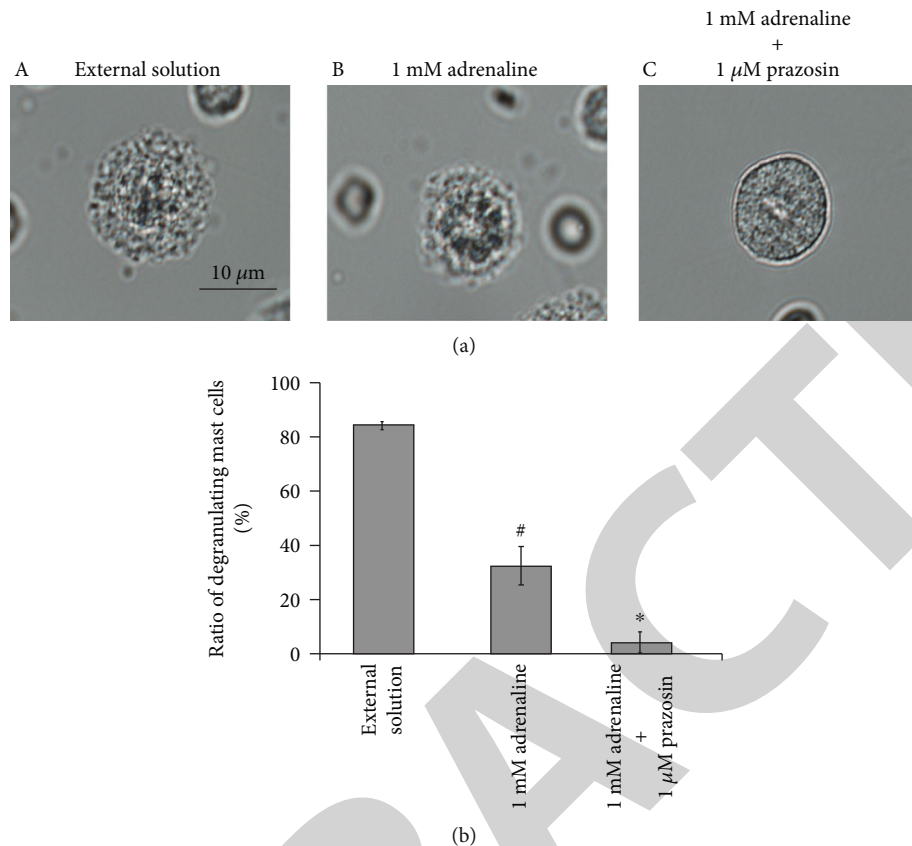
FIGURE 7: Effects of α_1-adrenergic receptor antagonist on adrenaline-induced inhibition of mast cell degranulation. (a) Differential-interference contrast (DIC) microscopic images were taken after exocytosis was externally induced by compound 48/80 in mast cells incubated in the external solutions containing no drug (A), 1 mM adrenaline (B), or 1 mM adrenaline in the presence of 1 μM prazosin (C). (b) After exocytosis was induced in mast cells incubated in the external solutions containing no drug and 1 mM adrenaline with or without the presence of 1 μM prazosin, the numbers of degranulating mast cells were expressed as percentages of the total mast cell numbers in selected bright fields. #$p < 0.05$ vs. incubation in the external solution alone. *$p < 0.05$ vs. incubation in the external solution containing 1 mM adrenaline. Values are means ± SEM. Differences were analyzed by ANOVA followed by Tukey's test.

findings obtained from previous studies [9]. Additionally, we further revealed for the first time that adrenaline with higher doses, such as 10 and 100 μM and 1 mM, more markedly suppressed the degranulation of mast cells dose-dependently (Figure 1(b)). These findings could be clinically applied to the topical use of adrenaline on the nasal mucosa [40], where higher concentrations are locally required before the drug is absorbed into the venous circulation by the transcellular diffusion [43]. In the present study, exocytosis was externally induced by compound 48/80 after pretreating mast cells with adrenaline. Similar to the antigen binding to IgE on mast cells that causes quick anaphylactic reaction, compound 48/80 initiates the degranulation of mast cells as immediately as 10 seconds after its addition [44]. Therefore, it would be difficult to examine the "therapeutic" effects of adrenaline on reversing the ongoing degranulation of mast cells. However, our study clearly demonstrated the "prophylactic" effects of adrenaline on suppressing the further initiation of exocytosis in mast cells. In our whole experiments, we used mast cells isolated from the peritoneal cavity of rats less than 25 weeks old, since mast cells isolated form these relatively younger rats were viable enough to be easily induced exocytosis by

the exogenous or endogenous pharmacological stimuli [13–16, 45].

In the present study, butoxamine, a β_2-adrenergic receptor antagonist, almost totally restored the adrenaline-induced inhibition of mast cell degranulation (Figure 4). This confirmed the previous findings that the β_2-adrenergic pathway is the major pathway in which adrenaline transduces inhibitory signals for the degranulation of mast cells [3, 33]. In addition to β_2-adrenergic receptors, previous in vitro studies demonstrated the expression of α_1-adrenergic receptors on mast cell membranes [4] or provided in vivo evidence indicating the presence of α_2-adrenergic receptors [11, 34]. There are two types of mast cells that exist throughout the body [46]. One is the connective tissue type, which primarily exists in loose connective tissues, such as the peritoneal cavity or skin. The other is the mucosal type, which primarily exists in the airway or gastrointestinal mucosa. In contrast to β_2-adrenergic receptors that are expressed in both types of mast cells [47], α_1-adrenergic receptors were shown to be expressed in mast cells isolated from heart connective tissue [4]. However, several in vitro studies using α-adrenergic agonists functionally demonstrated the presence of α-adrenergic

receptors in mucosal-type mast cells, such as human lung mast cells [5]. From our results, α_2-adrenergic receptors were not likely to be involved in the process of exocytosis in mast cells, since both agonist and antagonist of the receptors did not affect the degranulation of mast cells (Figures 5(b) and 6(b)). On the other hand, we noted for the first time that high-dose prazosin, an α_1-adrenergic receptor antagonist, significantly suppressed the degranulation of mast cells (Figure 6(a)) and synergistically potentiated the adrenaline-induced inhibition of exocytosis (Figure 7). In previous in vitro studies using human lung mast cells, stimulation of α_1-adrenergic receptors increased the release of chemical mediators [5]. Based on this, later studies further demonstrated in humans that the pharmacological blockade of α_1-adrenergic receptors actually ameliorated the airway hyperresponsiveness in patients with asthma [7, 8]. In this context, our results strongly suggested that the blockade of α_1-adrenergic receptor by prazosin may also be useful in the treatment of anaphylaxis by potentiating the therapeutic efficacy of adrenaline. However, to exert such effects, prazosin with doses much higher than those of the physiological concentration was required (Figure 6(a)), which can deteriorate hypotension due to the blockade of vascular α_1-adrenergic receptors [48]. In such cases, the use of omalizumab or talizumab that directly inhibits the binding of IgE to FcεRI may be considered [49], since these reagents are more selective to immune systems compared to prazosin.

As we have shown in our patch-clamp studies, the elevation of the intracellular Ca^{2+} concentration ($[Ca^{2+}]_i$) primarily triggers exocytosis in mast cells [14]. According to previous studies using human lung mast cells, the elevation of the $[Ca^{2+}]_i$ was primarily ascribable to the activity of Ca^{2+}-activated K^+ channels (KCa 3.1), because these channels facilitate the Ca^{2+} influx through store-operated calcium channels (SOCs) [50]. Upon activation, α_1-adrenergic receptors stimulate phospholipase C (PLC) via the coupling of G proteins [51]. This enzymatically cleaves phosphatidylinositol triphosphate (PIP_2) into inositol triphosphate (IP_3) and diacylglycerol (DAG), which leads to the activation of protein kinase C (PKC) [52]. Since PKC is known to stimulate the activity of KCa 3.1 [53] or SOC, such as transient receptor potential canonical (TRPC) 1 and 6 [54, 55], the upstream blockade of the α_1-adrenergic receptor by prazosin may inhibit the activity of these channels. Such induced decrease in $[Ca^{2+}]_i$ was thought to be the mechanism by which prazosin exerts mast cell-stabilizing property. Alternatively, as we previously demonstrated in antiallergic drugs or macrolide antibiotics [13, 14, 16], highly lipophilic prazosin [56], which is prone to penetrate into the plasma membrane and accumulate there, may have induced membrane stretch in mast cells. Such mechanical stimuli to the membranes would rearrange the cytoskeletal structures, influencing the activity of the K^+ or Ca^{2+} channels expressed in mast cells. Consequently, such induced changes in the $[Ca^{2+}]_i$ were thought to contribute to the prazosin-induced inhibition of exocytosis.

In summary, this study provided electrophysiological evidence for the first time that adrenaline dose-dependently inhibits the process of exocytosis, confirming its usefulness as a potent mast cell stabilizer. The pharmacological blockade of the α_1-adrenergic receptor by prazosin synergistically potentiated such mast cell-stabilizing property of adrenaline, which is primarily mediated by β_2-adrenergic receptors.

Data Availability

The data used to support the findings of this study are available from the corresponding author upon request.

Conflicts of Interest

The authors declare no conflicts of interest.

Acknowledgments

References

[1] H. A. Sampson, A. Muñoz-Furlong, R. L. Campbell et al., "Second symposium on the definition and management of anaphylaxis: Summary report—Second National Institute of Allergy and Infectious Disease/Food Allergy and Anaphylaxis Network symposium," *Journal of Allergy and Clinical Immunology*, vol. 117, no. 2, pp. 391–397, 2006.

[2] S. F. Kemp, R. F. Lockey, and F. E. R. Simons, "Epinephrine," *World Allergy Organization Journal*, vol. 1, Supplement, pp. S18–S26, 2008.

[3] H. S. Kuehn and A. M. Gilfillan, "G protein-coupled receptors and the modification of FcepsilonRI-mediated mast cell activation," *Immunology Letters*, vol. 113, no. 2, pp. 59–69, 2007.

[4] W. Schulze and M. L. Fu, "Localization of alpha 1-adrenoceptors in rat and human hearts by immunocytochemistry," *Molecular and Cellular Biochemistry*, vol. 163-164, pp. 159–165, 1996.

[5] M. Kaliner, R. P. Orange, and K. F. Austen, "Immunological release of histamine and slow reacting substance of anaphylaxis from human lung," *The Journal of Experimental Medicine*, vol. 136, no. 3, pp. 556–567, 1972.

[6] F. Moroni, R. Fantozzi, E. Masini, and P. F. Mannaioni, "The modulation of histamine release by alpha-adrenoceptors: evidences in murine neoplastic mast cells," *Agents and Actions*, vol. 7, no. 1, pp. 57–61, 1977.

[7] P. J. Barnes, N. M. Wilson, and H. Vickers, "Prazosin, an alpha 1-adrenoceptor antagonist, partially inhibits exercise-induced asthma," *The Journal of Allergy and Clinical Immunology*, vol. 68, no. 6, pp. 411–415, 1981.

[8] C. Jenkins, A. B. Breslin, and G. E. Marlin, "The role of alpha and beta adrenoceptors in airway hyperresponsiveness to histamine," *The Journal of Allergy and Clinical Immunology*, vol. 75, no. 3, pp. 364–372, 1985.

[9] W. H. Ng, R. Polosa, and M. K. Church, "Adenosine bronchoconstriction in asthma: investigations into its possible mechanism of action," *British Journal of Clinical Pharmacology*, vol. 30, Suppl 1, pp. 89S–98S, 1990.

[10] E. E. Graevskaya, M. Y. Akhalaya, and E. N. Goncharenko, "Effects of cold stress and epinephrine on degranulation of peritoneal mast cells in rats," *Bulletin of Experimental Biology and Medicine*, vol. 131, no. 4, pp. 333–335, 2001.

[11] B. R. Lindgren, N. Grundstrom, and R. G. Andersson, "Comparison of the effects of clonidine and guanfacine on the histamine liberation from human mast cells and basophils and on the human bronchial smooth muscle activity," *Arzneimittel-Forschung*, vol. 37, no. 5, pp. 551–553, 1987.

[12] B. L. Gruber, "Mast cells in the pathogenesis of fibrosis," *Current Rheumatology Reports*, vol. 5, no. 2, pp. 147–153, 2003.

[13] A. Baba, M. Tachi, Y. Maruyama, and I. Kazama, "Olopatadine inhibits exocytosis in rat peritoneal mast cells by counteracting membrane surface deformation," *Cellular Physiology and Biochemistry*, vol. 35, no. 1, pp. 386–396, 2015.

[14] A. Baba, M. Tachi, Y. Ejima et al., "Anti-allergic drugs tranilast and ketotifen dose-dependently exert mast cell-stabilizing properties," *Cellular Physiology and Biochemistry*, vol. 38, no. 1, pp. 15–27, 2016.

[15] T. Mori, N. Abe, K. Saito et al., "Hydrocortisone and dexamethasone dose-dependently stabilize mast cells derived from rat peritoneum," *Pharmacological Reports*, vol. 68, no. 6, pp. 1358–1365, 2016.

[16] I. Kazama, K. Saito, A. Baba et al., "Clarithromycin dose-dependently stabilizes rat peritoneal mast cells," *Chemotherapy*, vol. 61, no. 6, pp. 295–303, 2016.

[17] I. Kazama, Y. Maruyama, S. Takahashi, and T. Kokumai, "Amphipaths differentially modulate membrane surface deformation in rat peritoneal mast cells during exocytosis," *Cellular Physiology and Biochemistry*, vol. 31, no. 4-5, pp. 592–600, 2013.

[18] I. Kazama, Y. Maruyama, and S. Nakamichi, "Aspirin-induced microscopic surface changes stimulate thrombopoiesis in rat megakaryocytes," *Clinical and Applied Thrombosis/Hemostasis*, vol. 20, no. 3, pp. 318–325, 2014.

[19] I. Kazama, Y. Maruyama, and Y. Murata, "Suppressive effects of nonsteroidal anti-inflammatory drugs diclofenac sodium, salicylate and indomethacin on delayed rectifier K+-channel currents in murine thymocytes," *Immunopharmacology and Immunotoxicology*, vol. 34, no. 5, pp. 874–878, 2012.

[20] I. Kazama, Y. Maruyama, and M. Matsubara, "Benidipine persistently inhibits delayed rectifier K(+)-channel currents in murine thymocytes," *Immunopharmacology and Immunotoxicology*, vol. 35, no. 1, pp. 28–33, 2013.

[21] I. Kazama and Y. Maruyama, "Differential effects of clarithromycin and azithromycin on delayed rectifier K(+)-channel currents in murine thymocytes," *Pharmaceutical Biology*, vol. 51, no. 6, pp. 760–765, 2013.

[22] I. Kazama, A. Baba, and Y. Maruyama, "HMG-CoA reductase inhibitors pravastatin, lovastatin and simvastatin suppress delayed rectifier K(+)-channel currents in murine thymocytes," *Pharmacological Reports*, vol. 66, no. 4, pp. 712–717, 2014.

[23] A. Baba, M. Tachi, Y. Maruyama, and I. Kazama, "Suppressive effects of diltiazem and verapamil on delayed rectifier K+-channel currents in murine thymocytes," *Pharmacological Reports*, vol. 67, no. 5, pp. 959–964, 2015.

[24] I. Kazama, Y. Ejima, Y. Endo et al., "Chlorpromazine-induced changes in membrane micro-architecture inhibit thrombopoiesis in rat megakaryocytes," *Biochimica et Biophysica Acta*, vol. 1848, no. 11, pp. 2805–2812, 2015.

[25] I. Kazama, A. Baba, Y. Endo et al., "Salicylate inhibits thrombopoiesis in rat megakaryocytes by changing the membrane micro-architecture," *Cellular Physiology and Biochemistry*, vol. 35, no. 6, pp. 2371–2382, 2015.

[26] K. Saito, N. Abe, H. Toyama et al., "Second-Generation Histamine H1 Receptor Antagonists Suppress Delayed Rectifier K+-Channel Currents in Murine Thymocytes," *BioMed Research International*, vol. 2019, Article ID 6261951, 12 pages, 2019.

[27] J. M. Fernandez, E. Neher, and B. D. Gomperts, "Capacitance measurements reveal stepwise fusion events in degranulating mast cells," *Nature*, vol. 312, no. 5993, pp. 453–455, 1984.

[28] D. Lorenz, B. Wiesner, J. Zipper et al., "Mechanism of peptide-induced mast cell degranulation. Translocation and patch-clamp studies," *The Journal of General Physiology*, vol. 112, no. 5, pp. 577–591, 1998.

[29] E. Neher, "The influence of intracellular calcium concentration on degranulation of dialysed mast cells from rat peritoneum," *The Journal of Physiology*, vol. 395, pp. 193–214, 1988.

[30] R. Penner and E. Neher, "Secretory responses of rat peritoneal mast cells to high intracellular calcium," *FEBS Letters*, vol. 226, no. 2, pp. 307–313, 1988.

[31] B. D. McNeil, P. Pundir, S. Meeker et al., "Identification of a mast-cell-specific receptor crucial for pseudo-allergic drug reactions," *Nature*, vol. 519, no. 7542, pp. 237–241, 2015.

[32] H. R. Katz, "Inhibitory receptors and allergy," *Current Opinion in Immunology*, vol. 14, no. 6, pp. 698–704, 2002.

[33] L. K. Chong, A. H. Morice, W. W. Yeo, R. P. Schleimer, and P. T. Peachell, "Functional desensitization of beta agonist responses in human lung mast cells," *American Journal of Respiratory Cell and Molecular Biology*, vol. 13, no. 5, pp. 540–546, 1995.

[34] B. Lindgren, A. Brundin, and R. Andersson, "Inhibitory effects of clonidine on the allergen-induced wheal-and-flare reactions in patients with extrinsic asthma," *The Journal of Allergy and Clinical Immunology*, vol. 79, no. 6, pp. 941–946, 1987.

[35] P. C. Rubin, L. Butters, R. A. Low, and J. L. Reid, "Clinical pharmacological studies with prazosin during pregnancy complicated by hypertension," *British Journal of Clinical Pharmacology*, vol. 16, no. 5, pp. 543–547, 1983.

[36] J. Vincent, P. A. Meredith, J. L. Reid, H. L. Elliott, and P. C. Rubin, "Clinical pharmacokinetics of prazosin–1985," *Clinical Pharmacokinetics*, vol. 10, no. 2, pp. 144–154, 1985.

[37] S. M. Yu, S. Y. Tsai, J. H. Guh, F. N. Ko, C. M. Teng, and J. T. Ou, "Mechanism of catecholamine-induced proliferation of vascular smooth muscle cells," *Circulation*, vol. 94, no. 3, pp. 547–554, 1996.

[38] R. Penner, "Multiple signaling pathways control stimulus-secretion coupling in rat peritoneal mast cells," *Proceedings of the National Academy of Sciences of the United States of America*, vol. 85, no. 24, pp. 9856–9860, 1988.

[39] J.-J. Body, P. E. Cryer, K. P. Offord, and H. Heath III, "Epinephrine is a hypophosphatemic hormone in man. Physiological effects of circulating epinephrine on plasma calcium, magnesium, phosphorus, parathyroid hormone, and calcitonin," *Journal of Clinical Investigation*, vol. 71, no. 3, pp. 572–578, 1983.

[40] K. M. Sarmento Junior, S. Tomita, and A. O. Kos, "Topical use of adrenaline in different concentrations for endoscopic sinus surgery," *Brazilian Journal of Otorhinolaryngology*, vol. 75, no. 2, pp. 280–289, 2009.

Research Article

A Static Magnetic Field Inhibits the Migration and Telomerase Function of Mouse Breast Cancer Cells

Zhu Fan [ID],[1] **Pingdong Hu** [ID],[2,3] **Lekang Xiang,**[1] **Ying Liu** [ID],[1] **Rongqiao He,**[2] **and Tao Lu** [ID][1]

[1]*School of Life Sciences, Beijing University of Chinese Medicine, Beijing 100029, China*
[2]*State Key Laboratory of Brain and Cognitive Science, Institute of Biophysics, CAS, Beijing 100101, China*
[3]*University of Chinese Academy of Sciences, Beijing 100101, China*

Correspondence should be addressed to Ying Liu; yingliu@bucm.edu.cn and Tao Lu; taolu@bucm.edu.cn

Zhu Fan and Pingdong Hu contributed equally to this work.

Static magnetic field (SMF) has a potential as a cancer therapeutic modality due to its specific inhibitory effects on the proliferation of multiple cancer cells. However, the underlying mechanism remains unclear, and just a few studies have examined the effects of SMF on metastasis, an important concern in cancer treatment. In this study, we evaluated the effects of moderate SMF (~150 mT) on the proliferation and migration of 4T1 breast cancer cells. Our results showed that SMF treatment accelerated cell proliferation but inhibited cell migration. Further, SMF treatment shortened the telomere length, decreased telomerase activity, and inhibited the expression of the cancer-specific marker telomerase reverse transcriptase (TERT), which may be related to expression upregulation of e2f1, a transcription repressor of TERT and positive regulator of the mitotic cell cycle. Our results revealed that SMF repressed both, cell migration and telomerase function. The telomerase network is responsive to SMF and may be involved in SMF-mediated cancer-specific effects; moreover, it may function as a therapeutic target in magnetic therapy of cancers.

1. Introduction

Static magnetic fields, such as the natural geomagnetic field (GMF, ~50 μT) and artificial magnetic fields produced by magnetic materials or instruments, are widely present in the environment. Magnetic fields of different intensities play an important role in the diagnosis and treatment of diseases [1]. For example, strong magnetic field (>1 T) are used in magnetic resonance imaging to help diagnose diseases, whereas moderate magnetic fields (1 mT–1 T) are widely used in the alternative and complementary treatment of various diseases [2–4]. Potential applications of SMF in cancer treatments have been indicated because of the specific inhibitory effects of SMF on the growth of multiple types of cancer cells. However, there is no consensus regarding the effect of SMF on cancer cells, and understanding the effects and underlying mechanism of SMF is critical before this method can be clinically applied.

Many studies have shown that SMF inhibits the proliferation of multiple tumor cells, and tumor cells could be more sensitive to magnetic fields compared to nontumor cells. Zhang et al. [5] treated seven human solid cancer cell lines and five human noncancer cell lines with 1-T magnetic field and found that the SMF significantly affected the proliferation of cancer cells but not noncancer cells. These results indicate that cancer-specific molecules are involved in cell proliferation regulation by SMF. Telomerase is cancer-specific marker rarely expressed in noncancer cells, and telomerase activation is a key factor in maintaining the telomere length for the immortal division of cancer cells [6]. Therapies targeting telomeres trigger DNA damage responses in tumor cells and lead to aging or apoptosis [7–9]. We speculate that SMF may cause alterations in telomerase to affect the proliferation of cancer cells.

In addition, metastatic cancer is more fatal than nonmetastatic cancer [10]. However, few studies have evaluated the

(a)   (b)
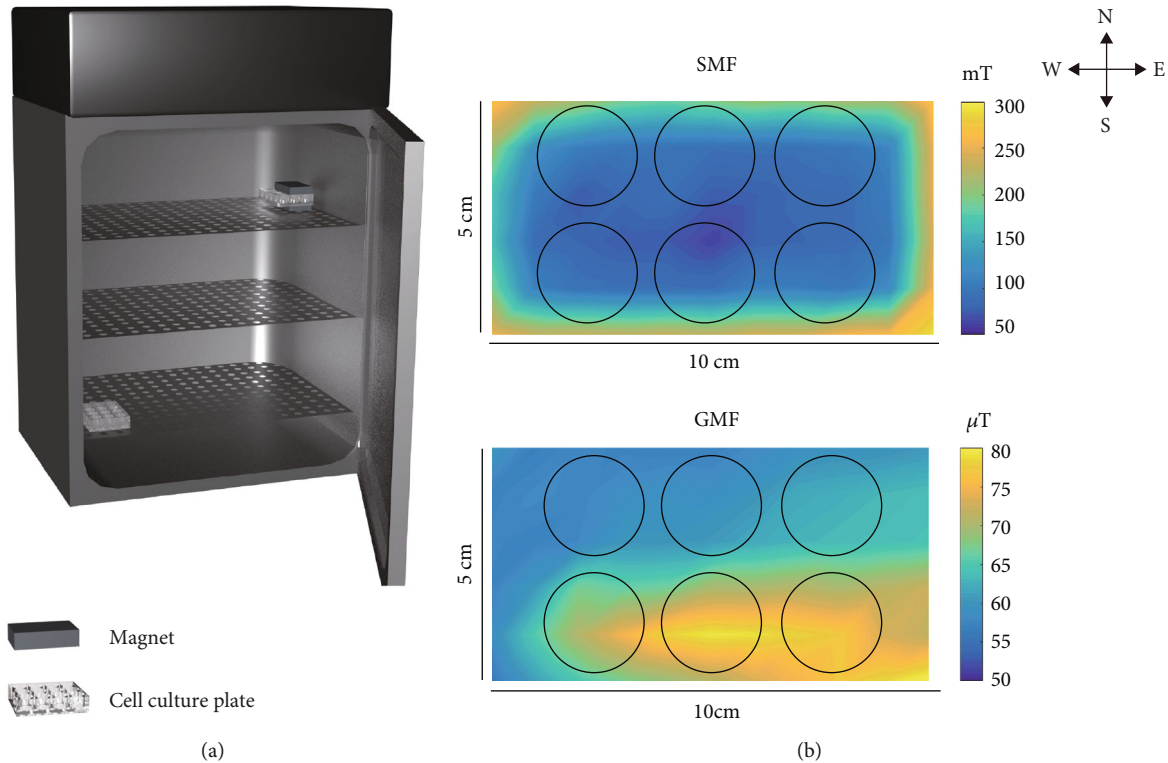
FIGURE 1: Experimental setups for SMF treatment. (a) The cell incubation system for MF treatment. A pair of magnets placed upon and under the cell plate provided the SMF. GMF control and SMF-exposed cells were incubated on different floors. (b) Distributions of the magnetic fields (vector sum) at the bottom plane of the cell plate for SMF (~153 mT) and GMF (~65 μT) treatment. Magnetic field was measured at an interval of 1×1 cm. (Black circles represent the exposed cell wells of a 12-well plate).

effects of moderate SMF on the migration of cancer cells. We previously found that GMF shielding (<200 nT) accelerated the proliferation but inhibited the cell motility of human neuroblastoma cells, but the specific effects were difficult to determine in the absence of a molecular marker [11, 12]. In addition to its classic role in affecting telomere length, telomerase is also related to the migration of cancer cells, and the expression of the subunit telomerase reverse transcriptase (TERT) can be used to distinguish benign from malignant tumors. The overexpression of TERT promotes cell migration, whereas a reduction in TERT expression results in decreased cell migration and adhesion [13, 14]. Coanalysis of the effects of SMF on cell proliferation, migration, and telomeres will increase the understanding of the effects and underlying mechanisms, as well as the risk of magnetic therapy.

Breast cancer cells are commonly used as a model for analyzing cancer metastasis and are sensitive to SMF treatment. SMF can inhibit the proliferation of different breast cancer cells and enhance the efficacy of specific chemotherapy drugs both *in vivo* [15] and *in vitro* [16–18]. Therefore, in this study, we evaluated the effects of a moderate SMF (~150 mT) on 4T1 breast cancer cells. We found that SMF treatment accelerated cell proliferation but inhibited cell migration and telomerase function, which were related to decreased telomerase activity and TERT expression. Our findings revealed that cancerous features of cells were reduced by SMF. The telomerase network responds to SMF and may act as a target in magnetic therapy for breast cancer.

2. Materials and Methods

2.1. Cell Culture and Treatment. Mouse breast cancer cell line 4T1 was purchased from the Cell Culture Bank of the Chinese Academy of Sciences' Culture Collection Committee. Cells were maintained in Dulbecco's Modified Eagle Medium (DMEM) (high D-glucose) supplemented with 10% fetal bovine serum (FBS; Gibco, Grand Island, NY, USA), 100 U/mL penicillin, and 100 μg/mL streptomycin (Gibco) and cultured at 37°C with 5% CO_2. The medium was changed every 2 days.

For magnetic field treatment, cells in the logarithmic growth phase were seeded at a density of 1×10^4 cells/mL at 1 mL/well in a 12-well plate except for in the Transwell assay. After incubation for 12 h, the cells were exposed to a moderate SMF. Cells cultured in the GMF area without SMF treatment were used as controls.

2.2. MF Conditions. The SMF and GMF conditions were set up in a CO_2 incubator (width × height × depth: $63 \times 92 \times 69$ cm, INCO 153 med, Memmert, Schwabach, Germany) on different layers. The untreated GMF control samples were placed at a position with an average SMF of 65.08 ± 7.18 μT, which is similar to the local magnetic field in the laboratory. A 150-mT rectangular magnet (neodymium iron boron, 10×5 cm, Genchang, Jiangsu, China) was applied for SMF treatment. The cell plate was placed between a pair of magnet blocks as shown in Figure 1(a), and no more than

TABLE 1: Magnetic field conditions[a].

Group	Position	$|B|$[b]	$|Bx|$[c]	$|By|$[d]	$|Bz|$[e]
SMF (mT)	Center	75.92 ± 7.76	6.5 ± 3.14	2.83 ± 1.46	75.5 ± 7.91
	Southeast	97.97 ± 13.16	24.83 ± 6.06	15.66 ± 11.17	92.83 ± 14.45
	Southwest	88.96 ± 10.82	4.5 ± 2.75	17.66 ± 16.42	85.66 ± 9.14
	Northeast	95.5 ± 10.39	14.83 ± 6.71	4.16 ± 4.41	94 ± 9.52
	Northwest	97.55 ± 16.2	3.5 ± 2.98	6.33 ± 4.71	97.16 ± 15.56
	Average	153.9 ± 72.0			
GMF (μT)	Center	64.85 ± 4.27	25.86 ± 3.96	56.93 ± 5.45	16.28 ± 2.07
	Southeast	92.62 ± 0.63	23.45 ± 2.3	55.65 ± 0.43	17.63 ± 0.19
	Southwest	73.42 ± 3.11	29.71 ± 4.9	63.11 ± 6.63	21.13 ± 4.37
	Northeast	58.29 ± 0.88	20.46 ± 1.83	51.09 ± 1.27	19.05 ± 0.85
	Northwest	67.4 ± 4.46	18.93 ± 14.05	60.6 ± 10.76	14.51 ± 2.79
	Average	65.08 ± 7.18			

[a] Data are the mean ± sd of measurement reads at the same layer; [b] Net static magnetic field (vector sum of the three directions); [c–e] Magnetic field directions: x, south to north; y, east to west; z, downward. *: $|B| = \sqrt{(Bx)^2 + (By)^2 + (Bz)^2}$.

2 sets of SMF/GMF plates were placed in one incubator to prevent the MFs from disturbing the other plates. The average SMF was 153.9 ± 72.0 mT (vector sum, Table 1), which was calculated from measurements performed at an interval of 1×1 cm on the bottom of the plate attached to the magnet (Figure 1 and Table 1). The five positions represent the mean field strength in the cell culture wells in the southeast, southwest, northeast, and northwest, and center of the magnetic field. The SMFs were measured with a permanent magnet digital gauss meter (HT20, Shanghai Hengtong, Shanghai, China).

2.3. Cell Proliferation Assays.
Cell proliferation was analyzed hemocytometry for cell counting and in a cell division assay by carboxyfluorescein diacetate succinimidyl ester (CFSE) staining.

CFSE staining was conducted according to the manufacturer's instructions (Cat. No. 565082, BD Horizon, BD Biosciences, Franklin Lakes, NJ, USA). Briefly, the cells were stained with 25μM CFSE for 20 min at 37°C. After two washes with phosphate-buffered saline, the CFSE-stained cells were seeded into 12-well plates for magnetic field treatment as described in section 2.1. The cells were collected after 24 and 48 h of exposure, and CFSE fluorescence was measured with a FACS Caliburflow cytometer (BD Biosciences) and analyzed with the Cell Quest Pro software.

2.4. Wound Healing Assay.
Cells were seeded into 12-well plates containing DMEM with 10% FBS and grown into monolayers. After confluence reached greater than 90%, wounds were made with a pipette tip to form a cross area on the cells. Detached cells were removed using serum-free DMEM, and 4T1 cells were exposed to an SMF for 24 h. The wound width was imaged at 0 (D0) and 24 h (d) and analyzed using the ImageJ software (NIH, Bethesda, MD, USA). The migration efficiency was calculated as $(D0 - d)/d \times 100\%$.

2.5. Transwell Assay.
Cell migration was detected in 24-well Transwell chambers (Corning, Inc., Corning, NY, USA). 4T1 cells (5×10^4 cells) were resuspended in DMEM (200μL) with 1% FBS added to the upper chamber, and 400μL DMEM with 10% fetal bovine serum added to the lower chamber. 4T1 cells were exposed to GMF and SMF for 24 h. After fixation, the cells were stained with 0.1% Hoechst and photographed with a DM5000 B microscope (Leica, Wetzlar, Germany). Five randomly selected fields of each membrane were counted. Cell numbers were calculated using the ImageJ software.

2.6. Reverse Transcription Real-Time Quantitative Polymerase Chain Reaction (RT-qPCR).
The expression of *TERT*, *e2f1*, *mzf1*, and *sp1* was analyzed by RT-qPCR. After 72 h of exposure, RNA was extracted using a RNeasy Mini kit according to the manufacturer's instructions (Qiagen, Hilden, Germany). Reverse transcription from total RNA was performed to synthesize cDNA (Qiagen), and a Rotor gene Q PCR Cycler (Qiagen, Valencia, CA, USA) was used for detection. Primer sequences were designed using Primer bank (https://pga.mgh.harvard.edu/primerbank/) [19], as shown in Table 2. *Gapdh* was used as an internal control.

2.7. Telomerase Activity Assay.
The telomerase activity of the cell extracts was measured with a TRAPeze RT Telomerase Detection Kit (Cat. No. S7710; Millipore, Billerica, MA, USA). The cells were inoculated into 12-well plates, and the inoculation density and treatment conditions were the same as those described in section 2.1. After 72 h of treatment, we tested the telomerase activity according to the manufacturer's instructions. Each assay mixture consisted of 5μL 5x TRAPeze RT reaction mixture, 17.6μL PCR grade water, 0.4μL 50x TITANIUM Taq DNA polymerase (Clontech, Mountain View, CA, USA), and 2μL cell extract or control template. A series of diluted TSR8 control templates was prepared in CHAPS lysis buffer to prepare a standard curves.

Target gene	Forward primer (5′-3′)	Reverse primer (3′-5′)
TERT	GCACTTTGGTTGCCCAATG	GCACGTTTCTCTCGTTGCG
E2f1	CTCGACTCCTCGCAGATCG	GATCCAGCCTCCGTTTCACC
Mzf1	AATTGCCACTGAACCTACCAATG	TGTCGCTATGAGGAGAGGTCT
Sp1	GCCGCCTTTTCTCAGACTC	TTGGGTGACTCAATTCTGCTG
Gapdh	AGGTCGGTGTGAACGGATTTG	TGTAGACCATGTAGTTGAGGTCA

Two additional replicate wells were used for each sample. The PCR amplification of the telomerase substrate was detected by real-time PCR with a Rotor gene Q PCR Cycler (Qiagen, Valencia, CA, USA) using the following cycle parameters: 30 min at 30°C, 2 min at 95°C, 45 cycles of 94°C for 15 s, 59°C for 1 min, and 45°C for 30 s. The linear plot of the log 10 and Ct values from the amount of the TSR8 control template standard was used to determine the amount of expanded telomerase substrate produced in each well from the telomerase activity of 2 μL cell extract within 30 min. The average of the two replicate wells for each sample was calculated. This number was divided by the amount of protein (mg) contained in the 2 μL extract and then divided by 30 min to determine the amount of extended telomerase substrate produced in every minute per milligram protein.

2.8. Telomere Length Detection. After 72 h of treatment, the cells were collected, and DNA was extracted using a DNeasy Blood and Tissue Kit (Cat. No. 69504, Qiagen). The average telomere length of total genomic DNA was determined by qPCR as described by Cawthon [20] and Callicott et al. [21] The telomere primer sequences (5′-3′) were as follows: forward, CGGTTTTTTGGTTTTTGGTTGGTTG GTTGGTTGGGTGTGTGTGTGT; and reverse, GGGTTG GCCTTACHCCTTACHCCTTACHCCTTACHCCTTACH CCTTACHCT. The reference control gene primer (mouse 36B4 single-copy gene) sequences were as follows: forward, TGAAGTGCTTGACATCACGAGGA; and reverse, CTGC AGACATCGCTGGCAAATT. An equal amount of DNA (35 ng) was used for each reaction and both, the telomere and 36B4 gene, were amplified under the same conditions. For each PCR, a standard curve was generated by serially diluting a known amount of DNA. The telomere (T) signal was normalized to the signal obtained from a single-copy (S) gene to generate a T/S ratio indicating the relative telomere length.

2.9. Bioinformatics. Transcription Factor Database TRRUST (version 2) [22] (https://www.grnpedia.org/trrust/) is a manually curated database of transcription factors (TF) and TF-target regulatory relationships, which contains 8,444 and 6,552 TF-target regulatory relationships of 800 human TFs and 828 mouse TFs. We input the transcription factors of interest into TRRUST (version 2), selected "mouse" as the species, obtained all genes regulated by the TFs, and classified the genes regulated according to "Activation," "Repression," and "Unknown".

Metascape [23] (http://www.metascape.org/, 2019/8/14) was used to further analyze the gene function and enrichment pathway. We uploaded the gene list to the website,

selected "M. musculus" for "Input as fields" and "Analysis as fields", and analyzed the gene according to "Custom Analysis." In Custom Analysis, we only checked "GO Biological Processes" in the "Pathway" option of "Membership" and "Enrichment"; the other options were used with default values, Min overlap: 3, P value cutoff: 0.01, Min enrichment: 1.5.

2.10. Statistical Analysis. Each experiment was repeated at least three times in triplicate. Unless otherwise indicated, t test was used to compare the means. Results showing P values of less than 0.05 were considered as significant.

3. Result

3.1. SMF Treatment Accelerated Proliferation and Inhibited Migration of 4 T1 Cells. The effect of SMF treatment on the proliferation of 4T1 cells was analyzed by cell counting and CFSE staining (Figures 2(a) and 2(b)). First, we monitored the number of 4T1 cells exposed to the magnetic field for 24, 48, and 72 h. The results showed that the cell number in the SMF group was the same as that in the GMF group at 24 h, and higher at 48 h (11.02%), reaching a significant increase at 72 h (19.28%) of treatment. These effects on proliferation acceleration were confirmed by CFSE staining, with the rate of cell division inversely proportioned to the fluorescence intensity remaining in the daughter cells (Figure 2(b)). The fluorescence ratio in SMF-treated cells was significantly lower than that in the GMF group at 24 h of exposure (10.39%), and the reduction became greater at 48 h (20.16%). Thus, the proliferation of 4T1 cells was accelerated by SMF, and the cell response to MF was detectable within 24 h.

The effects of SMF treatment on the migration of 4T1 cells were measured in wound healing and Transwell assays at 24 h of exposure in serum-free and low-serum medium, respectively, to abolish the effect on proliferation. As observed in the wound healing assays (Figures 2(c) and 2(d)), the width of the "wound" healed in SMF was smaller than that in the GMF control, and the cell migration efficiency in SMF was only 71.68% of that in the GMF ($P < 0.05$). The results of the Transwell assays (Figures 2(e) and 2(f)) also revealed fewer transported cells in the SMF than in the GMF group ($P < 0.0001$), confirming that SMF treatment inhibited the migration ability of 4T1 cells.

3.2. SMF Treatment Decreased Telomerase Function in 4 T1 Cells. Considering the accelerated division of 4 T1 cells in the SMF, it is important to evaluate the effect on immortality, a characteristic of cancer cells. Telomerase is rarely expressed

(a)

(b)

(c)

(d)

(e)

(f)

FIGURE 2: SMF treatment accelerated proliferation and inhibited migration of 4T1 cells. (a) Cell numbers counted following SMF exposure to different magnetic fields for 24, 48, and 72 h (h). (b) The proliferation rates of 4T1 cells shown by CFSE fluorescence ratio of SMF/GMF at 24 and 48 h of exposure. (c) Representative images of the wound width and (d) migration efficiency of the SMF and GMF cell at 0 and 24 h of the exposure in the wound healing assay. Wound healing assays and Transwell assays (e) were used to detect the migration ability of cells. (e) Representative fluorescent images showing the nuclei (blue, stained by Hoechst) of the migrated cells exposed in GMF and SMF for 24 h. (f) Compared to the GMF group, SMF treatment significantly inhibited cell migration. Data are the means ± sem from three independent experiments ($n = 3$). $*P < 0.05$; $**P < 0.01$; $****P < 0.0001$, compared to the GMF group. SMF: static magnetic field; GMF: geomagnetic field.

in most normal cells but is activated in more than 90% of tumor cells [24, 25] and is a key factor in maintaining the proliferative ability and telomere length of tumor cells and determining cell life. Thus, we next evaluated the telomerase activity, telomere length, and expression of telomere-associated proteins at 72 h of MF exposure, when the greatest effect on cell proliferation was detected.

Our results showed that SMF treatment significantly inhibited telomerase activity and shortened telomeres in 4T1 cells compared to in the GMF group (Figures 3(a) and 3(b)), indicating decreased division related to telomerase and a tendency for accelerated exit from limitless cancerous growth.

Moreover, compared to the GMF group, the expression of telomerase (telomerase reverse transcriptase, *TERT*) was downregulated, as demonstrated in the RT-qPCR assay

(Figure 3(c)). These data indicate that decreased telomerase activity following SMF involves the response of upstream expression regulators rather than effects on telomerase alone.

3.3. SMF Treatment Upregulates e2f1 Expression in 4 T1 Cells. To further explore the SMF-responsive regulator of *TERT*, we examined the expression levels of TFs upstream of *TERT*, such as the activating TF sp1 and the inhibitory TFs e2f1 [26] and mzf1, by RT-qPCR. As shown in Figures 4(a)–4(c), the expression level of e2f1 was significantly higher in SMF-treated cells than in the GMF control, whereas the other TFs did not change significantly.

To determine whether e2f1 mediates the response of 4 T1 cells to the magnetic field, GO enrichment analysis was performed on genes activated by e2f1 (Figure 4(d)). The terms
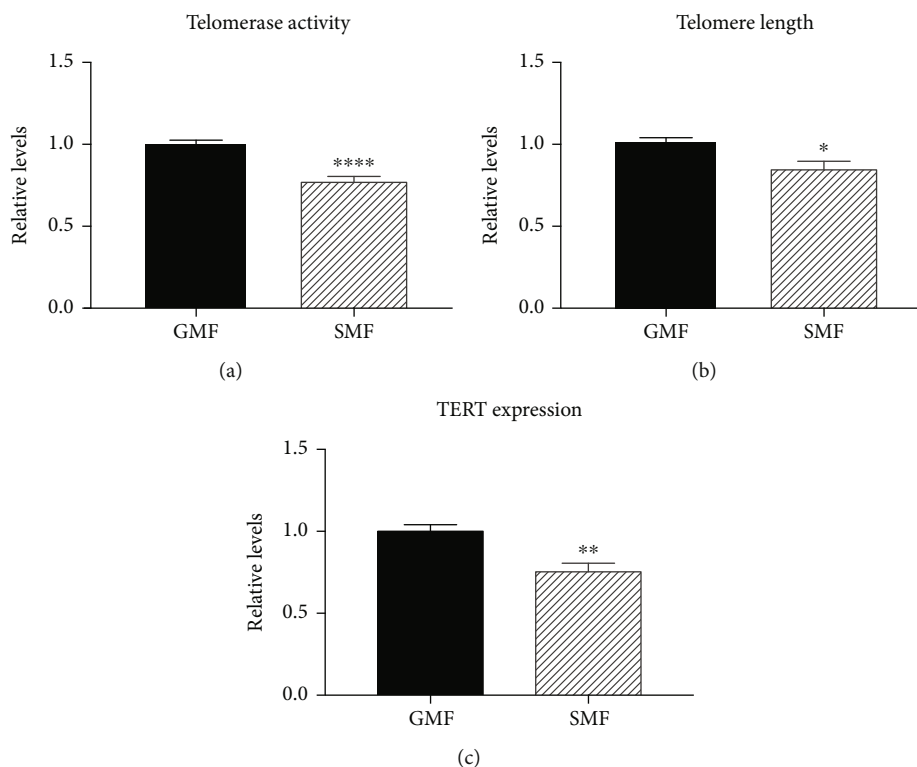
FIGURE 3: SMF treatment decreased telomerase function in 4T1 cells after 72 h exposure. (a) Relative telomerase activity, (b) relative telomere length, and (c) relative mRNA expression of TERT in GMF- or SMF-treated cells; data are the means ± sem normalized to the GMF control ($n = 9$ from three independent experiments). $*P < 0.05$, $**P < 0.01$, and $****P < 0.0001$ compared to the GMF group.

sorted based on the P values showed that 4 of the top 6 terms were related to the cell cycle, and the top was related to the mitotic cell cycle process, which may partially explain the accelerated proliferation of tumor cells. To further examine the relationship between terms, we chose a subset of enriched terms and constructed a network graph (Figure 4(e)). We found that the top three biological processes were enriched in mitotic cell cycle process, positive regulation of cell death, and cellular response to DNA stimulus. The possible activation of cell death indicates a tendency for the fate change of immortalized cancer cells.

4. Discussion

In this study, we examined the potential of SMF in cancer treatment by coanalysis of the effect on proliferation, migration, and telomeres and revealed the role of telomerase in response to SMF. We found that a moderate SMF (~150 mT) accelerated cell proliferation but inhibited breast cancer cell migration and shortened telomere length, which was associated with decreased telomerase activity and expression of TERT, as well as corresponding upregulation of e2f1 expression.

This is the first study to demonstrate an association of telomerase and the effects on cell proliferation and migration under SMF treatment. E2f1 is a transcription repressor of TERT and positive regulator of the mitotic cell cycle, as shown by GO enrichment analysis. Its upregulation may lead to downregulation of TERT and the acceleration of prolifer-

ation. Decreased TERT can mediate migration repression and telomere shortening. Thus, SMF treatment may antagonize tumor growth by restricting the uncontrolled division in addition to inhibit cell proliferation and cause cell death.

In this study, the proliferation and division of 4T1 cells were accelerated by SMF treatment, which contrasts previously reported results [27, 28]. This was expected, as the exact effects of SMFs on cells are largely dependent on the cell types and magnetic conditions [5]. Although SMF shows anticancer potential because of its ability to specifically inhibit the proliferation of cancer cells, accelerated proliferation may improve the efficacy of some chemotherapy drugs against rapidly dividing cells.

The inhibition effect on 4T1 migration was consistent with that observed in our previous study, as well as a few others evaluating different cell types and treatment condition [29, 30], suggesting the potential of using a SMF to inhibit metastasis in cancer treatment.

A unique feature of tumor cells is immortalization, in which telomerase activation is a key factor. Active telomerase, a reverse transcriptase, can directly increase telomere length [6]. As SMF can accelerate cell proliferation and reduce telomerase activity, further studies are needed to determine whether prolonging the SMF can shorten the telomere to a critical length and stop division, thus leading to the aging of tumor cells. Previous studies showed that SMF can accelerate senescence and shorten lifespan in nematodes. For example, Hung et al. [31] found that after 200 mT of steady SMF treatment, the development rate of wild-type
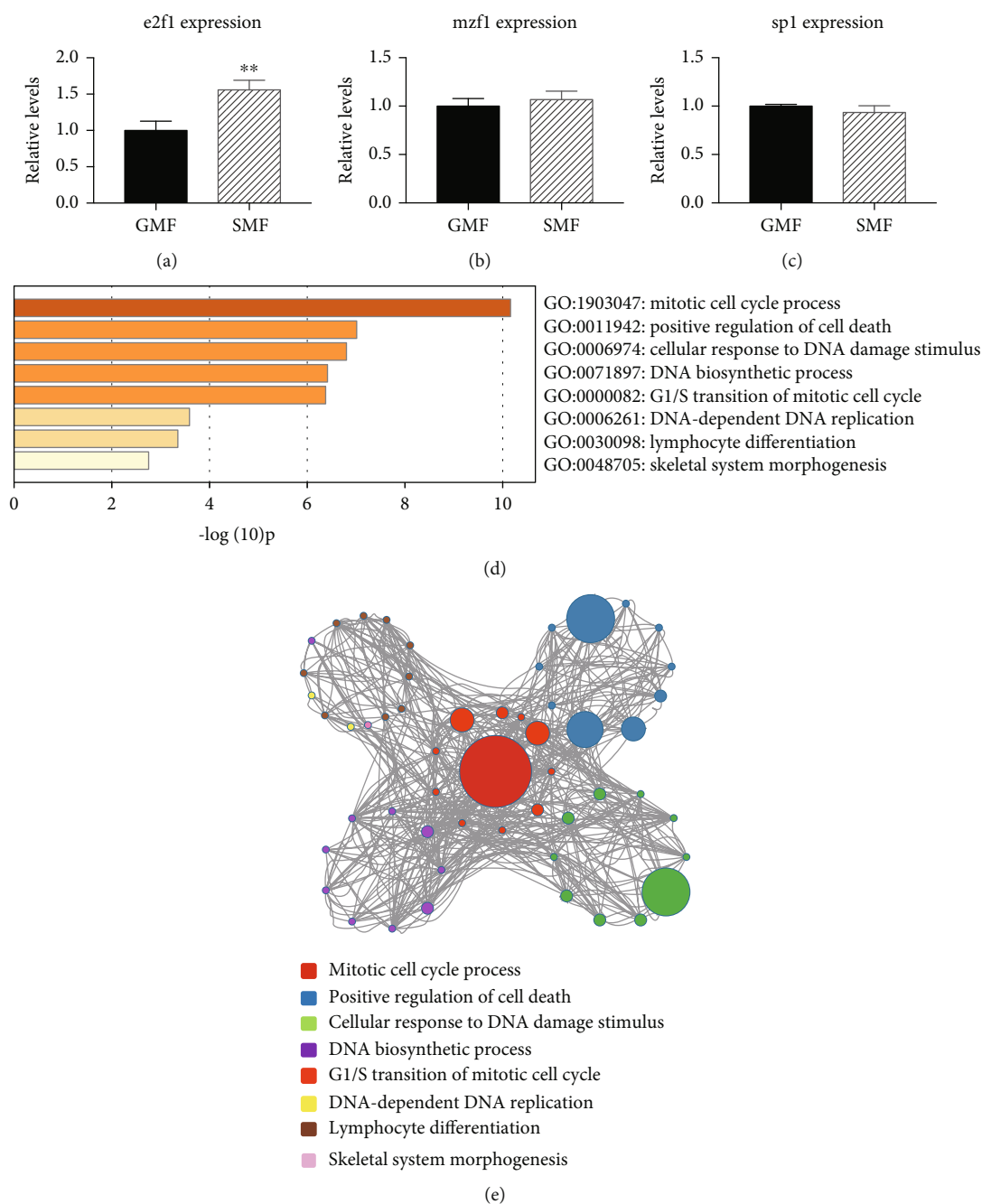
Figure 4: SMF treatment upregulates e2f1 expression in 4T1 cells. (a–c) The relative expression of transcription factors e2f1, mzf1, and sp1 in SMF-treated cells at 72 h of exposure detected by RT-qPCR. Data are the means ± sem normalized to GMF control, $n = 9$ from 3 independent experiments, $**P < 0.01$. (d) Columns illustration shows target genes activated by e2f1 from GO enrichment analysis, and the terms with $P < 0.01$ are listed. (e) Network relationship between enriched terms. The circle of the same color represents the same term; the size of the circle is positively correlated with the number of genes enriched in this term.

nematodes was increased by 20–31%, and the average lifespan decreased from 31 to 24 days. After SMF treatment, pathways involving development and senescence-related genes, such as *let-7*, *clk-1*, *unc-3*, and *age-1*, were significantly upregulated in nematodes [32]. Nematodes exposed to 8.5 T SMF also showed significant acceleration of aging and increased expression of superoxide dismutase-3.

Overall, SMF treatment inhibits cell migration and may accelerate/induce the exit from immortalizing division by repressing telomerase activity in tumor cells. The telomerase network can respond to the SMF and may be involved in cancer-specific effects and function as a target in magnetic therapy.

Data Availability

All data included in this study are available upon request from the corresponding author.

Conflicts of Interest

Acknowledgments

References

[1] S. Ghodbane, A. Lahbib, M. Sakly, and H. Abdelmelek, "Bioeffects of Static Magnetic Fields: Oxidative Stress, Genotoxic Effects, and Cancer Studies," *BioMed Research International*, vol. 2013, 12 pages, 2013.

[2] A. P. Alfano, A. G. Taylor, P. A. Foresman et al., "Static magnetic fields for treatment of fibromyalgia: a randomized controlled trial," *Journal of Alternative and Complementary Medicine*, vol. 7, no. 1, pp. 53–64, 2001.

[3] N. K. Eccles, "A critical review of randomized controlled trials of static magnets for pain relief," *Journal of Alternative and Complementary Medicine*, vol. 11, no. 3, pp. 495–509, 2005.

[4] J. R. Salvatore, J. Harrington, and T. Kummet, "Phase I clinical study of a static magnetic field combined with anti-neoplastic chemotherapy in the treatment of human malignancy: initial safety and toxicity data," *Bioelectromagnetics*, vol. 24, no. 7, pp. 524–527, 2003.

[5] L. Zhang, X. M. Ji, X. X. Yang, and X. Zhang, "Cell type- and density-dependent effect of 1 T static magnetic field on cell proliferation," *Oncotarget*, vol. 8, no. 8, pp. 13126–13141, 2017.

[6] H. W. Lee, M. A. Blasco, G. J. Gottlieb, J. W. Horner 2nd, C. W. Greider, and R. DePinho, "Essential role of mouse telomerase in highly proliferative organs," *Nature*, vol. 392, no. 6676, pp. 569–574, 1998.

[7] G. Li, J. Shen, J. Cao et al., "Alternative splicing of human telomerase reverse transcriptase in gliomas and its modulation mediated by CX-5461," *Journal of Experimental & Clinical Cancer Research*, vol. 37, no. 1, p. 78, 2018.

[8] X. H. Zheng, X. Nie, Y. Fang et al., "A Cisplatin Derivative Tetra-Pt(bpy) as an Oncotherapeutic Agent for Targeting ALT Cancer," *Journal of the National Cancer Institute*, vol. 109, no. 10, 2017.

[9] A. M. Rankin, D. V. Faller, and R. A. Spanjaard, "Telomerase inhibitors and T-oligo' as cancer therapeutics: contrasting molecular mechanisms of cytotoxicity," *Anti-Cancer Drugs*, vol. 19, no. 4, pp. 329–338, 2008.

[10] C. R. Bohl, S. Harihar, W. L. Denning, R. Sharma, and D. R. Welch, "Metastasis suppressors in breast cancers: mechanistic insights and clinical potential," *Journal of Molecular Medicine*, vol. 92, no. 1, pp. 13–30, 2014.

[11] W.-C. Mo, Z.-J. Zhang, D.-L. Wang, Y. Liu, P. F. Bartlett, and R. Q. He, "Shielding of the geomagnetic field alters actin assembly and inhibits cell motility in human neuroblastoma cells," *Scientific Reports*, vol. 6, no. 1, p. 22624, 2016.

[12] W. Mo, Y. Liu, P. F. Bartlett, and R. He, "Transcriptome profile of human neuroblastoma cells in the hypomagnetic field," *Science China Life Sciences.*, vol. 57, no. 4, pp. 448–461, 2014.

[13] H. Liu, Q. Liu, Y. Ge, Q. Zhao, X. Zheng, and Y. Zhao, "hTERT promotes cell adhesion and migration independent of telomerase activity," *Scientific Reports*, vol. 6, no. 1, p. 22886, 2016.

[14] V. Maggisano, M. Celano, G. E. Lombardo et al., "Silencing of hTERT blocks growth and migration of anaplastic thyroid cancer cells," *Molecular and Cellular Endocrinology*, vol. 448, pp. 34–40, 2017.

[15] J. R. Gray, C. H. Frith, and J. D. Parker, "In vivo enhancement of chemotherapy with static electric or magnetic fields," *Bioelectromagnetics*, vol. 21, no. 8, pp. 575–583, 2000.

[16] T. Lin, L. Wan, X. Qi, W. Shi, and J. Lin, "A moderate static magnetic field enhances TRAIL-induced apoptosis by the inhibition of Cdc2 and subsequent downregulation of survivin in human breast carcinoma cells," *Bioelectromagnetics*, vol. 35, no. 5, pp. 337–346, 2014.

[17] K. Aljarrah, N. M. Mhaidat, M. A. H. al-Akhras et al., "Magnetic nanoparticles sensitize MCF-7 breast cancer cells to doxorubicin-induced apoptosis," *World Journal of Surgical Oncology*, vol. 10, no. 1, p. 62, 2012.

[18] Y. Luo, X. Ji, J. Liu et al., "Moderate intensity static magnetic fields affect mitotic spindles and increase the antitumor efficacy of 5-FU and Taxol," *Bioelectrochemistry*, vol. 109, pp. 31–40, 2016.

[19] X. Wang, A. Spandidos, H. Wang, and B. Seed, "PrimerBank: a PCR primer database for quantitative gene expression analysis, 2012 update," *Nucleic Acids Research*, vol. 40, no. Database issue, pp. D1144–D1149, 2012.

[20] R. M. Cawthon, "Telomere measurement by quantitative PCR," *Nucleic Acids Research*, vol. 30, no. 10, article e47, 2002.

[21] R. J. Callicott and J. E. Womack, "Real-time PCR assay for measurement of mouse telomeres," *Comparative Medicine*, vol. 56, no. 1, pp. 17–22, 2006.

[22] H. Han, J. W. Cho, S. Lee et al., "TRRUST v2: an expanded reference database of human and mouse transcriptional regulatory interactions," *Nucleic Acids Research*, vol. 46, no. D1, pp. D380–D386, 2018.

[23] Y. Zhou, B. Zhou, L. Pache et al., "Metascape provides a biologist-oriented resource for the analysis of systems-level datasets," *Nature Communications*, vol. 10, no. 1, p. 1523, 2019.

[24] M. A. Jafri, S. A. Ansari, M. H. Alqahtani, and J. W. Shay, "Roles of telomeres and telomerase in cancer, and advances in telomerase-targeted therapies," *Genome Medicine*, vol. 8, no. 1, p. 69, 2016.

[25] J. W. Shay and W. E. Wright, "Telomeres and telomerase in normal and cancer stem cells," *FEBS Letters*, vol. 584, no. 17, pp. 3819–3825, 2010.

[26] E. Ko, H. W. Seo, E. S. Jung, B. H. Kim, and G. Jung, "The TERT promoter SNP rs2853669 decreases E2F1 transcription factor binding and increases mortality and recurrence risks in liver cancer," *Oncotarget*, vol. 7, no. 1, pp. 684–699, 2016.

[27] S. Tofani, D. Barone, M. Cintorino et al., "Static and ELF magnetic fields induce tumor growth inhibition and apoptosis," *Bioelectromagnetics*, vol. 22, no. 6, pp. 419–428, 2001.

[28] L. Zhang, J. Wang, H. Wang et al., "Moderate and strong static magnetic fields directly affect EGFR kinase domain orientation to inhibit cancer cell proliferation," *Oncotarget*, vol. 7, no. 27, pp. 41527–41539, 2016.

[29] F. J. Papatheofanis, "Use of calcium channel antagonists as magnetoprotective agents," *Radiation Research*, vol. 122, no. 1, pp. 24–28, 1990.

[30] Y. Li, L.-Q. Song, M. Q. Chen et al., "Low strength static magnetic field inhibits the proliferation, migration, and adhesion of human vascular smooth muscle cells in a restenosis model through mediating integrins β1-FAK, Ca 2+ signaling pathway," *Annals of biomedical engineering.*, vol. 40, no. 12, pp. 2611–2618, 2012.

[31] Y. C. Hung, J. H. Lee, H. M. Chen, and G. S. Huang, "Effects of static magnetic fields on the development and aging of Caenorhabditis elegans," *The Journal of Experimental Biology*, vol. 213, Part 12, pp. 2079–2085, 2010.

[32] C. H. Lee, Y. C. Hung, and G. S. Huang, "Static magnetic field accelerates aging and development in nematode," *Communicative & Integrative Biology*, vol. 3, no. 6, pp. 528-529, 2010.

Review Article

Space Radiation Biology for "Living in Space"

Satoshi Furukawa [iD],[1] Aiko Nagamatsu [iD],[1] Mitsuru Nenoi,[2] Akira Fujimori,[2]
Shizuko Kakinuma [iD],[2] Takanori Katsube [iD],[2] Bing Wang [iD],[2] Chizuru Tsuruoka [iD],[2]
Toshiyuki Shirai,[2] Asako J. Nakamura [iD],[3] Asako Sakaue-Sawano,[4] Atsushi Miyawaki,[4]
Hiroshi Harada [iD],[5] Minoru Kobayashi [iD],[5] Junya Kobayashi,[5] Takekazu Kunieda [iD],[6]
Tomoo Funayama [iD],[7] Michiyo Suzuki,[7] Tatsuo Miyamoto [iD],[8] Jun Hidema [iD],[9,10]
Yukari Yoshida [iD],[11] and Akihisa Takahashi [iD][11]

[1]Japan Aerospace Exploration Agency, 2-1-1 Sengen, Tsukuba, Ibaraki 305-8505, Japan
[2]National Institute of Radiological Sciences, National Institutes for Quantum and Radiological Science and Technology (QST), 4-9-1 Anagawa, Inage-ku, Chiba 263-8555, Japan
[3]Department of Biological Sciences, College of Science, Ibaraki University, 2-1-1, Bunkyo, Mito, Ibaraki 310-8512, Japan
[4]Lab for Cell Function and Dynamics, CBS, RIKEN, 2-1 Hirosawa, Wako, Saitama 351-0198, Japan
[5]Radiation Biology Center, Graduate School of Biostudies, Kyoto University, Yoshida Konoe-cho, Sakyo-ku, Kyoto 606-8501, Japan
[6]Department of Biological Sciences, Graduate School of Science, The University of Tokyo, 7-3-1 Hongo, Bunkyo-ku, Tokyo 113-0033, Japan
[7]Takasaki Advanced Radiation Research Institute, QST, 1233 Watanuki-machi, Takasaki, Gunma 370-1292, Japan
[8]Research Institute for Radiation Biology and Medicine, Hiroshima University, Kasumi 1-2-3, Minami-ku, Hiroshima 734-8553, Japan
[9]Graduate School of Life Sciences, Tohoku University, 2-1-1 Katahira, Aoba-ku, Sendai, Miyagi 980-8577, Japan
[10]Division for the Establishment of Frontier Sciences of the Organization for Advanced Studies, Tohoku University, 2-1-1 Katahira, Aoba-ku, Sendai, Miyagi 980-8577, Japan
[11]Gunma University Heavy Ion Medical Center, 3-39-22 Showa-machi, Maebashi, Gunma 371-8511, Japan

Correspondence should be addressed to Akihisa Takahashi; a-takahashi@gunma-u.ac.jp

Space travel has advanced significantly over the last six decades with astronauts spending up to 6 months at the International Space Station. Nonetheless, the living environment while in outer space is extremely challenging to astronauts. In particular, exposure to space radiation represents a serious potential long-term threat to the health of astronauts because the amount of radiation exposure accumulates during their time in space. Therefore, health risks associated with exposure to space radiation are an important topic in space travel, and characterizing space radiation in detail is essential for improving the safety of space missions. In the first part of this review, we provide an overview of the space radiation environment and briefly present current and future endeavors that monitor different space radiation environments. We then present research evaluating adverse biological effects caused by exposure to various space radiation environments and how these can be reduced. We especially consider the deleterious effects on cellular DNA and how cells activate DNA repair mechanisms. The latest technologies being developed, e.g., a fluorescent ubiquitination-based cell cycle indicator, to measure real-time cell cycle progression and DNA damage caused by exposure to ultraviolet radiation are presented. Progress in examining the combined effects of microgravity and radiation to animals and plants are summarized, and our current understanding of the relationship between psychological stress and radiation is presented. Finally, we provide details about protective agents and the study of organisms that are highly resistant to radiation and how their biological mechanisms may aid developing novel technologies that alleviate biological damage caused by radiation. Future research that furthers our understanding of the effects of space radiation on human health will facilitate risk-mitigating strategies to enable long-term space and planetary exploration.

1. Introduction

Yuri Gagarin was the first human to journey into outer space. He completed one orbit of Earth on 12 April 1961. Almost 60 years have passed since this event, and space mission durations have remarkably extended. Currently, it is possible for humans to spend more than 6 months in outer space on the International Space Station (ISS). The ISS circles the Earth at an altitude of approximately 400 km. The living environment on the ISS is challenging to astronauts because microgravity (μG) induces musculoskeletal atrophy, isolated and limited habitability causes psychological stress, and exposure to space radiation potentially endangers the health of the astronauts [1].

The next challenging steps for humankind include new missions to the Moon followed by human exploration of Mars. In a Mars mission, the long distance between Earth and Mars will make the total mission duration 800–1,100 days, of which approximately 500 days will be spent on the surface of the planet, depending on the final mission design [2]. As a result, radiation exposure is expected to be greater when compared with that of a 6-month mission on the ISS. One major health concern in such prolonged missions is the amount of radiation exposure that accumulates over the duration of the lives of the astronauts. Therefore, health risks associated with exposure to space radiation are an important topic in a human Mars mission. The focus of this review is space radiation. We will initially discuss the environment of space radiation. This will be followed by a description of the various kinds of research endeavors undertaken to evaluate and minimize adverse biological outcomes caused by space radiation exposure.

2. Environment of Space Radiation

2.1. Radiation Environment in Low-Earth Orbits (LEO). As mentioned in previous reviews [3–6], important ionizing radiation (IR) sources in the ISS orbits (altitude: 300 to 400 km; orbital inclination: 51.6°) include the three primary radiation sources (galactic cosmic rays (GCRs), which range widely from protons to Fe-ions, solar particle events (SPEs), and electrons and protons trapped in the Van Allen Belts (TPs)) outside the spacecraft. These combine to produce a complex radiation environment in and around the ISS, and the complexity of this radiation is dependent on the solar cycle, altitude, and shielding of each module of the ISS.

Primary GCRs comprise protons and high-energy heavy-ion (HZE) charged particles with energy spectra forming a broad peak around 1 GeV/n [3]. Fluxes of less than about 10 GeV/n are inversely related to solar activity [7]. The GCR fluxes depend heavily on the ISS altitude and are difficult to shield against using a realistic shielding mass for the ISS structure because of their high energy. Primary GCRs produce many secondary particles through projectile and target fragmentation in the ISS shielding materials and in the bodies of astronauts. The fluxes of primary TPs increase substantially as the altitude of the ISS increases [3, 7–9]. Although the fluxes of primary TPs can be effectively reduced by thin shielding (a few g/cm^2), secondary particles produced by nuclear reactions increase in number as shielding mass increases and become dominant in fluxes under thick shielding conditions [10, 11]. Thus, TPs play a role in increasing or decreasing the exposure of astronauts to radiation in LEO. The energies of TPs are generally lower than those of GCRs, and their maximum energy is approximately several hundred MeV.

Since the construction of ISS began in 1998, there have been more than 120 SPEs (counted by NOAA, Space Weather Prediction) that have affected the Earth environment over solar cycles 23 to 24. The emergency return of astronauts following flight rules [12] due to severe SPEs has never occurred before because of Earth's protective magnetic field.

Japan Aerospace Exploration Agency (JAXA) has conducted a series of monitoring experiments to evaluate the radiation environment inside and outside the Japanese Experiment Module Kibo, which is part of the ISS with Passive Dosimeter for Life-Science and Experiments in Space (PADLES) [9, 13, 14]: area radiation monitoring in the Japanese Experiment Module "Kibo" of the ISS (Area PADLES) [15]; dose measurements of biological samples exposed to space radiation (Bio PADLES) [16–19]; radiation dosimetry of Asian astronauts (Crew PADLES); various kinds of international cooperative experiments with ISS partners (Dosimetric-PADLES); measurement of the directional dependence of the radiation dose inside the Kibo module (Exp PADLES) [11, 20]; and measurement of outside doses and evaluation of the shielding effect of the ISS Kibo hull (Free-space PADLES). Those experiments were initiated in 2008 just after attachment of the Japanese Pressurized Module (JPM) to the ISS.

We concluded that the characteristics of the space radiation environment in LEO contain the following: (i) a high contribution from high-linear energy transfer (LET) radiation that have a high-quality factor (QF) up to 30; (ii) dose rates have values that are a few hundred times greater than those on the ground; (iii) the directional distribution of space radiation is nearly isotropic; and (iv) radiation effects occur under μG [13, 14, 19]. Space radiation for LET greater than several keV/μm causes more serious damage to living things than low-LET radiation. Measurements only of absorbed doses are insufficient for investigating biological effects or assessing radiation risk to astronauts. Dose equivalents taking into account the LET distributions of high-LET particles, their high radiation QFs, and relative biological effectiveness (RBE) must be measured considering space radiation environment.

Space radiation environments include fast neutrons with a wide energy range beyond several tens of MeV. The neutron dose contribution has been roughly estimated through the STS-89 space shuttle mission/Mir experiment with RRMD-III for charged particles and BBND for neutrons with energies less than 15 MeV, both loaded simultaneously [21]. Neutron doses contributing to total doses in LEO and around the Moon and Mars are still being estimated with various simulation codes. However, no practical measurement has been established so far with a neutron personal dosimeter applicable to energy exceeding ~20 MeV. The most physical

and practical approach for estimating the high-energy neutron dose is to theoretically and experimentally determine LET values of energetic charged particles released by interactions with the neutrons and an anthropomorphic phantom. The dose-equivalent part of the practical dose can be obtained using the relation between QFs and LET values via the Q–L relation ICRP 60 [22]. Therefore, dose equivalents taking into account the LET distributions are also important for evaluating neutron doses.

2.2. Radiation Environment beyond LEO (Deep Space, the Moon, and Mars). The space radiation environment differs in and beyond LEO, including the surface of the Moon [23–28], Mars [23], deep space [29, 30], and their comparisons [23, 31]. In past explorations, space radiation measurements have been conducted by three interplanetary missions in the orbital environment of both the Moon and Mars to generate global dosage maps and to measure energy spectra below 100 MeV [32–36]. In deep space outside Earth's protective magnetic field, HZE charged particles of GCRs and solar energetic particles (SEPs) strongly affect the dosimetry of astronauts. Space radiation doses change drastically because of the varying intensity and peak amplitude of SEP events in and near the Moon and Mars environments, where a protective magnetic field is almost completely absent.

Therefore, for radiation dose management of astronauts exposed to both SEPs and GCRs, it is essential to establish methods for estimating organ doses and effective doses that are both relative to career dose limits. These are obtained from the energy spectra of space radiation and doses from personnel dosimeters and environmental radiation monitoring systems.

Currently, as part of the NASA Artemis program, astronauts will land on the Moon by 2024. Under the umbrella of Artemis, the Lunar Orbital Platform-Gateway, which is a station orbiting the Moon, provides an international cooperation platform for scientific experiments and exploration of the lunar surface. The career dose limits for gateway are still under coordination between international partners. Currently, there is no interplanetary mission to measure the space environment in Japan. Thus, we must conduct actual measurements beyond LEO to determine effective materials, effective locations, and appropriate thicknesses or combinations on the basis of benchmark evaluations. This information will be useful for interplanetary space flight and travel expected in the near future.

2.3. Solar Ultraviolet (UV) Radiation. UV is part of the natural energy produced by the sun. UV radiation has electromagnetic radiation wavelengths from 10 nm to 400 nm, which are shorter than visible light (400–700 nm) but longer than X-ray. UV radiation reaches the Earth surface. UV radiation is classified into three regions based on their effects on biological processes: UV-C (<280 nm), UV-B (280–315 nm), and UV-A (315–400 nm). UV-C, which is a highly energetic wavelength, is eliminated by the stratospheric ozone layer and is not encountered by plants. Both UV-B and UV-A radiations reach the surface of Earth [37].

Cyanobacteria have created a foundation of the environment in which most organisms live today. The ozone layer completely absorbs harmful UV-C radiation (<285 nm), and through evolution, organisms were able to expand their habitat from water to land. The first land organisms, which resembled the liverworts, have evolved into the diverse range of plant species that exist. Sunlight-driven photosynthesis maintained the composition of the atmosphere, and plants serve as a food source for animals. Although sunlight is highly beneficial for life on Earth, it contains harmful UV-B radiation (280–315 nm) despite its efficient absorption by the ozone layer [38]. Although UV-B radiation accounts for <0.5% of the total solar energy on the surface of the Earth, its high energy causes damage to important cellular components, such as DNA, RNA, protein, and lipids, as it is readily absorbed by such macromolecules [39]. Among them, DNA, which stores genetic information, is a major target of UV-induced damage, and UV radiation can directly alter its structure. The main UV-induced photoproducts are cyclobutane pyrimidine dimers (CPDs) and pyrimidine-pyrimidone (6-4) photoproducts, which are also termed (6-4) photoproducts, and form between adjacent pyrimidines on the same strand [39, 40]. CPDs account for approximately 75% of DNA damage and the (6-4) photoproducts for the majority of the remaining 25%. DNA damage impedes replication and transcription, induces mutations, and may be lethal [39, 40]. Therefore, UV radiation causes damage to all organisms including plants. Most skin cancers are caused by UV radiation damaging the DNA in skin cells. Plants, which are sessile organisms, are at a higher risk of UV-B damage in comparison with motile organisms, which reduces growth and productivity.

The environment of space is characterized by low gravity, temperature oscillation, short-wavelength solar UV radiation, and complex cosmic IR. In particular, space is showered by a variety of different types of radiation, and thus, astronauts are exposed to a considerably large amount of space radiation [41, 42]. Moreover, in space, UV-C with shorter wavelengths than UV-B are much more prevalent, and its intensity is much higher than on Earth. On the surface of Mars, the UV-B radiation is remarkably higher than that on Earth and exceeds the safety limit for terrestrial life [43, 44]. Therefore, to establish sustainable life support systems for securing long-term human life in space, the effects of the complicated space environment not only for humans but also for plants must be understood. The growth and survival of plants will be required to supply nutrients and oxygen to humans under a resource-recycling system in space.

3. Irradiation Tests with Ground Facilities Similar to the Environment in Space

3.1. Low Dose Rate Irradiation Facilities. Humans are continuously exposed to low doses of background radiation and may also be exposed to low doses of IR from X-ray or CT scans and occupational usage of radiation as medical doctors, radiologists, or nuclear power plant workers. Residents in high background radiation areas or space station astronauts are exposed to low dose rates of IR for long periods. Residents

in the vicinity of the evacuated areas of Chernobyl and Fukushima Daiichi nuclear power plant disasters may also have been exposed to low dose rates of IR and have health risk concerns because of exposure to above-average levels of IR. Biological responses toward acute irradiation from high doses of IR have been well characterized, and the molecular mechanisms of cell cycle checkpoints and DNA repair have been studied extensively. However, the biological effects and the health risks with low dose or low-dose-rate radiation exposure remain poorly understood. Understanding the health risks (mainly cancer) due to low doses of IR has been provided by epidemiological studies of atomic bomb survivors [45]; however, the risk or biological effects from chronic exposure to low dose rates of IR has only recently been more examined. To understand the molecular mechanisms following exposure to low dose rates of IR, irradiation instruments for chronic exposure to low dose rates of IR have been established in Japan and other countries [46]. The instruments in Japan use ^{137}Cs as a radiation source and can irradiate biological specimens with γ-rays. Among them, the irradiation instrument for the Institute for Environmental Sciences (IES) can expose small animals such as mice with extremely low dose rates (about 0.05 mGy/day), and other instruments at IES can expose mice to different low dose rates (about 1 or 20 mGy/day). These instruments can perform chronic irradiation for a few years and have been supplying important information on the biological effects of chronic low dose rate irradiation to mice [46]. The instruments at the Research Institute for Radiation Biology and Medicine (RIRBM), Hiroshima University, Central Research Institute of Electric Power Industry (CRIEPI), University of Occupational and Environmental Health (UOEH), and National Institute of Radiological Sciences, National Institutes for Quantum and Radiological Science and Technology (QST-NIRS), can also perform chronic irradiation with dose rates that are higher than the instruments at IES. The instruments at CRIEPI and UOEH can irradiate cultured cells, and IES and RIRBM possess irradiation instruments for exclusive use on cultured cells. The chronic irradiation instrument at the Radiation Biology Center (RBC), Graduate School of Biostudies, Kyoto University, can be used to irradiate cultured cells and small fish [47]. The instruments have three different ^{137}Cs radiation sources and stands (where the CO_2 incubator for culture cells or aquarium for small fish is placed on) that can be placed at distances between 1.3 and 12 m from the radiation source. The machine exposes cultured cells or small fish to γ-rays over the range of 0.3–1,500 mGy/day by combining the radiation source choice and distance. The dose rate of space radiation in the ISS is 0.5 mGy/day [13–19]. Thus, the instrument at the RBC may provide important information about the health risks to astronauts at the ISS. The use of such chronic irradiation instruments in Japan is expected to provide important information to clarify the biological effects and health risks to humans under various chronic low dose rates of irradiation.

3.2. High-Energy Particle Irradiation Facilities.

Dose rates from cosmic radiation such as SEP and GCR are low at around 0.5 mGy/day as measured inside ISS Kibo [13–19].

Sometimes this increases to tens of mGy/day during SPE events lasting up to several days. However, this will become a serious health issue over long stay periods in future missions to Mars and other planets. SEP and GCR contain various radiations, including γ-ray, electron, neutron, proton, and heavier ions. In particular, GCR includes heavier ions up to Fe ($Z = 26$), and these heavier ions can significantly affect crew and electric devices in a manned spacecraft because of their high ionization density. The interesting energy range of GCR is from 100 MeV/u to several GeV/u. This energy spectrum is around the peak flux of GCR and difficult to shield against in a spacecraft. Experiments involving cosmic radiation in space are expensive and rather time-limited. Although it is difficult to reproduce the cosmic radiation environment on the ground, experiments using HZE accelerators are important.

The pioneer of radiation research of HZEs was Bevalac at the Lawrence Berkeley National Laboratory (LBL), USA. After the shutdown of Bevalac in 1993, the QST-NIRS in Japan started the operation of Heavy-Ion Medical Accelerator in Chiba (HIMAC) in 1994. Although NIRS is a dedicated facility for heavy-ion radiotherapy, it can provide various ion beams for other experiments outside treatment hours. The available ions are He, C, Ar, Fe, and Xe with an energy maximum of 800 MeV/u (ion species dependent). There are five experimental beam lines at HIMAC, and a 3D field can be formed by the wobbler beam delivery system. In the past 25 years, many studies have been carried out, including those examining biological effects, radiation shielding, development and comparison of cosmic radiation detectors, and radiation tests of electric devices [48].

At the almost same time, the GSI Helmholtz Center for Heavy Ion Research (GSI) started the operation of SIS-18. GSI covers the wide research fields of nuclear physics, atomic physics, material science, plasma physics, biophysics, and clinical research, based on the heavy-ion accelerator complex. This facility can provide various ions from proton to uranium. The energy range is up to 2 GeV/u (ion species dependent) and is suitable to study the radiation effects of GCRs. Furthermore, the new FAIR accelerator complex is under construction at GSI. Heavy ions with energies up to 10 GeV/u will be available for radiation research in the near future [49].

The Brookhaven National Laboratory (BNL) in the USA has operated a very large heavy-ion accelerator complex, RHIC/AGS, for the study of nuclear and particle physics. In 2003, the NASA Space Radiation Laboratory (NSRL) was founded to study the health risks of cosmic radiation to crews. NSRL uses the BNL Booster synchrotron, which can provide ions from protons to gold, ranging in energy from 50 MeV/u to 2,500 MeV/u (ion species dependent) [50]. Although one of the difficulties of ground-based experiments is that cosmic radiation consists of a wide variety of ion species and energy ranges, NSRL produces a GCR simulated beam using rapid switching technology of ion species and ion energies.

In addition to these three research facilities, some institutes provide HZE beams for cosmic radiation research. In particular, 12 C-ion radiotherapy facilities are now in

operation, including the Gunma University Heavy Ion Medical Center (GHMC) in Japan and the National Centre for Oncological Hadrontherapy (CNAO) in Italy. These facilities provide a C-ion beam from 100 MeV/u to 400 MeV/u, which is close to the GCR energy range. Researchers of cosmic radiation and the C-ion radiotherapy have common scientific interests in characterizing the biological effects of HZEs and contribute to this research field.

3.3. Microbeam Irradiation Facilities. Space radiation includes the HZE of GCRs, which is unlike radiation at ground level. Therefore, analysis of the hit effect of HZE is an important subject when evaluating space radiation risks for long-term manned missions.

HZE deposits concentrated energy along with its trajectory, and this manner of microdosimetric energy deposition of HZE is called the "ion track structure" [51]. The ion track structure is a characteristic of HZE and explains the difference between the biological effects of HZE and that of low-LET radiation. Because of this concentrated energy deposition of the ion track structure, a dose is deposited in close vicinity to the ion-hit position and does not extend further than a few micrometers away from this hit position. This results in a microscopic uneven dose distribution on radiation targets [52]. For example, when 1 Gy of HZEs with a LET higher than approximately 625 keV/μm was used to irradiate a population of cells with nuclei with areas of 100 μm^2 using broad field beam irradiation, less than one ion hits the nucleus of a cell on average. Thus, a mixture of cells hit and not hit by an ion occurs. Even with low-LET radiation, when the number of hit events becomes small, a similar uneven spatial distribution of hit events will occur. However, the dose given to the cells with a single hit event is too small and not sufficient to induce cellular responses. In contrast, a single hit of HZE with high LET deposits a sufficient dose to cells that is biologically effective. Therefore, investigating the effects of HZE on a cell population with broad field beam irradiation faces two problems that arise from not uniformly irradiating the cell population. The first problem is that each cell in a cell population will not be hit with the same count of ions, making it difficult to evaluate the exact effect of a single-ion hit. The second problem is the radiation-induced bystander effect [53, 54], which is a phenomenon that ion-hit cells induce radiation responses on nonhit nearby cells by transferring the hit signal *via* biological pathways. This second issue contributes much more to the overall radiation effect than the situation of low-LET radiation.

A microbeam is an experimental method that targets and irradiates biological samples with a radiation spot on the micrometer scale under microscopic observation. Because a microbeam is able to irradiate each cell with a defined dose accurately, analysis of an evenly irradiated cell population is possible. Moreover, by irradiating only a part of the cell population, we are able to induce and analyze the radiation-induced bystander effect. Therefore, a microbeam is a useful approach to analyze biological effects caused by radiation having a microscopically nonuniform dose distribution like HZE. To analyze the hit effect of HZE, it is necessary to irradiate HZEs as a microbeam. There are many international facilities where biological targets can be irradiated with a microbeam [55–57]; however, most of them are limited to irradiating only protons and alpha particles. The sites that are able to irradiate microbeams of HZE are GSI [58], Munich University [59], Institute of Modern Physics in China [60], and QST-Takasaki [52, 61]. Of these four sites, three sites, except QST-Takasaki, are only capable of irradiating cultured cells. However, to evaluate the effects of HZE on human health, experiments using model animals are necessary. The heavy-ion microbeam at QST-Takasaki is able to irradiate cultured cells and small model animals with a HZE. Therefore, this facility has contributed to the analysis of radiation effects of HZE to cultured cells from the viewpoint of single-ion-hit effects [62] and bystander effects [63–65], as well as analyzed the effects of local HZE radiation on the whole body using the nematode *Caenorhabditis elegans* [66, 67] and Medaka fish [68]. Moreover, at QST-Takasaki, the development of a new microbeam beamline that generates a finer beam spot than the current system is taking place [69]. In summary, heavy-ion microbeams will contribute more in future research examining the effect of HZE radiation, which is a significant health risk for astronauts undertaking long-term projects in space.

4. Adverse Events Caused by Space Radiation

4.1. DNA Damage and Detection. Radiation exposure induces various biological effects with the main effect being damage to DNA. There are various types of radiation-induced DNA damage, including base damage, single-strand breaks (SSBs), and double-strand breaks (DSBs) [70–73]. Among them, DNA DSBs are the most severe DNA lesion. Therefore, organisms have various DNA damage repair pathways to ensure genome stability [70, 71, 73, 74]. However, if a large amount of damage occurs or the damage is not repaired correctly, cell death, cellular senescence, and tumorigenesis may be induced [71, 72, 75, 76].

The energy of radiation is important when considering radiation exposure in space. Radiation exposure on the ground is at low-LET radiation levels and includes X-rays and γ-rays, while GCR contains high-LET radiation such as energetic protons and heavy particle beams, i.e., HZE particles [77–79]. High-LET radiation exposure leads to dense ionization along their radiation tracks and induces complex DNA damage. These localized dense DNA regions of damage, within a few helical turns of DNA, are called "complex DNA damage (lesion)" or "clustered DNA damage (lesion)" and are difficult to repair when compared with that of normal DNA damage [80–83]. Therefore, even if the radiation dose is the same on the ground as that in space, the quality and amount of DNA damage that occurs will be different, and evaluating the quality and quantity of DNA damage induced by GCRs for precise assessment of the biological effects in space is required.

Although clustered DNA damage induced by high-LET radiation exposure is detected using agarose gel electrophoresis or the comet assay, the results are sometimes controversial because their sensitivity is limited [82, 84–88]. In recent

years, several papers have reported visualization of DNA damage induced by high-LET radiation exposure using γ-H2AX, which is a marker of DNA DSB [17, 89–91]. These data have shown the different nature of DNA damage between low-LET radiation exposure and high-LET radiation exposure. Since γ-H2AX occurs in a DSB site-specific manner, it is used as a sensitive tool to detect DSB [92–94]. The Ohnishi group was the first to report that clear tracks of the γ-H2AX signal are detected in lymphoblastoid nuclei after spaceflight [17]. Additionally, a similar track of γ-H2AX was detected in fibroblast nuclei that had been cultured for 14 d at the ISS; however, these tracks were not observed for control samples on ground control samples [95]. Recently, we investigated DSB formation after exposure to different energy ion beams. Interestingly, our study indicated that the C-ion beam, which causes more complex DNA damage than the He-ion, induced larger γ-H2AX foci sizes than exposure to the He-ion beam. Both large and small sizes of foci formation were observed in C-ion and He-ion mixed beam irradiated cells (unpublished data). These results indicate that the radiation-induced γ-H2AX foci size depends on the energy of the radiation, suggesting that to correctly understand biological effects, not only the spatial formation of damage but also the size of damage needs to be considered.

Finally, radiation exposure in outer space occurs in a μG environment. Most studies conducted only analyze DNA damage caused by high-LET radiation exposure in a static environment, and it is unclear whether clustered DNA damage occurs and is repaired in a μG environment. Thus, to correctly understand the biological effects in outer space, it will be important to evaluate accurately the combined effects of μG and high-LET radiation exposure.

4.2. DNA Repair. As mentioned above, IR, including space radiation, generates various types of DNA damage. Among them, DNA DSB is the most serious damage, which can lead to tumorigenesis or cell death. Thus, organisms have developed DNA repair mechanisms to repair DSB damage. DSBs are mainly repaired by nonhomologous end-joining (NHEJ) and homologous recombination (HR) in eukaryotes [74]. Once DSB damages are generated following exposure to IR, the KU70/KU80 complex or MRE11/RAD50/NBS1 (MRN) complex is recruited to DSB damage sites. KU70/KU80 complex activates the NHEJ pathway with DNA-PKcs and the XRCC4/Lig4 complex, and these factors rejoin DSB ends. Since exposure of DNA to IR generates various forms of DSB ends, the resection of DSB ends by Artemis is essential for NHEJ progression. Such resection can lead to the loss of nucleotides and subsequent genomic instability. Hence, NHEJ is an error-prone repair system. Recruitment of the MRN complex activates the HR pathway, and this complex initiates the resection of the DSB ends with CtIP, followed by a longer resection with Exo1 or Dna2. As a result, more than 30 single-stranded DNA (ssDNA) tails are formed at both DSB ends. The replication protein A (RPA) complex then binds to ssDNA and is subsequently replaced with RAD51. Such ssDNA/RAD51 ends invade intact homologous DNA, and then error-free repair is completed using the intact homologous DNA as a template. Thus, as the HR mechanism needs an intact DNA template after replication, it is activated during the late S and G2 phase, whereas the NHEJ mechanism is activated at any point during the cell cycle [96]. NHEJ is used preferentially in higher eukaryotes such as humans. However, high-LET radiation such as heavy particle or α-rays, which is present in space radiation, generates various types of DNA damage (e.g., DSB, SSB, and oxidative damage) at the point of the irradiated areas. As NHEJ cannot repair such complicated DNA damage, HR is often activated for repair of this DNA damage in a cell cycle-independent manner [97]. However, cell cycle-independent use of HR, particularly in G1 may cause misrepair and subsequent genomic instability. Hence, RIF1 and 53BP1 can repress the unexpected activation of HR in G1 and function to select the correct repair pathway (i.e., NHEJ or HR) [96].

Acute exposure to 1 Gy of low-LET radiation such as a γ-ray could generate approximately 40 DSBs in a nucleus, ~1,000 SSB, and more than 1,000 base damages, as well as oxidation causing ~100,000 ionizations of various molecules in a nucleus simultaneously [98]. In the case of chronic irradiation by low-LET radiation, which is assumed to occur on space stations, the amount of DSB damage decreases to a negligible level. However, SSB and base damages remain and may represent a health risk. SSB damage and most types of base damage are repaired by base excision repair (BER), and cross-linked damage between adjacent bases such as a thymine dimer is repaired by nucleotide excision repair (NER) [99]. Some kinds of oxidative bases cause misinsertion of a base against the template DNA during DNA replication. Such misinserted bases are exchanged to correct bases by mismatch repair (MMR). Mistakes or incompletion of DNA repairs containing NHEJ and HR can lead to gene mutations and genomic instability, but the relationship with radiation carcinogenesis remains unclear.

4.3. Chromosomal Aberrations (CAs) and Micronuclei (MN). CAs are cytogenetic biomarkers for exposure to IR and other DNA-damaging agents [100]. CAs can be measured using many types of cells including peripheral blood cells and are used frequently in epidemiological studies of humans, laboratory animals, and *in vitro* cell and tissue systems. The frequency of CAs in peripheral blood lymphocytes may be associated with the risk of human cancer [101].

CAs are classified into unstable and stable types [102]. Unstable types are unrepaired broken chromosomes and rearranged acentric, multicentric, or ring chromosomes. Unstable CAs are frequently lost with cell division because they are associated with impaired DNA replication of broken termini without telomeres or in chromosome segregation. Dicentric chromosomes are the most popular cytogenetic biomarker of unstable CAs. They can be identified easily with the conventional Giemsa staining because of their typical structure with two centromeres. Dicentric chromosomes are the biomarker of choice for investigating recent exposure to IR.

Stable CAs are rearranged monocentric chromosomes, which can be transmitted stably to daughter cells after cell division, and hence used as biomarkers of past exposures to

IR. The conventional Giemsa staining cannot provide much information about stable CAs. The fluorescence *in situ* hybridization (FISH) technique with chromosome-specific DNA probes greatly improves the detection of stable CAs [103].

Chromosomes can be observed only in metaphase cells in their native forms. Premature chromosome condensation (PCC) techniques, which can induce condensation of chromosomes in cells at the interphase by fusion with mitotic cells or by chemical treatment, have improved CA analysis to detect DNA damage that has occurred in interphase cells [104, 105].

The MN assay is an alternative approach to detect DNA damage and used commonly because of its sensitivity, simplicity, and the speed by which cells can be scored [100]. MN are small pieces of DNA resulting from unrepaired DSBs or mitotic spindle damage that appears near the nucleus following cell division [106].

CAs in spacecraft crews have been analyzed since the 1960s to investigate genotoxic effects of space radiation and to estimate the received doses [107]. The frequency of total CAs seemed to be higher at postflight than at preflight, notably after flights longer than 180 days [107, 108]. However, the diversity of radiation history and personal susceptibility makes it difficult for epidemiological studies to estimate the risk of space radiation exposure. In addition, our knowledge of the effects of HZE particles involved in space radiation on induction of CAs is limited when compared with our understanding of low-LET IR. Studies using FISH painting revealed that HZE particles frequently induce highly complex chromosomal rearrangements when compared with the effect of low-LET IR [109]. Induction of mitotic CAs by HZE particles is complicated by their serious effects on cell cycle progression [110]. We recently compared induction of CAs and MN in C57BL/6J Jms mice at 1 and 2 months after exposure to several doses of X-rays (low-LET IR) or Fe-ions (HZE). FISH analysis of CAs in splenocytes showed that Fe particles are less effective at inducing translocations than X-rays when compared at the same physical dose. DNA DSBs induced by Fe-ions are probably not rejoined and mostly cause cell cycle arrest or cell death rather than result in induction of stable CAs [111]. Conversely, Fe-ions are more effective at inducing MN in bone marrow erythrocytes than X-rays, whereas the relative effectiveness of Fe-ions to X-rays was higher at a low dose (0.5 Gy) than that at a high dose (3.0 Gy) [112].

4.4. Genome Instability. Genomic instability refers to the accumulation of multiple changes within the genome of a cellular lineage to convert a stable genome to an unstable genome. Genomic instability is characterized by varied end points, for example, CAs, amplification of genetic material, micronucleus formation, and gene mutation.

Genomic instability can be induced by a high frequency of DNA damage [113] as DNA damages can cause inaccurate translesion synthesis past the damages or errors in repair, leading to mutation. IR can cause immediate effects such as mutation or cell death, observed within hours or a few days after irradiation. IR also induces delayed effects many cell generations after irradiation.
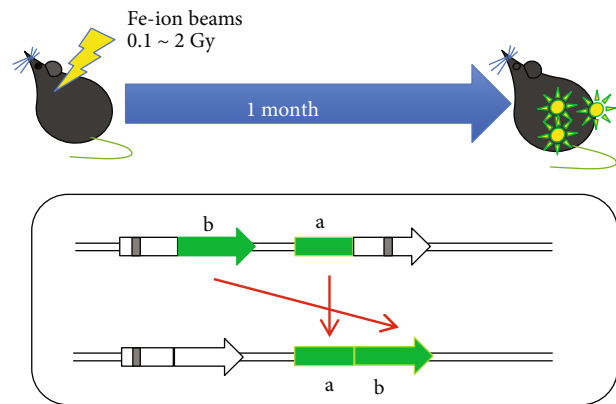
FIGURE 1: Wild-type EGFP (ab) fluorescence occurs as a result of HR between two *EGFP* genes (a and b) that are both inactive because of deletions (shadowed boxes).

Genomic instability (delayed effect) caused by IR was first demonstrated by Kadhim et al. after alpha particle irradiation and indicated that many of the clonally derived cells that exhibited the unstable phenotype were not likely to have been traversed by an alpha particle [114]. IR is capable of inducing genome instability in mammalian cells, manifesting as delayed HR *in vitro* and *in vivo* [115, 116], which is detected in the progeny of an irradiated cell multiple generations after initial exposure. Genome instability is the driving force responsible for radio carcinogenesis, which can initiate cancer and augment progression [117–119].

Cosmic radiation contains proton, various HZE particle beams, and electron beams. As the heavy ion has a higher biological effect than proton or γ-rays, it is very important to study the effects *in vivo* and *in vitro*. For astronauts on space missions or people traveling in space, it is important to evaluate the risk of exposure to cosmic radiation, such as carcinogenesis.

DNA DSBs are repaired by the NHEJ and HR pathways. The correct balance of NHEJ and HR is essential for preventing genomic instability [120, 121]. HR is essential for repair of DSBs; however, too much HR activity can be detrimental and increase "genomic instability because HR carries the risk of misalignments that cause insertions, deletions, and a loss of heterozygosity (LOH) [122, 123]. However, there has been no observation of such genomic instability in animal tissues. In recent years, a research group at Massachusetts Institute of Technology established a model mouse system (RaDR mice) that enables evaluation of genomic instability using the green fluorescence of the green fluorescence protein (GFP) as an indicator [124]. In the mouse genome, a direct repeat HR substrate is targeted to the ubiquitously expressed Rosa26 locus and HR between two truncated enhanced GFP (EGFP) expression cassettes can yield a fluorescent signal (Figure 1).

Before using the mouse model, we used an *in vitro* system (RKO cells), namely a GFP direct repeat homologous recombination system. We demonstrated that DHR increases several-fold in response to low-LET X-rays and high-LET C-ion radiation [116, 125].

Using the RaDR model mouse, we confirmed that the HR frequency is related to thymic lymphomas. When 5 weeks

old, RaDR mice were irradiated with 1.8 Gy γ-rays per week for 4 weeks (total dose 7.2 Gy), and about half of the individuals developed thymic lymphoma by 150 days. Our results indicated that a significant increase in GFP-positive cells was observed in infiltrated lymphoma. Two months after the irradiation, the frequency of GFP-positive nucleated cells (HR frequency) increased in the thymus, bone marrow, and spleen. In contrast, when model mice were irradiated with 0.5 Gy Fe-ion beam, the HR frequency in bone marrow or spleen cells was observed to increase significantly. Additionally, we found that the HR frequency significantly decreased under a radioadaptive response- (RAR-) inducible condition when compared with that under a non-RAR-inducible condition [126].

4.5. Carcinogenesis. Carcinogenesis is a major concern for future space missions, especially space missions that will be for long durations [127–129] because astronauts will be constantly exposed to IR from natural radiation sources. The radiation field in space contains electrons, protons, alpha particles, and heavier ions up to HZE-charged particles. In addition, inside spacecraft, various secondary radiations including neutrons are created by interactions between primary radiation and materials of the spacecraft.

The carcinogenic potential after radiation exposure has been revealed by epidemiological data from atomic bomb survivors [130]. However, there is insufficient data delineating the carcinogenic potential of HZE-charged particle radiation. Therefore, estimation of the cancer risk after exposure to each HZE particle or neutron using animal experiments is important. RBE values are given as the ratio of the absorbed doses of two types of radiation producing the same specified biological effect under identical irradiation conditions. Cucinotta et al. [131] used RBE values from various animal experiments for predicting the risk of cancer after exposure to HZE and fission neutrons, and the used RBE values were 2 to 10 and 4 to 20, respectively. Imaoka et al. [132] summarized RBE of the risk of cancer after exposure to protons, C-ions, or neutrons to estimate secondary cancer after radiation therapy. The RBE was less than 2 for protons and less than 20 for C-ions and neutrons. These animal data revealed that RBE values are variable for tissues type, radiation types, and age at the time of irradiation.

The greater carcinogenesis effects of HZE particle radiation have been analyzed from the viewpoint of a targeted effect (genetic change) and nontargeted effects. C-ion-induced lymphomas showed a marginal increase in the frequency of large interstitial deletions at various sites across the genome when compared with that of photon-induced lymphomas [133]. HZE particle irradiation promoted more aggressive cancers, such as increased growth rate, transcriptomic signatures, and metastasis when using a radiation/genetic mammary chimera mouse model of breast cancer [134]. This suggests that the nontargeting effects of HZE particles were more effective than the reference γ-radiation. Unfortunately, there is still a paucity of data on this subject.

Considering radiation exposure in deep space, the health risk of exposure at low dose and low-dose-rate radiation from GCR is also important. Chronic exposure to γ-rays or X-rays has been reported to reduce dramatically the risk of carcinogenesis when compared with that of acute exposure [135, 136]. Therefore, cancer risks after exposure to low-dose-rate HZE require further clarification. In future experiments, more animal data are required to determine the RBE of cancer risk after exposure to HZE particles or neutrons.

4.6. Central Nervous System (CNS) Response. In the last 10–20 years, risk assessment of space radiation has focused on the risks of cancer. In addition to the risk of cancer, NASA recently began focusing on the risks to the CNS. The CNS consists of the brain and spinal cord. The brain is the body's most complex organ and its spatial architecture. There are approximately 86 billion neurons and glia cells of the about the same number in the human brain [137, 138], all of which communicate to form circuits and share information. It is therefore very difficult to evaluate the radiation risk to the brain. Thus, it is necessary to evaluate the response of individual cells in the brain directly to radiation as a simple, accessible model.

The brain is a largely radioresistant organ [139]. However, ground-based animal studies indicate that space radiation alters neuronal tissue and neuronal functions such as excitability, synaptic transmission, and plasticity. HZE particles have been demonstrated to inhibit neuronal connectivity, neuronal proliferation, and neuronal differentiation and to change glial characterization [140]. We summarize the current knowledge of neuronal and glial responses caused by HZE irradiation less than 2 Gy (Table 1).

Thus, many researchers observed the response of the brain to radiation using short-term, higher-dose-rate exposures of radiation, which does not accurately reflect the conditions in space. The long-term effects of these doses of radiation on the CNS are largely unknown. Acharya et al. exposed mice to chronic, low-dose-rate (1 mGy/day) radiation for 6 months to investigate how deep space travel could affect the CNS [152]. They found that the radiation exposure impaired cellular signaling in the hippocampus, a part tied to learning and memory, and the prefrontal cortex, which plays a role in higher cognitive functions, resulting in learning and memory impairments. They predict that during a deep space mission, 1 in every 5.1 astronauts would experience anxiety-like behavior, and 1 in every 2.8 astronauts would experience certain levels of memory impairments. These results suggest that chronic, low-dose-rate radiation exposure from deep space travel may pose considerable risks for cognitive performance and health. For the assessment and management of human health in space, it is necessary to obtain more basic data of the effects of radiation on the brain. Additionally, it is important for us to progress with the developments of methods and protective materials that shield radiation effects.

4.7. Motility Disturbance. Adverse effects of high-LET radiation, an important component of cosmic rays, on the functions of biological systems are a potential risk in interplanetary manned space missions. Therefore, analysis of the effects of high-LET radiation on animals at an individual level and focusing on the impact of such radiation on biological

TABLE 1: Summary of brain cellular response to HZE irradiation (doses of less than 2 Gy).

Cells	Response	Irradiation	Dose rate (Gy/min)	Time after IR	Ref.
Neuron	Cell death	^{56}Fe: 1.5 Gy	0.88	1 m	[141]
		^{56}Fe: 1.6 Gy	1	12 m	[142]
	Deficits to proliferation and differentiation	^{28}Si: 0.2, 1 Gy	1	24 h, 3 m	[143]
		^{56}Fe: 0.3, 1 Gy	0.01–1	48 h, 1 m	[144]
		GCR (H+He+O): 0.5 Gy	0.0616	100+ d	[145]
		^{16}O, ^{48}Ti: 0.05, 0.3 Gy	0.05, 0.25	15 w	[146]
	Changes to dendritic, axonal, and synaptic properties	^{1}H: 1 Gy	0.55	3 m	[147]
		^{16}O, ^{28}Si, ^{4}He: 0.3 Gy		6 w	[148]
		^{56}Fe: 0.5 Gy		3 m	[149]
		^{1}H: 0.5 Gy + ^{16}O: 0.1 Gy	^{1}H: 0.18–0.19 ^{16}O: 0.18–0.33	3 m	[150]
Glia	Astrocyte activation	^{56}Fe: 1.6 Gy	1	12 m	[142]
		GCR (H+He+O): 0.5 Gy	0.0616	100+ d	[145]
	Microglial activation	^{16}O, ^{48}Ti: 0.05, 0.3 Gy	0.05, 0.25	15 w, 27 w	[146]
		^{4}He: 0.05, 0.3 Gy	0.05	12 m	[151]

h: hours; d: days; w: weeks; m: months.

functions are important for space missions. The effects of high-LET radiation exposure on several behaviors including muscle movements have been investigated using the nematode *C. elegans* [66, 67, 69, 153, 154], which is an experimental model organism and a powerful tool to study the effects of radiation. In this animal, locomotion, including forward and backward movements and turns, is carried out by 95 body wall muscle cells, for which the fate of each cell from its birth to death can be easily determined. Locomotion (motility) of adult *C. elegans* on an agar plate without food was reported to decrease in a dose-dependent manner immediately after whole-body irradiation was administered using both high-LET radiation (^{12}C, 18.3 MeV/u, LET = 113 keV/μm) [67, 153] and low-LET radiation (^{60}Co γ-rays) [155]. The RBE ratio of high-LET radiation relative to low-LET radiation for inhibition of locomotion was 1.4 [153]. If the radiation effects were mainly caused by DNA damage, it is generally thought that the effects of high-LET radiation would be several times higher than those of low-LET radiation. Therefore, the reduction of motility in *C. elegans* following exposure to high-LET radiation is not caused by DNA damage and is likely induced by another factor. Recovery of motility shortly after irradiation supports the hypothesis that DNA damage is not responsible for IR-induced reduction of motility. In particular, an important factor that induces radiation effects is reactive oxygen species (ROS) produced by IR. Exposure to IR results in the formation of free radicals such as OH• or H•, and the reactions of free radicals cause the production of ROS, including hydrogen peroxide (H_2O_2). Experimental results showed that *C. elegans* motility was H_2O_2 dose-dependent, indicating that radiation-induced reduction in motility is caused by IR-produced H_2O_2 [155]. Moreover, the results of region-specific irradiation showed that motility was not reduced significantly by irradiation of any of the individual tissues in a $\varnothing$ 20 μm region, including the CNS, intestines, and tail. This suggests that radiation reduces loco-

motion by a whole-body mechanism, potentially involving motor neurons and/or body wall muscle cells, rather than affecting motor control *via* the CNS and the stimulation response [67].

In studies of stress responses, disturbances to muscle cells induced by various stresses and stimulations have been well investigated. Wang et al. showed that mitochondrial dysfunction is related to muscle atrophy [156], and extracellular matrix (ECM) stability is necessary for maintaining muscle health. In addition, Momma et al. investigated alterations of Ca^{2+} homeostasis and mitochondrial morphology *in vivo* in body wall muscles of *C. elegans* exposed to an elevated temperature. The results showed that heat stress for 3 h at 35°C increased the concentration of free Ca^{2+} and led to mitochondrial fragmentation and subsequent dysfunction of the muscle cells [157]. Furthermore, it was reported that mitochondrial dysfunction acts as an intramuscular signal that, *via* excessive Ca^{2+} release, activates ECM-degrading enzymes to reduce ECM content and, subsequently, results in the structural and functional decline of muscles [158].

Although reduction in motility of body wall muscles recovers within several hours after whole-body irradiation with less than 1,000 Gy of high-LET radiation and the effects are masked, the disturbance observed after whole-body irradiation with more than 1,000 Gy of high-LET radiation might be induced by the above mitochondrial mechanisms. Further studies that focus on the effects of radiation to the homeostasis of muscle cells are required.

4.8. Visualization of Adverse Events. The cellular response to DNA damage varies according to the cell type, the stage of the cell cycle, and extent of damage [159]. More than 50 years have passed since the first observation of cell cycle-dependent DNA damage was made by using synchronized HeLa cell populations [160, 161]. These classical studies concluded that mitotic cells are hypersensitive to X-ray
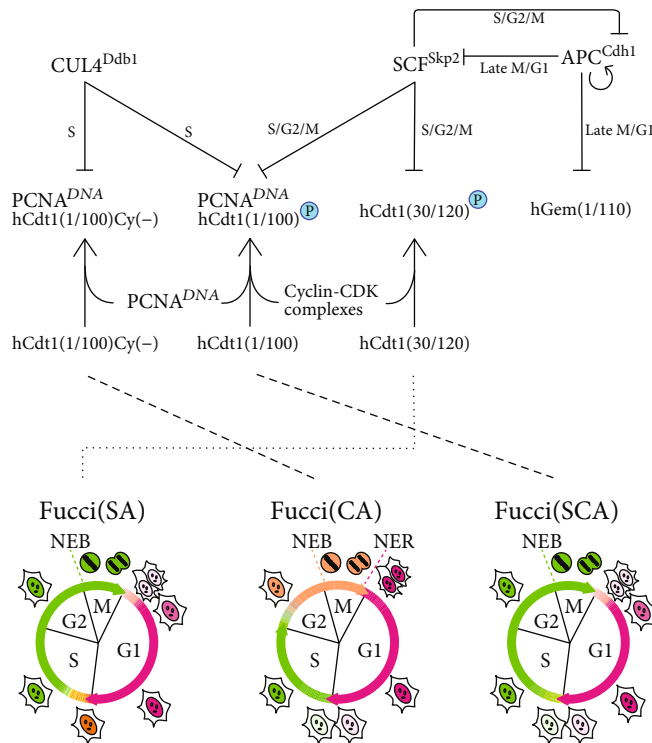
FIGURE 2: Cell cycle-phasing capabilities of the Fucci technology. Cell cycle regulations involving E3 ligase activities of CUL4^{Ddb1}, SCF^{Skp2}, and APC^{Cdh1}. Molecules whose intracellular concentrations or enzymatic activities change in a cell cycle-dependent manner are shown in color. PCNA^{DNA}: DNA-bound PCNA. Data adapted from Sakaue-Sawano et al. [164].

irradiation, which inactivates the DNA DSB repair pathway. Cell survival was maximal when cells were irradiated during the early postmitotic (early G1) and premitotic (S to G2) phases and was minimal during the mitotic (M) and late G1 or early DNA synthesis (early S) phases. However, the conventional "arrest-and-release" methods using pharmacological reagents or the mitotic shake-off method cause more or less adverse cellular perturbations and do not ensure complete cell cycle synchronization of tumor cells.

Recently, a variety of fluorescent protein- (FP-) based methods for visualizing cell cycle progression at the single cell level have been developed, enabling researchers to analyze cell cycle progression without affecting normal cellular functions. Fucci (fluorescent ubiquitination-based cell cycle indicator) harnesses the cell cycle-dependent proteolysis of Cdt1 and Geminin. Fucci highlights the cell cycle transition from G1 to S phase with high color contrast, like a traffic signal: red and green mean "stop" and "go," respectively, for the transition (Figure 2) [162, 163]. SCF^{Skp2} and APC^{Cdh1} E3 ligases are involved in the degradation of Cdt1 and Geminin, respectively. Over the course of the cell cycle, these two E3 ligase activities oscillate reciprocally and the protein levels of their direct substrates oscillate accordingly. To label S–G2–M-phase nuclei green, the Fucci probe has a green-emitting FP fused to the APC^{Cdh1}-mediated ubiquitylation domain (1–110) of human Geminin (hGem) (Fucci-S/G2/M-Green); this chimeric protein is the direct substrate of APC^{Cdh1} E3 ligase. To label G1-phase nuclei red, the probe has a red-emitting FP fused to residues 30–120 of human Cdt1 (hCdt1) (Fucci-G1-Red); it contains the Cy motif

(amino acids 68–70), which binds to the SCF^{Skp2} E3 ligase. The combination of the RFP-labeled hCdt1(30/120) and GFP-labeled hGem(1/110) can be called Fucci(SA) because they monitor the balance between SCF^{Skp2} and APC^{Cdh1} E3 ligase activities.

Eukaryotic cells spend most of their life in interphase of the cell cycle. Understanding the rich diversity of genomic regulation that occurs in interphase requires the demarcation of precise phase boundaries *in situ*. Although Fucci(SA) highlights the G1/S phase transition with yellow fluorescence, it does not provide a fluorescent readout for distinct interphase boundaries. Additionally, Fucci(SA) has a fluorescence gap in very early G1 phase, making it difficult to continuously track cell positions in all phases of the cell cycle.

In 2017, we engineered the hCdt1-based probe to be sensitive to CUL4^{Ddb1} in addition to or instead of SCF^{Skp2} [164]. As the PIP box (amino acids 1–10 of hCdt1) is a specific substrate of CUL4^{Ddb1}, hCdt1(1/100), which retains both the PIP box and Cy motif, is targeted by both SCF^{Skp2} and CUL4^{Ddb1}. We also constructed hCdt1(1/100)Cy(−), which is a specific substrate of CUL4^{Ddb1}. By combining hCdt1(1/100)- and hCdt1(1/100)Cy(−)-containing red-emitting probes with hGem(1/110)-containing green/yellow-emitting probes, we developed Fucci(SCA) and Fucci(CA) probes, respectively, which have increased the versatility of the Fucci technology for new biological studies of cell cycle interphase regulation. Although Fucci(CA) monitors the balance between CUL4^{Ddb1} and APC^{Cdh1} E3 ligase activities, Fucci(CA) can distinguish clear interphase boundaries between G1, S, and G2 phases.

TABLE 2: Biological effects of radiation and μG in space experiments.

Interactive effects	Species	Biological index	Flight time	Irradiation[a]	Ref.
No	Human blood	Chromosomal aberration	12 h	+ ^{32}P, β-rays	[167]
	E. coli, S. cerevisiae	DSB and SSB repair	14 d	Pre-X-rays	[168]
	S. cerevisiae	DSB repair	10 d	Pre-X-rays	[169]
	E. coli, S. cerevisiae	SOS response	2–4 d	Pre-X-rays	[170]
	Human blood	Chromosomal aberration	8 d	Pre- and post-γ-rays	[171]
Yes, ↑	D. melanogaster	Larval mortality	45 h	+ ^{85}Sr, γ-rays	[172]
	C. morosus	Abnormality	7 d	No	[173]
	S. cerevisiae	DSB repair	9 d	No	[174]
	D. melanogaster	Mutation	8 d	No	[175]
	D. discoideum	Spore formation	9 d	No	[176]
	Human blood	Chromosomal aberration	10–485 d	Pre- and post-X-rays	[177]
Yes, ↓	N. crassa	Cell killing, mutation	45 h	+ ^{85}Sr, γ-rays	[172]
	D. radiodurans	Cell killing	14 d	Pre-γ-rays	[178]

E. coli: Escherichia coli; S. cerevisiae: Saccharomyces cerevisiae; D. melanogaster: Drosophila melanogaster; C. morosus: Carausius morosus; D. discoideum: Dictyostelium discoideum; N. crassa: Neurospora crassa; D. radiodurans: Deinococcus radiodurans; DSB: DNA double-strand breaks; SSB: DNA single-strand breaks; h: hours; d: days. [a]+ means simultaneous irradiation with spaceflight.

We have demonstrated that Fucci(CA) can be used to

(1) fully highlight the short G1 phase of rapidly proliferating mESCs

(2) continuously track cell positions in all phases of the cell cycle

(3) detect cell cycle- (S phase) specific sensitivity (HeLa cells) to UV irradiation

(4) explore cell cycle-specific intracellular signaling

(5) visualize a cell cycle-specific response or homeostatic balance to space radiation

To investigate the impact of space radiation and μG on "Living in Space," a variety of FP-based approaches had been launched. Harada et al. introduced an EGFP-53BP1M FP probe to visualize the diversity of the radiation-induced DNA damage responses in real time [165]. Ishii's group reported that B16BL6 cells in the early S phase were the most susceptible to radiotherapy [166]. Live imaging technology using FPs is expected to make significant contributions to the direct visualization and detailed understanding of radiation adverse events.

5. Combined Biological Effects

5.1. Radiation and μG. The biological effects of radiation and μG in space experiments are summarized in Table 2. In a previous short mission, there was no appreciable difference in results between space and ground samples because exposure to space radiation occurred at a low dose. Therefore, various living systems have been irradiated before spaceflight to clarify the effect of μG on the radiation-induced DNA damage response, but there was no appreciable difference in results [167–171]. However, synergistic effects between radiation and μG have been reported [172–177], and they can sup-

press each other's effects [172, 178]. There is the still no consensus on whether radiation and μG have combined effects [179, 180]. JAXA developed not only the Cell Biology Equipment Facility (CBEF) [181] but also a mouse habitat unit cage (MHU) [182], which provides long-term artificial gravity for control experiments in space. This experimental platform provides the opportunity to investigate the specific impacts of space radiation and μG for future human space exploration [181].

The biological effects of radiation and simulated μG in ground experiments are summarized in Table 3. To clarify the effects of μG at ground level, researchers have used rotating devices, such as a rotating wall vessel bioreactor (RWV; Synthecone, Houston, TX, USA) and the random positioning machine (RPM; Dutch Space, Netherlands), which are pieces of equipment that continuously rotate a sample. These devices can equalize the gravity vector and cancel the effect of gravity, thereby simulating μG. However, there are two major limitations associated with this approach: (i) it is necessary to stop rotation during irradiation as the sample was exposed to radiation outside the incubator after or before rotation with a RWV [183–188] and (ii) nonuniformity of dose flatness in the irradiation area occurs because of chronical irradiation of a rotating sample with a RPM [189, 190]. To address these problems, we have developed a system of simultaneous irradiation in simulated-μG (SSS) using 3D clinostat [191, 192]. Our SSS is based on technologies related to X-ray irradiation with a high-speed shutter [191] and C-ion radiotherapy such as accelerator systems and respiratory gating systems [192].

Using this SSS, we reported that simultaneous exposure of human fibroblasts to simulated μG and radiation results in a greater frequency of chromosomal aberration than in cells exposed to radiation alone [193]. The expression of cell cycle-suppressing genes decreased and that of cell cycle-promoting genes increased after C-ion irradiation under simulated μG [194]. Assessment of the cancer risk associated

TABLE 3: Biological effects of radiation and simulated μG in ground experiments.

Interactive effects	Cells	Biological index	Devices	Irradiation[a]	Ref.
Yes, ↑	Lymphoblastoid	Mutation, micronuclei	RWV	Pre-^{60}Co, γ-rays	[183]
	Lymphocyte	Mutation	RWV	Pre-^{60}Co, γ-rays	[184]
	Lymphocyte	γ-H2AX	RWV	Pre-^{137}Cs, γ-rays	[185]
	Lymphoblast	Apoptosis, ROS	RWV	Post-C-ion	[186]
	Fibroblast	Gene induction	RPM	+ ^{252}Cf, neutron	[189]
	Neuron	Apoptosis, gene induction	RPM	+ ^{252}Cf, neutron	[190]
	Fibroblast	Chromosomal aberration	SSS	+ X-rays, + C-ion	[193]
	Fibroblast	Cell cycle-promoting genes	SSS	+ C-ion	[194]
Yes, ↓	Lymphocyte	Apoptosis	RWV	Pre-^{137}Cs, γ-rays	[187]
	Lymphoblastoid	Apoptosis	RWV	Pre-^{60}Co, γ-rays	[183]
	Lymphocyte	Micro-RNA	RWV	Pre-^{137}Cs, γ-rays	[188]
	Fibroblast	Cell cycle-suppressing genes	SSS	+ C-ion	[194]

ROS: reactive oxygen species; RWV: rotating wall vessel bioreactor; RPM: random positioning machine; SSS: system of simultaneous irradiation in simulated-microgravity. [a]+ means simultaneous irradiation with spaceflight.

with space radiation in the conventional manner based on data of radiation quality and quantity from cells irradiated under static conditions might underestimate the potential risk to astronauts. Nonetheless, examination of endpoints and *in vivo* model systems under the combined effects of radiation and μG are required.

In the near future, there is also a need to investigate the biological effect of partial gravity such as $1/6G$ and $3/8G$ on the response to radiation for manned missions to the Moon and Mars. Two simulated partial gravity devices using the RPM, one by applying specific software protocols to drive the RPM motors and the other involving integrating a centrifuge into the RPM, should become useful tools [195]. The actual effects should be tested either in a proper centrifuge experiment on the ISS, such as CBEF [181] and MHU [182], or actually on the surfaces of the Moon and Mars.

5.2. Combined Effects of μG and UV Radiation on Plants. Plants supply nutrients and oxygen to humans under a resource-recycling system on Earth and also in space. All organisms, including plants, have evolved protection mechanisms against environmental stresses. However, the environment in space differs dramatically from that on Earth. Can all organisms adapt to the environment in space and live healthy? In addition, there is the possibility that the higher intensity of UV radiation, which is a driving force of evolution, and the complex cosmic IR in space could lead to an increase in the mutation frequency. Currently, μG has been reported to cause cellular oxidative stress that leads to production of ROS and endoplasmic reticulum stress in experimental animals [196–198]. In addition, Sugimoto et al. reported that the environment during spaceflight induces oxidative stress and ROS gene network activation in the space-grown Mizuna plant [199]. The mechanisms by which μG elicits these cellular responses remain poorly understood, although very interesting results have been reported recently. For example, simulated μG induces autophagy *via* mitochondrial dysfunction in human Hodgkin's lymphoma cells [196] and TCam-2 cells [197]. The results

of proteomic and metabolomics analysis of human primary osteoblasts exposed to simulated μG suggest that μG suppresses bone cell function, impairing mitochondrial energy potential and the energy state of the cell [200].

To plan cultivation of plants in space including Mars, we need to identify what plants to use and whether to use sunlight or an artificial light source for growth. Negative effects of UV radiation can be avoided if plants are grown under artificial light without sunlight. However, we need to address some issues. For example, (1) it is difficult to grow plants uniformly in the same growth chamber, because the optimal wavelength and light intensity differ for different vegetable plants; and (2) growing plants in a growth chamber under artificial light is very costly because of the consumption of electric power. Conversely, if plants are grown using sunlight, the potential negative effects from UV radiation are unavoidable. It is unclear whether various UV-B protection mechanisms, which have evolved under $1G$, would function properly under lower gravity. It is thus important to investigate the potential ability of plants to adapt to the environment of space. For this purpose, utilization of facilities on orbiting space platforms such as the ISS is essential, although we cannot repeatedly and frequently conduct experiments on the ISS. To disturb the gravity direction or produce simulated μG on the ground, a 3D clinostat is useful and convenient (Figure 3).

Therefore, it is necessary to understand the combined environmental effects of space on plants at the molecular, cellular, and whole-plant levels and understand not only the transient, short-term (one generation) effects but also long-term (next, subsequent generations) effects under space environmental conditions through space experiments or experiments using equipment such as a 3D clinostat. Such experiments clarify direct and/or indirect gravity effects on vegetative and reproductive growth, provide new evidence of antigravity reactions, and possibly find not only novel biological knowledge, such as molecular mechanisms in gravity reactions, but also novel growth controls in crop production on Earth. In addition, experiments that include
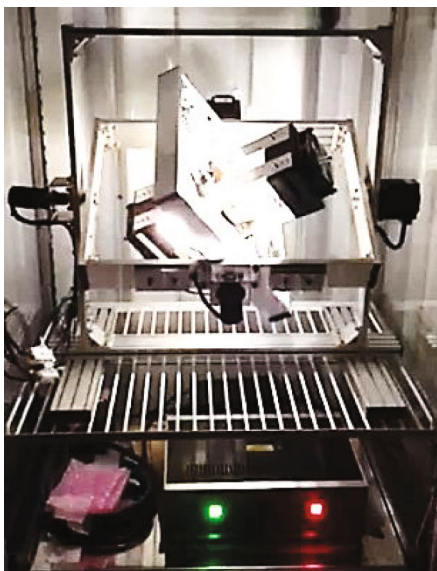
FIGURE 3: A 3D clinostat quipped with a UV-visible light unit. The UV-visible light unit is composed of white and UV-B- (280 nm) light-emitting diodes (LEDs).

the space-specific radiation environment will help elucidate the combined influence of low gravity and high-level visible UV and space radiations on plant growth and regeneration in a whole growth stage. However, a study about such combined effects on organisms as well as plants has only recently been initiated. Such studies, both on the ground and on orbiting space platforms such as the ISS, should be promoted to establish sustainable life support systems for securing long-term human life in space and on the Moon and Mars.

5.3. Radiation and Stress. Stress refers to conditions where an environmental demand exceeds the natural regulatory capacity of an organism, in particular situations that include unpredictability and uncontrollability, and psychological stress is one of two basic kinds of stress [201]. Psychological stress and radiation are known to cause various adverse effects on humans. Radiation is a carcinogen, and long-lasting psychological stress may affect the overall health and ability to cope with cancer. Whether psychological stress influences susceptibility to radiation, radiocarcinogenesis in particular, is of great concern for both academia and the public [202]. Using a laboratory mouse model for chronic restraint-induced psychological stress, the pioneering work on concurrent exposure of *Trp53* heterozygous C57BL/6 mice to psychological stress and total body γ-rays showed that psychological stress modulates susceptibility to radiation, causing increased susceptibility to radiocarcinogenesis in *Trp53*-heterozygous mice underlying the mechanism of *Trp53* function attenuation [203]. In recent years, studies using the same chronic restraint system, wild-type C57BL/6J male mice aged 5 weeks and total body exposure to 4 Gy X-rays, showed that psychological stress has minimal modifying effects on radiation-induced hematopoietic toxicity and genotoxicity measured as a peripheral blood histogram, MN in the erythrocytes of bone marrow, and splenocyte CAs (insertions, dicentrics, and fragments), suggesting that chronic restraint-

induced psychological stress does not appear to synergize with the clastogenicity of low-LET radiation in wild-type animals [204, 205]. Interestingly, in the animal model for psychosocial stress using 6- or 8-week-old male ddY mice (model mouse for spontaneous IgA nephropathy) and SAMP10 mice (model mouse for accelerated senescence), results of concurrent exposure to both psychosocial stress and X-rays at a dose of 3–6 Gy showed increased acute damage, namely, reduced 30-day survival, and decreased erythrocyte and leukocyte counts in the peripheral blood and hypocellular bone marrow, indicating psychological stress promotes radiosensitivity of bone marrow in these particular mice [206]. Interestingly, investigation using the mouse model for chronic restraint-induced psychological stress, *Trp53* heterozygous C57BL/6N male mice aged 6 weeks, and high-LET Fe particle irradiation at 0.1 or 2 Gy showed that concurrent exposure to psychological stress and 0.1 Gy Fe irradiation resulted in increased hematopoietic toxicity and genotoxicity measured as MN in the erythrocytes of the bone marrow and splenocyte CAs [207–209]. In contrast, in the mouse testis, concurrent exposure to 0.1 Gy Fe irradiation did not induce any increased apoptosis and autophagy inhibition [210]. These results indicate that psychological stress does not exacerbate radiation effects. These findings also suggest that studies on concurrent exposure should be performed using different endpoints in different tissues in both short- and long-term models for chronic restraint-induced psychological stress. In summary, concurrent exposure of wild-type mice to psychological stress and low-LET radiation did not suggest an additive effect for induction of hematopoietic toxicity and genotoxicity but promoted radiosensitivity of the bone marrow in some disease-prone mice. In contrast, concurrent exposure of *Trp53* heterozygous mice to psychological stress and high-LET radiation suggested an additive effect for induction of hematopoietic toxicity and genotoxicity. To reduce health risks from exposure to radiation by active intervention, further investigations are needed to collect more data that provide insights into the mechanisms underlying the alterations in susceptibility due to psychological stress modulation.

6. Radiation Exposure Management

To prevent IR-induced carcinogenesis, the exposure dose in spaceflight is limited to a level that will not result in exposure-induced death (REID) from fatal cancer over a career of more than 3%, at the 95% upper confidence interval of the risk calculation [129]. Based on this concept, missions in space are currently planned to last less than 180 days [211]. However, it has been suggested that there are individual differences in the IR-induced cancer risk within human populations [212]. Three factors that underlie individual IR-induced cancer risk, i.e., age, sex, and smoking, are already considered when determining the safe number of days in spaceflight [213]. Here, we review genetic variants in the DNA repair genes as an important factor underlying the individual differences in IR-induced cancer risk.

In human cells, DNA repair systems monitor and repair DNA DSBs to maintain genomic integrity. If IR-induced DSBs are left unrepaired, they can alter the information stored in the

genome to cause carcinogenesis. It is thus useful to measure the capacity of cells to repair DSBs to understand how prone individuals are to IR-induced carcinogenesis. The cytokinesis-blocked MN assay, a procedure established to evaluate the capacity of cells to repair DSBs by counting MN derived from unrepaired DSB-induced chromosomal fragments, has revealed the existence of cases in which the capacity to repair DSBs has been slightly decreased by IR within healthy individuals and those with breast cancer [214]. The FISH painting analysis, which monitors IR-induced unstable ring and multicentric chromosomes, also demonstrated the heterogeneity of the capacity to repair DSBs after IR within human populations [215]. Interestingly, genome-wide association studies (GWASs) have revealed that many nucleotide variants in DNA repair genes are linked to an enhanced risk of cancer in normal individuals [216]. These findings in the fields of radiation biology and epidemiology have suggested that the personalized risk of cancer after IR exposure might be attributable to variants in DNA repair genes.

To clarify whether variants in DNA repair genes are involved in the risk of IR-induced cancer, it is informative to compare chromosomal instability after IR exposure of primary cells with or without the variant of interest, such as skin fibroblasts and peripheral blood lymphocytes. However, the capacity of primary cells to repair DSBs is affected by the diverse genetic backgrounds within human populations [217]. It is therefore essential to evaluate the effects of candidate variants on the capacity of cells to repair DSBs in a uniform genetic background. Genome-editing technology is beneficial in this regard because it enables the introduction of candidate variants into human cultured cells with a uniform genetic background. Comparison of IR-induced chromosomal abnormalities in genome-edited cells can then reveal whether a candidate variant is able to repair DSBs within human populations. Previously, we used this approach to demonstrate that ataxia-telangiectasia mutated (*ATM*) heterozygous mutations, which are present at a rate of around 1% in human populations, are indeed associated with the individual capacity of cells to repair DSBs [217]. Besides *ATM* gene mutations, germline mutations of DNA repair genes in human populations have been reported, such as *MRE11A*, *NBS1*, *Rad50*, *Artemis*, and *DNA Lig-IV* [212]. These mutations are generally rare, while heterozygous *BRCA1* and *BRCA2* mutations for hereditary breast and ovarian cancers are estimated to be present at a rate of 0.05–1% in human populations [218, 219]. The extent to which these mutations contribute to the capacity to repair DSBs remains unclear but should be resolved to achieve personalized radiation exposure management. Further studies using an approach combining the fields of epidemiology and functional genomics are needed to understand the genetic basis of individual differences in IR-induced cancer risk.

7. Protection from Radiation

7.1. Protective Agents.
Many biological effects such as cell death and inflammatory responses due to radiation exposure are caused by DNA damage [71, 72, 75, 76]. Therefore, various drugs that aimed at decreasing induced DNA damage

have been studied as radioprotective agents. Radiation induces DNA damage both directly and indirectly through radicals generated in response to intracellular water molecules. Thus, there are numerous studies evaluating antioxidants that suppress radiation-induced radical generation [220–224]. In particular, the effects of vitamin C and vitamin E have been studied for many years as antioxidants with radioprotective effects. Our group has assessed radioprotective effects of ascorbic acid (AA) to patients before cardiac catheterization (CC) for diagnostic purposes. Although we did not find satisfactory evidence to show that AA treatment reduces γ-H2AX foci formation immediately after CC, a slight decrease in DNA damage in the group of AA treatment was detected [225]. However, the results vary depending on the animal model used, the radiation dose, and the method for evaluating the protective effect [226–230]. In addition to vitamins C and E, radioprotective effects of nitroxide compounds as strong radical scavengers have also been analyzed [220, 231–233].

Currently developed radioprotective drugs are unsuitable as radioprotectants in outer space because the situation of radiation exposure differs to that of previous ideas. In outer space, suitable radioprotective drugs should protect against chronic exposure to low dose and a low dose rate of high-LET radiation, and not the acute high-dose radiation exposure found in radiotherapy. Drugs suitable for humans living in space must treat both unexpected high-dose radiation exposure due to solar flares and the suppression of DNA damage by space radiation that occurs constantly. Therefore, it is necessary to validate a radioprotective drug that can be taken daily with minimal side effects. For this purpose, it may be effective to develop functional space foods with a radioprotective effect that can be ingested continuously in outer space [234, 235]. Currently, our group is examining the radioprotective effect of piceatannol, which is an ingredient of passion fruit and displays strong antioxidant activity. We have confirmed that suppression of DSB after not only low-LET radiation exposure but also various high-LET radiation exposures occurs when using piceatannol (unpublished data). The development of various radiation protection agents is expected to progress in the future. We emphasize that there is a need for the development of protective agents against not just space radiation but also various space environmental risks.

7.2. Historical Overview and Perspective of Basic Research for the Development of Biological Strategies.
Unfortunately, the development of a biological strategy for protection of our body from space radiation has not been achieved. To accomplish this, a basic knowledge about adverse effects of space radiation toward human health is required. In particular, we need to understand the radiosensitivity of each tissue. A French oncologist, Jean Alban Bergonié, and a French dermatologist, Louis Tribondeau, worked together between 1904 and 1906 and formulated a fundamental law in the field of radiation biology regarding the difference in radiosensitivity of normal tissues. They observed damage in the testis of male rats under a microscope after whole -body X-ray irradiation and found that biological effects of radiation were

TABLE 4: Classification of tissues based on their radiosensitivity.

Frequency of cell division	Tissue	Radiosensitivity
++	Lymphoid tissue, hematopoietic tissue (bone marrow), testicular epithelium, follicular epithelium, and intestinal epithelium	Extremely high
+	Oropharyngeal oral epithelium, skin epidermis, hair follicle epithelium, sebaceous gland epithelium, bladder epithelium, esophageal epithelium, lens epithelium, gastric gland epithelium, and ureteral epithelium	High
+/−	Connective tissue, small vessel tissue, and growing cartilage/bone tissue	Intermediate
−	Mature cartilage/bone tissue, mucous serous epithelium, sweat gland epithelium, nasopharyngeal epithelium, lung epithelium, renal epithelium, liver epithelium, pancreatic epithelium, pituitary epithelium, thyroid epithelium, and adrenal epithelium	Low
− −	Nerve tissue and muscle tissue	Extremely low

severer in the order of spermatogonia, spermatocyte, spermatid, and sperm. They generalized the result and formulated the so-called the Law of Bergonié and Tribondeau, which theorized that radiation causes severer damage to a tissue (1) when reproductive activity of cells in the tissue is greater, (2) when the karyokinetic fate of cells is longer (in other words, when the length of time that cells proliferate actively is longer), and (3) when morphology and function of cells are less differentiated. Based on this, radiosensitivity of representative tissues is classified as a summary in Table 4.

Accumulating evidence has demonstrated that the law certainly applies to many tissues; however, there are some exceptions. For example, Regaud claimed that spermatogonia in young rats are less radiosensitive than those in adults, though their proliferation rates are similar [236]. Using tobacco leaves, whose cell division rate significantly decreases as they grow, Haber and Rothstein demonstrated that radiosensitivity was almost the same between dividing and nondividing tissues [237]. Meyn and Jenkins measured the efficiency of DNA strand break formation in normal tissues of mice after whole-body irradiation and found that the least breaks were produced in the gut when compared with those of other tissues such as the bone marrow, spleen, brain, kidney, testis, and liver [238]. Ueno et al. recently found that quiescent melanocyte stem cells (McSCs) were more radiosensitive than coexisting nonquiescent McSCs and suggested that tissue radiosensitivity depends on the state of somatic stem cells under their microenvironment [239]. The law of Bergonié and Tribondeau needs to be revisited to integrate current knowledge about differences in radiosensitivity between various tissues.

Adverse effects of space radiation have been investigated under the various limitations of experimental settings; there is no way to separately evaluate radiosensitivity of each tissue using acute and monoenergetic beams [240]. To conduct more integrated analyses, our efforts in establishing a platform for *in vivo* animal studies are required. We can then analyze the effect of multiple factors (including low gravity and tissue microenvironment) on the efficiency of repair of DNA damage caused by space radiation. In particular, *in vivo* research using imaging techniques or genetically modified animals should provide spatiotemporal information about these factors. Moreover, we should conduct this research under various kinds of radiation that mimic space radiation with complex energy spectra and diverse ionic compositions. These approaches are expected to give us important information about radiosensitive tissues that should be protected from space radiation during ultralong spaceflights. Additionally, these approaches may lead to the development of radioprotective agents and also a system to select an astronaut who is potentially radioresistant.

8. Radioresistant Organisms

Organisms on Earth are protected from harmful space radiation by the electromagnetic field of our planet, most organisms including us are vulnerable to radiation, and radiation damage is one of the most severe risks to human health in long-term space flights. Some species on our planet, however, exhibit extraordinary resistance against high doses of radiation. Elucidating the molecular machinery responsible for these extraordinary radioresistance may aid the development of novel technologies that alleviate biological damage caused by radiation.

Most of the well-known radioresistant organisms are single-cellular prokaryotic organisms, such as archaea and bacteria. *Deinococcus radiodurans*, one of the most famous radioresistant bacteria, is reported to survive without loss of viability even after irradiation with 5,000 Gy of γ-rays [241, 242]. Although the genome DNA of *D. radiodurans* is heavily fragmented by high-dose irradiation, the DNA fragments are rapidly repaired to a complete circular genome by extensive DNA repair processes likely using their polyploid genome [243]. Mutation in the DNA repair pathways drastically compromises the radioresistance of *D. radiodurans*, suggesting that DNA is the most vulnerable target to radiation, and the powerful DNA repair system plays important roles in the high radioresistant capacity of this bacterium [243]. In addition to unicellular organisms, some animals such as tardigrades, bdelloid rotifers, and a sleeping chironomid, also exhibit exceptional tolerance against high doses of irradiation [244–248]. Intriguingly, these radioresistant animals also exhibit tolerance against almost complete dehydration. In a dehydrated state also known as "anhydrobiosis," they can withstand several thousand Gy of γ-irradiation. Some tardigrade species and a sleeping chironomid were reported to survive direct exposure to space in a desiccated state, suggesting that they are resistant even against space radiation [249,
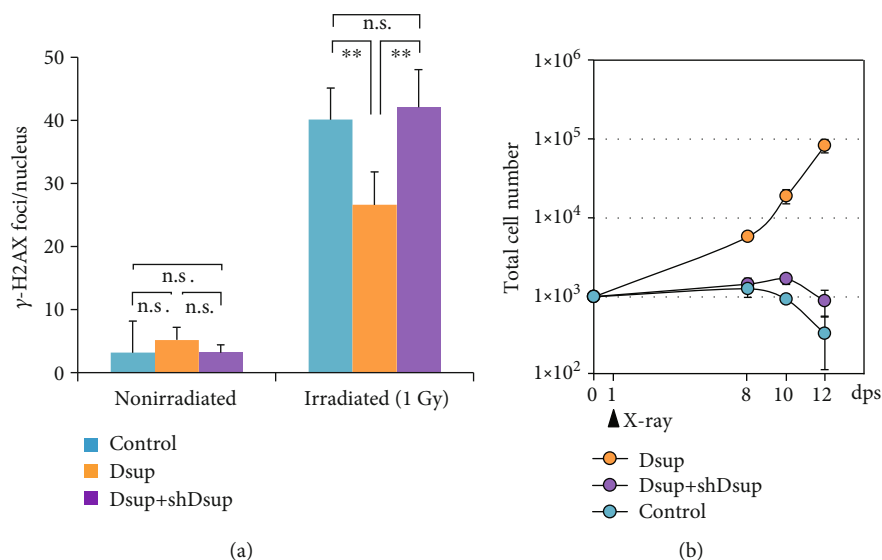
(a)

(b)

FIGURE 4: Dsup reduced X-ray-induced DNA damage (a) and improved viability of irradiated human cultured cells (b). The number of DNA-break marker, γ-H2AX foci in nonirradiated or 1 Gy-irradiated conditions (a), and growth curves after 4 Gy-irradiation (b) are compared among nonengineered human cultured cells (HEK293, control), Dsup-expressing cells (Dsup), and Dsup-knockdown cells (Dsup +shDsup). Reproduced from Hashimoto and Kunieda [253] under a Creative Commons Attribution-NonCommercial-ShareAlike 4.0 International License.

250]. Because biological damage by radiation, e.g., DNA lesions, partly overlaps with damage caused by desiccation, similar resistance machinery may be used to mitigate these two stressors, and coevolution of radioresistance and desiccation tolerance has been proposed [246].

Unlike other radioresistant animals, tardigrades exhibit high radiotolerance either in a hydrated state or in a dehydrated state, suggesting the presence of specific machinery that relieves the indirect effects of radiation in this animal group. *Ramazzottius varieornatus* is one of the most radiotolerant species in tardigrades [244]. A recent study identified a tardigrade-unique DNA-associating protein, termed damage suppressor (Dsup) as a DNA-protecting agent from a chromatin fraction of *R. varieornatus* [251]. Intriguingly, in a human cultured cell line engineered to express the Dsup protein, DNA damage caused by X-ray radiation (1–10 Gy) was reduced to nearly half of those in nonengineered cells (Figure 4). In addition, Dsup can also reduce DNA fragmentation in human cells treated with H_2O_2 significantly. Thus, Dsup is capable of protecting DNA from both X-ray irradiation and attack by ROS. The ability of Dsup to protect DNA from ROS could explain the high radiation resistance of tardigrades even in wet conditions in which radiation causes biological damage *via* generation of ROS, which is known as indirect effects. After irradiation with a near lethal dose (4 Gy) of X-ray, nonengineered human cultured cells lose their proliferative ability (Figure 4), but surprisingly, Dsup-expressing cells survive the irradiation and even retain proliferative ability that is comparable with those of nonirradiated cells (Figure 4) [251]. Considering these results, Dsup is able to not only confer DNA protection but also improve radiotolerance to human cultured cells. A recent *in vitro* study also confirmed that Dsup can protect chromatin DNA from hydroxyl radicals [252]. Currently, a Dsup homolog has only

been found in another tardigrade species, *Hypsibius exemplaris*, which belongs to the same taxonomic family of *R. varieornatus* [252–254]. These findings indicate that tardigrades have evolved their own stress-resistant machinery in their lineages and such unique machinery can also function in human cells. Radiation-resistant organisms including tardigrades are a valuable resource of undiscovered resistance genes and machineries, which might be used to enhance radiation resistance in other animal species including human.

9. Conclusions

In this review, discussion started with the environment of space radiation followed by a variety of simulated space radiation environments. Then, various adverse events by space radiation were discussed. In that chapter, state-of-the-art visualization technology of adverse events was discussed. Next, combined biological effects were discussed, and we reported that a newly developed 3D clinostat with synchronized irradiation capability would enable us to examine combined effects of radiation and μG. Radiation exposure management and radiation protection were then discussed. Finally, radioprotective organisms were presented because these organisms may aid the development of novel technologies that alleviate biological damage caused by radiation.

Understanding these topics in greater detail should facilitate better prediction of the risks and provide risk-mitigating strategies for future exploration space missions. In addition, meticulous use of available astronaut data, in particular long-duration mission crew members, should be beneficial. Furthermore, the use of rodent models in a Gateway program around the Moon orbit, for example, should provide important information required for a future human Mars mission.

Conflicts of Interest

The authors declare no conflicts of interest.

Acknowledgments

References

[1] J. C. McPhee and J. B. Charles, *Human health and performance risks of space exploration missions*, Government Printing Office, Washington, DC, USA, 2009.

[2] B. G. Drake, *Human exploration of mars design reference architecture 5.0*, National Aeronautics and Space Administration, 2009.

[3] E. R. Benton and E. V. Benton, "Space radiation dosimetry in low-Earth orbit and beyond," *Nuclear Instruments and Methods*, vol. 184, no. 1–2, pp. 255–294, 2001.

[4] E. V. Benton, K. Ogura, A. L. Frank, T. M. Atallah, and V. Rowe, "Response of different types of CR-39 to energetic ions," *Nuclear Tracks and Radiation Measurements*, vol. 12, no. 1-6, pp. 79–82, 1986.

[5] NCRP, "Radiation protection guidance for activities in low-Earth-orbit," *NCRP Report, no. 132*, 2000.

[6] NCRP, "Operational radiation safety program for astr5onauts in low-Earth orbit: a basic framework," *NCRP Report, no. 142*, 2002.

[7] G. D. Badhwar, F. A. Cucinotta, L. A. Braby, and A. Konradi, "Measurements on the shuttle of the LET spectra of galactic cosmic radiation and comparison with the radiation transport model," *Radiation Research*, vol. 139, no. 3, pp. 344–351, 1994.

[8] F. Spurny, "Radiation doses at high altitudes and during space flights," *Radiation Physics and Chemistry*, vol. 61, no. 3-6, pp. 301–307, 2001.

[9] A. Nagamatsu, "Space radiation dosimetry in the ISS, spearheading the following steps on the pathway to human space exploration beyond low-Earth orbit," in *The 15th International Congress of Radiation Research*, Kyoto, Japan, 2015.

[10] Z. Kolísková (Mrázová), L. Sihver, I. Ambrožová, T. Sato, F. Spurný, and V. A. Shurshakov, "Simulations of absorbed dose on the phantom surface of MATROSHKA-R experiment at the ISS," *Advances in Space Research*, vol. 49, pp. 230–236, 2012.

[11] A. Nagamatsu, M. Casolino, O. Larsson et al., "Space radiation dosimetry to evaluate the effect of polyethylene shielding in the Russian segment of the International Space Station," *Physics Procedia*, vol. 80, pp. 25–35, 2015.

[12] S. McKenna-Lawlor, the SG3.19/1.10 team, and Team members, "Feasibility study of astronaut standardized career dose limits in LEO and the outlook for BLEO," *Acta Astronautica*, vol. 104, no. 2, pp. 565–573, 2014.

[13] A. Nagamatsu, M. Masukawa, S. Kamigaichi et al., "Development of the space radiation dosimetry system 'PADLES'," in *20th Workshop on Radiation Detectors and Their Users*, pp. 23–36, Tsukuba, Japan, 2006.

[14] A. Nagamatsu, K. Murakami, S. Araki, H. Kumagai, K. Kitajo, and H. Tawara, "Space radiation dosimetry in low Earth orbit by a passive and integrating dosimeter 'PADLES'," in *22nd Workshop on Radiation Detectors and Their Uses, KEK Proceedings 2008–14*, pp. 167–177, Tsukuba, Japan, 2009.

[15] A. Nagamatsu, K. Murakami, K. Kitajo, K. Shimada, H. Kumagai, and H. Tawara, "Area radiation monitoring on ISS increments 17 to 22 using PADLES in the Japanese Experiment Module Kibo," *Radiation Measurements*, vol. 59, pp. 84–93, 2013.

[16] A. Takahashi, H. Ikeda, and Y. Yoshida, "Role of high-linear energy transfer radiobiology in space radiation exposure risks," *International Journal of Particle Therapy*, vol. 5, no. 1, pp. 151–159, 2018.

[17] T. Ohnishi, A. Takahashi, A. Nagamatsu et al., "Detection of space radiation-induced double strand breaks as a track in cell nucleus," *Biochemical and Biophysical Research Communications*, vol. 390, no. 3, pp. 485–488, 2009.

[18] A. Takahashi, A. Nagamatsu, X. Su et al., "The first life science experiments in ISS: reports of "Rad Gene"-Space radiation effects on human cultured cells-," *Biological Sciences in Space*, vol. 24, no. 1, pp. 17–41, 2010.

[19] S. Wakayama, Y. Kamada, K. Yamanaka et al., "Healthy offspring from freeze-dried mouse spermatozoa held on the International Space Station for 9 months," *Proceedings of the National Academy of Sciences of the United States of America*, vol. 114, no. 23, pp. 5988–5993, 2017.

[20] G. Reitz, T. Berger, P. Bilski et al., "Astronaut's organ doses inferred from measurements in a human phantom outside the International Space Station," *Radiation Research*, vol. 171, no. 2, pp. 225–235, 2009.

[21] K. Terasawa, "Development of Position Sensitive Tissue Equivalent Proportional Counter (PS-TEPC) and establishment of dosimetric technique in the International Space Station (ISS) with PS-TEPC," *Space Utilization Research*, vol. 24, pp. 322–325, 2008.

[22] ICRP, "1990 Recommendations of the International Commission on Radiological Protection," *Annals of the ICRP*, vol. 21, no. 1–3, pp. 1–201, 1991.

[23] R. Donald, "Radiation effects and shielding requirements in human missions to the Moon and Mars," *The MARS Journal*, vol. 2, pp. 46–71, 2006.

[24] R. K. Tripathi, J. W. Wilson, F. F. Badavi, and G. de Angelis, "A characterization of the moon radiation environment for radiation analysis," *Advances in Space Research*, vol. 37, no. 9, pp. 1749–1758, 2006.

[25] G. de Angelis, F. F. Badavi, S. R. Blattnig et al., "Modeling of the martian environment for radiation analysis," *Nuclear Physics B*, vol. 166, pp. 184–202, 2007.

[26] K. Hayatsu, M. Hareyama, S. Kobayashi et al., "Radiation doses for human exposed to galactic cosmic rays and their

secondary products on the lunar surface," *Biological Sciences in Space*, vol. 22, no. 2, pp. 59–66, 2008.

[27] P. M. O'Neill, "Galactic cosmic ray flux model- revised," *IEEE Transactions on Nuclear Science*, vol. 57, no. 6, pp. 3148–3153, 2010.

[28] Y. Jia and Z. W. Lin, "The radiation environment on the Moon from galactic cosmic rays in a lunar habitat," *Radiation Research*, vol. 173, no. 2, pp. 238–244, 2010.

[29] J. W. Wilson, M. S. Clowdsley, F. A. Cucinotta, R. K. Tripathi, J. E. Nealy, and G. de Angelis, "Deep space environments for human exploration," *Advances in Space Research*, vol. 34, no. 6, pp. 1281–1287, 2004.

[30] M.-H. Y. Kim, G. de Angelis, and F. A. Cucinotta, "Probabilistic assessment of radiation risk for astronauts in space missions," *Acta Astronautica*, vol. 68, no. 7-8, pp. 747–759, 2011.

[31] T. Sato, A. Nagamatsu, H. Ueno et al., "Comparison of cosmic-ray environments on Earth, Moon, Mars and in SPACECRAFT using PHITS," *Radiation Protection Dosimetry*, vol. 180, no. 1–4, pp. 146–149, 2018.

[32] K. T. Lee, T. Cleghorn, F. A. Cucinotta, L. Pinsky, and C. Zeitlin, "Heavy ion observations by MARIE in cruise phase and Mars orbit," *Advances in Space Research*, vol. 33, no. 12, pp. 2211–2214, 2004.

[33] H. E. Spence, A. W. Case, M. J. Golightly et al., "CRaTER: the cosmic ray telescope for the effects of radiation experiment on the lunar reconnaissance orbiter mission," *Space Science Reviews*, vol. 150, no. 1-4, pp. 243–284, 2010.

[34] C. Zeitlin, D. M. Hassler, F. A. Cucinotta et al., "Measurements of energetic particle radiation in transit to Mars on the Mars Science Laboratory," *Science*, vol. 340, no. 6136, pp. 1080–1084, 2013.

[35] D. M. Hassler, C. Zeitlin, R. F. Wimmer-Schweingruber et al., "Mars' surface radiation environment measured with the Mars Science Laboratory's Curiosity rover," *Science*, vol. 343, no. 6169, article 1244797, 2014.

[36] C. Zeitlin, D. M. Hassler, B. Ehresmann et al., "Measurements of radiation quality factor on Mars with the Mars Science Laboratory Radiation Assessment Detector," *Life Sciences in Space Research*, vol. 22, pp. 89–97, 2019.

[37] R. Singh, P. Parohar, S. Singh, M. Singh, V. P. Singh, and S. M. Prasad, "An introduction to UV-B research in plant science 1," in *UV-B radiation: From Environmental Stressor to Regulator of Plant Growth*, V. P. Singh, S. Singh, S. M. Prasad, and P. Parohar, Eds., pp. 1–6, Wiley, 2017.

[38] J. Jankowski and A. B. Cader, "The effect of depletion of the earth ozone layer on the human health condition," *International Journal of Occupational Medicine and Environmental Health*, vol. 10, no. 4, pp. 349–364, 1997.

[39] A. B. Britt, "DNA damage and repair in plants," *Annual Review of Plant Physiology and Plant Molecular Biology*, vol. 47, no. 1, pp. 75–100, 1996.

[40] A. Sancar, "Photolyase and cryptochrome blue-light photoreceptors," *Advances in Protein Chemistry*, vol. 69, pp. 73–100, 2004.

[41] G. A. Nelson, "Fundamental space radiobiology," *Gravitational and Space Biology Bulletin*, vol. 16, no. 2, pp. 29–36, 2003.

[42] J. C. Chancellor, R. S. Blue, K. A. Cengel et al., "Limitations in predicting the space radiation health risk for exploration astronauts," *npj Microgravity*, vol. 4, no. 1, p. 8, 2018.

[43] A. Yamagishi, S. Yokobori, Y. Yoshimura et al., "Japan Astrobiology Mars Project (JAMP): search for microbes on the Mars surface with special interest in methane-oxidizing bacteria," *Biological Sciences in Space*, vol. 24, no. 2, pp. 67–82, 2010.

[44] G. Rontó, A. Bérces, H. Lammer et al., "Solar UV irradiation conditions on the surface of Mars," *Photochemistry and Photobiology*, vol. 77, no. 1, pp. 34–40, 2003.

[45] E. J. Grant, A. Brenner, H. Sugiyama et al., "Solid cancer incidence among the life span study of atomic bomb survivors: 1958-2009," *Radiation Research*, vol. 187, no. 5, pp. 513–537, 2017.

[46] I. Braga-Tanaka III, S. Tanaka, A. Kohda et al., "Experimental studies on the biological effects of chronic low dose-rate radiation exposure in mice: overview of the studies at the Institute for Environmental Sciences," *International Journal of Radiation Biology*, vol. 94, no. 5, pp. 423–433, 2018.

[47] K. Ishizaki, Y. Hayashi, H. Nakamura, Y. Yasui, K. Komatsu, and A. Tachibana, "No induction of p53 phosphorylation and few focus formation of phosphorylated H2AX suggest efficient repair of DNA damage during chronic low-dose-rate irradiation in human cells," *Journal of Radiation Research*, vol. 45, no. 4, pp. 521–525, 2004.

[48] J. Miller, "Applications of charged particle accelerators -Impact of the NIRS-HIMAC facility, 5.1   Space Radiation Physics and Biology," *Radioisotopes*, vol. 68, no. 6, pp. 403–405, 2019.

[49] https://www.gsi.de/en/work/research/biophysics/biophysical_research/space_radiation_physics.htm.

[50] C. La Tessa, M. Sivertz, I.-H. Chiang, D. Lowenstein, and A. Rusek, "Overview of the NASA space radiation laboratory," *Life Sciences in Space Research*, vol. 11, pp. 18–23, 2016.

[51] A. Chatterjee and H. J. Schaefer, "Microdosimetric structure of heavy ion tracks in tissue," *Radiation and Environmental Biophysics*, vol. 13, no. 3, pp. 215–227, 1976.

[52] T. Funayama, "Heavy-ion microbeams for biological science: development of system and utilization for biological experiments in QST-Takasaki," *Quantum Beam Science*, vol. 3, no. 2, p. 13, 2019.

[53] N. Hamada, H. Matsumoto, T. Hara, and Y. Kobayashi, "Intercellular and intracellular signaling pathways mediating ionizing radiation-induced bystander effects," *Journal of Radiation Research*, vol. 48, no. 2, pp. 87–95, 2007.

[54] H. Matsumoto, N. Hamada, A. Takahashi, Y. Kobayashi, and T. Ohnishi, "Vanguards of paradigm shift in radiation biology: radiation-induced adaptive and bystander responses," *Journal of Radiation Research*, vol. 48, no. 2, pp. 97–106, 2007.

[55] S. Gerardi, "Ionizing radiation microbeam facilities for radiobiological studies in Europe," *Journal of Radiation Research*, vol. 50, Supplement A, pp. A13–A20, 2009.

[56] A. Bigelow, G. Garty, T. Funayama, G. Randers-Pehrson, D. Brenner, and C. Geard, "Expanding the question-answering potential of single-cell microbeams at RARAF, USA," *Journal of Radiation Research*, vol. 50, Supplement A, pp. A21–A28, 2009.

[57] Y. Kobayashi, T. Funayama, N. Hamada et al., "Microbeam irradiation facilities for radiobiology in Japan and China," *Journal of Radiation Research*, vol. 50, Supplement A, pp. A29–A47, 2009.

[58] B. E. Fischer, K.-O. Voss, and G. du, "Targeted irradiation of biological cells using an ion microprobe - Why a small beam spot is not sufficient for success," *Nuclear Instruments and Methods in Physics Research Section B*, vol. 267, no. 12-13, pp. 2122–2124, 2009.

[59] G. A. Drexler, C. Siebenwirth, S. E. Drexler et al., "Live cell imaging at the Munich ion microbeam SNAKE – a status report," *Radiation Oncology*, vol. 10, no. 1, p. 42, 2015.

[60] N. Guo, G. du, W. Liu et al., "Live cell imaging combined with high-energy single-ion microbeam," *Review of Scientific Instruments*, vol. 87, no. 3, article 034301, 2016.

[61] T. Funayama, N. Hamada, T. Sakashita, and Y. Kobayashi, "Heavy-ion microbeams - development and applications in biological studies," *IEEE Transactions on Plasma Science*, vol. 36, no. 4, pp. 1432–1440, 2008.

[62] T. Funayama, S. Wada, Y. Kobayashi, and H. Watanabe, "Irradiation of mammalian cultured cells with a collimated heavy-ion microbeam," *Radiation Research*, vol. 163, no. 2, pp. 241–246, 2005.

[63] N. Hamada, M. Ni, T. Funayama, T. Sakashita, and Y. Kobayashi, "Temporally distinct response of irradiated normal human fibroblasts and their bystander cells to energetic heavy ions," *Mutation Research*, vol. 639, no. 1–2, pp. 35–44, 2008.

[64] M. Iwakawa, N. Hamada, K. Imadome et al., "Expression profiles are different in carbon ion-irradiated normal human fibroblasts and their bystander cells," *Mutation Research*, vol. 642, no. 1-2, pp. 57–67, 2008.

[65] Y. Mutou-Yoshihara, T. Funayama, Y. Yokota, and Y. Kobayashi, "Involvement of bystander effect in suppression of the cytokine production induced by heavy-ion broad beams," *International Journal of Radiation Biology*, vol. 88, no. 3, pp. 258–266, 2012.

[66] T. Sugimoto, K. Dazai, T. Sakashita et al., "Cell cycle arrest and apoptosis in *Caenorhabditis elegans* germline cells following heavy-ion microbeam irradiation," *International Journal of Radiation Biology*, vol. 82, no. 1, pp. 31–38, 2006.

[67] M. Suzuki, Y. Hattori, T. Sakashita, Y. Yokota, Y. Kobayashi, and T. Funayama, "Region-specific irradiation system with heavy-ion microbeam for active individuals of *Caenorhabditis elegans*," *Journal of Radiation Research*, vol. 58, no. 6, pp. 881–886, 2017.

[68] T. Yasuda, M. Kamahori, K. Nagata et al., "Abscopal activation of microglia in embryonic fish brain following targeted irradiation with heavy-ion microbeam," *International Journal of Molecular Sciences*, vol. 18, no. 7, article 1428, 2017.

[69] T. Funayama, T. Sakashita, M. Suzuki et al., "An irradiation device for biological targets using focused microbeams of cyclotron-accelerated heavy ion," *Nuclear Instruments and Methods in Physics Research Section B*, vol. 465, pp. 101–109, 2020.

[70] P. L. Olive, J. P. Banáth, R. E. Durand, and J. P. Banath, "Heterogeneity in radiation-induced DNA damage and repair in tumor and normal cells measured using the "comet" assay," *Radiation Research*, vol. 122, no. 1, pp. 86–94, 1990.

[71] P. Jeggo and M. Löbrich, "Radiation-induced DNA damage responses," *Radiation Protection Dosimetry*, vol. 122, no. 1–4, pp. 124–127, 2006.

[72] K. Sankaranarayanan, R. Taleei, S. Rahmanian, and H. Nikjoo, "Ionizing radiation and genetic risks. XVII. Formation mechanisms underlying naturally occurring DNA deletions in the human genome and their potential relevance for bridging the gap between induced DNA double-strand breaks and deletions in irradiated germ cells," *Mutation Research/Reviews in Mutation Research*, vol. 753, no. 2, pp. 114–130, 2013.

[73] W. L. Santivasi and F. Xia, "Ionizing radiation-induced DNA damage, response, and repair," *Antioxidants & Redox Signaling*, vol. 21, no. 2, pp. 251–259, 2014.

[74] R. Scully, A. Panday, R. Elango, and N. A. Willis, "DNA double-strand break repair-pathway choice in somatic mammalian cells," *Nature Reviews Molecular Cell Biology*, vol. 20, no. 11, pp. 698–714, 2019.

[75] P. A. Jeggo, L. H. Pearl, and A. M. Carr, "DNA repair, genome stability and cancer: a historical perspective," *Nature Reviews Cancer*, vol. 16, no. 1, pp. 35–42, 2016.

[76] D. B. Lombard, K. F. Chua, R. Mostoslavsky, S. Franco, M. Gostissa, and F. W. Alt, "DNA repair, genome stability, and aging," *Cell*, vol. 120, no. 4, pp. 497–512, 2005.

[77] F. Cortese, D. Klokov, A. Osipov et al., "Vive la radiorésistance!: converging research in radiobiology and biogerontology to enhance human radioresistance for deep space exploration and colonization," *Oncotarget*, vol. 9, no. 18, pp. 14692–14722, 2018.

[78] U. Hagen, "Radiation biology in space: a critical review," *Advances in Space Research*, vol. 9, no. 10, pp. 3–8, 1989.

[79] K. Ohnishi and T. Ohnishi, "The biological effects of space radiation during long stays in space," *Biological Sciences in Space*, vol. 18, no. 4, pp. 201–205, 2004.

[80] L. J. Eccles, P. O'Neill, and M. E. Lomax, "Delayed repair of radiation induced clustered DNA damage: friend or foe?," *Mutation Research/Fundamental and Molecular Mechanisms of Mutagenesis*, vol. 711, no. 1-2, pp. 134–141, 2011.

[81] E. Sage and N. Shikazono, "Radiation-induced clustered DNA lesions: repair and mutagenesis," *Free Radical Biology & Medicine*, vol. 107, pp. 125–135, 2017.

[82] M. Hada and A. G. Georgakilas, "Formation of clustered DNA damage after high-LET irradiation: a review," *Journal of Radiation Research*, vol. 49, no. 3, pp. 203–210, 2008.

[83] B. Rydberg, "Radiation-induced DNA damage and chromatin structure," *Acta Oncologica*, vol. 40, no. 6, pp. 682–685, 2001.

[84] B. Rydberg, "Clusters of DNA damage induced by ionizing radiation: formation of short DNA fragments. II. Experimental detection," *Radiation Research*, vol. 145, no. 2, pp. 200–209, 1996.

[85] D. Tsao, P. Kalogerinis, I. Tabrizi, M. Dingfelder, R. D. Stewart, and A. G. Georgakilas, "Induction and processing of oxidative clustered DNA lesions in ^{56}Fe-ion-irradiated human monocytes," *Radiation Research*, vol. 168, no. 1, pp. 87–97, 2007.

[86] J. R. Milligan, J. A. Aguilera, R. A. Paglinawan, J. F. Ward, and C. L. Limoli, "DNA strand break yields after post-high LET irradiation incubation with endonuclease-III and evidence for hydroxyl radical clustering," *International Journal of Radiation Biology*, vol. 77, no. 2, pp. 155–164, 2001.

[87] A. G. Georgakilas, S. M. Holt, J. M. Hair, and C. W. Loftin, "Measurement of oxidatively-induced clustered DNA lesions using a novel adaptation of single cell gel electrophoresis (comet assay)," *Current Protocols in Cell Biology*, vol. 49, no. 1, pp. 6.11.1–6.11.17, 2010.

[88] I. Testard and L. Sabatier, "Assessment of DNA damage induced by high-LET ions in human lymphocytes using the comet assay," *Mutation Research*, vol. 448, no. 1, pp. 105–115, 2000.

[89] N. Desai, M. Durante, Z. W. Lin, F. A. Cucinotta, and H. Wu, "High LET-induced H2AX phosphorylation around the Bragg curve," *Advances in Space Research*, vol. 35, no. 2, pp. 236–242, 2005.

[90] N. Desai, E. Davis, P. O'Neill, M. Durante, F. A. Cucinotta, and H. Wu, "Immunofluorescence detection of clustered γ-H2AX foci induced by HZE-particle radiation," *Radiation Research*, vol. 164, no. 4, pp. 518–522, 2005.

[91] E. L. Leatherbarrow, J. V. Harper, F. A. Cucinotta, and P. O'Neill, "Induction and quantification of γ-H2AX foci following low and high LET-irradiation," *International Journal of Radiation Biology*, vol. 82, no. 2, pp. 111–118, 2006.

[92] E. P. Rogakou, D. R. Pilch, A. H. Orr, V. S. Ivanova, and W. M. Bonner, "DNA double-stranded breaks induce histone H2AX phosphorylation on serine 139," *Journal of Biological Chemistry*, vol. 273, no. 10, pp. 5858–5868, 1998.

[93] W. M. Bonner, C. E. Redon, J. S. Dickey et al., "γH2AX and cancer," *Nature Reviews Cancer*, vol. 8, no. 12, pp. 957–967, 2008.

[94] C. E. Redon, A. J. Nakamura, O. Sordet et al., "γ-H2AX detection in peripheral blood lymphocytes, splenocytes, bone marrow, xenografts, and skin," *Methods in Molecular Biology*, vol. 682, pp. 249–270, 2011.

[95] T. Lu, Y. Zhang, M. Wong et al., "Detection of DNA damage by space radiation in human fibroblasts flown on the International Space Station," *Life Sciences in Space Research*, vol. 12, pp. 24–31, 2017.

[96] A. Shibata, "Regulation of repair pathway choice at two-ended DNA double-strand breaks," *Mutation Research/Fundamental and Molecular Mechanisms of Mutagenesis*, vol. 803-805, pp. 51–55, 2017.

[97] H. Yajima, H. Fujisawa, N. I. Nakajima et al., "The complexity of DNA double strand breaks is a critical factor enhancing end-resection," *DNA Repair*, vol. 12, no. 11, pp. 936–946, 2013.

[98] D. T. Goodhead, "Initial events in the cellular effects of ionizing radiations: clustered damage in DNA," *International Journal of Radiation Biology*, vol. 65, no. 1, pp. 7–17, 1994.

[99] G. Slupphaug, B. Kavli, and H. E. Krokan, "The interacting pathways for prevention and repair of oxidative DNA damage," *Mutation Research/Fundamental and Molecular Mechanisms of Mutagenesis*, vol. 531, no. 1–2, pp. 231–251, 2003.

[100] E. Pernot, J. Hall, S. Baatout et al., "Ionizing radiation biomarkers for potential use in epidemiological studies," *Mutation Research/Reviews in Mutation Research*, vol. 751, no. 2, pp. 258–286, 2012.

[101] S. Bonassi, H. Norppa, M. Ceppi et al., "Chromosomal aberration frequency in lymphocytes predicts the risk of cancer: results from a pooled cohort study of 22 358 subjects in 11 countries," *Carcinogenesis*, vol. 29, no. 6, pp. 1178–1183, 2008.

[102] D. G. Harnden and H. P. Klinger, "An international system for human cytogenetic nomenclature (1985) ISCN 1985. Report of the standing Committee on Human Cytogenetic Nomenclature," *Birth Defects Original Article Series*, vol. 21, no. 1, pp. 1–117, 1985.

[103] A. L. Brooks, "Biomarkers of exposure, sensitivity and disease," *International Journal of Radiation Biology*, vol. 75, no. 12, pp. 1481–1503, 1999.

[104] M. Durante, Y. Furusawa, H. Majima, T. Kawata, and E. Gotoh, "Association between G2-phase block and repair of radiation-induced chromosome fragments in human lymphocytes," *Radiation Research*, vol. 151, no. 6, pp. 670–676, 1999.

[105] G. E. Pantelias and H. D. Maillie, "A simple method for premature chromosome condensation induction in primary human and rodent cells using polyethylene glycol," *Somatic Cell Genetics*, vol. 9, no. 5, pp. 533–547, 1983.

[106] M. Fenech, M. Kirsch-Volders, A. T. Natarajan et al., "Molecular mechanisms of micronucleus, nucleoplasmic bridge and nuclear bud formation in mammalian and human cells," *Mutagenesis*, vol. 26, no. 1, pp. 125–132, 2011.

[107] M. Maalouf, M. Durante, and N. Foray, "Biological effects of space radiation on human cells: history, advances and outcomes," *Journal of Radiation Research*, vol. 52, no. 2, pp. 126–146, 2011.

[108] K. George, J. Rhone, A. Beitman, and F. A. Cucinotta, "Cytogenetic damage in the blood lymphocytes of astronauts: effects of repeat long-duration space missions," *Mutation Research*, vol. 756, no. 1–2, pp. 165–169, 2013.

[109] K. A. George, M. Hada, L. Chappell, and F. A. Cucinotta, "Biological effectiveness of accelerated particles for the induction of chromosome damage: track structure effects," *Radiation Research*, vol. 180, no. 1, pp. 25–33, 2013.

[110] S. Ritter and M. Durante, "Heavy-ion induced chromosomal aberrations: a review," *Mutation Research*, vol. 701, no. 1, pp. 38–46, 2010.

[111] T. Katsube, B. Wang, K. Tanaka et al., "FISH analysis of chromosomal aberrations in mouse splenocytes following total body irradiation with heavy ions (iron-56 ions) and X-rays," in *The 63rd Annual Radiation Research Society Meeting*, Cancun, Mexico, 2017.

[112] B. Wang, K. Tanaka, T. Katsube et al., "Relative effectiveness of heavy ion irradiations from accelerated iron-56 particles for induction of genotoxicity in the hematopoietic system in mice: hematological abnormality in the peripheral blood and residual damage in the bone marrow erythrocytes (Part II)," in *The 63rd Annual Radiation Research Society Meeting*, Cancun, Mexico, 2017.

[113] P. Møller, "Genotoxicity of environmental agents assessed by the alkaline comet assay," *Basic Clinical Pharmacology and Toxicology*, vol. 96, pp. 1–42, 2005.

[114] M. A. Kadhim, D. A. Macdonald, D. T. Goodhead, S. A. Lorimore, S. J. Marsden, and E. G. Wright, "Transmission of chromosomal instability after plutonium α-particle irradiation," *Nature*, vol. 355, no. 6362, pp. 738–740, 1992.

[115] L. Huang, S. Grim, L. E. Smith et al., "Ionizing radiation induces delayed hyper-recombination in mammalian cells," *Molecular and Cellular Biology*, vol. 24, no. 11, pp. 5060–5068, 2004.

[116] C. P. Allen, H. Hirakawa, N. I. Nakajima et al., "Low- and high-LET ionizing radiation induces delayed homologous recombination that persists for two weeks before resolving," *Radiation Research*, vol. 188, no. 1, pp. 82–93, 2017.

[117] C. L. Limoli, B. Ponnaiya, J. J. Corcoran et al., "Genomic instability induced by high and low LET ionizing radiation,"

Advances in Space Research, vol. 25, no. 10, pp. 2107–2117, 2000.

[118] W. F. Morgan, J. P. Day, M. I. Kaplan, E. M. McGhee, and C. L. Limoli, "Genomic instability induced by ionizing radiation," *Radiation Research*, vol. 146, no. 3, pp. 247–258, 1996.

[119] Y. Yao and W. Dai, "Genomic instability and cancer," *Journal of Carcinogenesis and Mutagenesis*, vol. 5, no. 2, article 1000165, 2014.

[120] E. M. Kass and M. Jasin, "Collaboration and competition between DNA double strand break repair pathways," *FEBS Letters*, vol. 584, no. 17, pp. 3703–3708, 2010.

[121] M. E. Moynahan and M. Jasin, "Mitotic homologous recombination maintains genomic stability and suppresses tumorigenesis," *Nature Reviews Molecular Cell Biology*, vol. 11, no. 3, pp. 196–207, 2010.

[122] P. K. Gupta, A. Sahota, S. A. Boyadjiev et al., "High frequency *in vivo* loss of heterozygosity is primarily a consequence of mitotic recombination," *Cancer Research*, vol. 57, no. 6, pp. 1188–1193, 1997.

[123] R. Reliene, A. J. R. Bishop, and R. H. Schiestl, "Involvement of homologous recombination in carcinogenesis," *Advances in Genetics*, vol. 58, pp. 67–87, 2007.

[124] M. R. Sukup-Jackson, O. Kiraly, J. E. Kay et al., "Rosa26-GFP direct repeat (RaDR-GFP) mice reveal tissue- and age-dependence of homologous recombination in mammals *in vivo*," *PLoS Genetics*, vol. 10, no. 6, article e1004299, 2014.

[125] A. Fujimori, H. Hirakawa, and C. Liu, "Visualization of *in vivo* DNA damage responses to galactic cosmic radiation," in *The 5th International Symposium on Space Radiation and Particle Radiotherapy*, Suzhou, China, 2017.

[126] C. Liu, H. Hirakawa, K. Tanaka et al., "Reduction of delayed homologous recombination by induction of radioadaptive response in RaDR-GFP mice (Yonezawa effect): an old player with a new role," *Dose Response*, vol. 17, no. 1, article 1559325819833840, 2019.

[127] F. A. Cucinotta and M. Durante, "Cancer risk from exposure to galactic cosmic rays: implications for space exploration by human beings," *Lancet Oncology*, vol. 7, no. 5, pp. 431–435, 2006.

[128] M. Durante and F. A. Cucinotta, "Heavy ion carcinogenesis and human space exploration," *Nature Reviews Cancer*, vol. 8, no. 6, pp. 465–472, 2008.

[129] Task Group on Radiation Protection in Space, ICRP Committee 2, G. Dietze et al., "Assessment of radiation exposure of astronauts in space Internal Commission on Radiological Protection, ICRP publication 123," *Annual Report of ICRP*, vol. 42, pp. 1–339, 2013.

[130] K. Ozasa, Y. Shimizu, A. Suyama et al., "Studies of the mortality of atomic bomb survivors, Report 14, 1950-2003: an overview of cancer and noncancer diseases," *Radiation Research*, vol. 177, no. 3, pp. 229–243, 2012.

[131] F. A. Cucinotta, K. To, and E. Cacao, "Predictions of space radiation fatality risk for exploration missions," *Life Sciences in Space Research*, vol. 13, pp. 1–11, 2017.

[132] T. Imaoka, M. Nishimura, K. Daino et al., "Risk of second cancer after ion beam radiotherapy: insights from animal carcinogenesis studies," *International Journal of Radiation Biology*, vol. 95, no. 10, pp. 1431–1440, 2019.

[133] B. J. Blyth, S. Kakinuma, M. Sunaoshi et al., "Genetic analysis of T cell lymphomas in carbon ion-irradiated mice reveals frequent interstitial chromosome deletions: implications for second cancer induction in normal tissues during carbon ion radiotherapy," *PLoS ONE*, vol. 10, no. 6, article e0130666, 2015.

[134] M. H. Barcellos-Hoff and J. H. Mao, "HZE radiation non-targeted effects on the microenvironment that mediate mammary carcinogenesis," *Frontiers in Oncology*, vol. 6, p. 57, 2016.

[135] C. Tsuruoka, B. J. Blyth, T. Morioka et al., "Sensitive detection of radiation-induced medulloblastomas after acute or protracted gamma-ray exposures in *Ptch1* heterozygous mice using a radiation-specific molecular signature," *Radiation Research*, vol. 186, no. 4, pp. 407–414, 2016.

[136] T. Imaoka, M. Nishimura, K. Daino et al., "Prominent dose-rate effect and its age dependence of rat mammary carcinogenesis induced by continuous gamma-ray exposure," *Radiation Research*, vol. 191, no. 3, pp. 245–254, 2019.

[137] R. Hodson, "The brain," *Nature*, vol. 571, no. 7766, p. S1, 2019.

[138] C. S. von Bartheld, J. Bahney, and S. Herculano-Houzel, "The search for true numbers of neurons and glial cells in the human brain: a review of 150 years of cell counting," *Journal of Comparative Neurology*, vol. 524, no. 18, pp. 3865–3895, 2016.

[139] P. J. Tofilon and J. R. Fike, "The radioresponse of the central nervous system: a dynamic process," *Radiation Research*, vol. 153, no. 4, pp. 357–370, 2000.

[140] E. Cekanaviciute, S. Rosi, and S. Costes, "Central nervous system responses to simulated galactic cosmic rays," *International Journal of Molecular Sciences*, vol. 19, no. 11, article 3669, 2018.

[141] K. Manda, M. Ueno, and K. Anzai, "Memory impairment, oxidative damage and apoptosis induced by space radiation: Ameliorative potential of α-lipoic acid," *Behavioural Brain Research*, vol. 187, no. 2, pp. 387–395, 2008.

[142] S. Suman, O. C. Rodriguez, T. A. Winters, A. J. Fornace Jr., C. Albanese, and K. Datta, "Therapeutic and space radiation exposure of mouse brain causes impaired DNA repair response and premature senescence by chronic oxidant production," *Aging*, vol. 5, no. 8, pp. 607–622, 2013.

[143] C. W. Whoolery, A. K. Walker, D. R. Richardson et al., "Whole-body exposure to ^{28}Si-Radiation dose-dependently disrupts dentate gyrus neurogenesis and proliferation in the short term and new neuron survival and contextual fear conditioning in the long term," *Radiation Research*, vol. 188, no. 5, pp. 532–551, 2017.

[144] T. B. Sweet, S. D. Hurley, M. D. Wu, J. A. Olschowka, J. P. Williams, and M. K. O'Banion, "Neurogenic effects of low-dose whole-body HZE (Fe) ion and gamma irradiation," *Radiation Research*, vol. 186, no. 6, pp. 614–623, 2016.

[145] K. Krukowski, K. Grue, E. S. Frias et al., "Female mice are protected from space radiation-induced maladaptive responses," *Brain, Behavior, and Immunity*, vol. 74, pp. 106–120, 2018.

[146] V. K. Parihar, B. D. Allen, C. Caressi et al., "Cosmic radiation exposure and persistent cognitive dysfunction," *Scientific Reports*, vol. 6, no. 1, article 34774, 2016.

[147] I. V. Sokolova, C. J. Schneider, M. Bezaire, I. Soltesz, R. Vlkolinsky, and G. A. Nelson, "Proton radiation alters intrinsic and synaptic properties of CA1 pyramidal neurons

of the mouse hippocampus," *Radiation Research*, vol. 183, no. 2, pp. 208–218, 2015.

[148] D. L. Dickstein, R. Talty, E. Bresnahan et al., "Alterations in synaptic density and myelination in response to exposure to high-energy charged particles," *Journal of Comparative Neurology*, vol. 526, no. 17, pp. 2845–2855, 2018.

[149] A. R. Allen, J. Raber, A. Chakraborti, S. Sharma, and J. R. Fike, "^{56}Fe irradiation alters spine density and dendritic complexity in the mouse hippocampus," *Radiation Research*, vol. 184, no. 6, pp. 586–594, 2015.

[150] F. Kiffer, H. Carr, T. Groves et al., "Effects of ^{1}H $^{+16}$O charged particle irradiation on short-term memory and hippocampal physiology in a murine model," *Radiation Research*, vol. 189, no. 1, pp. 53–63, 2018.

[151] V. K. Parihar, M. Maroso, A. Syage et al., "Persistent nature of alterations in cognition and neuronal circuit excitability after exposure to simulated cosmic radiation in mice," *Experimental Neurology*, vol. 305, pp. 44–55, 2018.

[152] M. M. Acharya, J. E. Baulch, P. M. Klein et al., "New concerns for neurocognitive function during deep space exposures to chronic, low dose-rate, neutron radiation," *eNeuro*, vol. 6, no. 4, pp. ENEURO.0094–ENEU19.2019, 2019.

[153] T. Sakashita, M. Suzuki, N. Hamada et al., "Behavioral resistance of *Caenorhabditis elegans* against high-LET radiation exposure," *Biological Sciences in Space*, vol. 26, pp. 7–11, 2012.

[154] T. Sakashita, M. Suzuki, N. Hamada et al., "Effects of low- and high-LET radiation on the salt chemotaxis learning in *Caenorhabditis elegans*," *Biological Sciences in Space*, vol. 26, pp. 21–25, 2012.

[155] M. Suzuki, T. Sakashita, S. Yanase et al., "Effects of ionizing radiation on locomotory behavior and mechanosensation in *Caenorhabditis elegans*," *Journal of Radiation Research*, vol. 50, no. 2, pp. 119–125, 2009.

[156] X. Wang, H. Li, A. Zheng et al., "Mitochondrial dysfunction-associated OPA1 cleavage contributes to muscle degeneration: preventative effect of hydroxytyrosol acetate," *Cell Death & Disease*, vol. 5, no. 11, article e1521, 2014.

[157] K. Momma, T. Homma, R. Isaka, S. Sudevan, and A. Higashitani, "Heat-induced calcium leakage causes mitochondrial damage in *Caenorhabditis elegans* body-wall muscles," *Genetics*, vol. 206, no. 4, pp. 1985–1994, 2017.

[158] S. Sudevan, M. Takiura, Y. Kubota et al., "Mitochondrial dysfunction causes Ca^{2+} overload and ECM degradation–mediated muscle damage in *C. elegans*," *FASEB Journal*, vol. 33, no. 8, pp. 9540–9550, 2019.

[159] L. Krenning, J. van den Berg, and R. H. Medema, "Life or death after a break: what determines the choice?," *Molecular Cell*, vol. 76, no. 2, pp. 346–358, 2019.

[160] T. Terasima and L. J. Tolmach, "Changes in x-ray sensitivity of HeLa cells during the division cycle," *Nature*, vol. 190, no. 4782, pp. 1210-1211, 1961.

[161] T. Terasima and L. J. Tolmach, "Variations in several responses of HeLa cells to X-irradiation during the division cycle," *Biophysical Journal*, vol. 3, no. 1, pp. 11–33, 1963.

[162] A. Sakaue-Sawano, H. Kurokawa, T. Morimura et al., "Visualizing spatiotemporal dynamics of multicellular cell-cycle progression," *Cell*, vol. 132, no. 3, pp. 487–498, 2008.

[163] A. Sakaue-Sawano, T. Kobayashi, K. Ohtawa, and A. Miyawaki, "Drug-induced cell cycle modulation leading to cell-cycle arrest, nuclear mis-segregation, or endoreplication," *BMC Cell Biology*, vol. 12, no. 1, p. 2, 2011.

[164] A. Sakaue-Sawano, M. Yo, N. Komatsu et al., "Genetically encoded tools for optical dissection of the mammalian cell cycle," *Molecular Cell*, vol. 68, no. 3, pp. 626–640.e5, 2017.

[165] Y. Zhu, T. Zhao, S. Itasaka et al., "Involvement of decreased hypoxia-inducible factor 1 activity and resultant G$_1$-S cell cycle transition in radioresistance of perinecrotic tumor cells," *Oncogene*, vol. 32, no. 16, pp. 2058–2068, 2013.

[166] K. Otani, Y. Naito, Y. Sakaguchi et al., "Cell-cycle-controlled radiation therapy was effective for treating a murine malignant melanoma cell line *in vitro* and *in vivo*," *Scientific Reports*, vol. 6, no. 1, article 30689, 2016.

[167] M. A. Bender, P. C. Gooch, and S. Kondo, "The Gemini-XI S-4 spaceflight-radiation interaction experiment: the human blood experiment," *Radiation Research*, vol. 34, no. 1, pp. 228–238, 1968.

[168] G. Horneck, P. Rettberg, S. Kozubek et al., "The influence of microgravity on repair of radiation-induced DNA damage in bacteria and human fibroblasts," *Radiation Research*, vol. 147, no. 3, pp. 376–384, 1997.

[169] H. D. Pross and J. Kiefer, "Repair of cellular radiation damage in space under microgravity conditions," *Radiation and Environmental Biophysics*, vol. 38, no. 2, pp. 133–138, 1999.

[170] A. Takahashi, K. Ohnishi, S. Takahashi et al., "The effects of microgravity on induced mutation in *Escherichia coli* and *Saccharomyces cerevisiae*," *Advances in Space Research*, vol. 28, no. 4, pp. 555–561, 2001.

[171] H. Wu, K. George, V. Willingham, and F. A. Cucinotta, "Comparison of chromosome aberration frequencies in pre- and post-flight astronaut lymphocytes irradiated *in vitro* with gamma rays," *Physica Medica*, vol. 17, Supplement 1, pp. 229–231, 2001.

[172] B. B. Shank, *Space biology and related topics*, Academic Press, 1974.

[173] H. Bücker, G. Horneck, G. Reitz et al., "Embryogenesis and organogenesis of *Carausius morosus* under spaceflight conditions," *Naturwissenschaften*, vol. 73, no. 7, pp. 433-434, 1986.

[174] H. D. Pross, M. Kost, and J. Kiefer, "Repair of radiation induced genetic damage under microgravity," *Advances in Space Research*, vol. 14, no. 10, pp. 125–130, 1994.

[175] M. Ikenaga, I. Yoshikawa, M. Kojo et al., "Mutations induced in *Drosophila* during space flight," *Biological Sciences in Space*, vol. 11, no. 4, pp. 346–350, 1997.

[176] A. Takahashi, K. Ohnishi, M. Fukui et al., "Mutation frequency of *Dictyostelium discoideum* spores exposed to the space environment," *Biological Sciences in Space*, vol. 11, no. 2, pp. 81–86, 1997.

[177] O. Greco, M. Durante, G. Gialanella et al., "Biological dosimetry in Russian and Italian astronauts," *Advances in Space Research*, vol. 31, no. 6, pp. 1495–1503, 2003.

[178] Y. Kobayashi, M. Kikuchi, S. Nagaoka, and H. Watanabe, "Recovery of *Deinococcus radiodurans* from radiation damage was enhanced under microgravity," *Biological Sciences in Space*, vol. 10, no. 2, pp. 97–101, 1996.

[179] M. Moreno-Villanueva, M. Wong, T. Lu, Y. Zhang, and H. Wu, "Interplay of space radiation and microgravity in DNA damage and DNA damage response," *npj Microgravity*, vol. 3, no. 1, p. 14, 2017.

[180] F. Yatagai, M. Honma, N. Dohmae, and N. Ishioka, "Biological effects of space environmental factors: a possible

interaction between space radiation and microgravity," *Life Sciences in Space Research*, vol. 20, pp. 113–123, 2019.

[181] N. Ishioka, H. Suzuki, M. Asashima et al., "Development and verification of hardware for life science experiments in the Japanese Experiment Module "Kibo" on the International Space Station," *Journal of Gravitational Physiology*, vol. 11, no. 1, pp. 81–91, 2004.

[182] D. Shiba, H. Mizuno, A. Yumoto et al., "Development of new experimental platform 'MARS'–Multiple Artificial-gravity Research System–to elucidate the impacts of micro/partial gravity on mice," *Scientific Reports*, vol. 7, no. 1, article 10837, 2017.

[183] S. Canova, F. Fiorasi, M. Mognato et al., "Modeled microgravity affects cell response to ionizing radiation and increases genomic damage," *Radiation Research*, vol. 163, no. 2, pp. 191–199, 2005.

[184] M. Mognato and L. Celotti, "Modeled microgravity affects cell survival and *HPRT* mutant frequency, but not the expression of DNA repair genes in human lymphocytes irradiated with ionising radiation," *Mutation Research*, vol. 578, no. 1–2, pp. 417–429, 2005.

[185] M. Mognato, C. Girardi, S. Fabris, and L. Celotti, "DNA repair in modeled microgravity: double strand break rejoining activity in human lymphocytes irradiated with γ-rays," *Mutation Research*, vol. 663, no. 1–2, pp. 32–39, 2009.

[186] B. Dang, Y. Yang, E. Zhang et al., "Simulated microgravity increases heavy ion radiation-induced apoptosis in human B lymphoblasts," *Life Sciences*, vol. 97, no. 2, pp. 123–128, 2014.

[187] D. Risin and N. R. Pellis, "Modeled microgravity inhibits apoptosis in peripheral blood lymphocytes," *In Vitro Cellular & Developmental Biology-Animal*, vol. 37, no. 2, pp. 66–72, 2001.

[188] C. Girardi, C. de Pittà, S. Casara et al., "Analysis of miRNA and mRNA expression profiles highlights alterations in ionizing radiation response of human lymphocytes under modeled microgravity," *PLoS ONE*, vol. 7, no. 2, article e31293, 2012.

[189] M. Beck, M. Moreels, R. Quintens et al., "Chronic exposure to simulated space conditions predominantly affects cytoskeleton remodeling and oxidative stress response in mouse fetal fibroblasts," *International Journal of Molecular Medicine*, vol. 34, no. 2, pp. 606–615, 2014.

[190] G. Pani, M. Verslegers, R. Quintens et al., "Combined exposure to simulated microgravity and acute or chronic radiation reduces neuronal network integrity and survival," *PLoS ONE*, vol. 11, no. 5, article e0155260, 2016.

[191] H. Ikeda, H. Souda, A. Puspitasari et al., "A new system for three-dimensional clinostat synchronized X-irradiation with a high-speed shutter for space radiation research," *Biological Sciences in Space*, vol. 30, pp. 8–16, 2016.

[192] H. Ikeda, H. Souda, A. Puspitasari et al., "Development and performance evaluation of a three-dimensional clinostat synchronized heavy-ion irradiation system," *Life Sciences in Space Research*, vol. 12, pp. 51–60, 2017.

[193] M. Hada, H. Ikeda, J. Rhone et al., "Increased chromosome aberrations in cells exposed simultaneously to simulated microgravity and radiation," *International Journal of Molecular Sciences*, vol. 20, no. 1, article 43, 2019.

[194] H. Ikeda, M. Muratani, J. Hidema et al., "Expression profile of cell cycle-related genes in human fibroblasts exposed simulta-

neously to radiation and simulated microgravity," *International Journal of Molecular Sciences*, vol. 20, no. 19, article 4791, 2019.

[195] A. Manzano, R. Herranz, L. A. den Toom et al., "Novel, Moon and Mars, partial gravity simulation paradigms and their effects on the balance between cell growth and cell proliferation during early plant development," *npj Microgravity*, vol. 4, no. 1, p. 9, 2018.

[196] A. J. Jeong, Y. J. Kim, M. H. Lim et al., "Microgravity induces autophagy *via* mitochondrial dysfunction in human Hodgkin's lymphoma cells," *Scientific Reports*, vol. 8, no. 1, article 14646, 2018.

[197] C. Morabito, S. Guarnieri, A. Catizone, C. Schiraldi, G. Ricci, and M. A. Mariggio, "Transient increases in intracellular calcium and reactive oxygen species levels in TCam-2 cells exposed to microgravity," *Scientific Reports*, vol. 7, no. 1, article 15648, 2017.

[198] Y. Tian, X. Ma, C. Yang, P. Su, C. Yin, and A. R. Qian, "The impact of oxidative stress on the bone system in response to the space special environment," *International Journal of Molecular Sciences*, vol. 18, no. 10, article 2132, 2017.

[199] M. Sugimoto, Y. Oono, O. Gusev et al., "Genome-wide expression analysis of reactive oxygen species gene network in Mizuna plants grown in long-term spaceflight," *BMC Plant Biology*, vol. 14, no. 1, p. 4, 2014.

[200] A. Michaletti, M. Gioia, U. Tarantino, and L. Zolla, "Effects of microgravity on osteoblast mitochondria: a proteomic and metabolomics profile," *Scientific Reports*, vol. 7, no. 1, article 15376, 2017.

[201] J. M. Koolhaas, A. Bartolomucci, B. Buwalda et al., "Stress revisited: a critical evaluation of the stress concept," *Neuroscience and Biobehavioral Reviews*, vol. 35, no. 5, pp. 1291–1301, 2011.

[202] B. Wang, T. Katsube, N. Begum, and M. Nenoi, "Revisiting the health effects of psychological stress - its influence on susceptibility to ionizing radiation: a mini-review," *Journal of Radiation Research*, vol. 57, no. 4, pp. 325–335, 2016.

[203] Z. Feng, L. Liu, C. Zhang et al., "Chronic restraint stress attenuates p53 function and promotes tumorigenesis," *Proceedings of the National Academy of Sciences of the United States of America*, vol. 109, no. 18, pp. 7013–7018, 2012.

[204] B. Wang, K. Tanaka, T. Katsube et al., "Chronic restraint-induced stress has little modifying effect on radiation hematopoietic toxicity in mice," *Journal of Radiation Research*, vol. 56, no. 5, pp. 760–767, 2015.

[205] T. Katsube, B. Wang, K. Tanaka et al., "Effects of chronic restraint-induced stress on radiation-induced chromosomal aberrations in mouse splenocytes," *Mutation Research*, vol. 813, pp. 18–26, 2017.

[206] T. Nakajima, "Psychosocial stress promotes radiation-induced acute damage in mice," in *The 16th International Congress of Radiation Research*, Manchester, 2019.

[207] B. Wang, K. Tanaka, T. Katsube et al., "Effects from chronic restraint-induced stress and total body Fe irradiation on the hematopoietic system in Trp53-heterozygous mice," in *The 64th Annual Radiation Research Society Meeting*, Chicago, 2018.

[208] T. Katsube, B. Wang, K. Tanaka et al., "Effects from chronic restraint-induced stress and total body Fe-particle irradiation on the induction of chromosomal aberrations in splenocytes

of Trp53-heterozygous mice," in *The 64th Annual Radiation Research Society Meeting*, Chicago, 2018.

[209] T. Katsube, B. Wang, K. Tanaka et al., "Effects of chronic restraint-induced stress and Fe-particle irradiation on induction of chromosomal aberrations in Trp53-heterozygous mice," in *The 16th International Congress of Radiation Research*, Manchester, 2019.

[210] H. Li, B. Wang, H. Zhang, T. Katsube, Y. Xie, and L. Gan, "Apoptosis induction by iron radiation *via* inhibition of autophagy in *Trp53*$^{+/-}$ Mouse testes: is chronic restraint-induced stress a modifying factor?," *International Journal of Biological Sciences*, vol. 14, no. 9, pp. 1109–1121, 2018.

[211] F. A. Cucinotta, M. Alp, B. Rowedder, and M. H. Y. Kim, "Safe days in space with acceptable uncertainty from space radiation exposure," *Life Sciences in Space Research*, vol. 5, pp. 31–38, 2015.

[212] T. Miyamoto, S. N. Akutsu, H. Tauchi et al., "Exploration of genetic basis underlying individual differences in radiosensitivity within human populations using genome editing technology," *Journal of Radiation Research*, vol. 59, Supplement 2, pp. ii75–ii82, 2018.

[213] P. A. Locke and M. M. Weil, "Personalized cancer risk assessments for space radiation exposures," *Frontiers in Oncology*, vol. 6, p. 38, 2016.

[214] D. Scott, J. B. P. Barber, E. L. Levine, W. Burrill, and S. A. Roberts, "Radiation-induced micronucleus induction in lymphocytes identifies a high frequency of radiosensitive cases among breast cancer patients: a test for predisposition?," *British Journal of Cancer*, vol. 77, no. 4, pp. 614–620, 1998.

[215] L. V. R. Distel, S. Neubauer, U. Keller, C. N. Sprung, R. Sauer, and G. G. Grabenbauer, "Individual differences in chromosomal aberrations after *in vitro* irradiation of cells from healthy individuals, cancer and cancer susceptibility syndrome patients," *Radiotherapy and Oncology*, vol. 81, no. 3, pp. 257–263, 2006.

[216] B. Koberle, B. Koch, B. M. Fischer, and A. Hartwig, "Single nucleotide polymorphisms in DNA repair genes and putative cancer risk," *Archives of Toxicology*, vol. 90, no. 10, pp. 2369–2388, 2016.

[217] E. Royba, T. Miyamoto, S. Natsuko Akutsu et al., "Evaluation of *ATM* heterozygous mutations underlying individual differences in radiosensitivity using genome editing in human cultured cells," *Scientific Reports*, vol. 7, no. 1, article 5996, 2017.

[218] D. Thompson, D. Easton, and Breast Cancer Linkage Consortium, "Variation in *BRCA1* cancer risks by mutation position," *Cancer Epidemiology, Biomarkers & Prevention*, vol. 11, no. 4, pp. 329–336, 2002.

[219] J. D. Fackenthal and O. I. Olopade, "Breast cancer risk associated with *BRCA1* and *BRCA2* in diverse populations," *Nature Reviews Cancer*, vol. 7, no. 12, pp. 937–948, 2007.

[220] T. A. Smith, D. R. Kirkpatrick, S. Smith et al., "Radioprotective agents to prevent cellular damage due to ionizing radiation," *Journal of Translational Medicine*, vol. 15, no. 1, p. 232, 2017.

[221] V. S. Kuntić, M. B. Stanković, Z. B. Vujić, J. S. Brborić, and S. M. Uskoković-Marković, "Radioprotectors - the evergreen topic," *Chemistry & Biodiversity*, vol. 10, no. 10, pp. 1791–1803, 2013.

[222] S. J. Hosseinimehr, "Trends in the development of radioprotective agents," *Drug Discovery Today*, vol. 12, no. 19–20, pp. 794–805, 2007.

[223] K. N. Prasad, "Rationale for using multiple antioxidants in protecting humans against low doses of ionizing radiation," *The British Journal of Radiology*, vol. 78, no. 930, pp. 485–492, 2005.

[224] J. A. Brink and J. D. Boice Jr., "Science to practice: can antioxidant supplements protect against the possible harmful effects of ionizing radiation from medical imaging?," *Radiology*, vol. 264, no. 1, pp. 1-2, 2012.

[225] L. Sun, T. Igarashi, R. Tetsuka et al., "Pilot clinical study of ascorbic acid treatment in cardiac catheterization," *Journal of Radiation Research*, vol. 60, no. 5, pp. 573–578, 2019.

[226] M. Konopacka and J. Rzeszowska-Wolny, "Antioxidant Vitamins C, E and β-carotene reduce DNA damage before as well as after γ-ray irradiation of human lymphocytes *in vitro*," *Mutation Research*, vol. 491, no. 1–2, pp. 1–7, 2001.

[227] M. Konopacka, M. Widel, and J. Rzeszowska-Wolny, "Modifying effect of vitamins C, E and beta-carotene against gamma-ray-induced DNA damage in mouse cells," *Mutation Research*, vol. 417, no. 2–3, pp. 85–94, 1998.

[228] E. C. Halperin, L. Gaspar, S. George, D. Darr, and S. Pinnell, "A double-blind, randomized, prospective trial to evaluate topical vitamin C solution for the prevention of radiation dermatitis," *International Journal of Radiation Oncology, Biology, Physics*, vol. 26, no. 3, pp. 413–416, 1993.

[229] M. K. O'Connor, J. F. Malone, M. Moriarty, and S. Mulgrew, "A radioprotective effect of vitamin C observed in Chinese hamster ovary cells," *The British Journal of Radiology*, vol. 50, no. 596, pp. 587–591, 1977.

[230] S. M. el-Nahas, F. E. Mattar, and A. A. Mohamed, "Radioprotective effect of vitamins C and E," *Mutation Research*, vol. 301, no. 2, pp. 143–147, 1993.

[231] S. M. Hahn, F. J. Sullivan, A. M. DeLuca et al., "Evaluation of Tempol radioprotection in a murine tumor model," *Free Radical Biology and Medicine*, vol. 22, no. 7, pp. 1211–1216, 1997.

[232] S. M. Hahn, M. C. Krishna, A. M. DeLuca, D. Coffin, and J. B. Mitchell, "Evaluation of the hydroxylamine Tempol-H as an *in vivo* radioprotector," *Free Radical Biology and Medicine*, vol. 28, no. 6, pp. 953–958, 2000.

[233] J. M. Metz, D. Smith, R. Mick et al., "A phase I study of topical Tempol for the prevention of alopecia induced by whole brain radiotherapy," *Clinical Cancer Research*, vol. 10, no. 19, pp. 6411–6417, 2004.

[234] R. Yahyapour, D. Shabeeb, M. Cheki et al., "Radiation protection and mitigation by natural antioxidants and flavonoids: implications to radiotherapy and radiation disasters," *Current Molecular Pharmacology*, vol. 11, no. 4, pp. 285–304, 2018.

[235] N. Fischer, E. J. Seo, and T. Efferth, "Prevention from radiation damage by natural products," *Phytomedicine*, vol. 47, pp. 192–200, 2018.

[236] G. Vogin and N. Foray, "The law of Bergonié and Tribondeau: a nice formula for a first approximation," *International Journal of Radiation Biology*, vol. 89, no. 1, pp. 2–8, 2013.

[237] A. H. Haber and B. E. Rothstein, "Radiosensitivity and rate of cell division: "Law of Bergonie and Tribondeau"," *Science*, vol. 163, no. 3873, pp. 1338-1339, 1969.

[238] R. E. Meyn and W. T. Jenkins, "Variation in normal and tumor tissue sensitivity of mice to ionizing radiation-induced DNA strand breaks *in vivo*," *Cancer Research*, vol. 43, 12 Part 1, pp. 5668–56673, 1983.

[239] M. Ueno, T. Aoto, Y. Mohri, H. Yokozeki, and E. K. Nishimura, "Coupling of the radiosensitivity of melanocyte stem cells to their dormancy during the hair cycle," *Pigment Cell & Melanoma Research*, vol. 27, no. 4, pp. 540–551, 2014.

[240] F. R. Tang and K. Loganovsky, "Low dose or low dose rate ionizing radiation-induced health effect in the human," *Journal of Environmental Radioactivity*, vol. 192, pp. 32–47, 2018.

[241] J. R. Battista, "Against all odds: the survival strategies *of Deinococcus radiodurans*," *Annual Review of Microbiology*, vol. 51, no. 1, pp. 203–224, 1997.

[242] I. Narumi, "Unlocking radiation resistance mechanisms: still a long way to go," *Trends in Microbiology*, vol. 11, no. 9, pp. 422–425, 2003.

[243] K. Zahradka, D. Slade, A. Bailone et al., "Reassembly of shattered chromosomes in *Deinococcus radiodurans*," *Nature*, vol. 443, no. 7111, pp. 569–573, 2006.

[244] D. D. Horikawa, T. Kunieda, W. Abe et al., "Establishment of a rearing system of the extremotolerant tardigrade *Ramazzottius varieornatus*: a new model animal for astrobiology," *Astrobiology*, vol. 8, no. 3, pp. 549–556, 2008.

[245] D. D. Horikawa, T. Sakashita, C. Katagiri et al., "Radiation tolerance in the tardigrade *Milnesium tardigradum*," *International Journal of Radiation Biology*, vol. 82, no. 12, pp. 843–848, 2006.

[246] K. I. Jönsson, "Radiation tolerance in tardigrades: current knowledge and potential applications in medicine," *Cancers*, vol. 11, no. 9, article 1333, 2019.

[247] E. Gladyshev and M. Meselson, "Extreme resistance of bdelloid rotifers to ionizing radiation," *Proceedings of the National Academy of Sciences of the United States of America*, vol. 105, no. 13, pp. 5139–5144, 2008.

[248] M. Watanabe, T. Sakashita, A. Fujita et al., "Biological effects of anhydrobiosis in an African chironomid, *Polypedilum vanderplanki* on radiation tolerance," *International Journal of Radiation Biology*, vol. 82, no. 8, pp. 587–592, 2006.

[249] K. I. Jönsson, E. Rabbow, R. O. Schill, M. Harms-Ringdahl, and P. Rettberg, "Tardigrades survive exposure to space in low Earth orbit," *Current Biology*, vol. 18, no. 17, pp. R729–R731, 2008.

[250] N. Novikova, O. Gusev, N. Polikarpov et al., "Survival of dormant organisms after long-term exposure to the space environment," *Acta Astronautica*, vol. 68, no. 9-10, pp. 1574–1580, 2011.

[251] T. Hashimoto, D. D. Horikawa, Y. Saito et al., "Extremotolerant tardigrade genome and improved radiotolerance of human cultured cells by tardigrade-unique protein," *Nature Communications*, vol. 7, no. 1, article 12808, 2016.

[252] C. Chavez, G. Cruz-Becerra, J. Fei, G. A. Kassavetis, and J. T. Kadonaga, "The tardigrade damage suppressor protein binds to nucleosomes and protects DNA from hydroxyl radicals," *eLife*, vol. 8, article e47682, 2019.

[253] T. Hashimoto and T. Kunieda, "DNA protection protein, a novel mechanism of radiation tolerance: lessons from tardigrades," *Life*, vol. 7, no. 2, p. 26, 2017.

[254] Y. Yoshida, G. Koutsovoulos, D. R. Laetsch et al., "Comparative genomics of the tardigrades *Hypsibius dujardini* and *Ramazzottius varieornatus*," *PLoS Biology*, vol. 15, no. 7, article e2002266, 2017.

Retraction

Retracted: Dielectrophoresis-Based Method for Measuring the Multiangle Mechanical Properties of Biological Cells

BioMed Research International

This article has been retracted by Hindawi following an investigation undertaken by the publisher [1]. This investigation has uncovered evidence of one or more of the following indicators of systematic manipulation of the publication process:

(1) Discrepancies in scope

(2) Discrepancies in the description of the research reported

(3) Discrepancies between the availability of data and the research described

(4) Inappropriate citations

(5) Incoherent, meaningless and/or irrelevant content included in the article

(6) Manipulated or compromised peer review

The presence of these indicators undermines our confidence in the integrity of the article's content and we cannot, therefore, vouch for its reliability. Please note that this notice is intended solely to alert readers that the content of this article is unreliable. We have not investigated whether authors were aware of or involved in the systematic manipulation of the publication process.

Wiley and Hindawi regrets that the usual quality checks did not identify these issues before publication and have since put additional measures in place to safeguard research integrity.

We wish to credit our own Research Integrity and Research Publishing teams and anonymous and named external researchers and research integrity experts for contributing to this investigation.

The corresponding author, as the representative of all authors, has been given the opportunity to register their agreement or disagreement to this retraction. We have kept a record of any response received.

References

[1] B. Zhu, W. Li, M. Zhu, P.-L. Hsu, L. Sun, and H. Yang, "Dielectrophoresis-Based Method for Measuring the Multiangle Mechanical Properties of Biological Cells," *BioMed Research International*, vol. 2020, Article ID 5358181, 9 pages, 2020.

Research Article

Dielectrophoresis-Based Method for Measuring the Multiangle Mechanical Properties of Biological Cells

Botao Zhu,[1] Wanting Li,[1] Mingjie Zhu,[1] Po-Lin Hsu,[2] Lining Sun,[1] and Hao Yang [1]

[1]*Robotics and Microsystems Center, School of Mechanical and Electric Engineering, Soochow University, Suzhou, Jiangsu, China*
[2]*Artificial Organ Technology Laboratory, School of Mechanical and Electric Engineering, Soochow University, Suzhou, Jiangsu, China*

Correspondence should be addressed to Hao Yang; yhao@suda.edu.cn

The mechanical properties of cells are closely related to their physiological functions and states. Analyzing and measuring these properties are beneficial to understanding cell mechanisms. However, most measurement methods only involve the unidirectional analysis of cellular mechanical properties and thus result in the incomplete measurement of these properties. In this study, a microfluidic platform was established, and an innovative microfluidic chip was designed to measure the multiangle cellular mechanical properties by using dielectrophoresis (DEP) force. Three unsymmetrical indium tin oxide (ITO) microelectrodes were designed and combined with the microfluidic chip, which were utilized to generate DEP force and stretch cell from different angles. A series of experiments was performed to measure and analyze the multiangle mechanical properties of red blood cells of mice. This work provided a new tool for the comprehensive and accurate measurement of multiangle cellular mechanical properties. The results may contribute to the exploration of the internal physiological structures of cells and the building of accurate cell models.

1. Introduction

The mechanical properties of cells affect cellular growth, differentiation, division, and apoptosis [1, 2]. Changes in these properties are the external manifestations of a decline in cell physiological functions; this decline eventually leads to various diseases [3–5]. Numerous advanced technologies and equipment, such as atomic force microscope, microinjection, micropipette, and optical tweezers, are used to measure cellular mechanical properties [1, 6–9]. Among these methods, devices and equipment are in direct contact with cells, which may cause damage. Dielectrophoresis (DEP) has attracted increasing attention because of its advantages, such as label-free, low cost, high throughput, and minimal damage [10, 11].

In many experiments that use DEP to measure the cellular mechanical properties, precious metal electrodes, such as gold and platinum, require magnetron sputtering, which is complex and expensive. Indium tin oxide (ITO) electrodes have low cost and are simple to manufacture and thus widely used in measuring the mechanical properties of cells, such as

red blood cells and NB_4 [12–14]. However, the majority of previous studies only performed a unidirectional measurement of the cellular mechanical properties and therefore resulted in incomprehensive measured data. In addition, the cytoplasm and nucleus are not completely symmetrical because of the nonuniformity of the physiological structures of the cells [15–17], and cellular mechanical properties in different directions may be inconsistent. Measuring the multiangle cellular mechanical properties can provide comprehensive and accurate data, and this process is convenient for studying the physiological structures of cells and building cell models. Therefore, a method that can quickly and accurately measure multiangle cellular mechanical properties must be developed.

In this study, an innovative platform based on the principle of DEP that can measure the multiangle mechanical properties of cells was built. This platform mainly included a microscope, a voltage signal generator, two microfluidic pumps, and a microfluidic chip. The microfluidic chip contained three ITO electrodes to form nonuniform electric fields in different directions for the measurement of

multiangle cellular mechanical properties. A series of experiments were performed to stretch the red blood cells of mice by using ITO electrodes. The analytical results showed that the mechanical properties of the red blood cell were almost the same in different directions. The proposed method also provides a new technique for studying the cellular mechanisms at the single-cell level, which helps to explore the internal physiological structure of cells. The designed microfluidic chip increases the DEP force (resultant force) at low voltages, thereby reducing damage in cells and increasing the efficiency of cell manipulation processes, such as cell rotation, separation, and transportation.

2. Materials and Methods

2.1. Sample Preparation. Blood samples were collected from the veins of healthy mice, and ethylenediaminetetraacetic acid anticoagulant was added to the samples to prevent blood clotting. Then, the samples were stored in a sterile environment at 4°C before the experiment. Appropriate amounts of red blood cells were added to the DEP buffer, which contained 8.5% w/w sucrose, 0.3% w/w glucose, and 20 mg/L $CaCl_2$. The electrical conductivity and relative permittivity were 10 mS/m and 78, respectively [18, 19]. Prior to the experiment, the microchannels were rinsed with deionized water and absolute ethanol and treated with 1% BSA to prevent cell adhesion. Experiments were completed within 2 h for the maintenance of cell viability.

2.2. Design and Manufacture of Microfluidic Chip. The microfluidic chip can be divided into two functional regions, namely, the cell focusing and stretching regions (Figure 1). Three inlets were designed in the cell focusing region. The middle microchannel was the cell injection microchannel, while the other two microchannels on both sides were used to inject the DEP buffer. The cell microchannel has a height of 50 μm, a width of 600 μm, and a length of 3 cm. The buffer microchannel has a height of 50 μm, a width of 200 μm, and a length of 600 μm. The appropriate flow rate was adjusted. The cells were made to continuously flow in the middle of the microchannel because of the laminar flow, which facilitated a more efficient capture of the cells at the edge of the ITO electrodes. The cell stretching region mainly included three ITO electrodes, in which sine wave signals were applied in different ways between the three ITO electrodes to generate a multidirectional DEP force to measure and analyze the multiangle cellular mechanical properties.

The manufacture of the microfluidic chips was mainly based on soft photolithography. First, a mask version of the ITO electrode and polydimethylsiloxane (PDMS) microchannel was designed with CAD 2014. The PDMS microchannel was manufactured as follows. First, the negative photoresist (SU-8 2050) was uniformly poured onto a silicon wafer, spin-coated at 800 rpm for 10 s through a homogenizer, and spin-coated for 30 s at 2500 rpm to produce a 50 μm high PDMS microchannel. After spin-coating, the silicon wafer was baked on a hot plate at 65°C for 2 min and 95°C for 7 min. After baking, the silicon wafer was exposed under 365 nm UV light of the lithography machine
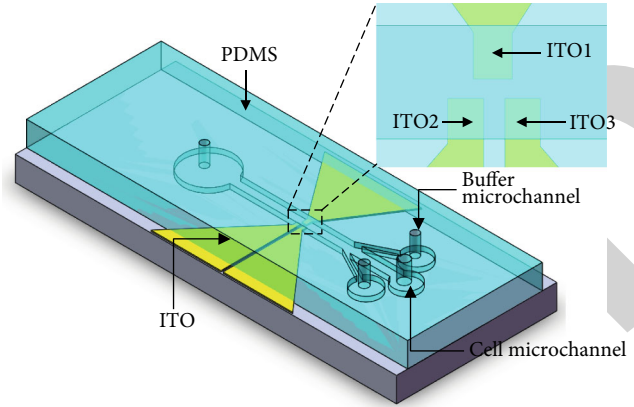

FIGURE 1: Scheme of microfluidic chip. Microfluidic chip consisting of three ITO electrodes and three microchannels.

for 10 s. The energy density was 12.4 mJ/cm². Then, the silicon wafer was baked with the same parameters on a hot plate. Finally, the wafer was washed twice in the developing solution and dried with nitrogen to obtain a PDMS microchannel mold. Then, 30 g of PDMS and the curing agent were mixed in a weight ratio of 10 : 1. PDMS was poured into the mold, which was then placed in a vacuum oven for 5 min. After baking at 85°C for 30 min, the PDMS microchannels were separated from the mold and cut to the appropriate size. The ITO electrode was manufactured as follows. First, a positive photoresist (RZJ-304) was applied to the ITO conductive glass at 3500 rpm to produce a 2 μm thick photoresist layer. The electrode was baked at 100°C for 3 min and then exposed to 365 nm UV for 2 s at an energy density of 12.4 mJ/cm². After exposure, the electrode was placed in a developer (RZX-3038) for 2 min and blow dried with nitrogen. The exposed ITO conductive glass was then etched away with hydrochloric acid and blown dry with nitrogen to make a patterned electrode. Finally, the PDMS microchannel and ITO electrode were placed in a plasma cleaner for 2 min by oxygen plasma treatment and then baked at 95°C for 15 min to ensure tight bonding. The inlet and outlet of the microfluidic chip were connected to a polytetrafluoroethylene tube.

2.3. Manipulation System. The experimental system for measuring and analyzing the multiangle cellular mechanical properties mainly included the following parts (Figure 2). First, a PDMS-based microfluidic chip was designed and manufactured for the cell stretching experiments. Second, a microfluidic pump (longer pump) was used to inject cells into the microchannels, and then, a signal generator (BK 4014B) was used to generate a sinusoidal voltage waveform. Third, the cell deformation was observed and recorded using a microscope (Nikon) and a CCD camera.

2.4. Theoretical Analysis. The DEP force F_{DEP} can be estimated by the following formula, in which the red blood cells stretched by DEP were assumed to have an ellipsoid structure [20, 21]:

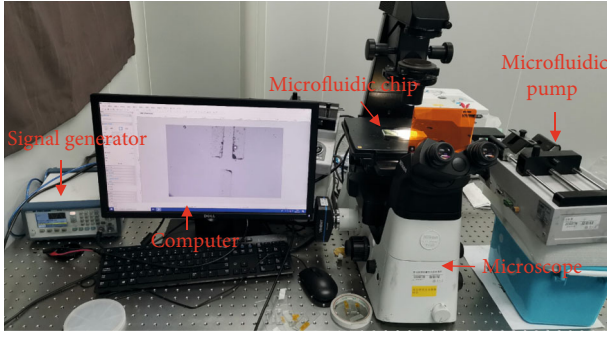$$F_{DEP} = \pi abc\varepsilon_m \, \text{Re} \, [f_{CM}]\nabla E_{rms}^2, \tag{1}$$

Figure 2: Manipulation system consisting of a signal generator, a microscope, and two microfluidic pumps.

Figure 3: Values of Re (f_{CM}) with electrical frequency between 1 kHz and 100 MHz.

where a and b denote the major and minor radii of the red blood cell, respectively; c denotes the thickness of the red blood cell. Radii a and b were measured by a CCD camera, and c was assumed as constant ($2\,\mu$m) [21]. f_{CM} denotes the Clausius–Mossotti factor, ε_m denotes the permittivity of the suspending medium, Re $[f_{CM}]$ denotes the actual compo-

nent of f_{CM}, and ∇E_{rms}^2 denotes the gradient of the square of the applied electric field E. The effective permittivity of the red blood cell was estimated with a single-shell structure model as follows [22, 23]:

$$f_{CM} = \frac{1}{3} \frac{(\varepsilon_{mem}^* - \varepsilon_m^*)\left[\left(\varepsilon_{mem}^* + A_1\left(\varepsilon_{cyto}^* - \varepsilon_{mem}^*\right)\right)\right] + \rho\left(\varepsilon_{cyto}^* - \varepsilon_{mem}^*\right)\left[\left(\varepsilon_{mem}^* - A_1(\varepsilon_{mem}^* - \varepsilon_m^*)\right)\right]}{(\varepsilon_m^* + A_1(\varepsilon_{mem}^* - \varepsilon_m^*))\left[\left(\varepsilon_{mem}^* + A_1\left(\varepsilon_{cyto}^* - \varepsilon_{mem}^*\right)\right)\right] + \rho A_2(1 - A_1)\left(\varepsilon_{cyto}^* - \varepsilon_{mem}^*\right)(\varepsilon_{mem}^* - \varepsilon_m^*)}, \tag{2}$$

where ω denotes the angular frequency; ε denotes the dielectric permittivity; $j = \sqrt{-1}$; the subscripts cyto, mem, and m represent the cytoplasm, membrane, and medium, respectively; and $\varepsilon^* = \varepsilon - j\sigma/\omega$. The electrical conductivity is $\rho = (a - t)(b - t)^2/ab^2$, where t denotes the thickness of the cell membrane, which was set to 4.5 nm in this study. $\varepsilon_{mem} = 4.44$, $\varepsilon_{cyto} = 59$, $\sigma_{mem} = 10^{-6}$ S/m, and $\sigma_{cyto} = 0.31$ S/m [24]. A_i is the depolarization factor which can be given as follows:

$$A_i = \frac{1 - e_i^2}{2e_i^3}\left[\log\frac{1 - e_i}{1 + e_i} - 2e_i\right], \quad i = 1, 2, \tag{3}$$

where $e_1 = \sqrt{1 - (b/a)^2}$ and $e_2 = \sqrt{1 - ((b - 2t)/(a - 2t))^2}$. The values of Re (f_{CM}) with the change in the electric field frequency for the red blood cells were calculated by MATLAB R2014a (Figure 3). Therefore, stretching the red blood cell with a frequency of megahertz is more efficient.

2.5. Cell Stretching Protocol. The multiangle stretching of cells could be divided into the following parts. First, the DEP buffer containing red blood cells was passed through the middle microchannel at a flow rate of $5\,\mu$l/min, whereas the DEP buffer without red blood cells was passed through the microchannels at both sides at a flow rate of $10\,\mu$l/min. This flow rate could concentrate the cells in the middle part of the microchannel and improve the capture efficiency of the cells.

Second, a sine wave with a frequency of 1.5 MHz and a peak-to-peak value of 2 Vpp was applied between ITO electrodes 1 and 2. The flow direction of the cells was from right to left (Figure 4(a)). First, ITO electrodes 1 and 2 were connected to increase the probability of capturing red blood cells at the middle edge of ITO electrode 1. The cells were prevented from being caught at the edges of the ITO electrode 2 or 3. When one red blood cell was captured at the edge of the ITO electrode 1, the microflow pump was turned off. The injection of red blood cells and DEP buffer was stopped. Then, the voltage between ITO electrodes 1 and 2 was increased from 2 Vpp to 10 Vpp, and the deformation of the cell between the ITO electrodes 1 and 2 was recorded by a CCD (Figure 4(b)). Second, the voltage applied between ITO electrodes 1 and 2 was turned off. Then, a sine wave signal with a frequency of 1.5 MHz and a peak-to-peak value of 2 Vpp was applied between ITO electrodes 1 and 3. The voltage was increased from 2 Vpp to 10 Vpp. The deformation of the cells in the other direction was recorded by the CCD (Figure 4(c)). Finally, a sine wave signal with the same parameters was applied simultaneously between ITO electrodes 1 and 2 and between ITO electrodes 1 and 3 (Figure 4(d)). Then, the voltage was increased from 2 Vpp to 10 Vpp to record the deformation of the cells in the third direction.

Figure 5(a) shows the connection between the three ITO electrodes. ITO electrode 1 was connected to ITO electrodes 2 and 3. Figures 5(b)–5(d) illustrate the simulated electric field gradients of the three ITO electrodes under different
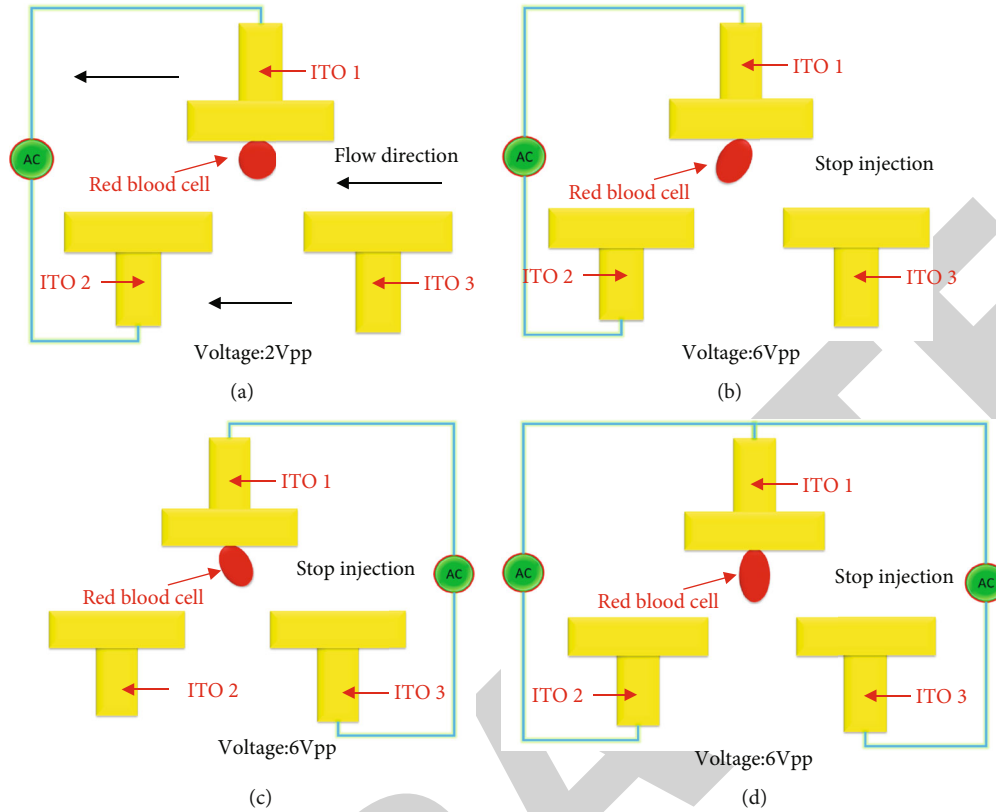
FIGURE 4: Scheme of the cell-stretching process: (a) the microfluidic syringe pump was on, and a sine wave with 2 Vpp and a frequency of 1.5 MHz was applied to capture the red blood cell on the middle of ITO electrode 1; (b–d) injection of DEP buffer was stopped, and the voltage was increased to stretch the cell in different directions.
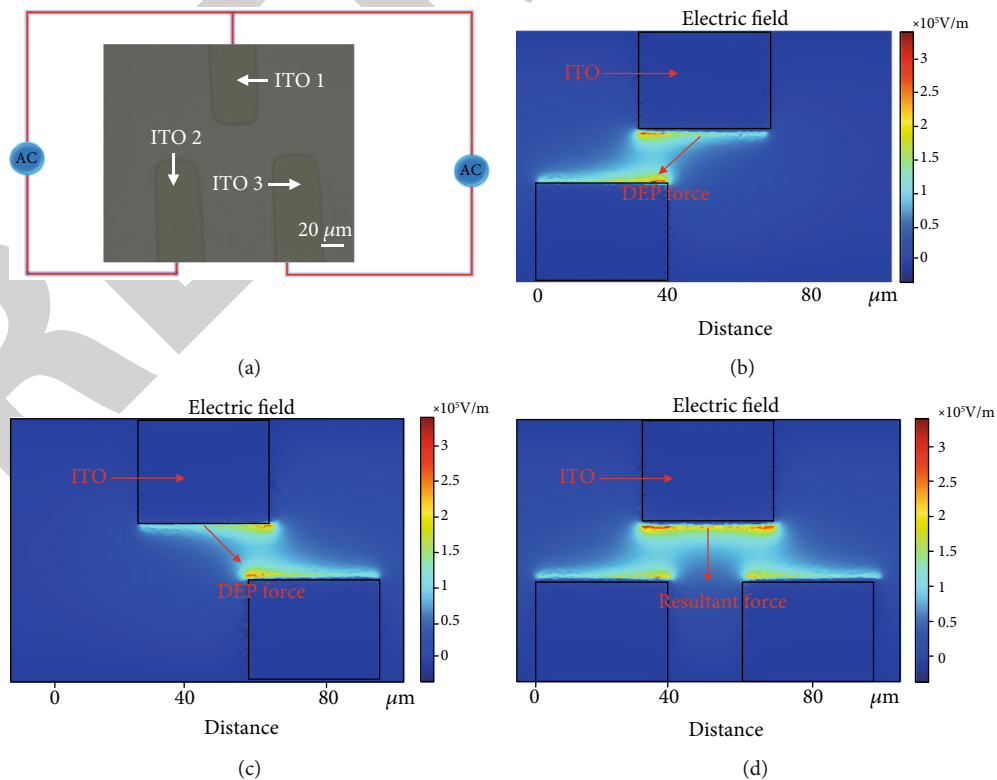

FIGURE 5: Simulation of the electric field gradient between the ITO electrodes and the direction of the DEP force.
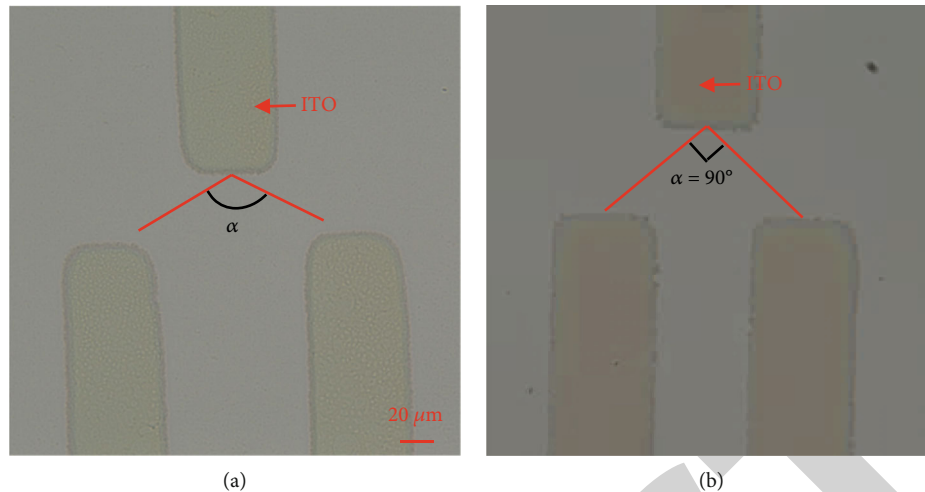
(a)

(b)

FIGURE 6: Schematic diagram of the distance between ITO electrodes (scale bar was 20 μm).

connection states. When a sine wave with a frequency of 1.5 MHz and a peak-to-peak value of 6 Vpp was applied between ITO electrodes 1 and 2, the direction of the DEP force applied to the cell was deviated to ITO electrode 2 at this time. Similarly, when the same voltage was applied between ITO electrodes 1 and 3, the direction of the DEP force applied to the cells was deviated to ITO electrode 3. When a sine wave with a frequency of 1.5 MHz and a peak-to-peak value of 6 Vpp was simultaneously applied between ITO electrodes 1 and 2 and between ITO electrodes 1 and 3, the cell received a resultant force on the directions of ITO electrodes 2 and 3.

3. Results and Discussion

3.1. Analysis of ITO Electrode Layout. The width of the ITO electrodes and the distance between them affect the efficiency of cell capture and stretching. Therefore, the arrangement of the ITO electrodes should be specially designed according to the type and size of the cells (Figure 6). In this experiment, the diameter of the red blood cells was approximately 6 μm. Therefore, the width of the ITO electrode was set to 40 μm, which could increase the efficiency of capturing and stretching at the single-cell level. We defined an angle α to quantitatively describe the distance between the three ITO electrodes. When $\alpha > 90°$, the distance between ITO electrodes 1 and 2 was too large. When a sine wave with a frequency of 1.5 MHz and a peak-to-peak value of 2 Vpp was applied between ITO electrodes 1 and 2, the cells in the middle of ITO electrode 1 were difficult to capture. By contrast, the cells were more easily captured on the left side of ITO electrode 1, affecting the efficiency of the multiangle stretch measurement of the cells. When $\alpha < 90°$, the cells were easy to capture in the middle of the ITO electrode 1. However, the fabrication of the ITO electrode became more difficult, because the distance between ITO electrodes 2 and 3 was very close. The direction of the DEP force changed slightly, and the effect of the multiangle stretching was not obvious. In summary, we set α to 90°, in which the fabrication of the ITO electrodes was relatively simple. When a sine wave with a fre-
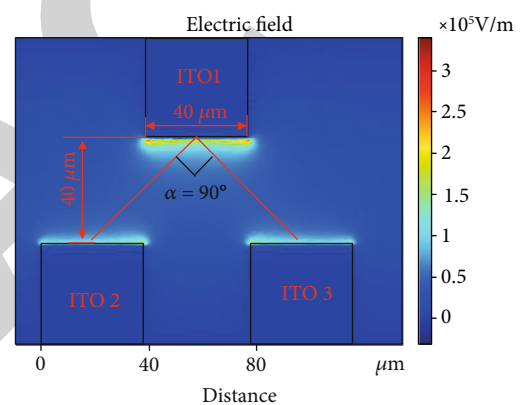

FIGURE 7: Diagram of the electric field between ITO electrodes when $\alpha = 90°$.

quency of 1.5 MHz and a peak-to-peak value of 2 Vpp was applied between ITO electrodes 1 and 2, the cells were easily captured in the middle of the ITO electrode 1. The effect of multiangle stretching on the cells was more obvious.

The ITO electrode parameters in this experiment are shown in Figure 7. The width of the ITO electrode is 40 μm, the distance between the ITO electrode 2 and the ITO electrode 3 is 40 μm, and the distance between the upper and lower ITO electrodes is also 40 μm.

When $\alpha = 90°$, the electric field at the center and the corners of the ITO electrode 1 is approximately the same, which facilitates capturing cells at the center of the ITO electrode 1. If the cells are not captured in the middle of the ITO electrode 1, the DEP force applied on the cell would be different, which makes it difficult to evaluate the mechanical properties of cells at different angles. When the cell type and size change, it is flexible to adjust the voltage and frequency by using this electrode arrangement. Meanwhile, this electrode form is more convenient for measuring three-angle mechanical properties of cells.

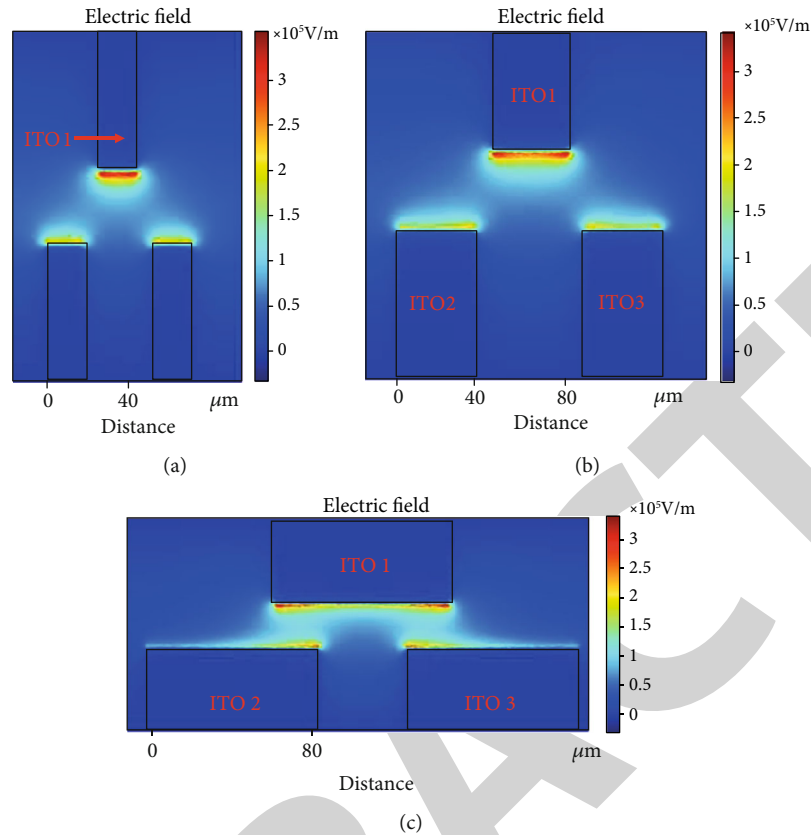As is shown in Figure 8, the distance between the upper and lower ITO electrodes is 40 μm. When the width of the

Figure 8: Diagram of the electric field between ITO electrodes. The width of the ITO electrode was set to (a) 20 μm, (b) 40 μm, and (c) 80 μm.
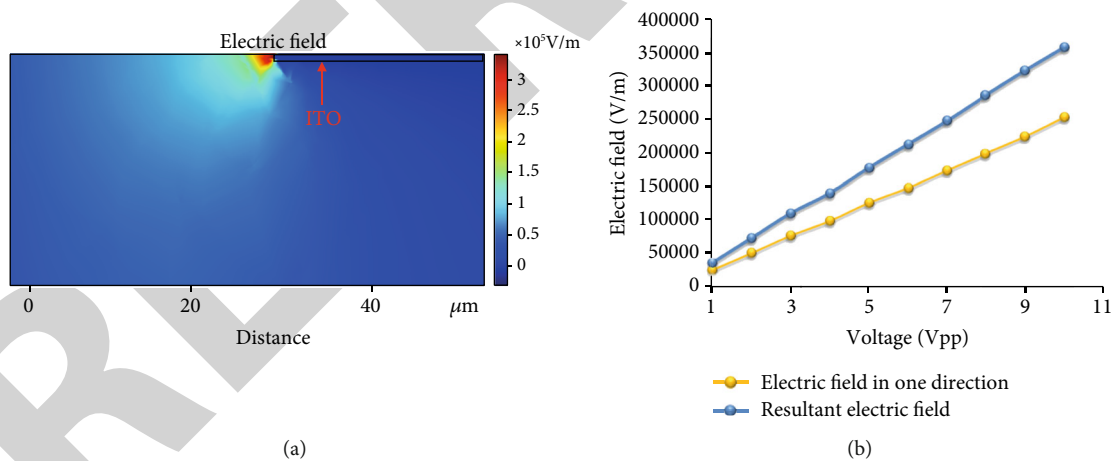

Figure 9: (a) Simulation diagram of the electric field in the middle part of ITO electrode 1; (b) diagram of the resultant electric field and the electric field in one direction.

ITO electrode is 20 μm and 40 μm, the electric field at the center and the corners of the ITO electrode 1 is approximately the same when $\alpha = 90°$, which facilitates capturing cells at the center of the ITO electrode 1. As the width of the ITO electrode 1 is increased to 80 μm, it can be found that the electric field at the corners of the ITO electrode 1 is greater than that of the center. At this time, the distance between the upper and lower electrodes needs to be increased to make $\alpha = 90°$. However, according to the size of the red

blood cells (6-8 μm) in this experiment, if the ITO electrode is too wide, many cells may be captured at the edge of the ITO electrode at the same time, and higher voltage is needed to stretch the cells. Therefore, we set α to 90°, the width of the ITO electrode to 40 μm, the distance between the ITO electrode 2 and the ITO electrode 3 to 40 μm, and the distance between the upper and lower ITO electrodes to 40 μm.

Figure 9(a) shows the simulation diagram of the electric field gradient in the middle of the ITO electrode 1 at $\alpha =$
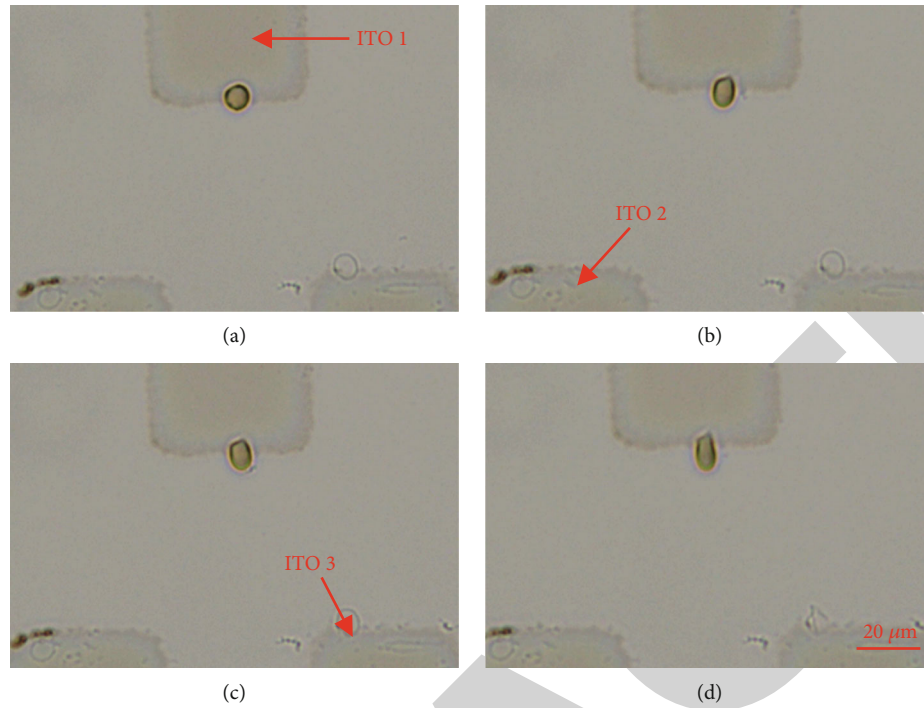
(a)

(b)

(c)

(d)

FIGURE 10: Experimental images of cell stretching. (a) A red blood cell was captured in the middle of ITO electrode 1. (b) A sine wave with 9 Vpp and a frequency of 1.5 MHz was applied between ITO electrodes 1 and 2. (c) A sine wave with the same parameters was applied between ITO electrodes 1 and 3. (d) Two same sine waves were applied between ITO electrodes 1 and 2 and between ITO electrodes 1 and 3.
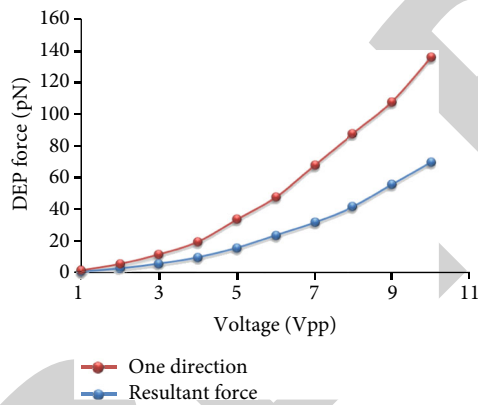

FIGURE 11: Relationship between the DEP force and voltage. The blue line represents the DEP force in one direction, and the red line represents the resultant force.

TABLE 1: DEP force and cell deformation.

Voltage (Vpp)	DEP force in one direction (pN)	$D(u1)$	$D(u2)$	Resultant DEP force (pN)	$D(u3)$
1	1	1.0	1.0	2	1.0
2	3	1.02	1.02	6	1.03
3	6	1.04	1.03	12	1.07
4	10	1.05	1.06	20	1.11
5	16	1.10	1.10	36	1.15
6	24	1.13	1.13	48	1.17
7	32	1.15	1.14	68	1.20
8	42	1.16	1.15	88	1.25
9	56	1.19	1.18	108	1.38
10	70	1.21	1.21	136	1.38

90°. The yellow polyline in Figure 9(b) denoted the electric field gradient in the middle of ITO electrode 1 when a sine wave with the same parameters was applied between ITO electrodes 1 and 2 or 3. The magnitude of the electric field gradient at the center of ITO electrode 1 was almost the same because ITO electrodes 2 and 3 were symmetrically arranged at both sides of ITO electrode 1. As the peak-to-peak voltage increased from 1 Vpp to 10 Vpp, the electric field increased from 2.5×10^4 V/m to 2.5×10^5 V/m. The blue polyline in Figure 9(b) denotes the resultant electric field t that two sine waves with a frequency of 1.5 MHz were applied between ITO electrodes 1 and 2 and between ITO electrodes 1 and 3. As the peak-to-peak voltage increased from 1 Vpp to

10 Vpp, the resultant electric field increased from 4×10^4 V/m to 3.6×10^5 V/m.

3.2. Cell Stretching Experiments. Figure 10 shows the experimental process of the multiangle stretching of cells. First, a red blood cell was captured in the middle of ITO electrode 1. A sine wave with a frequency of 1.5 MHz was applied between ITO electrodes 1 and 2. Then, the peak-to-peak voltage was gradually increased from 1 Vpp to 10 Vpp. Figures 10(b)–10(d) show the deformation of the red blood cell when the voltage was set to 9 Vpp. As the voltage increased, the DEP force on the red blood cells located in the middle of the ITO electrode 1 also gradually increased.
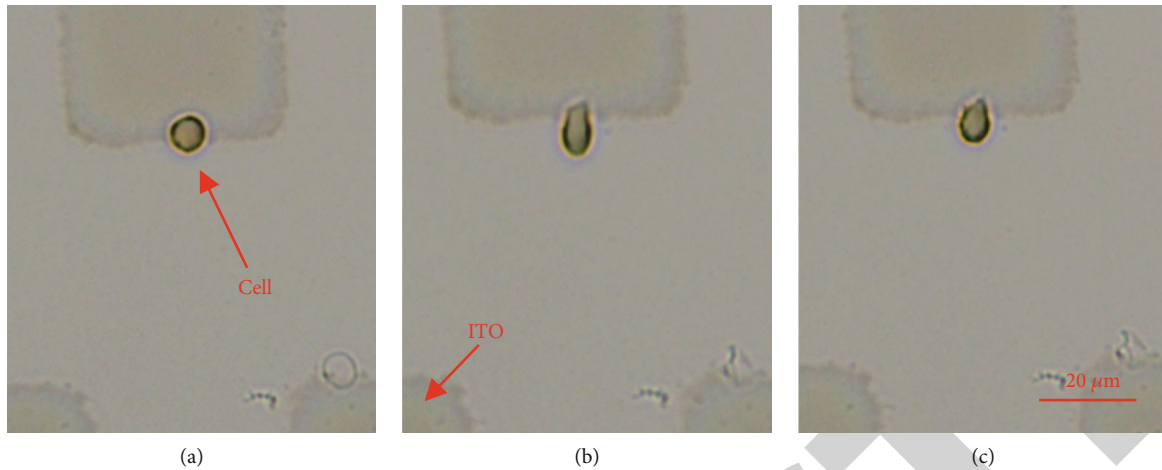
Figure 12: After applying a 10 Vpp sine wave to the ITO electrodes to stretch the cell, the cell did not return to its original shape. The scale bar was 20 μm.

The deformation of the cell along the direction of ITO electrode 2 was recorded by the CCD. Second, a sine wave with the same frequency was applied between ITO electrodes 1 and 3. The voltage between these electrodes was also increased from 1 Vpp to 10 Vpp; the deformation of the cell along the direction of ITO electrode 3 was recorded. Finally, two sine waves with a frequency of 1.5 MHz were applied between ITO electrodes 1 and 2 and between ITO electrodes 1 and 3. The deformation of the cell along the direction of the resultant force was recorded. Figure 11 shows the change in the DEP force on the red blood cell in the middle of ITO electrode 1 with the increase in voltage. When a sine wave with the same parameters was applied between ITO electrodes 1 and 2 or 3, the cell was subjected to the same DEP force, which was increased from 1 pN to 70 pN. When two sine waves with the same parameters were applied between ITO electrodes 1 and 2 and between ITO electrodes 1 and 3, the resultant force the cell received increased from 2 pN to 136 pN.

The degree of cell deformation was defined as D by the following formula:

$$D(u) = \frac{l(u)}{l_0},\qquad(4)$$

where u denotes the peak-to-peak voltage of the sine wave, $l(u)$ denotes the length of the cell after deformation at the voltage of u, and l_0 denotes the original length of the cell. As shown in Table 1, the amount of deformation of the cell gradually increased as the voltage was increased from 1 Vpp to 10 Vpp. $D(u1)$ indicated the deformation of the cell when a voltage was applied between ITO electrodes 1 and 2. $D(u2)$ indicated the deformation of the cell when a voltage was applied between ITO electrodes 1 and 3. $D(u3)$ represented the deformation of the cell when all three ITO electrodes were connected. The DEP force in one direction and the resultant DEP force were also included in Table 1 to show intuitively the relationship between cell deformation and DEP force. Analytical results of $D(u1)$, $D(u2)$, and $D(u3)$

show that when the DEP force received by the cell was below 70 pN, the maximum deformation was 1.21. The deformation of the cell in all directions was proportional to the value of the DEP force. Hence, the mechanical properties of the red blood cells were inferred to be almost the same in all directions. Analysis of $D(u3)$ shows that when the red blood cell was subjected to a DEP force of 100 pN, the deformation reaches a maximum value of 1.38. When the voltage was continuously increased, the DEP force was increased, but the cell deformation did not increase. However, the deformation of the cell continued to increase when the voltage was increased to above 10 Vpp, and this process was irreversible (Figure 12). The cell did not return to its original state after being stretched, and the physiological structure of the red blood cell was destroyed.

4. Conclusions

A microfluidic chip with three unsymmetrical ITO electrodes was innovatively designed to measure and analyze the multiangle cellular mechanical properties. The designed chip had wide practicability, and the measurement and analysis of the multiangle mechanical characteristics of different kinds of cells were achieved by only adjusting the distance between the ITO electrodes. These properties enabled an accurate and comprehensive measurement. An efficient and accurate platform for measuring and analyzing cellular mechanical properties was established. A series of experiments was performed to measure and analyze the multiangle mechanical properties of mouse red blood cells. The results showed that the mechanical properties of red blood cells were almost the same in all directions. This work provides an efficient and low-cost tool for evaluating the multiangle cellular mechanical properties of cells to obtain comprehensive and accurate data. In addition, a new method for generating larger DEP force (resultant force) at low voltages was proposed. This method may increase the efficiency of cell manipulation.

Research Article

Transcriptome Analysis Reveals the Negative Effect of 16 T High Static Magnetic Field on Osteoclastogenesis of RAW264.7 Cells

Ting Huyan,[1,2] **Hourong Peng,**[1] **Suna Cai,**[1] **Qi Li** ⓘ,[1] **Dandan Dong,**[1] **Zhouqi Yang** ⓘ,[1] **and Peng Shang** ⓘ[1,3]

[1]*Key Laboratory for Space Biosciences and Biotechnology, Institute of Special Environment Biophysics, School of Life Sciences, Northwestern Polytechnical University, Xi'an, China*
[2]*Institute of Flexible Electronics (IFE), Northwestern Polytechnical University, 127 Youyi Xilu, Xi'an, 710072 Shaanxi, China*
[3]*Research & Development Institute in Shenzhen, Northwestern Polytechnical University, Shenzhen 518057, China*

Correspondence should be addressed to Zhouqi Yang; yangzhouqi@nwpu.edu.cn and Peng Shang; shangpeng@nwpu.edu.cn

The magnetic field is the most common element in the universe, and high static magnetic field (HiSMF) has been reported to act as an inhibited factor for osteoclasts differentiation. Although many studies have indicated the negative role of HiSMF on osteoclastogenesis of RANKL-induced RAW264.7 cells, the molecular mechanism is still elusive. In this study, the HiSMF-retarded cycle and weakened differentiation of RAW264.7 cells was identified. Through RNA-seq analysis, RANKL-induced RAW264.7 cells under HiSMF were analysed, and a total number of 197 differentially expressed genes (DEGs) were discovered. Gene ontology (GO) enrichment analysis and Kyoto Encyclopedia of Genes and Genomes (KEGG) pathway analysis indicated that regulators of cell cycle and cell division such as Bub1b, Rbl1, Ube2c, Kif11, and Nusap1 were highly expressed, and CtsK, the marker gene of osteoclastogenesis was downregulated in HiSMF group. In addition, pathways related to DNA replication, cell cycle, and metabolic pathways were significantly inhibited in the HiSMF group compared to the Control group. Collectively, this study describes the negative changes occurring throughout osteoclastogenesis under 16 T HiSMF treatment from the morphological and molecular perspectives. Our study provides information that may be utilized in improving magnetotherapy on bone disease.

1. Introduction

The static magnetic fields (SMF) are an important element of the earth's mechanical environment. SMF can be clarified into hypo (lower than $5\,\mu$T), weak (range from $5\,\mu$T to 1 mT), moderate (range from 1 mT to 1 T), and high (stronger than 1 T) SMF according to the magnetic intensity [1–3]. Each organism on Earth usually lives and sustains in 30-60 μT geomagnetic field (GMF). However, man-made SMF can produce High-SMF (HiSMF). For example, Magnetic Resonance Imaging (MRI), one of the most essential medical equipment, can provide 1.5-3 T HiSMF, which is 30,000 to 60,000 times bigger than the natural SMF on earth [4]. To improve the diagnosis and therapy, efforts have been put into increasing the intensity of SMF in medical research areas. Nowogrodzki recently made the world's strongest

MRI machines with a 10.5 T magnetic field [5]. Currently, the use of MRI with 7 T in clinical diagnosis has been approved by the Food and Drug Administration (FDA) [6]. At the same time, the high-intensity magnetotherapy, a noninvasion approach, has been applied in the treatment of various diseases including osteoporosis [7], rheumatoid arthritis [8], diabetic wound healing [9], and cancer [10]. Therefore, the application of HiSMF medical equipment is megatrends in the near future. However, the effect of HiSMF on biological objects still needs to be established.

Some pioneering studies revealed the multiple effects of SMF on biological systems, for example, (1) regulate plant functions, growth, and enhance tolerance against environmental stresses [11]; (2) promote chromosome break repair [12]; (3) delay the early development of zebrafish [13]; and (4) accelerate diabetic wound healing [9]. Recently, as a

crucial mechanical environment, the effect of SMF on the bone system attracts more attention. Bone is an essential organ of vertebrates, and the remolding process between bone formation and bone resorption needs to keep balanced because the remolding process is sensitive to alterations in the mechanical environment [14]. Turner reported that in SMF, magnetic nanocomposite could stimulate osteoblastic and vasculogenic potentials by mechanically stimulating the progenitor cell function [15]. Osteoclasts play an important role in mediating calcium metabolism and bone resorption. SMF could mediate inhibition of osteoclastogenesis and bone resorption by Receptor Activator of Nuclear Factor-κ B Ligand- (RANKL-) induced Akt, GSK3β, MAPK, and NF-κB pathways by Kim et al. [16]. Our previous works have revealed the vital role of HiSMF on osteoclasts, such as suppressing human preosteoclasts FLG29.1 cells survival and differentiation [17] as well as inhibiting NF-κ-B ligand-induced osteoclastogenesis via mediating the iron metabolism of RAW264.7 cells [4]. We further found that the effect of SMF on osteoclasts differentiation varies with the increase of the magnetic field intensity. Weak and moderate SMF facilitated osteoclastogenesis and bone resorption activity. In contrast, HiSMF (16 T) had a negative effect, which is related with the downregulated expression of osteoclastogenic genes such as matrix metalloproteinase 9 (MMP9), V-ATPase, carbonic anhydrase II (Car2), and RANK. Furthermore, HiSMF altered osteoclast cytoskeleton organization, which destructed the formation of filamentous actin ring and downregulated the expression of integrin β3 [18].

To further comprehensively understanding the role of HiSMF on osteoclastogenesis and bone remolding, next generation sequencing (NGS) was used to explore the crucial underlying factor at transcriptome level in this study. By screening and validating key differentially expressed genes between RANKL-induced RAW264.7 cells under HiSMF and normal conditions, the key functional genes profile and related regulatory networks of HiSMF on osteoclastogenesis were drawn to build the foundation of HiSMF-based magnetotherapy on bone metabolic diseases in future. A more profound knowledge of molecular mechanism of HiSMF-induced inhibitory effects on osteoclasts and the relationship between HiSMF and biological responses could render enhancement in the therapeutic method of bone disorders and help to extend novel clinical applications.

2. Materials and Methods

2.1. HiSMF Exposure System. The superconducting magnet (JASTEC, Kobe, Japan) could create a high static magnetic field (HiSMF) with a corresponding magnetic field intensity of 16 T. In the superconducting magnet, we have established a cell culture platform, which has been described in previous studies [4, 19]. The CO_2 concentration in the cell culture platform is controlled at 5%, and the temperature is controlled at 37°C. In this work, RAW264.7 cells were placed in 16 T magnetic field.

2.2. Cell Culture. The murine osteoclast precursor RAW264.7 cells (the Cell Collection Center of Shanghai, Shanghai, China) were cultivated in α-minimum essential medium (α-MEM; Gibco, Carlsbad, USA) with 100 units/mL penicillin, 0.1 mg/mL streptomycin, and 10% fetal bovine serum (Gibco, Carlsbad, USA) in 5% CO_2 atmosphere at 37°C. The cells were induced with RANKL (50 ng/mL, PeproTech, NJ, USA) to differentiate into mature osteoclasts and were continuously exposed to 16 T HiSMF for 3 days. In this study, it considered RANKL-induced RAW264.7 cells treated with the 16 T magnetic field as the HiSMF group and cells cultured in the ground-based condition as the Control group.

2.3. TRAP Staining. RAW264.7 cells, at the phase of the logarithmic growth, were seeded into the 96-well plate with a density of 2×10^5 cells per well, and $100 \mu L$ of the medium was added to each well. After the cells adhered to the plates, the cell culture medium was changed with osteoclast differentiation induction medium with 50 ng/mL RANKL, and the cells were placed to the HiSMF system for 3 days. TRAP staining assay was applied by using a Leukocyte kit (Sigma-Aldrich, USA) according to the manufacturer's instructions. Briefly, RAW264.7 cells were treated with 4% formaldehyde for 5 min, and 0.1% Triton X-100 was applied for cell permeabilization in 5 min. Then, the cells were stained with the leukocyte acid phosphatase reagent. Finally, the cells were removed from the wells for climbing slides and photographed under a microscope. TRAP-positive cells were defined as cells that have more than three nuclei and were burgundy.

2.4. Cell Proliferation Assay. For the cell proliferation assay, RAW264.7 cells were seeded into the 96-well plate with a density of 1×10^5 cells and $100 \mu L$ of the medium in each well. After treatment with the HiSMF system, cell proliferation at day 1, day 2, and day 3 were detected by the Cell Counting Kit-8 (CCK8; Beyotime, Shanghai, China) according to the manufacturer's instructions. Briefly, RAW264.7 cells were cultured in the 96-well plate. Then, $20 \mu L$ of the CCK8 solution was added to each well (up to $100 \mu L$ per well), the cells were continuously incubated at 37°C for 2 hours, and the optical density (OD) values were recorded at 450 nm by a multifunctional microplate reader (Bio-Rad Laboratories, Hercules, CA, USA). The average value of duplicate wells was used as the cell viability value.

2.5. Cell Cycle Assay. RAW264.7 cells, at the phase of the logarithmic growth, were seeded in 35 mm dishes with 2×10^5 cells per dish. After 24 hours of culture, the cell culture system was changed with the serum-free medium and cultured for 24 hours for cell cycle synchronization. Immediately after, the medium was changed with induction medium containing 50 ng/mL RANKL, and the cells were placed to the HiSMF system for 3 days. Then, cells were washed twice with ice-cold PBS and fixed with 75% ice-cold ethanol overnight. Subsequently, cells were stained by $50 \mu g/mL$ propidium iodide (PI; Sigma-Aldrich, Louis, MO, USA) and 1 mg/mL RNase A (Sigma-Aldrich, Louis, MO, USA) for 60 min. Finally, the cell cycle of samples was performed on a flow cytometer (FACSCalibur, BD, USA).

2.6. Library Construction and Sequencing. First, total RNA of RAW264.7 was obtained by using Trizol reagent (Invitrogen, Carlsbad, CA, USA). Second, the mRNA was enriched with magnetic beads and cut into short fragments; the first strand of cDNA was synthesized. After the end repair, base A and the sequencing adapter was added, agarose gel electrophoresis was used to recover the target size fragments, and PCR amplification was performed to complete the entire library preparation. Finally, the constructed library was sequenced using the Illumina HiSeq 2000 by GENE DENOVO (Guangzhou, China).

2.7. RNA-Seq Analysis. Low-quality portions of reads and adapter sequences were wiped out by using Trimmomatic (version 0.32) [20]. The amount of paired-end clean reads of each sample was in Table 1. Cleaned reads to the mouse reference genome (version: GRCm38) were aligned by using Bowtie2. Then RSEM program [21, 22] was applied for quantifying the level of gene expression. Differential expression was determined by using the DESeq2 package [23].

2.8. Gene Ontology and KEGG Pathway Enrichment Analysis. We used online resources (https://david.ncifcrf.gov) implemented in DAVID to conduct the gene ontology overrepresentation analysis and pathway analysis [24] to associate the identified DEGs with biological functions and processes and pathways. Gene ontology functional annotation consists of three parts, including cellular components (CC), molecular functions (MF), and biological processes (BP). KEGG pathway enrichment analysis was carried out by using the database (https://www.genome.jp/kegg/).

2.9. Quantitative Real-Time PCR Analysis. Ten candidate DEGs were selected to confirm the RNA-seq results. Total RNA was isolated from osteoclasts using Trizol (Invitrogen Corp). After the obtained RNA was reversely transcribed and qPCR was performed, the relative expression of mRNA was determined by the CFX96 Touch qPCR system (Bio-Rad Laboratories, Hercules, CA, USA). SYBR Green Real-Time PCR Master Mixes (Applied Biosystems, Carlsbad, CA, USA) were used in this experiment according to the manufacturer's instructions. The primers of candidate DEGs were obtained from the Primer-BLAST online tool [25], and GAPDH was used as the reference gene [4]. The detailed sequences were showed in Table 2. The reaction was performed under the following amplification conditions: initial denaturation at 50°C for 2 minutes, 95°C for 10 minutes, then 40 reaction cycles at 95°C for 15 seconds, and 60 cycles at 60°C. Gene expression was assessed and analyzed by the $2^{-\Delta\Delta Ct}$ method.

2.10. Statistical Analysis. All experiments were biologically replicated 3 times with 3 technical replicates. The results of the experiment were represented by the mean values of three experiments. The data are expressed as mean ± SD. The Student's *t*-test was used to calculate *P* values, and $P < 0.05$ was considered a statistically significant difference. The graphs and statistical analysis in this paper were generated by the GraphPad Prism (version 6, GraphPad Software, California, USA).

TABLE 1: The number of clean reads in the Control and 16 T-HiSMF treated group.

Sample	Number of reads
CONTROL1_R1.clean.fastq	14253190
CONTROL1_R2.clean.fastq	14253190
CONTROL2_R1.clean.fastq	14084434
CONTROL2_R2.clean.fastq	14084434
EXP1_R1.clean.fastq	14394195
EXP1_R2.clean.fastq	14394195
EXP2_R1.clean.fastq	14270708
EXP2_R2.clean.fastq	14270708
EXP3_R1.clean.fastq	13193553
EXP3_R2.clean.fastq	13193553

3. Results

3.1. HiSMF Inhibited the Osteoclasts Activity, Cell Proliferation, and Cell Cycle. RAW264.7 cells were inoculated in 18 mm dishes and were induced for 3 days in a HiSMF system with osteoclast induction medium to obtain mature osteoclasts. The TRAP staining results (Figure 1(a)) showed that a larger amount of giant TRAP-positive multinucleated cells were in the Control group than in the HiSMF group. These results indicated that differentiation of RAW264.7 cells was inhibited by HiSMF. To determine whether HiSMF had a negative effect on osteoclastogenesis of RAW264.7 cells, we primarily observed that HiSMF inhibited the proliferation of RAW264.7 cells (Figure 1(c)). For further study, cell cycle distribution was investigated to determine whether it was associated with this inhibitory effect on cell proliferation. It showed that the ratio of cells at the G1 phase raised in the HiSMF group (Figure 1(b)) compared with the Control group. Inversely, the ratio of cells in the S phase had a significant reduction in the HiSMF group versus the Control group. However, the ratio of cells in the G2 phase had no significant difference.

3.2. Differentially Expressed Genes (DEGs) Analysis. Initially, there were six samples sequenced; however, due to contamination, one of the samples in the Control group was not able to pass the quality control. Therefore, we only used 2 control samples and 3 HiSMF samples sequenced data for further analysis. DEGs were identified between Control and HiSMF groups using the DESeq2 package. The significance level was defined as a false discovery rate (FDR) less than 0.01 and $\log_2$ fold change ($\log_2$FC) larger than ±0.5. In total, a number of 197 DEGs were obtained. Upregulated and downregulated DEGs were showed in volcano plots (Figure 2(a)). After identifying the DEGs, we first did a hierarchical cluster analysis and the upregulated and downregulated genes were showed in a heatmap (Figure 2(b)). Gene counts were $\log_{10}$ transformed and normalized as *Z*-score. In Figure 2(b), two clusters were clearly displayed; all control groups were in one cluster and the HiSMF groups in another cluster, which showed high intragroup consistency and high intergroup variability.

Table 2: Primer sequences of selected 10 target genes used for quantitative real time PCR [4, 25].

Gene name	Primer sequences (5′-3′)
CtsK (ENSMUST00000015664)	Forward: TTCTGCTGCTACCCATGGTG
	Reverse: TGCACGTATTGGAAGGCAGT
Ube2c (ENSMUST00000088248)	Forward: GTTGCCGCGGTTCGAAAAG
	Reverse: TCAGGGATCTTGGCTGGAGA
Kif11 (ENSMUST00000012587)	Forward: GCAGAGCGGAAAGCTAATGC
	Reverse: CAAGGTTGCTGCAGTTGTCC
Nusap1 (ENSMUST00000068225)	Forward: GTGACCCCAGTTCCTCCAAG
	Reverse: CACCCAGGTTTCTTCGAGCT
Bub1b (ENSMUST00000038341)	Forward: GCCCAGAGAAGACCCCTTTC
	Reverse: CGGTCGGTCTTCCACAGAAA
Rbl1 (ENSMUST00000029170)	Forward: AAGCCCTGGATGACTTCACG
	Reverse: AGATCAGGTCCAAGCAGCAC
Pcna (ENSMUST00000028817)	Forward: CCTGAAGAAGGTGCTGGAGG
	Reverse: TGTTCCCATTGCCAAGCTCT
Gm10696 (ENSMUST00000161475)	Forward: TGCCAAGTGAGCATAGTGGG
	Reverse: TGCTTCAGCTACCAAGTGGG
Gm4737 (ENSMUST00000059524)	Forward: TCTGTCAGGCATCCGAGGTA
	Reverse: CCTGGGGCTTGATGTTCACT
Gm8994 (ENSMUSG00000094973)	Forward: CACACAGGTCGTTCTCGTCA
	Reverse: CGATGTCCCTGAGAATCCGG
GAPDH (ENSMUST00000073605)	Forward: TGCACCACCAACTGCTTAG
	Reverse: GGATGCAGGGATGATGTTC

3.3. Enriched GO Ontology and Pathway Analysis of DEGs. The GO function annotation and Kyoto Encyclopedia of Genes and Genomes (KEGG) pathway provide background knowledge on gene function classification and gene function research. We performed GO analysis and pathway analysis on DEGs, taking $P < 0.05$ as a significance threshold. Based on the GO analysis results, a GO enrichment classification map of DEGs was drawn (Figure 3). From Figure 3, the GO function enrichment results showed that significant biological process (BP) in our analysis were cell cycle, cell division, and mitotic nuclear division. DEGs involved in these processes were Benzimidazoles 1 homolog beta (Bub1b), Retinoblastoma-like protein 1 (Rbl1), Ubiquitin-conjugating enzyme E2C (Ube2c), Kinesin family member 11 (Kif11), and Nucleolar spindle associated protein 1 (Nusap1). These genes have been considered as the important factors in regulating cell cycle and spindle assembly processes. Therefore, we chose these genes as candidate genes for validation of RNA-seq results. In cellular component (CC), the nucleoplasm had the highest number of genes. In Molecular Function (MF), it was mainly concentrated in DNA binding, ATP binding, and protein homodimerization activity.

In the KEGG enrichment analysis, significant pathways were plotted in the bubble diagram, which shows that DEGs were mainly in the cell cycle and DNA replication-related pathways (Figure 4). Genes involved in these pathways are considered to be candidate DEGs for validation. Therefore, proliferating cell nuclear antigen (Pcna, the DNA replication related gene) and cathepsin K (CtsK, the marker gene of osteoclastogenesis), which were vital genes in cell proliferating and differentiation, were selected for further confirmation analysis. Besides these well-known genes, there were also some new genes which refer to the sequence known, but its biological function has not been experimentally confirmed. Therefore, we were interested in testing these new DEGs, and then the top 3 new genes in DEGs were also selected as the candidate genes for validation.

3.4. Validation of the DEGs. Based on DEGs analysis, Go ontology, and pathway analysis, ten candidate genes were selected (Table 3) for further qPCR validation. In these selected 10 DEGs, 7 were upregulated and 3 were downregulated. The qPCR assay was applied on these mRNAs to verify the results of RNA-seq. The results of qPCR confirmed that the expression trends of 9 DEGs coincided to the RNA-seq results except for one gene, indicating that the RNA-seq results were reliable (Figure 5), which provides valuable information for the downstream analysis. The gene not confirmed by qPCR was Pcna. We further took a closer look at this gene and found that the expression of this gene showed large variances across three replicates (large SD in the HiSMF group), leading to the failure of confirmation.

4. Discussion

The research on the use of HiSMF technology in magnetotherapy in clinics has been increasing due to its useful effects in many diseases, including cancers, edema, inflammation, wounds healing, and bone disorders [7–10, 26]. Due to its safety and noninvasiveness, magnetotherapy has been approved as an instructive novel strategy by the US Food and Drug Administration (FDA) [16]. Especially, HiSMF has been considered as a regulator in bone metabolism, such as bone formation and bone resorption [27]. Bone
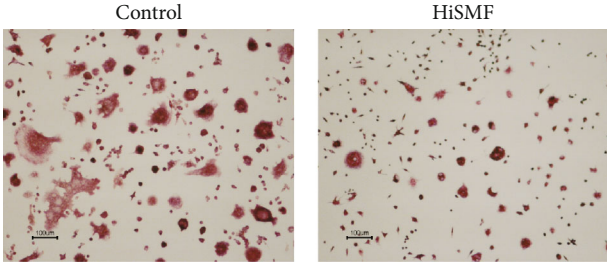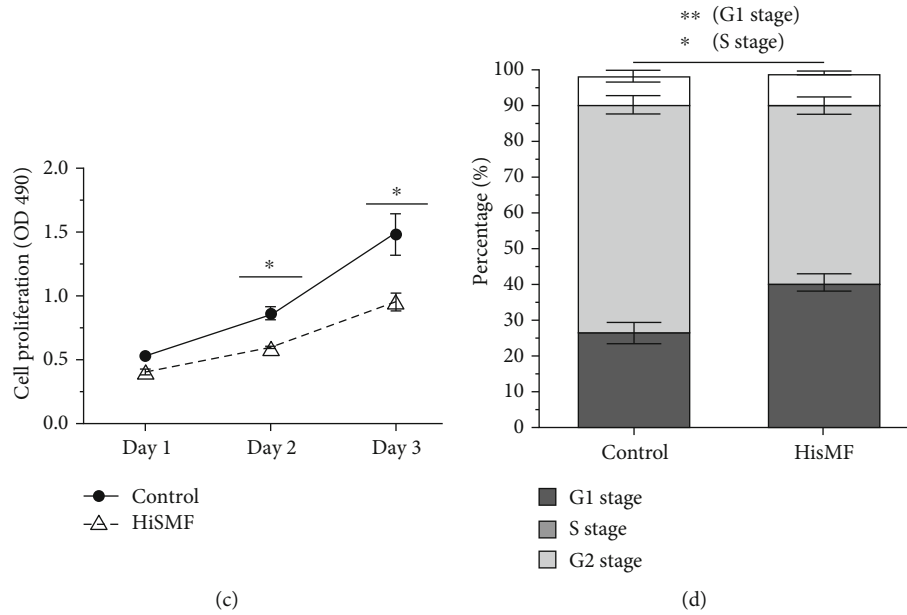
(a)
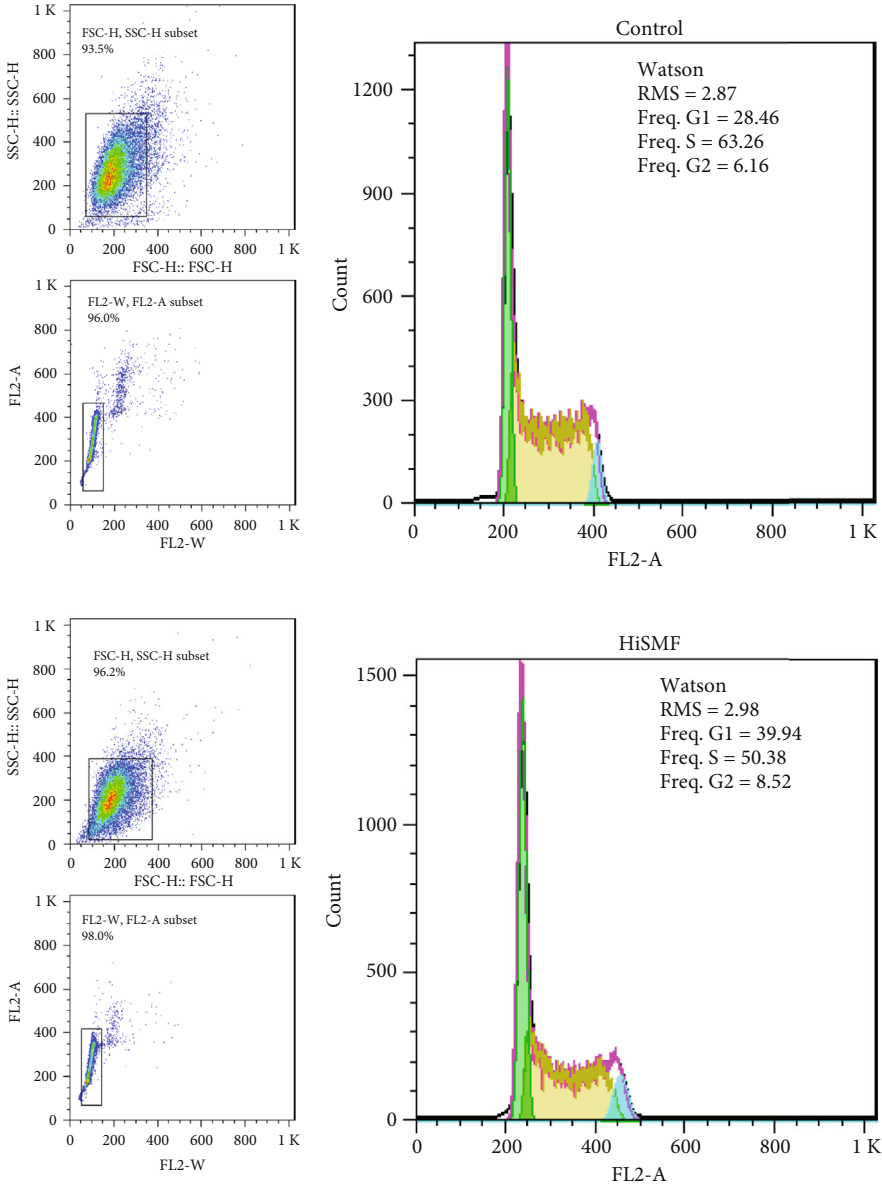
(b)

Figure 1: Continued.

(c)

(d)

FIGURE 1: Effect of HiSMF on osteoclastogenesis, cell proliferation, and cell cycle of preosteoclast RAW264.7 cells. (a) TRAP staining of mature osteoclasts generated by RANKL-induced preosteoclast RAW264.7 cells at day 3 ($n = 3$), Bar = 100 μm. (b) Cell cycle distribution of RAW264.7 cells in HiSMF. Cell cycle distribution was determined by flow cytometry with PI staining ($n = 3$). (c) Proliferation of RAW264.7 cells in the Control and HiSMF group. Proliferation of RAW264.7 cells were examined by CCK8 assay, and the results were shown as OD450. (d) The percentage of RAW264.7 cell cycle distribution in the bar graph. All groups were compared with the Control group ($n = 3$). Data shown are mean ± SD, $^{*}P < 0.05$, $^{**}P < 0.01$.
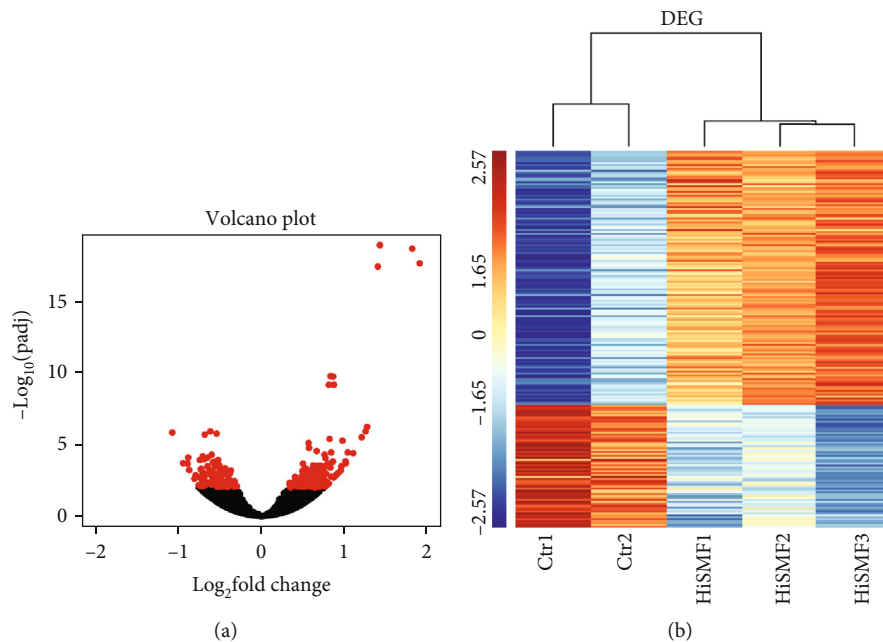

(a)

(b)

FIGURE 2: Differentially expressed genes (DEGs) expression profiles of osteoclasts after HiSMF treatment. (a) Volcano plot of DEGs between Control and HiSMF groups. The red dots on the left side of the figure indicate downregulated genes, and the red dots on the right side indicate upregulated genes. (b) Heatmap of cluster analysis of DEGs. Red color indicates highly expressed DEGs, and blue color indicates lower expressed DEGs.

remodeling, a dynamic equilibrium between degradation by osteoclasts and formation by osteoblasts, maintains the structural integrity of the bone. Accumulated studies indicated that HiSMF enhanced activities of osteoblasts and inhibited

differentiation of osteoclasts [18, 28]. However, most studies focused on osteoblast because of its important role in bone formation, and few studies were related to osteoclast, which is responsible for bone resorption. Recently, our previous
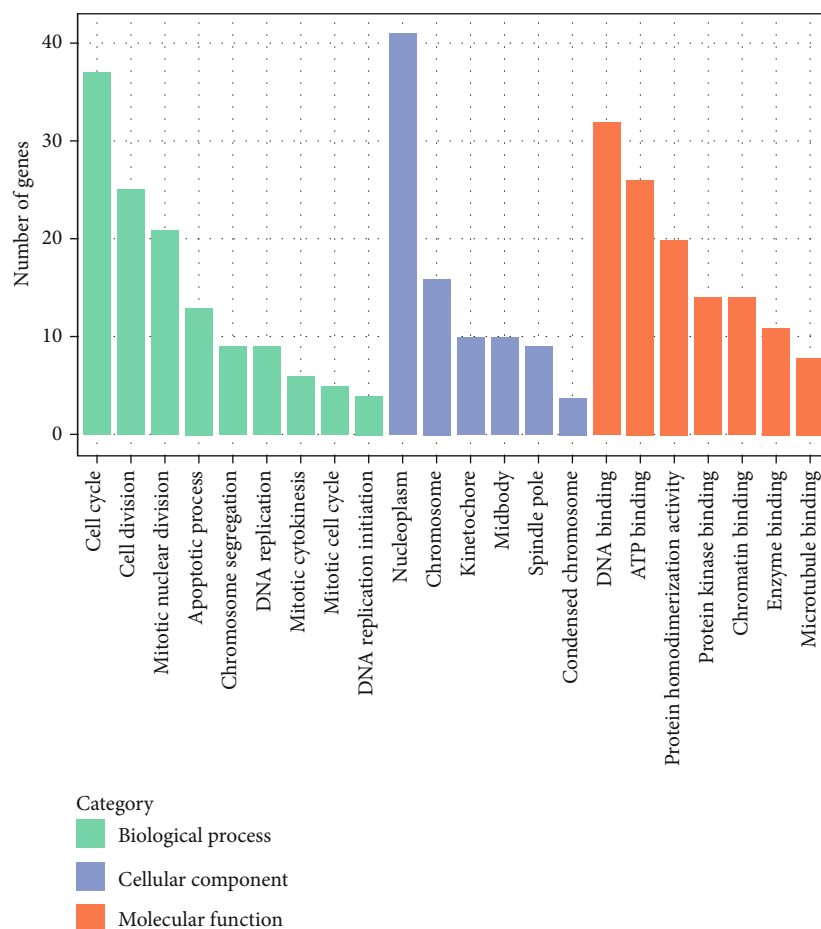
FIGURE 3: GO enrichment classification map of differentially expressed genes (DEGs). GO enrichment analysis consists of 3 parts: biological processes (BP, green bars), cellular components (CC, blue bars), and molecular functions (MF, orange bars). The y-axis is the number of DEGs enriched in each part.

studies *in vitro* have suggested that HiSMF could suppress the osteoclast formation in preosteoclast FLG29.1 and RAW264.7 cells [4, 17, 18, 28]. Although, there were a few studies that reported the differential expression genes of osteoclasts responding to HiSMF exposure, the systematical gene expression change at the transcriptome level was not clear. Therefore, we used RNA-seq analysis to identify the molecular mechanisms of HiSMF towards osteoclastogenesis.

In this study, a well-characterized cell linage, RAW264.7 cells were used as the osteoclast precursor cell line because the primary osteoclast precursor cells which originated from bone marrow may raise some issues including availability and variation in response pattern for cellular study [29, 30]. In addition to primary osteoclast precursor cells, RAW264.7 cells had been proved to respond to stimuli *in vitro* and differentiate to mature osteoclasts with the hallmark characteristics, so it offered advantages of the cellular model system compared to the primary osteoclast precursor cells [31]. Because of these reasons, we initially performed cytological assays on RANKL-induced RAW264.7 cells to determine whether HiSMF can cause different cellular phenotypes of RAW264.7 cells. Consistent with our previous results [4, 18, 28], the amount of TRAP-positive RAW264.7 cells signifi-

cantly reduced in HiSMF. Moreover, the RAW264.7 cells proliferation was also decreased in HiSMF associated with the G1 phase arresting. These data confirmed that osteoclastic differentiation and maturation were negatively regulated by HiSMF.

The high throughput NGS has been considered the most comprehensive method for transcriptome analysis and exploring molecular mechanisms [32]. In our transcriptome study, we observed significant changes in the expression levels of 197 genes of RANKL-induced RAW264.7 cells after exposure to HiSMF, of which 133 genes were upregulated, and 64 genes were downregulated (FDR less than 0.01, and $\log_2$FC larger than ±0.5). Among these DEGs, some of them are new genes. It is important and interesting to identify new genes because the genome of mouse was sequenced, and one of the annotation was predicting genes. As a result, there are many genes predicted by bioinformatics tools, but their functions have not been confirmed by biological experiments. Therefore, these new genes, which the sequence is known, but its biological function has not been experimentally confirmed, were identified to be associated with HiSMF in our study. This provides new information and knowledge of understanding the regulatory network/pathway under HiSMF.
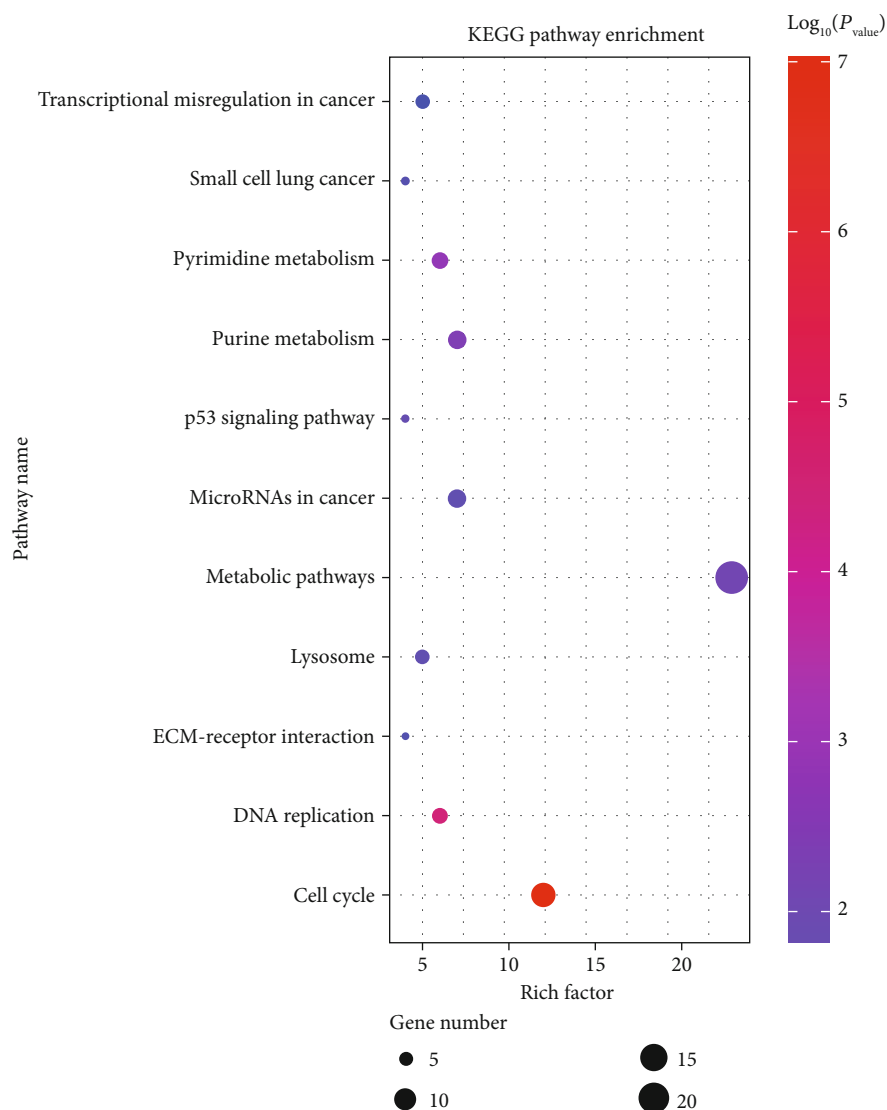
FIGURE 4: The bubble map of KEGG pathway enrichment analysis of differentially expressed genes (DEGs). The size of the bubbles represents the number of DEGs enriched in each pathway. The color of the bubbles represents the significance level.

TABLE 3: Differential expression of selected 10 target genes in control and HiSMF treated group.

| Gene name	Description	Con-expression	HiSMF-expression	log2FoldChange	Adjusted P value
CtsK	Cathepsin K	201359	137884	-0.528987973	0.0000315
Ube2c	Ubiquitin-conjugating enzyme E2C	270.5	490.4	0.654515154	0.0000886
Kif11	Kinesin family member 11	315.5	542.7	0.603638084	0.000208588
Nusap1	Nucleolar and spindle associated protein 1	166	312.3	0.674634071	0.000104789
Bub1b	BUB1B mitotic checkpoint serine/threonine kinase	442	846	0.726751612	0.0000085
Rbl1	RB transcriptional corepressor like 1	176.5	336.3	0.702550004	0.0000322
Pcna	Cell proliferation proliferating cell nuclear antigen	1390.5	2320.3	0.61344962	0.0000102
Gm10696	Predicted gene 10696	453.2	216.34	-0.880892972	0.000000216
Gm4737	Predicted gene 4737	623.7	1047.2	0.619442963	0.00000731
Gm8994	Predicted gene 8994	407.5	216.4	-0.708009712	0.000119099
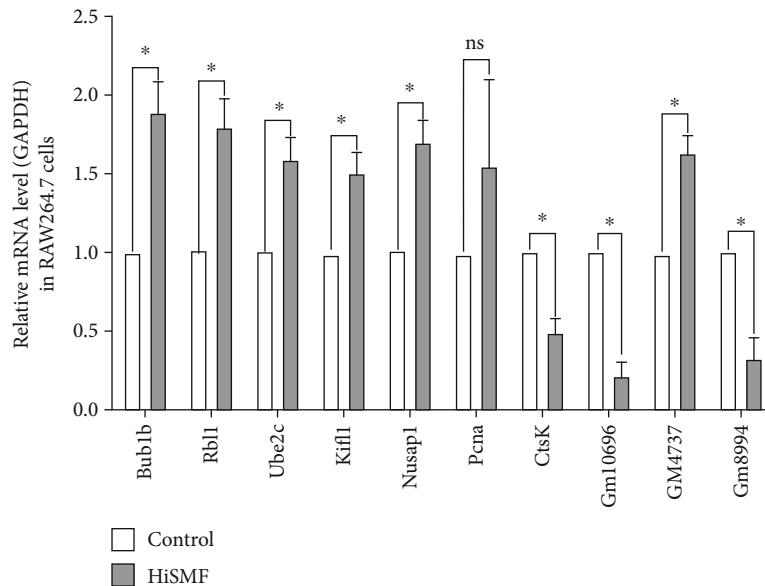
FIGURE 5: The validation of 10 selected DEGs through qPCR. Relative mRNAs expression level was calculated by fold change. Each group represented as the mean ± SD from three separate experiments ($*P < 0.05$).

In GO and pathway analysis, the most significant term was cell cycle, indicating that this cellular process was altered in HiSMF. It was consistent with our cytological results. In the GO category of molecular functions, DEGs were mainly involved in DNA binding and ATP binding, suggesting that many factors took part in the transcriptional regulation of RAW264.7 cells. As the primary public pathway-related database, KEGG analysis could effectively enrich signal transduction pathways and metabolic pathways in DEGs [33]. Analogously, in the KEGG pathway analysis, 8 pathways were significantly enriched, including cell cycle, DNA replication, ECM-receptor interaction, lysosome, purine metabolism, metabolic pathways, pyrimidine metabolism, and p53 signaling pathway. Among them, cell cycle was the most significantly pathway and played a vital role in cell growth and differentiation.

Cell cycle has multiple functions in physiological processes, including embryonic morphogenesis, cell proliferation and differentiation, and stem cell pluripotency [34, 35]. It commonly appeared that cell cycle arrest temporally couple with cell differentiation [36]. For the differentiation of osteoclasts, this process is also mediated by cell cycle related genes, such as cyclin-dependent kinase (Cdk), Cdk inhibitors, and checkpoint factors [37]. Previous result showed that RANKL could induce osteoclastogenic via arresting cell cycle at the G1 phase in connection with overexpression of the CDK inhibitor p27 [38]. Another work showed that RANKL-induced cell cycle arrest with both upregulation of two Cdk inhibitors (p21 and p27) may be relevant to osteoclastogenesis [39, 40]. In this study, the inhibition effect of HiSMF on cell cycle was coordinated with osteoclast differentiation in cytological and RNA-Seq results.

Through RNA-seq analysis, 10 DEGs involved in cell cycle (Bub1b, Rbl1, Ube2c, Kif11, and Nusap1), cell proliferation (Pcna), cell differentiation (CtsK), and newly predicted genes (Gm10696, Gm4737, and Gm8994) were selected for validation by qPCR. Nine out of ten DEGs were confirmed the expression trend. However, one gene, Pcna, was not significantly upregulated in qPCR results. It might be due to the inconsistent expression level among replicates, which produces the difficulty of repeating RNA-seq results. In the present study, cell cycle was more systematically analyzed, and the DEGs involved in cell cycle were investigated and validated, which could provide more information for further study.

The five cell cycle related genes in the validated DEGs were all upregulated in the HiSMF group. Among them, Benzimidazoles 1 homolog beta (Bub1b), an important spindle checkpoint gene, regulates multiple functional domains, including mitotic timing and mitotic checkpoint control [41]. The upregulation of Bub1b may result in chromosomal aneuploidy and instability and finally affect cell cycle process [42, 43]. Ubiquitin-conjugating enzyme E2C (Ube2c) could interact with the anaphase-promoting complex/cyclostome (APC/C) to regulate the cell cycle progression [44]. Overexpression of Ube2c may participate in the transition of G1 phase to G2 phase [45]. Kinesin family member 11 (Kif11), a molecular motor, regulates the separation of centrosome and development of the bipolar mitotic spindle [46]. Upregulated Kif11 can cause inordinate cell cycle arrest and cell division in mitosis process [47]. Nucleolar spindle associated protein 1 (Nusap1), a microtubule-associated molecular, plays an important role in the aggregation of microtubule with mitotic chromosomes during cell cycle regulation [48]. Retinoblastoma-like protein 1 (Rbl1), an important controller of entry into cell division [49], has been demonstrated that its phosphorylation status was in the transition from S to M phase, and its dephosphorylation status was in the G1 phase [50]. Future work needs to explore the phosphorylation status of Rbl1 in osteoclastogenesis.

Besides genes involved in cell cycle, we also identified an osteoclast-specific marker gene, *CtsK*, which was significantly downregulated in the HiSMF group. The previous study has provided evidence for the expression of the osteoclast-specific markers in SMF condition, such as *TRAP* and *CtsK* [4]. Our results supported and confirmed that the *CtsK* might be a critical molecular target in HiSMF. What is more, *CtsK* could be further investigated in this process, which may demonstrate the molecular mechanism of HiSMF toward osteoclast differentiation.

Based on our findings, there are several experiments to do in the future. Initially, the data measured by cytological experiments could apply as an in vivo study, which is the advanced level to verify the molecular functions in osteoclastogenesis under HiSMF. In addition to cell cycle, other pathways such as DNA replication and metabolic have been proved to be related to essential DEGs, but not further studied. How to explore the other DEGs in combination with multiple processes during osteoclastogenesis is the focus of future work. Thirdly, the function of the predicted genes in our results needs to be further validated and may provide more biological information for the mechanism for the osteoclastogenesis under HiSMF. Finally, current studies mainly analyze the dynamic changes of genes in time series based on RNA-seq technology. In future, it is necessary to apply a more comprehensive gene expression map by using advanced technology, such as single-cell sequencing, which reflects more detail in the intracellular network [51, 52]. We firmly believe that single-cell sequencing data will effectively build more reliable and accurate networks for future work.

5. Conclusion

Here, we employed NGS to identify, at the transcriptome level, significant DEGs related to cell cycle, cell division, and osteoclasts differentiation in HiSMF condition. The GO and KEGG functional enrichment analyses of the DEGs revealed that the cell cycle, cell division, and DNA replication play a vital role in the regulation of HiSMF on osteoclasts differentiation. The cell cycle was significantly inhibited. Furthermore, nine out of ten DEGs were confirmed the result, and three of them were new genes, which may be related to the differentiation of RAW264.7 cells into mature osteoclasts. Taken together, these findings provided potential new molecular targets for studying the mechanism of the osteoclast differentiation, which may contribute to improving magnetotherapy on bone disease in the future.

Data Availability

The data used to support the findings of this study are available from the corresponding author upon request.

Conflicts of Interest

The authors report no conflicts of interest.

References

[1] H. Tabenkin, A. Tamir, L. Epstein, and P. Shvartzman, "Characteristics and perceptions of physician managers in Israel," *Harefuah*, vol. 122, no. 2, pp. 65–69, 1992.

[2] A. D. Rosen, "Mechanism of action of moderate-intensity static magnetic fields on biological systems," *Cell Biochemistry and Biophysics*, vol. 39, no. 2, pp. 163–173, 2003.

[3] W. Mo, Y. Liu, and R. He, "Hypomagnetic field, an ignorable environmental factor in space?," *Science China Life Sciences*, vol. 57, no. 7, pp. 726–728, 2014.

[4] D. Dong, J. Yang, G. Zhang, T. Huyan, and P. Shang, "16 T high static magnetic field inhibits receptor activator of nuclear factor kappa-B ligand-induced osteoclast differentiation by regulating iron metabolism in RAW264.7 cells," *Journal of Tissue Engineering and Regenerative Medicine*, vol. 13, no. 12, pp. 2181–2190, 2019.

[5] A. Nowogrodzki, "The world's strongest MRI machines are pushing human imaging to new limits," *Nature*, vol. 563, no. 7729, pp. 24–26, 2018.

[6] C. A. Park, C. K. Kang, Y. B. Kim, and Z. H. Cho, "Advances in MR angiography with 7T MRI: from microvascular imaging to functional angiography," *NeuroImage*, vol. 168, pp. 269–278, 2018.

[7] Z. Bao, M. Fan, L. Ma, Q. Duan, and W. Jiang, "The effects of pulsed electromagnetic fields combined with a static magnetic intramedullary implant on the repair of bone defects: a preliminary study," *Electromagnetic Biology and Medicine*, vol. 38, no. 3, pp. 210–217, 2019.

[8] J. Zwolinska, M. Gasior, E. Sniezek, and A. Kwolek, "The use of magnetic fields in treatment of patients with rheumatoid arthritis. Review of the literature," *Reumatologia*, vol. 54, no. 4, pp. 201–206, 2016.

[9] W. Shang, G. Chen, Y. Li et al., "Static magnetic field accelerates diabetic wound healing by facilitating resolution of inflammation," *Journal Diabetes Research*, vol. 2019, article 5641271, 11 pages, 2019.

[10] M. Ognjanović, M. Radović, M. Mirković et al., "99mTc-,90Y-, and177Lu-Labeled iron oxide nanoflowers designed for potential use in dual magnetic hyperthermia/radionuclide cancer therapy and diagnosis," *ACS Applied Materials & Interfaces*, vol. 11, no. 44, pp. 41109–41117, 2019.

[11] R. Radhakrishnan, "Magnetic field regulates plant functions, growth and enhances tolerance against environmental stresses," *Physiology and Molecular Biology of Plants*, vol. 25, no. 5, pp. 1107–1119, 2019.

[12] A. M. Burgos-Molina, S. Mercado-Saenz, F. Sendra-Portero, and M. J. Ruiz-Gomez, "Effect of low frequency magnetic field

on efficiency of chromosome break repair," *Electromagnetic Biology and Medicine*, vol. 39, no. 1, pp. 30–37, 2020.

[13] S. Ge, J. Li, D. Huang et al., "Strong static magnetic field delayed the early development of zebrafish," *Open Biology*, vol. 9, no. 10, p. 190137, 2019.

[14] P. Zhang, K. Hamamura, and H. Yokota, "A brief review of bone adaptation to unloading," *Genomics, Proteomics & Bioinformatics*, vol. 6, no. 1, pp. 4–7, 2008.

[15] P. Turner, "Recent observations on drugs and human fertility," *Postgraduate Medical Journal*, vol. 64, no. 754, pp. 578–580, 1988.

[16] E. C. Kim, J. Park, G. Noh et al., "Effects of moderate intensity static magnetic fields on osteoclastic differentiation in mouse bone marrow cells," *Bioelectromagnetics*, vol. 39, no. 5, pp. 394–404, 2018.

[17] S. Di, Z. Tian, A. Qian et al., "Large gradient high magnetic field affects FLG29.1 cells differentiation to form osteoclast-like cells," *International Journal of Radiation Biology*, vol. 88, no. 11, pp. 806–813, 2012.

[18] J. Zhang, X. Meng, C. Ding, L. Xie, P. Yang, and P. Shang, "Regulation of osteoclast differentiation by static magnetic fields," *Electromagnetic Biology and Medicine*, vol. 36, no. 1, pp. 8–19, 2017.

[19] J. Zhang, C. Ding, and P. Shang, "Alterations of mineral elements in osteoblast during differentiation under hypo, moderate and high static magnetic fields," *Biological Trace Element Research*, vol. 162, no. 1-3, pp. 153–157, 2014.

[20] A. M. Bolger, M. Lohse, and B. Usadel, "Trimmomatic: a flexible trimmer for Illumina sequence data," *Bioinformatics*, vol. 30, no. 15, pp. 2114–2120, 2014.

[21] B. Li and C. N. Dewey, "RSEM: accurate transcript quantification from RNA-Seq data with or without a reference genome," *BMC Bioinformatics*, vol. 12, no. 1, 2011.

[22] B. Li, V. Ruotti, R. M. Stewart, J. A. Thomson, and C. N. Dewey, "RNA-Seq gene expression estimation with read mapping uncertainty," *Bioinformatics*, vol. 26, no. 4, pp. 493–500, 2010.

[23] M. I. Love, W. Huber, and S. Anders, "Moderated estimation of fold change and dispersion for RNA-seq data with DESeq2," *Genome Biology*, vol. 15, no. 12, p. 550, 2014.

[24] D. W. Huang, B. T. Sherman, and R. A. Lempicki, "Bioinformatics enrichment tools: paths toward the comprehensive functional analysis of large gene lists," *Nucleic Acids Research*, vol. 37, no. 1, pp. 1–13, 2009.

[25] J. Ye, G. Coulouris, I. Zaretskaya, I. Cutcutache, S. Rozen, and T. L. Madden, "Primer-BLAST: a tool to design target-specific primers for polymerase chain reaction," *BMC Bioinformatics*, vol. 13, no. 1, 2012.

[26] G. Bertolino, A. de Freitas Braga, K. de Oliveira Lima do Couto Rosa, L. C. de Brito Junior, and J. E. de Araujo, "Macroscopic and histological effects of magnetic field exposition in the process of tissue reparation in Wistar rats," *Archives of Dermatological Research*, vol. 298, no. 3, pp. 121–126, 2006.

[27] J. Zhang, C. Ding, X. Meng, and P. Shang, "Nitric oxide modulates the responses of osteoclast formation to static magnetic fields," *Electromagnetic Biology and Medicine*, vol. 37, no. 1, pp. 23–34, 2018.

[28] T. Pesqueira, R. Costa-Almeida, and M. E. Gomes, "Magnetotherapy: the quest for tendon regeneration," *Journal of Cellular Physiology*, vol. 233, no. 10, pp. 6395–6405, 2018.

[29] P. Collin-Osdoby and P. Osdoby, "RANKL-mediated osteoclast formation from murine RAW 264.7 cells," *Methods in Molecular Biology*, vol. 816, pp. 187–202, 2012.

[30] P. Collin-Osdoby, X. Yu, H. Zheng, and P. Osdoby, "RANKL-mediated osteoclast formation from murine RAW 264.7 cells," *Methods in Molecular Medicine*, vol. 80, pp. 153–166, 2003.

[31] L. Kong, W. Smith, and D. Hao, "Overview of RAW264.7 for osteoclastogensis study: phenotype and stimuli," *Journal of Cellular and Molecular Medicine*, vol. 23, no. 5, pp. 3077–3087, 2019.

[32] K. O. Mutz, A. Heilkenbrinker, M. Lonne, J. G. Walter, and F. Stahl, "Transcriptome analysis using next-generation sequencing," *Current Opinion in Biotechnology*, vol. 24, no. 1, pp. 22–30, 2013.

[33] M. Kanehisa and S. Goto, "KEGG: Kyoto encyclopedia of genes and genomes," *Nucleic Acids Research*, vol. 28, no. 1, pp. 27–30, 2000.

[34] S. Champeris Tsaniras, N. Kanellakis, I. E. Symeonidou, P. Nikolopoulou, Z. Lygerou, and S. Taraviras, "Licensing of DNA replication, cancer, pluripotency and differentiation: an interlinked world?," *Seminars in Cell & Developmental Biology*, vol. 30, pp. 174–180, 2014.

[35] S. Masri, M. Cervantes, and P. Sassone-Corsi, "The circadian clock and cell cycle: interconnected biological circuits," *Current Opinion in Cell Biology*, vol. 25, no. 6, pp. 730–734, 2013.

[36] D. L. Myster and R. J. Duronio, "To differentiate or not to differentiate?," *Current Biology*, vol. 10, no. 8, pp. R302–R304, 2000.

[37] M. Kwon, J. M. Kim, K. Lee et al., "Synchronized cell cycle arrest promotes osteoclast differentiation," *International Journal of Molecular Sciences*, vol. 17, no. 8, p. 1292, 2016.

[38] A. C. Bharti, Y. Takada, S. Shishodia, and B. B. Aggarwal, "Evidence that receptor activator of nuclear factor (NF)-κB ligand can suppress cell proliferation and induce apoptosis through activation of a NF-κB-independent and TRAF6-dependent mechanism," *The Journal of Biological Chemistry*, vol. 279, no. 7, pp. 6065–6076, 2004.

[39] T. Ogasawara, M. Katagiri, A. Yamamoto et al., "Osteoclast differentiation by RANKL requires NF-kappaB-mediated downregulation of cyclin-dependent kinase 6 (Cdk6)," *Journal of Bone and Mineral Research*, vol. 19, no. 7, pp. 1128–1136, 2004.

[40] T. Mizoguchi, A. Muto, N. Udagawa et al., "Identification of cell cycle-arrested quiescent osteoclast precursors in vivo," *The Journal of Cell Biology*, vol. 184, no. 4, pp. 541–554, 2009.

[41] A. Musacchio and E. D. Salmon, "The spindle-assembly checkpoint in space and time," *Nature Reviews. Molecular Cell Biology*, vol. 8, no. 5, pp. 379–393, 2007.

[42] M. M. Hahn, L. Vreede, S. A. S. A. Bemelmans et al., "Prevalence of germline mutations in the spindle assembly checkpoint gene BUB1B in individuals with early-onset colorectal cancer," *Genes, Chromosomes & Cancer*, vol. 55, no. 11, pp. 855–863, 2016.

[43] E. Myslinski, M. A. Gerard, A. Krol, and P. Carbon, "Transcription of the human cell cycle regulated BUB1B gene requires hStaf/ZNF143," *Nucleic Acids Research*, vol. 35, no. 10, pp. 3453–3464, 2007.

[44] C. Xie, C. Powell, M. Yao, J. Wu, and Q. Dong, "Ubiquitin-conjugating enzyme E2C: a potential cancer biomarker," *The International Journal of Biochemistry & Cell Biology*, vol. 47, pp. 113–117, 2014.

[45] G. Liu, J. Zhao, B. Pan, G. Ma, and L. Liu, "UBE2C overexpression in melanoma and its essential role in G2/M transition," *Journal of Cancer*, vol. 10, no. 10, pp. 2176–2184, 2019.

[46] O. I. Kahn, V. Sharma, C. Gonzalez-Billault, and P. W. Baas, "Effects of kinesin-5 inhibition on dendritic architecture and microtubule organization," *Molecular Biology of the Cell*, vol. 26, no. 1, pp. 66–77, 2015.

[47] L. Liu, X. Liu, M. Mare et al., "Overexpression of Eg5 correlates with high grade astrocytic neoplasm," *Journal of Neuro-Oncology*, vol. 126, no. 1, pp. 77–80, 2016.

[48] M. Hetzer, D. Bilbao-Cortes, T. C. Walther, O. J. Gruss, and I. W. Mattaj, "GTP hydrolysis by Ran is required for nuclear envelope assembly," *Molecular Cell*, vol. 5, no. 6, pp. 1013–1024, 2000.

[49] F. Schmit, M. Korenjak, M. Mannefeld et al., "LINC, a human complex that is related to pRB-containing complexes in invertebrates regulates the expression of G2/M genes," *Cell Cycle*, vol. 6, no. 15, pp. 1903–1913, 2007.

[50] D. Pan, Y. Chen, Y. Du, Z. Ren, X. Li, and B. Hu, "Methylation of promoter of RBL1 enhances the radioresistance of three dimensional cultured carcinoma cells," *Oncotarget*, vol. 8, no. 3, pp. 4422–4435, 2017.

[51] D. Grun and A. van Oudenaarden, "Design and analysis of single-cell sequencing experiments," *Cell*, vol. 163, no. 4, pp. 799–810, 2015.

[52] Y. Wang and N. E. Navin, "Advances and applications of single-cell sequencing technologies," *Molecular Cell*, vol. 58, no. 4, pp. 598–609, 2015.

Research Article

Physiological Acclimatization of the Liver to 180-Day Isolation and the Mars Solar Day

Hailong Chen [iD],[1] **Ke Lv,**[1] **Guohua Ji,**[1] **Yanhong Yuan,**[1] **Liang Lu,**[1] **Fengji Liang,**[1] **Kai Li,**[1] **Zi Xu,**[2] **Jianghui Xiong,**[1] **Lina Qu** [iD],[1] **and Yinghui Li** [iD][1]

[1]*State Key Laboratory of Space Medicine Fundamentals and Application, China Astronaut Research and Training Center, 26 Beiqing Road, Haidian District, Beijing, China*
[2]*Department of health technology research and development, SPACEnter Space Science and Technology Institute (Shenzhen), 4 Shamiao Road, Pingdi Street, Longgang District, Shenzhen 518117, China*

Correspondence should be addressed to Lina Qu; linaqu@263.net and Yinghui Li; yinghuidd@vip.sina.com

Physiological changes in humans are evident under environmental conditions similar to those on a Mars mission involving both a space factor (long-term isolation) and a time factor (the Mars solar day). However, very few studies have investigated the response of the liver to those conditions. Serum protein levels, bilirubin levels, aminotransferase activities, blood alkaline phosphatase, gamma-glutamyltransferase, lipid levels, and serum cytokines interleukin-6 and interferon-γ levels were analyzed 30 days before the mock mission; on days 2, 30, 60, 75, 90, 105, 120, 150, and 175 of the mission; and 30 days after the mission, in four subjects in 4-person 180-day Controlled Ecological Life Support System Experiment. Serum protein levels (total protein and globulin) decreased and bilirubin increased under the isolation environment from day 2 and exhibited chronic acclimatization from days 30 to 175. Effects of the Mars solar day were evident on day 75. Blood lipid levels were somewhat affected. No obvious peak in any enzyme level was detected during the mission. The change tendency of these results indicated that future studies should explore whether protein parameters especially globulin could serve as indicators of immunological function exposure to the stress of a Mars mission.

1. Introduction

During a future manned mission to Mars, long-term isolation [1] and the Mars solar day [2] will be major stressors of astronauts. Long-term isolation impairs sleep, mood, and alertness [3]; compromises muscle strength [4]; induces changes in stress hormone levels and glucose metabolism [5, 6]; weakens the extent of healthy qi; triggers a free-fall in "Gan" (liver) failure; and disrupts the relationship between "Gan" and "Wei" (the stomach) [7]. The human circadian system evolved to synchronize strictly to the 24 h Earth day, but must entrain to the Mars solar day, almost 40 min longer than the Earth day, during a Mars mission [2]. Failure to entrain to the Mars solar day over several days will disrupt sleep; compromise endocrine phys-

iology; impair cognition, alertness, mood, and vigilance; and predispose to poor performance [8–11]. The liver, a complex multifunctional organ, maintains bodily homeostasis [12], regulates substance and energy metabolism [13], and plays a front-line role in removing microbial components and toxins from portal blood [14]. However, the response of protein as well as bilirubin to long-term isolation, and the Mars solar day has not been characterized. To investigate changes in human liver function under such conditions, we evaluated human liver function markers in four subjects in the Controlled Ecological Life Support System (CELSS) experiment, which commenced in June 2016 to explore physiological, psychological, and behavioral changes during long-term isolation and exposure to the Mars solar day [15].
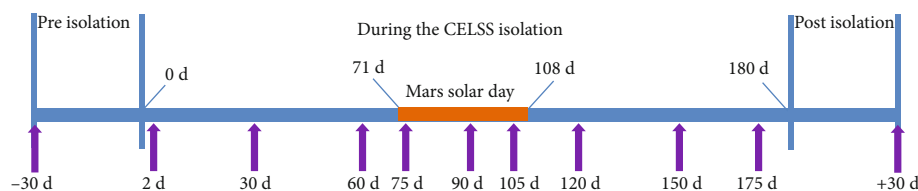
FIGURE 1: Experiment timeline and serum collecting time points.

2. Materials and Methods

2.1. Subjects and Experiments.
Four subjects (three males and one female, aged 29–43 years) participated in 4-person 180-day CELSS Experiment at the SPACEnter Space Science and Technology Institute (Shenzhen, China) from June to December 2016; this featured 180 days of isolation and a Mars solar day from $10:30$ PM on day 71 to $10:30$ PM on day 108. The CELSS featured six cabins. A cabin for crew and life support system facilitated daily work, cooking, and sleeping, and a cabin for resource system was used to dispose of nonedible plant materials and to produce CO_2, and four Greenhouses used to cultivate 25 kinds of plants including wheat, potatoes, sweet potatoes, soybeans, peanuts, lettuce, cabbage, edible amaranth, cherry radish, tomatoes, and strawberries. The indoor air of each cabin was usually not ventilated, but was when the oxygen ratio became lower than 19.0% or the CO_2 level lower than 500 ppm. The subjects and experimental environment have been described in detail elsewhere [15, 16].

2.2. Sample Collection and Storage.
Serum were collected from the four (fasting) subjects 30 days before the mission (−30d); on days 2, 30, 60, 75, 90, 105, 120, 150, and 175 during the mission (2d, 30d, 60d, 75d, 90d, 105d, 120d, 150d, 175d); and 30 days after the mission (+30d) (Figure 1). There was no smoking or alcohol consumption in the four subjects. Food, physical activity, temperature, and wakefulness cycle were all controlled well before each blood collection. All samples were stored at −80°C prior to analysis.

2.3. Measurement of Proteins, Enzymes, Bilirubins, and Lipids.
The serum levels of total protein (TP), albumin (ALB), and globulin (GLB); the activities of alanine aminotransferase (ALT), aspartate aminotransferase (AST), alkaline phosphatase (ALP), and gamma-glutamyltransferase (GGT); and the levels of bilirubin (BIL), total bilirubin (TBIL), direct bilirubin (DBIL), indirect bilirubin (IBIL), and total triglycerides (TG) were measured. The levels of total cholesterol (TC), high-density lipoprotein cholesterol (HDL-C), and low-density lipoprotein cholesterol (LDL-C) were analyzed via the hexokinase method using a Hitachi 7600 Autoanalyzer (Hitachi Ltd., Tokyo, Japan).

2.4. Detection of Serum IL-6 and IFN-γ.
The serum level of interleukin-6 (IL-6) was detected with enzyme-linked immunosorbent assay (ELISA) Kit (R&D, D6050, USA) and that of interferon-γ (IFN-γ) was detected with ELISA Kit (R&D, DIF50, USA).

2.5. Data Analysis.
Data are presented as mean ± SEM. The small sample (four subjects) with mixed gender (three males and one female) limited the utility of statistical tests, so we only use average value to locate the difference in those time points and provide descriptive statistics and descriptive analyses.

3. Results

3.1. Protein Levels.
The tendency of average total protein (TP) and globulin (GLB) levels was lower from 2d to 60d (minimum value was 88% or 62% of that on −30d, respectively), recovered to −30d levels by 75d, and lower again from 90d onwards (86% or 70% of that on −30d, respectively). However, the ALB level remained constant before, during, and after the mission, except for brief rises on 2d (1.1 fold of that on −30d) and 75d (1.1 fold of that on -30d). Therefore, the changes in the ALB to GLB (A/G) ratios showed exactly the opposite tendency in contrast with the observed results in the TP and GLB levels: the ratio was very high on 2d (1.8 fold of that on −30d), relatively lower on 75d, and relatively higher from 90d onwards (1.3 fold of that on −30d) (Figures 2(a)–2(d)).

3.2. Bilirubin Levels.
The tendency of average total bilirubin (TBIL) level increased on 2d (to 2.3-fold −30d level) and 175d (to 1.6-fold −30d level). The direct bilirubin (DBIL) and indirect bilirubin (IBIL) levels exhibited similar changes (Figure 2(e)).

3.3. Serum Aminotransferase Activities.
Tendency of alanine aminotransferase (ALT) activity was decreased from 105d to 150d (minimum value was 65% of that on −30d), but was reactivated on +30d (to 1.5-fold that on −30d). Similarly, aspartate aminotransferase (AST) activity was reduced on 30d, 105d, and 150d during the mission (minimum value was 73% of that on −30d), but then rose to the level of −30d. The AST to ALT (AST/ALT) ratio did not change during or after the mission (Figures 3(a) and 3(b)).

3.4. Serum ALP and GGT Activities.
Similar to the AST activity, the alkaline phosphatase (ALP) activity fell on 30d and after 90d; the minimum level was 68.9% that on −30d. Gamma-glutamyltransferase (GGT) activity was also low on 30d, 120d, and 175d (minimum value was 75% of that on −30d) (Figures 3(c) and 3(d)).

3.5. Blood Lipid Levels.
Except for a low total triglycerides (TG) concentration on 120d (86% of that on −30d) and high-density lipoprotein cholesterol (HDL-C) level on +30d
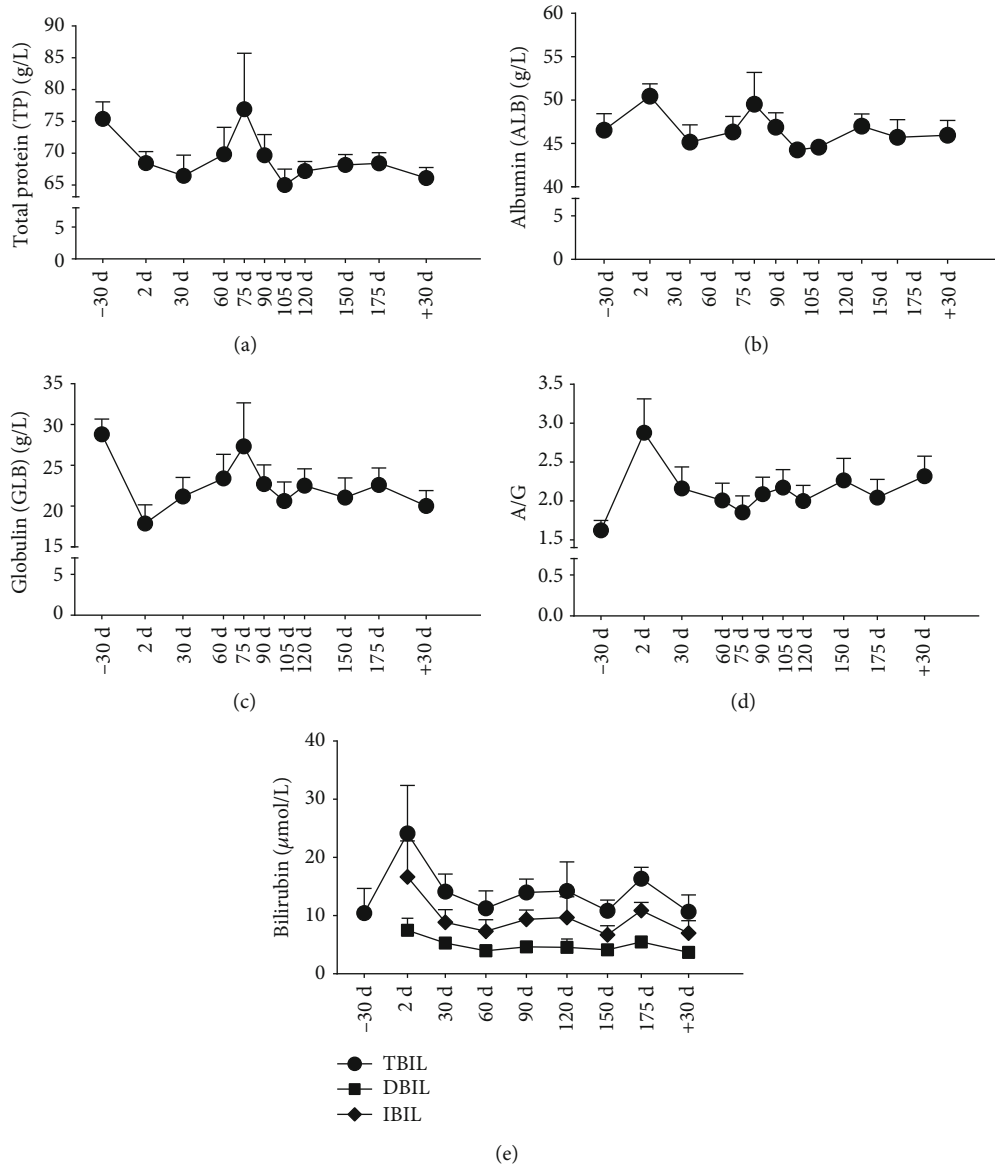
FIGURE 2: Protein and bilirubin levels. (a) TP; (b) ALB; (c) GLB; (d) A/G; (e) TBIL, DBIL, and IBIL; Data are expressed as means ± SEM.

(1.2 fold of that on −30d), we found no change in blood lipid levels during or after the mission (Figure 4).

3.6. Serum IL-6 and IFN-γ Levels. Both of them decreased from 2d to 60d (minimum value was 49% or 93% of that on −30d, respectively), recovered to −30d levels by 75d (for interleukin-6 (IL-6)) or by 90d (for interferon-γ (IFN-γ)), and decreased again after 90d (60% of that on −30d for IL-6) or on 105d (61% of that on −30d for IFN-γ) (Figure 5).

4. Discussion

We found that both protein and bilirubin level changes under long-term (180-day) isolation might reflect the probable adaptation to isolation. Initial effects were followed by a recovery toward baseline; this persisted for a short time, followed by chronic acclimatization to a new steady state. We found decreases in TP and GLB levels, but increases in

ALB and BIL levels and the A/G ratio, on day 2; blood homeostasis, in terms of both protein and bilirubin levels, was changed. These functions then rapidly recovered. However, long-term isolation (from day 30 to 175) was associated with new steady-state levels (between the normal and initial levels). Similar effects were evident for blood lipids (TG, TC, HDL-C, or LDL-C). The observed "initial effects–recovery–chronic acclimatization" process is similar to the effect of gravity on circadian timing [17].

The intrinsic human circadian period averages 24.2 h [18, 19], about 0.45 h less than the Mars solar day (24.67 h). Protein levels such as TP, ALB, and GLB rose and triggered effects exposure to the Mars solar day. However, the human circadian period can entrain to the Mars solar day, avoiding disturbance of the circadian rhythm, which can impair sleep, alertness, mood, and cognitive function [8, 9, 20]. We used fluorescent lamps in the six cabins and LED lamps [15, 16] to assist entrainment to the Mars
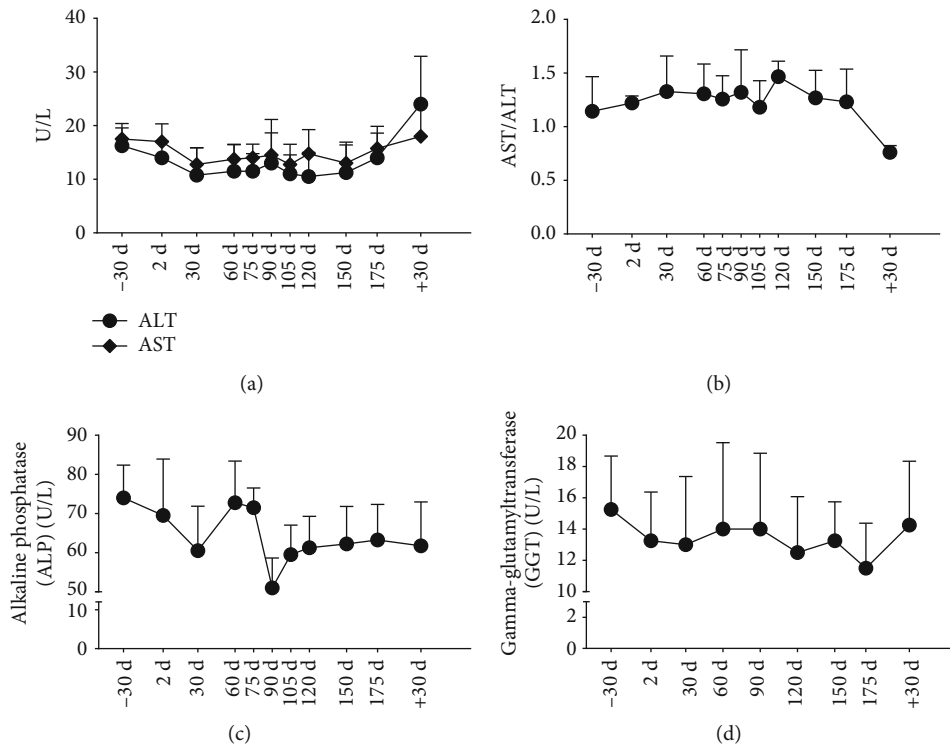
Figure 3: Enzymes. (a) ALT and AST; (b) AST/ALT; (c) ALP; (d) GGT. Data are expressed as means ± SEM. Presentation of results for ALT and AST with 8 time points has been permitted by *Frontiers in Physiology*.
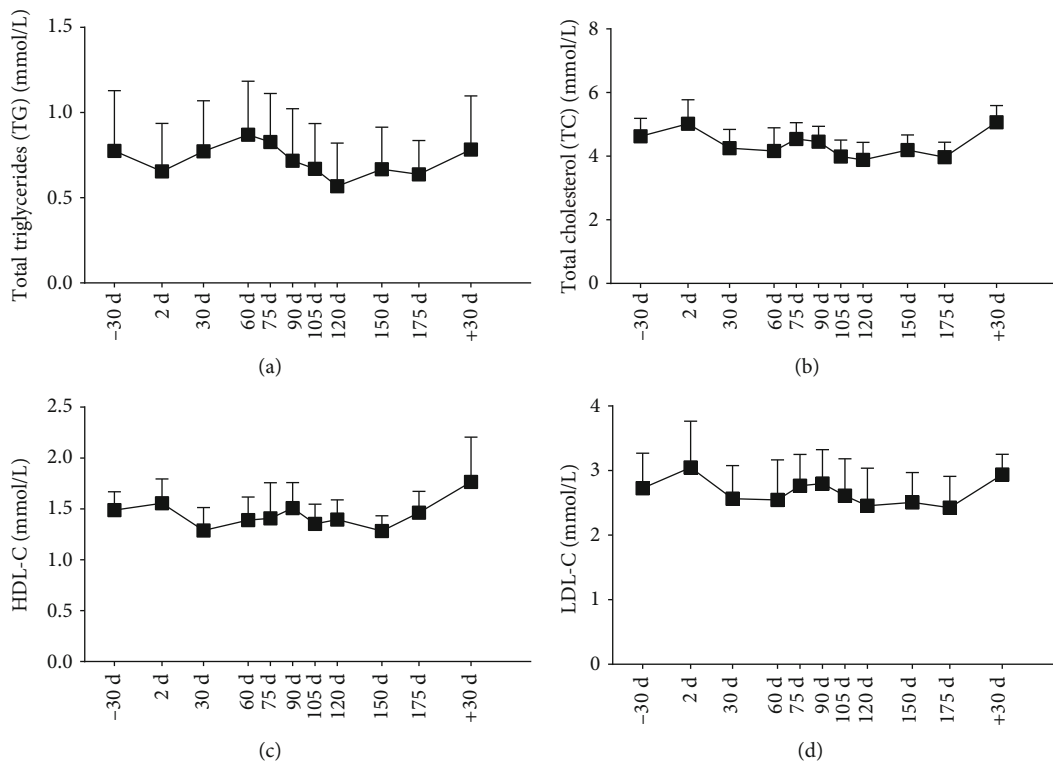

Figure 4: Blood lipid levels. (a) TG; (b) TC; (c) HDL-C; (d) LDL-C. Data are expressed as means ± SEM. Presentation of results for lipids with 8 time points has been permitted by *Frontiers in Physiology*.
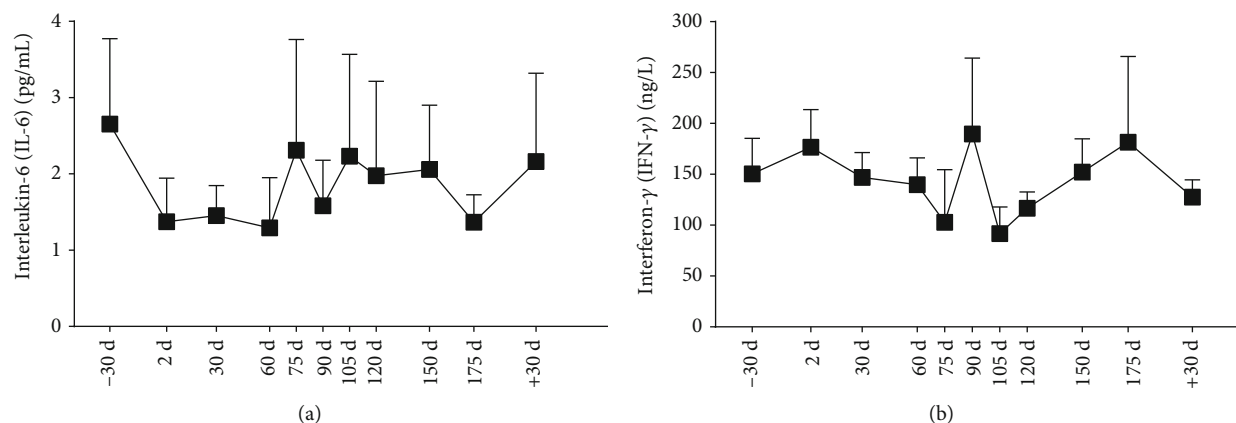
Figure 5: Serum IL-6 and IFN-γ levels. (a) IL-6; (b) IFN-γ. Data are expressed as means ± SEM.

solar day, and the effects on protein levels disappeared soon after day 75 of the mission.

A reduction in GLB level and an increase in the A/G ratio are indicators of poor immunological status and high susceptibility to infection. As a decrease in GLB level and a high A/G ratio were observed during the mission, the immunological profile may diverge from that characteristic of life on Earth. A prior report found a decrease in leukocyte numbers and increases in lymphocyte and monocyte numbers during 131 days of isolation [21].

To verify the relationship between GLB change and immunological function, we detected the serum IL-6 and IFN-γ levels and found that IL-6 change was consistent with the change of GLB. It was reported that IL-6 could promote GLB production and in particular regulate immunoglobulin synthesis through facilitating T-follicular helper-cell differentiation and IL-21 production [22, 23]. In addition, ALB could be used to predict the prognosis of cancer patients. Patients with high A/G ratio have better survival than patients with low A/G ratio [23]. Moreover, as both proinflammatory and anti-inflammatory cytokine, IL-6 might probably predominantly present anti-inflammatory effect opposite to that of IFN-γ. This intriguing phenomenon needs to be further studied.

Hepatocyte enzymes such as ALT and AST are released into the bloodstream when hepatocytes are injured or cell membrane integrity is compromised. Therefore, high serum ALT or AST activity levels reflect liver damage [24]. The serum activities of ALT, AST, ALP, and GGT did not change during the mission; thus, neither 180-day isolation nor the Mars solar day caused liver damage. Unexpectedly, ALT was activated on day +30, possibly associated with a burdensome postmission task.

A recent short-term study found no obvious changes in neurophysiological, neuropsychological, or cognitive function during 30 days of isolation [25]. However, this does not indicate that behavioral, psychological, physiological, and/or biochemical changes will not develop during long-term isolation (>100 days). Further research is needed.

Yuan et al. [26] showed that body weight decreased (mainly lean mass) on the 6th month during the isolation environment. We found that concentration of TP as well as

GLB also reduced on 175th day. This suggested that the change of protein level was in accordance with that of lean mass, which may be multiple factors including isolation, diet, workload, and training. However, there may be no relationship between lipid change and fat mass change, because fat mass was without clear trends under isolation station, as shown in the results of Yuan et al.

A limitation of the study is that we included only four subjects. We thus lack data of proteins, bilirubins, and lipids on a large sample and only give a descriptive analysis for the change tendency instead of statistical analysis. Additionally, we did not measure BIL concentration or GGT activity on day 75 of the mission, as the samples were lost. Another limitation is that we did not investigate the daily rhythmic changes of the proteins, bilirubins, enzymes, and lipids during Earth solar day and Mars solar day.

In summary, this study provides useful insights into how the protein and bilirubin react to long-term isolation and the Mars solar day. Our findings will contribute to planning a manned Mars mission. Future studies are required to clarify whether protein and bilirubin parameters especially GLB can serve as indicators of immunological function changes during a prolonged Mars mission.

Data Availability

All data are available.

Ethical Approval

All procedures involving human participants were in accordance with the ethical standards of the China Astronaut Research and Training Center Medical Ethics Committee and those of the 1964 Helsinki declaration and later amendments or comparable ethical standards. All volunteers provided written informed consent prior to participation in the experiment.

Consent

Informed consent was obtained from all participants in the study.

Conflicts of Interest

No author has any conflict of interest.

Authors' Contributions

Hailong Chen and Ke Lv equally contributed to this work.

Acknowledgments

References

[1] L. A. Palinkas, "Psychosocial issues in long-term space flight: overview," *Gravitational and Space Research*, vol. 14, no. 2, p. 14, 2007.

[2] L. K. Barger, J. P. Sullivan, A. S. Vincent et al., "Learning to live on a Mars day: fatigue countermeasures during the Phoenix Mars Lander mission," *Sleep*, vol. 35, no. 10, pp. 1423–1435, 2012.

[3] M. Basner, D. F. Dinges, D. J. Mollicone et al., "Psychological and behavioral changes during confinement in a 520-day simulated interplanetary mission to mars," *PLoS One*, vol. 9, no. 3, article e93298, 2014.

[4] C. J. Gaffney, E. Fomina, D. Babich, V. Kitov, K. Uskov, and D. A. Green, "The effect of long-term confinement and the efficacy of exercise countermeasures on muscle strength during a simulated mission to Mars: data from the Mars500 study," *Sports Medicine - Open*, vol. 3, no. 1, 2017.

[5] F. Strollo, G. Vassilieva, M. Ruscica et al., "Changes in stress hormones and metabolism during a 105-day simulated Mars mission," *Aviation, Space, and Environmental Medicine*, vol. 85, no. 8, pp. 793–797, 2014.

[6] F. Strollo, C. Macchi, I. Eberini et al., "Body composition and metabolic changes during a 520-day mission simulation to Mars," *Journal of Endocrinological Investigation*, vol. 41, no. 11, pp. 1267–1273, 2018.

[7] H.-z. Shi, Q.-c. Fan, J.-y. Gao et al., "Evaluation of the health status of six volunteers from the Mars 500 project using pulse analysis," *Chinese Journal of Integrative Medicine*, vol. 23, no. 8, pp. 574–580, 2017.

[8] K. P. Wright Jr., R. Hughes, R. E. Kronauer, D. J. Dijk, and C. A. Czeisler, "Intrinsic near-24-h pacemaker period determines limits of circadian entrainment to a weak synchronizer in humans," *Proceedings of the National Academy of Sciences of the United States of America*, vol. 98, no. 24, pp. 14027–14032, 2001.

[9] K. P. Wright Jr., J. T. Hull, R. J. Hughes, J. M. Ronda, and C. A. Czeisler, "Sleep and wakefulness out of phase with internal biological time impairs learning in humans," *Journal of Cognitive Neuroscience*, vol. 18, no. 4, pp. 508–521, 2006.

[10] F. A. J. L. Scheer, K. P. Wright, R. E. Kronauer, and C. A. Czeisler, "Plasticity of the intrinsic period of the human circadian timing system," *PLoS One*, vol. 2, no. 8, article e721, 2007.

[11] C. Gronfier, K. P. Wright, R. E. Kronauer, and C. A. Czeisler, "Entrainment of the human circadian pacemaker to longer-than-24h days," *Proceedings of the National Academy of Sciences of the United States of America*, vol. 104, no. 21, pp. 9081–9086, 2007.

[12] S. Ghosh, C. Kruger, S. Wicks et al., "Short chain acyl-CoA dehydrogenase deficiency and short-term high-fat diet perturb mitochondrial energy metabolism and transcriptional control of lipid-handling in liver," *Nutrition & Metabolism*, vol. 13, no. 1, p. 17, 2016.

[13] L. D. Fonseca, J. P. Eler, M. A. Pereira et al., "Liver proteomics unravel the metabolic pathways related to feed efficiency in beef cattle," *Scientific Reports*, vol. 9, no. 1, p. 5364, 2019.

[14] A. Abu-Shanab and E. M. Quigley, "The role of the gut microbiota in nonalcoholic fatty liver disease," *Nature Reviews Gastroenterology & Hepatology*, vol. 7, no. 12, pp. 691–701, 2010.

[15] Z. Xu, Q. N. Yu, L. C. Zhang, J. H. Xiong, W. D. Ai, and L. N. Qu, "Overview of 4-person 180-day integrated experiment in controlled ecological life support system," *Space Medicine & Medical Engineering*, vol. 31, no. 2, pp. 264–272, 2018.

[16] K. Dai, Q. Yu, Z. Zhang, Y. Wang, and X. Wang, "Aromatic hydrocarbons in a controlled ecological life support system during a 4-person-180-day integrated experiment," *Science of The Total Environment*, vol. 610-611, pp. 905–911, 2018.

[17] C. A. Fuller, T. M. Hoban-Higgins, D. W. Griffin, and D. M. Murakami, "Influence of gravity on the circadian timing system," *Advances in Space Research*, vol. 14, no. 8, pp. 399–408, 1994.

[18] C. A. Czeisler, J. F. Duffy, T. L. Shanahan et al., "Stability, precision, and near-24-hour period of the human circadian pacemaker," *Science*, vol. 284, no. 5423, pp. 2177–2181, 1999.

[19] J. F. Duffy, S. W. Cain, A. M. Chang et al., "Sex difference in the near-24-hour intrinsic period of the human circadian timing system," *Proceedings of the National Academy of Sciences of the United States of America*, vol. 108, Supplement 3, pp. 15602–15608, 2011.

[20] C. Gronfier, K. P. Wright, R. E. Kronauer, and C. A. Czeisler, "Entrainment of the human circadian pacemaker to longer-than-24-h days," *Proceedings of the National Academy of Sciences of the United States of America*, vol. 104, no. 21, pp. 9081–9086, 2007.

[21] G. Sonnenfeld, J. Measel, M. R. Loken et al., "Effects of isolation on interferon production and hematological and immunological parameters," *Journal of Interferon Research*, vol. 12, no. 2, pp. 75–81, 1992.

[22] T. Tanaka, M. Narazaki, and T. Kishimoto, "IL-6 in inflammation, immunity, and disease," *Cold Spring Harbor Perspectives in Biology*, vol. 6, no. 10, p. a016295, 2014.

[23] M. Gundog and H. Basaran, "Pretreatment low prognostic nutritional index and low albumin-globulin ratio are predictive for overall survival in nasopharyngeal cancer," *European Archives of Oto-Rhino-Laryngology*, vol. 276, no. 11, pp. 3221–3230, 2019.

[24] M. L. G. M. L. de Araujo, G. G. P. de Carvalho, M. C. C. Ayres et al., "Assessment of the metabolic, protein, energy, and liver profiles of lambs finished in a feedlot and receiving diets containing groundnut cake," *Tropical Animal Health and Production*, vol. 46, no. 2, pp. 433–437, 2014.

[25] J. Weber, F. Javelle, T. Klein et al., "Neurophysiological, neuro-psychological, and cognitive effects of 30 days of isolation," *Experimental Brain Research*, vol. 237, no. 6, pp. 1563–1573, 2019.

[26] M. Yuan, M. A. Custaud, Z. Xu et al., "Multi-system adaptation to confinement during the 180-day controlled ecological life support system (CELSS) experiment," *Frontiers in Physiology*, vol. 10, p. 575, 2019.

Research Article

The Potential Regulatory Roles of lncRNAs in DNA Damage Response in Human Lymphocytes Exposed to UVC Irradiation

Dan Xu (ID)**, Yue Wang, Jia Wang, Fei Qi, and Yeqing Sun**

Institute of Environmental Systems Biology, College of Environmental Science and Engineering, Dalian Maritime University, Dalian, Liaoning, Linghai Road 1, 116026, China

Correspondence should be addressed to Dan Xu; jotan1995@163.com

Long noncoding RNAs (lncRNAs) are a class of noncoding RNAs that modulate gene expression, thereby participating in the regulation of various cellular processes. However, it is not clear about the expression and underlying mechanism of lncRNAs in irradiation-induced DNA damage response. In the present study, we performed integrative analysis of lncRNA-mRNA expression profile in human lymphocytes irradiated with ultraviolet-C (UVC). The results showed that exposure to UVC irradiation dose-dependently increased the fluorescence intensity of γ-H$_2$AX and induced cell death. Microarray analysis revealed that up-regulated lncRNAs were more common than down-regulated lncRNAs with the increase of radiation dose in UVC-radiated cells. Stem analysis demonstrated the relationship between lncRNA expression level and radiation dose. qPCR results confirmed that LOC338799 and its coexpressed genes such as LCE1F and ISCU showed the increase in expression levels with the increase of UVC radiation dose. We utilized Cytoscape to screen out 5 lncRNAs and 13 coexpressed genes linking to p53, which might participate in the regulation of DNA damage, cell cycle arrest, apoptosis, and cell death. These findings suggest that lncRNAs might play a role in UVC-induced DNA damage response through regulating expression of genes in p53 signaling pathway.

1. Introduction

Ultraviolet (UV) radiation belongs to the nonionizing part of the electromagnetic spectrum, which is subdivided into UVA (wavelengths 315-400 nm), UVB (280-315 nm), and UVC (200-280 nm). Recently, UVC radiation gained more attention because UVC has direct damaging effects to cellular DNA and results in DNA single- and double-strand breaks [1, 2]. Cellular DNA has a higher absorption peak at 260 nm within the UVC band, so UVC is often used as the easiest and fastest way to produce DNA damage. UVC can induce immediate DNA damage and energy-dependent biological effects in a variety of cells. It is reported that UVC radiation-induced DNA damage provoked highly divergent responses in human skin fibroblasts exposed to low (10 J/m^2) and high doses (50 J/m^2) of UVC radiation [3]. Another report showed that UVC could affect the transcriptional profile in human primary cultured fibroblasts irradiated with even a low dose (0.5 or 5 J/m^2) of UVC [4].

Cell viability and apoptosis of mouse embryonic fibroblasts were investigated after exposure to three doses (50, 75, and 300 J/m^2) of UVC radiation [5].

When cells are exposed to environmental stress, DNA damage often occurs and subsequently causes DNA-damage response (DDR) including cell cycle arrest, apoptosis, and DNA repair [6]. DNA damage can also result in cell death unless it is repaired or tolerated [7]. TP53 is one of the major regulators in DDR after irradiation, which can activate many downstream genes including p21WAF1/-CIP1 (CDKN1A), Bcl-2-Associated X Protein (BAX), Bcl-2-Binding Component 3 (BBC3), Cyclin Dependent Kinase 6 (CDK6), DNA Damage 45 alpha (GADD45A), and Late Cornified Envelope Group I (LCE1) family [8–12]. It is reported that most of p53 target genes together construct the p53 network in response to irradiation [13, 14]. Therefore, p53 signaling pathway is considered to be the most important pathway and a number of genes have been suggested to become potential radiation dosimeters [15].
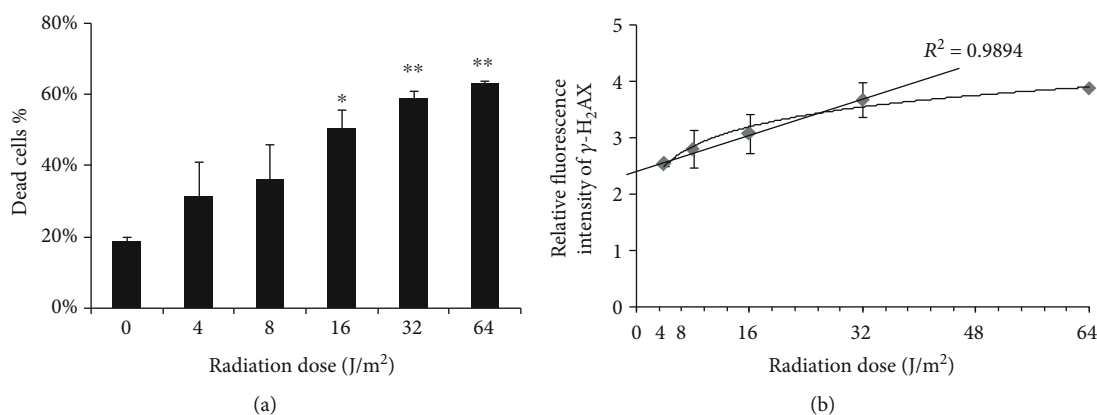
(a)

(b)

FIGURE 1: The effects of UVC on DNA damage and cell death in CD4 cells. (a) The percentage of dead cells was calculated in CD4 cells at 24 h after UVC irradiation. (b) The relative fluorescence intensity of γ-H$_2$AX was examined in CD4 cells at 30 min after UVC irradiation. The straight line indicates a linear relationship between the fluorescence intensity of γ-H$_2$AX and the radiation dose within the dose range of 4-32 J/m^2. The results are displayed as the mean $\pm$ SD ($n = 3$). $^*P < 0.05$, $^{**}P < 0.01$ compared with the control group.

Long noncoding RNAs (lncRNAs) are defined as RNA molecules longer than 200 nucleotides in length, which can modulate gene expression through a variety of mechanism [16]. A number of reports revealed that lncRNAs could affect not only gene expression but also protein translation and stability [17]. LncRNAs are less conserved in sequence and only about 12% of lncRNAs can be found other than humans. Deep sequencing recently has been utilized to discover novel lncRNAs. LincRNA-p21 is first identified as a direct transcriptional target of p53. The induction of lincRNA-21 by UVB irradiation was primarily through a p53-dependent pathway and had a proapoptotic function in keratinocytes [18]. It is reported that HULC promoted UVB-induced cell injury via the activation of JAK/STAT (1/3) signaling pathway in HaCaT cells [19]. HOTAIR resulted in apoptosis and inflammation in UVB-exposed keratinocytes [20]. However, it is not clear about the expression and underlying mechanism of lncRNAs in DDR induced by UVC irradiation.

Human lymphocytes have been widely used in the field of radiation research about DNA damage. We select human CD4$^+$ T lymphocytes (CD4) because they are nucleated cells and easily separated from human blood. Here, we aimed to study the dose-dependent expression changes of lncRNAs in CD4 cells exposed to UVC irradiation. We performed coexpression network analysis of lncRNA-mRNA and revealed that novel lncRNAs might play a crucial role in DDR induced by UVC through p53 signaling pathway. Our study will provide important experimental guide for screening lncRNAs as new radiation dosimeters in the future.

2. Materials and Methods

2.1. Cell Culture and UVC Radiation. The human CD4$^+$ T lymphocytes (CD4) (ATCC, Manassas, VA) were cultured in RPMI 1640 Medium (GIBCO, Carlsbad, CA) containing 10% fetal bovine serum (GIBCO) and antibiotic in an incubator. CD4 cells were cultured in T25 flasks and passaged every 4 days.

CD4 cells were suspended in 1 ml culture medium, evenly covering with the bottom of 60 mm petri dish. The lid was open when cells were irradiated with 4-64 J/m^2 UVC light (0.11 J/m^2/s at 254 nm) in a dark box. Control cells were treated similarly with the exception that they did not undergo UVC irradiation. Subsequent to UVC exposure, the cells were placed in an incubator for indicated time until their use.

2.2. γ-H$_2$AX Fluorescence Assay. CD4 cells were untreated or radiated with UVC at different doses, and then cultured in an incubator for 30 min. Phosphorylated histone H$_2$AX (γ-H$_2$AX) was detected by γ-H$_2$AX Fluorescence Assay Kit according to the manufacturer's instructions (Upstate Biotechnology Inc., NY, USA). In brief, the cells were collected, fixed, permeabilized, and stained with FITC-conjugated antiphospho-histone H$_2$AX (Ser139). Cells are then scanned in a flow cytometer (BD Biosciences, San Jose, CA) to quantitate the number of cells staining positive for γ-H$_2$AX. The relative fluorescence intensity was used to reflect the appearance of γ-H$_2$AX in comparison to nonradiated samples.

2.3. Quantitative PCR (qPCR). Total RNA was extracted using the TRIzol reagent. The expression levels of mRNAs and lncRNAs were quantified by qPCR. Real-time PCR reactions were performed with SYBR Green Master Mix using a Light Cycler®48 II real-time PCR system (Applied Biosystems, CA). The primer sequences in qPCR were listed in Table. S1. The relative expression level was calculated using the comparative delta CT method ($2^{-\triangle\triangle Ct}$) after normalization with reference to the expression of GAPDH.

2.4. LncRNA-mRNA Microarray Analysis. After UVC irradiation, CD4 cells were placed in an incubator for 24 hours and then used for microarray analysis using Affymetrix Human HTA2.0. LncRNA-mRNA microarray analysis was supplied by Shanghai OE Biotechnology Company. The sample treatments were based on the manufacturer's standard protocols. The expression level of each lncRNA or mRNA was presented as fold change. Differentially expressed lncRNAs or mRNAs ($\geq$2-fold) were identified to be significant. A filtering
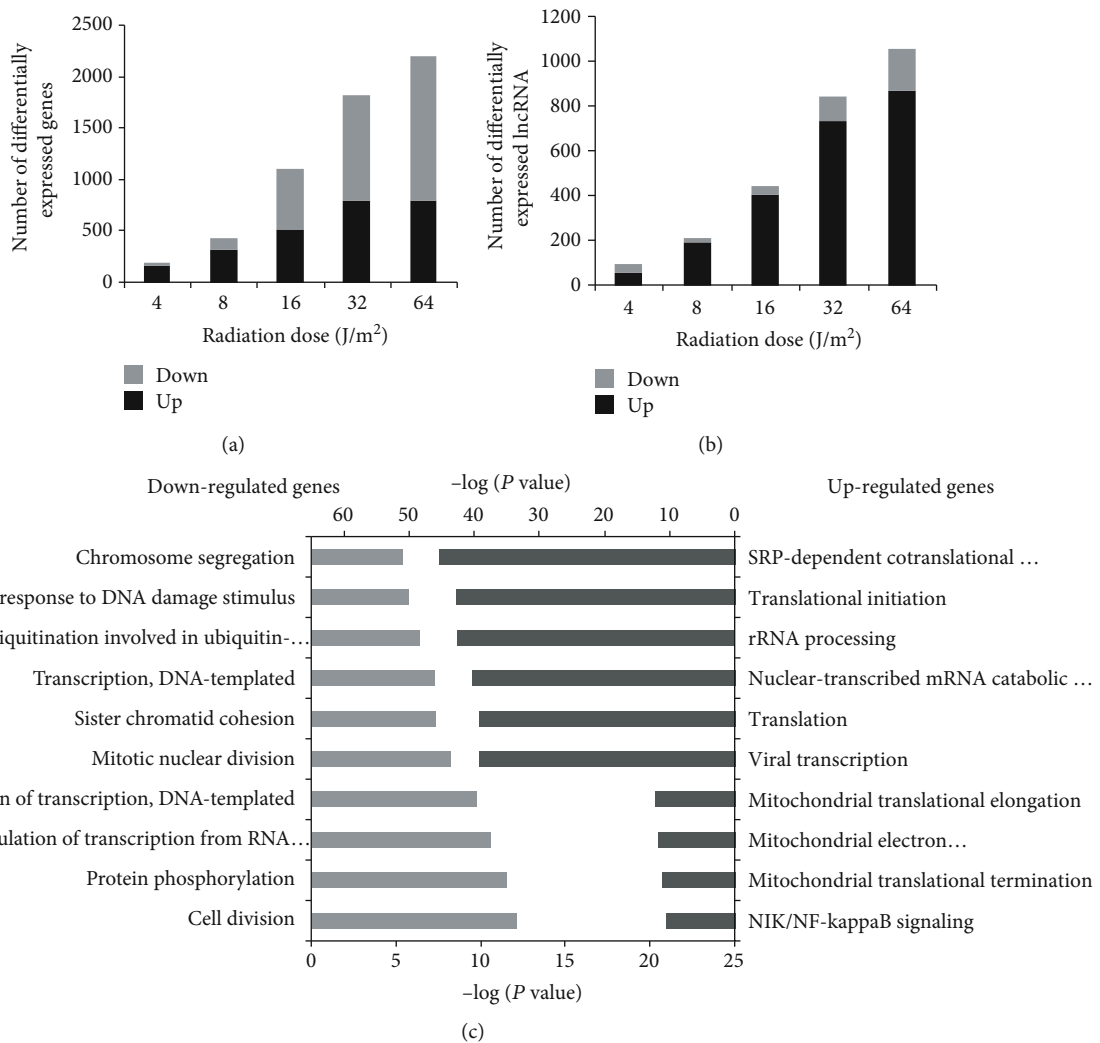
(a)

(b)

(c)

FIGURE 2: Microarray analysis of gene and lncRNA expression profiles under UVC irradiation. (a, b) The number of differentially expressed genes (a) and lncRNAs (b) was shown in the five radiation dose groups. (c) Function analysis of down-regulated genes and up-regulated genes.

step was applied to reduce the number of multiple hypotheses. Only those genes annotated with NM_numbers or ENST-numbers, and those lncRNAs annotated with NR_ numbers or ENST-numbers, were included in the final analysis.

2.5. Stem Analysis and Coexpression Analysis of lncRNA-mRNA. Stem analysis and coexpression analysis for lncRNA-mRNA were supplied by Shanghai OE Biotechnology Company. In stem analysis, differentially expressed genes or lncRNAs were divided into 30 categories and the upper left-hand digit of each small graph was the category number. No. 21 and No. 4 had significant differences (fold changes ≥2 and $P \leq 0.05$), whereas the others had no significant differences.

The Pearson correlation between expression value of each lncRNA and expression value of its coexpressed mRNA was calculated. When P value of the coefficient correlation was not higher than 0.05 and the absolute value of correlation was not less than 0.7, they were considered to be relevant.

The top 30 coexpressed mRNAs of each lncRNA were selected to discuss the regulatory relationship between lncRNA and coexpressed mRNA using Cytoscape 3.6.1 (https://cytoscape.org/) [21].

2.6. Statistical Analysis. All data are presented as means ± standard deviations (SD). Regression analysis and Student's T-test analysis were performed using SPSS version 17.0. $P < 0.05$ were considered statistically significant.

3. Results

3.1. Effect of UVC Irradiation on DNA Damage and Cell Death in CD4 Cells. We firstly identified that the optimal radiation dose range of UVC was 4-64 J/m^2, within which the percentage of dead cells was 30-70% in CD4 cells at 24 h after UVC irradiation. UVC irradiation caused cell death in a dose-dependent manner, showing the significant increase in the percentage of dead cells in the 16, 32, and 64 J/m^2 groups compared with the control group
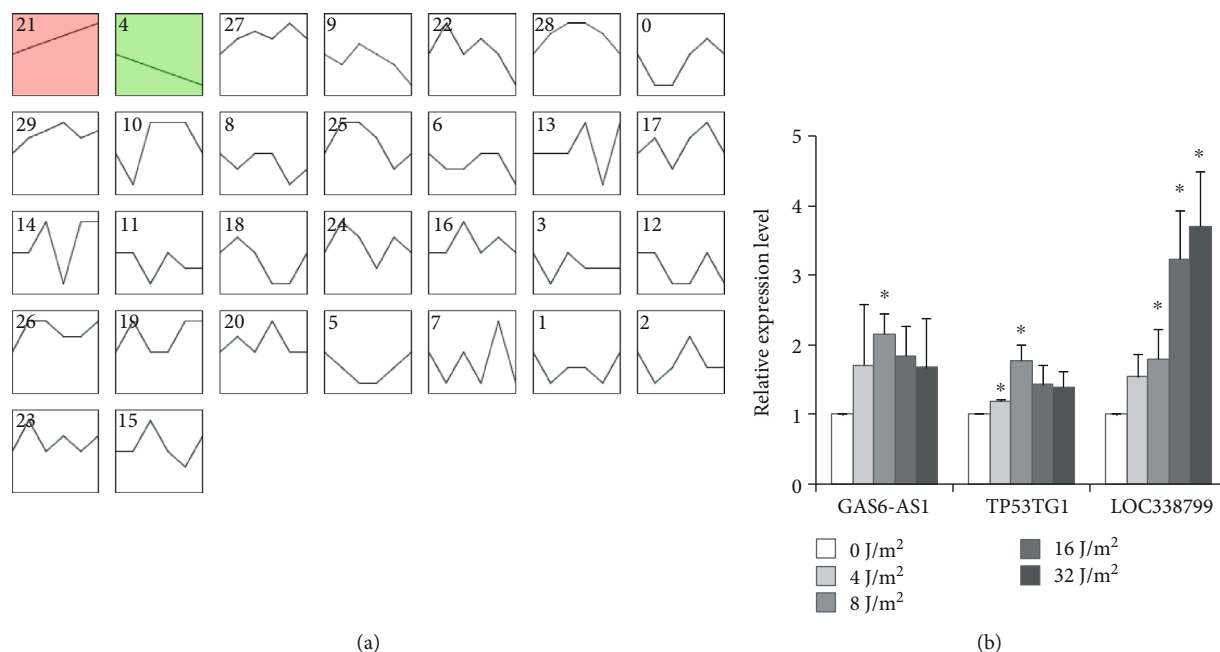
(a)

(b)

FIGURE 3: Stem analysis and validation of lncRNA expression alterations. (a) Differentially expressed lncRNAs are divided into 30 categories, and the category number No. 21 represents the expression of lncRNAs increased significantly with the increase of UVC radiation dose, No.4 represents the expression of lncRNAs decreased significantly with the increase of UVC radiation dose. (b) qPCR results confirmed the expression alterations of three lncRNAs in CD4 cells at 24 h after UVC irradiation. $^*P < 0.05$ compared with control group.

(Figure 1(a)). We then examined relative fluorescent intensity of γ-H$_2$AX in CD4 cells at 30 min after UVC radiation. The results showed that UVC radiation increased relative fluorescent intensity of γ-H$_2$AX in a dose-dependent manner. There was a linear relationship ($R^2 = 0.9894$) between the fluorescence intensity of γ-H$_2$AX and the radiation dose within the dose range of 4-32 J/m^2 (Figure 1(b)).

3.2. Effect of UVC Radiation on Differentially Expressed mRNA and lncRNAs.

We performed microarray analysis of gene and lncRNA expression profiles. The results showed that UVC radiation induced the increase in the number of differentially expressed genes and lncRNAs ($\geq$2-fold) in a dose-dependent manner (Figures 2(a) and 2(b)). The number of 2-5-fold up- or down-regulated genes (Table. S2) and lncRNAs (Table. S3) was listed in detail. We observed that there were much more up-regulated genes in lower dose groups and much more down-regulated genes in higher dose groups (Figure 2(a)). In contrast, most of lncRNAs were up-regulated in all UVC-radiated groups (Figure 2(b)). GO analysis showed that most of down-regulated genes function on cell division, protein phosphorylation, transcription, and cellular response to DNA damage stimulus. Those up-regulated genes may be involved in various translation processes (Figure 2(c)).

3.3. Relationship Analysis between Expression Alteration and Radiation Dose.

To observe the relationship between expression alteration of gene or lncRNA and radiation dose, we performed stem analysis. The results showed that the expression of 729 genes and 797 lncRNAs increased significantly with the increase of UVC radiation dose whereas 1372 genes and

133 lncRNAs showed the significant decrease in expression levels with the increase of UVC radiation dose (Fig. S1 and Figure 3(a)).

UV radiation is an environmental hazard and mutagen, leading to an increased risk of human cancers. We utilized lncRNA disease database, and found that three lncRNAs including GAS6 antisense RNA 1 (GAS6-AS1), TP53 target 1 (TP53TG1), and Telomerase RNA component (TERC) were known to be associated with human cancers [22–24]. qPCR results confirmed the up-regulation of GAS6-AS1 and TP53TG1 in 4-32 J/m^2 dose groups (Figure 3(b)), although the expression of TERC showed an increased trend with the increase of radiation dose without statistical significance (data not shown). Notably, the expression of LOC338799 increased significantly with the increase of UVC radiation dose whereas TP53TG1 expression showed the significant increase in 4 and 8 J/m^2 dose groups.

3.4. Coexpression Network Analysis of lncRNA-mRNA.

Each lncRNA had a positive or negative regulation relationship with coexpressed gene. We searched for some lncRNAs such as LOC338799, TERC, and USP17L6P from significantly up-regulated lncRNAs with the increase of UVC radiation dose, based on the results from stem analysis. We focused on LOC338799, which had positive regulation relationship with 20 genes while it had negative regulation relationship with 10 genes (Figure 4(a)). The up-regulation of LCE1F and ISCU showed an exponential trend with the increase of radiation dose (Figure 4(b)). qPCR results confirmed the up-regulation of LCE1F and ISCU in a dose-dependent manner within the dose range of 4-32 J/m^2 (Figure 4(c)). Similarly, we found that TERC had a positive regulation relationship with
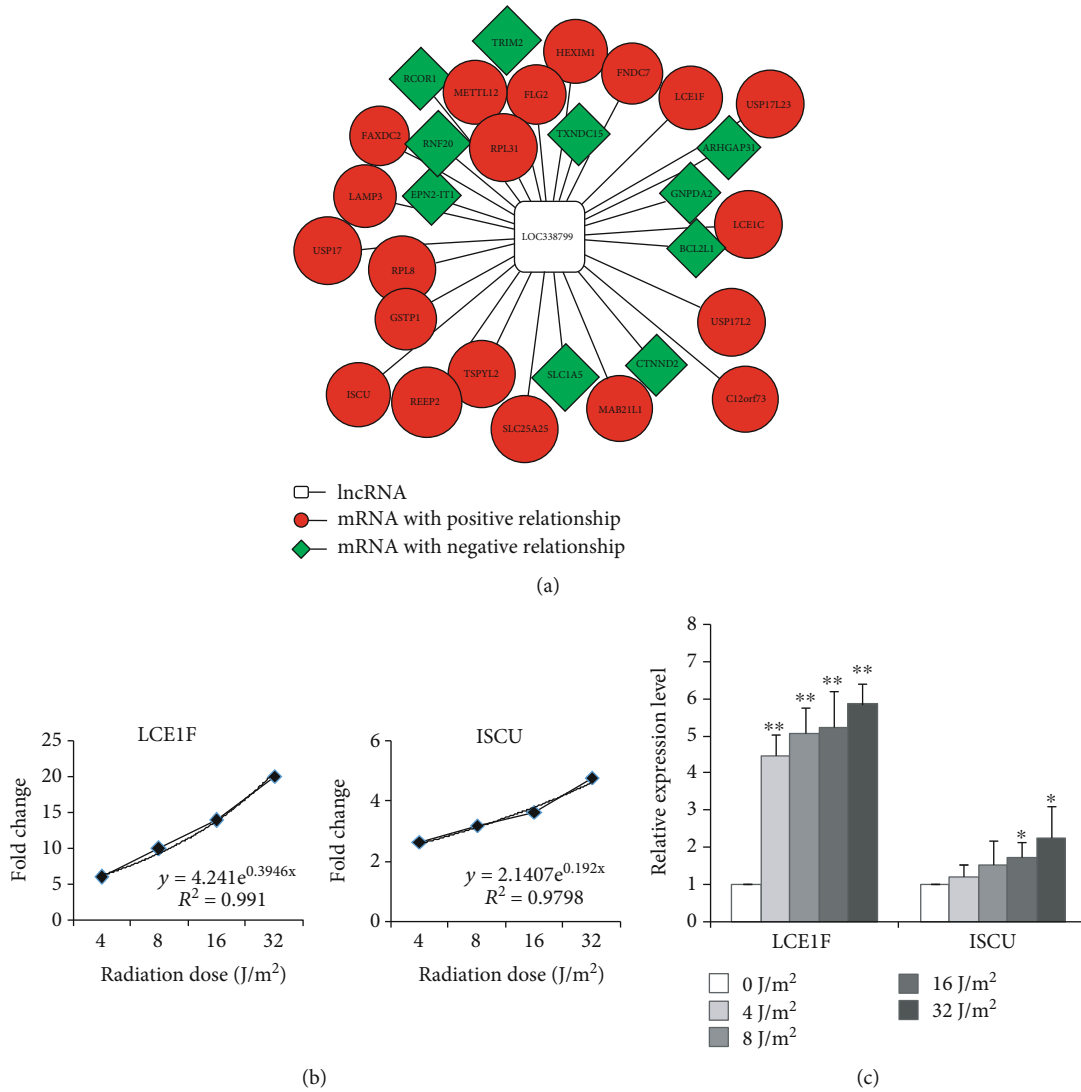
(a)

(b)

(c)

Figure 4: Regulation network of LOC338799 and coexpressed mRNAs. (a) LOC338799 has 30 coexpressed genes, including 20 positively regulated genes (red) and 10 negatively regulated genes (green). (b) Regression analyses of coexpressed genes LCE1F and ISCU show dose-dependent relationships between gene expression alteration and the radiation dose within the dose range of 4-32 J/m^2. (c) qRT-PCR results confirmed the expression alterations of LCE1F and ISCU in CD4 cells at 24 h after UVC irradiation. $^*P < 0.05$, $^{**}P < 0.01$ compared with the control group.

15 genes such as apoptotic regulator 1 (MOAP1) and eukaryotic translation initiation factor 3 subunit D (EIF3D) that were reported to regulate cell cycle, apoptosis, and cell death [25, 26]. USP17L6P had a positive regulation relationship with TP53-regulated inhibitor of apoptosis (TRIAP1) that was associated with apoptosis and cell death [27].

Further, Cytoscape were utilized for coexpression network analysis of lncRNA-mRNA. We wonder how many coexpressed genes of lncRNAs may be regulated by p53. We screened out 13 coexpressed genes of 5 lncRNAs, possibly involved in DDR via p53 signaling pathway (Figure 5). All the lncRNAs were up-regulated and most of the genes except CDK6 showed the increase in expression levels in UVC-radiated groups although the induction levels varied (Table 1). GAS6-AS1 had 4 coexpressed genes including GADD45A, MDM2, Tumor Protein P53 Inducible

Protein 3 (TP53I3), and inhibitor of DNA binding 3 (ID3). LOC338799 had 8 coexpressed genes including GADD45A, TP53I3, CDK6, BAX, CDKN1A, LCE1C, LCE1F, and ISCU. TRIAP1 is coexpressed gene of USP17L6P. TP53I3 and ID3 are coexpressed genes of LOC644656. qPCR results confirmed the up-regulation of CDKN1A, GADD45A, and TRIAP1 within the dose range of 4-32 J/m^2 (Fig. S2). Taken together, these genes may participate in the regulation of DDR including cell cycle arrest, DNA damage, cell death, and apoptosis.

4. Discussion

In the present study, we investigated the expression alterations of lncRNAs in human lymphocytes exposed to five doses of UVC radiation. We found that most of lncRNAs
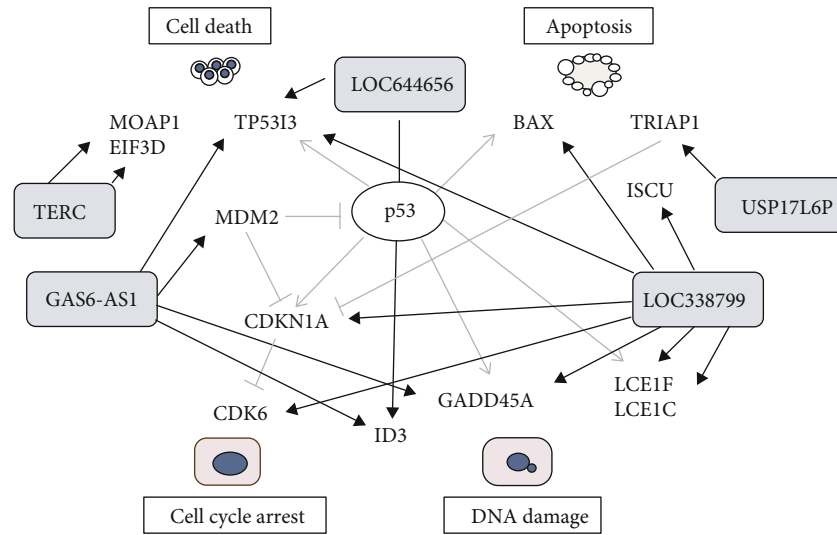
FIGURE 5: Regulatory network diagram of lncRNAs and coexpressed genes linking to p53. Regulatory network diagram of 5 lncRNAs and 13 coexpressed genes linking to p53 were constructed. They together play important roles in UVC-induced DDR including DNA damage, cell cycle arrest, cell death, and apoptosis.

TABLE 1: Coexpressed genes of lncRNAs function in DDR via p53 signaling pathway.

LncRNAs	Gene symbol	4	8	16 Fold change	32	64 (J/m^2)	Function
GAS6-AS1 LOC338799	**GADD45A**	2.28	2.54	1.86	2.08	1.47	DNA damage, cell cycle, apoptosis
GAS6-AS1 LOC644656	ID3	1.10	1.29	1.75	1.49	1.57	DNA damage
GAS6-AS1 LOC338799 LOC644656	**TP53I3**	3.18	4.23	3.73	2.29	1.82	Cell death
GAS6-AS1	**MDM2**	3.49	3.35	3.30	2.26	1.21	Cell cycle arrest, apoptosis
LOC338799	**BAX**	1.71	2.4	2.45	2.46	1.99	Apoptosis
LOC338799	**CDKN1A**	2.28	3.56	3.04	2.50	1.95	Cell cycle arrest, apoptosis
LOC338799	CDK6	-1.03	-1.25	-1.96	-2.75	-3.46	G1 arrest
LOC338799	**ISCU**	2.63	3.17	3.62	4.76	4.10	-
LOC338799	**LCE1C**	3.92	7.72	6.48	9.92	5.15	DNA damage
LOC338799	**LCE1F**	6.01	9.96	14	20	13.6	DNA damage
USP17L6P	**TRIAP1**	3.74	6.56	8.69	18.5	13.4	Apoptosis
TERC	MOAP1	1.12	1.18	1.31	1.55	1.65	Cell death, apoptosis
TERC	EIF3D	1.12	1.47	1.51	1.94	1.99	Cell death, apoptosis

Genes in bold show more than 2-fold increase in expression levels in at least three groups.

were up-regulated at 24 h after UVC irradiation. We performed lncRNA-mRNA coexpression network analysis, demonstrating the potential regulatory role of lncRNAs in UVC-induced DDR via p53 signaling pathway. Especially, LOC338799 and coexpressed genes such as LCE1F and ISCU showed the increase in expression levels with the increase of UVC radiation dose. We suppose that five candidate lncRNAs including LOC338799, LOC644656, GAS6-AS1, TERC, and USP17L6P could be involved in DNA damage, cell cycle, apoptosis, and cell death through the regulation of coexpressed genes.

We selected the optimal dose range of UVC radiation, based on determining the status of live and dead cells after UVC radiation. We identified the percentage of dead cells was 30-70% in CD4 cells at 24 h after 4-64 J/m^2 of UVC irradiation. Therefore, the optimal dose range of UVC radiation was 4-64 J/m^2 in our experimental settings. It is known that γ-H$_2$AX is a highly specific and sensitive molecular marker for the detection of DNA damage. The detection of γ-H$_2$AX foci in DNA strand break (DSB) sites or the increase in γ-H$_2$AX fluorescent intensity indicates the occurrence of DNA damage [28]. We found that UVC increased the

relative fluorescence intensity of γ-H_2AX in a dose-dependent manner within the dose range of 4-32 J/m^2 except 64 J/m^2, suggesting that 4-32 J/m^2 may be the optimal dose range to study the dose-dependent expression alterations and regulation mechanisms of lncRNAs in the further experiments.

PLK2 plays a key role in cell cycle progression, which is activated at the G1-S transition of cell cycle [29]. TRIAP1 overexpression inhibited cell death and apoptosis by inhibiting p21, which contributed to mitochondrial-dependent apoptosis resistance [27]. In this study, we found that PLK2 and TRIAP1 were up-regulated in UVC-irradiated CD4 cells and qPCR results confirmed the increase in their expression levels with the increase of UVC radiation dose (Fig. S2). ISCU is the main scaffold protein for Fe-S cluster assembly, involved in the regulation of cell metabolism [30]. LCE1F belongs to LCE1 family, which are target genes of p53. LCE1F protein interacts with protein arginine methyltransferase 5 (PRMT5) in response to DNA damage [10]. MOAP1 participates in the internal and external pathways of cell death and activates the apoptotic protein BAX of Bcl-2 family [25]. Studies have shown that knockout of EIF3D significantly induces G2/M arrest and apoptosis by down-regulating cyclin B1 and up-regulating p21 [26].

Among the top 30 coexpressed genes of GAS6-AS1, GADD45A, MDM2, TP53I3, and ID3 have been reported to maintain genomic stability. GADD45A is known downstream gene of p53 and regulate many cellular processes such as DNA damage, cell cycle, and apoptosis [31, 32]. MDM2 is a key regulator of the expression and function of p53, which inhibits p53-mediated cell cycle arrest and apoptosis [33]. TP53I3 is induced by p53 and involved in p53-mediated cell death [34]. It is reported that knockout of ID3 resulted in a significant increase in DNA damage accumulation and chromosomal aberration. After ionizing radiation, ID3 is phosphorylated by ATM and MDC1, resulting in the recruitment of additional DDR factor at DSB sites [35].

In this study, we found that LOC338799 showed the increase in expression levels with the increase of UVC radiation dose. LOC338799 had 8 coexpressed genes, among which most of the genes showed the increased expression levels ($\geq$2-fold) except LCE1C whereas CDK6 was down-regulated in a dose-dependent manner. qPCR results also confirmed positive relationship between LOC338799 and coexpressed genes such as ISCU and LCE1F. CDK6 promotes cell cycle progression from G1 to S, inhibited by CDKN1A [36]. BAX induces apoptosis as a direct transcriptional target of p53 [37]. LCE1C and LCE1F belong to LCE1 family as p53 downstream targets. It is reported that induction of LCE1 expressions was caused by UV irradiation in a p53-dependent manner and might have functions on DNA damage through modulation of the PRMT5 activity [10]. Taken together, LOC338799 might play a critical role in p53-mediated DDR through regulating the expression of its coexpressed genes.

It is known that some lncRNAs have been associated with human diseases, implicated in the progression of human cancer. GAS6-AS1 was down-regulated in 50 cases of non-small-cell lung cancer, negatively correlated with lymph node metastasis and advanced lymph node metastasis [22]. The expression of TP53TG1 was significantly increased in human glioma tissues or cell lines. In the case of sugar deficiency, TP53TG1 knockout decreased cell proliferation and migration [23].

Although the number of novel lncRNAs is increasing, cellular functions of many lncRNAs remain unknown. Our results suggest that specific lncRNAs might be involved in DDR induced by UVC irradiation via p53 signaling pathway. We also performed sequence analysis of lncRNA and coexpressed genes, and confirmed that there were the same short sequences (>10 nt) between some lncRNAs and their coexpressed genes (data not shown), indicating that they might work together to participate in DDR. Further, it is necessary to do knockout or overexpression experiments to understand their contributions to DDR in the near future.

5. Conclusions

In this study, we at the first time investigated the expression alterations of mRNAs and lncRNAs in CD4 cells after UVC radiation. We propose an integrated molecular mechanism of lncRNAs in UVC-induced DNA damage in human lymphocytes. LOC338799 showed the increase in expression levels with the increase of UVC radiation dose. LOC338799 and 8 coexpressed genes were most likely involved in the regulation of DNA damage, cell cycle, apoptosis, and cell death via p53 signaling pathway.

Data Availability

The data used to support the findings of this study are available from the corresponding author upon request.

Conflicts of Interest

The authors declare that there is no conflict of interest regarding the publication of this paper.

Acknowledgments

Supplementary Materials

Table S1: PCR primer sequences of genes and lncRNAs used in RT reaction and real-time reaction. Table S2: number of differentially expressed genes in UVC-radiated CD4 cells. Table S3: number of differentially expressed lncRNAs in UVC-radiated CD4 cells. Fig. S1: stem analysis of differentially expressed genes in UVC-radiated CD4 cells. Fig. S2: regression analysis of regulated genes and validation of lncRNA expression alterations. (a) Regression analyses of coexpressed genes TRIAP1, PLK2, NFKBIE, and ZPLD1 show dose-dependent relationships between expression alteration and the radiation dose within the range of 4-32 J/m2. (b) qRT-PCR results confirmed the expression

alterations of CDKN1A1, GADD45A, TRIAP1, and PLK2 in CD4 cells at 24 h after UVC irradiation. $^*P < 0.05$, $^{**}P < 0.01$ compared with control group. (Supplementary Materials)

References

[1] R. Barrios, P. Skurski, and J. Simons, "Mechanism for damage to DNA by low-energy electrons," The Journal of Physical Chemistry B, vol. 106, no. 33, pp. 7991–7994, 2002.

[2] E. Lipiec, R. Sekine, J. Bielecki, W. M. Kwiatek, and B. R. Wood, "Molecular characterization of DNA double strand breaks with tip-enhanced Raman scattering," Angewandte Chemie International Edition, vol. 53, no. 1, pp. 169–172, 2014.

[3] M. Gentile, L. Latonen, and M. Laiho, "Cell cycle arrest and apoptosis provoked by UV radiation-induced DNA damage are transcriptionally highly divergent responses," Nucleic Acids Research, vol. 31, no. 16, pp. 4779–4790, 2003.

[4] S. Takeuchi, T. Matsuda, R. Ono, M. Tsujimoto, and C. Nishigori, "Mitotic genes are transcriptionally upregulated in the fibroblast irradiated with very low doses of UV-C," Scientific Reports, vol. 6, no. 1, 2016.

[5] L. Begović, M. Antunovic, I. Matic et al., "Effect of UVC radiation on mouse fibroblasts deficient for FAS-associated protein with death domain," International Journal of Radiation Biology, vol. 92, no. 8, pp. 475–482, 2016.

[6] S. Yan, M. Sorrell, and Z. Berman, "Functional interplay between ATM/ATR-mediated DNA damage response and DNA repair pathways in oxidative stress," Cellular and Molecular Life Sciences, vol. 71, no. 20, pp. 3951–3967, 2014.

[7] S. Nakajima, L. Lan, S. Kanno et al., "UV light-induced DNA damage and tolerance for the survival of nucleotide excision repair-deficient human cells," The Journal of Biological Chemistry, vol. 279, no. 45, pp. 46674–46677, 2004.

[8] P. W. Hastwell, L. L. Chai, K. J. Roberts et al., "High-specificity and high-sensitivity genotoxicity assessment in a human cell line: Validation of the GreenScreen HC GADD45a-GFP genotoxicity assay," Mutation Research, vol. 607, no. 2, pp. 160–175, 2006.

[9] K. H. Vousden and D. P. Lane, "p53 in health and disease," Nature Reviews Molecular Cell Biology, vol. 8, no. 4, pp. 275–283, 2007.

[10] Z. Deng, K. Matsuda, C. Tanikawa et al., "Late Cornified Envelope Group I, a novel target of p53, regulates PRMT5 activity," Neoplasia, vol. 16, no. 8, pp. 656–664, 2014.

[11] M. Tajnik, M. Strazisar, M. Volavsek, E. Bostjancic, and D. Glavac, "BBC3 is down-regulated with increased tumor size independently of p53 expression in head and neck cancer," Cancer Biomarkers, vol. 11, no. 5, pp. 197–208, 2012.

[12] F. Bellutti, A. S. Tigan, S. Nebenfuehr et al., "CDK6 antagonizes p53-induced responses during tumorigenesis," Cancer Discovery, vol. 8, no. 7, pp. 884–897, 2018.

[13] H. K. Dressman, G. G. Muramoto, N. J. Chao et al., "Gene expression signatures that predict radiation exposure in mice and humans," PLoS Medicine, vol. 4, no. 4, p. e106, 2007.

[14] S. Paul, "Dysfunction of the ubiquitin-proteasome system in multiple disease conditions: therapeutic approaches," BioEssays: News and Reviews in Molecular, Cellular and Developmental Biology, vol. 30, no. 11-12, pp. 1172–1184, 2008.

[15] A. Prasad, S. Visweswaran, K. Kanagaraj et al., "^{18}F-FDG PET/CT scanning: Biological effects on patients: Entrance surface dose, DNA damage, and chromosome aberrations in lymphocytes," Mutation Research/Genetic Toxicology and Environmental Mutagenesis, vol. 838, pp. 59–66, 2019.

[16] C. P. Ponting, P. L. Oliver, and W. Reik, "Evolution and functions of long noncoding RNAs," Cell, vol. 136, no. 4, pp. 629–641, 2009.

[17] S. U. Schmitz, P. Grote, and B. G. Herrmann, "Mechanisms of long noncoding RNA function in development and disease," Cellular and Molecular Life Sciences: CMLS, vol. 73, no. 13, pp. 2491–2509, 2016.

[18] J. R. Hall, Z. J. Messenger, H. W. Tam, S. L. Phillips, L. Recio, and R. C. Smart, "Long noncoding RNA lincRNA-p21 is the major mediator of UVB-induced and p53-dependent apoptosis in keratinocytes," Cell Death & Disease, vol. 6, no. 3, p. e1700, 2015.

[19] L. Zhao, Y. Man, and S. Liu, "Long non-coding RNA HULC promotes UVB-induced injury by up-regulation of BNIP3 in keratinocytes," Biomedicine & Pharmacotherapy = Biomedecine & Pharmacotherapie, vol. 104, pp. 672–678, 2018.

[20] G. Liu and W. Zhang, "Long non-coding RNA HOTAIR promotes UVB-induced apoptosis and inflammatory injury by up-regulation of PKR in keratinocytes," Brazilian Journal of Medical and Biological Research = Revista brasileira de pesquisas medicas e biologicas, vol. 51, no. 8, p. e6896, 2018.

[21] X. Wang, K. B. Hu, Y. Q. Zhang, C. J. Yang, and H. H. Yao, "Comprehensive analysis of aberrantly expressed profiles of lncRNAs, miRNAs and mRNAs with associated ceRNA network in cholangiocarcinoma," Cancer Biomarkers: Section A of Disease Markers, vol. 23, no. 4, pp. 549–559, 2018.

[22] L. Han, R. Kong, D. D. Yin et al., "Low expression of long noncoding RNA GAS6-AS1 predicts a poor prognosis in patients with NSCLC," Medical Oncology (Northwood, London, England), vol. 30, no. 4, p. 694, 2013.

[23] A. Diaz-Lagares, A. B. Crujeiras, P. Lopez-Serra et al., "Epigenetic inactivation of the p53-induced long noncoding RNA TP53 target 1 in human cancer," Proceedings of the National Academy of Sciences of the United States of America, vol. 113, no. 47, pp. e7535–e7544, 2016.

[24] E. M. Bolton, A. V. Tuzova, A. L. Walsh, T. Lynch, and A. S. Perry, "Noncoding RNAs in prostate cancer: the long and the short of it," Clinical Cancer Research: an official journal of the American Association for Cancer Research, vol. 20, no. 1, pp. 35–43, 2014.

[25] J. Law, M. Salla, A. Zare et al., "Modulator of apoptosis 1 (MOAP-1) is a tumor suppressor protein linked to the RASSF1A protein," The Journal of Biological Chemistry, vol. 290, no. 40, pp. 24100–24118, 2015.

[26] X. W. Pan, L. Chen, Y. Hong et al., "EIF3D silencing suppresses renal cell carcinoma tumorigenesis via inducing G2/M arrest through downregulation of Cyclin B1/CDK1 signaling," International Journal of Oncology, vol. 48, no. 6, pp. 2580–2590, 2016.

[27] Y. Li, X. Tang, Q. He et al., "Overexpression of mitochondria mediator gene TRIAP1 by miR-320b loss is associated with progression in nasopharyngeal carcinoma," PLoS Genetics, vol. 12, no. 7, p. e1006183, 2016.

[28] L. J. Kuo and L. X. Yang, "Gamma-H2AX - a novel biomarker for DNA double-strand breaks," In vivo, vol. 22, no. 3, pp. 305–309, 2008.

[29] S. Warnke, S. Kemmler, R. S. Hames et al., "Polo-like kinase-2 is required for centriole duplication in mammalian cells," Current Biology: CB, vol. 14, no. 13, pp. 1200–1207, 2004.

[30] O. Berteau, "A missed Fe-S cluster handoff causes a metabolic shakeup," *The Journal of Biological Chemistry*, vol. 293, no. 21, pp. 8312-8313, 2018.

[31] J. Hildesheim, D. V. Bulavin, M. R. Anver et al., "Gadd45a protects against UV irradiation-induced skin tumors, and promotes apoptosis and stress signaling via MAPK and p53," *Cancer Research*, vol. 62, no. 24, pp. 7305–7315, 2002.

[32] T. Maeda, A. N. Hanna, A. B. Sim, P. P. Chua, M. T. Chong, and V. A. Tron, "GADD45 regulates G2/M arrest, DNA repair, and cell death in keratinocytes following ultraviolet exposure," *The Journal of Investigative Dermatology*, vol. 119, no. 1, pp. 22–26, 2002.

[33] Y. Zhu, B. Dai, H. Zhang, G. Shi, Y. Shen, and D. Ye, "Long non-coding RNA LOC572558 inhibits bladder cancer cell proliferation and tumor growth by regulating the AKT-MDM2-p53 signaling axis," *Cancer Letters*, vol. 380, no. 2, pp. 369–374, 2016.

[34] P. M. Flatt, K. Polyak, L. J. Tang et al., "p53-dependent expression of PIG3 during proliferation, genotoxic stress, and reversible growth arrest," *Cancer Letters*, vol. 156, no. 1, pp. 63–72, 2000.

[35] J. H. Lee, S. J. Park, G. Hariharasudhan et al., "ID3 regulates the MDC1-mediated DNA damage response in order to maintain genome stability," *Nature Communications*, vol. 8, no. 1, article 1051, p. 903, 2017.

[36] A. L. Gartel and S. K. Radhakrishnan, "Lost in transcription: p21 repression, mechanisms, and consequences," *Cancer Research*, vol. 65, no. 10, pp. 3980–3985, 2005.

[37] T. Miyashita and J. C. Reed, "Tumor suppressor p53 is a direct transcriptional activator of the human bax gene," *Cell*, vol. 80, no. 2, pp. 293–299, 1995.

Research Article

Developmental Timing Determines the Protective Effect of Maternal Electroacupuncture on Perinatal Nicotine Exposure-Induced Offspring Lung Phenotype

Jian Dai [iD],[1] **Bo Ji** [iD],[1] **Guozhen Zhao,**[1] **Yawen Lu** [iD],[1] **Yitian Liu** [iD],[1] **Qiujie Mou,**[1] **Reiko Sakurai,**[2] **Yana Xie,**[1] **Qin Zhang,**[1] **Shuang Xu,**[1] and **Virender K. Rehan** [iD][2]

[1]*School of Acupuncture-Moxibustion and Tuina, Beijing University of Chinese Medicine, Beijing 100029, China*
[2]*Department of Pediatrics, Lundquist Institute for Biomedical Innovation at Harbor-UCLA Medical Center, David Geffen School of Medicine at UCLA, Los Angeles, CA 90502, USA*

Correspondence should be addressed to Bo Ji; jibo678@163.com and Virender K. Rehan; vrehan@lundquist.org

Introduction. Environmental exposure of the developing offspring to cigarette smoke or nicotine is an important predisposing factor for many chronic respiratory conditions, such as asthma, emphysema, pulmonary fibrosis, and so forth, in the exposed offspring. Studies showed that electroacupuncture (EA) applied to maternal "Zusanli" (ST36) acupoints during pregnancy and lactation protects against perinatal nicotine exposure- (PNE-) induced lung damage. However, the most effective time period, that is, prenatal vs. postnatal, to attain this effect has not been determined. *Objective.* To determine the most effective developmental timing of EA's protective effect against PNE-induced lung phenotype in the exposed offspring. *Methods.* Pregnant rats were given (1) saline ("S" group); (2) nicotine ("N" group); (3) nicotine + EA, exclusively prenatally ("Pre-EA" group); (4) nicotine + EA, exclusively postnatally ("Post-EA," group); and (5) nicotine + EA, administered both prenatally and postnatally ("Pre- and Post-EA" group). Nicotine was injected once daily (1 mg/kg, 100 μl) and EA was administered to bilateral ST36 acupoints once daily during the specified time-periods. At the end of the experimental periods, key hypothalamic pituitary adrenal (HPA) axis markers in pups and dams, and lung function, morphometry, and the central molecular markers of lung development in the offspring were determined. *Results.* After nicotine exposure, alveolar mean linear intercept (MLI) increased, but mean alveolar number (MAN) decreased and lung PPARγ level decreased, but glucocorticoid receptor (GR) and serum corticosterone (Cort) levels increased, in line with the known PNE-induced lung phenotype. In the nicotine exposed group, maternal hypothalamic corticotropin releasing hormone (CRH) level decreased, but pituitary adrenocorticotropic hormone (ACTH) and serum Cort levels increased. In the "Pre- and Post-EA" groups, PNE-induced alterations in lung morphometry, lung development markers, and HPA axis were blocked. In the "Pre-EA" group, PNE-induced changes in lung morphometry, GR, and maternal HPA axis improved; lung PPARγ and serum Cort levels were slightly but not significantly improved. In contrast, the exclusive "Post-EA" group showed none of these benefits. *Conclusions.* Maternal EA applied to ST36 acupoints during both pre- and postnatal periods preserves offspring lung structure and function despite perinatal exposure to nicotine. EA applied during the "prenatal period" affords only limited benefits, whereas EA applied during the "postnatal period" is ineffective, suggesting that the EA's effects in modulating PNE-induced lung phenotype are limited to specific time-periods during lung development.

1. Introduction

Despite well-established dangers of tobacco to human health, exposure of pregnant women to mainstream or sidestream smoke remains extremely high [1]. Although among the high-income women, the number of smokers is decreasing, among low-income women, this number is increasing [2]. Importantly, over half of the smokers continue to smoke while pregnant [3]. Considerable evidence supports that nicotine is the main harmful substance in

cigarettes, which rapidly crosses the placenta and accumulates in the fetus in concentrations much higher than maternal serum concentrations [4]. Prenatal exposure to nicotine not only affects the survival and birth weight of infants [5, 6], but also adversely affects many developing systems including but not limited to the nervous, circulatory, immune, and respiratory systems [7–10]. Its effects are especially pronounced on the developing lung [11], as it predisposes the exposed offspring to many chronic respiratory conditions such as asthma, emphysema, pulmonary fibrosis, and so forth. [12–15]. These effects appear to be permanent, lasting to adulthood and some can even be potentially transmitted to future generations [16, 17].

Nicotine's effects on the developing lung have been largely attributed to a disruption in epithelial-mesenchymal paracrine signaling, the central component of which is the nuclear transcription factor peroxisome proliferator-activated receptor-γ (PPARγ). PPARγ is centrally involved in alveolar and airway development [18–20] and is a key determinant of the alveolar fibroblast differentiation to lipofibroblasts, which are essential for alveolar development, homeostasis, and injury repair [18, 21]. Lung-specific PPARγ knockout mice show enlarged alveolar sacs, increased apoptotic cells, and an enlarged lung volume, highlighting PPARγ's indispensable role in lung development [19, 20]. Nicotine, by down-regulating PPARγ, drives alveolar lipofibroblasts to transdifferentiate to myofibroblasts, which are the hallmarks of all chronic lung conditions including the perinatal nicotine exposure- (PNE-) induced lung damage [22, 23]. Supporting these observations, in experimental animal models, blocking lipofibroblast-to-myofibroblast differentiation, using PPARγ agonists blocks and/or reverses the PNE-induced lung damage in the exposed offspring [24, 25].

Hypothalamic pituitary adrenal (HPA) axis, by regulating the production of glucocorticoids, also performs an essential role in lung development and maturation [26]. Glucocorticoids act on the glucocorticoid receptor (GR), expressed in the developing lung, stimulating alveolar epithelial-mesenchymal cross-talk, and increase surfactant production. However, excessive glucocorticoids, either endogenous or administered exogenously, can hinder lung development, predisposing to conditions such as childhood asthma [27] and emphysema [28]. Evidence suggests that perinatal nicotine exposure disrupts maternal and offspring HPA axes, increasing maternal and offspring serum corticosterone (Cort) levels, which impacts offspring growth and development negatively [29–32]. Thereby, PNE-induced lung damage, at least, in part, can be attributed to altered maternal and offspring HPA axes.

Currently, there is no clinically safe and effective pharmacologic intervention to prevent or treat PNE-induced lung damage [25, 33–39]. Interestingly, electroacupuncture (EA) is known to treat a number of respiratory conditions, such as allergic asthma and acute lung injury [40, 41]. By regulating HPA axis, EA also improves airway inflammation associated with asthma [42]. More importantly, experimentally, we have recently

shown that EA applied to maternal "Zusanli" (ST36) acupoints during pregnancy and lactation (from embryonic day 6 [E6] to postnatal day 21 [PND21]) protects against PNE-induced lung damage [31, 32]. However, the most effective time-period, that is, prenatal vs. postnatal, to attain this effect has not been determined. Since lung morphogenesis is a complex, finely orchestrated program with specific signaling pathways involved at specific stages during development, we hypothesize that the EA's effect in modulating PNE-induced lung phenotype is limited to specific time-periods during lung development. Here we compare EA's protective effect against nicotine-induced lung phenotype, when it is administered exclusively "prenatally" (embryonic, pseudoglandular, canalicular, and early saccular stages of lung development), exclusively "postnatally" (late saccular and alveolar stages of lung development), or both "pre- and postnatally" (all stages of lung development).

2. Materials and Methods

2.1. Animals. Approval was obtained from the Beijing University of Chinese Medicine experimental animal Ethics Committee in 2017 and all animal procedures were performed in accordance with the "Guide to the Care and Use of Experimental Animals" of the China Animal Welfare Commission. Thirty female and ten male specific pathogen-free Sprague-Dawley rats (11 weeks old) without prior mating history were obtained (SPF, Beijing, Biotechnology Co., Ltd., production license number: SCXK (Beijing) 2006-0002). Animals were housed at a constant temperature and humidity environment with 12 hours of alternate light and dark cycle, with the provision of ad lib food and water. The feeding cages and water bottles were regularly disinfected.

2.2. Experimental Protocol. In line with a well-established model [31, 32], saline or nicotine injections (saline: 100 μl volume once daily and nicotine: 1 mg/kg in 100 μl volume once daily) were started on E6, and continued throughout pregnancy and lactation, that is, up to PND21 (except on the day of delivery). The saline group ("S" group) was injected saline once daily. The nicotine group ("N" group) was injected nicotine once daily. For the prenatal EA group ("Pre-EA group"), nicotine injection was the same as in the "N" group, but these dams were also administered EA to bilateral ST36 acupoints from E6 to the day of delivery. For the postnatal EA group ("Post-EA" group), nicotine injection was the same as in the "N" group, but these animals were administered EA to bilateral ST36 acupoints from PND1 to PND21. The prenatal and postnatal EA group ("Pre- and Post-EA" group) was administered nicotine similar to the "N" group, but these animals also received EA at bilateral ST36 acupoints from E6 to PND21 (except on the day of delivery). On PND21, pulmonary function testing was performed before sacrificing pups for lung tissue and serum collection and dams for the hypothalamus, pituitary, and serum collection.

2.3. Electroacupuncture Protocol.

The ST36 acupoints were identified at the posterolateral side of knee-joint about 5 mm below the head of the fibula, as detailed in "Experimental Acupuncture Science" [43]. Disposable sterile acupuncture needles (0.20 mm × 13 mm, Beijing Hanyi Medical Instruments Centre, China) were pierced to a depth of ~0.7 cm at bilateral ST36 acupoints (connecting to negative pole) and horizontally to a depth of ~0.2 cm into the skin below ST36 (connecting to positive pole). The EA parameters were, frequency 2/15 Hz; intensity 1 mA; and duration 20 minutes, administered once a day. For consistency, acupuncture was performed by the same operator between 10 a.m. to twelve noon throughout the study period.

2.4. Pulmonary Function Testing.

Pulmonary function testing was performed by the Respiratory Function Instrument with Buxco FinePointe software (Buxco, USA). The pups were intraperitoneally injected with 2% pentobarbital (5.5 mg/100g) for anesthesia, tracheotomized, cannulated, and connected to a ventilator for plethysmography. After a period of steady breaths, the lung resistance (RL), dynamic compliance (Cdyn), minute ventilation volume (MV), and peak expiratory flow (PEF) were recorded.

2.5. Lung Morphology.

At sacrifice, pup lungs were fully inflated with 4% paraformaldehyde (PFA) in PBS with constant pressure; after ligation, the lungs were submerged in 4% PFA for about 5 h, followed by immersion in 30% sucrose in PBS. The left lung was used for paraffin embedding, cut into 5 μm slices, which for lung morphometry were stained with hematoxylin and eosin (H&E). Subsequently, lung tissue morphology was assessed by determining mean linear intercepts (MLI) and mean alveolar numbers (MAN) using previously described methods [44].

2.6. Offspring Lung PPARγ and Glucocorticoid Receptor and Maternal Hypothalamic Corticotropic Releasing Hormone and Pituitary Adrenocorticotropic Hormone ELISA.

Offspring lung tissue and maternal hypothalamic and pituitary tissues were homogenized and the supernatants were collected for detecting PPARγ (Cusabio, China, Catalog#: CSBE08624r), GR (Cusabio, China, Catalog#: CSB-E08747r), CRH (Immunoway, USA, Catalog#: KE1318), and ACTH (Raybiotech, USA, Catalog#: EIAR-ACTH 0524197055) using ELISA as per manufacturer's instructions.

2.7. Radioimmunoassay for Serum Corticosterone Levels in Offspring and Mother.

Serum Cort levels in the mother and offspring rats were performed using radioimmunoassay as manufacturer's instructions (BioSino Bio-Technology and Science Inc. Catalog#: HY-068B).

2.8. Offspring Lung PPARγ mRNA Expression by Real-Time PCR.

The method for RNA extraction, Real-time PCR, and the primers information of PPARγ and GAPDH have been described previously [31].

2.9. Statistical Analysis.

The data are expressed as mean ± SD. Statistical analysis was performed using SPSS statistical software (SPSS Inc., USA). One-Way ANOVA-Bonferroni test was used for the comparison of differences between groups, and $P < 0.05$ was considered statistically significant.

3. Results

3.1. Effect of Maternal EA during Different Developmental Time-Periods on PNE-Induced Changes in Offspring Lung Function.

Compared with the "S" group, in the "N" group, Cdyn, MV, and PEF decreased ($P < 0.01$, <0.01, and <0.05, respectively), while RL increased ($P < 0.01$) significantly. Compared with the "N" group, in the "Pre-EA" group, Cdyn increased ($P < 0.01$) and RL decreased ($P < 0.01$) significantly; however, the MV and PEF were not different ($P > 0.05$). Compared with the "N" group, the RL decreased significantly ($P < 0.01$) in the "Post-EA" group; however, the Cdyn, MV, and PEF were not significantly different ($P > 0.05$). Furthermore, the Cdyn, MV, and PEF increased ($P < 0.01$, <0.05, and <0.05, respectively), while RL decreased ($P < 0.01$) significantly, in "Pre- and Post-EA" group vs. the "N" group (Figure 1).

3.2. Effect of Maternal EA during Different Developmental Time-Periods on PNE-Induced Changes in Offspring Lung Morphometry.

The photomicrographs of the H&E-stained sections showed that the alveolar structure in group "S" was intact and the alveolar septum relatively complete. Compared with the "S" group, the alveolar volume in the "N" group was significantly larger, as determined by the greater MLI ($P < 0.01$), accompanying a lower MAN ($P < 0.01$), and in parts ruptured and fused alveolar walls. Compared with the "N" group, the "Pre-EA" and the "Pre- and Post-EA" group had smaller alveolar volumes ($P < 0.05$ and <0.01, respectively, vs. the "N" group) and more alveoli ($P < 0.01$ vs. the "N" group), the rupture and fusion of alveolar walls improved; however, the "Post-EA" group was not different from the "N" group ($P > 0.05$ vs. the "N" group) (Figure 2).

3.3. Effect of Maternal EA during Different Developmental Time-Periods on PNE-Induced Changes in Offspring Lung PPARγ mRNA and Protein Levels.

Using Real-time PCR and ELISA, compared to the "S" group, PPARγ mRNA (Figure 3(a)) and protein (Figure 3(b)) levels decreased significantly in the "N" group ($P < 0.05$, and <0.01, respectively). Both of these changes were blocked in the "Pre- and Post-EA" group ($P < 0.05$, and<0.01 vs. the "N" group); although the "Pre-EA" group showed a significant increase, it did not reach statistical significance ($P > 0.05$ vs. the "N" group); however, the "Post-EA" group was not different from the "N" group in both PPARγ mRNA and protein levels ($P > 0.05$ for both).
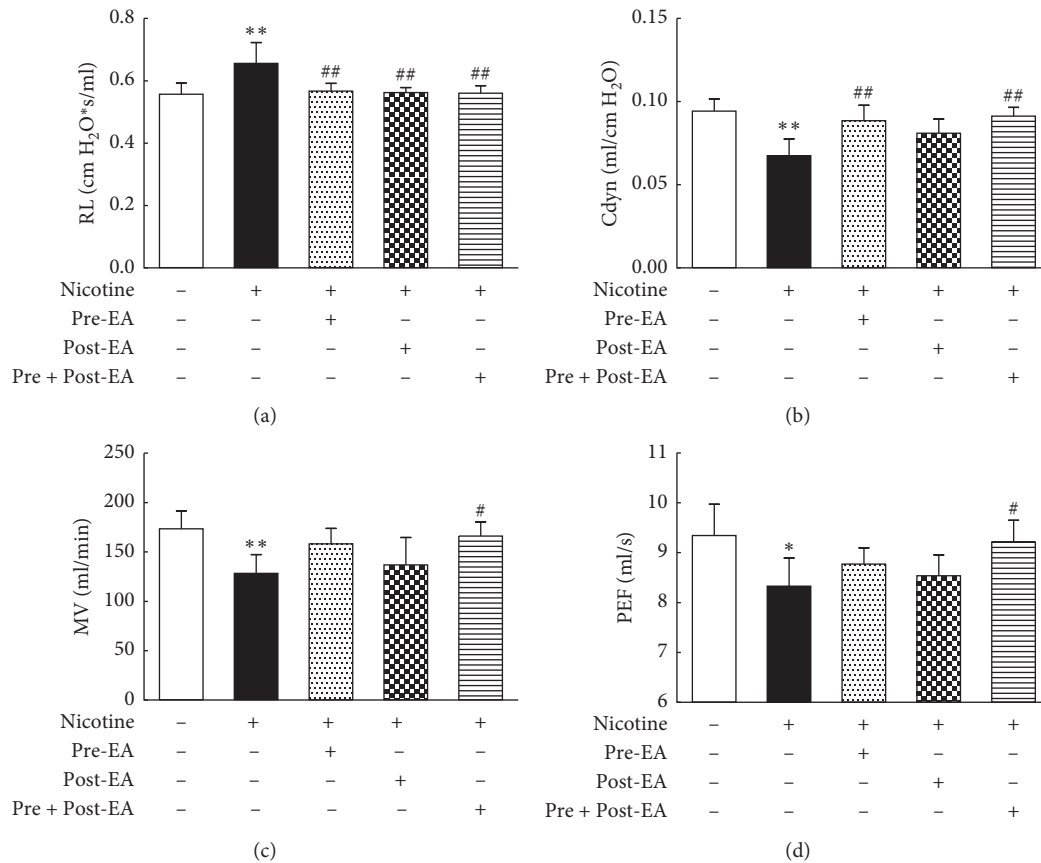
FIGURE 1: Effect of maternal EA during different developmental time-periods on PNE-induced changes in offspring pulmonary function. (a) RL. (b) Cdyn. (c) MV. (d) PEF. Values are mean ± SD; $n = 6$ per group. $^*P < 0.05$, $^{**}P < 0.01$ vs. control; $^\#P < 0.05$, $^{\#\#}P < 0.01$ vs. nicotine.

3.4. Effect of Maternal EA during Different Developmental Time-Periods on PNE-Induced Changes in Offspring HPA Axis. The results showed that serum Cort (Figure 4(a)) and lung GR (Figure 4(b)) levels in the "N" group were significantly higher than in the "S" group ($P < 0.05$, and <0.01, respectively), which normalized in the "Pre- and Post-EA" group ($P < 0.05$, and <0.01 vs. the "N" group). Furthermore, in the "Pre-EA" group, compared with the "N" group, though the lung GR decreased significantly ($P < 0.05$), serum Cort was not significantly different ($P > 0.05$). Furthermore, the "Post-EA" group was not different from the "N" group in both (lung GR and serum Cort levels) of these parameters ($P > 0.05$).

3.5. Effect of Maternal EA during Different Developmental Time-Periods on PNE-Induced Changes in Maternal HPA Axis. The results showed that compared to the "S" group, the levels of maternal hypothalamic CRH decreased ($P < 0.05$, Figure 5(a)), while the pituitary ACTH ($P < 0.01$, Figure 5(b)) and serum Cort ($P < 0.01$, Figure 5(c)) levels increased significantly in "N" group. These changes were blocked in the "Pre-EA" ($P < 0.01$, <0.05, and <0.05, respectively), "Post-EA" ($P < 0.05$, <0.05, and<0.01, respectively), and "Pre- and Post-EA" ($P < 0.01$, <0.01, and <0.01, respectively) group.

4. Discussion

Exposure to mainstream or sidestream smoke during pregnancy is an important healthcare risk worldwide. It adversely affects offspring development, especially having a long-term detrimental effect on the respiratory health of the exposed offspring [45–47]. Considering nicotine's strong addictive effect and the extensive advertising by the tobacco companies to target teens, the problem of smoke exposure during pregnancy is unlikely to go away soon. Hence, finding novel, safe, and effective intervention strategies to mitigate the impact of perinatal tobacco exposure is of great public health significance.

Electroacupuncture is a modification of acupuncture that stimulates acupoints with low-frequency pulsed electrical current. Biologically, it is a combination of acupuncture stimulation and its consequent electrophysiological effects. As a nonpharmacologic therapy, EA is easy to operate and has minimal side effects [48]. ST36 is an acupoint of the "Stomach Meridian" and has been identified to be important for general improvement in health. It is effective in treating diseases of many organ systems, including the respiratory system [49, 50]. It also modulates HPA axis stability [51]. In general, the effects of acupuncture are determined by factors, such as the functional state of the body, stimulation parameters, acupoint selection, and the timing and duration of treatment.
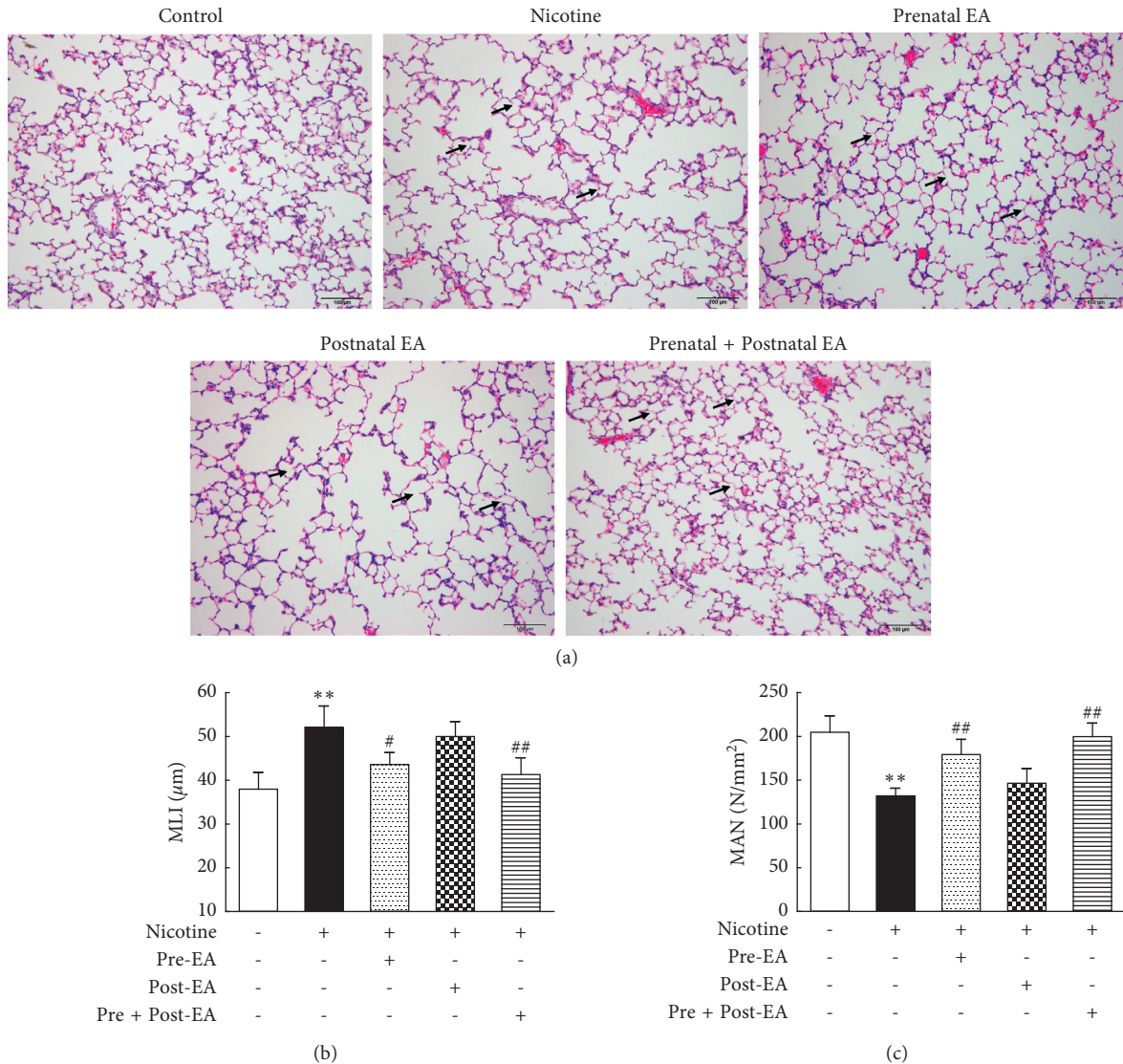
(a)

(b)

(c)

FIGURE 2: Effect of maternal EA during different developmental time-periods on PNE-induced changes in offspring lung morphometry. (a) Representative H&E-stained lung sections. Magnification ×20; arrows point to the integrity and/or rupture of alveolar walls. (b) MLI. (c) MAN. Values are mean ± SD; $n = 5$ per group; $^{**}P < 0.01$ vs. control; $^{#}P < 0.05$, $^{##}P < 0.01$ vs. nicotine.

Regarding the timing of treatment, it was demonstrated that acupuncture treatment 4–7 days after the onset of facial paralysis is better than its administration either within the first 1–3 days or after 8–10 days of the onset of facial paralysis [52]. Similarly, for establishing a more efficient bladder control of a neurogenic urinary bladder following spinal cord injury, earlier intervention is better than later [53]. These studies indicate that the efficacy of acupuncture at different disease stages is different.

Mammalian lung morphogenesis is a complex, finely orchestrated program, which progresses through well-defined, sequential stages to result in fully functional lung; for example, the rat lung development proceeds through the embryonic (E11–13), pseudoglandular (E13–18.5), canalicular (E18.5–20), saccular (E20-PND4), and alveolar (PND4–21) stages. Specific growth factors and signaling mechanisms regulate each stage and drive its progression to

the next stage [54]. By comparing EA's protective effects against nicotine-induced lung phenotype, administered exclusively during the "prenatal period" (embryonic, psuedoglandular, canalicular, and early saccular stage of lung development), "postnatal period" (late saccular and alveolar stages of lung development), or both "prenatal and postnatal periods" (all stages of lung development), we found that the PNE-induced lung morphometric (MLI and MAN) and functional (Cdyn, PEF, MV, and RL) changes were effectively blocked only when EA was administered during both "prenatal and postnatal periods." This is in line with our previous findings [31, 32]. However, its application exclusively during the "prenatal period" resulted in incomplete mitigation of perinatal nicotine-induced pulmonary functional changes, for example, nicotine's effects on Cdyn and RL were blocked, but not on PEF and MV. The application of EA exclusively during the "postnatal period"
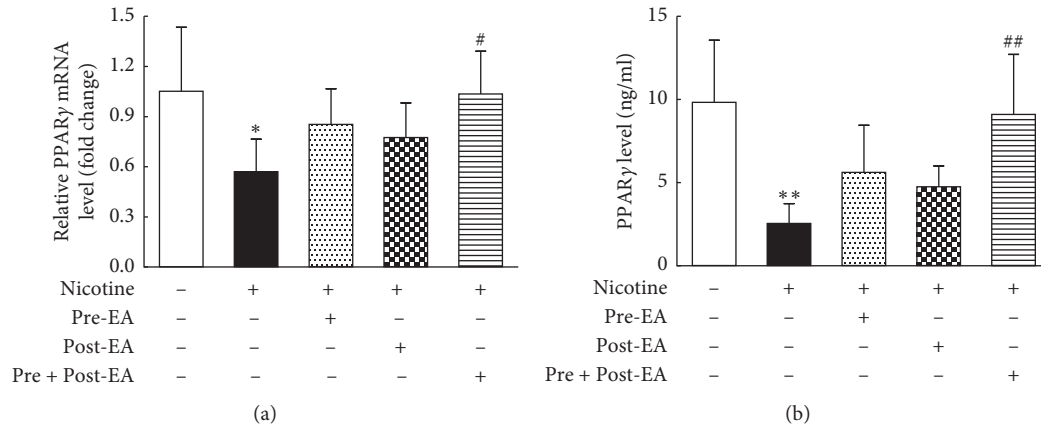
FIGURE 3: Effect of maternal EA during different developmental time-periods on PNE-induced changes in offspring lung PPARγ mRNA and protein levels. (a) PPARγ mRNA. (b) PPARγ protein. Values are mean ± SD; $n = 6$ per group. $^*P < 0.05$, $^{**}P < 0.01$ vs. control; $^{\#}P < 0.05$, $^{\#\#}P < 0.01$ vs. nicotine.
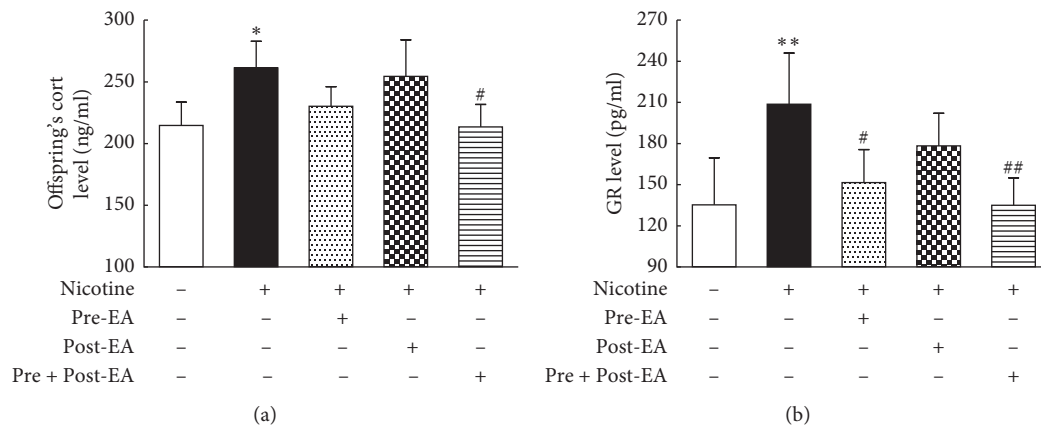

FIGURE 4: Effect of maternal EA during different developmental time-periods on PNE-induced changes in offspring. (a) Serum Cort of offspring. (b) Lung GR of offspring. Values are mean ± SD; $n = 5$-6 per group. $^*P < 0.05$, $^{**}P < 0.01$ vs. control; $^{\#}P < 0.05$, $^{\#\#}P < 0.01$ vs. nicotine.

had even fewer effects; that is, it only blocked PNE-induced changes in RL but not in other pulmonary functional indices. These data suggest a graded efficacy of EA's beneficial effects when administered during both "prenatal and postnatal periods," exclusively "prenatal period," or exclusively "postnatal period," with administration during both "pre- and postnatal periods" providing the maximum beneficial effect, while its administration exclusively during the "postnatal period" had the least beneficial effect.

PPARγ is a ligand-activated transcription factor that plays a key role in regulating lipid storage and metabolism in various organs including the lung [55–57]. Experimentally, in a rat model, PNE down-regulated PPARγ expression in the developing lung along with the associated nicotine-induced pulmonary structural and functional phenotype [25, 58]. EA applied to maternal ST36 acupoints during "pre- and postnatal periods" completely prevented the nicotine-induced decrease in pulmonary PPARγ protein levels, in conjunction with blockage of the perinatal nicotine-induced pulmonary structural and functional changes.

Interestingly, EA applied exclusively during the "prenatal period" only slightly blocked the PNE-induced decrease in pulmonary PPARγ protein levels, which, not surprisingly, was accompanied by incomplete protection against PNE-induced pulmonary effects; that is, although the lung morphology improved, it only partially blocked nicotine's effects on pulmonary function. In contrast, administration of EA exclusively during the "postnatal period," neither improved pulmonary PPARγ protein levels nor nicotine's effects on lung structure and function.

To understand the mechanism of EA's effects on nicotine-induced pulmonary morbidity in the developing lung, it is important to understand nicotine's effects on maternal and fetal HPA axes and how these are affected by EA. Glucocorticoids are key players in mediating stress response on the HPA axis, both before and after birth [59, 60]. In general, maternal and fetal/neonatal glucocorticoid levels correlate closely. High maternal glucocorticoid levels can result in high blood circulatory levels in the fetus and infant through the placenta and breast milk,
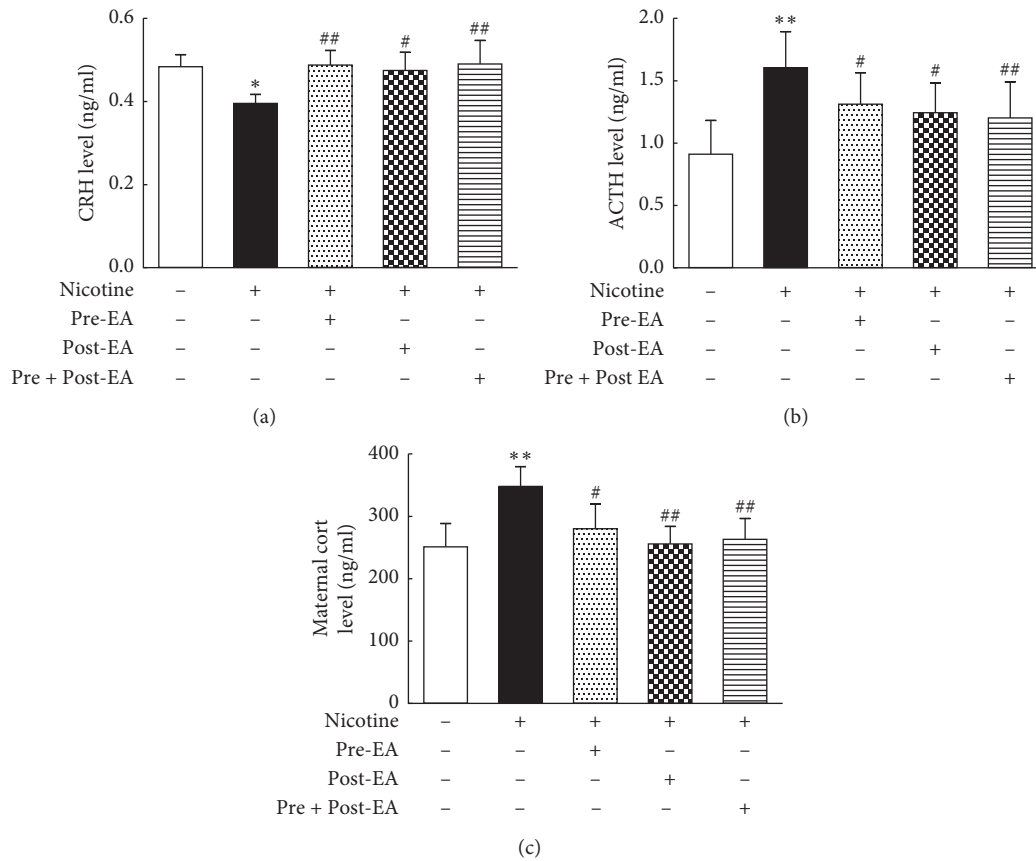
(a)

(b)

(c)

FIGURE 5: Effect of maternal EA during different developmental time-periods on PNE-induced changes in maternal HPA axes. (a) Maternal CRH. (b) Maternal ACTH. (c) Maternal Cort; Values are mean ± SD; $n = 5$-6 per group. $^*P < 0.05$, $^{**}P < 0.01$ vs. control; $^{\#}P < 0.05$, $^{\#\#}P < 0.01$ vs. nicotine.

respectively [61, 62]. Nicotine increases glucocorticoid synthesis in maternal adrenals, decreases placental 11β-HSD-2 activity, and compromises the placental barrier to maternal glucocorticoids, which leads to fetal overexposure to maternal glucocorticoids, which in turn affects fetal HPA axis and growth [29, 30]. In line with our previous studies, with nicotine exposure, we found decreased maternal hypothalamic CRH, but increased pituitary ACTH and serum Cort levels; in addition, fetal serum Cort and lung GR levels increased [31, 32]. Previously, it has been shown that the negative feedback from elevated serum Cort and ACTH levels during pregnancy results in inhibited maternal hypothalamic CRH secretion, which normalizes after delivery [63]. It is likely that perinatal smoke/nicotine-induced lung injury in the exposed offspring, at least in part, is causally related to maternal glucocorticoid overexposure. In contrast, EA applied at ST36 throughout pregnancy and lactation results in increased maternal hypothalamic CRH, but decreased pituitary ACTH and serum Cort levels. This effectively restores the maternal HPA axis, avoiding offspring overexposure to maternal glucocorticoids, which normalizes the offspring's serum Cort and lung GR levels, thereby preventing nicotine-induced lung injury.

Our data suggest that maternal EA during pregnancy can have lasting effects on the maternal HPA axis, that is, at least until the end of lactation. Long lasting effects after

acupuncture have been demonstrated in other conditions as well [64, 65]. For example, in a rat model, it has been demonstrated that inhibition of morphine withdrawal syndrome lasted 7 days after the end of the treatment [64]. As another example, the beneficial effects of acupuncture anesthesia have been shown to last well into the postoperative recovery period [65]. However, these effects gradually wane, which might explain the lack of beneficial effects in pulmonary function and in PPARγ and serum Cort levels at PND21 following prenatal EA. We also found that although EA applied to ST36 acupoints during lactation modulated maternal HPA axis, it had no apparent effect on offspring rats. It is likely to be due to relatively limited transfer to maternal glucocorticoids via breast milk to offspring. A previous study showed that PPARγ agonists administered during lactation (PND1- PND21) could reverse nicotine-induced lung damage in rat offspring [24]. The contrasting data from that study and our present study are possibly related to the fact that in the previous study the PPARγ agonist was directly administered to rat pups, whereas in the present study, the protective effect was dependent upon transmission of protective factors via breast milk. Overall, our data support that for the optimal benefit of EA at ST36 acupoints against perinatal nicotine-induced lung damage, it needs to be administered both pre- and postnatally.

5. Conclusion

In conclusion, in an experimental rat model, maternal EA applied to ST36 acupoints, during both "pre- and postnatal periods," preserves offspring lung structure and function despite perinatal exposure to nicotine. This effect is accompanied by blockage of PNE-induced changes in HPA axes in both the mother and the offspring, thus preventing offspring exposure to excessive maternal glucocorticoids, which occurs with perinatal nicotine exposure. Maternal EA at ST36, administered exclusively during the "prenatal period," affords only limited benefit, while its administration exclusively during the "postnatal period" does not afford obvious protection.

Data Availability

The data used to support the findings of this study are available from the corresponding author (Bo Ji) upon request.

Conflicts of Interest

The authors declare that they have no conflicts of interest.

Acknowledgments

References

[1] N. L. Lee, J. M. Samet, G. Yang et al., "Prenatal secondhand smoke exposure and infant birth weight in China," *International Journal of Environmental Research and Public Health*, vol. 9, no. 10, pp. 3398–3420, 2012.

[2] B. R. Hunt and S. Whitman, "Maternal smoking in Chicago: a community-level analysis," *Journal of Health Care for the Poor & Underserved*, vol. 22, no. 1, pp. 194–210, 2011.

[3] E. Passmore, R. Mcguire, P. Correll, and J. Bentley, "Demographic factors associated with smoking cessation during pregnancy in New South Wales, Australia, 2000–2011," *BMC Public Health*, vol. 15, no. 1, p. 398, 2015.

[4] J. E. Fewell, F. G. Smith, and V. K. Y. Ng, "Threshold levels of maternal nicotine impairing protective responses of newborn rats to intermittent hypoxia," *Journal of Applied Physiology*, vol. 90, no. 5, pp. 1968–1976, 2001.

[5] K. Wisborg, U. Kesmodel, T. B. Henriksen, S. F. Olsen, and N. J. Secher, "Exposure to tobacco smoke in utero and the risk of stillbirth and death in the first year of life," *American Journal of Epidemiology*, vol. 154, no. 4, pp. 322–327, 2001.

[6] K. B. Ashford, E. Hahn, L. Hall, M. K. Rayens, M. Noland, and J. E. Ferguson, "The effects of prenatal secondhand smoke exposure on preterm birth and neonatal outcomes," *Journal of Obstetric, Gynecologic & Neonatal Nursing*, vol. 39, no. 5, pp. 525–535, 2010.

[7] L. Wang, J. Ke, Y. Li et al., "Inhibition of miRNA-210 reverses nicotine-induced brain hypoxic-ischemic injury in neonatal rats," *International Journal of Biological Sciences*, vol. 13, no. 1, pp. 76–84, 2017.

[8] J. Ke, N. Dong, L. Wang et al., "Role of DNA methylation in perinatal nicotine-induced development of heart ischemia-sensitive phenotype in rat offspring," *Oncotarget*, vol. 8, no. 44, pp. 76865–76880, 2017.

[9] N. G. Barra, M. Lisyansky, T. A. Vanduzer, S. Raha, A. C. Holloway, and D. B. Hardy, "Maternal nicotine exposure leads to decreased cardiac protein disulfide isomerase and impaired mitochondrial function in male rat offspring," *Journal of Applied Toxicology*, vol. 37, no. 12, pp. 1517–1526, 2017.

[10] J. Gyekis, K. Anthony, J. E. Foreman, L. C. Klein, and D. J. Vandenbergh, "Perinatal nicotine exposure delays genital development in mice," *Reproductive Toxicology*, vol. 29, no. 3, pp. 378–380, 2010.

[11] H. S. Sekhon, J. A. Keller, N. L. Benowitz, and E. R. Spindel, "Prenatal nicotine exposure alters pulmonary function in newborn rhesus monkeys," *American Journal of Respiratory and Critical Care Medicine*, vol. 164, no. 6, pp. 989–994, 2001.

[12] K. Tanaka, Y. Miyake, S. Furukawa, and M. Arakawa, "Secondhand smoke exposure and risk of wheeze in early childhood: a prospective pregnancy birth cohort study," *Tobacco Induced Diseases*, vol. 15, no. 1, p. 30, 2017.

[13] G. S. Maritz and M. Mutemwa, "The effect of grand maternal nicotine exposure during gestation and lactation on lung integrity of the F2 generation," *Pediatric Pulmonology*, vol. 49, no. 1, pp. 67–75, 2014.

[14] C. Dasgupta, D. Xiao, Z. Xu, S. Yang, and L. Zhang, "Developmental nicotine exposure results in programming of alveolar simplification and interstitial pulmonary fibrosis in adult male rats," *Reproductive Toxicology*, vol. 34, no. 3, pp. 370–377, 2012.

[15] L.-T. Huang, H.-C. Chou, C.-M. Lin, T.-F. Yeh, and C.-M. Chen, "Maternal nicotine exposure exacerbates neonatal hyperoxia-induced lung fibrosis in rats," *Neonatology*, vol. 106, no. 2, pp. 94–101, 2014.

[16] C. J. Lodge, L. Bråbäck, A. J. Lowe, S. C. Dharmage, D. Olsson, and B. Forsberg, "Grandmaternal smoking increases asthma risk in grandchildren: a nationwide Swedish cohort," *Clinical & Experimental Allergy*, vol. 48, no. 2, pp. 167–174, 2018.

[17] V. K. Rehan, J. Liu, E. Naeem et al., "Perinatal nicotine exposure induces asthma in second generation offspring," *BMC Medicine*, vol. 10, no. 1, p. 129, 2012.

[18] V. K. Rehan and J. S. Torday, "PPARγ signaling mediates the evolution, development, homeostasis, and repair of the lung," *PPAR Research*, vol. 2012, Article ID 289867, 8 pages, 2012.

[19] D. M. Simon, M. C. Arikan, S. Srisuma et al., "Epithelial cell PPARγ contributes to normal lung maturation," *The FASEB Journal*, vol. 20, no. 9, pp. 1507–1509, 2006.

[20] J.-H. Kim, S. Yamaori, T. Tanabe et al., "Lack of epithelial PPARγ causes cystic adenomatoid malformations in mouse fetal lung," *Biochemical and Biophysical Research Communications*, vol. 491, no. 2, pp. 271–276, 2017.

[21] V. K. Rehan and J. S. Torday, "The lung alveolar lipofibroblast: an evolutionary strategy against neonatal hyperoxic lung injury," *Antioxidants & Redox Signaling*, vol. 21, no. 13, pp. 1893–1904, 2014.

[22] V. K. Rehan, Y. Wang, S. Sugano et al., "Mechanism of nicotine-induced pulmonary fibroblast transdifferentiation," *American Journal of Physiology Lung Cellular and Molecular Physiology*, vol. 289, no. 4, pp. 667–676, 2005.

[23] V. K. Rehan, R. Sakurai, Y. Wang, J. Santos, K. Huynh, and J. S. Torday, "Reversal of nicotine-induced alveolar lipofibroblast-to-myofibroblast transdifferentiation by stimulants of parathyroid hormone-related protein signaling," *Lung*, vol. 185, no. 3, pp. 151–159, 2007.

[24] J. Liu, R. Sakurai, and V. K. Rehan, "PPAR-γ agonist rosiglitazone reverses perinatal nicotine exposure-induced asthma in rat offspring," *American Journal of Physiology-Lung Cellular and Molecular Physiology*, vol. 308, no. 8, pp. L788–L796, 2015.

[25] J. Liu, R. Sakurai, E. M. O'Roark, N. J. Kenyon, J. S. Torday, and V. K. Rehan, "PPARγ agonist rosiglitazone prevents perinatal nicotine exposure-induced asthma in rat offspring," *American Journal of Physiology-Lung Cellular and Molecular Physiology*, vol. 300, no. 5, pp. L710–L717, 2011.

[26] A. D. Bird, Y. L. Choo, S. B. Hooper, A. R. McDougall, and T. J. Cole, "Mesenchymal glucocorticoid receptor regulates the development of multiple cell layers of the mouse lung," *American Journal of Respiratory Cell and Molecular Biology*, vol. 50, no. 2, pp. 419–428, 2013.

[27] J. D. Pole, C. A. Mustard, T. To, J. Beyene, and A. C. Allen, "Antenatal steroid therapy and childhood asthma: is there a possible link?," *Medical Hypotheses*, vol. 70, no. 5, pp. 981–989, 2008.

[28] S. Okajima, T. Matsuda, K. Cho, Y. Matsumoto, Y. Kobayashi, and S. Fujimoto, "Antenatal dexamethasone administration impairs normal postnatal lung growth in rats," *Pediatric Research*, vol. 49, no. 6, pp. 777–781, 2001.

[29] M. Chen, T. Wang, Z. X. Liao, X. L. Pan, Y. H. Feng, and H. Wang, "Nicotine-induced prenatal overexposure to maternal glucocorticoid and intrauterine growth retardation in rat," *Experimental and Toxicologic Pathology*, vol. 59, no. 3-4, pp. 245–251, 2007.

[30] D. Xu, G. Liang, Y. E. Yan et al., "Nicotine-induced overexposure to maternal glucocorticoid and activated glucocorticoid metabolism causes hypothalamic-pituitary-adrenal axis-associated neuroendocrine metabolic alterations in fetal rats," *Toxicology Letters*, vol. 209, no. 3, pp. 282–290, 2012.

[31] Y. Liu, B. Ji, G. Zhao et al., "Protective effect of electroacupuncture at maternal different points on perinatal nicotine exposure-induced pulmonary dysplasia in offspring based on HPA axis and signal transduction pathway," *Biochemical and Biophysical Research Communications*, vol. 505, no. 2, pp. 586–592, 2018.

[32] B. Ji, G. Z. Zhao, R. Sakurai et al., "Effect of maternal electroacupuncture on perinatal nicotine exposure-induced lung phenotype in offspring," *Lung*, vol. 194, no. 4, pp. 535–546, 2016.

[33] J. Kung and R. R. Henry, "Thiazolidinedione safety," *Expert Opinion on Drug Safety*, vol. 11, no. 4, pp. 565–579, 2012.

[34] B. J. Proskocil, H. S. Sekhon, J. A. Clark et al., "Vitamin C prevents the effects of prenatal nicotine on pulmonary function in newborn monkeys," *American Journal of Respiratory and Critical Care Medicine*, vol. 171, no. 9, pp. 1032–1039, 2005.

[35] G. S. Maritz and S. S. Rayise, "Effect of maternal nicotine exposure on neonatal rat lung development: protective effect of maternal ascorbic acid supplementation," *Experimental Lung Research*, vol. 37, no. 1, pp. 57–65, 2011.

[36] S. M. Scott and S. R. Rose, "Use of glucocorticoids for the fetus and preterm infant," *Clinics in Perinatology*, vol. 45, no. 1, pp. 93–102, 2018.

[37] R. J. Wapner, Y. Sorokin, L. Mele et al., "Long-term outcomes after repeat doses of antenatal corticosteroids," *New England Journal of Medicine*, vol. 357, no. 12, pp. 1190–1198, 2007.

[38] A. Yildiz, N. Vardi, M. Karaaslan, B. Ates, E. Taslidere, and M. Esrefoglu, "The protective effect of melatonin in lungs of newborn rats exposed to maternal nicotine," *Biotechnic & Histochemistry*, vol. 93, no. 6, pp. 442–452, 2018.

[39] R. Fallah, F. Shoroki, and F. Ferdosian, "Safety and efficacy of melatonin in pediatric migraine prophylaxis," *Current Drug Safety*, vol. 10, no. 2, pp. 132–135, 2015.

[40] Y.-l. Liu, L.-d. Zhang, T.-m. Ma et al., "Feishu acupuncture inhibits acetylcholine synthesis and restores muscarinic acetylcholine receptor M2 expression in the lung when treating allergic asthma," *Inflammation*, vol. 41, no. 3, pp. 741–750, 2018.

[41] C.-L. Huang, C.-J. Huang, P.-S. Tsai, L.-P. Yan, and H.-Z. Xu, "Acupuncture stimulation of ST-36 (Zusanli) significantly mitigates acute lung injury in lipopolysaccharide-stimulated rats," *Acta Anaesthesiologica Scandinavica*, vol. 50, no. 6, pp. 722–730, 2006.

[42] Y. Wei, M. Dong, L. Zhong et al., "Regulation of hypothalamic-pituitary-adrenal axis activity and immunologic function contributed to the anti-inflammatory effect of acupuncture in the OVA-induced murine asthma model," *Neuroscience Letters*, vol. 636, pp. 177–183, 2017.

[43] L. F. Zhang, *The Experimental Acupuncture and Moxibustion Science*, Chemical Industry Press, Beijing, China, 2010.

[44] L. Lin, G. Hou, D. Han, J. Kang, and Q. Wang, "Ursolic acid protected lung of rats from damage induced by cigarette smoke extract," *Frontiers in Pharmacology*, vol. 10, p. 700, 2019.

[45] M. R. Hayatbakhsh, S. Sadasivam, A. A. Mamun, J. M. Najman, G. M. Williams, and M. J. O'Callaghan, "Maternal smoking during and after pregnancy and lung function in early adulthood: a prospective study," *Thorax*, vol. 64, no. 9, pp. 810–814, 2009.

[46] J. Stocks, A. Hislop, and S. Sonnappa, "Early lung development: lifelong effect on respiratory health and disease," *The Lancet Respiratory Medicine*, vol. 1, no. 9, pp. 728–742, 2013.

[47] C. I. Vardavas, C. Hohmann, E. Patelarou et al., "The independent role of prenatal and postnatal exposure to active and passive smoking on the development of early wheeze in children," *European Respiratory Journal*, vol. 48, no. 1, pp. 115–124, 2016.

[48] Y. Zeng, B. Liu, T. Luo, Y. Chen, G. Chen, and D. Chen, "Effects of acupuncture on preeclampsia in Chinese women: a pilot prospective cohort study," *Acupuncture in Medicine*, vol. 34, no. 2, pp. 144–148, 2016.

[49] X.-F. Zhang, Q. Qin, W.-Y. Geng et al., "Electroacupuncture reduces hypothalamic and medullary expression of orexins and their receptors in a rat model of chronic obstructive pulmonary disease," *Acupuncture in Medicine*, vol. 36, no. 5, pp. 312–318, 2018.

[50] W.-y. Geng, Z.-b. Liu, N.-n. Song et al., "Effects of electroacupuncture at Zusanli (ST36) on inflammatory cytokines in a rat model of smoke-induced chronic obstructive pulmonary disease," *Journal of Integrative Medicine*, vol. 11, no. 3, pp. 213–219, 2013.

[51] J.-j. Le, T. Yi, L. Qi, J. Li, L. Shao, and J.-C. Dong, "Electroacupuncture regulate hypothalamic-pituitary-adrenal axis and enhance hippocampal serotonin system in a rat model of depression," *Neuroscience Letters*, vol. 615, pp. 66–71, 2016.

[52] L. Feng and W. Z. Ma, "Impacts on the curative effect of peripheral facial paralysis treated with acupuncture and moxibustion at different times," *Chinese Acupuncture & Moxibustion*, vol. 33, no. 12, pp. 1085–1087, 2013, in Chinese.

[53] J. Qin, Y. J. Zhao, X. X. Shi et al., "Effects of acupuncture intervention at different stages on urinary function reconstruction of neurogenic bladder after spinal cord injury," *Chinese Acupuncture & Moxibustion*, vol. 35, no. 2, pp. 132–136, 2015, in Chinese.

[54] M. Hussain, C. Xu, M. Lu, X. Wu, L. Tang, and X. Wu, "Wnt/β-catenin signaling links embryonic lung development and asthmatic airway remodeling," *Biochimica et Biophysica Acta (BBA)-Molecular Basis of Disease*, vol. 1863, no. 12, pp. 3226–3242, 2017.

[55] M. G. Belvisi, D. J. Hele, and M. A. Birrell, "Peroxisome proliferator-activated receptor gamma agonists as therapy for chronic airway inflammation," *European Journal of Pharmacology*, vol. 533, no. 1–3, pp. 101–109, 2006.

[56] P. Tontonoz, E. Hu, and B. M. Spiegelman, "Regulation of adipocyte gene expression and differentiation by peroxisome proliferator activated receptor γ," *Current Opinion in Genetics & Development*, vol. 5, no. 5, pp. 571–576, 1995.

[57] J. N. Feige, L. Gelman, L. Michalik, B. Desvergne, and W. Wahli, "From molecular action to physiological outputs: peroxisome proliferator-activated receptors are nuclear receptors at the crossroads of key cellular functions," *Progress in Lipid Research*, vol. 45, no. 2, pp. 120–159, 2006.

[58] M. Krebs, R. Sakurai, J. S. Torday, and V. K. Rehan, "Evidence for in vivo nicotine-induced alveolar interstitial fibroblast-to-myofibroblast transdifferentiation," *Experimental Lung Research*, vol. 36, no. 7, pp. 390–398, 2010.

[59] B. C. Bingham, C. S. Sheela Rani, A. Frazer, R. Strong, and D. A. Morilak, "Exogenous prenatal corticosterone exposure mimics the effects of prenatal stress on adult brain stress response systems and fear extinction behavior," *Psychoneuroendocrinology*, vol. 38, no. 11, pp. 2746–2757, 2013.

[60] L. Duthie and R. M. Reynolds, "Changes in the maternal hypothalamic-pituitary-adrenal axis in pregnancy and postpartum: influences on maternal and fetal outcomes," *Neuroendocrinology*, vol. 98, no. 2, pp. 106–115, 2013.

[61] A. K. Smith, D. J. Newport, M. P. Ashe et al., "Predictors of neonatal hypothalamic-pituitary-adrenal axis activity at delivery," *Clinical Endocrinology*, vol. 75, no. 1, pp. 90–95, 2011.

[62] J. J. Hollanders, A. C. Heijboer, B. van der Voorn, J. Rotteveel, and M. J. J. Finken, "Nutritional programming by glucocorticoids in breast milk: targets, mechanisms and possible implications," *Best Practice & Research Clinical Endocrinology & Metabolism*, vol. 31, no. 4, pp. 397–408, 2017.

[63] G. Mastorakos and I. Ilias, "Maternal hypothalamic-pituitary-adrenal axis in pregnancy and the postpartum period: postpartum-related disorders," *Annals Of the New York Academy Of Sciences*, vol. 900, no. 1, pp. 95–106, 2000.

[64] L. Z. Wu, C. L. Cui, and J. S. Han, "Cumulative and lasting effects of multiple 100 Hz electroacupuncture stimulation suppressed the morphine withdrawal syndrome in rats," *Chinese Journal of Pain Medicine*, vol. 7, no. 2, pp. 105–108, 2001, in Chinese.

[65] Z. Yang, C. Q. Li, L. J. Ye, and L. M. Xiang, "Unique post acupuncture effect of acupuncture anesthesia," *Acupuncture Research*, vol. 1-2, p. 251, 1989, in Chinese.

Research Article

Comparison of Protective Effects of Electroacupuncture at ST 36 and LU 5 on Pulmonary and Hypothalamic Pituitary Adrenal Axis Changes in Perinatal Nicotine-Exposed Rats

Yawen Lu ⓘ,[1] **Bo Ji** ⓘ,[1] **Guozhen Zhao,**[1] **Jian Dai,**[1] **Reiko Sakurai,**[2] **Yitian Liu** ⓘ,[1] **Qiujie Mou,**[1] **Yana Xie,**[1] **Qin Zhang,**[1] **Shuang Xu,**[1] **and Virender Kumar Rehan**[2]

[1]*School of Acupuncture-Moxibustion and Tuina, Beijing University of Chinese Medicine, Beijing 100029, China*
[2]*Department of Pediatrics, Lundquist Institute for Biomedical Innovation at Harbor-UCLA Medical Center, Torrance, CA 90502, USA*

Correspondence should be addressed to Bo Ji; jibo678@163.com

Background. Maternal smoking and/or exposure to environmental tobacco smoke continue to be significant factors in fetal and childhood morbidity and are a serious public health issue worldwide. Nicotine passes through the placenta easily with minimal biotransformation, entering fetal circulation, where it results in many harmful effects on the developing offspring, especially on the developing respiratory system. *Objectives.* Recently, in a rat model, electroacupuncture (EA) at maternal acupoints ST 36 has been shown to block perinatal nicotine-induced pulmonary damage; however, the underlying mechanism and the specificity of ST 36 acupoints for this effect are unknown. Here, we tested the hypothesis that compared with EA at ST 36, EA at LU 5 acupoints, which are on lung-specific meridian, will be equally or more effective in preventing perinatal nicotine-induced pulmonary changes. *Methods.* Twenty-four pregnant rat dams were randomly divided into 4 groups: saline ("S"), nicotine ("N"), nicotine + ST 36 (N + ST 36), and nicotine + LU 5 (N + LU 5) groups. Nicotine (1 mg/kg, subcutaneously) and EA (at ST 36 or LU 5 acupoints, bilaterally) were administered from embryonic day 6 to postnatal day 21 once daily. The "S" group was injected saline. As needed, using ELISA, western analysis, q-RT-PCR, lung histopathology, maternal and offspring hypothalamic pituitary adrenal axes, offspring key lung developmental markers, and lung morphometry were determined. *Results.* With nicotine exposure, alveolar count decreased, but mean linear intercept and septal thickness increased. It also led to a decrease in pulmonary function and PPARγ and an increase of β-catenin and glucocorticoid receptor expression in lung tissue and corticosterone in the serum of offspring rats. Electroacupuncture at ST 36 normalized all of these changes, whereas EA at LU 5 had no obvious effect. *Conclusion.* Electroacupuncture applied to ST 36 acupoints provided effective protection against perinatal nicotine-induced lung changes, whereas EA applied at LU 5 acupoints was ineffective, suggesting mechanistic specificity and HPA axis' involvement in mediating EA at ST 36 acupoints' effects in mitigating perinatal nicotine-induced pulmonary phenotype. This opens the possibility that other acupoints, besides ST 36, can have similar or even more robust beneficial effects on the developing lung against the harmful effect of perinatal nicotine exposure. The approach proposed by us is simple, cheap, quick, easy to administer, and is devoid of any significant side effects.

1. Introduction

The concept that smoking is harmful to health has been deeply rooted among the populace, but tobacco smoking continues to hurt, particularly, the most vulnerable members of the society, i.e., fetuses and newborns. Maternal smoking

and/or exposure to environmental tobacco smoke continue to be significant factors in fetal and childhood morbidity and are a serious public health problem worldwide. According to the World Health Organization, more than 1 billion people around the world smoke, and 5 million die from cigarettes each year. In China, the current smoking rate for adults, aged

15 and over, is 27.7, percent and the total number of smokers is more than 300 million (China Adult Tobacco Survey, 2015). Even though the rate of active smoking during pregnancy in China is relatively low, the exposure rate to secondhand smoke during pregnancy is alarmingly high (>50%) [1]. Globally, the rate of smoking during pregnancy varies from 5% to 40% in European countries [2], and about 10% of women in the United States smoke during pregnancy [3]. Currently, many people choose e-cigarettes instead of traditional tobacco products, but the harm caused by nicotine is almost equivalent [4, 5].

There are hundreds of toxicants in tobacco smoke, among which nicotine is the main chemical with known toxicity for the developing lungs and brain [6, 7]. Nicotine easily crosses placenta with minimal biotransformation, and it enters fetal circulation, potentially exceeding 15% of maternal circulation levels. Nicotine levels in the amniotic fluid can exceed maternal plasma levels by 88% [8, 9]. Perinatal nicotine exposure is harmful to the health of the offspring in many aspects; it results in low birth weight, preterm delivery, stillbirth, neurobehavioral deficits, sudden infant death syndrome, and a range of neuroendocrine, craniofacial, and immune system abnormalities [10–16]. In addition to these problems, it is especially harmful to the developing respiratory system. Previous studies have shown lifelong and even transgenerational pulmonary structural and functional changes, consistent with asthma phenotype, among other respiratory morbidities [17].

Despite aforementioned concerns, at present, other than smoking cessation and avoiding cigarette smoke exposure altogether, there is no effective preventive or therapeutic option. Unfortunately, due to aggressive advertising strategies from the tobacco industry, especially towards the youth, and the highly addictive property of nicotine and negative reinforcement of withdrawal symptoms [18, 19], it is unlikely that the problem of smoke/nicotine exposure will go away anytime soon. Therefore, newer, effective approaches are needed to deal with a public health issue of huge clinical, financial, and societal implications.

While pharmacological interventions remain far-fetched, interestingly, perinatal electroacupuncture (EA) offers a promising, practical approach that can be, safely and relatively easily, translated to clinical practice. Using a rat model, we recently showed that EA at ST 36 acupoints (Zusanli) effectively blocked perinatal nicotine-induced pulmonary phenotype in the exposed offspring [20, 21]. However, the specificity of the acupoints ST 36 in blocking perinatal nicotine-induced pulmonary phenotype is not established.

Zusanli (ST 36) is a commonly used acupuncture modality, utilized mainly, for general well-being and gastrointestinal ailments, although it has been also shown to be effective against respiratory conditions such as allergic asthma [22], chronic obstructive pulmonary disease [23], lung injury [24], and pulmonary fibrosis [25]. ST 36 acupoint is located on the Stomach Meridian of Hand-Yangming. In contrast, Chize (LU 5) belongs to the Lung Meridian of Hand-Taiyin (LU), which connects with the lung. Ancient and modern literature studies confirm that LU

5 can treat pulmonary diseases. Although LU 5 and ST 36 belong to different meridians, located on corresponding locations on elbow and knee joints, respectively, both can treat lung diseases. The purpose of this study was to determine whether EA applied at LU 5 acupoints could replicate or surpass the protective effect of EA at ST 36 on perinatal nicotine-induced lung phenotype. By examining the specificity of the beneficial effects of EA at ST 36 acupoints on perinatal nicotine-induced lung phenotype, we hope to gain better mechanistic insights and advance acupuncture's clinical translation for its potential benefits. We hypothesized that compared with EA at ST 36, EA at LU 5 acupoints would be equally or more effective in preventing perinatal nicotine-induced pulmonary phenotype.

1.1. Experimental Equipment and Reagents.

Nicotine bitartrate (99% purity) and pentobarbital (2%) were purchased from Sigma-Aldrich, USA. HAN's acupoint stimulation equipment (LH202H) was obtained from Beijing Huawei Industrial Development Co., Ltd., and Huatuo brand aseptic acupuncture needles (0.20 mm × 13 mm) were acquired from Suzhou Medical supplies Factory Co., Ltd. Pulmonary function studies were performed using AniRes2005 animal lung function analysis system.

1.2. Animal Model and Grouping.

Twenty-four specific pathogen-free (SPF) Sprague Dawley female (11-weeks old, weighing 210 ± 20 g) and eight male (11-weeks old, weighing 240 ± 30 g) rats were purchased from Beijing Weitong Lihua Experimental Animal Technology Co., Ltd. (certificate no. SCXK (Beijing) 2006-0009). The experiments were performed in the barrier animal room of the SPF Animal Research Center of Beijing University of Chinese Medicine. Before the experiment, the animals were allowed to acclimatize for 72 h at room temperature $(23 \pm 1)°C$ in $55 \pm 5\%$ relative humidity and 12 : 12 h light:dark cycle. All animal procedures were conducted in accordance with the Guidelines for the Animal Care and Use advocated by the U. S. National Institutes of Health, as well as the "3R" principle of animal experimentation with reduction, substitution, and optimization. The animal protocol passed the Ethics Committee of Beijing University of Chinese Medicine.

In line with our previously described model [26], pregnant dams were randomly divided to the saline ("S"), nicotine ("N"), nicotine plus Zusanli (N + ST 36), and nicotine plus LU 5 (N + LU 5) groups with 6 dams in each group. At term, dams delivered vaginally. The pups were culled to eight pups/litter and allowed to breast feed ad libitum. Nicotine (1 mg/kg/day~moderate cigarette exposure) in $100 \mu L$ volumes was administered to dams subcutaneously from embryonic day (E) 6 to postnatal day (PND) 21 except on the day of delivery. The "S" group was administered the same amount of saline subcutaneously as the "N" group from E6 to PND 21. The N + ST 36 group, in addition to nicotine, was administered acupuncture at acupoints ST 36, which are located in the posterolateral aspect of the knee joint, 5 mm below the fibulae capitulum (Figure 1). Similarly, the N + LU 5 group was administered
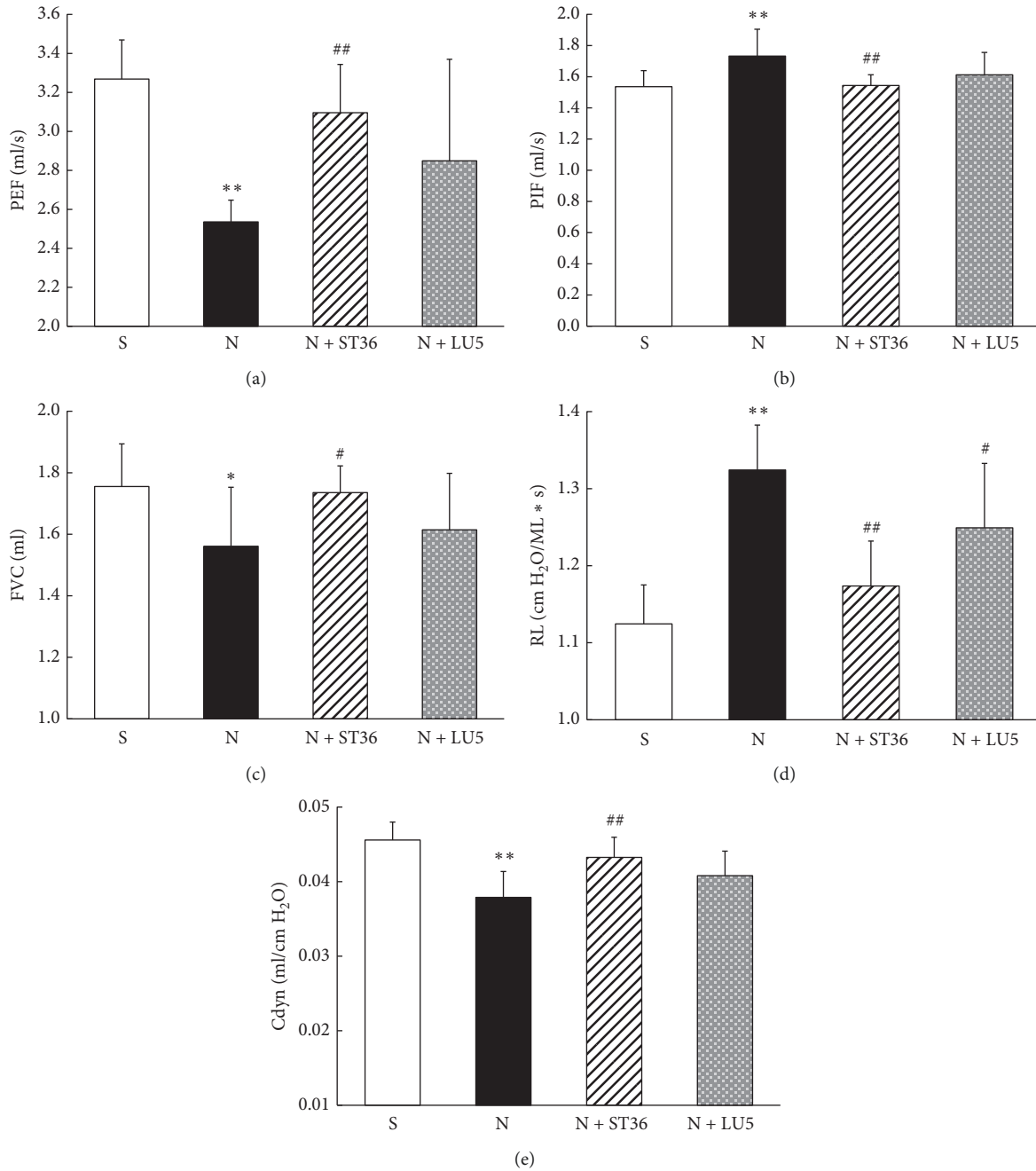
FIGURE 1: Effects of maternal EA on the lung function in perinatal nicotine exposure offspring ($n = 8$; $^{*}<0.05$ vs. control; $^{#}<0.05$ vs. nicotine; $^{**}<0.01$ vs. control; $^{##}<0.01$ vs. nicotine).

acupuncture at LU 5 acupoints, which are located in the transverse cubital crease, on the radial side of the tendon of biceps brachii, i.e., located in the depression of the elbow transverse line on the radial side (Figure 1). The treatment method of EA was the same as that of N + ST 36 group.

For EA application, rat dams were held in a locally made restraining bag with head and legs outside of the bag at opposite ends, taped in prone position on a tabletop. When the dam was quiet, the Huatuo brand acupuncture needles (0.20 mm × 13 mm) were inserted perpendicularly 7 mm into ST 36 or LU 5 acupoints (connected to the EA negative

electrode) and 2 mm subcutaneously below ST 36 or LU 5 (connected to the EA positive electrode). The EA parameters were set as follows: Sparse-dense wave frequency, 2/15 Hz; intensity, 1 mA; and duration, 20 minutes, administered by the same operator, once a day between 10 AM–12 noon every day.

1.3. Pulmonary Function Testing. For pulmonary function studies, on PND 21, after instrument calibration for airway pressure and lung volume, rat pups were weighed and

anesthetized using 2% pentobarbital sodium (55 mg/kg), followed by tracheostomy, cannulation, and ventilation for plethysmography. After respiratory stability was achieved, using AniRes2005 software, airway resistance (RL), peak inspiratory flow (PIF), peak expiratory flow (PEF), forced vital capacity (FVC), and dynamic pulmonary compliance (Cdyn) were derived.

1.4. Sample Collection and Processing

1.4.1. Lung Tissue Morphology. At sacrifice, the lungs were collected and instilled with ice-cold 4% paraformaldehyde (PFA) dissolved in $1 \times$ PBS. These were kept immersed in 4% PFA for 4-5 hours and then moved to 30% sucrose dissolved in PBS. When settled to the bottom of the container, the lungs were removed, and the left lung was paraffin-embedded. An investigator unaware of experimental groups performed lung morphometry on $5 \mu m$ thickness hematoxylin and eosin-stained tissue slices from different experimental groups. Using Image-Pro Plus 6.0 software, alveolar count, mean linear intercept, and septal thickness were determined as described by us previously [27].

1.4.2. Determination of Lung PPARγ, β-Catenin, Serum Corticosterone (Cort), and Pituitary Glucocorticoid Receptor (GR) Levels in Offspring and Pituitary Adrenocorticotropic Hormone (ACTH), Adrenal Melanocortin 2 Receptor (MC2R), and Serum Cort in Maternal Rats. At the end of the experimental period (PND 21), dams and pups were euthanized (pentobarbital 200 mg/kg, injected intraperitoneally), and blood was collected via cardiac puncture. Serum was separated by centrifugation, and samples were frozen at −80°C until processing. Offspring lungs and maternal pituitary and adrenal glands were collected and immediately flash-frozen in liquid nitrogen. Lung PPARγ and β-catenin, serum Cort, and pituitary GR, ACTH, and adrenal MC2R levels were determined using ELISA according to manufacturers' instructions. As needed, the lung tissue, pituitary, and adrenal glands were ground, lysed, and centrifuged. ELISA kits used were PPARγ from LifeSpan BioSciences Co., Ltd. (LS-F15392); β-catenin from Enzo Life Sciences Co., Ltd. (ADI-900-135); ACTH, MC2R, and GR from WUHAN CUSABIO Co., Ltd. (CSB-E06875r; CSB-E013559RA; and CSB-E08747r, respectively).

1.4.3. Detection of PPARγ and β-Catenin in Offspring Lung by Quantitative RT-PCR. RNA extraction was performed using Qiagen RNAeasy Mini kit (category no. 74106) obtained from Life Technologies. The extracted RNA was qualitatively analyzed using Agilent nucleic acid and protein analyzer (Agilent 2100, Germany) and quantified using Nanodrop micronucleic acid protein analyzer (UVS-99ASP-3700ASP, USA) and stored at −80°C until needed for assay. Reverse transcription of RNA to cDNA was performed using SuperScript VILOTM cDNA Synthesis Kit (category no. 11754) for qRT-PCR System (Life Technologies, USA) and the PCR automatic analyzer (PX2 Thermal, USA). Real-time

PCR was performed using the upstream and downstream primers, obtained from Sangon Biotech Co., Ltd., Shanghai, China (Table 1). SYBR Green PCR Master Mix of PPARγ and β-catenin were obtained from Invitrogen (USA) and amplified by the real-time fluorescence quantitative PCR (GeneAmp 7000 Sequence Detection System, Applied Biosystems). The reaction was carried out by activating the DNA polymerase at 95°C for 10 minutes, and then up to 40 PCR denaturation cycles at 95°C for 15 s and annealing at 60°C for 1 minute were performed. The relative quantitative value of each gene was calculated using the 2ΔΔCT method based on CT values.

1.4.4. Statistical Analysis. All data were analyzed using the statistical software (IBM SPSS 20.0). The data are expressed as mean ± SD. The differences between the groups were compared by one-way analysis of variance, followed by the Tukey test. $P < 0.05$ indicated statistically significant difference.

2. Results

2.1. Effect of EA at ST 36 and LU 5 Acupoints of Perinatal Nicotine-Induced Pulmonary Phenotype in Offspring Rats. Compared with the "S" group, the PEF, FVC, and Cdyn in the "N" group decreased significantly ($P < 0.01$, $P < 0.05$, and $P < 0.01$, respectively), while the PIF and RL increased significantly ($P < 0.01$). Compared with the "N" group, the PEF, FVC, and Cdyn in the N + ST 36 group increased ($P < 0.01$, $P < 0.05$, and $P < 0.01$, respectively), and the PIF and RL decreased significantly ($P < 0.01$). Furthermore, compared with the "N" group, while the PEF, FVC, and Cdyn in the N + LU 5 group showed an upward and the RL, a downward trend; these changes did not reach statistical significance ($P > 0.05$) (Figure 1).

The results of ELISA showed that compared with the "S" group, PPARγ protein level decreased, and β-catenin protein increased significantly in the "N" ($P < 0.05$). Compared with the "N" group, in the N + ST 36 group, PPARγ protein level increased, and β-catenin levels decreased significantly ($P < 0.05$). However, in the N + LU 5 group, while there was a trend towards normalization, the changes did not statistical significance ($P > 0.05$) (Figure 2).

The results of qRT-PCR for PPARγ and β-catenin expression were in-line with the ELISA data outlined above, i.e., compared with the "S" group, "N" group showed a significant decrease in PPARγ and a significant increase in β-catenin expression ($P < 0.05$). While these changes were corrected in the N + ST 36 group, there was no statistically significant effect in the LU 5 group ($P > 0.05$), even though there was a trend towards normalization (Figure 3).

2.2. Effect of EA at ST 36 and LU 5 Acupoints on Perinatal Nicotine-Induced Changes in Maternal HPA Axis. The results of ELISA showed that pituitary ACTH, adrenal MC2R, and serum Cort levels of rat dams in "N" group were significantly higher than that in "S" group ($P < 0.01$, $P < 0.01$, and

TABLE 1: Primer sequence and length of amplification segment.

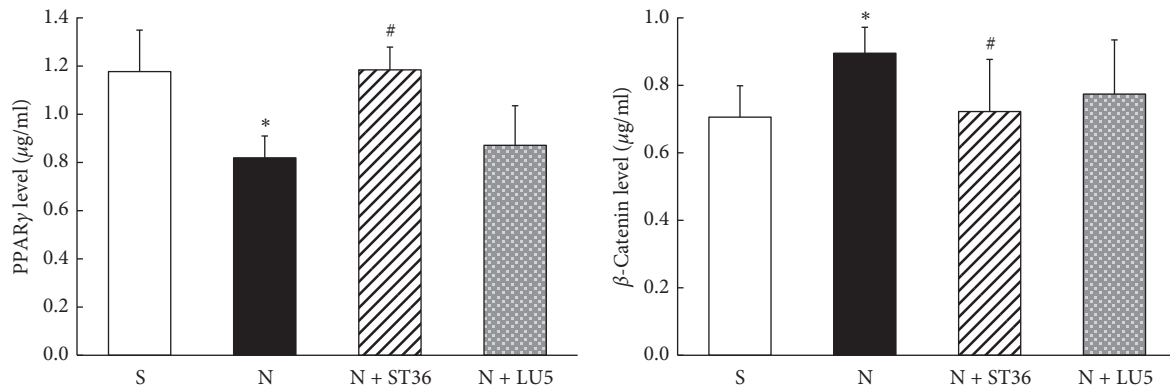| Gene name (rat)	Primer sequence (5′ to 3′)	Length of amplification segment
PPARγ	Forward CCAAGTGACTCTGCTCAAGTATGG Reverse CATGAATCCTTGTCCCTCTGATATG	106 bp
β-Catenin	Forward GTGCAATTCCTGAGCTGACC Reverse CGGGCTGTTTCTACGTCATT	184 bp
GAPDH	Forward GACATGCCGCCTGGAGAAAC Reverse AGCCCAGGATGCCCTTTAGT	92 bp

FIGURE 2: Effects of maternal EA on the levels of lung PPARγ and β-catenin protein in PNE offspring ($n = 6$; * <0.05 vs. control; # <0.05 vs. nicotine).
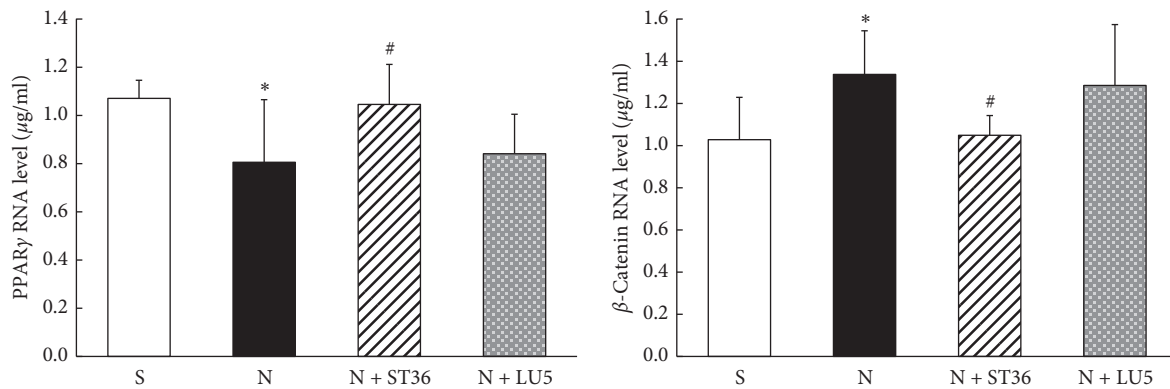

FIGURE 3: Effects of maternal EA on the lung PPARγ and β-catenin mRNA in PNE offspring ($n = 6$; * <0.05 vs. control; # <0.05 vs. nicotine).

$P < 0.05$, respectively). Compared with the "N" group, pituitary ACTH, adrenal MC2R, and serum Cort levels in N + ST 36 group were significantly lower ($P < 0.05$, $P < 0.01$, and $P < 0.05$, respectively) and not statistically different from the "S″" group; however, compared with the "N" group, there was no significant change in the levels of all these biomarkers in the N + LU 5 group ($P > 0.05$) (Figure 4).

2.3. Effect of EA at ST 36 and LU 5 Acupoints on Perinatal Nicotine-Induced Changes in Offspring HPA Axis.
Compared with the "S" group, lung GR and serum Cort levels in the offspring rats in the "N" group were significantly higher ($P < 0.01$, $P < 0.05$, respectively). The GR and Cort levels in the N + ST 36 group were significantly lower compared with the "N" group ($P < 0.01$ and $P < 0.05$, respectively) and were not statistically different from the "S"

group ($P > 0.05$). In contrast, in the N + LU 5 group, while there was a downward trend, these levels were not statistically different compared with the "N" group ($P > 0.05$) (Figure 5).

2.4. Lung Morphometry.
Compared with the "S" group, the mean linear intercept increased and alveolar count decreased significantly in the "N" group ($P < 0.01$ for both). Compared with the "N" group, these changes improved significantly in the N + ST 36 group ($P < 0.05$) and were not statistically different from the "S" group ($P > 0.05$). In contrast, in the N + LU 5 group, while there was an improving trend in these parameters, these did not reach statistical significance vs. the "N" group ($P > 0.05$). Note that lung morphometry data outlined here have been published previously [27].
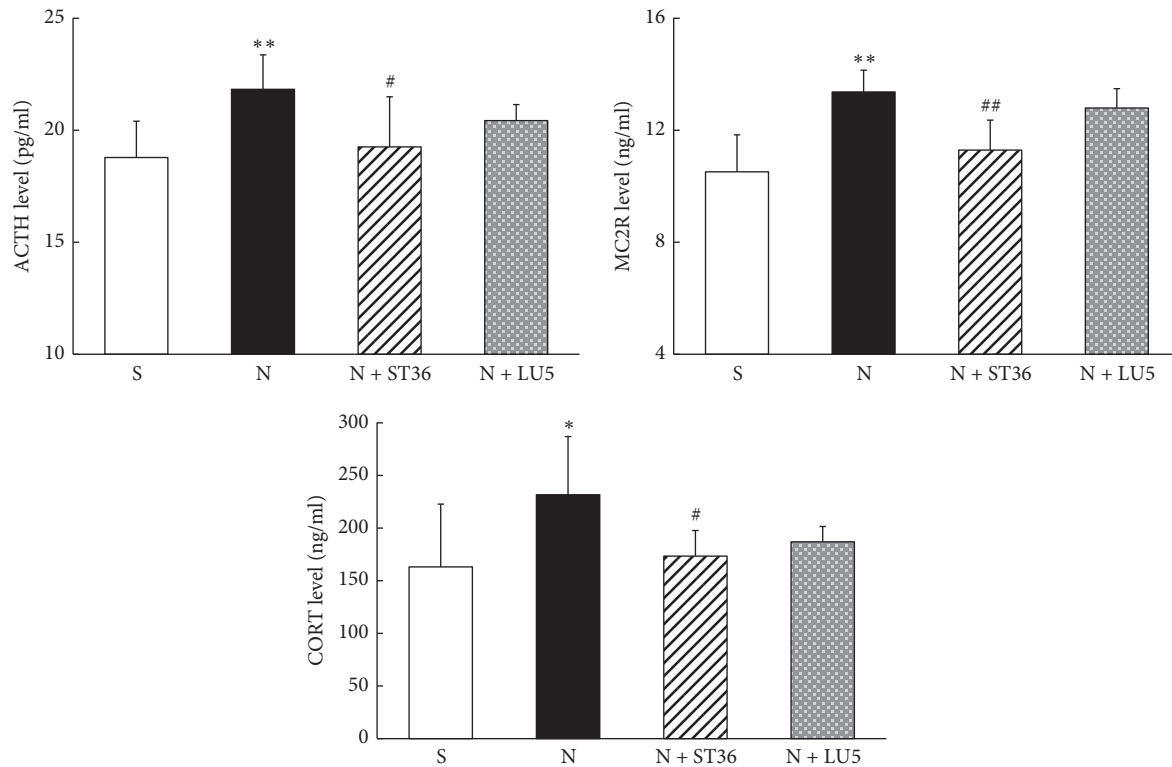
FIGURE 4: Effects of EA on PNE mother of maternal CORT and MC2R and ACTH ($n = 6$) ($^*<0.05$ vs control; $^\#<0.05$ vs. nicotine; $^{**}<0.01$ vs. control; $^{\#\#}<0.01$ vs nicotine).
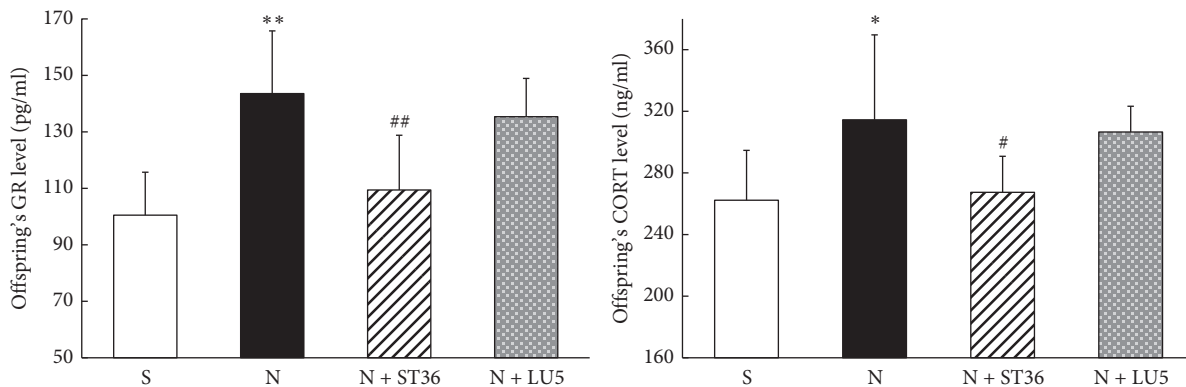

FIGURE 5: Effects of EA on PNE of offspring GR and CORT ($n = 6$; $^*<0.05$ vs. control and $^\#<0.05$ vs. nicotine; $^{**}<0.01$ vs. control; $^{\#\#}<0.01$ vs. nicotine).

3. Discussion

Our data demonstrate that EA at ST 36 blocked the perinatal nicotine-induced changes in maternal (hypothalamic CRH, adrenal MC2R, and serum ACTH and Cort levels) and offspring (serum Cort level and lung GR expression) HPA axes. It also blocked perinatal nicotine-induced changes in key lung developmental signaling pathways (PPARγ downregulation and β-catenin upregulation), lung morphometry (radial alveolar count, mean linear intercept, and septal thickness), and pulmonary function (RL, PIF, PEF, FVC, and Cdyn). In contrast, EA at LU 5 acupoints had no

significant effect on either maternal/fetal HPA axis, or lung molecular, structural, and functional phenotypes.

As outlined above, at present, there is no effective pharmacologic intervention against the harmful effects of perinatal smoke/nicotine exposure on the developing lung; however, our recent work has suggested acupuncture to be a promising, potential approach. Recently, we demonstrated that EA at ST 36 could regulate maternal HPA axis, promote PPARγ and inhibit Wnt signaling in offspring lung, and preserve lung development and function in offspring perinatally exposed to nicotine [20, 21]. All of these findings have been reconfirmed in the present study, along with

contrasting futility of EA at LU 5 in replicating these beneficial effects.

PPARγ signaling is vital for lung lipid differentiation programming, which is essential for normal lung development and homeostasis [28]. PPARγ signaling in turn interacts with Wnt signaling, which is involved in many key developmental biological processes involved in lung development and maturation [29–31]. A balanced PPARγ and Wnt signaling is critically important during lung development [32], a balance that is clearly adversely impacted on perinatal smoke/nicotine exposure [33–36]. Additionally, the HPA axis regulates glucocorticoid levels, which also modulate pulmonary maturation and surfactant synthesis. Briefly, the hypothalamus secretes CRH, which regulates pituitary secretion of ACTH. ACTH regulates adrenocortical secretion of Cort, which, in turn, regulates the secretion of CRH via HPA axis feedback loop [37]. The maternal HPA axis promotes ACTH synthesis and cortisol release into the maternal circulation, which is transported across placenta. Under normal circumstances, the mother, placenta, and fetus work together to regulate the level of glucocorticoids in the uterine environment and prevent fetal exposure to excessive maternal glucocorticoids. Our results show that following perinatal nicotine exposure, maternal pituitary ACTH, adrenal MC2R, and serum Cort levels increase, indicating activated maternal HPA axis. Since nicotine has been shown to disrupt maternal-fetal placental barrier and reduce placental 11β-HSD-2 expression, it results in fetal exposure to a high glucocorticoid environment. This high fetal glucocorticoid environment potentially disrupts fetal neuroendocrine environment, inhibiting fetal HPA axis, intrauterine growth retardation [38], and elicitation of fetal compensatory responses, which, at least, partially explain a likely mechanism for how perinatal nicotine exposure might affect offspring lung development and how acupuncture might modulate it. In line with this paradigm, acupuncture has been shown to modulate HPA axis and regulate PPARγ and β-catenin expressions [38–41]. In particular, EA at ST 36 blocked all perinatal nicotine-induced changes in maternal/offspring HPA axis in conjunction with the protected lung morphologic, molecular, and functional phenotype. In contrast, EA at LU 5 acupoints had no obvious effects on either maternal/offspring HPA axis or the resultant offspring lung phenotype. These results suggest that EA at ST 36 acupoints likely protects against the harmful effects of perinatal nicotine exposure on offspring lung development by primarily modulating maternal/offspring HPA axis, whereas EA at LU 5 acupoints had no such effect.

In the theory of traditional Chinese medicine, the main effects of acupoints' stimulation are directly related to the meridians and position to which they belong. The acupoints on the meridians can treat the diseases of the Zang-fu organs, which the meridians belong to, and the diseases of the Zang-fu organs and tissues, through which the meridians travel, as well as the disease of the adjacent areas. In addition, some acupoints have special therapeutic effects. The therapeutic effects of meridian acupoints are specific, an important factor affecting the beneficial effects of acupuncture. There are differences in functional effects between acupoints and nonacupoints, different acupoints of the same meridian, and different acupoints of different meridians. However, the specificity is relative, as one meridian point can treat multiple viscera and multisystem diseases, different meridian points can treat the same meridian or the same visceral diseases, and different meridian points have different effects on the same disease [42]. The two acupoints selected for this study belong to different meridians. ST 36 belongs to the Stomach Meridian Foot-Yangming (ST), which connects with the stomach. However, both ancient and modern literature supports that acupuncture at ST 36 has beneficial effects on not only gastrointestinal diseases but also on lung diseases. This is not surprising, since, embryologically, lung is derived from the foregut and maintains some functional commonality with gut, e.g., surfactant synthesis and secretion occurs in both organs. Moreover, in traditional Chinese medicine, invigoration of stomach and spleen in enhancing vital energy has been suggested to be the first important point of physical strength. Therefore, ST 36 has been often targeted to strengthen the physique and regulate the body as a whole. The recent work shows that ST 36 has a wide range of regulatory effects on various systems of the whole body, such as the neuroendocrine and immune systems [43]. In particular, by targeting neuroendocrine and immune mechanisms, it enhances the physique and self-repair and modulates various diseases. It is possible that the protective effect of ST 36 on lung development of offspring exposed to perinatal nicotine is related to its strong overall regulatory effect on whole body rather than a specific therapeutic effect on lung development per se. In contrast, since the LU 5 acupoints are connected to lungs, the main treatment targets of the acupoints on this meridian are related to the lung system. Chize (LU 5), the main point of the LU, can treat lung diseases. In addition, studies from ancient times to now have shown that although LU5 can also treat some nonlung diseases, e.g., diarrhoea and low back pain [44, 45]; there is very limited information on LU5 role in overall regulation of the whole body and effect commonly seen with ST 36 acupoints.

It is also important to highlight that in our previous studies, we did not observe any significant effects of EA at sham acupoints on lung morphometry and lung maturation supporting specific mechanisms involved in mediating ST 36 acupoints' effects on the developing lung. However, since we applied EA during both antenatal and postnatal periods, it is difficult to distinguish between the effects for each period, and to determine if postnatal intervention has any effect.

To sum up, comparing the effects of EA at ST 36 and LU 5 acupoints on lung development of the perinatally nicotine exposed offspring, we conclude that the mechanism underlying the beneficial effects of EA at ST 36 acupoints is via modulation of maternal/offspring HPA axis. This likely helps in avoiding offspring exposure to excessive maternal glucocorticoid environment induced by nicotine exposure, which, in turn, blocks the perinatal nicotine-induced decrease in alveolar PPARγ and increase in Wnt signaling, and provides a more homeostatic milieu for offspring lung development. In contrast, even though LU 5 is on the lung meridian and has been used to treat many lung diseases, it

did not prove to be useful against perinatal nicotine's exposure on the developing lungs. It reinforces that the beneficial effects of EA at ST 36 on the developing lung are via its effect on maternal/offspring HPA axis, rather than on offspring lung directly. This opens the possibility that other acupoints besides ST 36 having similar or even more robust beneficial effects on the developing lung against the harmful effect of perinatal nicotine exposure. The approach proposed by us is simple, cheap, quick, easy to administer, and is devoid of any significant side effects.

Data Availability

The data used to support the findings of this study are available from the corresponding author upon request.

Conflicts of Interest

The authors declare that they have no conflicts of interest.

Acknowledgments

References

[1] L. Zhang, J. Hsia, X. Xia et al., "Exposure to secondhand tobacco smoke and interventions among pregnant women in China: a systematic review," *Preventing Chronic Disease*, vol. 12, no. 3, p. E35, 2015.

[2] J. Smedberg, A. Lupattelli, A.C. Mårdby et al., "Characteristics of women who continue smoking during pregnancy: a cross-sectional study of pregnant women and new mothers in 15 European countries," *BMC Pregnancy & Childbirth*, vol. 14, no. 1, p. 213, 2014.

[3] K. Filion, H. Abenhaim, S. Mottillo et al., "The effect of smoking cessation counselling in pregnant women: a meta-analysis of randomised controlled trials," *BJOG: An International Journal of Obstetrics & Gynaecology*, vol. 118, no. 12, pp. 1422–1428, 2011.

[4] T. L. Wagener, E. L. Floyd, I. Stepanov et al., "Have combustible cigarettes met their match? The nicotine delivery profiles and harmful constituent exposures of second-generation and third-generation electronic cigarette users," *Tobacco Control*, vol. 26, no. e1, pp. e23–e28, 2017.

[5] J.-F. Etter and C. Bullen, "A longitudinal study of electronic cigarette users," *Addictive Behaviors*, vol. 39, no. 2, pp. 491–494, 2014.

[6] D. A. Dempsey and N. L. Benowitz, "Risks and benefits of nicotine to aid smoking cessation in pregnancy," *Drug Safety*, vol. 24, no. 4, pp. 277–322, 2001.

[7] M. Eriksen, J. Mackay, and H. Ross, *The Tobacco Atlas*, World Lung Foundation, New York, NY, USA, 2013.

[8] R. L. Andres and M. C. Day, "Perinatal complications associated with maternal tobacco use," *Seminars in Neonatology*, vol. 5, pp. 231–241, 2000.

[9] N. L. Benowitz, *Nicotine Safety and Toxicity*, Oxford University Press, Oxford, UK, 1998.

[10] H. M. Vesterinen, R. Morellofrosch, S. Sen et al., "Cumulative effects of prenatal-exposure to exogenous chemicals and psychosocial stress on fetal growth: systematic-review of the human and animal evidence," *PLoS One*, vol. 12, no. 7, 2017.

[11] J. Schechter, E. K. Do, J. J. Zhang et al., "Effect of prenatal smoke exposure on birth weight: the moderating role of maternal depressive symptoms," *Nicotine & Tobacco Research*, vol. 10, 2018.

[12] J. B. Dwyer, S. C. Mcquown, and F. M. Leslie, "The dynamic effects of nicotine on the developing brain," *Pharmacology & Therapeutics*, vol. 122, no. 2, pp. 125–139, 2009.

[13] T. Alkam, T. Mamiya, N. Yoshida et al., "Prenatal nicotine exposure decreases the release of dopamine in the medial frontal cortex and induces atomoxetine-responsive neurobehavioral deficits in mice," *Psychopharmacology*, vol. 234, no. 12, pp. 1853–1869, 2017.

[14] M. R. Orzabal, E. R. Lunde-Young, J. I. Ramirez et al., "Chronic exposure to e-cig aerosols during early development causes vascular dysfunction and offspring growth deficits," *Translational Research*, vol. 207, pp. 70–82, 2019.

[15] C. Zhu, Y. Guo, H. Luo et al., "Synergistic effects of prenatal nicotine exposure and post-weaning high-fat diet on hypercholesterolaemia in rat offspring of different sexes," *Basic & Clinical Pharmacology & Toxicology*, vol. 124, no. 6, pp. 730–740, 2019.

[16] W. Qu, W.-h. Zhao, X. Wen et al., "Prenatal nicotine exposure induces thymic hypoplasia in mice offspring from neonatal to adulthood," *Toxicology Letters*, vol. 304, pp. 30–38, 2019.

[17] C. T. Mcevoy and E. R. Spindel, "Pulmonary effects of maternal smoking on the fetus and child: effects on lung development, respiratory morbidities, and Life long lung health," *Paediatric Respiratory Reviews*, vol. 10, 2016.

[18] C. G. Aguirre, M. S. Bello, N. Andrabi et al., "Gender, ethnicity, and their intersectionality in the prediction of smoking outcome expectancies in regular cigarette smokers," *Behavior Modification*, vol. 40, no. 1-2, pp. 281–302, 2016.

[19] S. D. Rahmanian, P. T. Diaz, and M. E. Wewers, "Tobacco use and cessation among women: Research and treatment-related issues," *Journal of Women's Health*, vol. 20, no. 3, pp. 349–357, 2011.

[20] B. Ji, G.-Z. Zhao, R. Cao et al., "Effect of maternal electroacupuncture on perinatal nicotine exposure-induced lung phenotype in offspring," *Lung*, vol. 194, no. 4, pp. 535–546, 2016.

[21] Y. Liu, B. Ji, G. Zhao et al., "Protective effect of electroacupuncture at maternal different points on perinatal nicotine exposure-induced pulmonary dysplasia in offspring based on HPA axis and signal transduction pathway," *Biochemical and Biophysical Research Communications*, vol. 10, 2018.

[22] C. Liang-liang, Li An-sheng, T. Jian-ning et al., "Clinical and experimental studies on preventing and treating anaphylactic athma with Zusanli point immunotherapy," *Chinese Journal of Integrated Traditional and Western Medicine*, vol. 12, pp. 709–712, 1996.

[23] J.-h. Xie and J.-h. Yu, "Effect of warming needle moxibustion on pulmonary function of elderly patients with stable chronic obstructive pulmonary disease," *World Journal of Acupuncture–Moxibustion*, vol. 24, no. 3, pp. 21–24, 2014.

[24] W. Huang, X. Zhang, Z. Liu et al., "Effect of electroacupuncture pretreatment on inflammatory cytokines and aquaporin-5 in acute lung injury rats induced by

lipopolysaccharide," *Journal of Yunnan University of Traditional Chinese Medicine*, vol. 40, no. 5, pp. 13–17, 2017.

[25] G. Liu, S. Liu, C. Zhang, F. LI, Y. LIU, and Q. Du, "Clinical observation on the treatment of pulmonary fibrosis in rats through huangqi injection in acupoint Zusanli combined with shaoshang bloodletting," *Journal of Liaoning University of Traditional Chinese Medicine*, vol. 18, no. 8, pp. 154–157, 2016.

[26] R. Sakurai, J. Liu, M. Gong et al., "Perinatal nicotine exposure induces myogenic differentiation, but not epithelial-mesenchymal transition in rat offspring lung," *Pediatric Pulmonology*, vol. 10, 2016.

[27] G. E. Yun-peng, J. I. Bo, Z. H. A. O. Guo-zhen et al., "Electroacupuncture at "Zusanli" (ST36) and "Chize" (LU5) of mother rats exposed to nicotine during pregnancy and lactation has a protective effect on development of lung function and morphology in neonatal rats," *Acupuncture Research*, vol. 44, no. 2, pp. 85–89, 2019.

[28] A. Karadag, R. Sakurai, Y. Wang et al., "Effect of maternal food restriction on fetal rat lung lipid differentiation program," *Pediatric Pulmonology*, vol. 44, no. 7, pp. 635–644, 2009.

[29] M. K. Guo, C. Shao, J. Wang et al., "Wnt/β-catenin signaling plays an ever-expanding role in stem cell self-renewal, tumorigenesis and cancer chemoresistance," *Genes & Diseases*, vol. 3, no. 1, pp. 11–40, 2016.

[30] H. Clevers, K. M. Loh, and R. Nusse, "An integral program for tissue renewal and regeneration: Wnt signaling and stem cell control," *Science*, vol. 346, no. 6205, p. 1248012, 2014.

[31] M. Königshoff and O. Eickelberg, "WNT signaling in lung disease," *American Journal of Respiratory Cell and Molecular Biology*, vol. 42, no. 1, pp. 21–31, 2010.

[32] J. S. Torday and V. K. Rehan, "Up-regulation of fetal rat lung parathyroid hormone-related protein gene regulatory network down-regulates the sonic hedgehog/wnt/βcatenin gene regulatory network," *Pediatric Research*, vol. 60, no. 4, pp. 382–388, 2006.

[33] V. K. Rehan, K. Asotra, and J. S. Torday, "The effects of smoking on the developing lung: insights from a biologic model for lung development, homeostasis, and repair," *Lung*, vol. 187, no. 5, pp. 281–289, 2009.

[34] C. T. Mcevoy, D. Schilling, N. Clay et al., "Vitamin C supplementation for pregnant smoking women and pulmonary function in their newborn infants: a randomized clinical trial," *Jama*, vol. 311, no. 20, pp. 2074–2082, 2014.

[35] A.-F. Hoo, M. Henschen, C. Dezateux, K. Costeloe, and J. Stocks, "Respiratory function among preterm infants whose mothers smoked during pregnancy," *American Journal of Respiratory and Critical Care Medicine*, vol. 158, no. 3, pp. 700–705, 1998.

[36] J. P. Hanrahan, I. B. Tager, M. R. Segal et al., "The effect of maternal smoking during pregnancy on early infant lung function," *American Review of Respiratory Disease*, vol. 145, no. 5, pp. 1129–1135, 1992.

[37] A. Allen, I. Schenkenberger, R. Trivedi et al., "Inhaled fluticasone furoate/vilanterol does not affect hypothalamic-pituitary-adrenal axis function in adolescent and adult asthma: randomised, double-blind, placebo-controlled study," *The Clinical Respiratory Journal*, vol. 7, no. 4, pp. 397–406, 2013.

[38] B. Jia, Z. Li, Y. Shi et al., "Effect of electroacupuncture on changes of behavior and some relat ed hormones of hypothalamus-pituitary-adrenal Axis in chronic stress model rats," *Acupuncture Research*, vol. 29, no. 4, pp. 252–256, 2004.

[39] Y. Cai, Z. Liu, S. Wang et al., "Influence of electroacupuncture of meridian acupoints on the related hormones of the hypothalamus-pituitary-adrenal Axis in rats with cerebral ischemia reperfusion injury," *Acupuncture Research*, vol. 34, no. 5, pp. 297–303, 2009.

[40] X. Jing, C. Ou, H. Chen et al., "Electroacupuncture reduces weight gain induced by rosiglitazone through PPARγ and leptin receptor in CNS," *Evidence-Based Complementary and Alternative Medicine*, vol. 2016, no. 2, Article ID 8098561, 2016.

[41] J. Liu, V. K. R. Sakurai, and V. K. Rehan, "PPAR-γ agonist rosiglitazone reverses perinatal nicotine exposure-induced asthma in rat offspring," *American Journal of Physiology-Lung Cellular and Molecular Physiology*, vol. 308, no. 8, pp. L788–L796, 2015.

[42] F. Liang, F. Zeng, L. Zhao et al., "Specificity of acupoint effect and its fundamental laws," *World Journal of Acupuncture-Moxibustion*, vol. 19, no. 1, pp. 1–5, 2009.

[43] W. Niu, X. Niu, Z. Lei et al., "Effect of acupuncture and moxibustion at Zusanli point on neuroendocrine immune network system," *Journal of Shaanxi University of Chinese Medicine*, vol. 2, pp. 101–103, 2014.

[44] F. Wang, "Treatment of 84 cases of acute tonsillitis by pricking blood on the back of the ear at LU5," *Journal of Clinical Acupuncture and Moxibustion*, vol. 40, no. 3, 2004.

[45] D. Kong, "Discussion on the treatment of backache by using chize (LU5) point," *Modern Traditional Chinese Medicine*, vol. 33, no. 4, pp. 55-56, 2013.

Research Article

Determination of Lymphocyte Cytokinesis-Block Micronucleus Values in Apparently Healthy Children by means of Age and Sex

Burak Durmaz [ID],[1] **Hasan Taslidere,**[1] **Guldane Koturoglu,**[2] **Cumhur Gunduz,**[3] **Mehmet Orman,**[4] **and Ozgur Cogulu** [ID][1,2]

[1]*Department of Medical Genetics, Ege University, Faculty of Medicine, Izmir, Turkey*
[2]*Department of Pediatrics, Ege University, Faculty of Medicine, Izmir, Turkey*
[3]*Department of Medical Biology, Ege University, Faculty of Medicine, Izmir, Turkey*
[4]*Department of Biostatistics, Ege University, Faculty of Medicine, Izmir, Turkey*

Correspondence should be addressed to Burak Durmaz; burak.durmaz@ege.edu.tr

The cytokinesis-block micronucleus (MN) assay on blood lymphocytes is one of the most important tests implemented in cytogenetics for the measurement of genotoxicity. For the purpose of biological dosing, it is crucial to know the spontaneous frequency of MN and its normal values in general population, especially in children, which are used for the population databases. In this study, MN levels were investigated in cytokinesis-blocked lymphocytes of 150 apparently healthy children aged 1 to 15. Our aim was to assess the variability of MN values according to age and sex. The mean MN frequency among boys was $3.69 \pm 1.747‰$ and $4.12 \pm 1.867‰$ in girls where there was no significant difference in relation to age and sex. However, when we separated age groups as 0–2 years, 3–5 years, 6–10 years, and 11–15 years, one-way ANOVA test showed significant association. Significance was obvious in the 0–2 years age group with the 3–5 years age group and 6–10 years age group. When we grouped our study population as 0–2 years and 3–15 years, the mean MN frequency among the 0–2 years age group was $2.85 \pm 1.599‰$ and $4.07 \pm 1.867‰$ in the 3–15 years age group which was also statistically significant. This difference may be attributed to age-related increase of close contact with environmental hazardous agents. In conclusion, normal values of MN obtained in this study will add valuable information in regard to update the current childhood population data and will act as a reference for further genotoxicity studies.

1. Introduction

Maintaining the normal function of a cell is crucial for a living organism, and it depends largely on proper DNA replication and repair mechanisms. In our daily lives, we are increasingly exposed to genotoxic effects including ionizing radiation, detrimental chemicals, and harmful physical agents. These genotoxic agents gradually damage the genetic information within a cell and may predispose to cancer, chronic diseases, or apoptosis [1, 2]. The effect of those factors on genomic stability could be determined by the measurement of micronuclei (MN) [3]. MN which originates from chromosome fragments or whole chromosomes is a measure of chromosome breakage or loss. The most commonly applied method for assessing genotoxicity by MN

assay is the cytokinesis-block technique in which cytochalasin-B is used for this purpose [4]. Elevated MN frequency in lymphocytes has been shown to be associated with an increased risk of cancer, severe adverse cardiovascular events in coronary artery disease patients, diabetes, mild cognitive impairment, Alzheimer's, and Parkinson's diseases [5–8]. Most of the studies investigating MN have been conducted in adults. In parallel, the great majority of studies performed in children has been on the effects of environmental factors, although there have been some reports of increased MN values among children with malnutrition, obesity, iron deficieny, and low blood levels of vitamin B12 [9–12]. Although this test has been reported to be reliable and useful, large variations are observed in the literature [13, 14]. This variability has been linked to study designs, different

experimental conditions, and population characteristics such as genetic and lifestyle factors [15]. In the light of those observations and reports, requirement of normal reference values has been pointed out by some authors [14, 15]. In this study we aimed to present the age-specific MN values in 150 apparently healthy children aged 1 to 15.

2. Materials and Methods

2.1. Patient Selection. Local Ethics Committee approval of the Institute of Medical Research was obtained before starting this work, and this study was performed in accordance with the ethical standards laid down in the Declaration of Helsinki. All the patients and parents were properly informed before and during the procedure, and they signed the informed content. The study population consisted of 150 apparently healthy children who were referred to pediatric outpatient clinic for routine follow-up. The selected children were all selected from the same locality in the summer period (June-August) where there is very limited air pollution and infections. The families were questioned about smoking habits, occurrence of cancer and malignancies, and history of vaccination, and the subjects were selected accordingly. The participants were grouped as age 1 to 15, each consisting of 10 children (5 boys and 5 girls). Inclusion criteria for the study comprised that all the subjects were healthy at the time of blood sampling, none of them had been exposed to ionizing or nonionizing radiation for diagnostic or other purposes during the six-month period, none of them took any medication and none of them had inherited genetic disorders or chronic diseases, and all the children were having a balanced diet and they were all within normal body mass index.

2.2. Blood Sampling. Peripheral whole blood samples were collected in heparinized tubes under aseptic conditions in the morning hours. After collection, the samples were randomly coded and transferred to the laboratory and processed on the same day.

2.3. Cytokinesis-Block Micronucleus (CBMN) Assay. The CBMN assay was performed using cytochalasin B (Cyt-B) as described elsewhere [2]. The cells from peripheral venous blood were cultured in the RPMI medium supplemented with fetal bovine serum, phytohaemagglutinin, penicillin, and streptomycin at 37°C for 72 hours. Cyt-B at a final concentration of $3 \mu g/ml$ was added to each sample on the 44th hour of incubation to accumulate cells that had divided once and incubated for another 18 hours, and then the cultures were harvested. They were centrifuged at 1100 rpm for 10 minutes. After the supernatant was removed, 10 mL of prewarmed hypotonic solution was added to the pellet and incubated for 23 min at 37°C. The cultures were centrifuged at 1100 rpm for 10 minutes and the supernatant was removed, and cells were fixed with a fixative, methanol-acetic acid (3 : 1, v/v). The cells were resuspended in a small volume of fixative and dropped onto clean cold slides. Finally, the slides were stained for 10 minutes in 5% Giemsa dye. Every

subject was analysed for the total number of micronuclei per 1000 binucleated cells according to criteria previously published by Fenech [16]. To prevent commentary differences, the cells were scored under the light microscope by two different qualified and experienced Medical Genetics specialists. Only cells with well-defined cytoplasmic border were evaluated for scoring (Figure 1). Microscopic analysis was done with an optical microscope with a final magnification of 400x (Olympus BX50, Tokyo, Japan).

2.4. Statistical Analysis. The statistical analysis was performed using SPSS 25.0 (SPSS Inc., IL, USA) statistical program package. The Student's *t*-test was used to compare the frequencies of MN among study groups. The Pearson method (*r*) was performed to evaluate the association between age, gender, and MN frequencies. The one-way ANOVA test was used to evaluate the association between MN frequencies and different age groups, and the Bonferroni test was conducted for multiple comparisons of age groups. The value of $p < 0.05$ was considered statistically significant.

3. Results

The study population consisted of 150 healthy children, 75 girls (50%), and 75 boys (50%) with ages ranging from 0 to 15 years. Each age group consisted of 10 subjects (5 boys and 5 girls). Figure 2 presents the error bar graph of MN frequencies within this group. The distribution of MN frequencies dispersed evenly when compared with age and sex. The mean MN frequency among boys was $3.69 \pm 1.747‰$ and $4.12 \pm 1.867‰$ in girls (95% confidence interval (CI)). Student's *t*-test showed there was not any significant correlation between males and females in regard to MN results ($p = 0.151$) (Table 1). The Pearson correlation revealed that there was no significant difference between males and females in relation to age ($r = 0.073$; $p = 0.372$) and sex (male $r = 0.55$, $p = 0.639$ and female $r = 0.92$, $p = 0.435$) (Table 2). However, when we compared different age groups, we were able to find significant results. We separated age groups as 0–2 years, 3–5 years, 6–10 years, and 11–15 years, and the one-way ANOVA test revealed significant association between these groups ($p = 0.021$) (Table 3). Bonferroni posthoc test for multiple comparisons showed significant association of MN frequencies of the 0–2 years age group with 3–5 years age group ($p = 0.046$) and 6–10 years age group ($p = 0.021$). When we grouped our study population as 0–2 years and 3–15 years, the mean MN frequency among the 0–2 years age group was $2.85 \pm 1.599‰$ and $4.07 \pm 1.867‰$ in the 3–15 years age group (95% confidence interval (CI)). Student's *t*-test revealed significant association of MN frequencies between these groups ($p = 0.005$) (Table 4). Figures 3 and 4 show the error bar graphs of MN frequencies among different age groups.

4. Discussion

In parallel with advances in civilization and developments in technology, the rate of exposure of human life to many
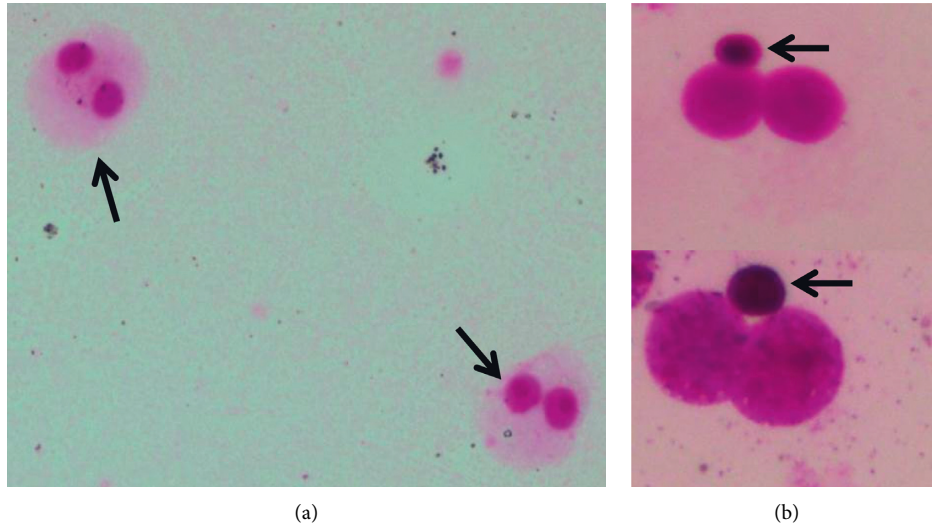
FIGURE 1: Representative of images of cells scored in the micronucleus study: (a) normal binucleated cells, shown by black arrows and (b) close-up view of binucleated cells with a micronucleus. The micronuclei are shown with black arrows.
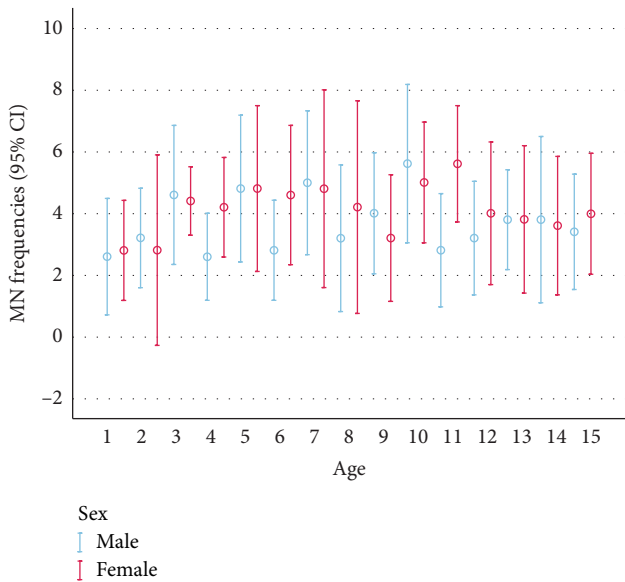

FIGURE 2: Error bar chart representing the MN frequencies, ages, and sexes of the study group. The frequency of MN dispersed evenly among sex and age (95% confidence interval) (MN: micronucleus, CI: confidence interval).

TABLE 1: Comparison of MN frequencies by means of sex. There was no significant correlation ($p > 0.05$).

Sex	Number (%)	MN mean $\pm$ SD	p
Male	75 (50)	3.69 ± 1.747	0.151
Female	75 (50)	4.12 ± 1.867	
Total	150 (100)		

MN: micronucleus, SD: standard deviation.

TABLE 2: The Pearson correlation revealed no significant difference between MN results, sex, and age (MN: micronucleus).

	Pearson correlation (r)	p
Sex		
Male	0.55	0.639
Female	0.92	0.435
Age	0.073	0.372

TABLE 3: The number of cases and MN frequencies are given among different age groups. The one-way ANOVA test showed significant correlation between these groups.

Age group (years)	Number (n)	MN Mean $\pm$ SD	p
0–2	20	2.85 ± 1.599	
3–5	30	4.23 ± 1.654	
6–10	50	4.24 ± 1.985	0.021*
11–15	50	3.80 ± 1.678	
Total	150	3.91 ± 1.815	

MN: micronucleus, SD: standard deviation, * = statistically significant p value.

TABLE 4: The Benferroni test revealed significant association of MN frequencies of the 0–2 years age group with the 3–5 years and 6–10 years age groups (upper part). Student's t-test revealed significant association of MN frequencies between the 0–2 years age group and 3–15 years age group (lower part).

Compared age group (years)	Age group (years)	p
	3–5	0.046*
0–2	6–10	0.021*
	11–15	0.268
0–2	3–15	0.005*

* = statistically significant p value.

genotoxic agents has been increasing over time. The foods taken, the drugs used, and the different causes of radiation are some of those leading agents which come to mind in the first place. Therefore, it is important to measure the

genotoxic capacity of these agents on human health. By this way, it can be possible to screen new chemicals which may be hazardous for the environment, to determine the acceptable
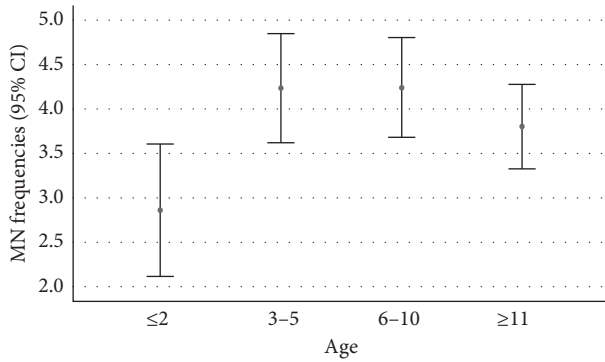
FIGURE 3: Error bar chart shows the MN frequencies between different age groups. There is a significant association of MN frequencies of the 0–2 years age group with the 3–5 years age group and 6–10 years age group (95% confidence interval) (MN: micronucleus, CI: confidence interval).
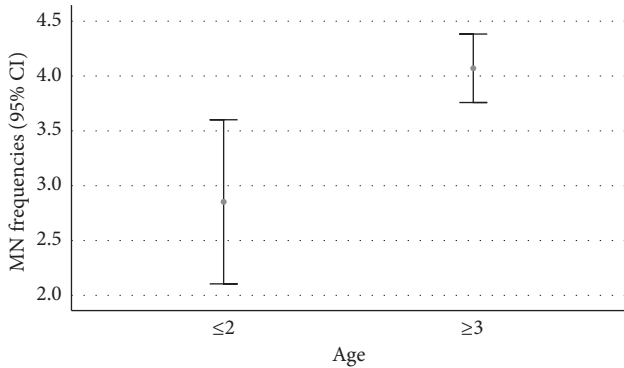

FIGURE 4: Error bar chart reveals the MN frequencies of 0–2 years age group and 3–15 years age group. There is a significant association of MN frequencies between these 2 groups (95% confidence interval) (MN: micronucleus, CI: confidence interval).

level of genetic damage, to identify individuals who are at risk for a specific genotoxic agent. Among the methods measuring genotoxicity in different situations, micronucleus assay is one of the most preferred methods. A number of studies were carried out to determine the baseline frequencies of MN measured with the CBMN method in standard healthy populations. The main factors to affect the frequency of MN were analysed, and they are confirming the age and sex as the main factors associated with the frequency. However, as pointed out by some studies, normal values for micronucleus test in healthy populations has been suggested by some authors due to the wide range of results of this test [14, 15, 17]. Considering this valuable information, the mean MN frequency of all participants in our study was found to be $3.91 \pm 1.82‰$, $3.69 \pm 1.75‰$ in female group, and $4.12 \pm 1.87‰$ in male group. Whereas those values were reported to be higher in adults such as $5.06 \pm 3.11‰$ in all subjects, $5.16 \pm 2.98‰$ in females, and $4.79 \pm 3.44‰$ in males by Gajski et al. [15]. The major difference between those studies and our study is the age groups of the participants. Gajski et al. included adult individuals between 19–80 years of age into their study and separated the study groups as <30, 31–40, 41–50, 51–60, 61–70, and >70. The highest value was

$6.47 \pm 2.42‰$ in the 61–70 age group, and the lowest was in the <30 age group which was $4.15 \pm 2.79‰$. Considering much lower value obtained in our study, increased ratios of MN in previous similar studies could be attributed to age-dependent increasing exposure of environmental conditions which may cause genomic damages.

In our study, no significant correlation was detected between male and female groups. The mean MN frequency of the female group was higher compared with the male group. Age and sex were found to have significant influences on MN frequency by Gajski et al. [15]. Although not being significant, a higher mean value of MN in the female group in our study may be associated with many factors such as growth characteristics of two sexes. In parallel with our study, Bonassi et al. reported not significant but higher level of MN frequency in females compared with males [18].

One of the interesting finding of our study was the detection of significant difference between the 0–2-year-old age group and the other age groups except 11–15. The lowest value in all studies including our study was detected in 0–2 age group. This difference may be due to the fact that children in this age group are exposed to environmental effects much less compared with other age groups because they are in infancy. The fact that children end up in infancy and transition to early childhood brings with it many problems. Common view of the researchers is that the early childhood period is the most important development period in life. They begin to learn the world around them and become vulnerable to harmful external effects such as food or physical and chemical agents by spending more time in the outdoor environment. Therefore, this close contact with hazardous agents increases with age as it progresses to an age-related relationship. Nevertheless, no linear correlation was found with the increasing age in our study except the mean MN values between the different age groups which were identified according to the growth and human development. The fact that there is no linear significant correlation related to each age can be attributed to individual differences in each age group.

In conclusion, our study is one of the few studies discussing the age-related baseline MN frequencies in the pediatric age group. Normal values in this study will be used to update the current pediatric population data regarding micronucleus and will act as a reference for future genotoxicity studies.

Data Availability

The data used to support the findings of this study are included within the article.

Conflicts of Interest

The authors declare that there are no conflicts of interest regarding the publication of this article.

Acknowledgments

References

[1] R. P. Araldi, T. C. de Melo, T. B. Mendes et al., "Using the comet and micronucleus assays for genotoxicity studies: a review," *Biomedicine and Pharmacotherapy*, vol. 72, pp. 74–82, 2015.

[2] T. Nohmi, "Thresholds of genotoxic and non-genotoxic carcinogens," *Toxicological Research*, vol. 34, no. 4, pp. 281–290, 2018.

[3] L. Luzhna, P. Kathiria, and O. Kovalchuk, "Micronuclei in genotoxicity assessment: from genetics to epigenetics and beyond," *Frontiers in Genetics*, vol. 4, p. 131, 2013.

[4] M. Mišík, A. Nersesyan, C. Bolognesi, M. Kundi, F. Ferk, and S. Knasmueller, "Cytome micronucleus assays with a metabolically competent human derived liver cell line (Huh6): a promising approach for routine testing of chemicals?," *Environmental and Molecular Mutagenesis*, vol. 60, no. 2, pp. 134–144, 2019.

[5] S. Bonassi, A. Znaor, M. Ceppi et al., "An increased micronucleus frequency in peripheral blood lymphocytes predicts the risk of cancer in humans," *Carcinogenesis*, vol. 28, no. 3, pp. 625–631, 2007.

[6] C. Federici, N. Botto, S. Manfredi, A. Rizza, M. D. Fiandra, and M. G. Andreassi, "Relation of increased chromosomal damage to future adverse cardiac events in patients with known coronary artery disease," *The American Journal of Cardiology*, vol. 102, no. 10, pp. 1296–1300, 2008.

[7] L. Migliore, R. Scarpato, F. Coppede', L. Petrozzi, U. Bonuccelli, and V. Rodilla, "Chromosome and oxidative damage biomarkers in lymphocytes of Parkinson's disease patients," *International Journal of Hygiene and Environmental Health*, vol. 204, no. 1, pp. 61–66, 2001.

[8] L. Migliore, N. Botto, R. Scarpato, L. Petrozzi, G. Cipriani, and U. Bonuccelli, "Preferential occurrence of chromosome 21 malsegregation in peripheral blood lymphocytes of Alzheimer disease patients," *Cytogenetic and Genome Research*, vol. 87, no. 1-2, pp. 41–46, 1999.

[9] M. Neri, D. Ugolini, S. Bonassi et al., "Children's exposure to environmental pollutants and biomarkers of genetic damageII. Results of a comprehensive literature search and meta-analysis," *Mutation Research/Reviews in Mutation Research*, vol. 612, no. 1, pp. 14–39, 2006.

[10] E. Cervantes-Ríos, R. Ortiz-Muñiz, A. L. Martínez-Hernández, L. Cabrera-Rojo, J. Graniel-Guerrero, and L. Rodríguez-Cruz, "Malnutrition and infection influence the peripheral blood reticulocyte micronuclei frequency in children," *Mutation Research/Fundamental and Molecular Mechanisms of Mutagenesis*, vol. 731, no. 1-2, pp. 68–74, 2012.

[11] C. Minnet, A. Koc, A. Aycicek, and A. Kocyigit, "Vitamin B12 treatment reduces mononuclear DNA damage," *Pediatrics International*, vol. 53, no. 6, pp. 1023–1027, 2011.

[12] D. Prá, A. Bortoluzzi, L. L. Müller et al., "Iron intake, red cell indicators of iron status, and DNA damage in young subjects," *Nutrition*, vol. 27, no. 3, pp. 293–297, 2011.

[13] A. Nersesyan, M. Fenech, C. Bolognesi et al., "Use of the lymphocyte cytokinesis-block micronucleus assay in occupational biomonitoring of genome damage caused by in vivo exposure to chemical genotoxins: past, present and future," *Mutation Research/Reviews in Mutation Research*, vol. 770, pp. 1–11, 2016.

[14] C. Bolognesi, L. Bonelli, A. Compalati et al., ""Normal values" for the lymphocyte cytokinesis-block micronucleus cytome parameters: repeatability and reproducibility in a healthy reference population," *Science of The Total Environment*, vol. 652, pp. 513–522, 2019.

[15] G. Gajski, M. Gerić, V. Oreščanin, and V. Garaj-Vrhovac, "Cytokinesis-block micronucleus cytome assay parameters in peripheral blood lymphocytes of the general population: contribution of age, sex, seasonal variations and lifestyle factors," *Ecotoxicology and Environmental Safety*, vol. 148, pp. 561–570, 2018.

[16] M. Fenech, "Cytokinesis-block micronucleus cytome assay," *Nature Protocols*, vol. 2, no. 5, pp. 1084–1104, 2007.

[17] M. Coşkun, A. Cayır, M. Coşkun, and H. Tok, "Evaluation of background DNA damage in a Turkish population measured by means of the cytokinesis-block micronucleus cytome assay," *Mutation Research/Genetic Toxicology and Environmental Mutagenesis*, vol. 757, no. 1, pp. 23–27, 2013.

[18] S. Bonassi, M. Fenech, C. Lando et al., "Human MicroNucleus project: international database comparison for results with the cytokinesis-block micronucleus assay in human lymphocytes: I. Effect of laboratory protocol, scoring criteria, and host factors on the frequency of micronuclei," *Environmental and Molecular Mutagenesis*, vol. 37, no. 1, pp. 31–45, 2001.